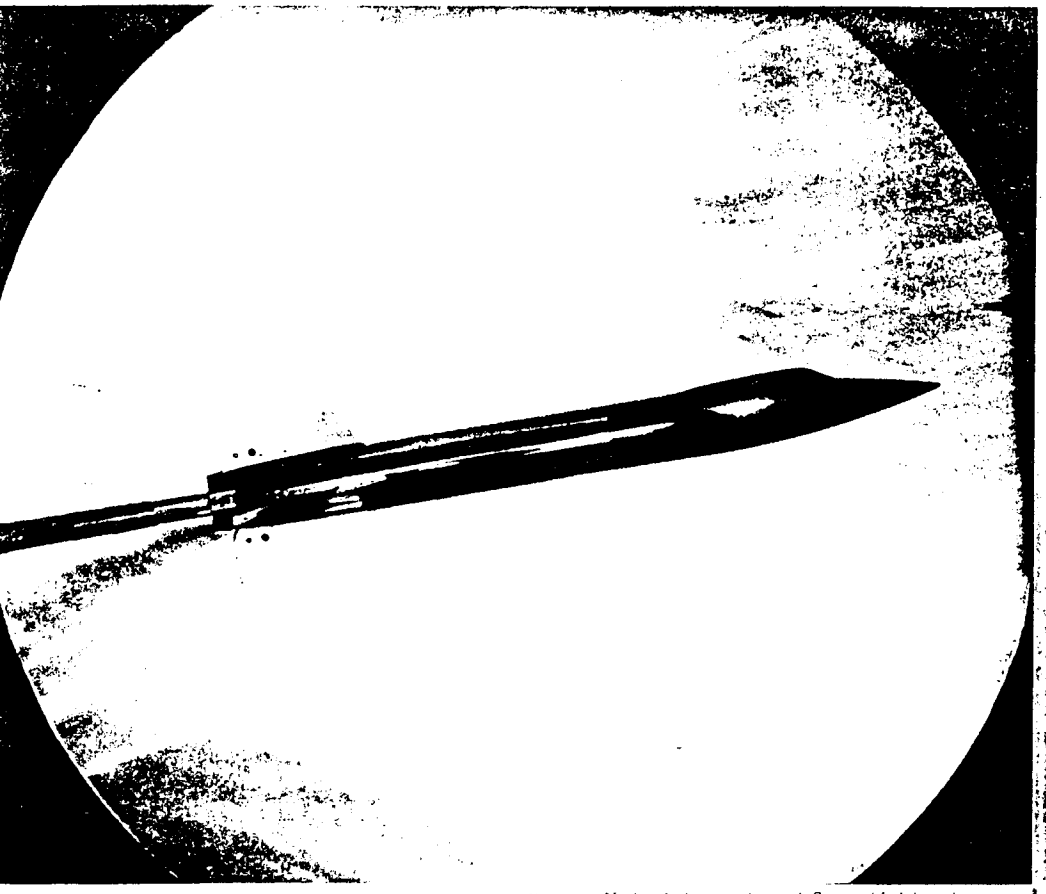


Courtesy National Aeronautics and Space Administration

Schlieren photograph of the flow field around the X-15 aircraft (Mach 3.24, $\alpha = 8°$, $\beta = 0°$).

DIRECCION DE PROYECTOS Biblioteca GETAFE (Madrid)

High-Speed Wind Tunnel Testing

Alan Pope

Director of Aerospace Projects, Sandia Corporation

Kennith L. Goin

Staff Member, Aerodynamic Testing Division, Sandia Corporation

John Wiley & Sons, Inc., New York | London | Sydney

DIRECCION DE PROYECTOS BIBLIOTECA

Copyright © 1965 by John Wiley & Sons, Inc.

All Rights Reserved
This book or any part thereof
must not be reproduced in any form
without the written permission of the publisher.

Library of Congress Catalog Card Number: 65-21435
Printed in the United States of America

Preface

The extension of the field of wind tunnel testing into the higher-speed regimes has made it advisable to revise *Wind Tunnel Testing* into low- and high-speed coverages. In this, the high-speed edition, the design, calibration, and operation of nearsonic, transonic, supersonic, and hypersonic tunnels are covered. This book is a separate entity for all but the relatively rare field of nearsonic testing, where low-speed wall corrections may have to be obtained from *Wind Tunnel Testing*.

The purpose of *High-Speed Wind Tunnel Testing* remains the same as that of its parent book: to furnish a reference for engineers using tunnels, to help students taking laboratory wind tunnel courses, and to aid beginners in the field of wind tunnel design.

Attention should be called to the format of the book. Nearly all types of tests may be performed in any of the speed ranges, and to avoid duplication we have had to select a place to discuss a test and make only such additions as seem necessary in the remaining speed ranges. We suggest, therefore, that when studying a particular type of test the reader check the speed ranges of reduced interest to see if the material contained therein is of use.

We wish to acknowledge the help we have received from our associates. Without it this book would have been substantially delayed.

Albuquerque, New Mexico
June, 1965

ALAN POPE
KENNITH L. GOIN

Contents

	Abbreviations	ix
1.	High-Speed Wind Tunnel Theory	1
2.	Design of Intermittent Blowdown Tunnels	66
3.	Design of Intermittent Indraft Tunnels	135
4.	Design of Pressure-Vacuum Tunnels	146
5.	Design of Continuous Closed-Circuit Tunnels	166
6.	Air Measuring Devices	198
7.	Force and Moment Measuring Devices	242
8.	Models, Testing, and Data Reduction	284
9.	Calibration and Use of Nearsonic and Transonic Tunnels	305
10.	Calibration and Use of Supersonic Tunnels	349
11.	Calibration and Use of Hypersonic Tunnels	402
12.	Hypervelocity Facilities	442
	Index	469

Abbreviations

In view of the large number of aeronautical research centers being set up, a list such as this must be considered incomplete. However, it may be of help in identifying the source of particular publications.

Abbreviation	Complete Meaning
AAL	Ames Aeronautical Laboratory (NASA), Moffett Field, California
ACA	Australian Council for Aeronautics, CSIR
AEDC	Arnold Engineering Development Center (Air Force), Tullahoma, Tennessee
AFAC	Air Force Armament Center, Eglin Field, Florida
AFCRC	Air Force Cambridge Research Center, Cambridge, Massachusetts
AFFTC	Air Force Flight Test Center, Muroc, California
AFMTC	Air Force Missile Test Center, Cocoa, Florida
AFSWC	Air Force Special Weapons Center, Albuquerque, New Mexico
AFWL	Air Force Weapons Laboratory, Albuquerque, New Mexico
AGARD	Advisory Group for Aeronautical Research and Development, a division of the North Atlantic Treaty Organization
AIAA	American Institute of Astronautics and Aeronautics
APL	Applied Physics Laboratory, Johns Hopkins University, Silver Spring, Maryland
ARA	Aeronautical Research Association, England
ARC	Air Research Committee, Australia
ARDC	Air Research and Development Center, Wright-Patterson Air Force Base, Ohio
ARDE	Armament Research and Development Establishment Fort Halstead, England
ARI, UT	Aerospace Research Institute, University of Tokyo (Japanese)
ARL	Aeronautical Research Laboratory, Whitley, England
ARL	Aerospace Research Laboratory, Wright-Patterson Air Force Base, Ohio
ASD	Aerospace Systems Division, Wright-Patterson Air Force Base, Ohio
ATL	Aeronautical Test Laboratory, U.S. Navy, Pt. Mugu, California
AVA	Aerodynamische Versuchsanstalt (Göttingen Institute for Aerodynamics), Göttingen, Germany
BAC	British Aircraft Corporation, England
BOE	Boeing Engineering Report, Boeing Company, Renton, Washington
BRL	Ballistic Research Laboratory, Aberdeen Proving Ground, Maryland

CAI	Central Aerohydrodynamic Institute, Moscow, U.S.S.R.
CSIR	Council for Scientific and Industrial Research, Australia
CNRC	Canadian National Research Council, Ottawa, Canada
DTMB	David Taylor Model Basin (Navy), Carderock, Maryland
DVL	Deutsche Versuchsanstalt für Luft- und Raumfahrt (German Institute for Aeronautical and Space Research) Berlin and Göttingen, Germany
ETH	Eidgenossische Technische Hochschule (Swiss Institute of Technology)
FFA	Flygtekniska Forsoksanstalten, Stockholm, Sweden
GALCIT	Guggenheim Aeronautical Laboratory of the California Institute of Technology, Pasadena, California
HMSO	Her Majesty's Stationery Office, London, England
IAS	Institute of Aeronautical Sciences (United States)
JAM	*Journal of Applied Mechanics*
JAS	*Journal of the Aeronautical Sciences* (United States)
JPL	Jet Propulsion Laboratory, California Institute of Technology, Pasadena, California
JRAS	*Journal of the Royal Aeronautical Society* (British)
LAL	Langley Aeronautical Laboratory (NACA), Langley Field, Virginia
LFA	Luftfahrtforschungsanstalt Hermann Göring (Hermann Göring Institute for Aeronautics), Braunschweig, Germany
LFPL	Lewis Flight Propulsion Laboratory (NACA), Cleveland, Ohio
LRBA	Laboratoire de Recherches Ballistique et Aerodynamique, Vernon, France
MAI	Moscow Aviation Institute, Moscow, U.S.S.R.
MIT	Massachusetts Institute of Technology, Cambridge, Massachusetts
NACA	National Advisory Committee on Aeronautics (now the National Aeronautics and Space Agency)
NAE	National Aeronautical Establishment, Bedford, England
NAE	National Aeronautical Establishment, Ottawa, Canada
NAL	National Aeronautical Laboratory, Tokyo, Japan
NASA	National Aeronautical and Space Agency, Washington, D.C.
NLRL	National Lucht-en-Ruimtevaartlaboratorium, Amsterdam, Netherlands
NOL	Naval Ordnance Laboratory, White Oaks, Maryland
NPL	National Physical Laboratory, Teddington, Middlesex, England
NRTS	National Reactor Testing Station, Arco, Idaho
NSL	Naval Supersonic Laboratory, Cambridge, Massachusetts
OAL	Ordnance Aerophysics Laboratory, Daingerfield, Texas
ONERA	Office National d'Études et de Recherches Aeronautiques (National Bureau of Aeronautical Research), Paris, France
ONR	Office of Naval Research, Washington, D.C.
ORNL	Oak Ridge National Laboratory, Oak Ridge, Tennessee
PRS	*Proceedings of the Royal Society of London* (British)

QAM	*Quarterly of Applied Mechanics*
R&M	*Reports and Memoranda* (of the Air Research Committee)
RAE	Royal Aeronautical Establishment, Farnborough, Hants, England
RM	*Research Memorandum of the NASA*
SAE	Society of Automotive Engineers (United States)
TCEA	Training Center for Experimental Aerodynamics, Belgium
TM	*Technical Memorandum of the NASA*
TN	*Technical Note of the NASA*
TR	*Technical Report of the NASA*
USNMC	United States Naval Missile Center, Pt. Mugu, California
WADC	Wright Air Development Center, Wright Patterson Air Force Base, Ohio
WRE	Weapons Research Establishment, Australia
ZAEA	Zhukovsky Aeronautical Engineering Academy, Moscow, U.S.S.R.

Chapter one

High-speed wind tunnel theory

1:1 Tunnel Types and Uses

Wind tunnels are devices which provide an airstream flowing under controlled conditions so that items of interest to aeronautical engineers can be tested. High-speed tunnels, as far as this textbook is concerned, are those whose usual operating speeds require the inclusion of compressible flow effects. This, it turns out, means that in the high-speed field we usually talk about "Mach number"—the ratio of a given velocity to the speed of sound in the air about the body—as a more typical parameter than velocity. A lower limit of "high speed" might be considered to be where the Mach number is approximately 0.5—about 380 mph for standard sea level conditions.

The power to drive a *low*-speed wind tunnel varies as the cube of the velocity in the wind tunnel. Although this rule does not hold into the high-speed regime, the implication of rapidly increasing power requirements with increasing test speed is correct. Because of the power requirements, high-speed wind tunnels are often of the "intermittent" type, in which energy is stored in the form of pressure or vacuum or both and is allowed to drive the tunnel only a few seconds out of each pumping hour.

Essential features of the "continuous" tunnel and three types of "intermittent" tunnels are shown in Figs. 1:1, 1:2, 1:3, and 1:4. The continuous tunnel (Fig. 1:1) is used throughout the speed range. The intermittent blowdown and indraft tunnels (Figs. 1:2 and 1:3) are normally used for Mach numbers from 0.5 to about 5.0, and the intermittent pressure-vacuum tunnels (Fig. 1:4) are normally used for higher Mach numbers. Both intermittent and continuous tunnels have their advantages and disadvantages.

Advantages claimed for intermittent tunnels are:

1. They are simpler to design and less costly to build.
2. A single drive may easily run several tunnels of different capabilities.

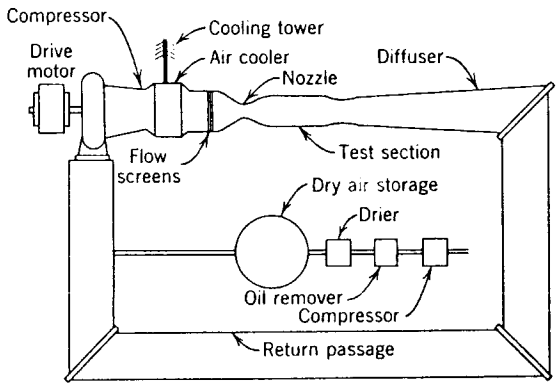


Fig. 1:1 Diagrammatic layout of closed-circuit, continuous flow, supersonic wind tunnel.

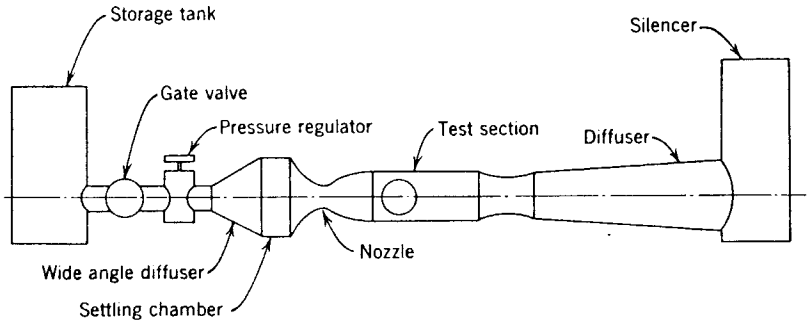


Fig. 1:2 Diagrammatic layout of intermittent blowdown tunnel.

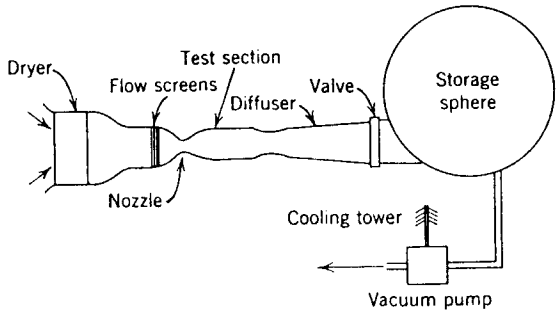


Fig. 1:3 Diagrammatic layout of intermittent indraft wind tunnel.

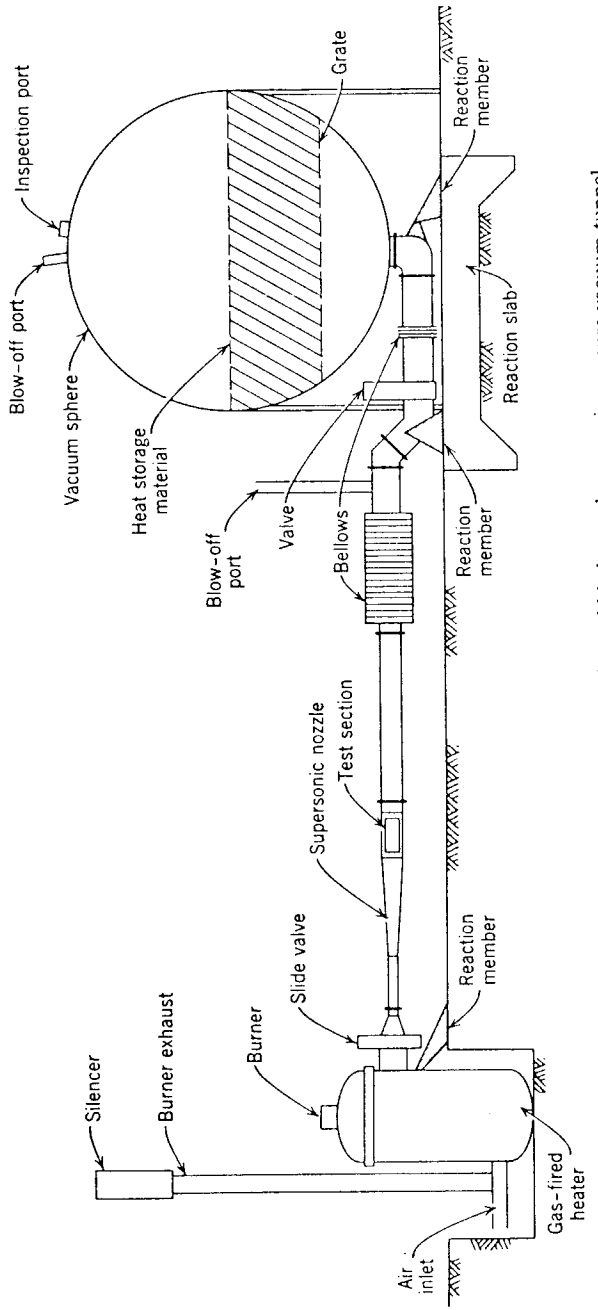


Fig. 1:4 Schematic drawing of Sandia Corporation pebble-heater hypersonic pressure-vacuum tunnel.

3. Model testing is more convenient, since a lot of time need not be spent in pumping down the whole circuit and getting the drive motors up to speed.
4. Failure of a model will usually not result in tunnel damage.
5. Extra "power" is available to start the tunnel.
6. Loads on a model during the establishment of high-speed flow (starting loads) are less severe because of faster starts.

Advantages claimed for the continuous tunnels are:

1. We are more in control of conditions, and may usually return to a given flow condition with more accuracy.
2. Since the "panic" of rapid testing is removed, check points are more easily obtained.
3. Testing conditions can be held constant over a long period of time.

Although intermittent tunnels seem to have more advantages, the fact remains that very few intermittent tunnels would be built if cost were of no consequence. We should also note that a tunnel's being continuous does not guarantee that it will turn out more data than an intermittent tunnel. For one thing, faster instrumentation is usually employed with intermittent tunnels, and even if continuous tunnels were to have such equipment (for some curious reason, they never seem to), the time lost pumping the pressure tunnels up and down, bringing the drive up to speed, and stopping it may offset the advantage of being able to run for longer periods. Particularly, pumping a continuous tunnel circuit up to a desired pressure may be a problem, since some tunnels require two hours or more.

It is sometimes amusing to listen to an operator of an intermittent tunnel and one of a continuous tunnel discuss their problems. It is almost as if they were talking two different languages. This is particularly true when the subject is the need for higher compression ratios (ratios of supply to discharge pressure) to start a tunnel than to keep it running. The intermittent tunnel—particularly the indraft or the pressure-vacuum type—almost automatically provides these ratios. When the valve on one of these intermittent tunnels is first snapped open, a near vacuum is provided against the stagnation pressure, and the pressure ratio is very large. Getting the tunnel started is no problem at all. On the other hand, the operator of a continuous tunnel is very well aware of the fact that his compressors will yield only a particular pressure ratio for a particular mass flow.

There is little choice in the type of intermittent tunnel to be used at the higher Mach numbers. The compression ratio requirements are so high that a pressure-vacuum tunnel is dictated. It is not practical to operate

with atmospheric inlet pressure (as with the indraft tunnel) or with atmospheric discharge pressure (as with the blowdown tunnel). However, there are many high-speed wind tunnels operating at Mach numbers for which both the indraft and blowdown tunnel are practical. Lists of the advantages of these two types of tunnels when compared with each other follow.

Some advantages of the *indraft* tunnel over the *blowdown* tunnel are:

1. Total air temperature at supply conditions (stagnation temperature) is constant during a run.
2. Total air pressure at supply conditions (stagnation pressure) is constant during a run although it may be lower than desired. There are no variations in total pressure such as those a pressure regulator may cause.
3. The airstream is free from contaminants such as compressor oil (but may contain dust from the desiccant of the air drier).
4. The headaches and dangers of pressure regulators are removed.
5. Loads on a model during the establishment of the high-speed flow (starting loads) are smaller.
6. Vacuum is safer to handle than pressure.
7. The noise level is lower.
8. Obtaining low air density (corresponding to high altitude) in the tunnel is not difficult.
9. The indraft tunnel can operate at higher Mach numbers before heating is required to prevent the liquefaction of air during the expansion to high speeds.
10. For a given cost, indraft tunnels are larger.

Advantages of the *blowdown* tunnel over the *indraft* tunnel are:

1. It is possible to vary the Reynolds number widely at a particular Mach number. In some cases the value corresponding to full-scale flight may be reached.
2. Cost is from slightly lower than to less than one-fourth of that of an indraft tunnel of equal Reynolds number.
3. Short-time burning tests are usually possible.

Although we risk antagonizing friends who swear by indraft tunnels by saying this, few such tunnels are built without the stimulus of strong external factors—such as gifts of equipment or free vacuum pumps.

1:2 Summary of Compressible Flow Theory

In low-speed aerodynamic work we assume that air is an incompressible fluid, that is, that the density of air does not change as the air flows

around a vehicle in flight or in a wind tunnel. This assumption is perfectly satisfactory from an engineering standpoint up to Mach numbers of 0.2, for flows to this speed will have only minor changes in air density. At Mach numbers above 0.2 the density changes increase, but the most important effects of compressibility are not realized until the local velocity at some point in the flow field exceeds the speed of sound. This, it turns out, almost never occurs below $M = 0.5$. We may count on it above $M = 0.85$.

The reason for the serious effects is a marked change in the character of the air flow which begins as soon as the speed of sound is exceeded. These effects include (1) the localizing of the effects of a body into a "zone of action" and a "zone of silence"; (2) a reversal of the subsonic laws governing "streamline flow"; and (3) the formation of "shock waves." We shall describe these effects, discuss their relation to the flow over an airfoil, and then summarize the laws of flow that govern their application.

The "Zone of Action" and "the Zone of Silence." An understanding of this phenomenon is based on the fundamental concept that disturbances in a fluid will propagate away from the point of a disturbance at the local speed of sound. This effect can be described by Fig. 1:5, which illustrates the propagation of sound waves relative to a particle in flight in different speed regimes. In Fig. 1:5*a* it may be considered that a particle has been fired into still air from a gun at time zero and at half the speed of sound ($M = 0.5$). At time zero, the particle rushing into the air sets up a disturbance that travels at the speed of sound a in all directions. At a time Δt later, the region affected by the initial disturbance is bounded by a sphere of radius $a\,\Delta t$. Meanwhile, the particle moving at half the speed of sound has moved through a distance of only $0.5a\,\Delta t$, so that the initial disturbance wave is preceding the particle. At time Δt, another disturbance is created. Between times Δt and $2\,\Delta t$, the sphere affected by the disturbance initiated at time zero expands to a radius of $2a\,\Delta t$, while that iniated at time Δt is expanding to a radius of $a\,\Delta t$. The particle is now preceded by both waves. Continuing in this manner in Fig. 1:5*a*, we see that the air ahead of the particle will always be affected by the disturbance waves before the particle reaches it. This is typical of subsonic flow. The disturbance waves, which are pressure pulses, go out ahead of the body to prepare the air ahead to move aside. Similarly, pressures at the rear of a body or behind it can reach forward and contribute to the flow pattern. Thus, the complete flow field is affected by every other point in the subsonic flow field, so that there is no "zone of silence."

Looking at Fig. 1:5*b*, which illustrates the case of a particle fired from a gun at the speed of sound ($M = 1.0$), we see that the disturbance

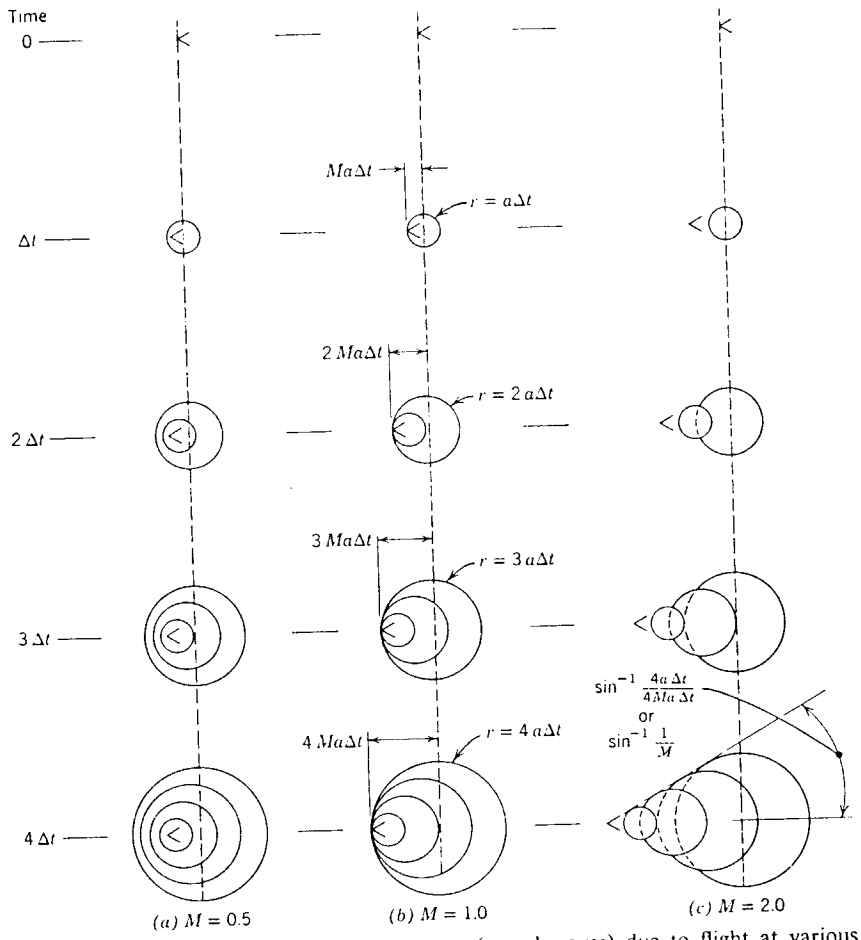


Fig. 1:5 Propagation of disturbance waves (sound waves) due to flight at various Mach numbers (M = Mach number, a = speed of sound).

propagation pattern is somewhat different. In this case the disturbances coalesce at the bow of the particle and form a concentrated wave front. For this case of Mach 1.0, the particle moves through the air at the speed of the advancing waves, so that the air ahead of the particle has not received a signal of the particles approach. Thus, the region ahead of the particle is a zone of silence.

For the case of the particle moving at a speed greater than the speed of sound, the disturbance propagation pattern is shown in Fig. 1:5*c*. In this case the radius of each disturbance wave increases at a rate less than the rate of movement of the particle. The result is that the disturbance

waves coalesce into a cone-shaped envelope that is a Mach wave having its apex at the particle. The region outside this cone is a zone of silence. As indicated in Fig. 1:5*c*, the half angle of the cone is $\sin^{-1}(1/M)$.

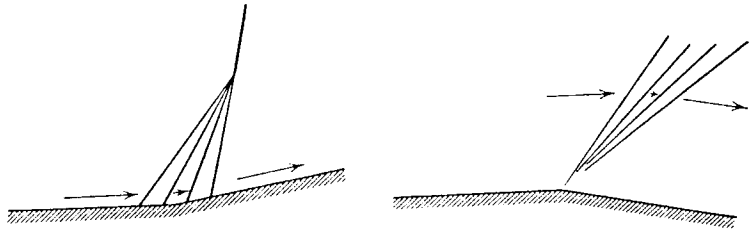
Streamline Flow. For air flowing through a duct at Mach numbers less than 1.0, increases in Mach number will be accompanied by increases in velocity and decreases in density. The velocity of the air increases faster than the density decreases; a 10 per cent increase of velocity, say, yields an 8 per cent decrease in density. In such a case the number of pounds per second *flowing through each square foot* of duct cross section increases with increasing Mach number. Consequently, the duct area must decrease if it is to remain filled with flow. (See also Ref. 1:15.)

Above $M = 1.0$, the phenomenon is reversed. As the Mach number increases, a 10 per cent increase in velocity might yield, say, a 12 per cent decrease in density. In this case, the number of pounds per second flowing *through each square foot* of duct cross section decreases, so that the duct area must be increased to accommodate the flow at increasing Mach number. Conversely, to decrease the Mach number of a supersonic flow, the duct area must be decreased, an action that would increase the Mach number of a subsonic flow.

In free air flows, we speak of "stream tubes" instead of ducts. Stream tubes are imaginary ducts in which constant mass is considered to flow. "Streamlines" are the lines forming the boundaries of two-dimensional stream tubes. Stream tubes, and therefore streamlines, assume the shape of perfectly designed ducts, decreasing in cross section when a subsonic flow is accelerated and increasing in cross section when a supersonic flow is accelerated. Thus, the subsonic laws governing streamline flow are reversed when the speed of sound is exceeded.

Shock Waves. As noted above and illustrated in Fig. 1:5, concentrated wave fronts are established when a particle is moving through the air at speeds of Mach 1.0 and above. If these waves are very weak, so that infinitely small changes in air properties occur as they pass through the air, the wave is said to be a "Mach wave" and is inclined at an angle $\sin^{-1}(1/M)$ with respect to the flow direction. Waves of finite strength (through which air properties change significantly) are caused by a concentration of Mach waves and are called "shock waves."

Figure 1:6 presents a comparison of the Mach wave formation caused by compression of a supersonic flow with that caused by the expansion of a supersonic flow. Changes in flow direction require a small, though finite, time. Thus, air approaching a corner tends to round the corner. When the corner is tending to compress the flow, disturbance waves will develop, as illustrated in Fig. 1:6*a*. A weak disturbance (Mach wave)



(*a*) Compression (*b*) Expansion

Fig. 1:6 Disturbance-wave formation in a compression and an expansion of supersonic flow.

develops, which will slow the flow very slightly and turn it very slightly. A number of following weak disturbances will do the same. The decreased flow velocity and changed flow direction are such that each successive disturbance wave has a greater inclination with respect to the original direction. The result is a coalescing of a large number of weak compression disturbances into a shock wave. When the corner is such as to cause the air to expand (Fig. 1:6*b*) a series of weak disturbance waves also develop. In this case, however, each succeeding disturbance occurs at a higher Mach number. The higher Mach number as well as the changed flow direction cause the disturbance waves to diverge, resulting in a series of expansion waves called a "Prandtl-Meyer expansion fan."

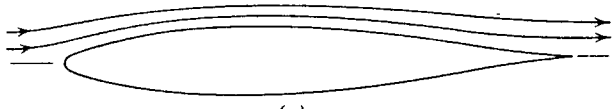
The shock wave in Fig. 1:6*a* is called an "oblique shock" because of its angle relative to the flow direction. If the turning angle of the flow is small, the velocity downstream of the oblique shock will be less than the mainstream flow velocity but will remain supersonic. If the turning angle is large, the shock will become normal to the flow and detached from the wedge, and the velocity downstream of the "normal shock" will be subsonic. Between these extreme turning angles, the oblique shock will become steeper and the downstream velocity lower as the turning angle increases.

Now that normal and oblique shocks have been introduced, we shall discuss the properties of shocks in more detail. Upon passing through a shock wave, the properties of the air change almost instantly. The pressure, temperature, and density increase and the velocity decreases. The entropy increases with the result that the total pressure of the air upstream of the shock cannot be recovered. The air can be brought to rest at the total temperature upstream of the shock but only at a pressure lower than the initial pressure.

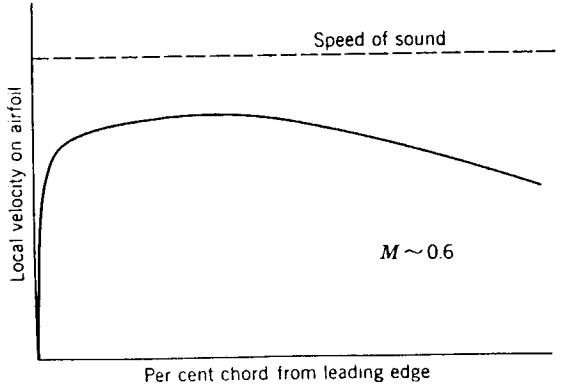
A shock will always develop when the flow velocity over an object is supersonic. If the flow over the object is slightly above Mach 1.0, the

shock will be normal and the losses through the shock will be small. If the flow velocity is higher, the shock may be either oblique or normal, depending on the angle through which the object turns the air. At a given Mach number losses through a normal shock are always greater than losses through an oblique shock. Normal shocks occur in the supersonic flow of air through a duct such as a wind tunnel when conditions are such as to require a reduction in speed to subsonic flow. The importance of normal shocks to wind tunnel operation will be discussed later.

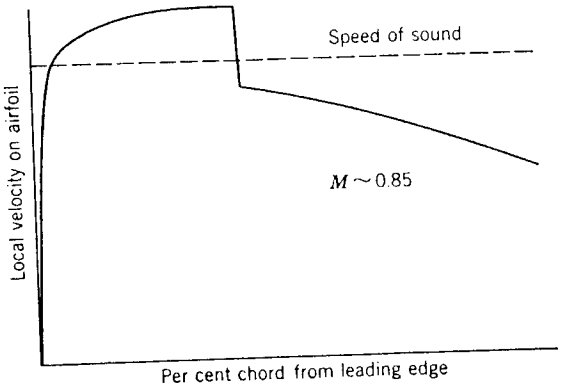
Now let us discuss the relation of the phenomena described above to the flow over the airfoil of Fig. 1:7*a*. The air passing over the surface of the airfoil must average faster than the mainstream flow because it has a greater distance to travel in the same length of time. Over the forward portion of the airfoil in subsonic flow where the thickness is increasing, the effective flow area is being reduced, so that the velocity is increasing and the stream tubes are getting smaller. Over the aft portion of the airfoil, where the thickness is decreasing, the effective flow area is being increased, so that the velocity is decreasing and the stream tubes are getting larger. The distribution of local velocity over the airfoil is illustrated in Fig. 1:7*b* for a flow Mach number of about 0.6. Note that for the ideal case an integration of the pressure loading over the airfoil at Mach 0.6 will yield a zero force in the flow direction (zero "drag").



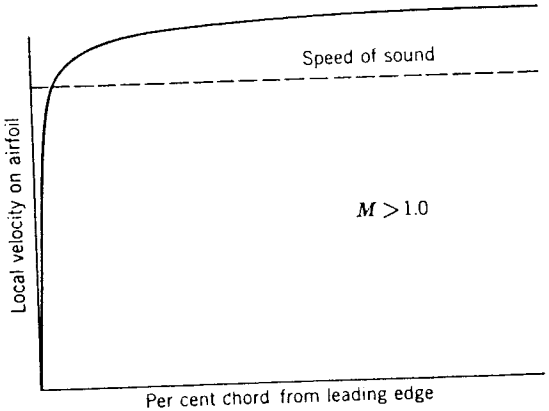
(*a*)



(*b*)



(*c*)



(*d*)

Fig. 1:7 Illustrative local velocity variation over surface of an airfoil at various freestream Mach numbers.

The high velocities over the forward portion of the airfoil are accompanied by reduced pressures, which tend to pull the airfoil forward. Similarly, the higher velocities over the aft portion are accompanied by reduced pressures, which tend to pull the airfoil aft. The forces in the two directions exactly cancel each other. In practice, the airfoil will have a slight pressure drag. The major portion of drag, however, will be due to friction between the airfoil surfaces and the air in proximity to these surfaces, that is, the boundary layer.

With the same airfoil in an airstream moving at about Mach 0.85 (Fig. 1:7*c*), the velocity of airflow in the stream tube again increases rapidly over the forward portion of the airfoil and in this case reaches

and passes through Mach 1.0. At the point where this occurs, the airfoil surface is turning away from the direction of local supersonic flow, which corresponds to an increasing stream tube area and consequently to an increasing velocity. The result is a tendency for the velocity to continue to increase with distance toward the trailing edge of the airfoil. Before rejoining the mainstream flow downstream of the airfoil, the flow must be decelerated to the original subsonic velocity. Deceleration is accomplished by a shock wave that forms on the surface of the airfoil. An integration of the ideal pressure loading for this case would yield little drag. In the actual case, however, the airfoil would exhibit a substantial increase in drag over that at Mach 0.6 because of interaction between the shock and the boundary layer.

Finally, when the airfoil is placed in a supersonic airflow (Fig. 1:7*d*) the flow over the airfoil bears no resemblence to incompressible flow. In this case, conditions exist for a shock wave ahead of the airfoil. A decreasing stream tube area and an increasing velocity are required to get the air approaching the airfoil around the leading edge of the airfoil. Since these conditions are consistent only for subsonic flow and the main flow is supersonic, a shock wave develops ahead of the airfoil, causing a decrease in speed to subsonic between the shock wave and the airfoil leading edge. From this subsonic velocity, the speed in the stream tube will rapidly increase to supersonic and then will continue to increase as it passes over the airfoil. At the trailing edge of the airfoil, the velocity will be above the main airstream velocity. A shock will occur at the trailing edge of the airfoil to bring the velocity back down to the mainstream velocity. In this case, the velocity over the forward portion of the airfoil is below freestream velocity, so that the pressure is above freestream. Over the aft portion, the velocity is above freestream, so that the pressure is below freestream. An integration of the pressure loading in this case yields a substantial drag because the drag components of the forward and aft portions of the airfoil are additive.

With this background in compressible flow theory, we shall now develop equations defining compressible flow. Air flow in general is governed by the five following laws.

1. At any point in a flow field, the pressure, density, and temperature are related by the *equation of state:*

$$p = \rho R_1 T \tag{1:1}$$

where p = pressure, lb/ft^2,
ρ = density, slugs/ft^3,
T = temperature, °R,
R_1 = gas constant, ft-lb/slug-°R.

2. For continuous flow in a duct or stream tube, the equivalence of mass flow at any two stations is specified by the *continuity equation.*

$$\rho_1 A_1 U_1 = \rho_2 A_2 U_2 \tag{1:2}$$

where A is the cross-sectional area of the duct at a given station (ft^2), U is the flow velocity (ft/sec), and subscripts 1 and 2 denote two stations in the duct.

3. If no energy is added or lost during the flow of a sample of fluid between two stations in a duct (that is, if the flow is adiabatic), the following *energy equation* is valid:

$$c_p T_1 + \frac{U_1^2}{2} = c_p T_2 + \frac{U_2^2}{2} = c_p T_t \tag{1:3}$$

where c_p is the specific heat at constant pressure (ft^2/sec^2-°R) and the subscript t denotes conditions at zero velocity or, identically, stagnation conditions.

4. If the change of state of a fluid during its flow from one station to another is *isentropic*, the following thermodynamic relation is applicable:

$$\frac{T_1}{p_1^{(\gamma-1)/\gamma}} = \frac{T_2}{p_2^{(\gamma-1)/\gamma}} \tag{1:4}$$

where γ is the ratio of specific heat at constant pressure, c_p, to specific heat at constant volume, c_v.

5. From the summation of forces between two stations in a constant area stream tube or duct with no friction, the following *momentum equation* is obtained:

$$p_1 + \rho_1 U_1^2 = p_2 + \rho_2 U_2^2 \tag{1:5}$$

In addition to the above equations, the following definitions are needed for the development of the desired relations for compressible flow:

$$U = aM \tag{1:6}$$

$$a = \sqrt{\gamma R_1 T} \tag{1:7}$$

$$c_p = \frac{\gamma R_1}{\gamma - 1} \tag{1:8}$$

where a is the speed of sound (ft/sec), M is Mach number, and R_1 is the gas constant (ft^2/sec^2-°R).

From the energy equation (1:3) and the definitions of eqs. (1:6) to (1:8) we get:

$$\frac{T_1}{T_2} = \frac{1 + [(\gamma - 1)/2]M_2^2}{1 + [(\gamma - 1)/2]M_1^2} \tag{1:9}$$

Combining eq. (1:9) with the equation for isentropic flow (1:4) yields:

$$\frac{p_1}{p_2} = \left\{\frac{1 + [(\gamma - 1)/2]M_2^2}{1 + [(\gamma - 1)/2]M_1^2}\right\}^{[\gamma/(\gamma-1)]} \tag{1:10}$$

Combining eqs. (1:9) and (1:10) with the equation of state (1:1) yields

$$\frac{\rho_1}{\rho_2} = \left\{\frac{1 + [(\gamma - 1)/2]M_2^2}{1 + [(\gamma - 1)/2]M_1^2}\right\}^{[1/(\gamma-1)]} \tag{1:11}$$

Adding in the continuity equation (1:2), we get

$$\frac{A_1}{A_2} = \frac{M_2}{M_1}\left\{\frac{1 + [(\gamma - 1)/2]M_2^2}{1 + [(\gamma - 1)/2]M_1^2}\right\}^{-[(\gamma+1)/2(\gamma-1)]} \tag{1:12}$$

From the definitions of eqs. (1:6) to (1:8), the following equation for dynamic pressure ($\rho U^2/2$) is obtained:

$$q = \frac{\gamma}{2} pM^2 \tag{1:13}$$

From the preceding equations, together with the knowledge that stagnation conditions will exist at $M = 0$, the following isentropic flow relations are obtained:

$$\frac{p}{p_t} = \left(1 + \frac{\gamma - 1}{2} M^2\right)^{-[\gamma/(\gamma-1)]} \tag{1:14}$$

$$\frac{\rho}{\rho_t} = \left(1 + \frac{\gamma - 1}{2} M^2\right)^{-[1/(\gamma-1)]} \tag{1:15}$$

$$\frac{T}{T_t} = \left(1 + \frac{\gamma - 1}{2} M^2\right)^{-1} \tag{1:16}$$

$$\frac{q}{p_t} = \frac{\gamma}{2} M^2\left(1 + \frac{\gamma - 1}{2} M^2\right)^{-[\gamma/(\gamma-1)]} \tag{1:17}$$

Using an area at $M = 1$ (A^*, corresponding to the throat of a supersonic nozzle) as a reference, we obtain the following from eq. (1:12):

$$\frac{A}{A^*} = \frac{1}{M}\left\{\frac{1 + [(\gamma - 1)/2]M^2}{[(\gamma + 1)/2]}\right\}^{[(\gamma+1)/2(\gamma-1)]} \tag{1:18}$$

The relations of eqs. (1:14) to (1:18) are tabulated in Table 1:1 for air at Mach numbers of 0.1 to 10.0.

When a normal shock wave exists in a flow, there is an entropy change across the shock. Consequently, the preceding isentropic flow equations are not valid. The equation of state (1:1), the continuity equation (1:2), the energy equation (1:3), and the momentum equation (1:5) are used in

Table 1:1

Isentropic Flow Parameters, $\gamma = 1.4$

The plus and minus numbers indicate the number of spaces the decimal is to be moved, plus to the right, minus to the left.

M	p/p_t	ρ/ρ_t	T/T_t	q/p_t	A/A^*
0.0	0.1000 + 01	0.1000 + 01	0.1000 + 01	0.0000 + 00	∞
0.1	0.9930 + 00	0.9950 + 00	0.9980 + 00	0.6951 − 02	5.822
0.2	0.9725 + 00	0.9803 + 00	0.9921 + 00	0.2723 − 01	2.964
0.3	0.9395 + 00	0.9564 + 00	0.9823 + 00	0.5919 − 01	2.035
0.4	0.8956 + 00	0.9243 + 00	0.9690 + 00	0.1003 + 00	1.590
0.5	0.8430 + 00	0.8852 + 00	0.9524 + 00	0.1475 + 00	1.340
0.6	0.7840 + 00	0.8405 + 00	0.9328 + 00	0.1976 + 00	1.188
0.7	0.7209 + 00	0.7916 + 00	0.9107 + 00	0.2473 + 00	1.094
0.8	0.6560 + 00	0.7400 + 00	0.8865 + 00	0.2939 + 00	1.038
0.9	0.5913 + 00	0.6870 + 00	0.8606 + 00	0.3352 + 00	1.009
1.0	0.5283 + 00	0.6339 + 00	0.8333 + 00	0.3698 + 00	1.000
1.1	0.4684 + 00	0.5817 + 00	0.8052 + 00	0.3967 + 00	1.008
1.2	0.4124 + 00	0.5311 + 00	0.7764 + 00	0.4157 + 00	1.030
1.3	0.3609 + 00	0.4829 + 00	0.7474 + 00	0.4270 + 00	1.066
1.4	0.3142 + 00	0.4374 + 00	0.7184 + 00	0.4311 + 00	1.115
1.5	0.2724 + 00	0.3950 + 00	0.6897 + 00	0.4290 + 00	1.176
1.6	0.2353 + 00	0.3557 + 00	0.6614 + 00	0.4216 + 00	1.250
1.7	0.2026 + 00	0.3197 + 00	0.6337 + 00	0.4098 + 00	1.338
1.8	0.1740 + 00	0.2868 + 00	0.6068 + 00	0.3947 + 00	1.439
1.9	0.1492 + 00	0.2570 + 00	0.5807 + 00	0.3771 + 00	1.555
2.0	0.1278 + 00	0.2300 + 00	0.5556 + 00	0.3579 + 00	1.687
2.1	0.1094 + 00	0.2058 + 00	0.5313 + 00	0.3376 + 00	1.837
2.2	0.9352 − 01	0.1841 + 00	0.5081 + 00	0.3169 + 00	2.005
2.3	0.7997 − 01	0.1646 + 00	0.4859 + 00	0.2961 + 00	2.193
2.4	0.6840 − 01	0.1472 + 00	0.4647 + 00	0.2758 + 00	2.403
2.5	0.5853 − 01	0.1317 + 00	0.4444 + 00	0.2561 + 00	2.637
2.6	0.5012 − 01	0.1179 + 00	0.4252 + 00	0.2371 + 00	2.896
2.7	0.4295 − 01	0.1056 + 00	0.4068 + 00	0.2192 + 00	3.183
2.8	0.3685 − 01	0.9463 − 01	0.3894 + 00	0.2022 + 00	3.500
2.9	0.3165 − 01	0.8489 − 01	0.3729 + 00	0.1863 + 00	3.850
3.0	0.2722 − 01	0.7623 − 01	0.3571 + 00	0.1715 + 00	4.235
3.1	0.2345 − 01	0.6852 − 01	0.3422 + 00	0.1577 + 00	4.657
3.2	0.2023 − 01	0.6165 − 01	0.3281 + 00	0.1450 + 00	5.121
3.3	0.1748 − 01	0.5554 − 01	0.3147 + 00	0.1332 + 00	5.629
3.4	0.1512 − 01	0.5009 − 01	0.3019 + 00	0.1224 + 00	6.184

Table 1:1 (*continued*)

M	p/p_t	ρ/ρ_t	T/T_t	q/p_t	A/A^*
3.5	0.1311 − 01	0.4523 − 01	0.2899 + 00	0.1124 + 00	6.790
3.6	0.1138 − 01	0.4089 − 01	0.2784 + 00	0.1033 + 00	7.450
3.7	0.9903 − 02	0.3702 − 01	0.2675 + 00	0.9490 − 01	8.169
3.8	0.8629 − 02	0.3355 − 01	0.2572 + 00	0.8722 − 01	8.951
3.9	0.7532 − 02	0.3044 − 01	0.2474 + 00	0.8019 − 01	9.799
4.0	0.6586 − 02	0.2766 − 01	0.2381 + 00	0.7376 − 01	10.719
4.1	0.5769 − 02	0.2516 − 01	0.2293 + 00	0.6788 − 01	11.715
4.2	0.5062 − 02	0.2292 − 01	0.2208 + 00	0.6251 − 01	12.792
4.3	0.4449 − 02	0.2090 − 01	0.2129 + 00	0.5759 − 01	13.955
4.4	0.3918 − 02	0.1909 − 01	0.2053 + 00	0.5309 − 01	15.210
4.5	0.3455 − 02	0.1745 − 01	0.1980 + 00	0.4898 − 01	16.562
4.6	0.3053 − 02	0.1597 − 01	0.1911 + 00	0.4521 − 01	18.018
4.7	0.2701 − 02	0.1464 − 01	0.1846 + 00	0.4177 − 01	19.583
4.8	0.2394 − 02	0.1343 − 01	0.1783 + 00	0.3861 − 01	21.264
4.9	0.2126 − 02	0.1233 − 01	0.1724 + 00	0.3572 − 01	23.067
5.0	0.1890 − 02	0.1134 − 01	0.1667 + 00	0.3308 − 01	25.000
5.1	0.1683 − 02	0.1044 − 01	0.1612 + 00	0.3065 − 01	27.070
5.2	0.1501 − 02	0.9620 − 02	0.1561 + 00	0.2842 − 01	29.283
5.3	0.1341 − 02	0.8875 − 02	0.1511 + 00	0.2637 − 01	31.649
5.4	0.1200 − 02	0.8197 − 02	0.1464 + 00	0.2449 − 01	34.175
5.5	0.1075 − 02	0.7578 − 02	0.1418 + 00	0.2276 − 01	36.869
5.6	0.9643 − 03	0.7012 − 02	0.1375 + 00	0.2117 − 01	39.740
5.7	0.8663 − 03	0.6496 − 02	0.1334 + 00	0.1970 − 01	42.797
5.8	0.7794 − 03	0.6023 − 02	0.1294 + 00	0.1835 − 01	46.050
5.9	0.7021 − 03	0.5590 − 02	0.1256 + 00	0.1711 − 01	49.507
6.0	0.6334 − 03	0.5194 − 02	0.1220 + 00	0.1596 − 01	53.180
6.1	0.5721 − 03	0.4829 − 02	0.1185 + 00	0.1490 − 01	57.077
6.2	0.5173 − 03	0.4495 − 02	0.1151 + 00	0.1392 − 01	61.210
6.3	0.4684 − 03	0.4187 − 02	0.1119 + 00	0.1301 − 01	65.590
6.4	0.4247 − 03	0.3904 − 02	0.1088 + 00	0.1218 − 01	70.227
6.5	0.3855 − 03	0.3643 − 02	0.1058 + 00	0.1140 − 01	75.134
6.6	0.3503 − 03	0.3402 − 02	0.1030 + 00	0.1068 − 01	80.323
6.7	0.3187 − 03	0.3180 − 02	0.1002 + 00	0.1001 − 01	85.805
6.8	0.2902 − 03	0.2974 − 02	0.9758 − 01	0.9395 − 02	91.594
6.9	0.2646 − 03	0.2785 − 02	0.9504 − 01	0.8820 − 02	97.702

Table 1:1 (*continued*)

M	p/p_t	ρ/ρ_t	T/T_t	q/p_t	A/A^*
7.0	0.2416 − 03	0.2609 − 02	0.9259 − 01	0.8285 − 02	104.143
7.1	0.2207 − 03	0.2446 − 02	0.9024 − 01	0.7788 − 02	110.931
7.2	0.2019 − 03	0.2295 − 02	0.8797 − 01	0.7326 − 02	118.080
7.3	0.1848 − 03	0.2155 − 02	0.8578 − 01	0.6895 − 02	125.605
7.4	0.1694 − 03	0.2025 − 02	0.8367 − 01	0.6494 − 02	133.520
7.5	0.1554 − 03	0.1904 − 02	0.8163 − 01	0.6120 − 02	141.841
7.6	0.1427 − 03	0.1792 − 02	0.7967 − 01	0.5771 − 02	150.585
7.7	0.1312 − 03	0.1687 − 02	0.7777 − 01	0.5445 − 02	159.767
7.8	0.1207 − 03	0.1589 − 02	0.7594 − 01	0.5140 − 02	169.403
7.9	0.1111 − 03	0.1498 − 02	0.7417 − 01	0.4855 − 02	179.511
8.0	0.1024 − 03	0.1414 − 02	0.7246 − 01	0.4589 − 02	190.109
8.1	0.9449 − 04	0.1334 − 02	0.7081 − 01	0.4339 − 02	201.215
8.2	0.8723 − 04	0.1260 − 02	0.6921 − 01	0.4106 − 02	212.846
8.3	0.8060 − 04	0.1191 − 02	0.6767 − 01	0.3887 − 02	225.022
8.4	0.7454 − 04	0.1126 − 02	0.6617 − 01	0.3682 − 02	237.762
8.5	0.6898 − 04	0.1066 − 02	0.6472 − 01	0.3489 − 02	251.086
8.6	0.6390 − 04	0.1009 − 02	0.6332 − 01	0.3308 − 02	265.014
8.7	0.5923 − 04	0.9558 − 03	0.6197 − 01	0.3138 − 02	279.567
8.8	0.5494 − 04	0.9059 − 03	0.6065 − 01	0.2978 − 02	294.766
8.9	0.5101 − 04	0.8590 − 03	0.5938 − 01	0.2828 − 02	310.633
9.0	0.4739 − 04	0.8150 − 03	0.5814 − 01	0.2687 − 02	327.189
9.1	0.4405 − 04	0.7737 − 03	0.5694 − 01	0.2554 − 02	344.458
9.2	0.4099 − 04	0.7348 − 03	0.5578 − 01	0.2428 − 02	362.463
9.3	0.3816 − 04	0.6982 − 03	0.5465 − 01	0.2310 − 02	381.227
9.4	0.3555 − 04	0.6638 − 03	0.5356 − 01	0.2199 − 02	400.775
9.5	0.3314 − 04	0.6313 − 03	0.5249 − 01	0.2094 − 02	421.131
9.6	0.3092 − 04	0.6008 − 03	0.5146 − 01	0.1994 − 02	442.321
9.7	0.2886 − 04	0.5719 − 03	0.5046 − 01	0.1901 − 02	464.370
9.8	0.2696 − 04	0.5447 − 03	0.4949 − 01	0.1812 − 02	487.304
9.9	0.2520 − 04	0.5191 − 03	0.4854 − 01	0.1729 − 02	511.151
10.0	0.2356 − 04	0.4948 − 03	0.4762 − 01	0.1649 − 02	535.937

the derivation of normal shock flow equations. Let subscripts 1 and 2, respectively, represent conditions upstream and downstream of a normal shock.

The solution of the energy equation (1:3) again yields eq. (1:9).

The combination of eqs. (1:1) and (1:5) gives

$$\frac{p_2}{p_1} = \frac{1 + \gamma M_1^2}{1 + \gamma M_2^2} \tag{1:19}$$

The combination of the continuity equation (1:2) with eqs. (1:9) and (1:19) gives

$$M_2^2 = \frac{[2/(\gamma - 1)] + M_1^2}{[2\gamma M_1^2/(\gamma - 1)] - 1} \tag{1:20}$$

When eq. (1:20) is used with eqs. (1:9) and (1:19), the following relations for flow across a normal shock, in terms of the upstream Mach number, are obtained.

$$\frac{T_2}{T_1} = \frac{\left[1 + \dfrac{\gamma - 1}{2} M_1^2\right]\left[\dfrac{2\gamma}{\gamma - 1} M_1^2 - 1\right]}{\dfrac{(\gamma + 1)^2}{2(\gamma - 1)} M_1^2} \tag{1:21}$$

$$\frac{p_2}{p_1} = \frac{2\gamma M_1^2 - (\gamma - 1)}{\gamma + 1} \tag{1:22}$$

When the equation of state (1:1) is combined with eqs. (1:21) and (1:22), the density ratio across the shock is obtained:

$$\frac{\rho_2}{\rho_1} = \frac{(\gamma + 1)M_1^2}{2 + (\gamma - 1)M_1^2} \tag{1:23}$$

The stagnation pressure downstream of a normal shock is less than that upstream of the shock. The relation of static to stagnation pressure downstream of the shock is obtained from eq. (1:14) when the Mach number downstream of the shock is used. A relation for the total pressure downstream of a normal shock is obtained as follows:

$$\frac{p_{t2}}{p_{t1}} = \frac{(p_1/p_{t1})(p_2/p_1)}{(p_2/p_{t2})} = \left[\frac{(\gamma + 1)}{2\gamma M_1^2 - (\gamma - 1)}\right]^{1/(\gamma-1)} \left[\frac{(\gamma + 1)M_1^2}{(\gamma - 1)M_1^2 + 2}\right]^{\gamma/(\gamma-1)} \tag{1:24}$$

The relations of eqs. (1:20) to (1:24) are tabulated in Table 1:2 for Mach numbers of 1 to 10. Also included in Table 1:2 is the parameter p_1/p_{t2}, which is obtained by dividing eq. (1:14) by eq. (1:24).

Table 1:2

Normal Shock Relations, $\gamma = 1.4$

M	p_2/p_1	ρ_2/ρ_1	T_2/T_1	p_{t2}/p_{t1}	p_1/p_{t2}	M_2
1.0	1.000	1.000	1.000	0.1000 + 01	0.5283 + 00	1.0000
1.1	1.245	1.169	1.065	0.9989 + 00	0.4689 + 00	0.9118
1.2	1.513	1.342	1.128	0.9928 + 00	0.4154 + 00	0.8422
1.3	1.805	1.516	1.191	0.9794 + 00	0.3685 + 00	0.7860
1.4	2.120	1.690	1.255	0.9582 + 00	0.3280 + 00	0.7397
1.5	2.458	1.862	1.320	0.9298 + 00	0.2930 + 00	0.7011
1.6	2.820	2.032	1.388	0.8952 + 00	0.2628 + 00	0.6684
1.7	3.205	2.198	1.458	0.8557 + 00	0.2368 + 00	0.6405
1.8	3.613	2.359	1.532	0.8127 + 00	0.2142 + 00	0.6165
1.9	4.045	2.516	1.608	0.7674 + 00	0.1945 + 00	0.5956
2.0	4.500	2.667	1.688	0.7209 + 00	0.1773 + 00	0.5774
2.1	4.978	2.812	1.770	0.6742 + 00	0.1622 + 00	0.5613
2.2	5.480	2.951	1.857	0.6281 + 00	0.1489 + 00	0.5471
2.3	6.005	3.085	1.947	0.5833 + 00	0.1371 + 00	0.5344
2.4	6.553	3.212	2.040	0.5401 + 00	0.1266 + 00	0.5231
2.5	7.125	3.333	2.137	0.4990 + 00	0.1173 + 00	0.5130
2.6	7.720	3.449	2.238	0.4601 + 00	0.1089 + 00	0.5039
2.7	8.338	3.559	2.343	0.4236 + 00	0.1014 + 00	0.4956
2.8	8.980	3.664	2.451	0.3895 + 00	0.9461 − 01	0.4882
2.9	9.645	3.763	2.563	0.3577 + 00	0.8848 − 01	0.4814
3.0	10.333	3.857	2.679	0.3283 + 00	0.8291 − 01	0.4752
3.1	11.045	3.947	2.799	0.3012 + 00	0.7785 − 01	0.4695
3.2	11.780	4.031	2.922	0.2762 + 00	0.7323 − 01	0.4643
3.3	12.538	4.112	3.049	0.2533 + 00	0.6900 − 01	0.4596
3.4	13.320	4.188	3.180	0.2322 + 00	0.6513 − 01	0.4552
3.5	14.125	4.261	3.315	0.2129 + 00	0.6157 − 01	0.4512
3.6	14.953	4.330	3.454	0.1953 + 00	0.5829 − 01	0.4474
3.7	15.805	4.395	3.596	0.1792 + 00	0.5526 − 01	0.4439
3.8	16.680	4.457	3.743	0.1645 + 00	0.5247 − 01	0.4407
3.9	17.578	4.516	3.893	0.1510 + 00	0.4987 − 01	0.4377
4.0	18.500	4.571	4.047	0.1388 + 00	0.4747 − 01	0.4350
4.1	19.445	4.624	4.205	0.1276 + 00	0.4523 − 01	0.4324
4.2	20.413	4.675	4.367	0.1173 + 00	0.4314 − 01	0.4299
4.3	21.405	4.723	4.532	0.1080 + 00	0.4120 − 01	0.4277
4.4	22.420	4.768	4.702	0.9948 − 01	0.3938 − 01	0.4255
4.5	23.458	4.812	4.875	0.9170 − 01	0.3768 − 01	0.4236
4.6	24.520	4.853	5.052	0.8459 − 01	0.3609 − 01	0.4217
4.7	25.605	4.893	5.233	0.7809 − 01	0.3459 − 01	0.4199
4.8	26.713	4.930	5.418	0.7214 − 01	0.3319 − 01	0.4183
4.9	27.845	4.966	5.607	0.6670 − 01	0.3187 − 01	0.4167

Table 1:2 (*continued*)

M	p_2/p_1	ρ_2/ρ_1	T_2/T_1	p_{t2}/p_{t1}	p_1/p_{t2}	M_2
5.0	29.000	5.000	5.800	0.6172 − 01	0.3062 − 01	0.4152
5.1	30.178	5.033	5.997	0.5715 − 01	0.2945 − 01	0.4138
5.2	31.380	5.064	6.197	0.5297 − 01	0.2834 − 01	0.4125
5.3	32.605	5.093	6.401	0.4913 − 01	0.2730 − 01	0.4113
5.4	33.853	5.122	6.610	0.4560 − 01	0.2631 − 01	0.4101
5.5	35.125	5.149	6.822	0.4236 − 01	0.2537 − 01	0.4090
5.6	36.420	5.175	7.038	0.3938 − 01	0.2448 − 01	0.4079
5.7	37.738	5.200	7.258	0.3664 − 01	0.2364 − 01	0.4069
5.8	39.080	5.224	7.481	0.3412 − 01	0.2284 − 01	0.4059
5.9	40.445	5.246	7.709	0.3179 − 01	0.2208 − 01	0.4050
6.0	41.833	5.268	7.941	0.2965 − 01	0.2136 − 01	0.4042
6.1	43.245	5.289	8.176	0.2767 − 01	0.2067 − 01	0.4033
6.2	44.680	5.309	8.415	0.2584 − 01	0.2002 − 01	0.4025
6.3	46.138	5.329	8.658	0.2416 − 01	0.1939 − 01	0.4018
6.4	47.620	5.347	8.905	0.2259 − 01	0.1880 − 01	0.4011
6.5	49.125	5.365	9.156	0.2115 − 01	0.1823 − 01	0.4004
6.6	50.653	5.382	9.411	0.1981 − 01	0.1768 − 01	0.3997
6.7	52.205	5.399	9.670	0.1857 − 01	0.1716 − 01	0.3991
6.8	53.780	5.415	9.933	0.1741 − 01	0.1667 − 01	0.3985
6.9	55.378	5.430	10.199	0.1634 − 01	0.1619 − 01	0.3979
7.0	57.000	5.444	10.469	0.1535 − 01	0.1573 − 01	0.3974
7.1	58.645	5.459	10.744	0.1443 − 01	0.1530 − 01	0.3968
7.2	60.313	5.472	11.022	0.1357 − 01	0.1488 − 01	0.3963
7.3	62.005	5.485	11.304	0.1277 − 01	0.1448 − 01	0.3958
7.4	63.720	5.498	11.590	0.1202 − 01	0.1409 − 01	0.3954
7.5	65.458	5.510	11.879	0.1133 − 01	0.1372 − 01	0.3949
7.6	67.220	5.522	12.173	0.1068 − 01	0.1336 − 01	0.3945
7.7	69.005	5.533	12.471	0.1008 − 01	0.1302 − 01	0.3941
7.8	70.813	5.544	12.772	0.9510 − 02	0.1269 − 01	0.3937
7.9	72.645	5.555	13.077	0.8982 − 02	0.1237 − 01	0.3933
8.0	74.500	5.565	13.387	0.8488 − 02	0.1207 − 01	0.3929
8.1	76.378	5.575	13.700	0.8025 − 02	0.1177 − 01	0.3925
8.2	78.280	5.585	14.017	0.7592 − 02	0.1149 − 01	0.3922
8.3	80.205	5.594	14.338	0.7187 − 02	0.1122 − 01	0.3918
8.4	82.153	5.603	14.662	0.6806 − 02	0.1095 − 01	0.3915
8.5	84.125	5.612	14.991	0.6449 − 02	0.1070 − 01	0.3912
8.6	86.120	5.620	15.324	0.6114 − 02	0.1045 − 01	0.3909
8.7	88.138	5.628	15.660	0.5799 − 02	0.1021 − 01	0.3906
8.8	90.180	5.636	16.000	0.5504 − 02	0.9983 − 02	0.3903
8.9	92.245	5.644	16.345	0.5226 − 02	0.9761 − 02	0.3901

Table 1:2 (*continued*)

M	p_2/p_1	ρ_2/ρ_1	T_2/T_1	p_{t2}/p_{t1}	p_1/p_{t2}	M_2
9.0	94.333	5.651	16.693	0.4964 − 02	0.9546 − 02	0.3898
9.1	96.445	5.658	17.045	0.4718 − 02	0.9338 − 02	0.3895
9.2	98.580	5.665	17.401	0.4486 − 02	0.9137 − 02	0.3893
9.3	100.738	5.672	17.760	0.4267 − 02	0.8943 − 02	0.3891
9.4	102.920	5.679	18.124	0.4061 − 02	0.8754 − 02	0.3888
9.5	105.125	5.685	18.492	0.3866 − 02	0.8572 − 02	0.3886
9.6	107.353	5.691	18.863	0.3683 − 02	0.8395 − 02	0.3884
9.7	109.605	5.697	19.238	0.3510 − 02	0.8223 − 02	0.3882
9.8	111.880	5.703	19.617	0.3346 − 02	0.8057 − 02	0.3880
9.9	114.178	5.709	20.001	0.3191 − 02	0.7895 − 02	0.3878
10.0	116.500	5.714	20.387	0.3045 − 02	0.7739 − 02	0.3876

1:3 Real Gas Effects

The preceding equations and relations which define the properties of air flow in wind tunnels are based on the premise that the specific heat ratio for air, γ, is invariable. This premise holds true for practical purposes as long as air temperatures of the flow are below about 1000°R. At these lower temperatures, the internal energy of the air is completely defined by the degree of excitation of the translational and rotational degrees of freedom of the molecule, and γ is constant.

At temperatures above 1000°R an additional degree of freedom of the molecule, termed the "vibrational degree of freedom," begins to reach significant proportions. When this occurs, the temperature increase of air with further additions of heat is less than it would have been at lower temperatures because a significant portion of the heat energy goes into excitation of the vibrational degree of freedom. This results in values of γ that vary with temperature.

Relations pertaining to the flow of air in wind tunnels with vibrational effects included have been derived in Ref. 1:1. From this reference the following equation for specific heat ratio, including the effects of molecular vibration, is obtained:

$$\gamma = 1 + \frac{\gamma_p - 1}{1 + (\gamma_p - 1)\left(\frac{\theta}{T}\right)^2 \frac{e^{\theta/T}}{(e^{\theta/T} - 1)^2}} \tag{1:25}$$

where θ = a constant, 5500°R for air,
γ = specific heat ratio,
γ_p = perfect gas value of specific heat ratio, 1.4 for air,
T = temperature, °R.

Equation (1:25) is satisfactory for engineering purposes at air temperatures up to 5000°R and yields the results of Fig. 1:8. Examination of eq. (1:25) quickly reveals that this is not one of the "slide rule" type of equations. Equations for flow relations pertinent to wind tunnels are similarly complicated. In fact, solutions for the case of a normal shock require iteration, and the reader is referred to Ref. 1:1, whose solutions in graphical form are reproduced in Figs. 1:9 to 1:18. Results of the figures are presented in terms of the ratio of the real gas flow parameter (including vibrational effects) to the same flow parameter calculated by assuming a value of $\gamma = 1.4$ throughout the flow. The subscript "therm perf" indicates a thermally perfect gas, which in turn indicates that the equation of state $p = \rho R_1 T$ is valid. This validity holds as long as the diatomic molecules of nitrogen and oxygen in air (N_2 and O_2) do not dissociate into atoms. The use of the figures is illustrated as follows.

Example 1:1 Determine the real gas static temperature of air in a Mach 5 flow with a total temperature of 3000°R.

From Fig. 1:11 at a Mach number of 5 and a total temperature of 3000°R, a value of 1.10 is read for the ratio

$$\frac{(T/T_t)_{\text{therm perf}}}{(T/T_t)_{\text{perf}}}$$

From Table 1:1, a value of $T/T_t = 0.1667$ is read for air at Mach 5.0 with $\gamma = 1.4$. Multiplying the ratio of 1.10 from the figure by 0.1667 yields 0.1834, which is the value of T/T_t including vibrational effects. Multiplying this value of T/T_t by the total temperature of 3000°R yields a static temperature of 550°R, as compared to 500°R when $\gamma = 1.4$.

1:4 Ideal Flow in a Supersonic Tunnel*

The establishment of a supersonic stream in a duct has many interesting facets, not the least of which is the odd-shaped passage that must be provided. In order for the flow to become supersonic, it must first become sonic. Because of the marked change in the characteristics of air flow that occurs at Mach 1.0, a sonic velocity can occur only at a minimum cross section of a duct. Hence a supersonic nozzle must first contract and then expand (see Fig. 1:19 and Ref. 1:15).

The relation between area and Mach number has been given in eq. (1:18). Unfortunately, however, the simple provision of the proper duct area will not assure uniform supersonic flow because increases in supersonic flow velocity do not occur through planes normal to the duct axis. As discussed previously, expansion disturbances in a supersonic flow are

* The not-inconsequential effects of viscosity will be discussed in the next section.

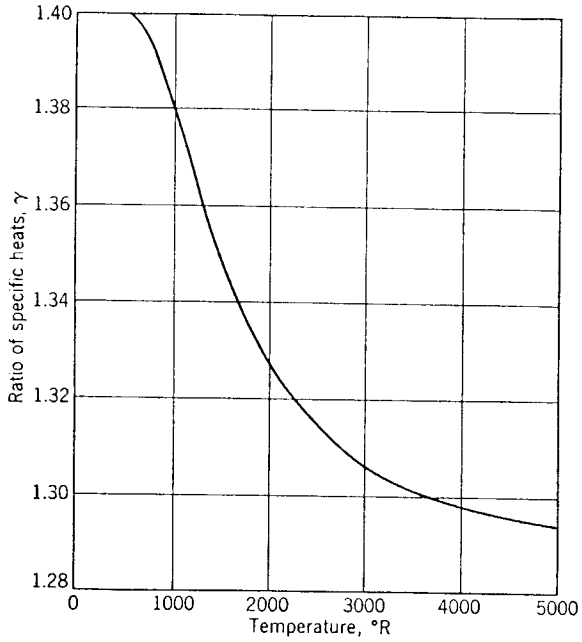


Fig. 1:8 The variation of the ratio of specific heats, γ, with temperature.

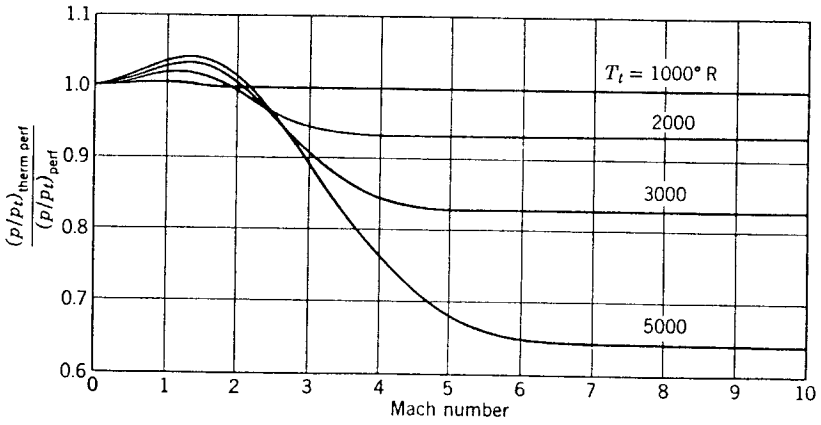


Fig. 1:9 Effect of caloric imperfections on the ratio of static pressure to total pressure.

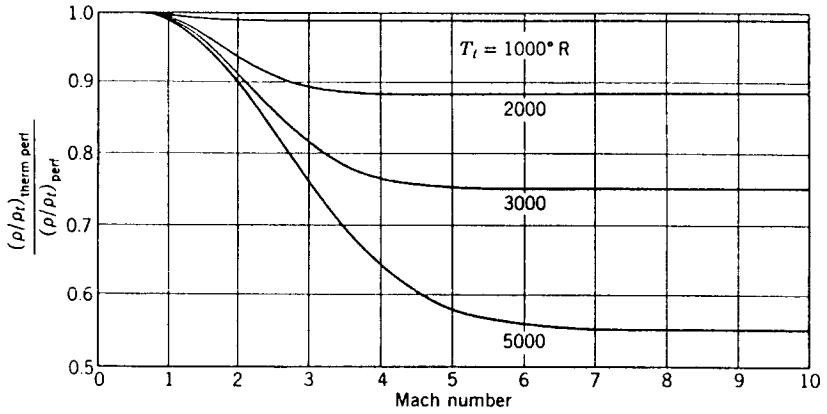


Fig. 1:10 Effect of caloric imperfections on the ratio of static density to total density.

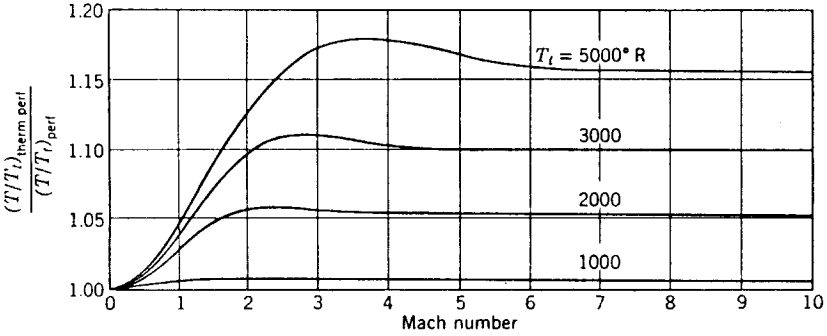


Fig. 1:11 Effect of caloric imperfections on the ratio of static temperature to total temperature.

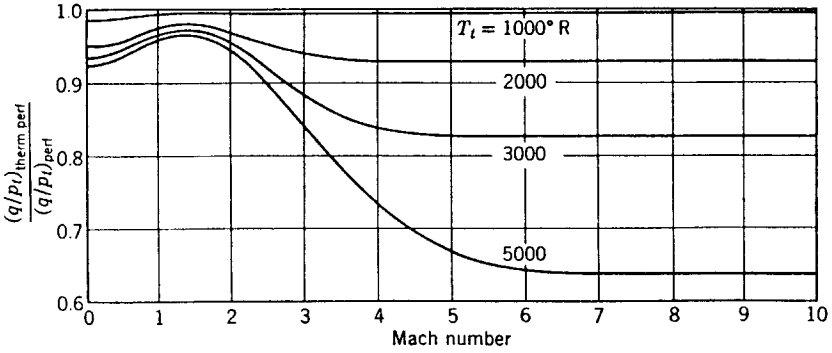


Fig. 1:12 Effect of caloric imperfections on the ratio of dynamic pressure to total pressure.

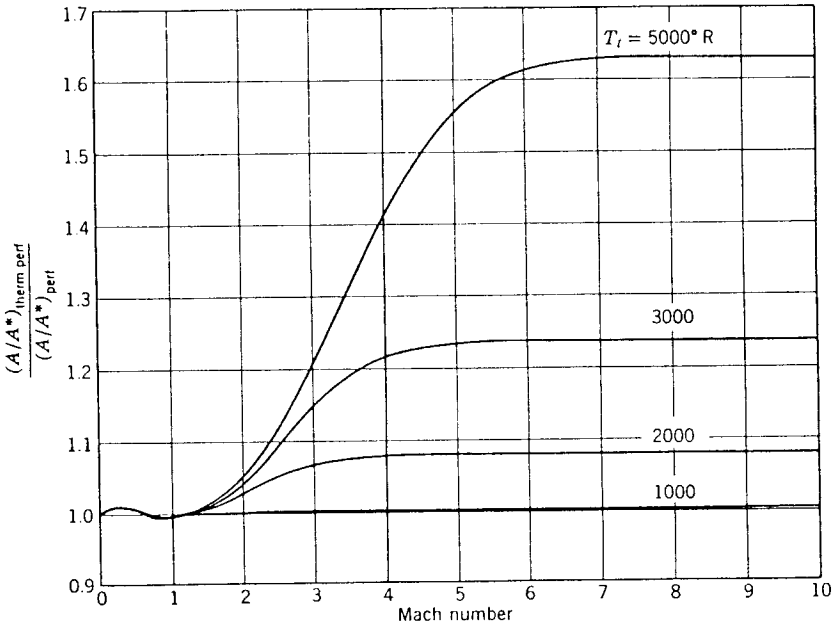


Fig. 1:13 Effect of caloric imperfections on the ratio of local cross-sectional area of a stream tube to the cross-sectional area at the point where $M = 1$.

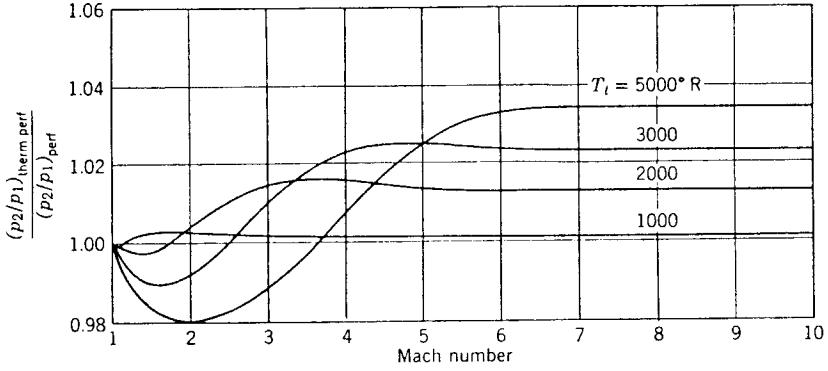


Fig. 1:14 Effect of caloric imperfections on the static pressure ratio across a normal shock wave.

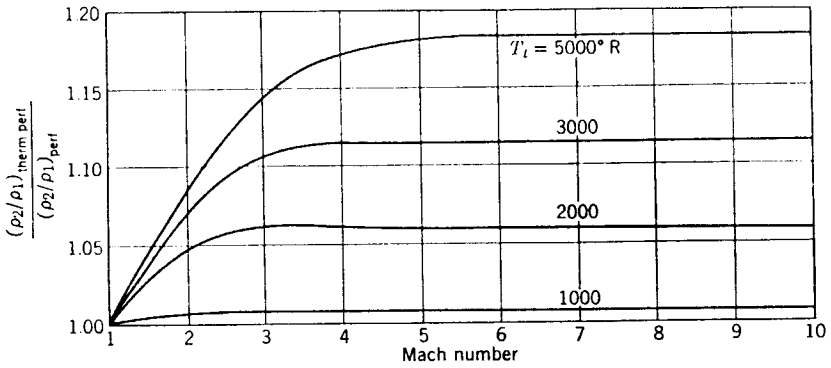


Fig. 1:15 Effect of caloric imperfections on the static density ratio across a normal shock wave.

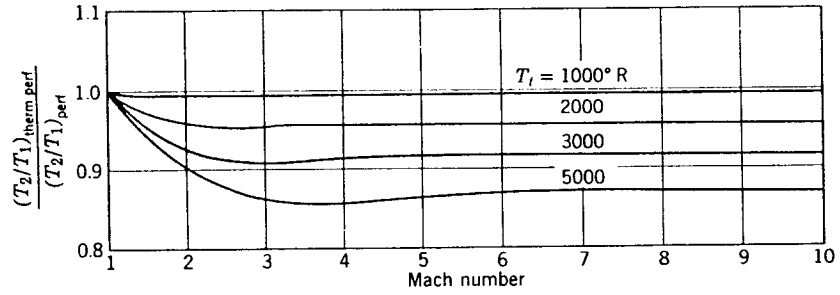


Fig. 1:16 Effect of caloric imperfections on the static temperature ratio across a normal shock wave.

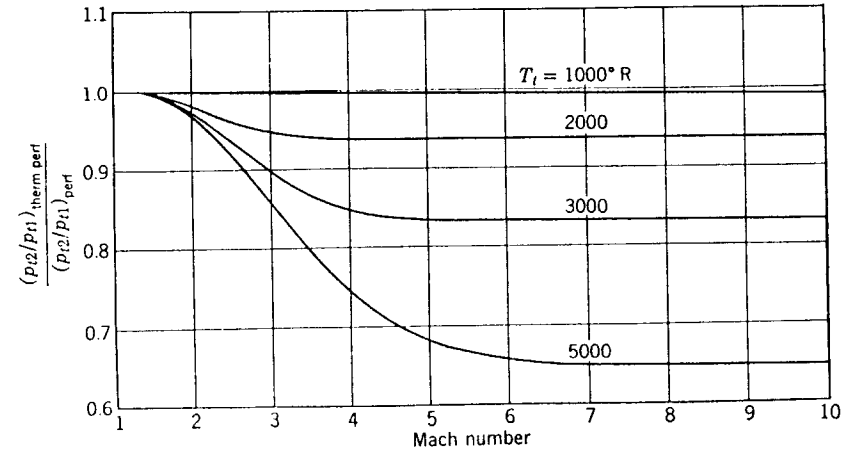


Fig. 1:17 Effect of caloric imperfections on the total pressure ratio across a normal shock wave.

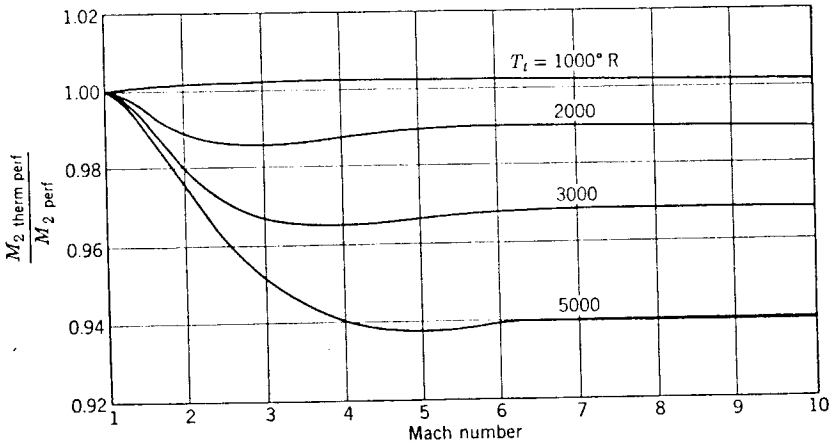


Fig. 1:18 Effect of caloric imperfections on the Mach number downstream of a normal shock wave.

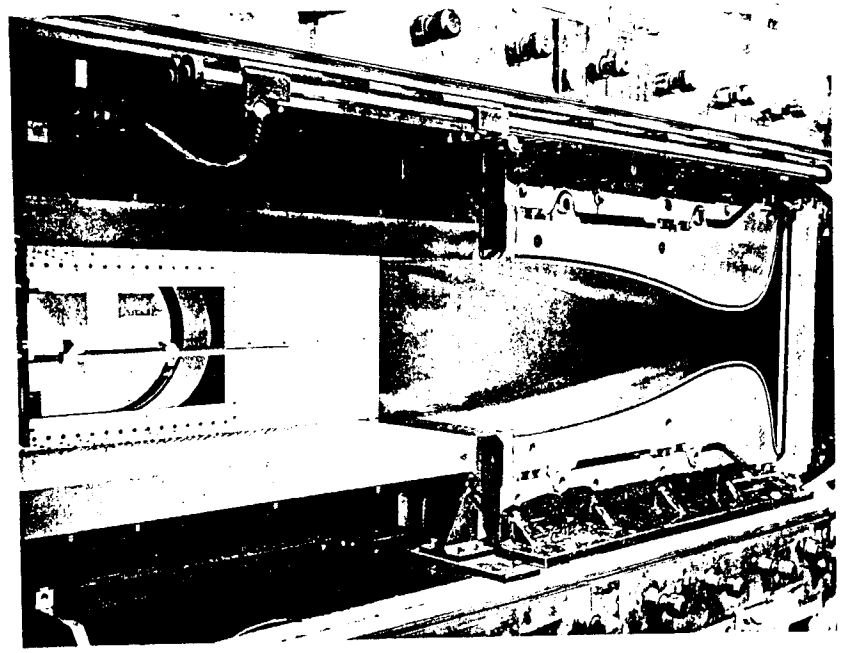


Fig. 1:19 A supersonic nozzle in a 12-inch transonic-supersonic wind tunnel. Flow is from right to left. (Courtesy Sandia Corporation.)

propagated along "Mach lines" or "characteristic lines," which are lines inclined at the angle $\sin^{-1}(1/M)$ with respect to the flow direction. Regions of flow upstream of the area bounded by the characteristic line are not influenced by the disturbance. Thus, an increase in duct area caused by diverging the walls of the duct does not affect the flow at the duct centerline until the characteristic lines originating at the beginning of the divergence cross the centerline as shown in Fig. 1:20. Because of this delayed effect of changing area ratio on the flow throughout the duct, great care must be exercised in obtaining the proper axial distribution of area ratio if uniform flow is to be obtained. We shall discuss the details of this problem in Section 1:8 on supersonic nozzle design.

The shock wave is the mechanism by which most supersonic flows, including those in a wind tunnel, are slowed down.* When a supersonic flow passes through a shock wave, a loss in total pressure occurs. The losses through the shock wave represent a large portion of the power requirements for higher Mach number supersonic tunnel operation. In the continuous-type wind tunnel the power loss through the shock is added to the other losses to be replaced by the tunnel drive compressor, and may under some conditions represent 90 per cent of the total loss.

The loss in total pressure associated with the return to subsonic speed through a normal shock is plotted in Fig. 1:21. Clearly it is a great waste of power to shock down at operating Mach number instead of reducing the Mach number before the final normal shock, particularly if the operating Mach number is above 1.5 or 2.0.

The above observation has led to the design of most supersonic wind tunnels with a diffuser† having a converging section, a minimum cross-section zone termed the "second throat," and then a diverging section. The purpose of this design is that the flow leaving the wind tunnel test section will be compressed and slowed down in the converging section of the diffuser, will pass through the second throat at a speed considerably below that of the test section, will begin to speed back up in the diverging section of the diffuser, and will establish a normal shock in the diverging portion of the diffuser at a Mach number considerably below the test section Mach number, and with a correspondingly smaller loss. It would be desirable to have a Mach number of 1.0 at the second throat in the hope that the normal shock would occur at a Mach number only slightly above 1.0 under conditions where the normal shock losses would be insignificant. It would appear, then, that the diffuser with a sonic flow in the second throat is the answer to the power requirements problem in

* They may also be slowed by friction or cooling.

† The diffuser is the section of the tunnel in which the flow is slowed from design conditions to a low subsonic speed.

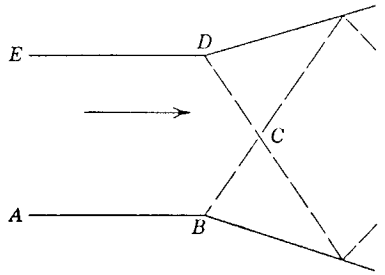


Fig. 1:20 Flow region affected by diverging duct walls. (The flow upstream of Mach waves *BC* and *DC* is unaffected by the divergence.)

a supersonic wind tunnel. Practical considerations, however, tend to negate this conclusion, as will be seen below.

As we start a supersonic tunnel there is at first a low subsonic speed throughout the tunnel circuit and the power required corresponds to the subsonic drag of the complete circuit. At this time the highest Mach number in the circuit occurs in the nozzle throat. As the power is increased, the speed throughout the circuit rises until the Mach number at the nozzle throat (Station *a*, Fig. 1:22) becomes 1.0 and a normal shock develops a short distance downstream of the throat. At this point the power required still corresponds to the subsonic drag of the complete circuit. A slight increase in power now will not change the Mach number *at the nozzle throat* but will move the normal shock further downstream

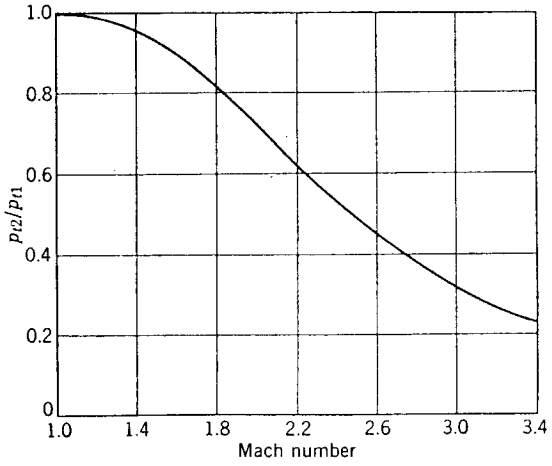


Fig. 1:21 Ratio of stagnation pressures across a normal shock wave.

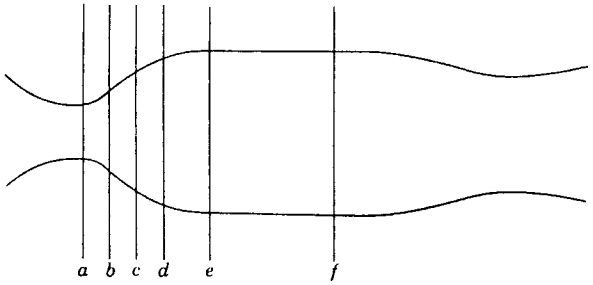


Fig. 1:22 Normal shock positions in a nozzle during the tunnel starting process.

of the throat (Station *b*), where the Mach number is supersonic and the losses through the normal shock are finite. The losses through the normal shock at this point account for the slight increase in power. As the power is further increased, the normal shock moves downstream through the nozzle (Stations *c*, *d*, *e*), and occurs at progressively higher Mach numbers. The resulting increased shock losses are added to the subsonic drag of the circuit and correspond to progressively increasing power requirements. Finally, the normal shock moves into the test section (Station *f*), where it occurs at the test section Mach number, and the power requirements correspond to the normal shock losses at the design Mach number. At this point in the tunnel starting process the power requirements are not influenced by the diffuser design because flow in the diffuser is still subsonic. Hence, in spite of the diffuser, the power requirements for getting a supersonic tunnel started correspond to normal shock losses at the design Mach number and are high at the higher Mach numbers. More customarily, the tunnel engineer, rather than speaking of "power," uses the ratio of necessary stagnation pressure to diffuser exit pressure, which he calls "pressure ratio." By including mass flow the two are affinely related. The theoretical pressure ratio required with a shock wave in the test section is shown as Case 3 in Fig. 1:23.

With the normal shock in the test section, only a slight increase in power should be required to move the shock through the second throat of the diffuser because the normal shock Mach number, and consequently the normal shock losses, should decrease as the shock moves through the converging section of the diffuser.

With the normal shock in the test section during the tunnel starting process, another limitation to the second-throat diffuser effectiveness appears. Downstream of the normal shock, the flow is subsonic. Hence the flow velocity in the converging section of the diffuser must be *increasing*, until a maximum velocity is reached in the second throat.

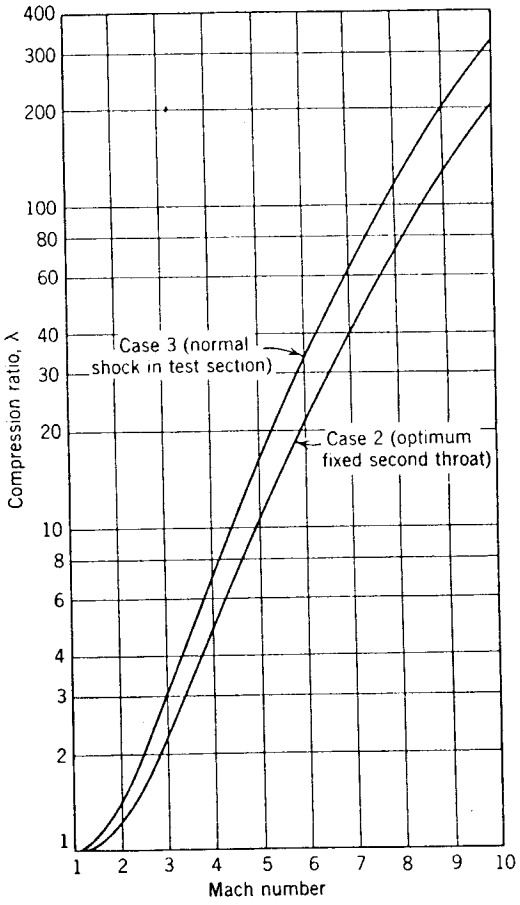


Fig. 1:23 Theoretical values of the compression ratio for Case 2 and 3 operation.

Since the Mach number in the second throat (minimum cross section) cannot exceed 1.0, the second throat must be sized to pass the mass flow of the nozzle with an expansion of the air downstream of the normal shock to a Mach number no greater than 1.0. Sizing of the second throat to allow the normal shock to pass through during the starting process is accomplished as follows. The Mach number in the second throat is assumed to be 1.0. The expansion of the air from the conditions *downstream* of the normal shock in the test section to Mach 1.0 at the second throat is assumed to be an isentropic process. With these assumptions eq. (1:12) is used to obtain the ratio of second throat area to test section area in terms of the Mach number downstream of the shock. The Mach

number downstream of the shock is related to the upstream Mach number by eq. (1:20). Combining these two equations and substituting $\gamma = 1.4$ yields

$$\frac{A_2^*}{A_T} = \frac{(5 + M^2)^{0.5}(7M^2 - 1)^{2.5}}{216\, M^6} \qquad (1:26)$$

where A_2^* = second-throat area, ft²,
A_T = test section area, ft²,
M = test section Mach number.

Values from eq. (1:26) are plotted in Fig. 1:24. The Mach number in the second throat after the tunnel has started, corresponding to isentropic flow between the two throats, may be obtained by using the area ratios of Fig. 1:24 in conjunction with eq. (1:12). When this is done we find that the requirement that the tunnel be able to *start* results in a fixed second throat considerably larger than that needed to bring the second-throat Mach number close to 1.0 during running. For example, when the test section Mach number is 6.0 and the second throat is sized for starting, its Mach number is 5.38. Similarly throughout the range, the second throats that permit starting do very little supersonic diffusing. The theoretical pressure ratios that would ensue for the optimum fixed second throat are shown as Case 2 in Fig. 1:23.

It is reasoned that if the second throat could be open enough to allow the tunnel to start and could then be closed down to a more nearly ideal

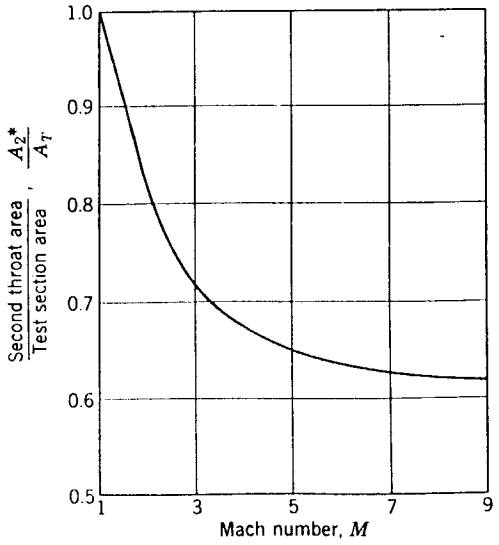


Fig. 1:24 The variation of the theoretical fixed geometry second throat area with Mach number, $\gamma = 1.4$.

area ratio after the shock has passed through, the pressure ratio requirements for running the tunnel could be reduced considerably. In theory, with a very gentle (no shock) diffuser, second throat Mach number could be made equal to 1.0.

Getting a little ahead of ourselves to consider a practical case, we note that several high-speed wind tunnels have incorporated this idea of an adjustable second throat, always with a degree of success far below ideal. As a matter of fact, the usefulness of such a technique has generally been so limited that many tunnels with variable second throats do not use them. High tunnel starting power requirements must be provided, and when they are, the power requirements for operation are no longer a problem.

1:5 Actual Flow in a Supersonic Tunnel

In Section 1:4 we discussed flow in a supersonic wind tunnel from the standpoint of ideal flow. Although this discussion is useful in describing the mechanism of the flow, the correlation with actual flow is quite poor unless viscous effects are included.

Viscous effects may be described in the following way. As air flows through a tunnel there is a friction force developed between the air and the walls. This causes a loss in velocity and momentum of air in a layer next to the wall called the "boundary layer." The boundary layer thickness and the total loss of momentum increase with increasing distance from the first throat of the nozzle and become quite important in the test section, particularly in high Mach number nozzles.

Viscous effects between the first throat and the test section of a nozzle are not usually of great importance during the steady-state operation of the tunnel. The growth of the boundary layer thickness with distance from the first throat is fairly predictable (see Section 1:9), and can be accounted for in nozzle design so that the desired flow outside the boundary layer can be achieved.

During the transient process in which the tunnel is started, viscous effects are extremely important and not very well understood. So important are these effects that compression ratios required to start most high Mach number tunnels now in operation are usually at least 100 per cent greater than the *normal shock pressure ratio* p_{t1}/p_{t2}. In effect, we are saying that losses due to viscous effects during the starting process are usually at least equal to the normal shock losses. The following explanation gives some insight into the flow complexities from which these high viscous losses occur.

Boundary layers are normally stable when the pressure is decreasing in the direction of boundary layer growth. However, they become unstable and have a tendency to break away or "separate" from the wall

when the pressure is increasing in the direction of growth. As a normal shock passes through a nozzle it imposes a severe unfavorable pressure gradient on the boundary layer, which will in some cases cause separation. If the boundary layer does separate, the flow across the nozzle will be severely altered over a large portion of the nozzle length. If the boundary layer does not separate, high pressure in the boundary layer downstream of the shock will cause air to flow forward into the subsonic portion of the boundary layer upstream of the shock, with the result that the boundary layer and consequently the flow in the duct are altered over a significant portion of the nozzle length.

In the diffuser of the wind tunnel viscous effects are probably predominant during starting and steady-state operation. In the starting case, after the normal shock moves into the converging section of the diffuser, an unfavorable pressure gradient is established at the beginning of the convergence. The unfavorable pressure gradient produced by the normal shock exists as in the general case mentioned above. "Oblique shocks" from the convergence create additional unfavorable pressure gradients when they strike the opposite wall. After the tunnel is started, all these effects still exist, with the difference that the normal shock has moved to a stable position downstream of the second throat—stable because small reductions in diffuser loss draw the shock farther downstream, where the greater area results in a higher Mach number and a larger loss.

In summary, there are six compression ratios (ratio of the total pressure in the settling chamber to that at the diffuser exit) that are of interest, three for ideal (theoretical) frictionless flow and three for the real or practical case.

1. The smallest is the ratio required to run the tunnel after an adjustable diffuser has been closed down to the minimum area. In theory, this ratio approaches 1.0, which corresponds to negligible loss.
2. The next is the ratio required to run the tunnel when a fixed diffuser (of throat area just large enough to let the tunnel start) is employed.
3. The largest is the ratio needed to start the tunnel. (This corresponds to the condition when the normal shock is in the test section.)

Compression ratios for Conditions 2 and 3 are shown in Fig. 1:23 for the theoretical case. The range of actual compression ratios for starting and running, as obtained from a number of wind tunnels, is shown in Fig. 1:25. The area between the curves for starting and running an actual tunnel has as its lowest values the compression ratios for tunnels with adjustable diffusers; higher values correspond to fixed diffusers. The actual starting ratios are higher yet, as shown.

The starting compression ratios in Fig. 1:25 may be reduced by using an adjustable nozzle and adjusting it to a higher Mach number after the tunnel has started. The running compression ratios may be reduced by means of injectors in the diffuser which reduce separation. (In one instance known to the author $M = 5.0$ was obtained by a compression ratio of 5.0, a very low figure.) Both alterations must be justified economically by special considerations of available equipment.

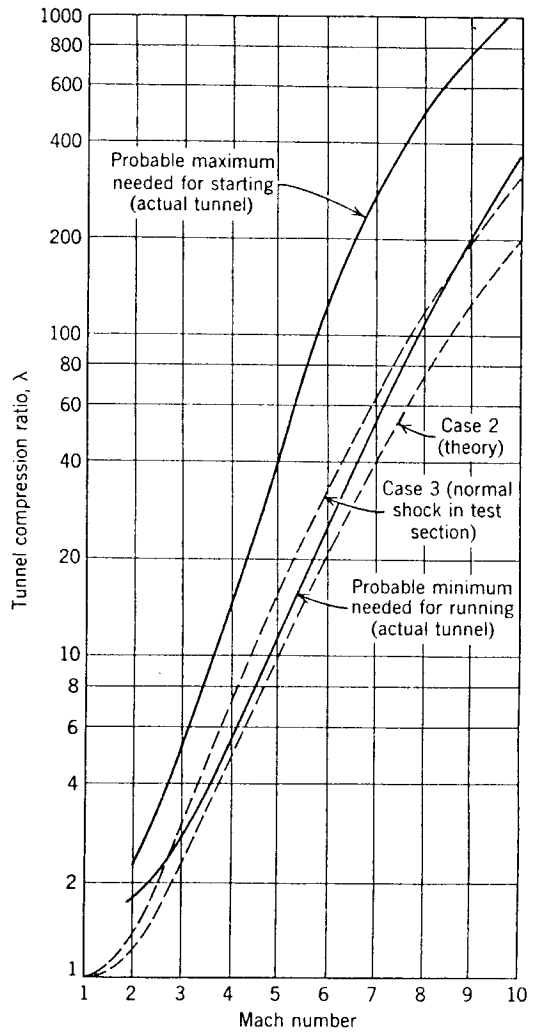


Fig. 1:25 The probable maximum pressure ratios needed for starting, and the minimum needed for running, as obtained from data from eleven tunnels over their range of Mach numbers. Data include tests with models installed.

In high-speed wind tunnel design the importance of providing adequate compression ratio cannot be overemphasized. The power supply is a major portion of the wind tunnel and cannot be easily altered in the event that sufficient compression ratio is not provided in the original design. It will be noted that a second throat as much as 30 per cent or more above the ideal size required for tunnel starting will be needed in order to make allowance for the increased losses produced when a model is installed in the test section. This allowance (see Section 1:6) is another extremely important item in wind tunnel design. It can be quite embarrassing to have enough compression ratio to operate a wind tunnel and to have a second throat too small to get it started.

In conclusion we note the following general items concerning flow in supersonic nozzles which have to this point only been implied:

1. The Mach number in a supersonic nozzle is locked in by the nozzle area ratio and will not be changed (as long as it remains supersonic) by either upstream or downstream pressure.
2. If the downstream stagnation pressure is lowered without changing the upstream pressure, there will be no change in the test section flow, but the losses in the diffuser shock system will be increased. This increased loss is usually attributed to the normal shock's being pulled farther downstream, where it occurs at a higher Mach number.
3. If the upstream pressure is increased, the flow in the test section will occur at a higher pressure but at the same Mach number.

Items 1 and 3 neglect secondary changes in Mach number produced by changes in boundary layer thickness and consequent changes in the effective area ratio.

1:6 Starting with a Model in the Test Section

Our discussion of flow in a supersonic tunnel has been generally limited so far to the case of a clear tunnel. Let us now consider the effects of a model in the test section on the starting of a supersonic tunnel.

It can be shown that the area of a second throat sized for Mach 1.0 flow during the starting process varies as the loss of total head in the test section. Using a value of $\gamma = 1.4$ and eq. (1:18), we obtain the ratio of area at the nozzle throat to area at the test section. Dividing the area ratio of eq. (1:26) by this area ratio gives the ratio of the second-throat area to the nozzle throat area. When this is done and the results are compared with eq. (1:24) we find that

$$\frac{A_2^*}{A_1^*} = \frac{p_{t1}}{p_{t2}} \qquad (1:27)$$

This relation implies that losses in total head resulting from the shocks on a model during the starting process require a second throat larger than that for the clear tunnel. This has been found to be true in actual wind tunnel operation.

Another important consideration is the maximum model size for tunnel starting. This may be studied in the manner of the second throat analysis. With a normal shock ahead of the model, the flow ahead of the model is subsonic. A minimum cross-sectional area will exist at the station where the cross-sectional area of the model is greatest. At this minimum area, the Mach number cannot exceed 1.0. Hence the model must be small enough to allow the mass flow of the nozzle to pass through the unobstructed nozzle cross section with an expansion of the air downstream of a normal shock to a Mach number no greater than 1.0. If the normal shock does not pass across the model during the starting process, the tunnel is said to be "choked." The theoretical unobstructed nozzle cross-sectional area at the model required for starting is the same as the second throat area of Fig. 1:24. In practice, it is wise to size a model somewhat smaller than this analysis suggests. If the model is particularly blunt, the model size may have to be further reduced. If the model is sufficiently small, the normal shock envelops the model in the manner illustrated by Fig. 1:26.

In Fig. 1:27, experimental data on model size for starting from several high-speed wind tunnels are summarized. At Mach numbers to 10.0, allowable model sizes are much smaller than theoretical, again indicating the danger of considering purely theoretical flow. Surprisingly, in a few instances, sharp models have permitted tunnel starts when their sizes were above the "theory" line.

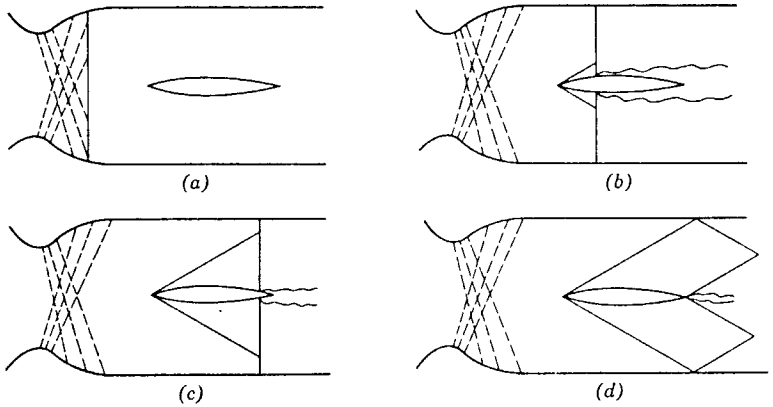


Fig. 1:26 Sketch showing the progress of the normal shock through a test section with a model. The flow is finally established in (*d*).

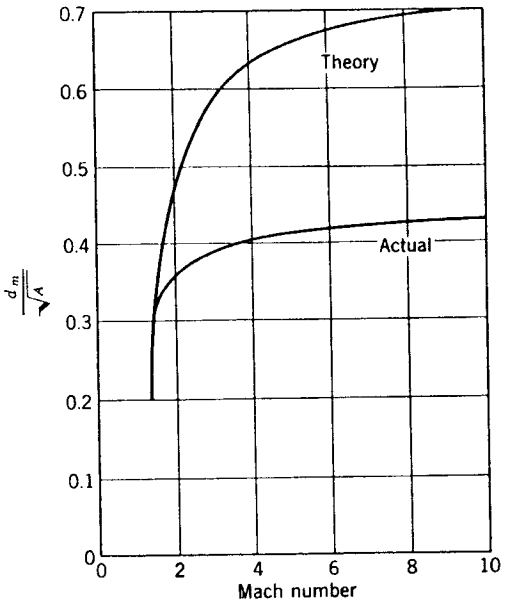


Fig. 1:27 Maximum model diameter for certain start of blunt models. (Ref. 1:2.) Sharp-nosed models may be larger than blunt ones. d_m = maximum model diameter; A = physicial test section cross-sectional area less the product of boundary layer displacement thickness and test section perimeter.

Occasionally a model is put in the tunnel and the tunnel will not start. The following actions (not in any particular order) may be tried, and good luck to all.*

1. Moving the model forward in the test section.
2. Squirting a spray of water in to the stagnation chamber.
3. Adding an afterbody to the model.
4. Blowing air out of holes near the nozzle throat.
5. Increasing the diffuser area.
6. Increasing the tunnel pressure ratio.
7. Adding a removable sharp nose to the model.

Since an increase in model angle of attack requires an increase of pressure ratio, the tunnel may "unstart" during a run. This effect is often accompanied by a change in tunnel noise that the operators may notice. However, visual means for detecting "unstarting" are much preferred.

* The authors know of one small (1-inch test section) indraft tunnel that starts when a wire is fed into the entrance cone and wiggled to "tickle the tunnel's throat."

Typical visual means include schlieren systems or manometers connected to test section pressure orifices.

1:7 The Method of Characteristics

The method of characteristics is a method for defining the properties of supersonic flows in the presence of varying boundaries such as in a wind tunnel nozzle or in the presence of some aerodynamic configuration in a supersonic air stream. The method as normally used requires constant entropy flow. Hence it cannot be used in a flow field having shock waves. In general, this limits the method of characteristics to the case of a continually expanding flow because weak compression waves have to be widely separated to avoid the formation of a shock and consequent entropy changes.

The method of characteristics is probably the most frequently used method for defining the internal contours of supersonic nozzles in the region between the first throat and the test section. It is this application which is of primary interest here.

The method of characteristics has been developed for both two-dimensional and three-dimensional flows. We shall discuss only the two-dimensional flow method. The two-dimensional flow considered is one in which flow changes occur in two dimensions such as a rectangular supersonic nozzle with parallel side walls and contoured upper and lower walls.

If a parallel flow at a Mach number of 1.0 is expanded around a corner, the direction of the flow will be changed and the Mach number will be increased. The Mach number to which the flow will be expanded by the corner is related to the angle of the corner. This relation is tabulated in Table 1:3, where ν is the turning angle. Also included in the table are angles of Mach lines with respect to the direction of flow, α_m, and ratios of static to total pressure, p/p_t. The data of Table 1:3 are based on the assumption of perfect gas flow. The values are not limited to cases in which the flow is expanded from Mach 1.0 by a single turn. They are applicable to cases in which the flow is turned from one direction to some maximum inclination with respect to that direction through any number of steps. They are also applicable to the case, as in a supersonic nozzle, where the flow is turned first to some maximum inclination with respect to the direction of flow at Mach 1.0 and then is turned back to the direction of flow at Mach 1.0. In this case, the angles of turning out and back are additive in determining the total turning angle, ν.

In order to describe the method of characteristics let us examine the flow around a corner illustrated in Fig. 1:28. The Mach number ahead of a 5-deg corner is 1.950. From Table 1:3 we find that in order to reach

Table 1:3

Prandtl-Meyer Corner Data, $\gamma = 1.4$

ν, Deg	Mach Number	α_m, Deg	p/p_t	ν, Deg	Mach Number	α_m, Deg	p/p_t
0.0	1.0000	90.00	0.5282	20.0	1.7743	34.31	0.1813
0.5	1.0508	72.10	0.4975	20.5	1.7915	33.93	0.1763
1.0	1.0808	67.70	0.4792	21.0	1.8090	33.54	0.1718
1.5	1.1078	64.50	0.4634	21.5	1.8268	33.19	0.1668
2.0	1.1328	61.96	0.4492	22.0	1.8445	32.83	0.1624
2.5	1.1559	59.89	0.4367	22.5	1.8622	32.48	0.1584
3.0	1.1770	58.17	0.4250	23.0	1.8795	32.15	0.1539
3.5	1.1973	56.68	0.4136	23.5	1.8973	31.82	0.1498
4.0	1.2170	55.29	0.4036	24.0	1.9150	31.49	0.1459
4.5	1.2362	53.99	0.3926	24.5	1.9325	31.16	0.1419
5.0	1.2554	52.77	0.3834	25.0	1.9502	30.85	0.1383
5.5	1.2745	51.66	0.3737	25.5	1.9680	30.54	0.1342
6.0	1.2935	50.63	0.3638	26.0	1.9861	30.23	0.1306
6.5	1.3120	49.66	0.3552	26.5	2.0041	29.93	0.1270
7.0	1.3300	48.75	0.3463	27.0	2.0222	29.64	0.1234
7.5	1.3478	47.90	0.3385	27.5	2.0402	29.35	0.1201
8.0	1.3649	47.11	0.3298	28.0	2.0585	29.06	0.1166
8.5	1.3825	46.33	0.3215	28.5	2.0770	28.78	0.1133
9.0	1 4005	45.57	0.3136	29.0	2.0957	28.49	0.1100
9.5	1.4178	44.58	0.3067	29.5	2.1145	28.23	0.1067
10.0	1.4350	44.18	0.2991	30.0	2.1336	27.97	0.1037
10.5	1.4522	43.52	0.2917	30.5	2.1530	27.68	0.1007
11.0	1.4688	42.92	0.2847	31.0	2.1723	27.41	0.0977
11.5	1.4858	42.30	0.2778	31.5	2.1913	27.16	0.0949
12.0	1.5028	41.72	0.2711	32.0	2.2105	26.90	0.0919
12.5	1.5195	41.15	0.2648	32.5	2.2298	26.65	0.0892
13.0	1.5365	40.60	0.2585	33.0	2.2492	26.40	0.0866
13.5	1.5540	40.05	0.2518	33.5	2.2688	26.15	0.0839
14.0	1.5710	39.53	0.2454	34.0	2.2885	25.91	0.0814
14.5	1.5875	39.04	0.2398	34.5	2.3090	25.66	0.0789
15.0	1.6045	38.54	0.2336	35.0	2.3288	25.43	0.0764
15.5	1.6213	38.08	0.2281	35.5	2.3485	25.21	0.0740
16.0	1.6380	37.63	0.2222	36.0	2.3688	24.99	0.0718
16.5	1.6550	37.17	0.2167	36.5	2.3895	24.77	0.0695
17.0	1.6723	36.73	0.2116	37.0	2.4108	24.53	0.0672
17.5	1.6892	36.30	0.2058	37.5	2.4316	24.29	0.0651
18.0	1.7061	35.88	0.2009	38.0	2.4525	24.07	0.0630
18.5	1.7230	35.48	0.1955	38.5	2.4730	23.86	0.0611
19.0	1.7401	35.08	0.1905	39.0	2.4942	23.64	0.0591
19.5	1.7572	34.69	0.1860	39.5	2.5156	23.43	0.0571

Table 1:3 (*continued*)

ν, Deg	Mach Number	α_m, Deg	p/p_t	ν, Deg	Mach Number	α_m, Deg	p/p_t
40.0	2.5372	23.22	0.0553	60.0	3.5937	16.16	0.0115
40.5	2.5590	23.01	0.0534	60.5	3.6270	16.01	0.0110
41.0	2.5810	22.80	0.0516	61.0	3.6610	15.86	0.0105
41.5	2.6028	22.59	0.0499	61.5	2.6948	15.71	0.00998
42.0	2.6254	22.38	0.0482	62.0	3.7288	15.56	0.00951
42.5	2.6484	22.19	0.0466	62.5	3.7632	15.41	0.00907
43.0	2.6716	21.98	0.0448	63.0	3.7980	15.26	0.00866
43.5	2.6948	21.79	0.0433	63.5	3.8332	15.12	0.00825
44.0	2.7179	21.59	0.0418	64.0	3.8690	14.98	0.00786
44.5	2.7412	21.39	0.0403	64.5	3.9052	14.84	0.00748
45.0	2.7643	21.21	0.0389	65.0	3.9417	14.70	0.00712
45.5	2.7879	21.02	0.0375	65.5	3.9788	14.56	0.00678
46.0	2.8120	20.83	0.0362	66.0	4.0164	14.42	0.00644
46.5	2.8361	20.65	0.0349	66.5	4.0548	14.28	0.00612
47.0	2.8610	20.46	0.0336	67.0	4.0940	14.14	0.00581
47.5	2.8855	20.28	0.0323	67.5	4.1338	14.00	0.00552
48.0	2.9105	20.09	0.0311	68.0	4.1738	13.86	0.00524
48.5	2.9360	19.91	0.0300	68.5	4.2135	13.73	0.00497
49.0	2.9616	19.73	0.0288	69.0	4.2543	13.60	0.00472
49.5	2.9873	19.56	0.0278	69.5	4.2960	13.46	0.00447
50.0	3.0131	19.38	0.0267	70.0	4.3385	13.33	0.00423
50.5	3.0393	19.21	0.0257	70.5	4.3820	13.19	0.00401
51.0	3.0660	19.06	0.0247	71.0	4.4257	13.06	0.00379
51.5	3.0925	18.87	0.0237	71.5	4.4704	12.92	0.00359
52.0	3.1193	18.70	0.0228	72.0	4.5158	12.79	0.00339
52.5	3.1463	18.53	0.0219	72.5	4.5620	12.66	0.00320
53.0	3.1737	18.38	0.0210	73.0	4.6086	12.53	0.00302
53.5	3.2015	18.21	0.0202	73.5	4.6558	12.40	0.00285
54.0	3.2293	18.04	0.0194	74.0	4.7031	12.28	0.00269
54.5	3.2576	17.87	0.0186	74.5	4.7505	12.15	0 00254
55.0	3.2865	17.72	0.0178	75.0	4.7979	12.02	0.00240
55.5	3.3158	17.55	0.0171	75.5	4.8504	11.89	0.00226
56.0	3.3451	17.40	0.0164	76 0	4.9032	11.76	0.00212
56.5	3.3747	17.24	0.0157	76.5	4.9557	11.64	0.00199
57.0	3.4055	17.08	0.0150	77.0	5.009	11.52	0.00187
57.5	3.4365	16.92	0.0144	78.0	5.119	11.27	0.00165
58.0	3.4675	16.76	0.0137	79.0	5.232	11.02	0.00145
58.5	3.4985	16.61	0.0131	80.0	5.349	10.78	0.00127
59.0	3.5295	16.46	0.0126	81.0	5.470	10.53	0.00111
59.5	3.5612	16.31	0.0120	82.0	5.595	10.29	0.000970

Table 1:3 (*continued*)

ν, Deg	Mach Number	α_m, Deg	p/p_t	ν, Deg	Mach Number	α_m, Deg	p/p_t
83.0	5.724	10.07	0.000845	98.0	8.622	6.67	0.0000628
84.0	5.867	9.81	0.000727	99.0	8.907	6.45	0.0000507
85.0	6.008	9.58	0.000628	100.0	9.210	6.23	0.0000407
86.0	6.155	9.35	0.000541	101.0	9.539	6.02	0.0000322
87.0	6.311	9.12	0.000463	102.0	9.887	5.80	0.0000254
88.0	6.472	8.88	0.000396	103.0	10.260	5.60	0.0000198
89.0	6.643	8.66	0.000336	104.0	10.658	5.38	0.0000154
90.0	6.820	8.43	0.000285	105.0	11.081	5.18	0.0000118
91.0	7.008	8.21	0.000240				
92.0	7.202	7.98	0.000202				
93.0	7.407	7.77	0.000169				
94.0	7.623	7.54	0.000140				
95.0	7.852	7.32	0.000116				
96.0	8.093	7.10	0.0000950				
97.0	8.350	6.88	0.0000776				

the Mach number of 1.950, the flow at this point has been turned through an angle of 25 deg from its direction at Mach 1.0. We also find that at a Mach number of 1.950, the angle of the Mach wave OA with respect to the direction of flow is 30.85 deg. Turning the flow through an additional 5-deg angle results in a total turning angle ν of 30 deg, so that the Mach number downstream of the corner is 2.134 and the Mach wave OB has an angle of 27.97 deg with respect to the new flow direction or 22.97 deg with respect to the original flow direction.

Between the Mach waves OA and OB the flow Mach number and

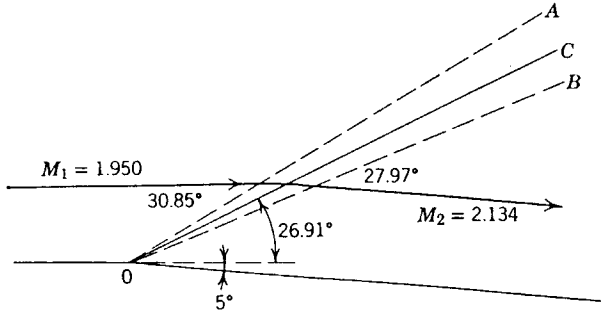


Fig. 1:28 Supersonic flow around a corner.

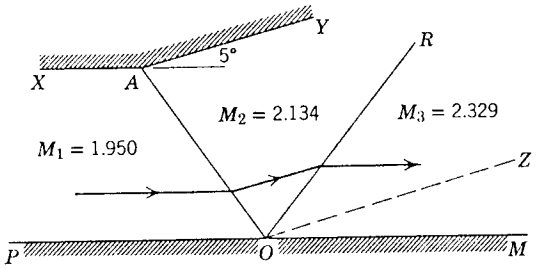


Fig. 1:29 Sketch demonstrating how characteristic lines from an expansion are reflected by a solid boundary.

direction are continuously changing. In the method of characteristics, these variations in the fan-shaped zone AOB are replaced by a step change from the conditions upstream of the corner to the conditions downstream of the corner across a line OC which bisects the fan shaped zone AOB. For the flow of Fig. 1:28, this corresponds to saying that the flow is at Mach 1.950 in its original direction until it reaches OC. When it crosses OC its Mach number is instantly changed to 2.134 and its direction is instantly changed by 5 deg. The line OC is called a characteristic line.

It is apparent that the changes in Mach number and flow direction across the fan-shaped zone AOB will be decreased as the turning angle is decreased. Thus, the assumptions of the method of characteristics approach the actual flow as the turning angle approaches zero.

In some supersonic flow problems, particularly in nozzle design, it is necessary to determine what happens when an expansion wave strikes a solid boundary. Let us examine this case by reference to Fig. 1:29. The initial flow is at a Mach number of 1.950 between the parallel walls XA and POM. At point A the upper wall makes a turn of 5 deg upward. From our previous example we have defined the characteristic AO and the Mach number downstream of AO. Now, let us draw a line OZ parallel to AY. If the area between AY and OZ is allowed to represent the flow channel downstream of AO, then no characteristics occur downstream of AO because no further turning of the flow is required. In this case the characteristic wave AO would be said to be "canceled" upon striking the boundary POZ. However, OM is the actual boundary of the flow downstream of AO and the flow along this boundary must be parallel to the boundary. Hence a characteristic wave is required to turn the flow from the 5-deg up direction to the horizontal direction. We can see that having the actual boundary OM instead of the boundary OZ for uniform flow allows more room for the air flow downstream of AO. Thus, the flow is expanded to a higher Mach number by the 5-deg turn

back to a horizontal direction. This being determined, the second characteristic line OR and the Mach number downstream of OR are obtained in the previously described manner.

1:8 Supersonic Nozzle Design

The supersonic nozzle consists of a subsonic portion which accelerates the settling chamber flow up to sonic speed, and a supersonic portion which further accelerates the flow and finally delivers it as a uniform stream to the test section. Considering first the subsonic portion, we find that it is exceedingly difficult to accelerate the settling chamber flow without having some areas of deceleration near the walls which tend to thicken the boundary layer undesirably. Usually this effect is neglected by nozzle designers, apparently without serious harm, and one of three completely arbitrary procedures is used to determine the subsonic shape:

1. Draw a smooth curve of Mach number against nozzle length from settling chamber Mach number to $M = 1.0$, and then using eq. 1:18 compute the corresponding area ratio. (The reason for not drawing the area curve directly is that the extra step yields a much more gradual curve than intuition would normally indicate.)
2. Draw an arc of $5h^*$ where h^* is the height of the sonic throat.
3. Use the curve made by an ellipse having the major axis equal to the throat height and the minor axis equal to one-half throat height. A 45-deg line is then faired from settling chamber to the ellipse.

In the usual case of fairing from a round settling chamber to a rectangular section at the sonic point (nozzle throat), about twenty control stations should be used. In actual construction the subsonic portion of the nozzle should end at $M = 0.9$ or below to avoid a joint at the sonic station, and whatever joint finally evolves should cause a step of no more than 0.001 inch.

For designing the portion of the nozzle between the throat and the test section, the method of characteristics is normally used. An outline of the steps required in the design of a two-dimensional nozzle by the method of characteristics will be given.

Note that use of the method of characteristics requires dividing the diverging portion of the nozzle into a series of straight sections in order to define the characteristic lines and their reflections and cancellations. However, after the characteristic calculations have been completed, it is possible to obtain a smooth curve which, after allowance has been made for the boundary layer, is suitable for creating a uniform supersonic stream of a predetermined Mach number. The general steps to take are as follows:

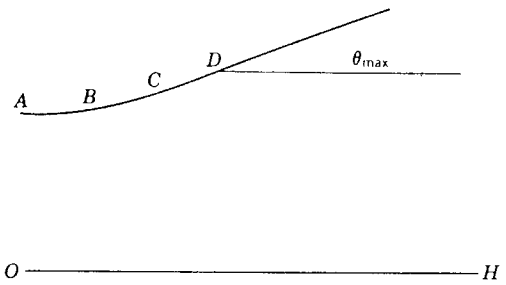


Fig. 1:30 Illustration of first step in supersonic nozzle design.

1. Read the turning angle ν for the desired Mach number from Table 1:3 and compute the maximum wall angle θ_{max} from $\theta_{max} = \nu/2$.
2. Since a nozzle symmetrical about a horizontal centerline will have symmetrical flow, the problem is somewhat shortened if we design only the upper half. Hence we now draw (Fig. 1:30) the centerline OH and a very short horizontal section AB representing the downstream end of the subsonic portion.
3. Construct a smooth and arbitrary curve BCD that expands the minimum section to θ_{max} at some distance downstream. Both the distance downstream and the curve are unimportant except in the way they effect the overall distance between the nozzle throat and the test section. In supersonic nozzles, this distance is usually in the range of 3 to 8 test section heights, with the lower values occurring at lower Mach numbers.
4. Divide the curve into enough equal straight sections to make an angle of not over 2 deg between each section. The shorter the sections are, the greater the accuracy, and, of course, the greater the number of calculations. Steps smaller than $\frac{1}{2}$ deg are probably unnecessary.
5. Construct the expansion waves and their reflections according to our previous work and the examples that follow Step 8.
6. Construct the section canceling all the expansion waves.
7. Redraw the nozzle to an expanded vertical scale and fair a smooth curve through the points of intersection of the waves with the wall.
8. Check the final result by comparing the area ratio of minimum to final section with that of eq. (1:18). Agreement should be within 1 per cent.

Example 1:2 Construct a single-step supersonic nozzle to obtain a final Mach number of 1.503, test section to be 9.44 inches high. ($M = 1.503$ is selected because it yields an even number of degrees of turn. Other Mach numbers merely require interpolation in the table.) Start with $M = 1.0$.

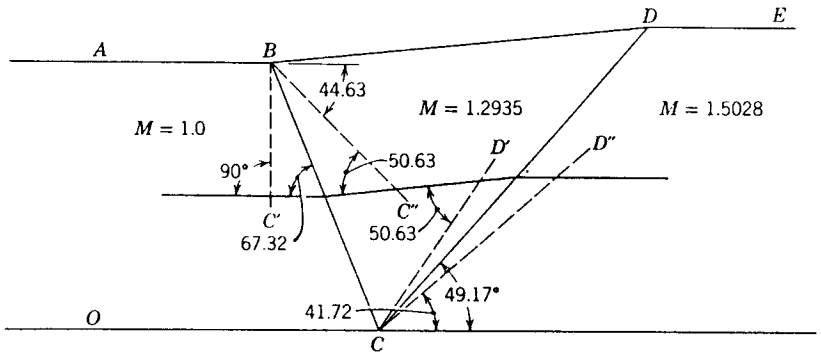


Fig. 1:31 Construction of a single-step characteristic net for a supersonic nozzle.

1. From Table 1:3 $\nu = 12$ deg for $M = 1.5028$. Hence $\theta_{max} = 6$ deg.

2. From eq. (1:18) the area ratio for $M = 1.5028$ is 1.180, so that distance AO of Fig. 1:31 should be constructed as $9.44/(2 \times 1.18) = 4.0$ inches.

3. Since we shall have only one step of 6 deg, no smooth curve need be laid in. It should be noted, of course, that 6-deg steps are too large, and this example is presented only as the simplest case, useful as a starting point.

4. The Mach number produced by a 6-deg turn is, from Table 1:3, 1.2935. The Mach angle for $M = 1.0$ is 90 deg, and for $M = 1.2935$ it is 50.63 deg. Sketching in the Mach wave for the initial flow BC' and the Mach wave for the turned flow BC'', and bisecting the angle thus formed, we get the first characteristic line BC, which is inclined 67.32 deg with respect to the horizontal.

5. We have determined that the Mach wave downstream of the first turn is inclined 50.63 deg with respect to the flow, so we sketch in such a wave CD'. When the 6-deg-up flow is turned down 6 deg to obtain the design Mach number of 1.5028, we find in Table 1:3 that the Mach wave is inclined 41.72 deg with respect to the flow. Such a wave, CD'', is sketched in. The angle between these two waves is bisected to obtain the second characteristic line CD, which has an angle of 49.17 deg with respect to the horizontal.

6. At the point of intersection of the characteristic line CD with the nozzle wall BD, the second 6-deg turn of the wall is made to form a horizontal segment DE. Since the flow everywhere downstream of the characteristic CD is parallel to the boundary DE, no further turning of the flow is required. Consequently the wave CD does not reflect when it strikes the wall. This portion of the nozzle where the characteristics strike the wall and are not reflected is called the "cancellation region."

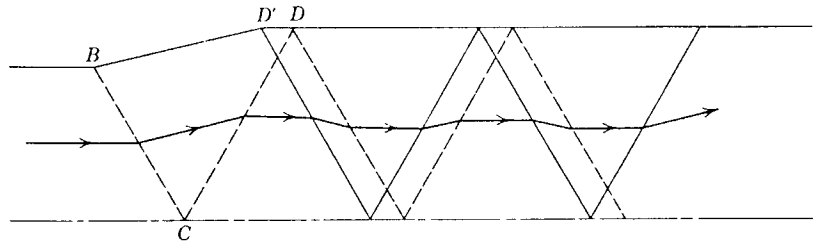


Fig. 1:32 Illustration of the effect of starting the constant-area section of a nozzle too far upstream.

This completes the single-step nozzle. Measurement of the area ratio yields 1.15, compared to 1.18 from eq. (1:18). It is noted that in the design of a nozzle by the characteristic method, the Mach waves of Fig. 1:31 are usually not sketched in because they increase the complexity of the drawing. Instead, the pertinent Mach wave angles are obtained, the angle formed by the two Mach waves are bisected analytically, and the characteristic line is drawn on the figure.

It is of interest to consider the result of starting the constant-area section too early, say at D' (Fig. 1:32). At D' the flow is up 6 deg, and the positively (to the flow) inclined surface would produce an over-pressure wave that would ricochet down the duct. Further, the rarefaction wavelet CD would not be canceled, and it too would continue downstream. The field in which the model is to be tested would have a lattice of horizontal, up-and-down-flow regions of varying speed, and successful testing would be most doubtful.

Example 1:3 Construct a two-step supersonic nozzle 9.44 inches high to yield a final Mach number of 1.5028. An additional step must be used, but this problem now embraces wave intersection and demonstrates the complete case, so that any number of steps may be employed in an identical manner.

1. In a manner similar to Example 1:2, θ_{max} is 6 deg.

2. The nozzle throat dimension OA is again 4 inches (Fig. 1:33). Fairing of a curve to define the length of steps in a two-step nozzle is unnecessary. The first step turning the flow up 3 deg is arbitrarily constructed with a length BE. At E, the second step turning the flow up an additional 3 deg is constructed.

3. The network of waves will form a number of spaces, each having its individual flow angle and Mach number. It is convenient to label each space according to a coordinate system (a, b) where a denotes the number of degrees of turn produced so far by waves from the upper

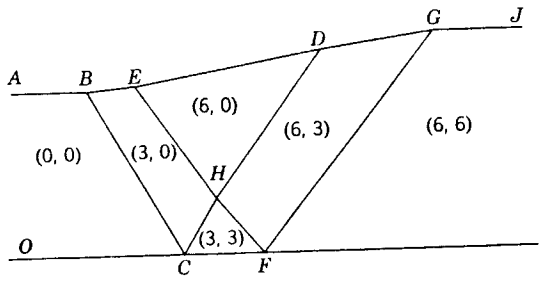


Fig. 1:33 The characteristic network for design of a nozzle with a two step expansion.

surface, and b is the number of degrees of turn produced so far by waves from the lower surface. Since waves from the upper wall turn the flow upward and those from the lower wall turn the flow downward, the local flow angle θ is equal to $a - b$, and the flow is hence horizontal when a is equal to b. The total ν is $(a + b)$ degrees. Our preliminary grid is hence as shown in Fig. 1:33.

4. An examination of the preliminary grid of Fig. 1:33 indicates that we will be concerned with total turning angles ν of 0, 3, 6, 9, and 12 deg. It is convenient to list in tabular form angles of pertinent Mach waves with respect to the horizontal as an aid in determining characteristic lines. It is noted that the inclination with respect to the horizontal of downward-moving Mach waves, δ_d, is the difference between the Mach angle and the upward flow angle, $\alpha_m - \theta$. Similarly, the inclination with respect to the horizontal of upward-moving Mach waves, δ_u, is $\alpha_m + \theta$. Using these two relations together with Table 1:3 allows the following tabulation:

			δ_d for Flow Up		δ_u for Flow Up	
ν	M	α_m	3°	6°	3°	6°
0	1.0000	90.00	—	—	—	—
3	1.1770	58.17	55.17	52.17	61.17	64.17
6	1.2935	50.63	47.63	44.63	53.63	56.63
9	1.4005	45.57	42.57	39.57	48.57	51.57
12	1.5028	41.72	38.72	35.72	44.72	47.72

5. The characteristic line BC is determined by averaging α_m for a zero turn angle with δ_d for a 3-deg turn angle and 3-deg up flow. The angle of BC with respect to the horizontal is thus $(90.00 + 55.17)/2 = 72.58$ deg.

6. The characteristic line EH is determined by averaging δ_d for a 3-deg turn angle and 3-deg up flow with δ_d for a 6-deg turn angle and 6-deg up flow: $(55.17 + 44.63)/2 = 49.90$ deg.

7. The characteristic line CH is determined by averaging δ_u for a 3-deg turn angle and 3-deg up flow with α_m for a 6-deg turn angle (horizontal flow): $(61.17 + 50.63)/2 = 55.90$.

8. The characteristic line HD is determined by averaging δ_u for a 6-deg turn angle and 6- deg up flow with δ_u for a 9-deg turn angle and 3-deg up flow: $(56.63 + 48.57)/2 = 52.60$ deg. Since the flow downstream of HD is 3 deg up, the nozzle contour must turn down 3 deg to that flow direction at D to avoid a reflection of HD from the wall.

9. The characteristic line HF is determined by averaging α_m for a 6-deg turn angle with δ_d for a 9-deg turn angle and 3-deg up flow: $(50.63 + 42.57)/2 = 46.60$ deg.

10. The characteristic line FG is determined by averaging δ_u for a 9-deg turn angle and 3-deg up flow with α_m for a 12-deg turn angle: $(48.57 + 41.72)/2 = 45.14$ deg. Since the flow downstream of FG is horizontal, the nozzle contour must turn down 3 deg to that flow direction at G to avoid a reflection of FG from the wall.

The use of θ_{max} is not obligatory. If DG were not inclined so as to cancel HD, then HD would be reflected and the flow passing through its reflection would be accelerated. Hence the Mach number that could be obtained with $\theta_{max} = 6$ deg, as in Fig. 1:33, could be increased by allowing CD and FG to be reflected and turning the wall where these intersections strike for wave cancellation. This technique is sometimes used for the lower supersonic Mach numbers because the more gradual acceleration has been found to yield more uniform flow. It is almost never used for Mach numbers above about 3. Nozzle length defined by the method of characteristics naturally increases with Mach number. The boundary layer thickness increases with distance at a higher rate as Mach number increases. Thus, the boundary layer growth poses a problem in high Mach number nozzles when the nozzles are short, and the problem becomes more pronounced when nozzle length is increased.

The method just described for defining uniform flow contours can be used for the design for any supersonic Mach number. It is noted, however, that it is not usually used above Mach numbers of 5 to 7, since axially symmetric (three-dimensional) nozzles then become much more practical. This fact may be illustrated by comparing the throat of a two-dimensional Mach 7.0 nozzle with a square test section with the throat of a three-dimensional Mach 7.0 nozzle. For purposes of illustration, let us assume that the two-dimensional nozzle has a 12-by-12-inch test section and the three-dimensional nozzle has a 12-inch diameter test section. From Table 1.1 we find that the test section to throat area ratio for a Mach 7.0 nozzle is 104.1. In the two-dimensional nozzle the throat would have a

12-inch width but would have a height of 12/104.1 = 0.115 inch. In the three-dimensional nozzle the throat would have a diameter of $12/\sqrt{104.1}$ = 1.18 inches. The precision of fabrication of the 1.18-inch diameter is greater than that for the fabrication of the 0.115-by-12-inch slit. Heating of the air becomes necessary at Mach numbers above about 5.0. Maintaining the stability of the slit in the presence of the hot air is much more difficult than maintaining stability of a circular cross section.

In three-dimensional nozzle design, the method of characteristics is also used. However, the method used here requires modification because of the third dimension. The reader is referred to Ref. 1:3 for a description of the three-dimensional method of characteristics. It is noted that this method is much more involved than the two-dimensional method and that no case of a three-dimensional wind tunnel nozzle designed by hand computation is known to the writer. High-speed computers have always been used.

1:9 Nozzle Boundary Layer Treatment

Because air, as well as any real fluid, is viscous, the flow of air over any surface results in the setting up of friction forces between the air and the surface. The result is a loss in velocity and momentum of the air stream as the surface is approached, with zero velocity occurring exactly at the surface. The region in which the loss in velocity and momentum occurs is termed the boundary layer.

Boundary layers have been divided into two general categories, laminar and turbulent. The laminar boundary layer may be described as one in which the flow in the boundary layer is divided into a number of stream tubes and each stream tube slides smoothly over the adjacent one, so that the only transfer of energy is due to a friction developed between stream tubes. There is no transfer of fluid from one stream tube to adjacent stream tubes. The turbulent boundary layer, on the other hand, may be described as one in which each stream tube has a mean velocity in the direction of flow but has imposed upon this, random velocity fluctuations in all directions. The result of these fluctuations is a mixing of fluids in and a transfer of energy between adjacent stream tubes.

Whether the flow in the boundary layer is laminar or turbulent depends primarily on the Reynolds number of the flow. At low Reynolds numbers the boundary layer will normally be laminar. As the Reynolds number is increased the boundary layer will change from laminar to turbulent. The condition of the surface over which the fluid is flowing is also important. If the surface is rough, the change from laminar to turbulent will occur at lower Reynolds numbers than if the surface is smooth. Also, for initial flows having a high degree of turbulence, the change from laminar to turbulent boundary layer will occur at lower Reynolds numbers than for initial flows having lesser degrees of turbulence. In any case, the point at which a change from a laminar to a turbulent layer occurs is termed the "transition point."

The study of flow in boundary layers is one to which an untold number of man years has been devoted and to which justice cannot possibly be done here. Consequently our presentation will be a general discussion of the relation of boundary layer to nozzle design and use. However, reference is made to the work of Schlicting in Ref. 1:4 for the status of boundary layer theory in general.

In a high-speed wind tunnel nozzle, the boundary layer adjacent to the wall of the nozzle is generally limited to a fraction of the distance from the nozzle wall to the nozzle centerline. An illustration of the velocity variation in the boundary layer is given in Fig. 1:34. At the nozzle wall the velocity is zero, and at the edge of the boundary layer the velocity is equal to the freestream velocity. The local velocity approaches the freestream velocity asymptotically as distance from the wall is increased. This makes the exact edge of the boundary layer difficult to define. It is common practice to define the edge of the boundary layer as the point at which the local velocity is 99 per cent of the freestream velocity. The boundary layer displacement thickness δ^* is the parameter most commonly

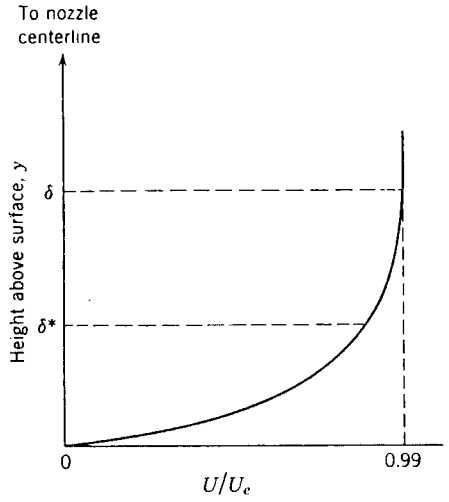


Fig. 1:34 The velocity profile in the boundary layer adjacent to the surface of a nozzle (y = distance from the nozzle surface, U = local velocity, U_e = velocity outside the boundary layer, δ = boundary layer thickness, δ^* = boundary layer displacement thickness).

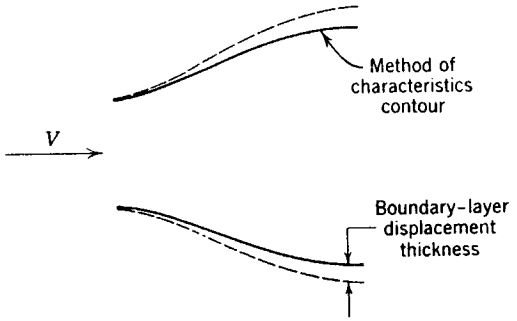


Fig. 1:35 Treatment of theoretical nozzle contours to allow for presence of boundary layer.

used in high-speed wind tunnel nozzle design. This is the amount by which the nozzle wall would have to be shifted out from that defined by the method of characteristics, to account for the boundary layer. It is the value of y that would be required at freestream flow conditions to make up for the deficiency of mass flow in the boundary layer. Displacement thickness is defined mathematically as follows:

$$\rho_e U_e \delta^* = \int_0^\delta (\rho_e U_e - \rho U)\, dy \qquad (1:28)$$

or

$$\delta^* = \int_0^\delta \left(1 - \frac{\rho U}{\rho_e U_e}\right) dy$$

where ρ = density, slugs/ft^3,
U = velocity, ft/sec,
y = distance from wall, ft,
δ = boundary layer thickness, ft.

The subscript e refers to conditions at the edge of the boundary layer.

When the boundary layer displacement thickness is determined, it is added to perfect fluid contours calculated by previously discussed techniques to obtain the ordinates to which the nozzle contours will actually be machined (Fig. 1:35).

Boundary layers in high-speed wind tunnels are usually turbulent. When flow is accelerated from a low speed in the settling chamber to a sonic velocity at the throat of a nozzle the boundary layer in general becomes negligibly thin at the throat. The boundary layer begins to get thicker as distance downstream of the throat and Mach number increase. Since this is the area of major importance with respect to developing uniform supersonic flow, the region between the throat and the test section

is the region in which boundary layer displacement thickness is calculated and resulting corrections are made to the ideal fluid contours.

If the nozzle has rectangular cross sections, as do most nozzles up to a Mach number of about 5.0, it is customary for the side walls of the nozzles to be parallel, with the other two walls generating the contour for developing uniform supersonic flow. In this type of nozzle, the boundary layer builds up on the side walls as well as on the contoured walls. Common practice is first to determine boundary layer thickness on both the sidewalls and the contoured walls, and then to make a correction to the contours adequate to handle the boundary layer flow of both the sidewalls and contoured walls, thus retaining parallel sidewalls. No cases of unusually poor quality flow resulting from the use of this technique have been noted, and it is apparent that nozzle fabrication is considerably simplified by this technique. If the nozzle has circular cross sections, as do most hypersonic nozzles, the displacement thickness is calculated as an increment in radius, which simply results in an increased radius at each station.

No exact method of calculating turbulent boundary layer displacement thicknesses for supersonic nozzles is currently available. Consequently, all calculating methods used to date have involved assumptions or approximations. For a brief summary of some of the methods most commonly used in the past together with a presentation of a more recent method, the reader is referred to the work of Sivells and Payne in Ref. 1:5. Comparisons of the theory of Ref. 1:5 with results of boundary layer surveys in actual tunnels are good.

An empirical method for estimating boundary layer thickness in two-dimensional nozzles with a minimum of calculations is presented in Ref. 1:6. A method for determining inviscid contours and boundary layer displacement thicknesses for axially symmetric nozzles is presented in Ref. 1:7. This reference also includes a high-speed computer program for complete three-dimensional nozzle contour calculations.

1:10 Condensation: The Need for Drying

The amount of moisture that can be held by a cubic foot of air increases with increasing temperature, but is independent of the pressure. Conditions are normally such that moist atmospheric air cooling as it expands isentropically through a wind tunnel may become supercooled (cooled to a temperature below dewpoint temperature). Moisture will then condense out and, if the moisture content is sufficiently high, will appear as a dense fog in the tunnel.

Condensation can result in changes in local Mach number and other flow characteristics such that data taken in a wind tunnel test may be erroneous. The flow changes are, naturally, a function of the amount of

heat released through condensation. They have been given in Ref. 1:8 as

$$\frac{dM^2}{M^2} = \frac{1 + \gamma M^2}{(1 - M^2)}\left[\frac{dQ}{H} - \frac{dA}{A}\right] \tag{1:29}$$

$$\frac{dp}{p} = -\frac{\gamma M^2}{1 - M^2}\left[\frac{dQ}{H} - \frac{dA}{A}\right] \tag{1:30}$$

where M = Mach number,
γ = specific heat ratio,
dQ = heat added through condensation, Btu/lb,
H = enthalpy per unit mass, Btu/lb,
A = duct area, ft^2,
p = static pressure, lb/ft^2.

These equations indicate that at supersonic speeds, the Mach number decreases and the pressure increases with condensation, whereas at subsonic speeds the reverse is true.

It is noted that the presence of water vapor without condensation is of no significance as far as temperature ratio, pressure ratio, and Mach number determined from isentropic relations are concerned. For example, the error in pressure ratio due to 0.003 pound of moisture per pound of dry air (relative humidity of 60 per cent at 40°F) is 0.3 per cent (see Ref. 1:9).

Whether condensation takes place is a function of four parameters: the amount of moisture in the stream, the static temperature of the stream (the air temperature that would be felt by an object moving with the stream as opposed to the total temperature that would be felt by a stationary object which stopped the air stream), the static pressure of the stream, and the time during which the stream is at a low temperature. These four parameters will be discussed in turn.

The amount of moisture that may be contained in normal atmospheric air is illustrated by Fig. 1:36 and usually varies in the range of 0.002 to 0.040 pound per pound of dry air. Many instruments and tables use grains per pound of dry air or grains per cubic foot. (A pound is equivalent to 7000 grains.)

The air temperature that can be reached in a supersonic nozzle is quite low. This is illustrated by assuming air with a total temperature of 100°F and using static to total temperature ratios from Table 1:1 to calculate static temperatures. When this is done we find that the static temperature will be +7°F at Mach 1.0, and −74°F at Mach 1.5, and will go to a low value of −367°F at Mach 5.0. The static temperatures reached during expansion of 100°F air to Mach numbers above 1.5 are considerably below dewpoint temperatures normally found in the atmosphere. Hence

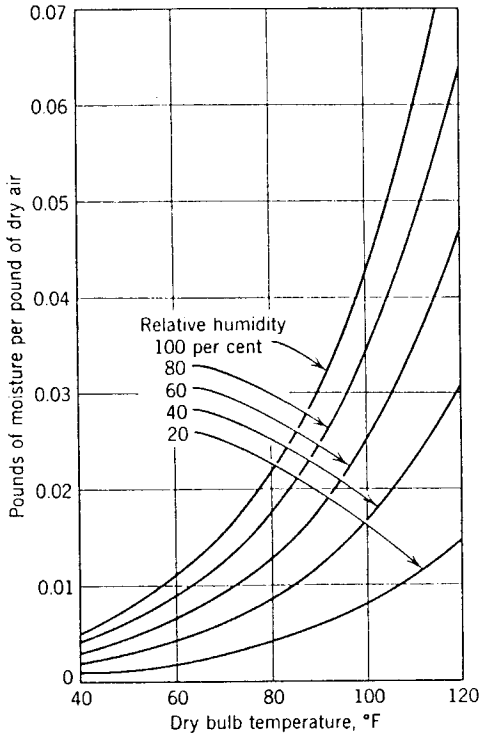


Fig. 1:36 The amount of moisture in atmospheric air at various relative humidities.

we see that the static air temperature in a supersonic tunnel can easily be low enough to condense out normal atmospheric water vapor.

The static pressure in a wind tunnel drops more rapidly with increasing Mach number than does the static temperature. The variation of dewpoint with pressure over a range of conditions is illustrated by Fig. 1:37.

The data of this figure indicate that the dewpoint decreases with decreasing pressure, which would correspond to increasing Mach number. This effect of pressure on dewpoint is desirable from the standpoint of preventing condensation. However, it turns out that the effect of pressure is secondary with regard to condensation of water vapor in supersonic nozzles. This is illustrated by Fig. 1:38, where the change in dewpoint due to the pressure decrease in a typical nozzle expansion is compared with the static temperature decrease.

Many investigators have studied the mechanics of moisture condensation in a supersonic wind tunnel. The work of Oswatich discussed by Lukasiewicz in Ref. 1:10 shows that the condensation of moisture in an airstream is the result of molecules colliding and combining and eventually

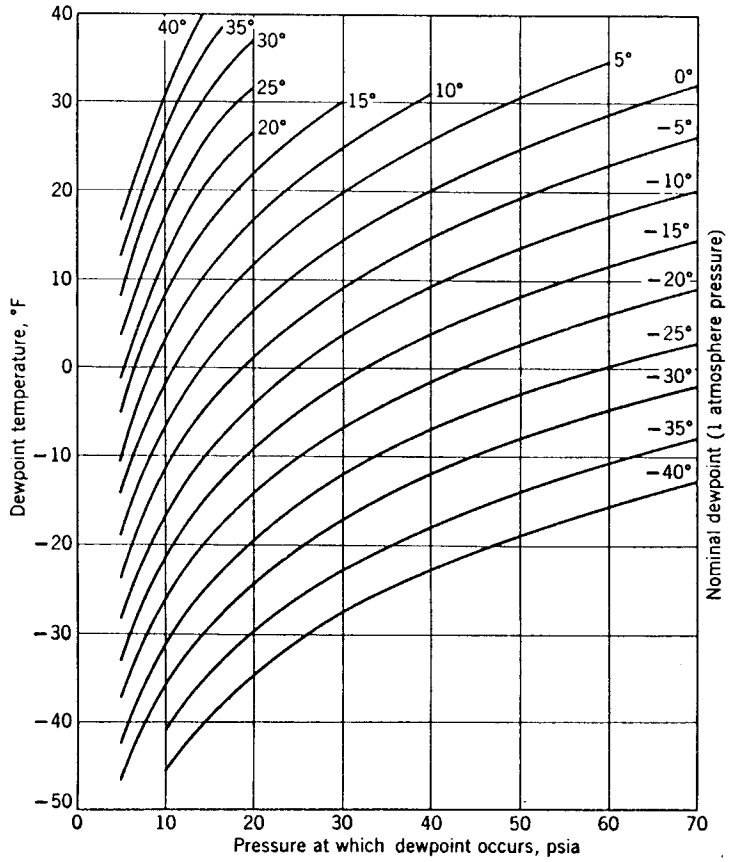


Fig. 1:37 Variation of dewpoint with pressure.

building up into droplet size. The likelihood of condensation in a supersonic tunnel with supercooling (cooling of the air below the dewpoint) of less than 55°F is negligible. Since condensation is a result of a gradual buildup from molecular to droplet size due to molecular collisions, it is obviously a time-dependent process. This has been verified by experiment. In a tunnel with a 1-foot-square test section, condensation has been found to remain low up to 90°F of supercooling. In Ref. 1:11, Lundquist reported 180°F of supercooling for a cooling rate of 460°F per inch. Because condensation is a time-dependent process and more time is required for air to traverse large tunnels than small tunnels designed for the same air speeds, less supercooling is tolerable in large tunnels than in small tunnels.

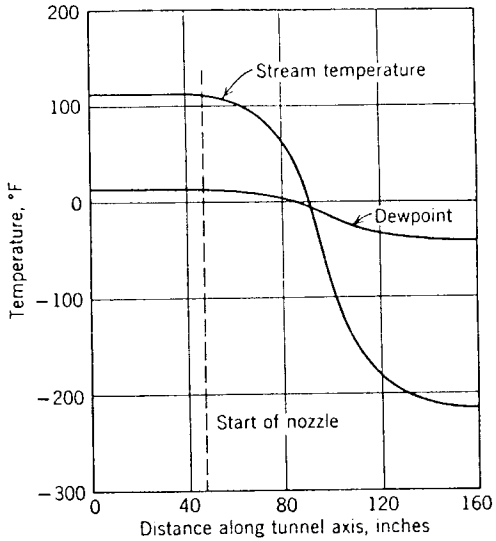


Fig. 1:38 Variation of stream temperature and dewpoint along the axis of a supersonic tunnel. Flow is expanding to $M = 2.56$ from $T_t = 110°F$ and $p_t = 25$ psia. Dewpoint = −1°F at one atmosphere.

There are two approaches to solving the problem of condensation in supersonic tunnels. The first is to heat the air so that upon expansion to the desired Mach number, its static temperature will be above the temperature corresponding to 55°F of supercooling. This approach turns out to be impractical because of the high temperature requirements. For example with a 39°F dewpoint, 55°F of supercooling would correspond to a static air temperature of −16°F. If this occurs at Mach 2.0, the total temperature required would be 340°F. And, of course, the required total temperature would increase very rapidly with increasing Mach number. The second approach is to dry the air, and this is the common procedure. Equipment for drying air to dewpoints in the neighborhood of −50°F is commercially available and not expensive. Although this dewpoint is considerably above static temperatures likely to exist in supersonic tunnels, the reasoning used is that the actual amount of water in the air at this dewpoint is so small that effects on tunnel flow conditions would be negligible even if it did condense.

The dewpoint of air passing through a supersonic wind tunnel is normally monitored by passing samples of supply air through a commercial dewpoint meter at atmospheric pressure. If condensation is suspected, any significant amount of condensation can normally be detected by the simultaneous measurement of three pressures. The total

pressure of the air in the settling chamber p_{t1}, a pitot probe (hollow tube with its open end facing into the air stream) pressure in the test section, and a static pressure in the test section. If condensation has occurred before the air reaches the test section, the air ahead of a pitot probe will be at a total pressure below p_{t1} and will include droplets of water. Upon striking the probe, the air temperature will rise to total temperature, the water droplets will evaporate, and consequently the pitot pressure will rise to p_{t2}, the value it would have been with no condensation. Thus, the ratio p_{t2}/p_{t1} generally shows no significant effect of condensation. On the other hand, a static pressure, such as one measured on the wall of a tunnel test section, is increased by condensation as previously noted. Consequently, inconsistencies between the ratios p_{t2}/p_{t1} and p/p_t from actual measurements and from previously developed flow relations may be an indication of condensation.

1:11 Liquefaction: The Need for Heating

In a manner that parallels the condensation of moisture in an airstream cooled below its saturation point, the components of air finally liquefy when the proper temperature and pressure conditions are met. Wegener (Ref. 1:12) gives the conditions for *static* saturation as

$$\log_{10} p = \frac{-605.4}{T} + 4.114 \qquad (1:31)$$

where p = pressure, atm, and
T = temperature, °R.

Values from eq. (1:31) are plotted in Fig. 1:39, where it is seen that liquefaction troubles might be expected to start around $M = 4.0$ for high-pressure air expanded from room temperature, although somewhat higher Mach numbers may be used without difficulty if the stagnation pressure is lowered. The conditions for static saturation presented in Fig. 1:39 have been used for several years to define design temperatures for hypersonic wind tunnels. Recent work by Daum (Ref. 1:13) has indicated that the required temperatures of Fig. 1:39 are quite conservative for wind tunnel design, particularly at test section pressures below about 4 mm mercury. Figure 1:40 shows a comparison of experimentally determined liquefaction temperatures in wind tunnels with static saturation temperatures through a range of pressures. The data of Fig. 1:40 have been interpreted to indicate, for example, that liquefaction will not occur at Mach numbers to 13 with total pressures of 100 psia and total temperatures above 900°R; at Mach numbers to 16 with total pressures of 400 psia and total temperatures above 1300°R; and at Mach numbers to 17 with total pressures of 1000 psia and total temperatures above 1700°R.

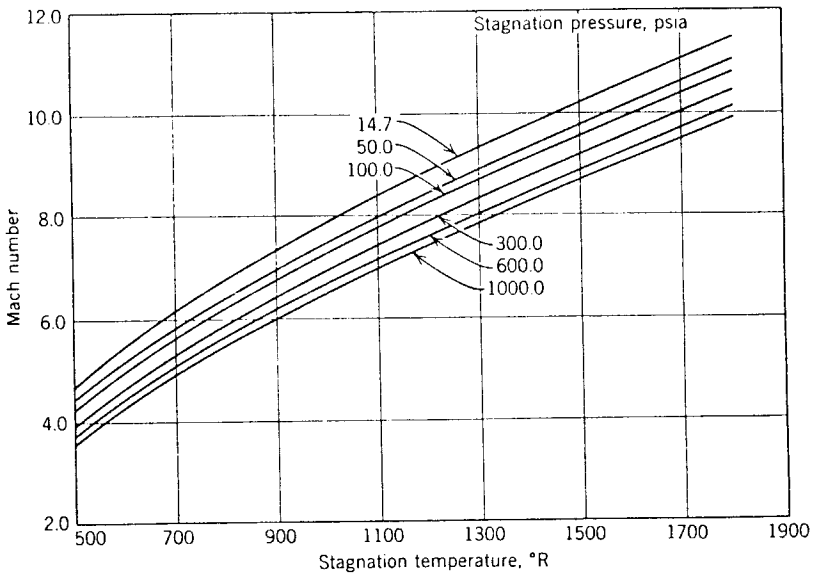


Fig. 1:39 Mach number for theoretical equilibrium condensation of air.

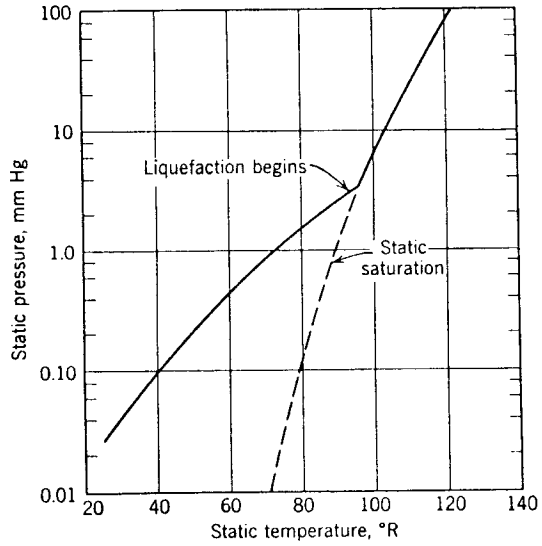


Fig. 1:40 Static pressure and temperature in the test sections of wind tunnel nozzles at beginning of liquefaction from experiment (Ref. 1:13). Liquefaction occurs *above* the solid line.

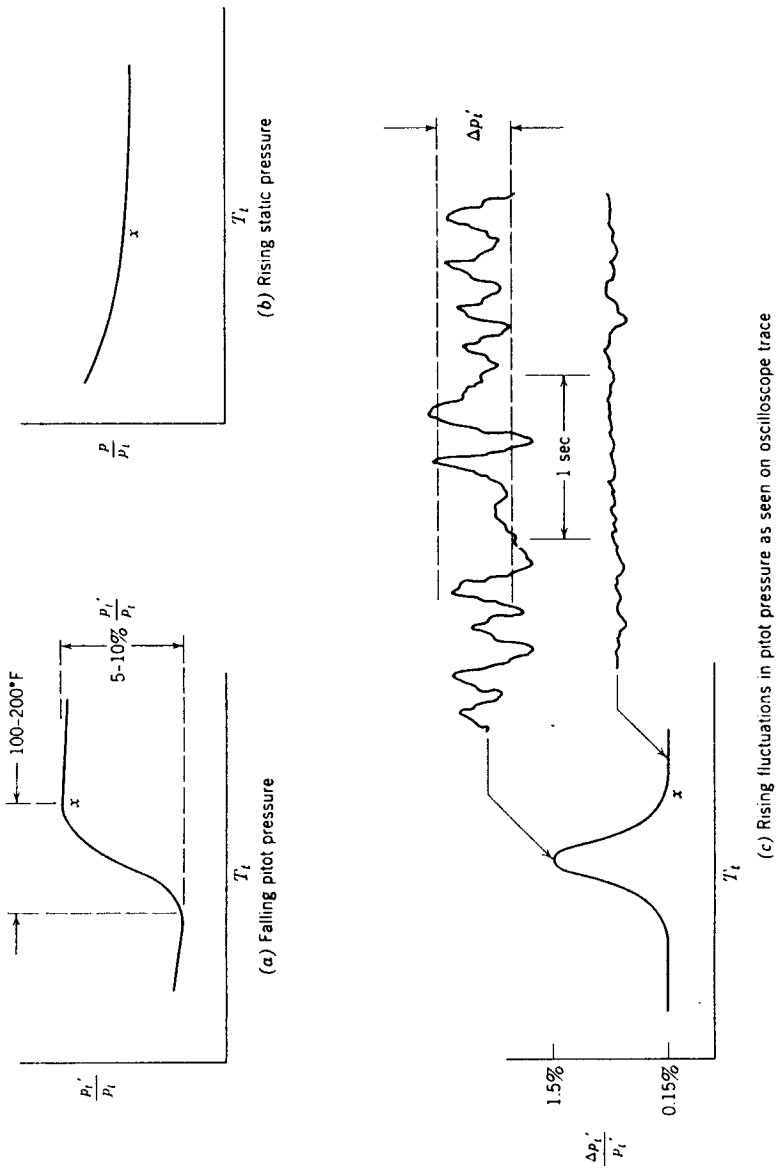


Fig. 1:41 Methods of detecting liquefaction of air in a hypersonic wind tunnel. No liquefaction occurs at temperatures above "x" on curves.

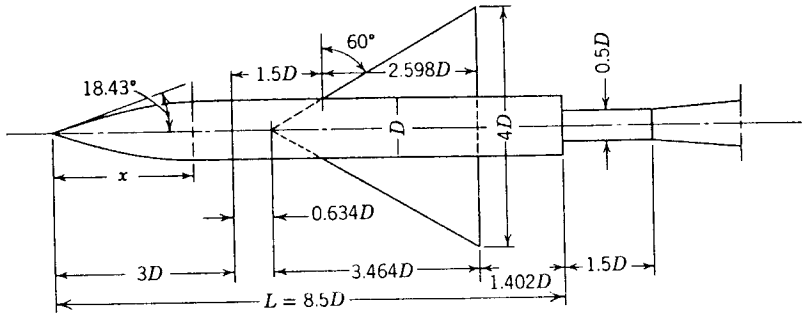


Fig. 1:42 AGARD Calibration Model B. Equation of nose $r = \frac{x}{3}\left[1 - \frac{1}{9}\left(\frac{x}{D}\right)^2 + \frac{1}{54}\left(\frac{x}{D}\right)^3\right]$. Wing profile lenticular 4% thick.

Sample data from measurements that may be made to detect the presence of liquefaction are shown in Fig. 1:41. The procedure followed in obtaining these data was to reduce the tunnel temperature progressively while holding the stagnation pressure constant, and to note (a) when the pitot pressure began to fall, (b) when the static pressure began to rise, or (c) when the fluctuations in pitot pressure began to rise.

The three methods correlate well, although the static-pressure method is least sensitive. The surprising result is that considerable liquefaction has essentially no effect on the normal-force and pitching-moment coefficients* of a typical model (AGARD Model B, Fig. 1:42) if the data are reduced by using the Mach number determined at temperatures high enough to avoid liquefaction. Tests of the model were made encompassing a temperature range from 140°F to 1000°F at $M = 8.0$ and a stagnation pressure of about 350 psia. Only small variations were found.

Although we do not claim that the above data are all-inclusive, it is apparent that some data may be safely taken when liquefaction exists. On the other hand, since doubt exists, it is preferable to avoid liquefaction whenever possible. The operation of existing high-speed tunnels at temperatures low enough to allow liquefaction is the exception rather than the rule. Daum's work indicates that it will be possible to operate at temperatures considerably below those which have for years been accepted as required to avoid liquefaction, particularly if the airstream can be kept free of particles that might act as nuclei for condensation droplets. The significance of being able to run colder without liquefaction lies in the capability of operating at higher Mach numbers at a given maximum air temperature.

* See Section 8:8 for nomenclature definition of coefficients.

1:12 Calibrating a Wind Tunnel

The calibration of a wind tunnel consists of determining the mean values and uniformity of various flow parameters in the region to be used for model testing. The parameters basic to any wind tunnel calibration are stagnation pressure and temperature, velocity or Mach number, and flow angularity. Other flow conditions of interest include static pressure and temperature, turbulence, and the amount of condensation or liquefaction.

Experience over the years has proven that the nozzle to test section flow of air in wind tunnels from the low subsonic to the hypersonic range can be considered isentropic when no shock waves, condensation of water vapor, or liquefaction of air exist. This fact has made the job of the wind tunnel calibrator much easier. If shocks, condensation, and liquefaction are avoided and isentropic flow is thus achieved, the total pressure in the test section is equal to the corresponding value when the air is at rest, a parameter that can be measured with relative ease in the wind tunnel settling chamber. Except for heated tunnels, where convective losses in the settling chamber become severe, the same is true of temperature. Since the ratios of total pressure and temperature to stream quantities are unique functions of Mach number, once settling chamber conditions are known, the calibrator has the choice of measuring any one of the test section parameters in order to define all the others. The existence of this choice is fortunate because by selecting specific parameters in particular speed ranges, one can obtain superior results, as we shall discuss in Chapters 9, 10, and 11. Also no simple, direct method of measuring has been derived for such parameters as velocity, static temperature, and Mach number.

1:13 Desirable Flow Qualities

Desirable flow qualities for a supersonic wind tunnel vary somewhat with both the model to be tested and the type of test. In general, one is justified in requiring higher flow quality in a tunnel to be used for research as compared to one employed only for development, but in either case good flow is essential.

Flow irregularities arise in a supersonic wind tunnel from a poor nozzle contour, from condensation of moisture, from liquefaction of air, or from excessive oil or dust in the airstream. Correction of a poor nozzle contour is difficult but approachable by tracing a bad wave to its source. We have discussed the problems of moisture condensation (Section 1:10) and liquefaction (Section 1:11). No system of measuring either the oil or dust content of the flow has been developed, nor do we have acceptance criteria.

The required accuracy of flow varies with the type of test to be conducted. Morris and Winter (Ref. 1:14) considered an "average" airplane model and devised the following criteria:

1. Errors in drag should be less than 1.0 per cent.
2. Errors in pitching moment should correspond to less than 0.1 degree in tail setting to trim.
3. Errors in center of pressure position should be less than 1.0 per cent wing mean aerodynamic chord.*

The criteria work out as follows:

DRAG. The error in drag is assumed to arise only from the longitudinal pressure gradient (i.e., a "buoyancy" effect). No secondary effects of, say, boundary layer changes due to pressure gradients are considered. It develops that the 1.0 per cent error in drag corresponds to a pressure gradient of 0.002 at $M = 1.4$, and to 0.0005 at $M = 3.0$, the gradient being expressed as the change in p/p_t per model length. The above gradient corresponds to a Mach number gradient of approximately 0.4 per cent of the nominal Mach number per model length.

PITCHING MOMENT. The error in pitching moment arises mostly from changes in flow angle at the tail.

CENTER OF PRESSURE POSITION. A 1 per cent shift in center of pressure position works out to be a gradient of 3 per cent in Mach number per body length.

To meet these criteria the Mach number in the test section must be uniform to about ± 0.2 per cent at $M = 1.4$, and to about ± 0.3 per cent at $M = 3.0$, and the flow direction must be uniform to ± 0.1 deg. Most tunnel engineers accept flow variations of double those stated above because it is difficult to do better.

1:14 Effects of Errors in Measuring

To provide an indication of the relation of Mach number variations to calibration accuracy, perfect gas flow equations have been differentiated with respect to static pressure and pitot pressure, with the following results:

a. The error in determining Mach number obtained by using static pressure and total head is given by

$$\frac{dM}{M} = \frac{1 + [(\gamma - 1)/2]M^2}{\gamma M^2}\left(\frac{dp_{t1}}{p_{t1}} - \frac{dp}{p}\right) \qquad (1:32)$$

* See Section 8:8 for nomenclature definition.

b. The error in determining Mach number obtained by using pitot pressure and total head is given by

$$\frac{dM}{M} = \frac{-(\gamma-1)[M^2 + 2/(\gamma-1)][2\gamma M^2 - (\gamma-1)]}{4\gamma(M^2-1)^2}\left(\frac{dp_{t1}}{p_{t1}} - \frac{dp_{t2}}{p_{t2}}\right) \tag{1:33}$$

c. The error in determining dynamic pressure obtained by using measured total pressure and calibrated Mach number is given by

$$\frac{dq}{q} = \frac{dM}{M}\left[2 - \frac{\gamma M^2}{1 + [(\gamma-1)/2]M^2}\right] + \frac{dp_t}{p_t} \tag{1:34}$$

To carry this tie-in of calibration accuracy to final data accuracy a step further, it would be necessary to consider the absolute accuracy of the pressure-measuring system, that is, to determine what errors are produced by, say, a 0.01-inch error in manometer reading. This step is necessary because of the great difference between the magnitude of static and pitot pressure previously indicated, but is not amenable to general treatment because of the wide range of total pressures used in wind tunnel work. Even this step will not give the complete picture because it ignores the fundamental fact that pitot pressure is much easier to measure than static pressure.

References

1:1 Ames Research Staff, Equations, Tables and Charts for Compressible Flow, *NACA* Report 1135, 1953.

1:2 C. J. Schueler, An Investigation of Model Blockage for Wind Tunnels at Mach Numbers 1.5 to 19.5, AEDC TN 59-165, 1960.

1:3 Antonio Ferri, *Elements of Aerodynamics of Supersonic Flows*, The Macmillan Company, 1949.

1:4 Hermann Schlichting, Boundary Layer Theory, McGraw-Hill Book Company, 1960.

1:5 James C. Sivells and Robert G. Payne, A method of Calculating Boundary Layer Growth at Hypersonic Mach Numbers, AEDC-TR-59-3, ASTIA Document AD-208774, 1959.

1:6 H. Maxwell and J. L. Jacocks, Nondimensional Calculation of Turbulent Boundary Layer Development In Two-Dimensional Nozzles of Supersonic Wind Tunnels, AEDC TN 61-153, 1962.

1:7 Charles B. Johnson, Lillian R. Boney, James C. Ellison, and Wayne D. Erickson, Real Gas Effects on Hypersonic Nozzle Contours With a Method of Calculation, NASA TN C-1622, 1963.

1:8 Paul Chambre and Lin Chia-Chiao, On the Steady Flow of Gas Through a Tube With Heat Exchange or Chemical Reaction, *JAS*, **13** (10), (1946) p. 537.

1:9 Richard M. Head, Investigation of Spontaneous Condensation Phenomena, Ph.D. Thesis, California Institute of Technology, 1949.

1:10 J. Lukasiewicz, Effects of Air Humidity in Supersonic Wind Tunnels, *R & M* 2563, June 1948.

1:11 G. A. Lundquist, Recent Experimental Work at NOL on Condensation in Compressible Flows, Geophysical Research Paper No. 37, ARDC, July 1955.

1:12 P. Wegener, On The Experimental Investigation of Hypersonic Flow, Naval Ordnance Laboratory Report 9629, 1948.

1:13 Fred L. Daum, Air Condensation in a Hypersonic Wind Tunnel, *AIAA Journal*, May 1963.

1:14 D. E. Morris and K. G. Winter, Requirements for Uniformity of Flow in Supersonic Wind Tunnels, RAE TN Aero 2340, 1954.

1:15 Alan Pope, *Aerodynamics of Supersonic Flight*, Pitman Publishing Corporation, 1958, p. 28.

Chapter two

Design of intermittent blowdown tunnels

2:1 General

The basic problems in the design of any high-speed wind tunnel are always those of providing suitable duct work and flow control devices to ensure that air will pass through the test section of the tunnel at the desired flow conditions. Going one step further, we can say that these problems always include those of providing air (1) with enough pressure ratio across the tunnel to achieve the desired flow velocity, (2) with enough mass per second and total mass to meet the tunnel size and run-time requirements, (3) dry enough to avoid condensation, and (4) hot enough to avoid liquefaction.

The ways of solving these problems result in four basic types of wind tunnels: blowdown, indraft, pressure-vacuum, and continuous. The following discussion of tunnel design is divided according to tunnel type in the order listed above, with the discussion of the blowdown tunnel in this chapter. The various types of wind tunnels have many common design problems and in the subsequent discussion of the other types of tunnels, reference is made to the discussion of blowdown tunnels where necessary to avoid repetition.

2:2 Design of Intermittent Blowdown Tunnels

Although some variations in arrangement are possible, the intermittent blowdown tunnel (Fig. 1:2), usually consists of a basic circuit of compressor, air storage tank, stagnation pressure control system, test section, and exhaust. The sizing of components and the selection and matching of components is a large portion of the science of blowdown tunnel design.

Often the design of a blowdown tunnel is greatly influenced by some special condition. For example, some major component (a building, a compressor, or an air storage tank) is already available and must be used for economy, or the tunnel will be used only for a particular type of test

and hence must be optimized for that type of test. Under such conditions, it is probable that the size, operating range, and versatility of the tunnel will be restricted somewhat. However, designing the tunnel is often made somewhat easier because some of the major decisions regarding the design are dictated by the special condition.

In our discussion we shall assume that there are no conditions imposed on the design of the tunnel, except that the desired operating Mach number range is known and there is a limitation on cost. Our discussion will not be completely relevant to the case when some special condition is imposed on the design but will be directly applicable to the most frequent case in which there is a cost for the tunnel that must not be exceeded.

Once a decision to build a tunnel is reached, one of the more important tasks is finding a place to put it. Buildings of some sort are required for every wind tunnel, and these can cost from a sizable fraction of to well over half the total cost of a wind tunnel, depending on the type of building, the amount of equipment that must be sheltered, whether office space is to be provided, the amount of floor space allowed for a work area and for setups, the amount of floor space allowed for controls, the type of equipment and instrumentation, the type and extent of heating and air conditioning, and many other factors common to building design. If the engineer can find a building suitable for his tunnel, he is spared the agonizing experience of seeing a large portion of his money go for buildings instead of tunnel.

2:3 Establishing the Minimum Allowable Operating Pressure

When the Mach numbers at which the tunnel is to operate are known, the minimum pressures at which operation is possible at these Mach numbers are obtained by using Fig. 1:25. Since the blowdown tunnel under discussion exhausts to atmosphere, the tunnel exit pressure is known and the minimum allowable operating pressure is easily determined by using a ratio from the figure. It is strongly suggested that in selecting ratios from Fig. 1:25 for determining minimum operating pressures, one use the top of the band rather than the middle or lower part of the band, or better yet, that one use a figure 25 per cent greater than that at the top of the band. The designers of tunnels whose data fall within the band were striving for operating efficiency, and it is doubtful that the uninitiated can do better. The construction of a tunnel that will not work because of insufficient compression ratio can be extremely embarrassing to the tunnel designer and can require extensive and expensive modifications.

If the design Mach number is below the lower limit of the band in Fig. 1:25, a minimum compression ratio of 2.0 is suggested for design

purposes. The selection of this compression ratio for design purposes instead of some lower ratio will affect the cost of the blowdown tunnel by only a small amount.

Once the minimum pressure to ensure satisfactory operation at the design Mach numbers is established, the tunnel designer may wish to consider higher operating pressures. However, at this point in the design he is in no position to do so because of the many ramifications of operating pressure on the design of components that have not yet been considered.

2:4 Determining the Size of Tunnels

The size of the wind tunnel test section is perhaps the most basic decision the tunnel designer must make with respect to cost. All wind tunnel components must be scaled in proportion to the test section and naturally the larger the test section, the greater the cost of each component and hence of the complete wind tunnel. Within reasonable cost limitations, the tunnel engineer usually wants to get the largest test section possible with the money he has available. Larger test sections make possible larger (and usually more costly) models. Larger models are more easily built in direct proportion to a full-scale aircraft or missile. They allow the installation of more instrumentation such as pressure orifices in the model surfaces, together with associated tubing to vent the individual pressures to measuring instruments outside the tunnel. They are much easier to work on than small models, and this, by the way, is extremely important because the person in wind tunnel work who has the talent and patience of a jeweler in working with very small mechanisms is rare indeed. Reynolds number, which is an important parameter with respect to correlating wind tunnel data of a model with flight characteristics, increases in direct proportion to model size. With all of these reasons for making the tunnel as large as possible, it is appropriate to state that useful and significant work has been accomplished in wind tunnels with test sections as small as 1 inch square.

It is appropriate to state the arguments for the *smallest* usable test section. Actually, for a given air supply and a given run time the largest Reynolds number is obtained by using the *smallest* test section and the highest available stagnation pressure. Except when maximum Reynolds number is the sole criterion, the arguments against extreme smallness given above are overwhelming. Probably, cost of a tunnel decreases with size in spite of designing (in this case) for higher pressure.

The possible options and the possible degrees of sophistication are too numerous to allow determination of the size of a wind tunnel that can be built with a specified amount of money. By contacting other people with wind tunnels of the type he wants to build, the tunnel designer can get a general idea of the size he can afford. This provides a starting point from which he can calculate his complete tunnel installation and come up with an estimated cost. If this estimate is less than he has available, he simply selects a larger test section size and goes through the complete tunnel installation calculations a second time to obtain a second estimated cost. In this manner he will arrive at a tunnel size compatible with the available money. A word of warning is appropriate at this point. The cost estimates should be thorough and carefully obtained because there is much equipment and often many subsystems in addition to the basic tunnel circuit which are required for satisfactory use of the tunnel and which can account for a very substantial portion of the complete tunnel cost.

2:5 Specifying Run Times

Tunnel run time is normally determined from considerations of the type and amount of data required during a given run. In turn, this depends on whether pressure or force tests are to be made. In pressure tests, several pressure orifices are normally installed at various locations in the surface of the wind tunnel model. Connections are made to these orifices with flexible tubes that run to the outside of the tunnel. Outside the tunnel, the tubes are connected to manometers or to some other form of pressure-measuring device from which the pressures are recorded. In this type of test, a significant amount of time is usually required for the pressure at the measuring device to stabilize at the orifice pressure, particularly if the orifice pressure is low. The reason for this is that air has to flow through the tube between the orifice and the measuring device. The tubes are normally quite small (because of model size) and a high resistance to air flow is developed. As the pressures at the orifice and at the measuring device approach each other, the pressure differential for air flow decreases, with the result that the measured pressure approaches the orifice pressure asymptotically. When the orifice pressure is lower than the measured pressure, the stabilization time is greater than when the reverse is true. While the measured pressure is approaching the orifice pressure and less differential is available for flow, the specific volume of air in the measuring device is getting greater and hence an increasing volume of flow is required for stabilization. This effect on stabilization time increases rapidly with pressures below 1 psia. In the blowdown tunnel it would be unwise to depend on pressure stabilization in less than 15 or 20 seconds with a system of the type described. This is an important factor in specifying run-time requirements. Of course, with a large tunnel, a large model, and pressure transducers located very near the orifices within the model a much faster response can be obtained.

In force tests the model is usually attached to a strain gage balance for

measurement of loads. During a test, the model is driven through a range of attitudes with respect to the airstream to obtain a record of forces and moments as a function of α. The time required to do this is, of course, dependent on the drive mechanism, the α range of interest, and the speed of the electronic data system that indicates and records the strain gage signals. However, for this type of test, a minimum run time of 15 seconds is usually required.

Because of the data recording times required for force and pressure tests, and the time for the pressure control valve to provide a stable operating pressure, blowdown wind tunnels are usually designed for minimum run times of 20 to 40 seconds. A run-time requirement of at least 30 seconds at each Mach number is probably reasonable, particularly at this point in the design. Later detailed analyses of data recording instrumentation and techniques and of the α drive mechanism may result in a change in the estimate of run-time requirements.

2:6 Calculating Air Flow Rates

The rate of flow of air through the tunnel is one of the primary considerations in sizing both the tunnel and the associated equipment. It is calculated as follows:

$$\dot{w} = \rho UA \tag{2:1}$$

where $\dot{w}$ = mass flow rate of air, slug/sec,
ρ = mass density of air, slug/ft^3,
U = velocity, ft/sec,
A = duct cross-sectional area, ft^2.

From eq. (1:15) with $\gamma = 1.4$, we get

$$\rho = \rho_t(1 + 0.2M^2)^{-5/2}$$

which, with the equation of state (1:1) becomes

$$\rho = (p_t/R_1T_t)(1 + 0.2M^2)^{-5/2} \tag{2:2}$$

where R_1 = gas constant, 1716 ft^2/sec^2 – °R,
p_t = total pressure, lb/ft^2,
T_t = total temperature, °R.

From eq. (1:16) with $\gamma = 1.4$, we get

$$T = T_t(1 + 0.2M^2)^{-1} \tag{2:3}$$

From eqs. (1:6) and (1:7), we get

$$U = M(1.4R_1T)^{1/2} \tag{2:4}$$

Combining eqs. (2:3) and (2:4), we have

$$U = M[1.4R_1T_t/(1 + 0.2M^2)]^{1/2} \tag{2:5}$$

Eq. (2:1) then becomes

$$\dot{w} = (1.4/R_1T_t)^{1/2}(Mp_tA)/(1 + 0.2M^2)^3$$

$$\dot{w} = 0.02856Mp_tA/[T_t^{1/2}(1 + 0.2M^2)^3] \tag{2:6}$$

If the flow rate being calculated is for a subsonic Mach number, eq. (2:6) is evaluated by using the test section Mach number in conjunction with the total temperature and pressure. If the flow rate being calculated is for a supersonic Mach number, it is usually convenient to make the calculation at the nozzle throat, where Mach number equals 1.0. For this case eq. (2:6) becomes:

$$\dot{w} = 0.01653p_tA^*/T_t^{1/2} \tag{2:7}$$

It is noted that blowdown tunnels invariably operate at an essentially constant pressure during each run. The primary purpose of this mode of operation is to obtain a steady flow while data are being recorded. Thus the total pressures to be used in evaluating eqs. (2:6) and (2:7) are the minimum allowable operating pressures determined as in Section 2:3. The area at the throat of a supersonic tunnel is of course obtained from the test section area, and the ratio of test section area to throat area (A/A^*) from eq. (1:18) or Table 1:1.

2:7 Calculating Run Times

There are two ways in which blowdown wind tunnels are customarily operated: (1), with constant q, and (2), with constant mass flow. For constant q operation, the only control necessary is a pressure regulator that holds the stagnation pressure constant. The stagnation temperature falls according to the polytropic process in the storage tank; $n = 1.4$ for short, high-mass runs, approaching $n = 1.0$ for long runs with thermal mass (open cans, spheres, etc.) in the tank.

For constant-mass runs the stagnation temperature must be held constant and either a heater or a thermal mass external to the tank is required. Since heat energy is added to the pressure energy for constant-mass running, a longer run time is obtained. Even more important, the constant temperature of the constant-mass run keeps the Reynolds number constant. Since a 200°F drop during a run is quite common without heat addition, this is a substantial point.

Assuming, then,

1. polytropic expansion in the storage tank,
2. a heater that keeps the temperature constant,
3. a pressure regulator that keeps the pressure constant,
4. no heat loss in the duct work,
5. isentropic expansion from the settling chamber to the test section, and
6. a *supersonic* tunnel,

we may proceed to compute run time.

The rate of mass flow through the tunnel is given by eq. (2:7). Setting the product of flow rate and run time equal to the change of mass in the tank, we get

$$0.01653 \frac{p_t A^*}{T_t^{1/2}} t = \rho_i V - \rho_f V$$

or

$$t = 60.5 \frac{T_t^{1/2} \rho_i}{p_t} \frac{V}{A^*} \left[1 - \frac{\rho_f}{\rho_i}\right]$$

where

t = run time, sec,

V = storage tank volume, ft^3,

and subscript i denotes initial conditions in the tank, and f denotes final conditions in the tank.

For a polytropic expansion of air in the tank

$$\frac{\rho_f}{\rho_i} = \left[\frac{p_f}{p_i}\right]^{1/n}.$$

The equation of state (1:1) yields $\rho_i = p_i/R_1 T_i$. The run time is then

$$t = 0.0353 \frac{V}{A^*} \frac{\sqrt{T_t}}{T_i} \frac{p_i}{p_t} \left\{1 - \left[\frac{p_f}{p_i}\right]^{1/n}\right\} \qquad (2:8)$$

Eq. (2:8) gives the run time for the general case of blowing down a tank under constant-mass-per-second conditions.

The maximum run time obviously occurs when p_f is a minimum. Note that the run does not continue until the tank pressure drops to the stagnation pressure p_t, but rather stops when the pressure reaches some higher value $p_f = p_t + \Delta p$, where Δp denotes the losses in the duct work and in the regulator. The value of Δp varies from about $0.1p_t$ for very-small-mass runs (hypersonic tunnels) to somewhere around $1.0p_t$ for high-mass runs.

Values for eq. (2:8) in parametric form have been plotted in Fig. 2:1 for the range of n. The proper value of n itself is a function of the rate at

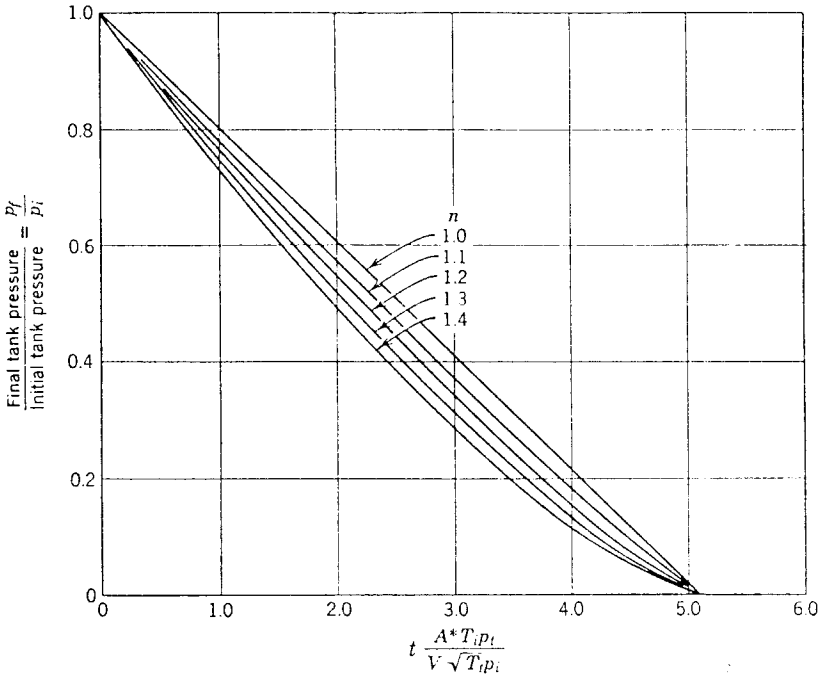


Fig. 2:1 Run time for blowdown tunnel; constant mass operation, $\gamma = 1.4$.

which the air is used, the total amount used, and the shape of the storage tank. From preliminary data is appears that n may be estimated from Fig. 2:2 for cylindrical tanks for which $l/d = 3.0$. The value of n for more spherical tanks tends more toward 1.4, and with heat storage material in the tank it approaches isothermal ($n = 1$). Equation (2:8) may also be used with good accuracy for constant-pressure runs in which the change in

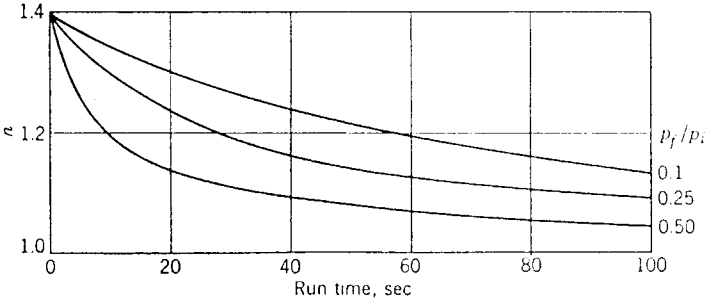


Fig. 2:2 Very approximate chart for estimating polytropic exponent n of expansion process in cylindrical pressure storage tank, length/diameter = 3.0.

total temperature is small, since these approach the constant-mass-rate condition.

Example 2:1 Compute the run time for a blowdown wind tunnel with the following specifications: $M = 2.5$, test section 12 by 12 inches, air storage 2600 ft^3 at 300 psig and 100°F. The storage tank has heat sink material in it.

1. From Fig. 1:25, a sufficient starting pressure ratio for $M = 2.5$ is 3.3, A satisfactory p_t will be $3.3 \times 14.7 = 48.5$ psia.
2. A reasonable duct and regulator valve pressure loss for $M = 2.5$ could be 50 per cent, yielding $p_t = (1.5)(48.5) = 72.8$ psia.
3. From eq. (1:18), the area ratio for $M = 2.5$ is 2.637.

Substituting in eq. (2:1), we have

$$t = \frac{(0.0353)(2600)(\sqrt{560})(314.7)}{(12 \times 12/144)(1/2.637)(560)(48.5)}\left[1 - \left(\frac{78.5}{314.5}\right)^{1/1.0}\right]$$

$$= 49.8 \text{ sec}$$

2:8 Specifying the Frequency of Runs

After calculating the air flow rates and specifying tunnel run times, we can readily calculate the amount of air to be used during a run at each design Mach number. This does not give us all the information we need for determining the size of the air supply system, however, unless it is correlated with the required run frequency. The specification of the frequency of runs is an item with numerous ramifications.

For example, if the blowdown tunnel is transonic (high subsonic and low supersonic speeds), changes in Mach number usually require only changes in operating pressure because one nozzle is normally used for this speed range. These changes require only changes in pressure regulator valve adjustment. Consequently, essentially no time is required for changes between runs. With this sort of operation there are two extreme possibilities regarding the air supply compressors and storage tanks. One possibility is to make the compressors and storage tanks of such a size that it would take 24 hours for the compressors to fill the air storage tanks, and when the tanks were full the air stored would be adequate to make perhaps a dozen runs during a one-hour period. With this arrangement the tunnel operating personnel would be busy with the test during the first hour of the day, would get the model changed and ready for the next series of runs in perhaps half an hour, and would be free for other work during a large part of the day. The other extreme possibility would be to make the compressors and storage tanks of such a size that the storage tanks would be essentially emptied during one run and it would take 20 or 30 minutes to refill the tanks. With this arrangement, there would be considerable time during which operating personnel would be idle but runs could be made at any time during the day.

If the blowdown tunnel is supersonic instead of transonic, a change in a model or a change in the wind tunnel nozzle is required between runs (except for occasional Reynolds number studies). Generally, a series of runs is made at one Mach number, and then the series of runs is repeated at the next Mach number. With this type of operation the time required for changing a model and getting set up for the next run is usually about 20 minutes. The time to change from one Mach number to the next typically varies from 5 minutes or less to more than an hour, depending on the design of the nozzle assembly for changing Mach number. To obtain the maximum utilization of a facility of this type and to have continuous operations chores for operating personnel, the compressors and air storage tanks should be of such a size that the pressure tanks will be pumped up and ready for the next run in about 20 minutes following a run. This is the reasoning usually followed by wind tunnel designers. However, it is not particularly recommended because each designer should have a good knowledge of the type of tunnel operation he is trying to get and should design accordingly.

2:9 Compressors and Pumping Time

There are various types of compressors that could be used for pumping up the storage tanks of a blowdown wind tunnel, but by far the most frequently used type is the piston compressor, the reasons generally being economy and commercial availablity in many sizes. Piston compressors can be obtained with one stage of compression for providing up to about 150 psia of discharge pressure, with two stages of compression for providing up to about 500 psia of discharge pressure, and with a third stage of compression for providing still higher pressure. For a given pumping capacity there is a marked difference between the cost of a single-stage and that of a double-stage compressor, as might be expected.

After calculating the minimum allowable operating pressure for each Mach number at which the tunnel is to be operated, the tunnel designer can look at the required operating pressure for the highest Mach number and usually can tell quickly whether he is going to require a single-stage or a double-stage compressor. The air storage pressure, and consequently the discharge pressure of the compressor, must of course be greater than the maximum tunnel operating pressure if the pressure control system is to work satisfactorily. The margin may be as small as 20 per cent, or possibly less, depending on the characteristics of the control system and the size of the air storage tank relative to the mass flow of the tunnel. A

tunnel designer would consider margins of this magnitude only if his minimum required operating pressures were on the verge of crossing over from a single- to a considerably more expensive double-stage compressor, and then only if the mass flow at the highest operating pressure were small compared to the maximum tunnel design mass flow. The latter is frequently the case when the tunnel is designed to cover a large range of Mach numbers. For low Mach numbers the pressures required for operation are low but the nozzle throat is large. As Mach number increases, the pressure required for operation increases but the nozzle throat decreases in area at a more rapid rate, with the result that the mass flow requirements are generally lowest at the highest Mach numbers.

In compressors a great deal of heat is added to air by the compression process. Because of this, cooling water is normally required to keep the temperature of the working parts of any sizable compressor at an acceptably low level. In multistage compressors, cooling water is also used between stages in order to take away the heat added by one stage of compression before the air enters the next stage. This is called "intercooling." If cooling water requirements are large, a cooling tower may be required along with associated piping, valving, and pumps in order to reuse rather than waste the cooling water. If the compressor is of significant size, several safety features are usually incorporated. Controls are provided to shut down the compressor if the cooling water stops flowing, if the lubricating oil level gets too low, or if the discharge pressure gets too high. It is usually desirable, also, to provide controls which will shut the compressor down when the storage tank reaches its design pressure and which will start the compressor back up when the tank pressure falls below some limit. In addition to the above "accessories" for a compressor, a motor control center is usually required for switching the large amounts of electrical power required in turning the compressor on and off. All of these extras must be taken into account in arriving at a reasonable cost estimate because they may represent a very significant portion of the compressor cost.

Small amounts of oil in high-pressure circuits present a considerable safety hazard, and several serious air–oil explosions have occurred in wind tunnel systems. Because of this hazard, it is important in wind tunnel design to minimize the oil entering the high-pressure system. The first step in doing this can be taken at the compressor. Compression cylinder piston rings of compressors are usually steel and require oil lubrication. With this arrangement the probability that some oil will get into the high-pressure circuit is high. However, at a very nominal cost the steel rings can be replaced by carbon or teflon rings, which do not require oil lubrication.

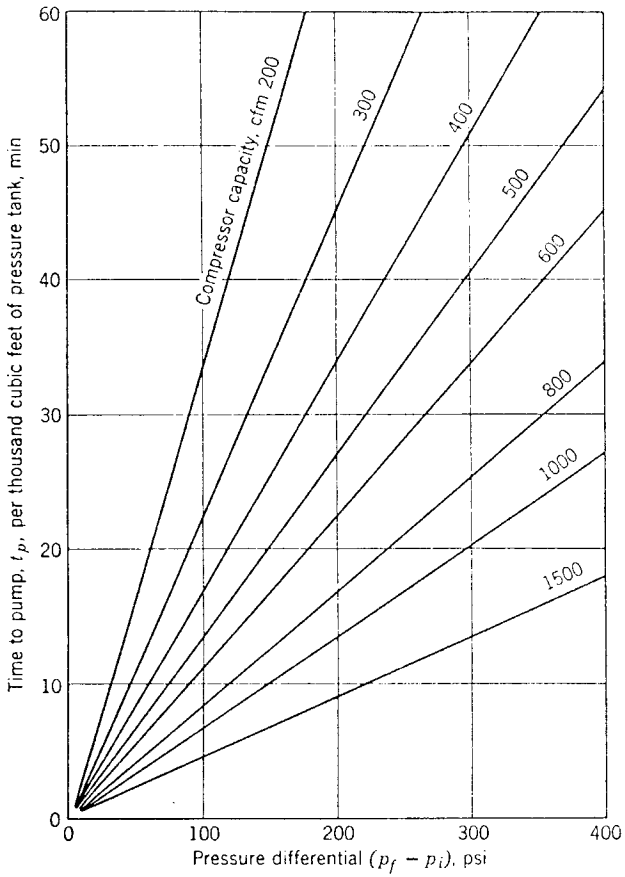


Fig. 2:3 Time to pump; standard sea level air.

The primary disadvantage of this substitution is that the carbon or teflon rings must be replaced more frequently than the steel rings. Carbon rings are normally expected to wear about 0.003 inch per year of 8-hour day operation, and in this case would have to be replaced after about 5 years. The newer teflon rings in some installations might have to be replaced as frequently as every 600 hours of compressor operation.

Compressors are rated at a specific number of cubic feet of sea level air per minute. The time to pump a tank from an initial pressure of p_i to a final pressure p_f may be found from

$$t_p = \frac{V_p}{14.7Q}(p_f - p_i) \tag{2:9}$$

where t_p = pump time, min,
Q = compressor rating (cfm at sea level),
p_f = final pressure, psia,
p_i = initial pressure, psia,
V_p = volume of pressure tank, ft³.

In practice p_f corresponds to the run start pressure, and p_i to the run end pressure. For computing pump times at altitude, the sea level constant of 14.7 in eq. (2:9) should be replaced with the corresponding atmospheric static pressure. Times required to pump each 1000 cubic feet of air storage tank are shown in Fig. 2:3.

Example 2:2 Compute the pump time to fill a 2600 ft³ tank from 14.7 psia to 300 psia using a compressor rated at 300 cfm.

$$t_p = \frac{2600}{(14.7)(300)}(300 - 14.7)$$
$$= 168 \text{ minutes.}$$

The number of cubic feet of inlet air pumped each minute (Q) is simply converted to pounds per minute by using the equation of state (1:1):

$$\dot{w}_c = \frac{gQp_0}{R_1T_0} \tag{2:10}$$

where $\dot{w}_c$ = rating of compressor, lb/min,
g = acceleration of gravity, 32.174 ft/sec²,
p_o = air pressure at compressor inlet, lb/ft²,
R_1 = gas constant, 1716 ft²/sec²-°R,
T_o = air temperature at compressor inlet, °R.

Using eq. (2:10) together with the mass flow through the tunnel from eq. (2:7), we can easily derive the relation of pumping time to running time:

$$\dot{w} \cdot t_r = \dot{w}_c \cdot t_p/g \tag{2:11}$$

where t_r = tunnel run time, sec. If the tunnel is to be designed so that following a maximum flow run the storage tanks will be back up to pressure and ready for the next run in some specified time, eqs. (2:10) and (2:11) can be combined to define the compressor capacity:

$$Q = \dot{w}\frac{R_1T_0}{p_0}\frac{t_r}{t_p} \tag{2:12}$$

For very small and simple blowdown wind tunnels, an ordinary "filling station" air compressor may be used. These compressors are usually air cooled and very economical to purchase and maintain. As they wear

they do put a lot of oil into the air which must be removed to eliminate the possibility of an air–oil explosion.

2:10 Aftercoolers

An aftercooler is usually provided to remove the heat of compression of air leaving the compressor. The aftercooler is a very simple device in which the hot air from the compressor is allowed to flow at low velocity through or over water-cooled tubes or pipes. A typical aftercooler consists of a straight section of large pipe, perhaps 25 to 50 diameters long, with several small pipes passing through the inside. The small pipes are manifolded together at each end and provide an air flow passage. The cooling water enters at the air-exit end of the large pipe, flows through the large pipe and over the small pipes that carry the air, and leaves at

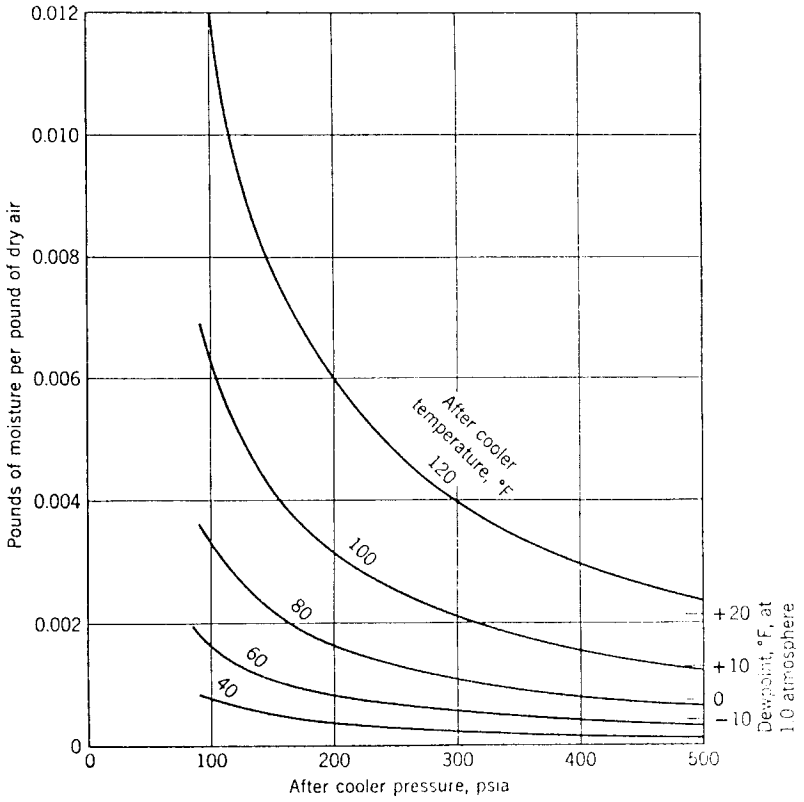


Fig. 2:4 Maximum amount of moisture remaining in atmospheric air after compression and cooling to indicated temperature (low pressure range).

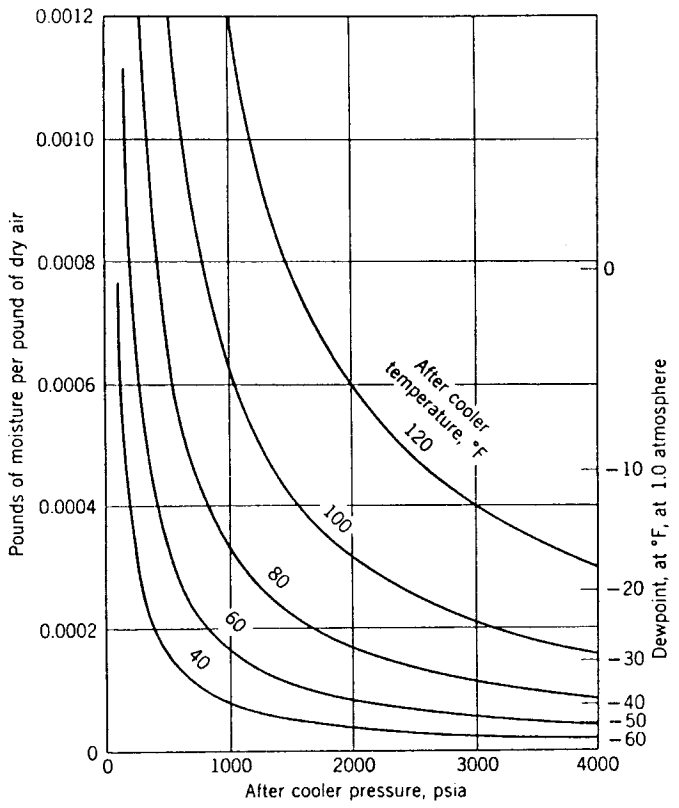


Fig. 2:5 Maximum amount of moisture remaining in atmospheric air after compression and cooling to indicated temperature (high pressure range).

the air-inlet end of the large pipe. The cooling water for the aftercooler would typically come from the circuit that supplies cooling water to the compressor.

Cooling the air immediately after it leaves the compressors serves several purposes. It reduces the temperature to a point where the oil filter and the air drier (Sections 2:11 and 2:12) can be effective. It reduces the temperature of piping, valves, and other components between the compressor and the air storage tank to a point where there is no danger of burns to personnel. It eases the requirements on valves to the point where regular commercial valves rather than high-temperature valves may be used. It reduces the volumetric flow rate and thus the size of oil filters and air driers between the compressor and the storage tank. It also reduces the moisture content of the air, as illustrated by Figs. 2:4 and 2:5. If saturated atmospheric air at 70°F is compressed to 10 atmospheres and

cooled back to 70°F, 90 per cent of the water will be condensed out. If the air is compressed to 3000 to 4000 psia and cooled, the moisture vapor content of the air will probably be reduced to levels satisfactory for high-speed tunnels without further drying. For more typical pressures, a drier will be required. In any event, a moisture separator to collect water and from which water may be drained should be installed downstream of the aftercooler.

2:11 Oil Filters

Oil filters are needed in most systems for the very obvious purpose of keeping oil with which the air comes in contact out of the system. The most important reason for keeping oil out of the compressed air systems is the danger of air–oil explosions. Other reasons are that oil passing through the air drier will rapidly reduce its effectiveness, and that oil may collect on windows of the nozzle test section and cause a deterioration of the quality of photographs.

Basically, the oil filter is a mechanical device that provides a great area upon which the oil vapor can condense. A sketch of an oil filter of the type often used in blowdown tunnels is shown in Fig. 2:6. In such a filter the air is forced to pass through a bed of desiccant (drying agent) in the form of granules. The granular form of the desiccant provides a large surface area on which oil vapor can condense. The desiccant used in the oil filter will usually be the same as that in the air drier for convenience of facility operation. If a large filter settling chamber is provided, one pound of alumina can clean 3000 pounds of air.

Usually, a commercial oil filter will be used rather than a homemade one for the simple reason that it is more economical when design time is considered. The filter is, of course, sized according to the air flow from the compressor. The desiccant in the filter will have to be removed and cleaned with an oil solvent or replaced periodically because it will lose its effectiveness when the surface of the granules becomes covered with oil. This operation may be necessary every few weeks or only after several months, depending on the amount of oil in the air leaving the compressors.

An oil filter of the type shown in Fig. 2:6 will serve as an effective moisture separator for collecting the water droplets condensed out by the aftercooler. Water will naturally collect in the cavity at the bottom of the filter and can be drained off.

2:12 Air Driers

Air driers for blowdown wind tunnels are usually "high-pressure" driers that operate somewhere between the maximum air storage tank pressure and the maximum compressor discharge pressure. Among the reasons for

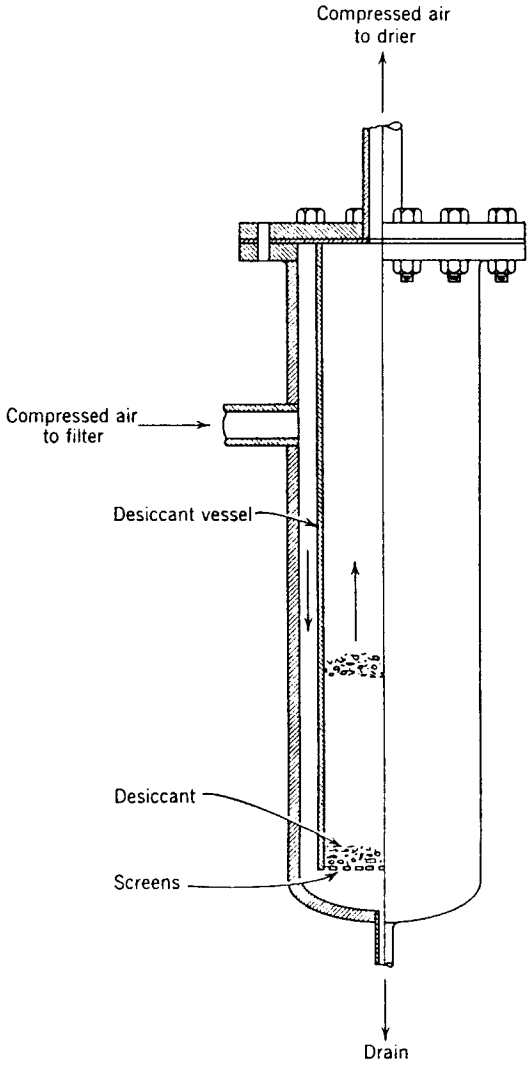


Fig. 2:6 Schematic drawing of oil filter.

the operation of the drier at high pressure are that the size and consequently the cost of the drier are reduced because the volumetric flow of air through the drier is less, and that the desiccant normally used in blowdown tunnel driers will hold more water at higher pressure. Of the various possible methods for drying, the method usually used in blowdown wind tunnels is the adsorption method in which moisture is collected in condensed form on the surfaces of a desiccant. The desiccant used in

blowdown wind tunnel driers is almost always either silica gel, activated alumina, or zirconia. These desiccants are in the form of granules having an extremely porous structure. Moisture condensing on the outer surfaces of the granules is drawn into the pores of the granules by capillary action. The moisture trapped by the desiccant is removed in a "reactivation" cycle in which the granules are simply heated to temperatures about 100°F above the boiling temperature of water.

The action of the desiccant is purely physical, no change in the size, shape, or appearance of the granules being noted as they become saturated. The granules adsorb water vapor until the pores are filled to a point where the internal pressure of the adsorbed fluid in the pores at a given temperature approaches as a limit the partial pressure of the vapor in the surrounding atmosphere at the same temperature.

When moisture is adsorbed by the desiccant, heat is liberated equivalent to the latent heat of evaporation of the adsorbed liquid plus an additional amount of heat known as the heat of wetting, the sum of the two being known as the heat of adsorption. This heat is dissipated into the adsorbent, its container, and the dried air. The temperature rise in the dried air in a typical installation amounts to 10°F for each grain of moisture removed per cubic foot of air at atmospheric pressure. In a typical system this amounts to a temperature rise of from 15 to 30°F during one drying cycle. While some tunnel engineers use silica gel, it is believed that most use activated alumina unless the higher temperature capacity of zirconia is required. The gel loses some of its drying capacity above 70°F, whereas the alumina, while less efficient than at lower temperatures can still dry to a dew point of −90°F while it is at 100°F. Alumina is also less susceptible to powdering. A comparison of pertinent characteristics of activated alumina and silica gel is given below.

	Activated alumina	*Silica gel*
Suggested moisture capacity, pounds of water per pound of desiccant	0.02	0.03
Suggested temperature for reactivation	275°F	325°F
Maximum temperature without damage	600°F	400°F
Specific heat, Btu/lb-°F	0.21	0.22
Density for typical granule size, lb/ft^3	50	40
Cost in small quantities, per pound	$0.20	$0.40

The capacity of a drier may be determined when the following are specified: (*a*) the desired dewpoint of the tunnel air, (*b*) the total amount of air to be passed through the drier between reactivation cycles, and (*c*) the amount of moisture in the air entering the drier.

The dewpoint required for condensation-free flow has been discussed in Section 1:10 and is readily obtained as a function of the maximum Mach number of the facility. It is sometimes suggested that regardless of the dewpoint required for condensation-free flow, the drier should be designed for a dewpoint of −40°F. This is easily and cheaply accomplished and provides air suitable for higher Mach numbers in the event that the operating Mach number range of the facility is increased in the future.

The total amount of air to be passed through the driers between reactivation cycles is, of course, dependent on the rate at which air is passed through the driers and the time between reactivation cycles. The rate at which air is passed through the drier depends only on the pumping capacity of the compressor, since all air leaving the compressor passes through the drier. The time between reactivation cycles is defined by the type of facility operation desired. If the facility is designed so that the compressors will operate 8 hours a day and be idle the remaining 16 hours, a drying cycle of at least 8 hours would be required, and the design would provide for reactivation during the idle hours. As in all components, a margin for trouble should be included in drier design, and in the above type of operation it would be reasonable to design the drier for 16 hours between reactivation cycles. In the event that the reactivation cycle fails one night, it would still be possible to run the next day. A more versatile drier system is obtained by using "twin tower" driers, which are simply two driers arranged so that one drier is always being reactivated while the other drier is being used. With "twin tower" driers the operating cycle is defined by the time required for reactivation.

As previously stated, the amount of moisture in the air leaving the aftercooler is essentially independent of the conditions of the air entering the compressor. If all the water condensed out of the air by the aftercooler is trapped, then the moisture content of the air entering the drier is dependent only on the pressure to which the air is compressed and the temperature to which it is cooled by the aftercooler (Figs. 2:4 and 2:5).

As an example of moisture-handling calculations, let us take a 500-cfm, 300-psia compressor handling atmospheric air at 80°F and 80 per cent relative humidity with an 8-hour cycle between reactivations and with an 80°F aftercooler. The atmospheric density is 0.075 lb/ft³, so that the air handled is 500 × 0.075 × 8 × 60 = 18,000 lb. From Fig. 1:36 we find the

moisture content of the atmospheric air to be 0.0176 lb per pound of dry air, so that the total moisture entering the compressor during a cycle is 0.0176 × 18,000 = 317 lb. This amount of water is not pertinent to the drier design but is an interesting figure to compare with the moisture handled by the drier. Following aftercooling the water vapor content of the air is 0.0011 lb per pound of dry air (Fig. 2:4), which yields a total of 0.0011 × 18,000 = 20 pounds of water entering the drier. If the air leaves the drier at −40°F dewpoint, the moisture content is less than 10 per cent of that entering the drier, so that the drier must collect about 20 lb of water during the cycle. For this 20 lb of water to be collected by the drier, it would be reasonable to provide 700 lb of silica gel (3 per cent moisture content) or 1000 lb of activated alumina (2 per cent moisture content) or, more typically, a commercial drier with a 20-lb water capacity at −40°F dewpoint. If the −40°F dewpoint is considerably below that for condensation-free flow at the highest tunnel Mach number, the above drier capacity is quite adequate because the drier capacity is increased as the dewpoint goes up. At a −20°F dewpoint the drier can hold about three times as much moisture as a dewpoint of −40°F.

Ordinarily, the blowdown tunnel engineer is not called upon to design an air drier system. Instead he gives a commercial drier supplier information

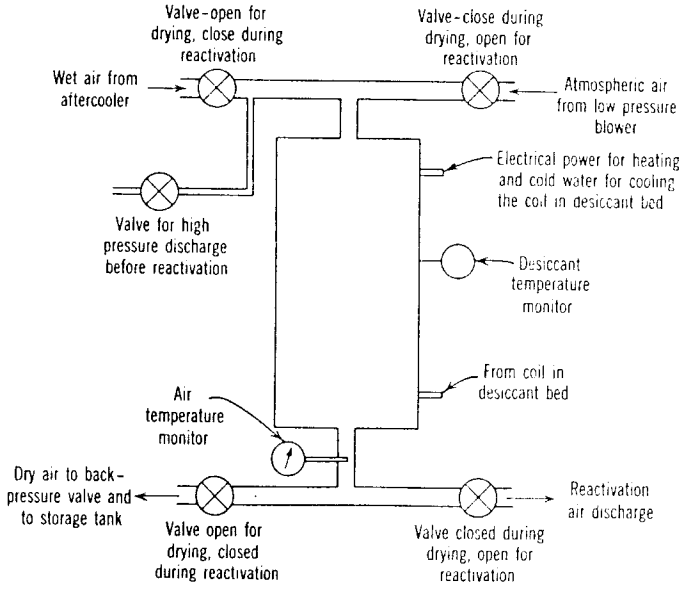


Fig. 2:7 Schematic drawing of typical high pressure drier system.

pertinent to the compressor, the aftercooler, and the drier use and reactivation cycles, and lets the supplier recommend a system.

A schematic drawing of a typical drier system is presented in Fig. 2:7. When it becomes time to reactivate the drier, the two valves that are open for drying air are closed, trapping pressure in the drier bed. This pressure is released slowly through a small valve exhausting to the outside of the building because rapid exhaust through a large valve could damage the desiccant bed or the grate and screen supporting the desiccant. When the pressure has been released, the two reactivation air valves are opened and a small blower turned on to circulate room air through the bed to carry out moisture that will be released during the reactivation. This air is usually exhausted outside the building. At the same time, a low-voltage electrical power is supplied to coils of copper tubing embedded in the desiccant. Over an extended period of time, electrical heating of the copper coils will raise the temperature of the desiccant to a temperature that will cause it to give up all its water and the air circulating through the bed will carry this water out. When the proper reactivation temperature is reached, the electrical power to the coils is turned off, the reactivation air blower is turned off, and cooling water is circulated through the coils embedded in the desiccant. This gradually removes the heat stored in the bed, and when the bed temperature is reduced to the neighborhood of 100°F, the reactivation cycle is complete and the bed is again ready for use.

The major deviations of existing drier systems from the schematic are usually in the method of heating the desiccant during the reactivation cycle. This may be accomplished by passing steam through the coils or by passing hot products of combustion directly through the bed.

Driers are usually designed for an automatic reactivation cycle because it is not practical from an economic standpoint to provide a person to monitor each reactivation cycle. A reactivation cycle can usually be set up on a time basis, so that each step in the reactivation process takes place at a specified time relative to starting time. When this is done there are several interlocks required to prevent drier damage in the event that something does not work properly. For example, the large reactivation valves must not be allowed to open until the pressure has been released through the small valve, and electrical power for heating coils must be turned off if the desiccant temperature or the reactivation air discharge temperature exceeds prescribed values.

Like any type of mechanical apparatus, driers have their difficulties. In most cases troubles may be located rapidly and corrected easily. Some typical troubles and their causes and corrections are outlined on the facing page.

Difficulty	*Possible Causes and Corrections*
Dust passing through the tunnel	1. Too rapid blowoff of drier pressure causing tumbling and rubbing of desiccant. Reduce size of blowoff line or add a constriction. 2. Pulsing from compressor is tumbling desiccant. Add a length of pipe for acoustic damping.
Poor dewpoints at all times	1. Aftercooler not working and air entering drier too hot or too wet. Repair aftercooler. 2. Improper reactivation. Check reactivation cycle. 3. Oil filter full of water and excessively moist air entering drier. Drain oil filter. 4. Desiccant covered with oil. Clean or replace desiccant.

Besides the heat-regenerated driers described above, there is a new type of drier now available that regenerates without any heat. It uses two towers and is arranged so that part of the air dried at high pressure in one tower is expanded (and made still drier) and bled through the second tower to regenerate it. A switching circuit sends the air from tower to tower in 2- to 4-minute cycles. A greatly reduced maximum electric load, less wear on the drier material, and less maintenance are advantages claimed for the new type of heatless drier.

2:13 Back-Pressure Valves

In Section 2:12 it was noted that air driers are almost always operated at high pressure. Since air leaving the drier is discharged into the air storage tank, which will always be below design pressure when the drier is being used, some means is required to maintain a high pressure in the drier. This is accomplished by a "back-pressure valve" between the drier and the air storage tank which is automatically adjusting to maintain a specified pressure in the drier regardless of the pressure in the air storage tank. The valve is, of course, designed to be compatible in size with the compressor capacity and pressure and is obtained commercially.

2:14 Air Storage Tanks

The major aspects of deciding on the size of the air storage tanks are covered in Sections 2:5 to 2:8. It is sufficient to say at this point that their size is dependent primarily on mass flows during a wind tunnel run and the frequency of runs desired.

Since a pressure regulator is used to reduce storage tank pressure to tunnel stagnation pressure, a choice will exist with respect to storage pressure selection if the available compressor discharge pressure is significantly

above the maximum tunnel stagnation pressure. It turns out that the cost of storing a given number of pounds of air is about the same no matter what the pressure, the higher pressures requiring smaller but stronger tanks. High pressure offers a margin of safety on compression ratio for starting the tunnel, has advantages from the standpoint of drying the air, and makes possible later tunnel changes for higher Mach numbers. On the other hand, from the standpoint of safety and minimum stagnation temperature drop during a run, low air storage pressure is advisable.

Pressure tanks are used by the oil, gas, and chemical industries (they call them "air receivers") and are hence usually available on an off-the-shelf basis. In the smaller sizes (400 to 4000 ft³) they are usually cylindrical, and may be mounted either horizontally or vertically, depending on the space available. Spherical tanks frequently prove less expensive for the larger sizes, and in some cases, especially for the highest storage pressures (5000 psi or so), high-pressure pipe or oxygen containers are used.

The tank should be installed with some sort of flexible joint between compressor and tank, and if installed horizontally, should be on a slight incline with the drain at the lowest point. There should be a lead-off pipe from the drain valve, so that if draining is necessary under pressure, the air blast will not strike the person operating the valve. The tank should be painted black in order to attain the maximum temperature produced by solar heating. However, if circumstances have resulted in a fairly long tank, say four or more diameters, it may well be worthwhile to forgo the heating, by using a sunshade over the tank, rather than risk excessive tank and inlet pipe bending. If the tank is outside and exposed to cold weather a commercial steam blanket will serve to keep it (and in turn the air in it) warm.

The tank should be equipped with a safety disc that is designed to fail at a pressure no greater than the design pressure of the tank. Such a safety disc, which can be obtained commercially, will fail and allow discharge of the tank pressure before the tank pressure can become dangerously high in the event of some malfunction.

The previously noted decrease in air stagnation temperature during a run is due to expansion of the air remaining in the tanks to a lower pressure as part of the air in the tanks is removed to operate the tunnel. The expansion of the air in the tanks is not an adiabatic process because as the air temperature in the tank drops, heat is transferred from the walls of the tank to the air. The result is a polytropic expansion process with a value of n between 1.0 (for isothermal) and 1.4 (for adiabatic) in the equation

$$\frac{T_i}{T_f} = \left(\frac{p_i}{p_f}\right)^{(n-1)/n} \qquad (2:13)$$

where T = temperature, °R,
p = pressure, lb/ft²,
i = initial conditions in tank,
f = final conditions in tank.

A chart showing approximate values of n for typical conditions is presented in Fig. 2:2. The final tank stagnation temperatures after expansion to lower pressures for an assumed expansion exponent $n = 1.2$ are presented in Fig. 2:8, where it may be seen that variations to about 200°R are possible.

This drop in stagnation temperature as the air leaves the storage tank can become bothersome. It affects the Mach number in the test section only secondarily through a change in boundary layer thickness, but it can affect balance strain gage readings significantly, and it does change the Reynolds number during a run. Some effort is therefore justified to see if the temperature drop can be reduced or perhaps completely nullified. Obviously a heater downstream of the tank could be designed to yield essentially zero temperature drop, and such heaters are sometimes employed. However, a simpler method is to fill the tank with crumpled metal or "tin" cans. As the air temperature drops, heat is transmitted to the air from the metal, and the drop is much reduced. The cheapest cans are those intended to contain dog food, but rimmed paint cans are worth the difference to avoid can crushing. The design of a can installation may be worked as follows:

1. Compute the amount of heat needed to bring the air expanded from p_i to p_f with $n = 1.2$ up to the desired temperature. (Use eq. (2:13) to obtain the final temperature.)
2. Select a can size and determine how many can be put in the tank. (Assume a packing factor of from 60 to 75 per cent.*)
3. From the specific heat of the metal of the cans and the total weight of the cans, determine the final can temperature if the required number of Btu's are removed.
4. From the required number of Btu's, the can surface area, the run time, and the heat transfer coefficient (assumed equal to 0.01 Btu/ft²-sec-°R), compute the difference between can and air temperature needed to effect the necessary heat transfer.

The example below will serve to illustrate the method.

Example 2:3 Compute the final air temperature for the conditions described below if cans are installed in the air storage tank:

tank volume 400 ft³	initial air temperature 520°R
initial pressure 150 psia	run time 30 sec
final pressure 50 psia	

* Some may have to be crushed to get this many in.

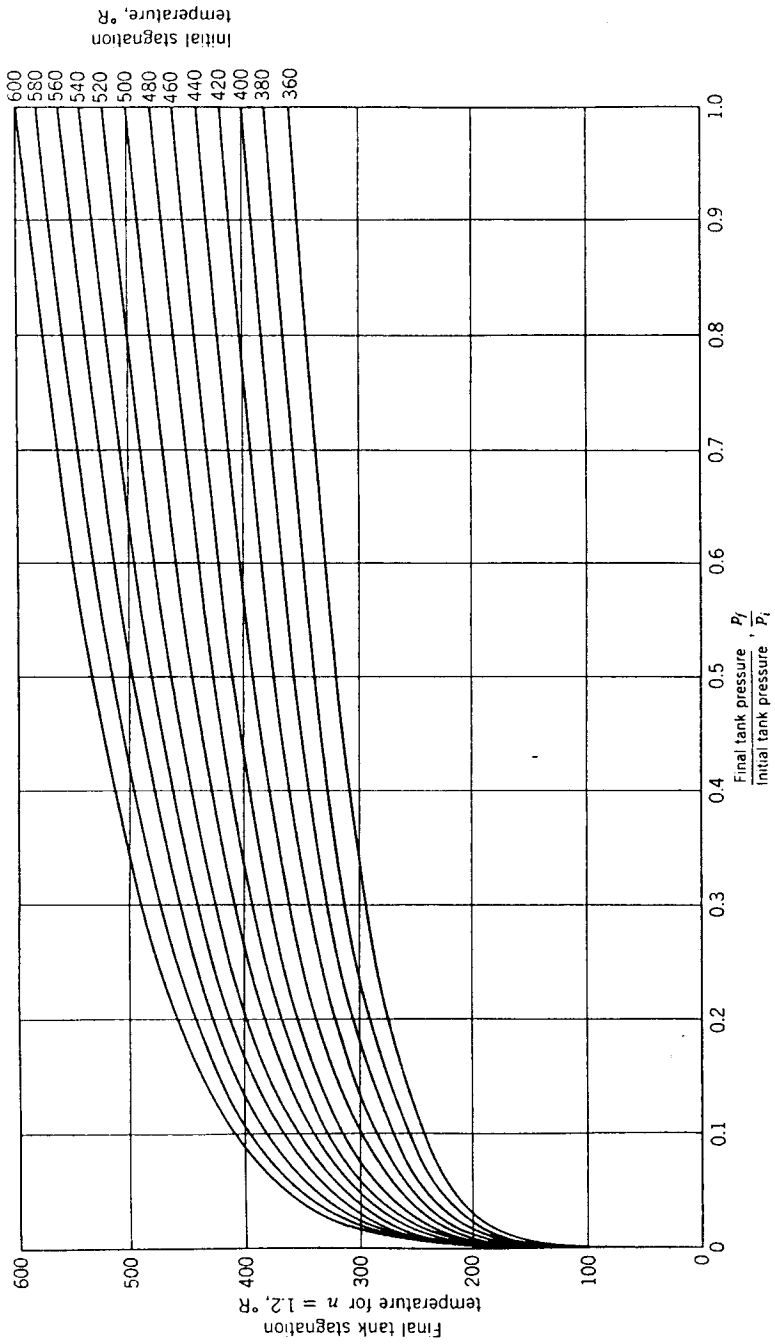


Fig. 2:8 Final temperatures in a storage tank assuming $n = 1.2$.

1. From the gas law the initial air density is 0.778 lb/ft³ and the initial weight of air is hence 311 lb.

2. From eq. (2:13), the final temperature would be 433°R with $n = 1.2$. The average temperature of the air leaving the tank would be 477°R.

3. If it is assumed that the cans permit no temperature drop, the final air density is 0.260 lb/ft³, and the final weight is 104 lb.

4. Using a specific heat of air of 0.24, we find that the heat needed by the air will be

$$\text{Btu} = 0.24(311 - 104)(520 - 477) = 2140$$

5. Assuming a can 3 inches in diameter and $4\frac{1}{2}$ inches long with an 0.013-inch wall (a commercial dog food can), we find that the surface area is 0.688 ft², the nominal volume is 0.0184 ft³, the metal volume is 0.000373 ft³ and the weight is 0.18 lb.

6. The maximum number of cans that can actually be put in the tank, assuming a packing factor of 0.75, will be $(400)(0.75)/(0.0184) = 16{,}300$. Their weight will be 2940 lb and their surface 11,200 ft².

7. The final temperature of the cans is found by letting the heat needed by the air equal the heat taken from the cans and using 0.11 as the specific heat of iron:

$$2140 = 0.11(2940)(520 - T_2)$$

$$520 - T_2 = 6.6°\text{R}$$

$$T_2 = 513.4°\text{R}$$

8. The next step is to find out how much temperature difference between the cans and the air is needed to develop the desired heating rate:

$$T = \frac{2140}{(0.01)(11{,}200)(30)} = 0.6°\text{R}$$

9. Thus, as the cans cool off, the air temperature follows the can temperature very closely. The first approximation of the final air temperature is 513.4 − 0.6 = 512.8°R.

10. Recalculating using 512.8°R as an end temperature of air in the tank is not justified, since the accuracy of the heat transfer coefficient is not that good.

The tank will be hydraulically pressure tested by the manufacturer, sometimes being supported during the process by being set in sand. Accordingly, should the need for retesting the tank arise because of age or the welding of additional fittings, a stress check should be made before filling it with water in the customary mounting saddle. Some tanks will be broken when loaded under such conditions. The very high pressure tanks have no such problem, since the density of air in the 5000-psi range approaches that of water.

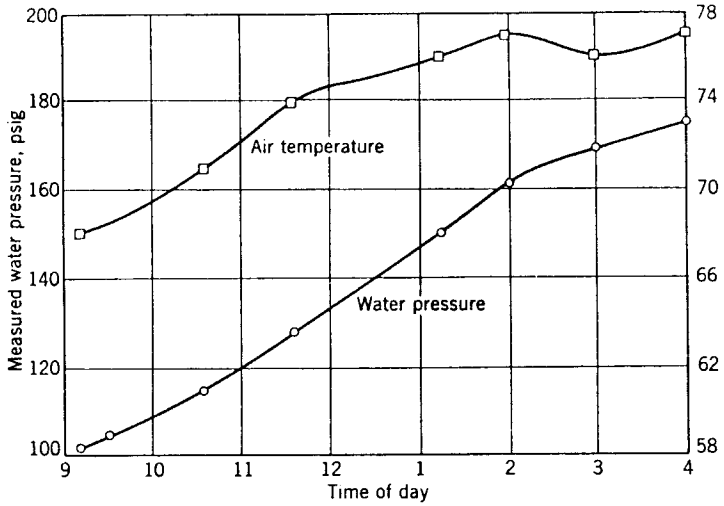


Fig. 2:9 The effect of solar heating during the hydrostatic pressure check of an air storage tank.

A problem to watch while checking for leaks and strength is the pressure increase due to solar heating if the tank is outside. The data from one such test are presented in Fig. 2:9, where it is seen that the tank pressure increased by 75 psi as the tank walls, heated by the sun, transmitted their heat to the water inside. This process, to the uninitiated, is a baffling thing, and many a student, sitting back with clipboard in hand to record a tank leakage rate has been terrified to see the pressure go up instead of down. The senior author had one such lad back off in awe, shake his head, and exclaim "I've got a negative leak!"

2:15 Pressure Regulators

Blowdown wind tunnels are almost invariably designed for operation at a constant stagnation pressure during any run. The pressure regulator is a special valve used to provide a constant wind tunnel stagnation pressure while the available pressure in the storage tank is decreasing. In theory, almost any valve could be used for this purpose. In practice, however, valves not designed for this purpose make very poor regulators.

Basically, the pressure regulator is a valve in which the opening through which the air passes varies fairly uniformly with valve position from fully closed to fully open. Fully open, the flow area through the valve should be approximately equal to that of the pipe supplying air to the valve. If the flow area through the valve is less than that of the lead-in pipe, higher storage tank pressures will be required to maintain a given tunnel stagnation pressure and tunnel run times will be reduced.

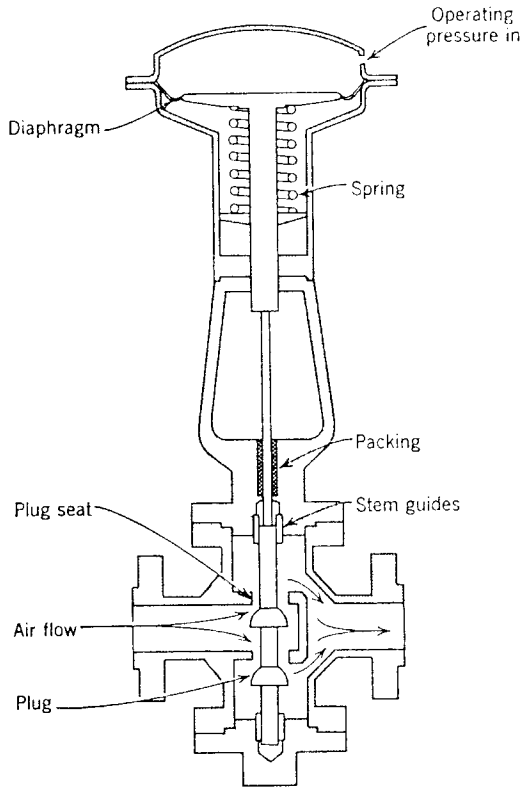


Fig. 2:10 Schematic of pressure control valve.

A schematic diagram illustrating the design principle of a pressure control valve is presented in Fig. 2:10. In the design, the flow opening is varied by gradually moving two spherical plugs out of their seats. Two plugs are used instead of one to increase the flow area through the valve. The plug-seat configuration of pressure control valves may vary considerably from that of Fig. 2:10. However, the basic idea of lifting a plug out of its seat to vary the flow area is very common. As illustrated in the figure, regulator valves are often operated by applying pressure to one side of a bellows to overcome the tension of a spring which is designed to keep the valve closed.

Pressure control systems can have almost any degree of sophistication that the designer is willing to pay for. With control valves similar to those of Fig. 2:10, satisfactory pressure control can be obtained manually by an experienced operator. In this case a pressure regulator valve to apply operating force to the valve and a pressure gage for the operator to watch

would be the only requirements. The other extreme of control system sophistication would be one in which the difference between desired and actual stagnation pressure is sensed, an electric signal proportional to this difference is fed into an analog computer, the computer continuously calculates regulator valve corrections from considerations of both difference between the desired and actual pressure and its rate of change, and a signal from the computer is continuously supplied to a device that regulates the pressure to the valve operator to make corrections to valve position. With this type of control system working properly, stagnation pressures may be controlled to within ½ of 1 per cent.

The regulator causes a drop in pressure and thus controls the downstream pressure by means of a throttling process. With the regulator valve only partially open the velocity in the constricted area of the valve is greater than in the pipe leading to the valve, and may vary anywhere from the velocity in the lead-in pipe to sonic, depending on the pressure drop across the valve, which is in turn dependent on mass flow rate and valve position. If the pressure drop across the valve is 47 per cent or greater (see Table 1:1) the flow through the constriction will be sonic. As the flow through the constriction fills the pipe downstream of the valve, it is at a lower total pressure and a higher velocity than in the pipe entering the valve (assuming the same pipe size). It may be at a *higher* or a *lower* stagnation temperature than the entering airstream, depending on its initial conditions. Throttled flow is known as "Joule-Thomson" flow, and is a constant-enthalpy process. However because of the changes in the coefficients of specific heat at constant pressure with temperature and pressure, the stagnation temperature of the stream may *rise* or *fall* as throttling occurs. The phenomenon is such that for low pressure storage, say around 300 psia, regulated to around 50 psia there is a loss of a few tens of degrees Fahrenheit. For very high pressure storage, moderately throttled, there may be a small rise in stagnation temperature. (See Fig. 2:11.)

Regulator valves are used in various ways in wind tunnel operation. Some tunnels are started by quickly opening the regulator valve and then adjusting its position either manually or automatically to maintain a constant stagnation pressure. Some tunnels have a quick-opening valve in series with and used in conjunction with the regulator valve. In these tunnels the regulator valve is pre-set to the approximate position required for the run. The tunnel is quickly started by operating the quick-opening valve and then the regulator valve takes over the control. In large tunnels, where it is necessary to conserve air, regulator valves have been used in still another way. In such tunnels, the operation of the regulator valve is programmed so that it is quickly opened to provide the pressure required

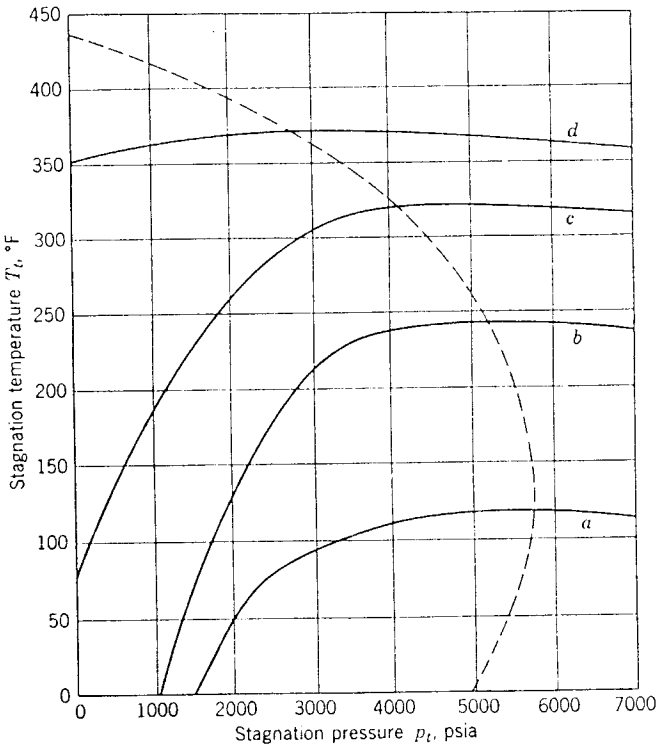


Fig. 2:11 The change of temperature with throttling. Curves *a*, *b*, *c*, and *d* are isenthalpy lines and show that in general the temperature falls during throttling. For very high pressures moderately throttled (points to the right of the dashed maxima line) there may be a small rise in temperature.

to start the tunnel, held in this position for 2 or 3 seconds to allow tunnel starting, closed down to a position needed to provide a minimum operating pressure ratio, and then allowed to control the pressure at this value during the run.

Pressure regulators should be fail-safe so that loss of operating air cannot permit the opening to increase and throw storage pressure into the wind tunnel. However, even those "fail-safe" regulators, after being put into operation, can sometimes be made to flop suddenly open if not used properly.

One fault with some regulators is that they seem to put a high-speed fluctuation ("noise") into the airstream. In instances known to the authors this fluctuation has been from ½ of 1 per cent to 3 per cent of the total head in magnitude and with a frequency of 500 to 700 cps. This oscillation must be in total head, since it represents as much as 200 per

cent of the dynamic pressure, but methods of alleviating it are as yet obscure. Another difficulty with some regulators concerns the asymmetrical flow created when the regulator is at a very small opening.

Pressure regulators are made which combine the duties of gate valves (sealing), butterfly valves (fast-opening), and regulators. These may be operated hydraulically, pneumatically, electrically, or manually, and give good control with fast action.

Even if such a regulator valve is used, however, it is highly desirable to have a quick-operating valve in series with it which can be used as a backup valve in the event of regulator valve failure.

The selection of a pressure regulator for a blowdown wind tunnel can sometimes be difficult. If the Mach number range of the tunnel is wide, the range of operating pressures and mass flows will also be wide. It is difficult to obtain a single regulator valve that will give satisfactory pressure control over a wide range of operating pressures and flows.

2:16 Piping and Valves

The cost of piping and valves increases rapidly with diameter (for a given pressure), and hence there is a natural tendency to use the smallest diameter possible. To avoid objectionable whistling and pressure losses, the piping should be selected so that, at the maximum mass flow (usually at the lowest operating Mach number of the tunnel), the Mach number in the pipe will be below 0.4. The pressure drop in the piping and valves between the air storage tank and the pressure regulator valve should be calculated because if the air storage capacity is marginal, this pressure drop may result in a significant reduction in available run time.

As mentioned in Section 2:15, some tunnels have a quick-opening valve in series with the regulator valve that is used in normal tunnel operation. In the event that such a valve is not used or that the valve used is not a tight shutoff valve, another valve will usually be required in series with the regulator to provide a tight shutoff and to double as a safety valve. The tight shutoff is required to prevent leakage of high-pressure air from the storage tanks through the tunnel. In addition to conserving air, the tight shutoff valve eliminates an annoying whistle and a draft of air through the tunnel which makes model changes immeasurably more difficult.

In view of the need for at least one valve in series with the regulator valve as well as the need for many valves in the various subsystems of the blowdown tunnel, some of the more common types of valves will be discussed briefly:

1. Butterfly valve. This valve consists of a disc in the flow passage which is rotated about an axis through its center. The disc is aligned with the flow when the valve is open and is essentially perpendicular to the flow when the valve is closed. Butterfly valves can be operated quickly because 90 deg of rotation of the valve stem changes the valve from fully closed to fully open. They are normally not tight shutoff valves but can be obtained with an inflatable sealing ring to provide tight shutoff for some applications.

2. Gate valve. This valve is essentially one on which a plate is slid across the flow passage of the pipe. In the closed position, sealing surfaces on the plate and on the valve body are forced into intimate contact by the pressure difference. The gate valve is not normally a quick-operating valve because of relatively large friction forces developed when the valve is closed and the pressure load holding the sealing surfaces together.

3. Plug valve. Plug valves consist of either a cylindrical or a conical plug in a seat with a hole through the plug equal to the inside diameter of the pipe. For operation the plug is rotated 90 deg, so that the hole in the plug is aligned with the pipe. Plug valves are quick-operating and tight-sealing valves. The conical plug has an advantage in severe flow environments in that it can be lifted out of its seat slightly, rotated, and then reseated, thus minimizing the torque required for operation.

4. Ball valve. Ball valves consist of a sphere with a through hole equal to the inside diameter of the pipe. Teflon rings around the inlet and outlet flow passages in the valve body maintain the proper ball position and provide a very good seal. These valves are quick-operating in that 90 deg of ball rotation opens or closes the valve.

2:17 Wide-Angle Diffusers

It has been known for many years that the uniformity of flow in a wind tunnel can be greatly improved if a large-area, low-velocity section is provided immediately upstream of the nozzle, so that a large contraction of the flow is provided as it enters the nozzle. This large-area, low-velocity section is termed the "settling chamber." As we have pointed out previously, it is desirable from an economic standpoint to use the smallest practical pipe size to deliver air from the storage tank to the tunnel proper and this small pipe size corresponds to high flow velocities. A diffuser is a device in which high-velocity flow, such as that in the small piping, is decelerated to a low-velocity flow, such as that in the settling chamber. Relatively long, shallow-angle diffusers have been tried between the piping and the settling chamber as a means of recovering the dynamic pressure in the piping while reducing the flow velocity. As far as the writers know, these have not been successful. Among the possible reasons is a turbulent and unsymmetrical flow leaving the pressure regulator valve which persists into the settling chamber and consequently into the nozzle.

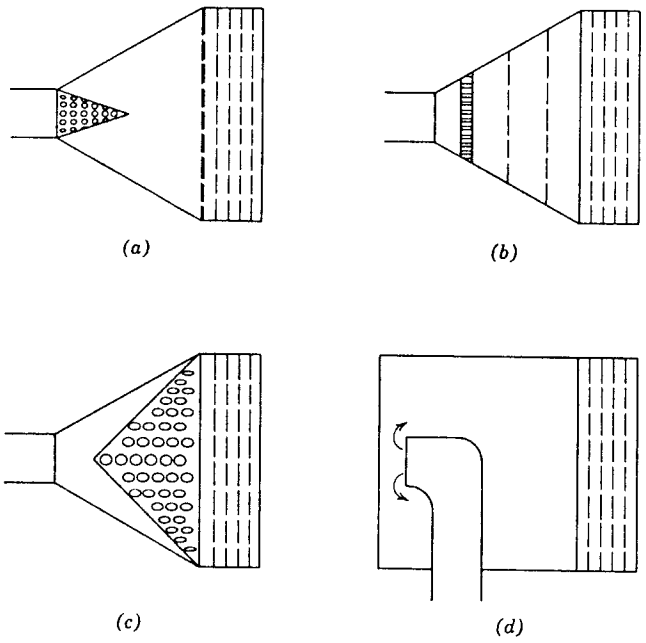


Fig. 2:12 Type of flow-spreaders. (*a*) Perforated can, perforated plate and screens. (*b*) Drilled plate, flow control screens. (*c*) Full perforated cone. (*d*) Reverse entry.

Blowdown tunnel designers typically use wide-angle diffusers for the transition from the pipe to the settling chamber. Commonly included angles between opposite walls are 45 to 90 deg. Because of the highly turbulent and non-uniform flow usually existing at the diffuser inlet, various devices are used to spread the flow from the inlet pipe to the settling chamber. There are almost as many spreader designs as there are tunnels. A few typical spreaders are illustrated in Fig. 2:12. Many failures of spreaders similar to those of Fig. 2:12*a* and 2:12*b* have occurred and these are attributed primarily to the high-pressure-drop design of the perforated can or plate in the small-diameter section. A recommended configuration is illustrated in Fig. 2:12*c*. The perforated cone facing upstream from the settling chamber allows ample perforations for a low-pressure-drop design and has been found to spread the flow satisfactorily. The perforations should be designed with a flow area sufficient to keep the average velocity through the perforations well below Mach 0.5 at the most severe operating conditions. This point should not be disregarded. In one tunnel using a perforated plate spreader with $\frac{1}{4}$-inch holes and insufficient flow area, the blast out of the holes was strong enough to tear out a welded screen four inches from the hole exit. The perforations should be positioned in the

cone to provide a uniform distribution of flow area over the duct. The spreader should be of rugged construction because it will be probably subjected to shock loads during starting and stopping of the tunnel in addition to pulsations from the control valve. An estimate of pressure drop through the spreader should be made because this could have a significant effect on the tunnel run time in some cases. A typical design value is $1.0q_e$, where q_e is the dynamic pressure in the inlet pipe.

2:18 The Settling Chamber

The settling chamber is usually a cylindrical shell, one diameter or more long, which accepts the air from the wide-angle diffuser, provides a length for settling to obtain uniform flow, provides screens for promoting uniformity of flow and for reducing turbulence in the air stream, and then exhausts into the subsonic portion (inlet) of the nozzle.

The static pressure in the settling chamber is higher than at any downstream point in the tunnel. However, it is normally considerably below that in the storage tanks or in the piping to the pressure regulator. Because it is economical, the settling chamber and downstream portions of the tunnel are usually designed for their normal operating pressures rather than the tank pressure. Because there is usually the possibility of a malfunction of a tunnel component which could result in excessive pressures in the settling chamber, such as the pressure regulator's suddenly being fully opened with maximum pressure in the air storage tanks, the settling chamber normally contains a blowoff stack extending through the roof of the building. The blowoff stack is equipped with a commercially available "safety disc" (or blowout diaphragm) rated to fail before an unsafe pressure is reached in the settling chamber. The exhaust stack and safety disc should be sized so that adequate flow passages are available to prevent over-pressurizing the settling chamber in the case of the worst conceivable malfunction. It is emphasized that the "worst conceivable malfunction" does not correspond to the most severe condition expected during normal operation. Often, it will be found that a blowoff stack and a safety disc with a flow area comparable to that of the pipe entering the wide-angle diffuser will be adequate.

It should be noted that blowout diaphragms come in two types, those for one-directional loads and those internally supported against vacuum failure, but designed for outward over-pressure blowout. The one-directional types are not satisfactory for blowdown tunnels, since sudden shutdowns can result in subatmospheric tunnel pressures as the momentum of the tunnel air carries it outside, dropping the tunnel pressure below ambient. The loss of diaphragm strength with temperature is shown in Fig. 2:13. If the flow spreader in the wide-angle diffuser is properly

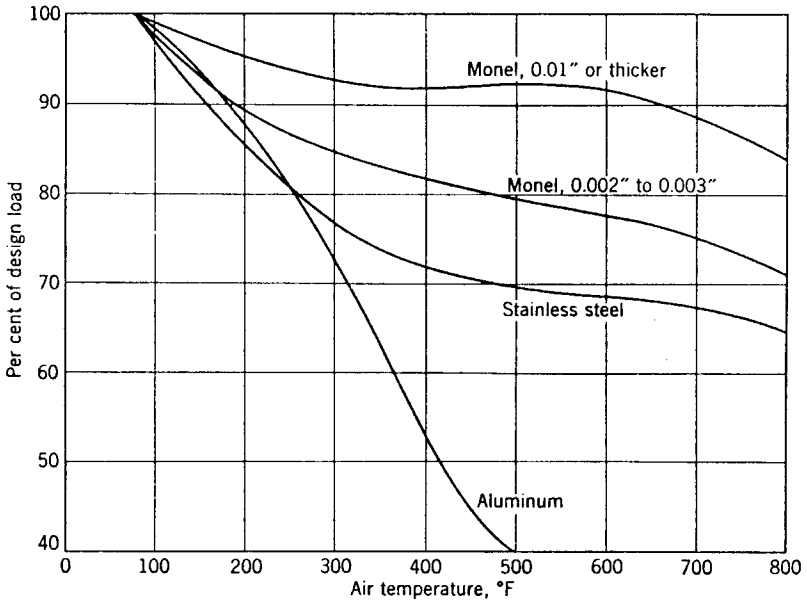


Fig. 2:13 Loss of strength with temperature for blowout diaphragms.

designed, air will enter the settling chamber with a fairly uniform distribution. In most spreader designs the air enters through perforations and a finite distance will be required for the individual jets of air from the individual perforations to coalesce to form a uniform flow. However, turbulence of the flow emanating from the control value or elsewhere will not be removed by the spreader. In fact, additional turbulence is almost certain to be induced by a perforated spreader.

The turbulence level of air in low-speed wind tunnels is extremely important because the point on a model at which a boundary layer has a transition from laminar to turbulent is related to the turbulence level. The aerodynamic drag of a model at low speeds is greatly influenced by this point of transition. The importance of turbulence level is generally considered to decrease as the wind tunnel speed increases into the transonic and supersonic range. At these speeds the model drag is primarily a function of pressure distribution and the effects of boundary layer transition are secondary. Nevertheless, most high-speed wind tunnels are designed with screens in the settling chamber to promote flow uniformity and to reduce the turbulence level before the air is expanded through the nozzle. Experiments to determine the turbulence damping accomplished by screens in low-velocity flows have been reported in Ref. 2:1. Results

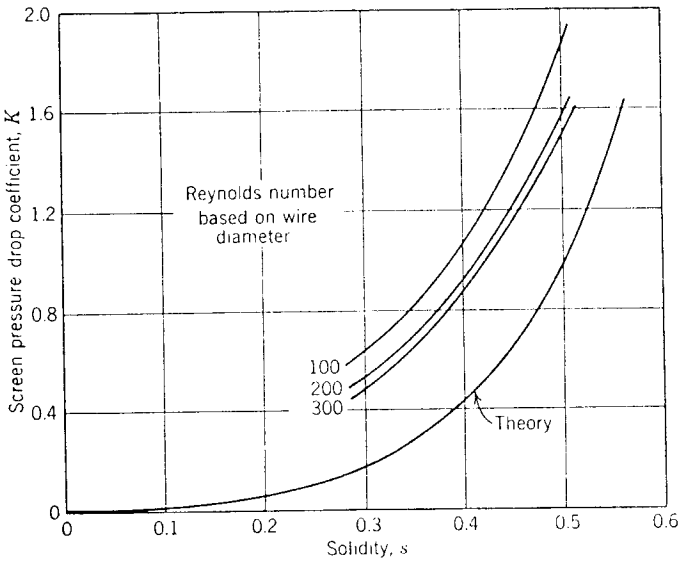


Fig. 2:14 Pressure drop through screens.

of these experiments indicated that the reduction in turbulence level is a function of the pressure drop through the screen:

$$f_u = \frac{1}{\sqrt{1 + K}} \tag{2:14}$$

where u' = root mean square of velocity fluctuation, ft/sec,

U = mean flow velocity, ft/sec,

$f_u = \dfrac{u'/U \text{ (with screen)}}{u'/U \text{ (without screen)}}$,

ρ = air density, slugs/ft^3,

Δp = pressure drop through a screen $= K \cdot \frac{1}{2}\rho U^2$.

Values of the screen pressure-drop coefficient as a function of Reynolds number and solidity (ratio of area blocked by wires of screen to total duct area) are presented in Fig. 2:14. Values of solidity and wire size for various screens are presented in Table 2:1. It is noted in Ref. 2:1 that at large pressure-drop coefficients, turbulence may be caused by screens and it is recommended that several low-pressure-drop screens are preferable to a single high-pressure-drop screen. This is the practice normally followed in blowdown tunnel design.

A characteristic of flow in wind tunnels is that the magnitude of velocity fluctuations in the settling chamber will remain essentially constant during the expansion of air through the nozzle. The result is that the turbulence

Table 2:1

Values of Solidity s for a Number of Screens

Screen Meshes per Inch	Wire Diameter	Solidity s
22	0.0075	0.303
30	0.0065	0.352
40	0.0065	0.452
50	0.0055	0.474

level u'/U is much lower in the test section of a high-speed tunnel than it is in the settling chamber.

The concensus of wind tunnel engineers is that settling chambers should be designed for flow velocities no greater than 80 to 100 feet per second. If possible, the lowest velocity in the settling chamber should be no less than about 10 feet per second. A low limit on velocity is desirable to prevent convection currents from causing a non-uniform temperature distribution that would persist from the settling chamber through the test section. Convection currents can become a problem any time there are significant differences between the air temperature in the settling chamber and the walls of the settling chamber, which is not unusual in blowdown tunnels. If the air is hotter than the walls, the air adjacent to the walls will be cooled. This cool air near the walls will have a tendency to drift toward the lower portion of the duct. If the flow velocity through the duct is small, there will be ample time for a temperature gradient to be set up before the air leaves the settling chamber. This problem is very important in high-temperature blowdown tunnels, but has been noted in tunnels with air temperature of about 200°F. It usually shows up in tunnels designed for a fairly large Mach number range. If a tunnel is designed for a settling chamber flow velocity of 100 feet per second at Mach 1.0 and is operated with the same size test section at a Mach number of 5.0, the settling chamber velocity at Mach 5.0 will be only 4 feet per second. An ideal solution for this problem has not been worked out. Possible solutions are the use of more than one settling chamber or the use of an air bleed system to maintain reasonable settling chamber velocities at the higher Mach numbers.

The settling chamber should be designed for easy removal or for easy access to its interior, since the screens will require some maintenance. It will have a provision for a connection to a pressure-measuring instrument. Normally this will need to be only a static pressure port because the velocity head will be negligible. If the tunnel is to have an automatic pressure

control system, a second pressure port will be required for obtaining a process pressure to be used by the control system. The settling chamber should also have a provision for measuring total air temperatures. Pressure and temperature measurements should, of course, be made downstream of the screens.

The settling chamber and wide-angle diffuser should be designed according to pressure vessel code and should have a hydraulic pressure check at 150 per cent of the design pressure. The pressure check will require blind flanges for the ends of the individual components or of the assembly. It will also require fittings for filling with water and bleeding off air.

2:19 Nozzles

Blowdown wind tunnel nozzles will be designed quite differently, depending on whether the tunnel is to operate at transonic speeds, supersonic speeds, or both. The entrance section for a transonic nozzle is usually designed to give a smooth variation of Mach number with distance between the settling chamber and the minimum section of the nozzle. Typical lengths for the entrance section are one or two test section heights. Downstream of the minimum, the nozzle usually has rectangular sections with parallel side walls and with flat top and bottom walls having provisions for being varied from parallel to perhaps ± 2 deg. The walls of the nozzle are vented from a point downstream of the minimum to the end of the rectangular section by means of slots or numerous holes either straight through the walls or inclined in a downstream direction, going from inside to outside the nozzle. Typical hole diameters in perforated nozzles are about equal to the wall thickness.

Work on ventilated test sections for transonic wind tunnels was pioneered by Wright of the NASA. The primary purpose of venting the nozzle walls is to minimize their effects on the air flow over the model. At transonic speeds (high subsonic and low supersonic), shocks and expansion waves developing in the vicinity of the model will be nearly normal to the flow. If shocks are allowed to strike a solid wall, they will reflect and strike the model, causing a flow over the model much different from that required to obtain data applicable to flight. If shocks are allowed to strike a free air boundary, they will be reflected as expansion waves and will again strike the model, causing bad data. The ventilated walls, being partly open and partly closed, are designed to minimize the effects of reflections of shock waves and similarly, of expansion waves. A second purpose of venting the walls is to generate a low supersonic Mach number. In Chapter 1 it was noted that the generation of supersonic flows in nozzles requires a convergence to a minimum area cross section and then a divergence to a larger area, with a specified area distribution required for

each individual Mach number. For tests in the transonic speed range, data are normally required at small Mach number intervals. This would require a large number of solid wall nozzles. However, by taking advantage of the ventilated walls, one can use a single nozzle to generate an almost unlimited number of low supersonic Mach numbers. To do this, the pressure outside the nozzle is reduced to a value near the static pressure at the desired operating Mach number and total pressure. In the portion of the nozzle upstream of the vents, the Mach number is 1.0 and the static pressure is above that outside the nozzle. When this higher-pressure air reaches the vented section of the nozzle, a flow to the lower pressure outside the nozzle begins. This flow through the vents continues until the pressure inside the nozzle becomes almost equal to that outside the nozzle. When this point is reached the air in the nozzle is flowing at the desired Mach number. Thus, the flow out through the vented walls gives the same end result as flow in a diverging solid wall nozzle.

Ventilations of the tunnel wall is usually accomplished in the manner illustrated in Fig. 2:15. The gradual increase of the slot or hole area allows a more gradual expansion of the nozzle flow to the desired Mach number and minimizes the likelihood of overexpansion with consequent nonuniform flow in the test section.

The ratio of open area to total wall area will typically be between about 16 and 30 per cent. With the smaller percentages of open area it will be more difficult to generate the higher transonic Mach numbers because the pressure drop through the ventilated area will be higher. No configuration for the vents has been found completely satisfactory from the standpoint of canceling both compression and expansion waves from the model. From published test results it appears that the best shock and expansion wave cancellation has been achieved with circular holes slanted 60 deg from a normal to the wall in a direction to encourage outward flow. The slanted holes provide cancellation of shock waves comparable to that of normal holes but do a better job of canceling expansion waves. The reader is referred to Refs. 2:2 and 2:3 for a bibliography of work on ventilated walls for transonic test sections.

Whether or not the previously mentioned variable-angle walls are used appears dependent to a large extent on the particular tunnel. They have been used to improve the test section flow or to improve the disturbance cancellation properties of the nozzles under specific operating conditions.

Generally the nozzle is enclosed in a plenum chamber and one of two means is used for reducing the pressure outside the nozzle (in the plenum chamber) Fig. 2:16. The most commonly used method is that of variable-angle flaps hinged on the diffuser walls and extending forward to the downstream end of the perforated walls. The diffuser is somewhat larger

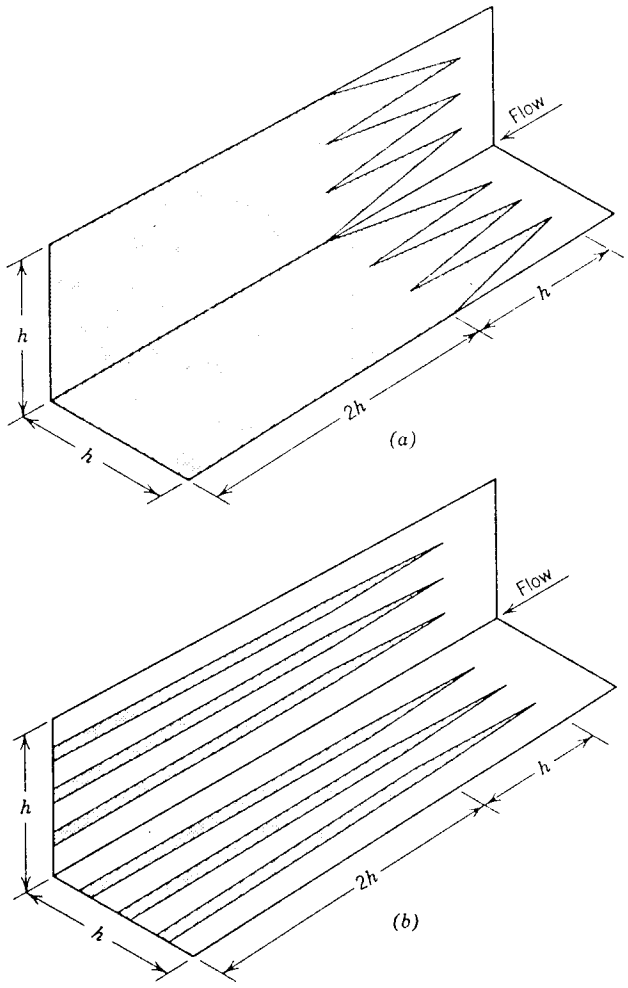


Fig. 2:15 Typical arrangement of ventilation in transonic test section. (Shading represents ventilation.) (*a*) Perforated; (*b*) slotted.

in cross section than the test section, so that air leaving the test section at a supersonic speed expands to a higher Mach number and lower pressure as it enters the diffuser. Rotation of the forward end of the flaps away from the tunnel centerline provides a gap through which the low-pressure air entering the diffuser can pull air from the plenum chamber, thus reducing its pressure. Flaps are sometimes located on only two walls and sometimes on all four walls.

The second method of controlling pressure in the test section is with an

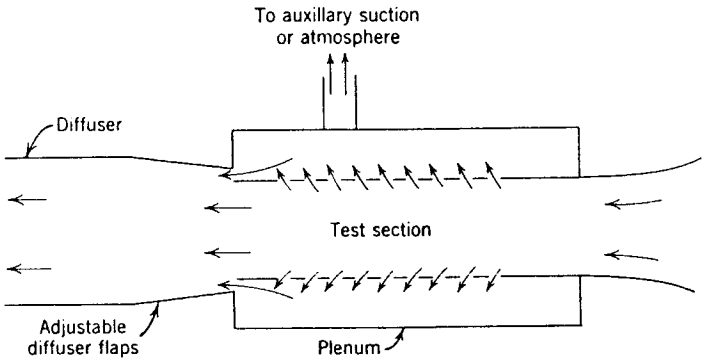


Fig. 2:16 Arrangement of devices to alter flow through ventilation.

auxiliary pumping system or by directly exhausting the plenum chamber to the atmosphere. When the plenum chamber is directly vented to the atmosphere, an excess of operating pressure is required in order to raise the test section static pressure and consequently the plenum pressure to the point where air will flow from the plenum to atmosphere.

It is noted that auxiliary suction is more commonly a part of large continuous tunnels than blowdown tunnels. In large tunnels with inadequate power for the desired operating Mach number, auxiliary suction with a relatively small pumping system is usually an economical means of increasing tunnel performance.

Some transonic tunnels use a choke for subsonic operation. Such a choke is sometimes a variable diffuser and sometimes a special diffuser design with a center body which can be moved to vary the diffuser minimum cross section. At a constant supply pressure, the choke can be used to vary the Mach number in the test section because it forms a sonic second throat. The choke may also be used to operate with increased tunnel stagnation pressure and consequently Reynolds number if it is used in conjunction with plenum chamber exhaust.

Operation at subsonic speeds does not require flow out through the ventilated walls of the test section. Consequently it is not necessary to reduce the pressure in the plenum chamber below that in the test section. This is fortunate because with subsonic flow, the air is compressed in passing from the nozzle into the diffuser and this compression has a tendency to increase the pressure in the plenum chamber above that in the nozzle. Some transonic tunnels are operated at subsonic and supersonic speeds with the same flap setting. When this type of operation is used, air flows from the plenum chamber into the nozzle, causing a thickening of the boundary layer but apparently having no adverse effects on the test section flow.

A point of importance with regard to safety is the design of the diffuser flaps. Positive means should be provided to ensure that the flaps will not come loose and block the diffuser. If they did, it could easily cause an overpressure in the plenum chamber with disastrous results. A safety disc is an excellent idea if there is any conceivable way for high pressures to be developed in the plenum chamber.

The aerodynamic design of supersonic nozzles has been discussed in Chapter 1. In translating the calculated nozzle coordinates into a mechanical design the allowable tolerances become an important factor. The cost of a nozzle will increase rapidly with decreasing tolerances on the nozzle contours. Experience has shown that a low tolerance on the actual coordinates of a nozzle is of considerably less importance than low tolerances on smoothness and continuity of curvature downstream of the initial expansion at the throat. Small supersonic nozzles with tolerances of 0.002 to 0.005 inch or even more may be expected to yield satisfactory flow if the contour is smooth and has a continuous curvature.

Nozzles for supersonic blowdown tunnels will generally be built according to one of four basic designs. (It is noted that only two-dimensional nozzles are considered inasmuch as axially symmetric nozzles are not commonly used in blowdown tunnels.) The first basic design is one in which the two side walls and the two contoured walls are fabricated into a rigid semi-permanent assembly and are inserted into the tunnel circuit as a piece of pipe would be with bolted flanges or with some other positive coupling device. Another basic design is one in which one side wall of the nozzle is a fixed part of the tunnel circuit. The other side wall and the two contoured walls are fabricated into a rigid semi-permanent assembly. This assembly is installed by placing it against the fixed side wall, using a positive coupling to attach it to the side wall, and then using positive coupling to the tunnel circuit at the upstream and downstream end. Another basic design is one in which a rectangular channel with a removable side wall is a fixed part of the tunnel circuit. The two contoured walls of the nozzle are secured in place in the channel and the movable side wall is then positively clamped to the channel. The last and by far the most complicated nozzle design is one in which the contoured walls of the tunnel are flexible plates (Fig. 2:17). Screw-type jacks are attached to the outer surfaces of the flexible plates and the nozzle contour is adjusted to that for the desired Mach number by use of the jacks. The flexible wall nozzle has advantages over the fixed wall nozzles in that Mach number can be set at any desired value in the operating range. This point is more theoretical than real, since few flexible nozzles have been arranged for more than a reasonable number of customarily used Mach numbers.

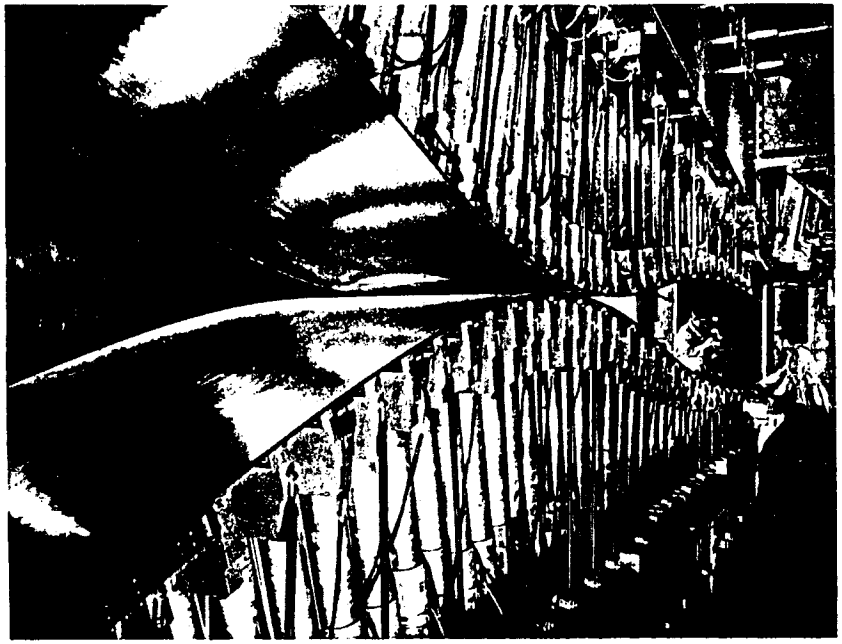


Fig. 2:17 A flexible plate nozzle. (Courtesy Arnold Engineering Development Center.)

However it is quite possible to miss developing the desired Mach number distribution, and this omission may easily be corrected without a lot of laborious recontouring by using flexible plates. Moreover, any nozzle contour is right for only one Reynolds number; flexible plates enable small corrections to be made simply.

Problems of using flexible wall nozzles include the extra cost of their construction and maintenance, and the difficulty of sealing the flexible plates where they contact the flat walls. This problem exists to a lesser degree with any built-up nozzle.

With the exception of the flexible wall nozzle, the material used for construction of the contoured walls is selected according to how much work can go into the nozzle and how long it is expected to last. Wood, aluminum, and steel all work well and last according to their strength.

When a nozzle is designed for use at both transonic and supersonic speeds, it will typically be designed as the transonic nozzle previously discussed with provisions for inserting contoured blocks in the upstream portion of the nozzle. These blocks form the converging–diverging portion of the nozzle and the test section of the transonic nozzle is not changed. A photograph of a transonic nozzle with contoured blocks for Mach 3.0

operation is presented in Fig. 1:19. The ventilated walls of the test section generally have no large adverse effects on the flow in the test section but may have an adverse effect on the pressure ratio required for operation.

2:20 The Test Section

The primary consideration in the design of a test section is to ensure that model length will not be limited by the length of the uniform flow portion of the nozzle. It is necessary in transonic tunnels to keep model sizes such that cross-sectional areas will not exceed 1 per cent of the test section area in order to minimize wall interference effects. For a cylindrical model in a square test section, this would mean that the model diameter should not exceed one-ninth of the test section height, and therefore that the model length for a fineness ratio (length to diameter) 9 model should not exceed one test section height. The aft end of the model should be at least 4 or 5 model diameters into the uniform flow region of the nozzle to minimize the effects of disturbances from the end of the nozzle on the wake behind the model and possibly on the flow over the model. Thus, a test section length of 1.5 test section heights should be adequate for testing fineness ratio 9 models. If tests of higher fineness ratio models are anticipated, the test section length should be increased accordingly.

In supersonic tunnels the model length will be limited by the reflections of bow shock waves from the tunnel walls. An exact procedure for determining allowable model lengths is not available. However, by making a few approximations, reasonable estimations of model lengths can be made. The problem is set up as illustrated in Fig. 2:18. The bow shocks are assumed to be reflected from a plane located a distance equal to the boundary layer displacement thickness inside the tunnel wall. Although it is certain that the bow wave will be reflected by the boundary layer rather than the tunnel wall, the point in the boundary layer at which reflection will actually take place cannot be specified. Although it would be more conservative to assume reflection at the surface of the boundary layer, it is reasonable to assume reflection from a plane equal to the displacement thickness away from the wall. The angle of the bow shock on a cone at an angle of attack cannot be readily determined. The assumption that this angle is equal to the shock wave angle on a cone at zero angle of attack is reasonable, particularly at moderate angles of attack (to between 5 and 10 deg). As the distance away from the cone apex increases, the bow shock will begin to curve toward the Mach angle, making the calculation conservative. The allowable proximity of the reflected shock to the base of the model depends to a large extent on the model configuration. For the model shown in Fig. 2:18, if the shock passes the model base 1.5 diameters from the model centerline, the only effect will be on the wake

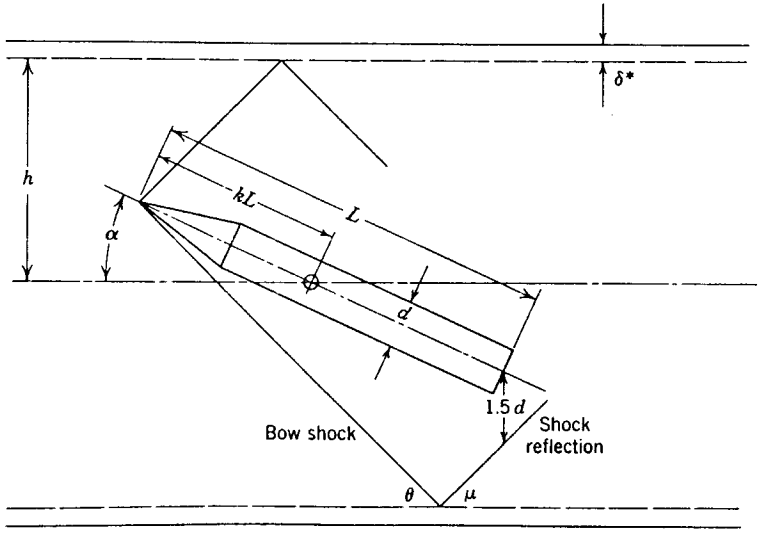


Fig. 2:18 Approximation of shock pattern for determining allowable model lengths at supersonic speeds. θ is the shock wave angle, and μ the angle of shock reflection. The Mach wave angle may often be used for both with little error.

behind the model. This is not particularly important because the wake is influenced to a large extent by the sting which holds the model to the tunnel, and model base pressures measured will not equal those of flight even in the absence of the reflected shock. If the model were boat-tailed at the base (having a diameter decreasing with model station), the flow over the boat-tailed portion could be influenced by the reflected shock. In this case, it would be desirable to specify an intersection of the shock with the wake a few diameters downstream of the model base. If the model were equipped with vertical fins, the model length would be specified from the consideration of proximity of the reflected shock to the fins.

It is obviously not possible to specify model length in completely general terms. However, the simple cone cylinder should be one of the longest models that can be tested in a particular supersonic tunnel. Since the test section is to be designed for the maximum allowable model lengths, an analysis of Fig. 2:18 should be applicable to the determination of test section length. From geometrical considerations the following equations can be derived. The model length limited by the shock reflection on the compression side of the model (L_c) is

$$L_c = \frac{h(1 + \tan\mu \cot\theta)}{1.5/(L/d) + \cos\alpha \tan\mu + \sin\alpha[1 - k(1 + \tan\mu \cot\theta)]} \quad (2:15)$$

The model length limited by the shock reflection on the expansion side of the model (L_e) is

$$L_e = \frac{h(1 + \tan\mu \cot\theta)}{1.5/(L/d) + \cos\alpha \tan\mu - \sin\alpha[1 - k(1 + \tan\mu \cot\theta)]} \quad (2:16)$$

Equations 2:15 and 2:16 indicate that L_c increases with increasing k and that L_e decreases with increasing k. Since allowable model length is limited by the lesser of L_c and L_e, it follows that maximum allowable model length (L_{max}) will occur when $L_c = L_e$. This condition is met when

$$k = \frac{1}{1 + \tan\mu \cot\theta} \quad (2:17)$$

$$L_{max} = \frac{h(1 + \tan\mu \cot\theta)}{1.5/(L/d) + \cos\alpha \tan\mu} \quad (2:18)$$

Equation 2:18 for maximum model length indicates that length will be limited by the zero angle of attack case.

It is noted that other factors may have a bearing on model length and should be considered before specifying test section length. These factors are (1) the nose of the model and the base of the model must be a reasonable distance outside the boundary layer at the highest angles of attack and (2) disturbances in the horizontal plane of the model must be examined in the manner of the preceding for the vertical plane of the model. Examinations of this type have resulted in some tunnels that have test sections with heights greater than their widths. (3) The possibility that disturbances from the viewing window will strike the model should be examined. Unless the window is flush with the inner walls of the tunnel, a disturbance will exist. It will be very difficult to keep such disturbances from striking the model if the window is large enough for good optical coverage and if the Mach number is less than about 2.

After defining maximum length models for a particular test section, it is sometimes advisable to examine the possibility of having a portion of the model located upstream of the test section (which is defined as the portion of the nozzle in which the flow is uniform over the complete duct with the exception of the boundary layer). Upstream of the test section, a wedge-shaped region of uniform flow at the test section Mach number exists. This wedge-shaped region has an apex on the tunnel centerline and is bounded by the last cancellation waves of the characteristic network, which intersect the nozzle wall at the beginning of the test section. At the lower Mach numbers there is not a great deal to be gained by shortening a nozzle to take advantage of this wedge-shaped uniform flow area. However, at Mach numbers of 4 or 5 and above, very significant reductions in nozzle length can be achieved. Such reductions are worthwhile because

of the rapid increase in viscous losses in long, high Mach number boundary layers with consequent increases in compression ratios required for operation. It is imperative that access to the test section be provided for model changes, and since time spent opening and closing doors is utterly wasted, a rapid lock system is essential, preferably single-lever operated. Doors should be put on both sides of the test section. Desirable features of doors include rapid opening, some sealing system to prevent leakage of air into the test section, protection of the window glass during model changes, and positive safety against falling should the door be raised to open. When possible, the door should provide a maximum of access to the model. If removable nozzle blocks are to be used, the door should provide access to them too.

2:21 Windows

Few if any wind tunnels have been built without windows with which to view the model and other important sections of the tunnel. Model viewing is necessary for optical analysis of the flow, as well as for simple observations of how badly the model is jumping around and whether the tail is still on. Glass has been found to be the most suitable of the various transparent substances. Plastics so far have not developed the abrasion resistance required, nor do they possess the desired optical properties.

Of the various glasses, borosilicate crown glass is probably the most suitable for the usual blowdown wind tunnel. Quartz windows are used in most high-temperature wind tunnels. It has a greater resistance to thermal shock and a smaller coefficient of expansion than glass. However, it is much more expensive than glass and is more difficult to obtain with satisfactory optical qualities.

A majority of wind tunnels are equipped with schlieren systems (described in Section 6:17), and it is primarily for this application that good optical qualities are required. For the schlieren system, the glass should have extremely flat surfaces, should have an extremely homogeneous structure, and should be free of internal imperfections such as "seeds" and "bubbles." If necessary, the windows may be made double with the volume between vented to the tunnel static pressure. This both makes the inner part (which is more likely to be scratched) easier to replace, and it relieves it from pressure loading so it is less likely to fail.

Glass is basically a silicon product that can be made of various compositions in much the same manner as metallic alloys. Mechanically, it loses its strength with time. The breaking strength of Foucault window-glass, for instance, is halved when load duration is increased from five seconds to thirty minutes. The final strength of glass is unknown; some believe it may be zero. When a load is applied to glass, no region of

plasticity appears, and Hooke's law (the proportionality of stress to strain) holds up to breaking. Fracture first occurs in tension, and consequently surface cracks or scratches materially reduce its strength. Curiously, the strength of glass containing cracks is influenced by the medium in contact with the glass surface. Water on the crack can reduce the strength by as much as 20 per cent, whereas substances that have dried on the surface usually increase the strength. The strength of glass decreases with increasing temperature. In the light of these facts, wind tunnel windows of glass are arbitrarily designed with a factor of safety of 10, using the following properties of glass:

Tensile strength (modulus of rupture)	6500 psi
Compression strength	36,000 psi
Young's modulus of elasticity	10,000,000
Poisson's ratio (average value)	0.24

Wind tunnel windows using the above values and factor of safety have resulted in essentially no failures. Glass may be tempered to a tensile strength of 30,000 psi, but it then becomes brittle and its optical qualities are not satisfactory for wind tunnel use. The maximum thickness of standard plate glass is $1\frac{1}{4}$ inches but greater thicknesses may be constructed by cementing thicknesses together using methyl methacrylate. The joint is typically 0.02 to 0.05 inch thick.

Windows that are highly loaded are normally round, but are sometimes square or rectangular with the corners rounded off. The proper thickness for a simply supported *round* window may be found from Ref. 2:4 as

$$t = \sqrt{\frac{3W(3m+1)}{8\pi m S_{\max}}} \tag{2:19}$$

where t = glass thickness, inches,
W = total of uniformly distributed load to be supported, lb
$m = 1/\mu$, where μ = Poisson's ratio,
$S_{\max}$ = maximum allowable stress, lb/inch^2 ($S_{\max}$ occurs at the center of the window).

Using the safety factor of 10, we have

$$S_{\max} = \frac{6500}{10} = 650 \text{ psi} \quad \text{and} \quad m = \frac{1}{0.24} = 4.17$$

Equation (2:19) reduces to

$$t = 0.0244\sqrt{W} \tag{2:20}$$

The maximum deflection occurs at the middle of the window and is

$$y_{max} = \frac{3W(m-1)(5m+1)r^2}{16\pi Em^2t^3} \qquad (2:21)$$

where r = window radius, inches,
E = Young's modulus for glass.
Equation (2:21) simplifies to

$$y_{max} = 0.237 \times 10^{-7} \frac{Wr^2}{t^3} \qquad (2:22)$$

Example 2:4 Compute the glass thickness and deflection for a 24-inch diameter simply supported window to withstand a pressure differential of 15 psi.

1. From eq. (2:20) the thickness is found to be

$$t = 0.0244\sqrt{\frac{\pi(24)^2(15)}{4}}$$
$$= 2.005 \text{ inches}$$

2. From eq. (2:22) the deflection at the middle of the window is

$$y_{max} = 0.237 \times 10^{-7} \frac{(6800)12^2}{(2.005)^3}$$
$$= 0.00290 \text{ inches}$$

The thickness of a simply supported *rectangular* window may be found by using the following steps (Ref. 2:4):

1. $$M_{max} = Bps^2$$

where M_{max} = maximum moment, lb (The maximum moment will occur as a result of the long dimension),
B = coefficient from ratio of long side to short side and Poisson's ratio, see Fig. 2:19,
p = unit pressure, psi,
s = length of short side, inches.

2. $$S_{max} = \frac{M_{max}\, c}{I}$$

where c = half the glass thickness = $t/2$,
I = moment of inertia for 1 inch wide strip = $t^3/12$,

$$S_{max} = \frac{6M_{max}}{t^2}.$$

$$\text{Hence } t = \sqrt{\frac{6M_{max}}{S_{max}}} \qquad (2:23)$$

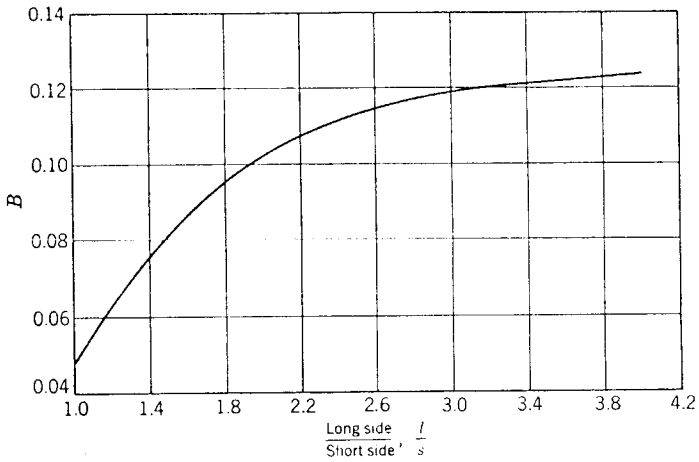


Fig. 2:19 Rectangular plate moment factor, B.

It must be noted that eq. (2:23) is for a simply supported plate, and stress concentrations will occur when the corners are restrained from curling up. Accordingly the corners should be radius cut or an additional factor of safety should be provided.

Example 2:5 Compute the acceptable glass thickness for a simply supported window 30 by 105 inches to withstand a 15-psi pressure differential.

1. $$M_{max} = (0.122)(15)(30)^2 \qquad (B = 0.122, \text{ Fig. } 2:19)$$
$$= 1648\text{-inch lb}$$

2. $$t = \sqrt{\frac{6 \times 1648}{650}}$$
$$= 3.90 \text{ inches}$$

A suitable window mounting arrangement is shown in Fig. 2:20. Positive holding against either pressure or mechanical loads in two directions is provided. The glue-filled gap provides resilience as well as a seal. Specifications for windows may take the following form:

1. State design pressure differential and factor of safety (usually 10, both for safety and for small distortion).
2. Windows to be of schlieren quality laminated from selected polished commercial plate 1 inch thick.

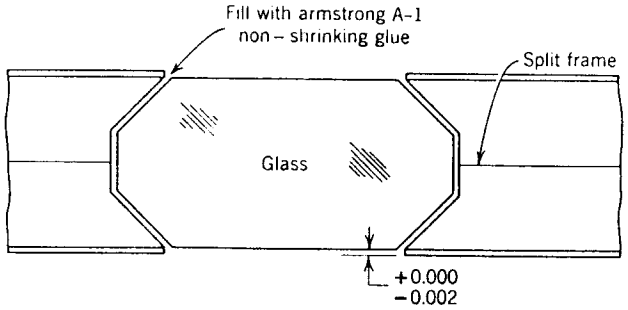


Fig. 2:20 Glass mounting detail.

3. Reasonable effort shall be expended in selection to meet the following specifications:

a. Windows shall be reasonably free of bubbles and seeds greater than 0.5 mm in diameter.
b. Bubbles and seeds less than 0.5 mm in diameter shall be sparsely and uniformly distributed when the plate is viewed by the unaided eye in normal daylight in a direction perpendicular to the polished surface of the plate.
c. The polished surface of the glass shall be reasonably free of scratches and chips in the central 60 per cent of the window area.
d. The central 60 per cent of the window area must be reasonably free of striae discernible by the unaided eye when inspected in a dark room by the usual striae inspection techniques.
e. The flatness and parallelism of the optical faces of the windows are defined by the appropriate sections of U.S. Air Force Specifications MIL-G-1366B. Additional polishing of the commercial plate may have to be employed to meet the specifications, but it should be avoided if at all possible (it is expensive). If additional polishing is deemed necessary, it should be so stated on the bid and the unit cost of the operation itemized (for future data and replacement).

4. Bonding plastic used to secure the glass laminations must have good optical qualities and maintain an air-tight bond for the temperature range +50 to 150°F and a pressure differential of 25 psi.

2:22 Free Jet Test Sections

Besides the more conventional solid wall test sections, the supersonic blowdown tunnel is sometimes arranged so that the testing is done in a free jet—either entirely open with no diffuser (Fig. 2:21) or as an enclosed free jet (Fig. 2:22). In either case the flow leaving the nozzle exit is surrounded by still air with a turbulent mixing zone for a boundary surface



Fig. 2:21 Free jet and model.

and constant pressure as a boundary condition. The advantages that arise from the use of a free jet include.

1. The lessening of choking and the consequent use of larger models than possible in a solid wall tunnel of the same nozzle exit diameter.
2. An improvement of access to the model.
3. In high-temperature tunnels, a lessening of the window-heating problems.
4. The starting and running compression ratios are nearly the same; no over-pressure to start is required.

The "price" of these above advantages is a usual increase of required compression ratio, and for the simple free jet, an enormous increase in noise. Usually, too, the flow quality is slightly poorer than in the solid wall tunnels.

The open free jet is by far the easiest type of all to construct and is particularly useful in engine work where the engine may be directly linked to it, or simply immersed in it. In many instances, a far larger model can be tested than in a conventional solid wall test section. It is of interest to note that the jet static pressure may be *below* ambient, a conditions not possible in subsonic flow. The starting pressure ratio (see Section 1:4) will be approximately that corresponding to a normal shock in the test section (Case 3 of Fig. 1:23), and the running ratio is about the same. The noise level from an open free jet is very serious, and a tunnel with such a test section should not be planned for installation in populated areas unless it is to be very small.

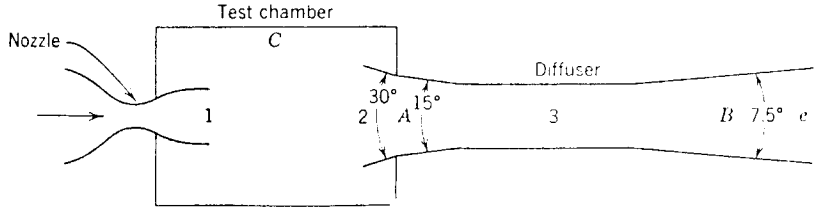


Fig. 2:22 Schematic diagram of a typical enclosed free jet test section.

The *enclosed* free jet avoids the noise problem and requires slightly less compression ratio than the open free jet. A model of the flow in the test chamber–diffuser portion of a free jet wind tunnel has been derived from theory in Ref. 2:5 and from experiments in Ref. 2:6. This model may be described by Fig. 2:22. The jet entering the test chamber (C) from the nozzle exit (1) contracts slightly during its passage through the test chamber because of mixing of the jet with the stagnant chamber air. Oblique shock waves exist in the supersonic portion of the jet and are terminated by a strong (nearly normal) shock wave system upstream of the diffuser throat (A). A very thick boundary layer exists between the supersonic jet and the walls of the contraction section of the diffuser. The flow passes through the remainder of the diffuser at subsonic speeds. With this flow configuration, the pressure at the diffuser exit (e) influences the pressure in the test chamber through flow upstream in the thick boundary layer. Increases in total pressure of the flow cause the normal shock to move downstream, with the result that test chamber pressure decreases. Also, increases in second-throat area cause the test chamber pressure to decrease.

It is usually desirable to maintain the test chamber pressure near the nozzle exit pressure to avoid strong shocks or expansions as the jet leaves the nozzle. There is a limiting value of second-throat area below which it is not possible to reduce the test chamber pressure to the value at the nozzle exit. However, if the second-throat area is slightly above this limiting value, relatively large increases in second-throat area can be made with very little effect on the tunnel operating efficiency (η = ratio of the tunnel exit pressure to the pressure behind a normal shock at the nozzle exit Mach number). In Ref. 2:6, second-throat (3) to nozzle exit (1) area ratios of 1.6 were found satisfactory for operation at Mach numbers of 2.0 to 4.3 with diffuser efficiencies of η varying from 0.62 at Mach 2.0 to 0.50 at Mach 4.3. For these conditions, free jet lengths (distance between the nozzle exit and diffuser inlet) to about 2¼ nozzle exit diameters had no apparent effect on tunnel operating efficiency. Figure 2:23 is a theoretical plot from Ref. 2:6 relating the ratio of diffuser inlet to nozzle exit area ratio A_2/A_1 to the ratio of test chamber to nozzle exit pressure p_c/p_1 and the tunnel operating efficiency η.

For the mode of operation of the enclosed free jet just described, the tunnel starting pressure ratio is less than the tunnel running pressure ratio, in contrast to the solid wall tunnel. The reason is that the strong shock is not driven through the diffuser throat. The mode of operation can be changed, however. The total pressure in the tunnel can be increased sufficiently to obtain sonic flow in the diffuser and a normal shock in the diverging diffuser. With this flow configuration the test chamber pressure remains essentially proportional to the nozzle exit pressure and the value

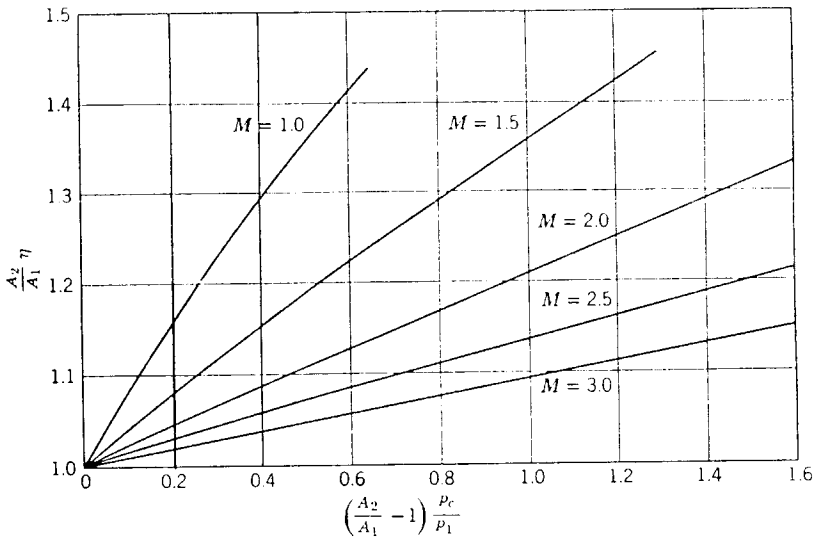


Fig. 2:23 Theoretical relation between diffuser inlet to nozzle area ratio (A_2/A_1), test chamber to nozzle exit pressure ratio (p_c/p_1) and tunnel operating efficiency η. (Ref. 2:6.)

of the proportion is dependent on diffuser throat area. As might be expected, the test chamber pressure increases as the diffuser throat area is decreased.

For the higher Mach numbers it is not essential to keep the test chamber pressure equal to the nozzle exit pressure. Disturbances resulting from pressure differences will have shallow angles and will not effect the flow in the center portion of the jet for a considerable distance downstream of the nozzle exit. With this reasoning, experiments were made at Mach numbers of 5 and 6 (Ref. 2:7) in an axially symmetric tunnel with diffuser throat areas less than the nozzle exit area. In these experiments it was found that tunnel operating efficiencies (η) were greater than 100 per cent in some cases. Also, it was found that the tunnel operation was similar to the solid wall tunnel in that the tunnel required less pressure ratio to run than to start. Results of these tests indicated that the free jet length should be no greater than 1.5 diameters.

2:23 Model Support Systems

The procedure most commonly used for obtaining aerodynamic force data in a high-speed wind tunnel is to establish flow in the tunnel with the model axis aligned with the airstream; to record data while changing the angular alignment of the model axis with respect to the airstream (angle of attack, α) from 0 deg to a negative angle, then to a positive angle,

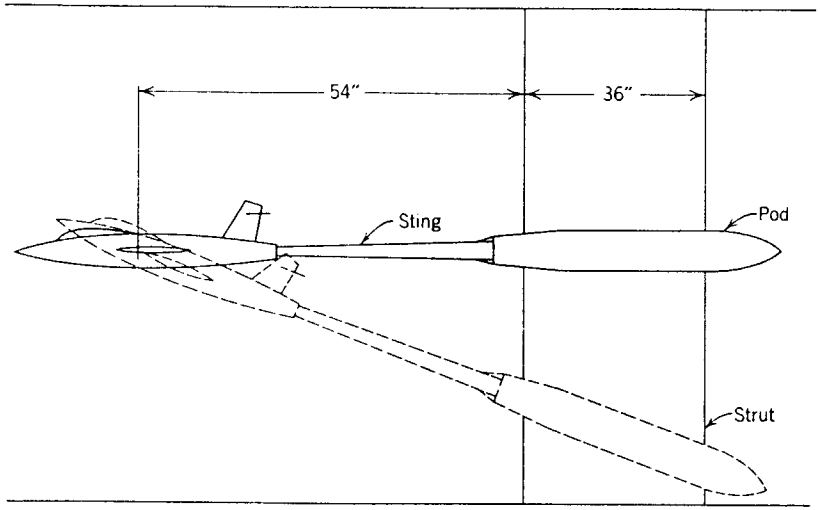


Fig. 2:24 Schematic of a vertical strut and sting installation.

then back to 0 deg; and then to stop the tunnel. The model support system is the means for holding the model in the tunnel and the mechanism for changing its angle of attack during the test.

By far the majority of models in high-speed wind tunnels are supported by means of a "sting" or small diameter rod extending downstream from the base of the model and aligned with the model axis (Fig. 2:24). The reasons for the sting-type mounting are twofold. First, the strut or struts extending from the walls of the wind tunnel to the lower surfaces of the model, as in many low-speed wind tunnels, would have major effects on the air flow around the model which could not be readily evaluated. The second is the fortuitous existence of blunt bases on high-speed aircraft to accommodate jet engines needed for the high speeds. With these blunt bases, the model can be sting supported without any alteration of model contour and with the minimum probability of interference of the support on air flow over the model.

Model stings are usually made of LaSalle fatigue-proof or Armco 17-4 stainless steel. The fatigue-proof steel develops a yield strength of 185,000 psi and an ultimate strength of 200,000 psi. Both of these values are for the un-heat-treated state, and hence machining is easy. The 17-4 has the advantage of withstanding higher temperatures and the corrosion sometimes found in tunnels with gas-fired heaters. It requires only a 700°F heat-treatment and hence has little warpage trouble. The final strength properties of 17-4 are a little above those of the fatigue-proof steel.

Usually, the model support system is designed to pitch (change α) the model in a vertical plane. The tunnel axis is normally horizontal and a reference alignment of the model with respect to the tunnel axis can easily be made with a small bubble level or an inclinometer. Also, schlieren systems used to view the flow over a model are preferably arranged to view the pitch plane. Schlieren systems require a lot of room and rigid installation of optical equipment, both of which are most convenient in a horizontal plane.

The first thing to decide in the design of the model support system is the location of the strut by which the model support sting is attached to the tunnel structure. The model will of course be mounted in the test section, where the flow is uniform, and the strut must be mounted a significant distance downstream of the test section. The sting leaving the model base must have a cross section which is small relative to that of the model and must have a length of small cross section equivalent to several model diameters to minimize effects of the sting on flow over the base region of the model. The long, slender sting has some severe disadvantages. First, it is inherently limber and is subject to buildup of stresses to high levels at the aft end of the small diameter, particularly during tunnel starting and stopping. Second, as the sting gets longer the angle of attack that can be achieved before the pod holding the sting to the strut hits the tunnel floor gets smaller. Angle of attack requirements to as high as 20 or 30 deg are common, and this places a severe limitation on sting length. Because of the conflicting requirements regarding sting length, compromises are usually involved in the location of the strut with respect to the test section location of the model. Distances from the leading edge of the strut to the point in the test section about which the model rotates when the angle of attack changes vary at least through the range of 1 to 2½ test section heights in existing wind tunnels. In some wind tunnels the solid walls are recessed to allow the pod on the strut to actually sink into the wall in order to obtain an increased α range. In the free jet wind tunnels, the wall restriction on angle of attack is of course no problem.

The strut should be designed with a streamlined leading edge and with a frontal area small enough to ensure that it will not cause any difficulties in starting the tunnel. Minimum flow areas for starting a tunnel have been discussed in Section 1:6. The frontal area of the strut should be small enough to keep the remaining flow area well above that theoretically required to start the tunnel. A good rule of thumb is to have a flow area at the strut which is well above that at the throat of the diffuser.

The model is usually driven through its α range by using either a rectangular vertical strut with a twin screw drive arrangement or a "sector" strut arrangement with a geared or screw-type drive (Fig. 2:25). The twin screw setup makes it possible to vary the model's center of rotation

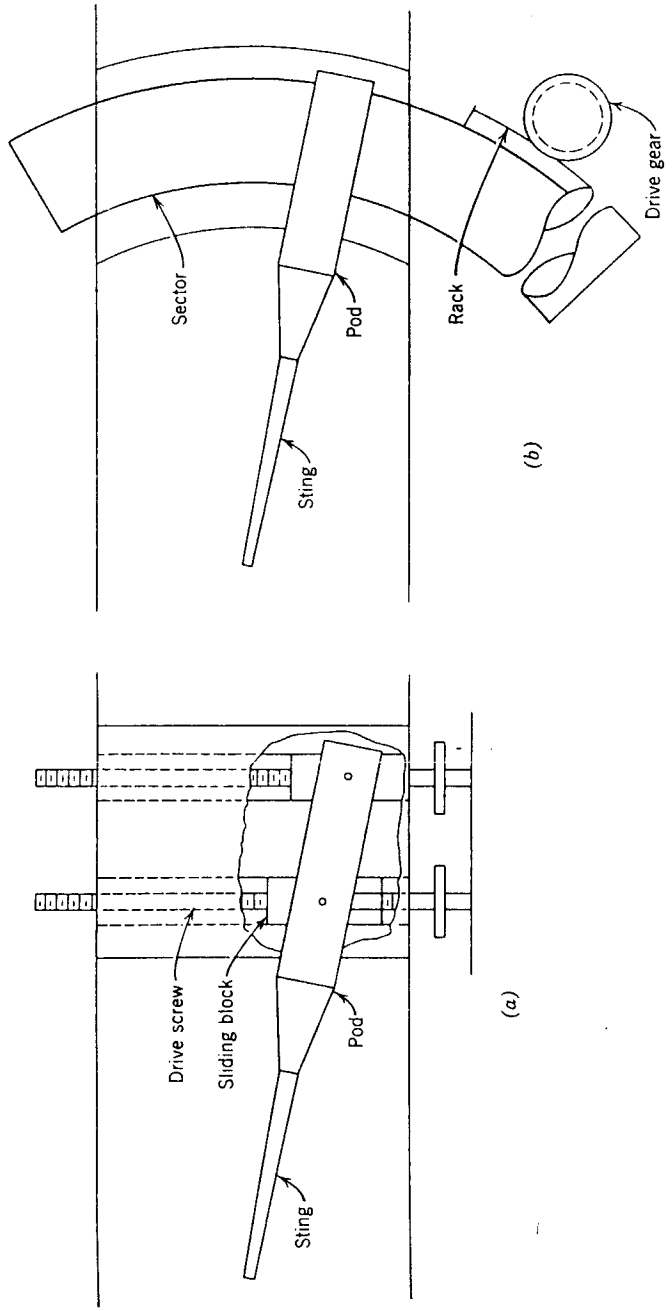


Fig. 2:25 Schematic drawings of two popular model support and drive mechanisms. (*a*) Twin screw; (*b*) sector.

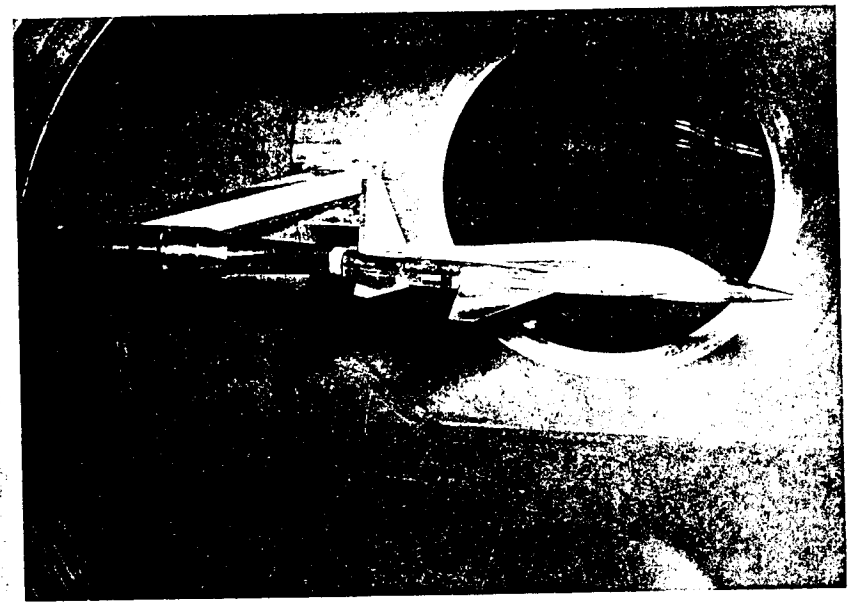


Fig. 2:26 A third method of pitching a model using a circular section in the tunnel wall. (Courtesy Northrop Corporation.)

by simply changing the drive gears. If drive gears are installed so that each screw turns at the same rate of speed, the twin screw setup provides a means for translation in the vertical plane of the tunnel. This arrangement is convenient for making vertical traverses with pressure probes during calibration of the tunnel or when it is necessary to survey the wake behind a model. The disadvantages of the twin screw arrangement are a fairly complicated design with many moving parts and a slight movement of model center of rotation with α. The sector arrangement requires fewer moving parts than the twin screw arrangement and has a fixed center of rotation. The primary disadvantages of the sector are that it takes considerably more room than the twin screw arrangement and poses a problem of sealing at points where the sector passes through the tunnel walls. (A third system is shown in Fig. 2:26.)

From an overall viewpoint, it is doubtful that one drive arrangement is truly superior to the other, and there are about as many of one as of the other. With either strut arrangement there are several general items of importance regarding the design. With regard to the aerodynamic flow over the model, the speed of rotation of the model is limited by two things. The model should have an insignificant change in angle of attack (less than 0.01 deg) during the time it takes a sample of air to pass from the

nose to the base of the model. The vertical translation velocity of every point on the model due to rotation should be less than 0.0002 times the air velocity. For a 1-foot-long model pitching about its nose or base in a 1000-ft/sec airstream, 10 deg of rotation per second would be the maximum rate. If the rotation speed is below that for aerodynamic flow effects, the data-recording system may have a limiting effect. Many wind tunnels record force data while the angular traverse is being made. The ability of the recording system to follow and record varying loads accurately may be the determining factor in specifying rotation speed. If continuous data recording is used, the drive speed must be constant to avoid measuring loads due to angular acceleration of the model mass. If a slow force data-recording system is used or if model pressures are to be measured during an α traverse, it is desirable to use a "pitch-pause" technique. In this technique, the model is driven to a new angle of attack, stopped, and held at a fixed attitude for a period of time to allow instrument stabilization. Data are then recorded and the model moved to the next α. If the pitch-pause system is to be used exclusively, the pitch rate is limited only by the economy and ease of design. On the other extreme, the model pitch rate must be compatible with available tunnel run time.

Provision should be made for automatic recording of the model angle of attack during the test. Ample room should be provided for taking electrical leads and pressure tubing from the model through the strut and to outside the tunnel. The model support and drive system should be very well engineered with large margins of safety on every point of design. They are the heart of the wind tunnel, are subject to a more severe environment than is usually estimated, and have to work essentially all the time the tunnel is running.

Quite rarely, swept struts instead of the sting support system are employed for mounting models in a high-speed wind tunnel (Fig. 2:27). When these are used they are usually as thin as structurally possible to minimize the interference of the strut on the flow over the model. Half-span models may also be mounted on a shielded plate (Fig. 2:28) or on the tunnel wall for zero yaw tests only. If the plate or the tunnel wall act as perfect reflection surfaces for shocks and expansion waves in supersonic flow, the flow patterns, with the exception of viscous effects, would be the same on the half span as if the other half span were present. Also, with the half-span model the balance system (for measuring forces and moments) can be located outside the tunnel where room is no problem. On the other hand, there are questions as to whether the plate or the tunnel wall act as perfect reflection planes, the effects of air flow through a gap which must be maintained between the plate or wall and the model are questionable, and the viscous effects are questionable. Consequently, the half-span

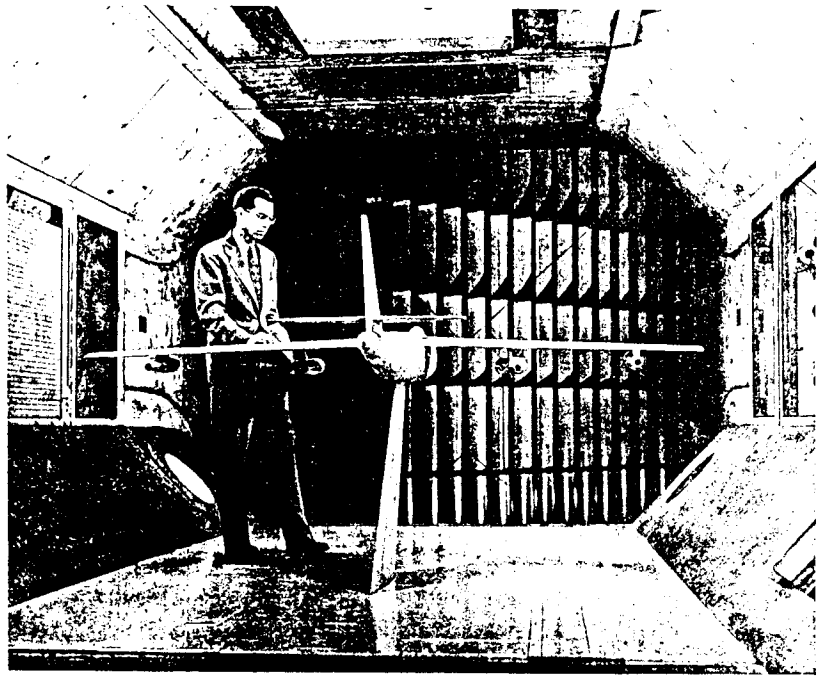


Fig. 2:27 B-47 model mounted on a single swept strut. (Courtesy Boeing Company.)

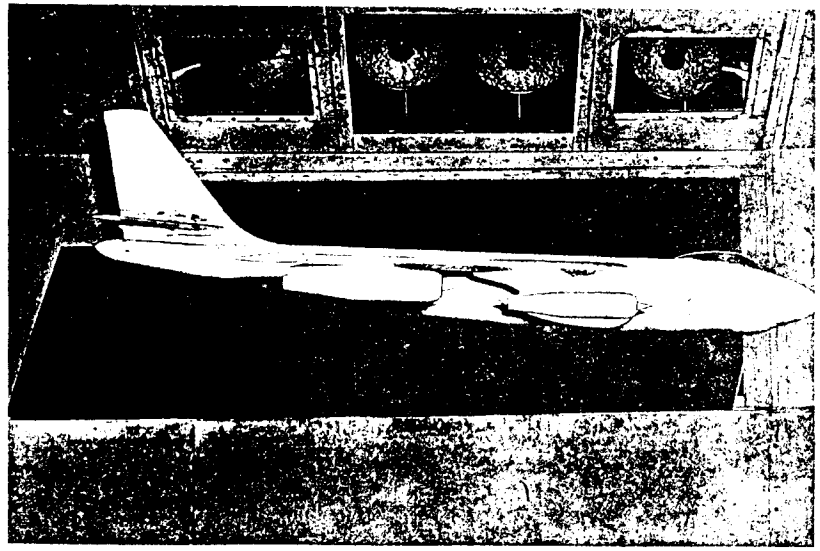


Fig. 2:28 B-47 model on plate mounting. Plate windshield occupies lower portion of picture. (Courtesy Boeing Company.)

technique is usually limited to obtaining increments in air loads due to model configuration changes in regions that would not be influenced by the plate or wall. A good example would be the measuring of increments of pitching moment and rolling moment due to the deflection of control surfaces. When a half-span model is tested on the tunnel wall, it is usually shimmed away from the wall, so that the plane in which the model is cut is located at the edge of the tunnel wall boundary layer. When a plate is used, it usually is located well above the tunnel wall boundary layer, has a perfectly flat surface aligned with the airstream on which the model is located, has a sharp leading edge to cleanly split the flow, and has a shield between the plate and the tunnel wall to prevent air loads on the member by which the model is attached to a balance outside the tunnel. A possible source of trouble with the plate is the chance of getting a "blocking" condition between the plate and the wall, with the result that the plate completely alters the flow over the model.

2:24 Diffusers

In transonic wind tunnels the section immediately downstream of the test section is somewhat larger in cross section than the test section. This enlarged section provides a means for expanding the air leaving the test section at low supersonic speeds and thus provides a suction to pull air out of the plenum chamber. In most transonic tunnels, a transition from a square or rectangular to a circular cross section is started near the downstream end of the diffuser flaps. When the section becomes circular it is usually joined with a conical diffuser having a maximum included angle of 7.5 deg. The cone continues until the area ratio is large enough for a low Mach number flow (perhaps $M = 0.1$ or less). It then joins a cylindrical section which makes a 90-deg turn, so that the air from the tunnel will be exhausted straight up. Compression ratios in transonic blowdown tunnels are seldom a problem because even single-stage compressors can supply air to 150 psia and stagnation pressures of 30 psia are adequate for the more inefficient tunnels.

The aerodynamic design of diffusers for supersonic wind tunnels has been discussed in Sections 1:4 and 1:5. It has been found that the diffuser should have a throat with a cross section less than that of the test section. Satisfactory throat areas have been defined in terms of the operating Mach number. However, the overall diffuser configuration has not been defined. Numerous studies have been made in the attempt to optimize such configuration variables as the angle of convergence between the test section and the diffuser throat and the length of the diffuser throat. Included angles of convergence from quite small up to 30 deg or more have been used, as have second throat lengths of zero to ten test section lengths.

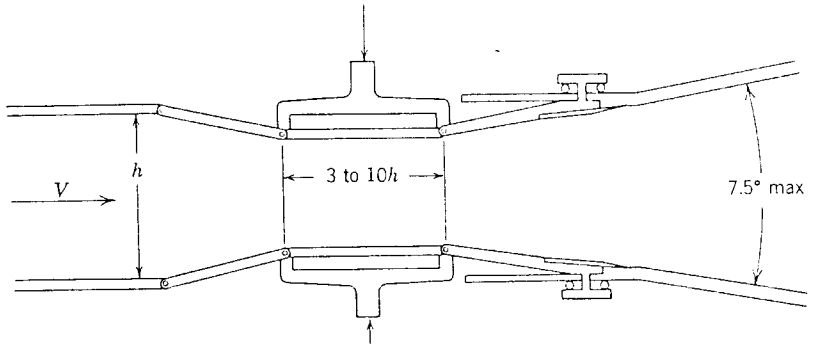


Fig. 2:29 Schematic diagram of adjustable diffuser design.

Results of these studies have not been conclusive and the tunnel designer must choose a configuration that he can reasonably expect to work on the basis of previous diffuser studies and hope it works well in his tunnel.

It has been pointed out in Section 1:4 that many supersonic tunnels have adjustable second-throat diffusers as in Fig. 2:29. These are fairly complex and costly items in a tunnel of significant size and frequently, if not usually, do not perform to the designers expectations. Our philosophy is that the designer will be ahead if a fixed diffuser is used and the cost of a variable diffuser is employed to increase the capability of the air supply system. Downstream of the second throat the diffuser of the supersonic tunnel should be the same as that of a transonic tunnel; that is, the angle between opposite walls should be kept below 6.0 deg.

2:25 Silencers

The scream of a high-speed wind tunnel varies from the threshold of pain at short distances to very annoying at large ones. Accordingly the few tunnels built without silencers rarely stay that way long. However the design of a silencer is beyond the scope of a wind tunnel engineer since silencers are available commercially and represent 2 per cent or less of the cost of a tunnel. For planning purposes the silencer diameter should be large enough to permit the air to be below 70 mph at the discharge end.

The simplest silencers are composed of two concentric cylinders with about a 6-inch gap between them. The inner one through which the air is discharged is perforated and the space between the cylinders is filled with a sound-absorbent such as glass wool. More complex silencers may have sound-absorbing curtains hung in the central passage. Typically silencers are from two and a half to four diameters long. The degree to which they silence the scream of a high-speed wind tunnel is quite impressive.

Since the silencer is the last part of the blowdown circuit, it should have

some sort of door to keep birds and insects out of the tunnel. This door should, however, not have any locking systems or spring loads apt to jam, since either action could result in over-pressurizing the tunnel circuit.

2:26 Injectors and Ejectors

The pressure ratios required for starting and running supersonic wind tunnels have been discussed in Section 1:4 and illustrated in Fig. 1:25. The discussion and figure lead to the conclusion that the blowdown tunnel must operate at some quite high stagnation pressures as the Mach number is increased and further that unless one cycles the pressure regulator to provide a higher pressure for a few seconds during starting, the tunnel will have to run at the starting pressure with a loss of maximum run time and a loss of maximum Mach number.

Injectors and ejectors are devices that work toward overcoming the above difficulties. Injectors are jets of relatively-high-energy air at the downstream end of the test section which add energy to the low-energy boundary layer and *reduce* the required compression ratio for a particular Mach number. Ejectors are nozzles located well downstream in the diffuser which are directed downstream and, by dropping the exit pressure, *provide* the needed pressure ratio. In many instances the injectors use main drive air which is at the tunnel stagnation pressure and by-passes the test section. More typically ejectors use pressures higher than tunnel stagnation values. For the amount of added tunnel performance, the efficency of the injector is far superior to that of the ejector, but the difference is usually not of importance.

A very effective configuration for an injector is shown in Fig. 2:30, wherein air at stagnation pressure is passed around the test section and enters the diffuser through flaps downstream of the test section. The injector air effectively forms a second throat. The performance of such a

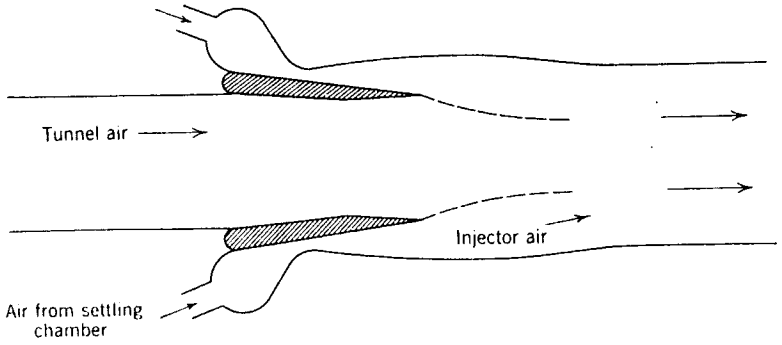


Fig. 2:30 Diffuser injector.

setup is shown in Fig. 2:31. Extrapolating the experimental values, we see that though a compression ratio of 5.5 is needed to start the tunnel at $M = 3.35$ without an injector, a ratio of only 2.7 is needed with the injector running and using twice as much air as the tunnel. If only the stagnation pressure corresponding to a ratio of 2.7 had been available without an injector, the maximum starting Mach number would have been about 2.3. A secondary benefit is that the starting and running pressures with the injector are essentially equal (Fig. 2:32).

Further improvements in injector tunnels have been described by Stokes in Ref. 2:8. With existing compressors of large mass flow rating but low pressure ratios, a Mach number of 7.0 has been achieved with an overall pressure ratio of 16 for nozzle flow and 4 for the injector flow when the mass flow of the injector was approximately 10 to 20 times the mass flow of the tunnel. The necessary test section arrangements were complex and costly, but the use of existing compressors resulted in a net economy. Still further, the new data generated on pressure recovery have been valuable.

The action of the injector may be explained in two ways. First, the rise in pressure associated with the diffusion produces a deleterious separation of the boundary layer flow, which the injector tends to overcome, and second, the injector air forms a second throat.

By contrast with the action of injectors, ejectors are simply pumping devices used to reduce the tunnel exit pressure and are not as efficient as injectors. They are used where extra air or steam is available locally. By using ejector flows of two to ten times the nozzle flow the tunnel exit pressure may be reduced by a factor of from two to ten. A setup of this type is shown in Fig. 2:33, and the performance of one ejector is shown in Fig. 2:34. Sometimes up to four or five ejectors are used in series where a low tunnel exit pressure is required.

Many variables of importance to the design and use of ejectors may be defined from Fig. 2:33 and are listed as follows together with reasonable values.

Item	Reasonable Values
1. Ejector pressure/Exit pressure p_1/p_5	3 to 8
2. Exit pressure/Tunnel pressure p_5/p_0	2 to 10
3. The area ratio A_3/A_{th}	6 to 8
4. The length/diameter ratio of the mixing length L/D	4 to 12
5. The projection ratio S/D	1.5 to 4.0
6. The tunnel inlet cone angle β	5 to 15°
7. The ejector nozzle angle α	10 to 20°
8. The outlet diffuser angle θ	4 to 7°
9. The mass ratio, tunnel mass/ejector mass m_t/m_e	0.05 to 0.50

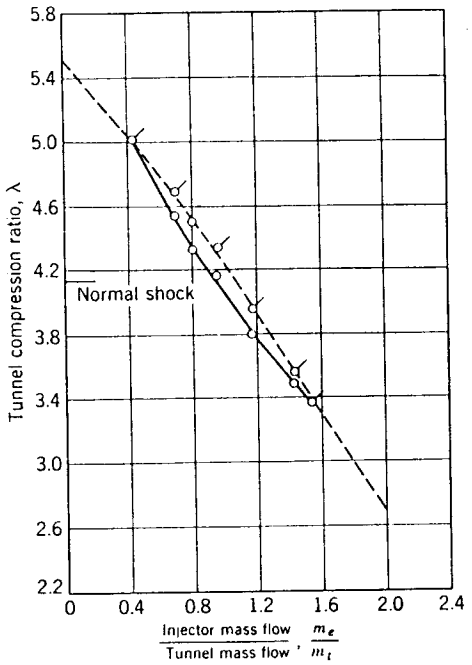


Fig. 2:31 Experimental performance of injector such as that shown in Fig. 2:30 at a tunnel Mach number of 3.35. Injector stagnation pressure is equal to tunnel stagnation pressure. Flagged points are for starting; others for running.

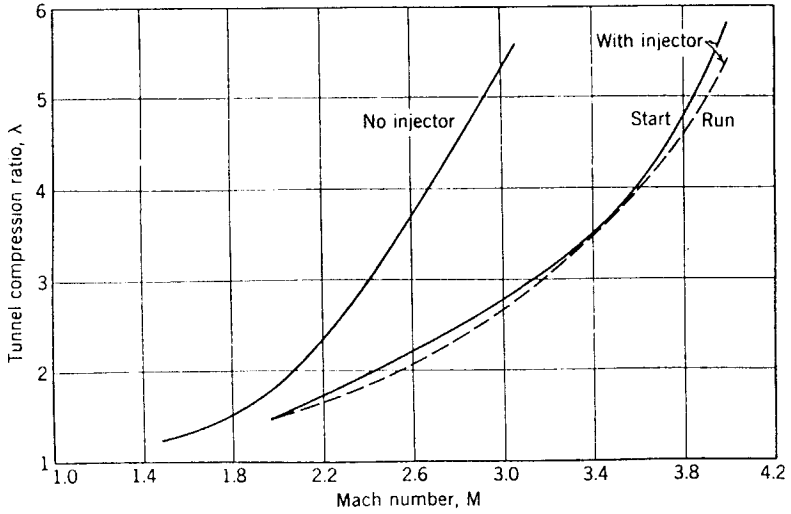


Fig. 2:32 Effect of injector on compression ratio needed to start and run.

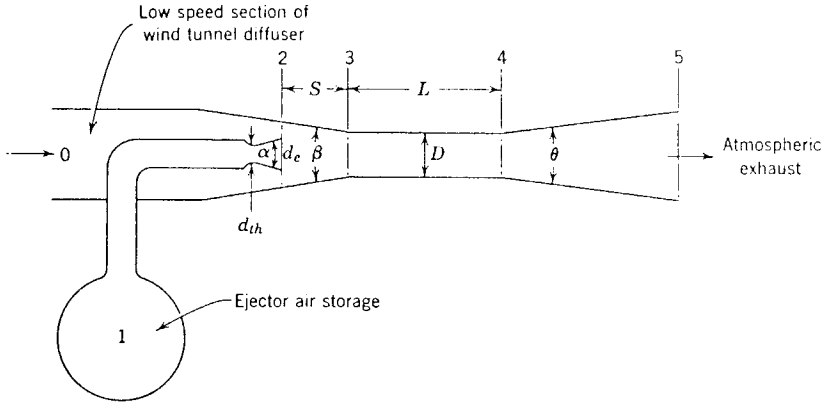


Fig. 2:33 Variables for ejector design.

References 2:9 and 2:10 should be consulted when an injector or ejector design is contemplated.

2:27 Safety and Fool-Proofing

Without equivocation the wind tunnel engineer must provide the maximum reasonable safety as far as the tunnel's structural integrity and operational procedures are concerned. Items to be considered include pop-off valves on storage tanks, blowout patches for ducting that might in any way be subjected to over-pressure, grids for blowout patch containment, air exit blast shields, door interlocks, heat shields, and so forth. Recently several catastrophic explosions of heavy ductwork containing air-oil mixtures have pointed out the requirement of oil-free high pressure air.

Among the most important safety requirements is to ensure that valves between the air storage tanks and the tunnel cannot be opened until the tunnel is completely closed up and secure. Several safety requirements have been pointed out in previous sections and others will be mentioned at relevant places throughout this book.

In addition to the safety requirement, fool-proofing of tunnel components to prevent destruction of equipment when personnel safety is not involved is an important aspect of wind tunnel design. If there is some way that a component can be damaged or destroyed through improper use, it very probably will be. Fool-proofing of a tunnel will vary widely according to the tunnel and only the designer or operator will be in a position to determine the many components that require fool-proofing. However, one good example of such a component that is common to most tunnels is the model support system. The angular travel of the system without

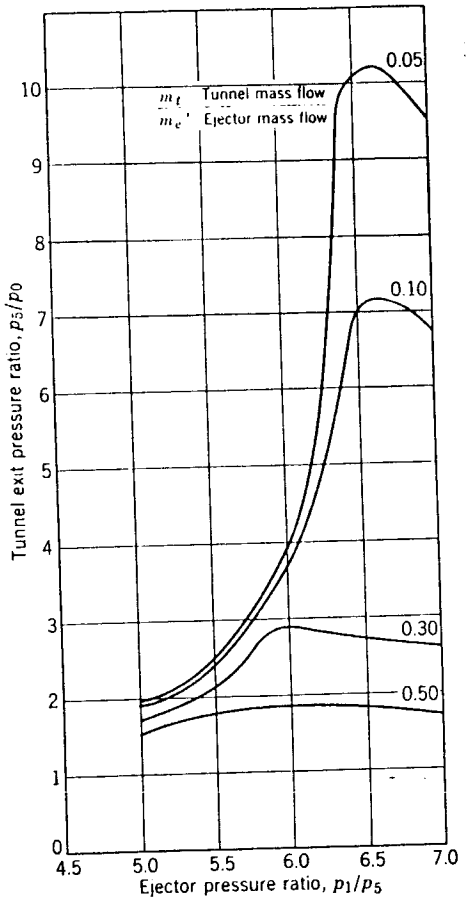


Fig. 2:34 Variation of tunnel exit pressure ratio with ejector pressure ratio and ejector mass flow. $A_3/A_{th} = 8.5$, $L/D = 10.0$ $\beta = 5°$, $S/D = 4.54$ (see Fig. 2:33 for nomenclature).

damage is limited. Provisions must be made to ensure that the drive power cannot force the system to travel until the pod hits the tunnel wall, or the model does. The authors speak with feeling on this point. Finally, though safety and fool-proofing devices are a very important part of wind tunnel design, they can be carried to the point where they are troublesome and fail in their intended purpose. Judgment on the part of the designer is the only prevention for this.

2:28 The Small Classroom Blowdown Tunnel

A satisfactory small blowdown tunnel is not difficult to build, and a discussion of its main features is in order. In essence the tunnel consists of

air drier, compressor, oil cleaner, storage tank, pressure regulator, gate valve, test section, and diffuser. All these items may be purchased new, but if the usual school economy prevails, most of the parts may be obtained used. Typical local sources are given when relevant.

DRIER. Both silica gel and activated alumina are commercially available and cheap and may be used for drying wind tunnel air according to Sections 1:10 and 2:12. The moisture adsorbed may be driven off by electric coil heating. Drying tunnel air may be omitted in many parts of the country as long as the Mach number is kept below 1.6.

COMPRESSOR. The customary filling-station type (150 psi) is adequate. Such compressors have a tendency to put considerable oil into the air-stream, but it may be removed with a porous filter. The filter will work much better if the compressed air is cooled by passing it through a coil of copper tubing before permitting it to enter the filter.

TANKS. Used pressure tanks of the 150-psi range are available in almost all cities for a few hundred dollars for a 160-ft^3 capacity. (This size will permit a 15-second run in a tunnel with a 4-inch-square test section.) According to code requirements the tank must have a safety valve and must be hydrostatically tested to $1\frac{1}{2}$ times the working pressure. Pressure tanks are always a potential source of danger and should be treated accordingly.

PRESSURE REGULATOR. Often a satisfactory pressure regulator may be borrowed from the local gas company. Such a regulator must be selected to withstand the maximum pressure, of course. Such regulators in general work well under much wider limits of volume and pressure than their rated values. Many regulators stabilize in 1 second.

GATE VALVE. A quick-acting gate valve is needed to save precious time in getting the tunnel up to operating Mach number. Gate valves are available at very reasonable cost.

TEST SECTION. The test section must be designed for ease in getting to the model and making changes. Usually the test section will be small, so that doors on both sides may be easily designed. The low pressure usually found in the test section of supersonic tunnels and the consequent large pressure difference from the test section to the room should be kept in mind and care taken that leaks do not occur. When they do the test section Mach number is changed. Although clear plastic may be used for windows in a small installation on a temporary basis, it scratches easily, and glass is preferred.

DIFFUSER. In a small installation the benefits resulting from the ease of getting to the test section without a diffuser usually outweigh the increase of running time with one. Diffusers do, however, reduce the noise. This may be an important point in some installations.

Instrumentation for the tunnel will usually start with manometers for pressure measurements. With such instrumentation, experiments may embrace comparison of Mach numbers as obtained by area ratios, stagnation to static pressure ratios, stagnation to pitot pressure ratios, pressures on simple bodies and comparison with theory, studies of the effects of sting diameters, and elementary diffuser studies.

References

2:1 G. B. Schubauer, W. G. Spangenberg, and P. S. Klebanoff, Aerodynamic Characteristics of Damping Screens, NACA TN 2001, 1950.

2:2 M. Pindzola and W. L. Chew, Jr., A Summary of Perforated Wall Wind Tunnel Studies at the Arnold Engineering Development Center, AEDC TR-60-9, 1960.

2:3 B. H. Little, Jr., and James M. Cubbage, Jr., The Development of an 8-inch by 8-inch Slotted Tunnel for Mach Numbers up to 1.28, NASA TN D-908, 1961.

2:4 S. Timonshenko, *Theory of Plates and Shells*, McGraw-Hill Book Company, 1940.

2:5 Rudolph Hermann, Diffuser Efficiency of Free-Jet Supersonic Wind Tunnels at Variable Test chamber pressure, *JAS*, **19** (6), June 1952.

2:6 J. D. Lee and G. L. Von Eschen, Critical Performance Parameters of an Intermittent High-Pressure Free-Jet Supersonic Wind Tunnel, Ohio State University Proj. 344, 1954.

2:7 William G. Harris and Ralph B. McCormick, Diffuser Investigation in an Axisymmetric Open Jet Hypersonic Wind Tunnel, *BOE*-Q-5, 1959.

2:8 George H. Stokes, Description of a 2-Foot Hypersonic Facility at the Langley Research Center, NASA TN D-939, September 1961.

2:9 J. M. Spiegel, R. U. Hofstetter, and D. M. Kuehn, Applications of Auxiliary Air Injectors to Supersonic Wind Tunnels, RM A 53 T 01, 1953.

2:10 W. G. E. Lewis and J. S. Drabble, Ejector Experiments, National Gas Turbine Establishment, R 151, 1954.

Chapter three

Design of intermittent indraft tunnels

3:1 General

Intermittent indraft tunnels are those that store energy as a pressure difference between a low-pressure tank and the atmosphere. During operation, the air flows from the atmosphere, through the tunnel, and into the vacuum tank, causing the tank pressure to rise. The run ends when the ratio of atmospheric pressure to tank pressure decreases below that required to drive the tunnel. The laws of flow, conditions for starting and running, and need for drying are the same as discussed in Chapter 1. The following are the main components of the intermittent indraft tunnel:

1. A door or valve at the tunnel inlet (sometimes).
2. A large-capacity drier that is capable of drying the air as it is used by the tunnel, or alternatively, a small-capacity compressor, a small high-pressure drier, and a dry air storage balloonet.
3. A settling chamber.
4. A nozzle.
5. A test section.
6. A diffuser.
7. A valve between the test section and the vacuum tank.
8. A vacuum storage tank.
9. A vacuum pump.

Each of these items will be discussed in some detail in the following sections.

3:2 Calculating Run Time

The run time of an indraft tunnel is limited by the rising pressure in the vacuum tank. When the vacuum tank pressure rises to the point where the pressure ratio across the tunnel is not sufficient to operate the tunnel at the desired Mach number, the run comes to an end. If the total pressure of the tunnel, the operating Mach number, and the corresponding pressure ratio required are known, the conditions in the vacuum tank at the end

of the run will be known. To calculate run time, the product of weight flow of air through the tunnel and run time is equated to the change in weight of air in the vacuum tank during the run:

$$\dot{w}t = V_v(\rho_e - \rho_i) \tag{3:1}$$

where $\dot{w}$ = mass flow through tunnel, slug/sec,
t = time of flow, sec,
V_v = vacuum tank volume, ft³,
ρ = mass density in vacuum tank, slug/ft³,
and the subscript e denotes end of run and i denotes beginning of run (initial conditions). Rearrangement of eq. (3:1) yields

$$t = \frac{V_v\rho_e}{\dot{w}}\left(1 - \frac{\rho_i}{\rho_e}\right) \tag{3:2}$$

The conditions in the tank during a run can be represented by a polytropic compression process, so that

$$\frac{\rho_i}{\rho_e} = \left(\frac{p_i}{p_e}\right)^{1/n} \tag{3:3}$$

where p = pressure, lb/ft²,
n = polytropic coefficient (to be discussed later).
Redefining ρ_e using the gas law and combining eqs. (3:2) and (3:3) yields

$$t = \frac{V_v p_e}{\dot{w}R_1T_e}\left[1 - \left(\frac{p_i}{p_e}\right)^{1/n}\right] \tag{3:4}$$

where T_e = temperature in tank at end of run,
R_1 = gas constant, ft²/sec² − °R.
All the air entering the tank will have a temperature approximately equal to the total temperature of the air entering the nozzle, T_t. The flow of air into the tank causes a compression of the air already in the tank with a consequent temperature rise. This has a relatively small overall effect and it is reasonable to assume a final tank temperature $T_e = T_t$. With this assumption, the rate flow from eq. (2:7), and the area ratio from eq. (1:18), eq. (3:4) becomes

$$t = 0.0205\ V_v \frac{(1 + 0.2M^2)^3}{MAT_t^{1/2}} \frac{p_e}{p_t}\left[1 - \left(\frac{p_i}{p_e}\right)^{1/n}\right] \tag{3:5}$$

The polytropic coefficient n in the above equation can only be estimated before the tunnel is operated. The possible variation of this coefficient is from 1.4 for an adiabatic process to 1.0 for an isothermal process. The larger the vacuum tank and the shorter the run time, the nearer this coefficient should approach 1.4. Experimental work by Lukasiewicz (Ref. 3:1) has yielded the following results:

Mach Number	Test Section Size	Run Time	Coefficient, n
1.4 to 2.0	10 × 10 inches	30 sec	1.10
1.0 to 1.6	30 × 16 inches	6 sec	1.20 to 1.24

For computations involving a new tunnel, a value of $n = 1.15$ is suggested. Values of total temperature and total pressure to be used in solving eq. (3:5) should be the values downstream of the drier, since the drier will cause a pressure drop and a temperature rise, both of which are discussed in Section 3:5.

Example 3:1 Compute the run time for an indraft wind tunnel with the following conditions: a 16 × 16-inch test section, initial tank pressure = 0.01 atmospheres, tank volume = 36,000 cu ft, $M = 2.5$, standard day with air temperature at 59°F and a dew point of 33°F, and a typical drier. Neglect the drier pressure drop.

1. From Fig. 1:25 a reasonable value of p_t/p_e for $M = 2.5$ is 2.5. Therefore the end pressure is 14.7/2.5 = 5.88 psia.
2. The initial tank pressure is 0.01 × 14.7 = 0.147 psia.
3. As just suggested, use $n = 1.15$.
4. From Fig. 3:1, a temperature rise through the drier of 20°F is reasonable, resulting in an air stagnation temperature of 460 + 59 + 20 = 539°R.
5. By substituting in eq. (3:5),

$$t = \frac{(0.0205)(36{,}000)[1 + 0.2(2.5)^2]^3}{(2.5)[(16)(16)/144](539)^{0.5}(2.5)}\left[1 - \left(\frac{0.147}{5.88}\right)^{1/1.15}\right]$$
$$= 31.0 \text{ sec}$$

3:3 Air Inlet

The air inlet for an indraft tunnel is usually sized to yield velocities low enough to avoid picking up paper and leaves; a value of 20 mph is probably adequate. A screen of 16 mesh or smaller is also desirable, or even a filter of the furnace type. Fine mesh screens or filters should be backed by a heavier screen for strength. It is also advisable to tip the screen a few degrees outward at the top to make it self-cleaning.

3:4 Upstream Door or Valve

Some method of closing the inlet when the tunnel is not in use is needed to prevent dust from entering the circuit. It is also needed to keep the weather outside the building when the tunnel test section is open. A draft of cold winter air would be most annoying to a person making a model

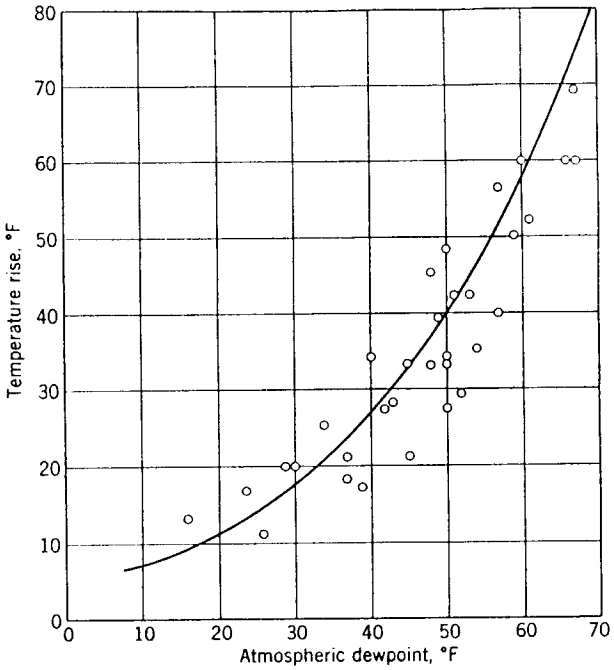


Fig. 3:1 Temperature rise of air passing through a typical indraft tunnel drier.

change in the test section. If the tunnel uses a dry air storage balloonet, a closure is required to prevent dry air leakage from the balloonet into the tunnel. For the purposes mentioned, a door consisting of a simple hinged plate with rubber gasket seals is satisfactory.

Although a valve at the tunnel inlet capable of sealing against the vacuum load is relatively expensive, it is sometimes used to serve the purpose of the door and also to add several advantages to the operation of the tunnel. When such a valve is installed, it is used for starting and stopping the tunnel. The valve between the test section and the vacuum tank is first opened, allowing equalization of the tunnel pressure and the vacuum tank pressure. The upstream valve is then rapidly opened or closed for starting or stopping the tunnel. Such a valve is necessary if operating pressure and hence Reynolds number of the tunnel are to be controlled at all. Partial opening of the valve creates a pressure drop of the air entering the tunnel and hence a reduction in the tunnel Reynolds number.

The possibility of equalizing the tunnel pressure and the vacuum tank pressure prior to a run has two advantages. It can be used as a means for checking the tunnel for leaks. It also serves the purpose of evacuating pressure lines from model or tunnel wall pressure orifices to pressures near

those to be measured during a test. This reduces the time required for stabilization of pressure-measuring manometers or transducers and consequently reduces the run time required to record pressure data.

In existing tunnels, valves in the upstream portion of the circuit are usually commercially available gate valves because of their good sealing qualities. However, butterfly valves are now available with an inflatable gasket that provides a better seal than the standard gate valve. This type of butterfly valve would probably be more practical in this application because it is much easier to obtain rapid operation of the butterfly valve than the gate valve.

3:5 Air Driers

Indraft tunnels may of course, operate without drying the tunnel air. If they do not dry the air, however, the maximum Mach number at which the tunnel can be operated without condensation is about 1.6, and this is possible only on a dry day. If the tunnel air is to be dried, it may be dried slowly over an extended period of time and stored in a balloonet, or it may be dried as it is used. If the first alternative is used, the method used for drying is identical to that described in Section 2:12 for a blowdown tunnel. The drying system consists of a compressor, an aftercooler, an oil filter, a high-pressure drier, a back-pressure valve, and a balloonet for storing the dry air. If the tunnel air is to be dried as it is used, the drier is more often a custom design than an off-the-shelf item and the tunnel designer is intimately concerned with its design.

A schematic drawing of a typical system for drying air as it is used in an indraft tunnel is presented in Fig. 3:2. When the tunnel is operating, dampers at *A*, *B*, and *C* are in the "1" position and the air enters the tunnel circuit, passes through the desiccant bed, and then flows on to the tunnel

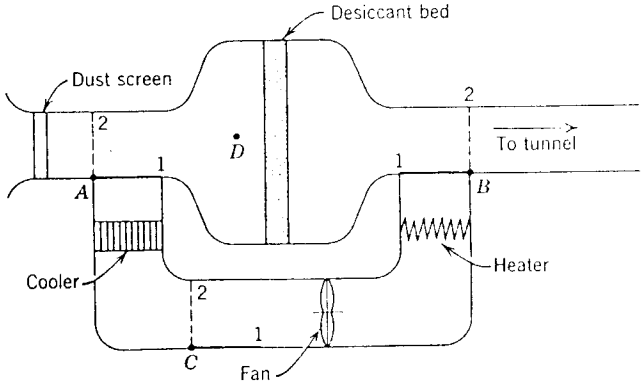


Fig. 3:2 Diagrammatic drier and regeneration circuit for an indraft tunnel.

proper. For reactivation of the drier, the dampers at *B* and *C* are put in the "2" position and the fan and heater are turned on. The fan forces air over the heater. The hot air leaving the heater passes through the desiccant bed and out of the circuit through the tunnel inlet. The air temperature is monitored at *D*, and when the temperature at this point reaches 250°F, the desiccant is hot and the moisture has been driven off. At this point in the reactivation cycle the heater is turned off, the cooler is turned on, and the damper at *A* is moved to position 2 and the damper at *C* to position 1. The fan is reversed and air is continuously circulated through the cooler, through the desiccant bed, and then through the fan. This circulation is continued until the desiccant temperature is reduced to 100°F, and the reactivation cycle is then complete.

The amount of desiccant to be provided for a given installation must be based on two factors, the amount of water to be removed between reactivation cycles and the permissible pressure drop sustained by the air as it passes through the drier. The amount of moisture to be removed should be based on the expected workday with a reasonable use factor for the tunnel. A reasonable value here is to plan to be able to dry for 75 per cent of the maximum possible run time based on the lowest Mach number of which the tunnel is capable (maximum mass flow). The 75 per cent maximum utility is adequate for the most critical condition, since being ready to run the instant the pressure is down is hardly a continuously achievable state. Providing for the low Mach number means plenty of capacity for higher Mach numbers. The amount of moisture to be removed is only rarely a function of locale, since one would want to be able to run on occasional damp days in the driest climate. From Fig. 1:36 a conservative specific humidity can be selected for any part of the country. Multiplication of the total mass of air passing through the tunnel between reactivation cycles by the specific humidity obtained from Fig. 1:36 yields the number of pounds of moisture that must be adsorbed by the drier. Dividing this amount of moisture by 0.02 or 0.03, depending on whether activated alumina or silica gel is to be used, yields the number of pounds of desiccant required in the drier.

A desiccant bed thickness of about 12 inches is normally selected to make certain that no air passes through the bed without coming in contact with the desiccant and to keep the pressure drop across the bed, which is proportional to bed thickness, to a minimum. Knowing the number of pounds of desiccant required and the density of the desiccant (Section 2:12), we can calculate the volume of desiccant. The cross-sectional area of the flow passage in which the desiccant is located is then simply calculated from the volume of desiccant and the thickness of the desiccant bed. A check should then be made to determine the maximum air velocity in the duct approaching the bed. With this air velocity, the pressure drop through the 12-inch-thick bed, in inches of mercury, is then calculated from the following experimentally derived equation:

$$\Delta p = 0.0883(1.715U)^{1.38} \tag{3:6}$$

where U = air velocity at the bed face, ft/sec.

There is no fixed criterion for an acceptable pressure drop across the bed but it should be kept to a practical minimum in order to keep the tunnel Reynolds number as high as practical and to alleviate the structural problem of retaining the desiccant bed. Successful driers have been built for pressure drops as high as 1.5 inches of mercury and this value is suggested as a maximum design value.

If the pressure drop calculated from the duct velocity exceeds 1.5 inches of mercury, corresponding to a velocity of about 4.5 ft/sec, the duct flow area should be increased in order to reduce the pressure drop to an acceptable value. This, of course, would mean increasing the desiccant mass above that needed for the required drying. On the other hand, if the pressure drop calculated is less than 1.5 inches of mercury, the flow area cannot be reduced because the desiccant mass would be inadequate. Note that in the design of a desiccant bed, an allowance should be made for covering about 10 per cent of the bed face by supporting structure.

Trays to hold the desiccant may be made of low-cost structural iron with 10 mesh stainless steel screen to hold the granules. Besides the weight load, the structure should be designed to withstand the pressure load, with a good factor for rigidity, because "working" the trays can cause dusting of the desiccant. In connection with dusting, new desiccant should be sifted before installation to remove the dust caused by shipping.

In most instances the regeneration is accomplished by air, heated by electricity, or by hot gases from natural gas burners, which are blown through the driers. The air (or combustion product) is supplied at about 350°F. Compared with the relatively small high-pressure drier, this drier will have several sources of significant heat loss and these must be considered in the design of the reactivation system. A breakdown showing the various heat requirements of the system together with rough percentages of the total heat based on a six-hour heating cycle follows:

1. to heat adsorbed water, evaporate it, and heat vapor to average temperature of about 250°F, 25 to 40 per cent (about 2000 Btu per pound of water);
2. to make up heat lost in discharged air, 30 to 40 per cent;
3. to heat adsorber to around 300°F, 20 to 30 per cent;
4. to heat up metal of desiccant bed, 2 to 5 per cent;
5. to make up heat lost in ductwork, 2 to 5 per cent.

The total heat requirements in typical driers correspond to 5000 to 7000 Btu per pound of water removed, compared to a figure nearer 2500 Btu per pound of water in a smaller high-pressure drier.

As the air passes through a drier, the adsorption process causes a temperature rise of the air with the result that the air leaves the drier at a temperature above atmospheric. The effect of the drier on the tunnel stagnation temperature is shown in Fig. 3:1 from Ref. 3:2.

3:6 Downstream Valve

A tight-sealing valve is required between the test section and the vacuum tank in order that the test section may be opened and model changes made while the vacuum tank is evacuated. This valve may be either a gate valve or a tight-sealing butterfly valve. If a valve is provided at the inlet end of the tunnel, it is not necessary that the downstream valve be fast acting because the upstream valve will be used to start and stop the tunnel. However, if no upstream valve exists, the downstream valve will be used for starting and stopping the tunnel and it must operate in 1 or 2 seconds.

3:7 Vacuum Tanks and Pumping Time

The size of a vacuum storage tank (usually a sphere) is, of course, a function of the size of the tunnel and the desired run time, and its cost will vary accordingly. At the present time one dollar per cubic foot for medium-sized tanks is not unreasonable. The tank must have a space to enter for inspection and painting, and a low-point drain. Leakage may be very small for a good tank installation. In one instance a 35,000 cubic foot tank had a pressure rise from 0.070 psia to 0.075 psia in 24 hours, certainly a very satisfactory performance.

If the piping from the tunnel diffuser leads straight into the vacuum tank, it is a good idea to install a "model catcher" just inside the vacuum tank to prevent damage to the tank by a heavy model that may come loose during a run. This model catcher should be installed in a way that will prevent any drop in pressure and therefore any decrease in run time. Lines leading from the vacuum tank to the vacuum pump should be arranged in a way that will prevent foreign objects which may get into the vacuum tank from entering the vacuum pump. A high location of the line on the tank together with a fine mesh screen at the line inlet is adequate.

The evacuation of the vacuum sphere takes place so slowly that heat is easily withdrawn from the walls to compensate for the drop in temperature that would normally accompany the drop in pressure. Hence the process may be taken as isothermal. Assuming that the pump withdraws a constant number of cubic feet per minute (a good assumption even with a wide variation in inlet conditions) the pump time becomes

$$t_{vp} = 2.305 \frac{V_v}{k} \log_{10} \frac{p_i}{p_f} \tag{3:7}$$

where p_i = initial pressure in the tank, psia,
p_f = final pressure in the tank, psia,
V_v = storage tank volume, ft^3,
k = pumping rate, ft^3/min,
t_{vp} = pumping time, min.

Example 3:2 Compute the pumping time to reduce the pressure in a 20,000 ft^3 storage tank from 14.7 psia to 0.1 psia if the pumping rate is 1200 ft^3/min:

$$t_{vp} = 2.305 \frac{20{,}000}{1200} \log_{10} \frac{14.7}{0.1}$$
$$= 83.5 \text{ min}$$

The exhaust from the vacuum tank need not be cooled if it is to be dumped into the atmosphere, but may need a cooler if it is to be saved for re-use with a balloonet.

3:8 Balloonets

Instead of being dried as it is used by the indraft tunnel (the usual procedure), the air may be dried by a low-capacity, high-pressure drier and stored in a fast-collapsing balloonet. The decision to use a balloonet is based on cost. Its cost and the cost of a structure to house it can be offset in areas where the cost of the power needed to regenerate a drier is large. This rarely is the case in the United States, but in many foreign countries (The United Kingdom, for instance) balloonets are economically justified. A number of fringe benefits also arise through the use of a balloonet. The air is free of contaminants such as natural or drier dust, it is free of the pressure drop through a drier and the setup is available for the use and recovery of gases other than air if desired.

A good balloonet material is nylon fabric impregnated with neoprene rubber and painted with a flexible aluminum paint. Such a material has a permeability of about 4×10^{-6} pounds of water per square foot per hour, and hence satisfactory dryness cannot be maintained for more than several days if the balloonet is exposed. Two attacks are available for this problem: the ductwork can be arranged so that some of the stored air may be recirculated through the drier, or the balloonet can be housed in a waterproof building. Such a building should be 7 to 10 per cent larger than the filled balloonet. Satisfactory balloonet collapse may be studied with models, a 10 per cent scale being adequate.

Note that an upstream door or valve becomes mandatory when a balloonet is used with an indraft tunnel to hold back the dry air while model changes are being made. Such a door or valve need not be able to withstand the full vacuum load unless it is to be used for starting and stopping the tunnel. Balloonets normally last many years in service.

3:9 Safety

Although the probability of injury is far less with an indraft tunnel than with a blowdown tunnel, since high pressure with its possibility of outward explosion is nonexistent, there are still safety problems that must be met. The most important of these is to make absolutely certain that the downstream valve cannot be inadvertently opened while someone is working on the model. The most direct solution to this problem is to interconnect the test section doors so that the valve cannot be opened unless the doors are closed. While not a safety item, the pressure seals in the nozzle and

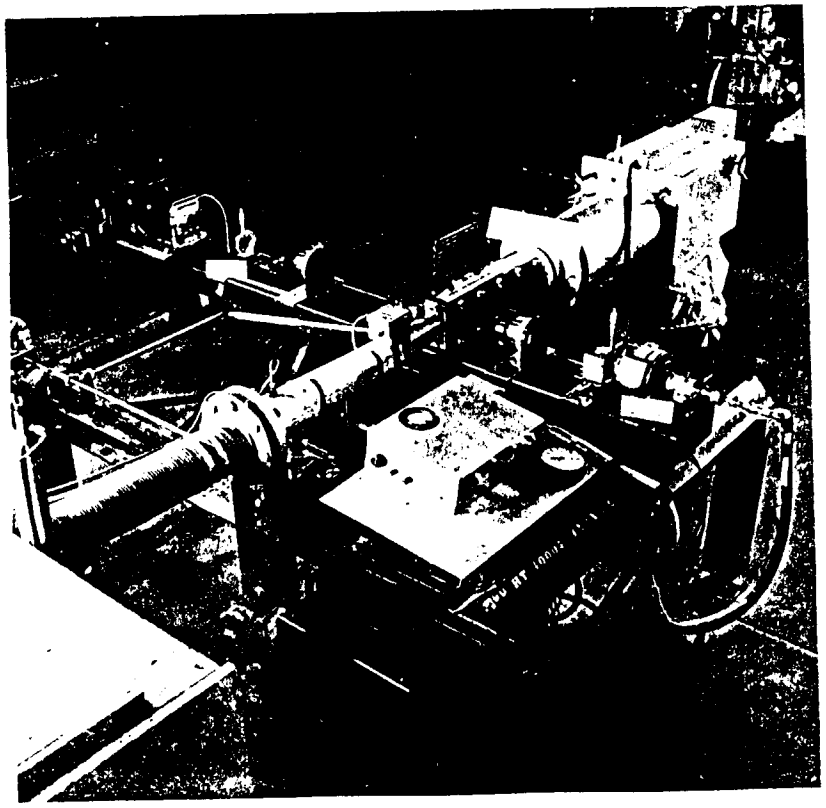


Fig. 3:3 The continuous indraft tunnel at the University of New Mexico.

test section are customarily also in this circuit in order to avoid taking worthless data with leaking seals. Interlocking the seals so that the main valve cannot be opened unless the seals are pressurized is a simple and convenient procedure.

3:10 Small Classroom Indraft Tunnels

A number of small indraft tunnels have been built for classroom demonstration purposes, of both the intermittent and the continuous type. The continuous ones, nominally movable, usually end up with a permanent installation, since the vacuum pumps need a steady flow of water for cooling or sealing or both. This type of tunnel, first used by the Air Force Academy, has no valves and starts when the motor is turned on. The tunnel at the University of New Mexico (Fig. 3:3) has had a small drier added, for even desert dryness is not enough to prevent condensation. Both tunnels, and that at the University of Texas (which is an intermittent tunnel) have test sections around one square inch in area. The experiments mentioned in Section 2:28 are easily run. Indeed, a very fine study of shock-boundary layer interaction was conducted in the University of New Mexico tunnel using exceedingly small pressure probes and measuring stations every few hundredths of an inch.

References

3:1 J. Lukasiewicz, Development of Intermittent Wind Tunnel Technique, AGARD Paper 17, 1954.

3:2 R. T. Patterson, The Design and Performance of an Air Drying System for a Supersonic Wind Tunnel, Navy Report DTMB 80, 1951.

Chapter four

Design of pressure-vacuum tunnels

4:1 General

Pressure-vacuum tunnels are those in which high-pressure air is stored as in blowdown tunnels and vacuum is stored as in indraft tunnels, for tunnel operation. The high-pressure air is introduced into the tunnel and the tunnel exhausts into the vacuum storage vessels. Pressure-vacuum tunnels are used when the pressures required for operating a blowdown tunnel become too high. By exhausting the tunnel to a low pressure, the overall tunnel pressure ratio required for operation at a given Mach number can be achieved at a greatly reduced operating pressure. These tunnels are almost invariably hypersonic tunnels. A drawing of a pressure-vacuum tunnel is presented in Fig. 1:4.

Pressure-vacuum tunnels are usually the same as blowdown tunnels from the air compressors through the pressure regulator valve. Downstream of the regulator valve, heaters are often installed. Normally the heaters are of the heat storage type, which can be charged over an extended period of time. A tunnel start-stop valve is usually located between the heater and the nozzle. Mixers may be required in the settling chamber to provide a uniform temperature of air entering the nozzle. Downstream of the diffuser, an air cooler and a valve for isolating the tunnel from the vacuum tanks are required. In this chapter, only tunnel design features different from those of other types of tunnels will be discussed. One difference will be the probable employment of an axisymmetric nozzle. Although one finds both two-dimensional and axisymmetric types in the low hypersonic range, at the higher Mach number the axisymmetric types have four arguments in their favor: they are easier to fabricate, have less throat distortion, have no high temperature seal problems, and are easier to cool.

4:2 Defining Tunnel Operating Conditions

Tunnel operating conditions are defined by the size of and the initial pressures in the pressure and vacuum storage tanks. An aid in defining

these conditions and therefore in determining the size of the vacuum tanks is obtained by combining equations 2:7 and 3:4 and rearranging to obtain

$$\frac{V}{p_t/p_e} = \frac{28.35A^*T_t t}{T_t^{1/2}\left[1 - \left(\frac{p_i}{p_e}\right)^{1/n}\right]} \tag{4:1}$$

In eq. (4:1) it is assumed that the air entering the vacuum tanks will be cooled to a constant temperature. Note that if the total operating temperature is above about 1000°R, the real gas effects begin to become significant. If eq. (4:1) is used without regard to real gas effects, the error will be less than 3 per cent to total operating temperatures of 3000°R, provided that the actual throat area (rather than a theoretical throat area based on perfect gas area ratio) is used. To illustrate how eq. (4:1) is used as an aid in defining tunnel operating conditions, let us consider the following example.

Example 4:1 A tunnel with a 15-inch test section diameter inside the boundary layer displacement thickness is to be operated at Mach 7 with a total temperature of 1000°R. The run time required is 45 sec. The tunnel air will be cooled to 540°R before it gets to the vacuum tanks. The throat area is

$$A^* = (\pi/4)(1.25)^2/104.1 = 0.01178 \text{ ft}^2$$

The value of n is expected to be about 1.1 (Section 3:2). Since most good vacuum pumps should be capable of evacuating the vacuum tanks to 0.1 psia, eq. (4:1) for this example becomes

$$\frac{V}{p_t/p_e} = \frac{(28.35)(0.01178)(540)(45)}{(1000)^{0.5}\left[1 - \left(\frac{0.1}{p_e}\right)^{0.909}\right]}$$

or

$$\frac{V}{p_t/p_e} = \frac{256}{\left[1 - \left(\frac{0.1}{p_e}\right)^{0.909}\right]} \tag{4:2}$$

The results of eq. (4:2) are presented in Fig. 4:1.

Since the value of $V/(p_t/p_e)$ does not decrease much with increasing p_e at the higher values, it would be practical to pick $p_e = 1.5$ psia as a design point. At this point the value of $V/(p_t/p_e)$ is 280. Then, since a compression ratio of 100 is required to run the tunnel (Fig. 1:25), the resulting sphere volume is 28,000 ft³ and the operating pressure is 150 psia. Now, let us suppose that we want to operate the tunnel at 1000 psia. With a compression ratio of 100 still required, the design value of p_e is 10. At this point the required sphere volume is only 26,000 ft³. Thus, if the sphere

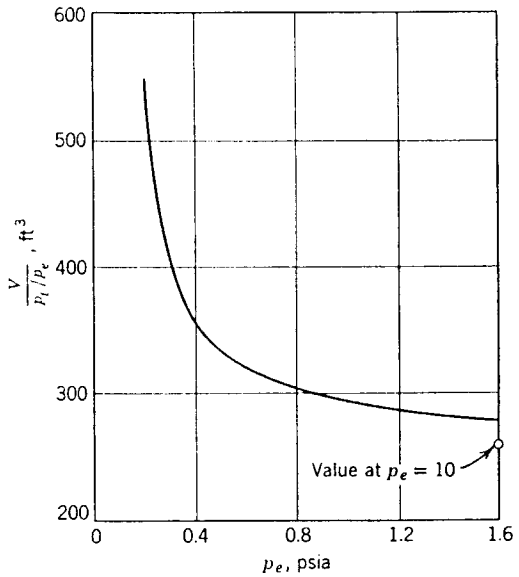


Fig. 4:1 Variation of sphere volume over compression ratio with sphere pressure at the end of a 45-second run at Mach 7 and 1000°R (eq. (4:2)).

volume is defined on the basis of a minimum desired p_t, and consequently a minimum required p_c, sphere volume will not limit the run time at higher values of p_t. The obvious exception to this is the case where the sphere pressure at the end of a run would have to be above the pressure for which the sphere is designed.

The above procedure affords a correspondence between vacuum tank volume and tunnel operation parameters which is a useful guide. However, in the end analysis, the definition of vacuum tank and pressure tank volume and of vacuum pump and compressor capacity and pressure capabilities will depend on many factors discussed in Sections 2:4 to 2:7.

4:3 Storage Heaters

Pressure-vacuum-type hypersonic tunnels normally use storage heaters, of which the most common are of the "pebble-bed" type. In these heaters, thermal energy is stored in refractory pebbles at a relatively slow rate by electrical heating or by a combustion heating process and then transferred from the pebbles to the air at a much higher rate during a relatively short period of wind tunnel operation.

Although storage heaters had been used previously for wind tunnels, the first pebble-bed heater for a hypersonic wind tunnel was developed by the Polytechnic Institute of Brooklyn Aeronautical Research Laboratory.

This heater (Ref. 4:1), which is designed to provide air at temperatures to 3000°R, is illustrated in Fig. 4:2. It consists primarily of a cylindrical pressure vessel lined with insulation, twelve "Globar" (silicon carbide) heating elements in a pattern concentric with the pressure vessel and with a diameter slightly greater than the diameter of the pebble bed, a tubular liner within the pattern of heating elements, a grate at the bottom of the tubular liner, and a bed of aluminum oxide pebbles retained by the tubular liner and resting on the grate at the bottom of the liner. In operation, electrical power to 75 kw is supplied to the 12 Globar heating elements. Heat is transferred from the heating elements to the surrounding refractory primarily by radiation, and from this refractory to the pebble-bed liner and the pebbles within by radiation and conduction. Heating is continued until the pebbles are thoroughly heat soaked. For running, cool air is introduced at the bottom of the heater. It flows upward through the bed of pebbles, absorbing heat, and then goes to the wind tunnel nozzle. A gas-fired pebble-bed heater also designed to supply air at 3000°R is illustrated

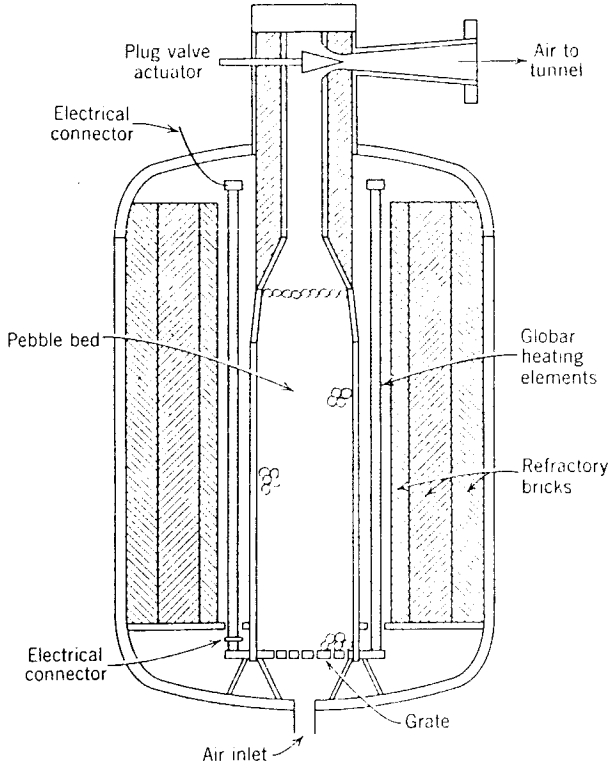


Fig. 4:2 Elements of an electrically heated pebble-bed heater.

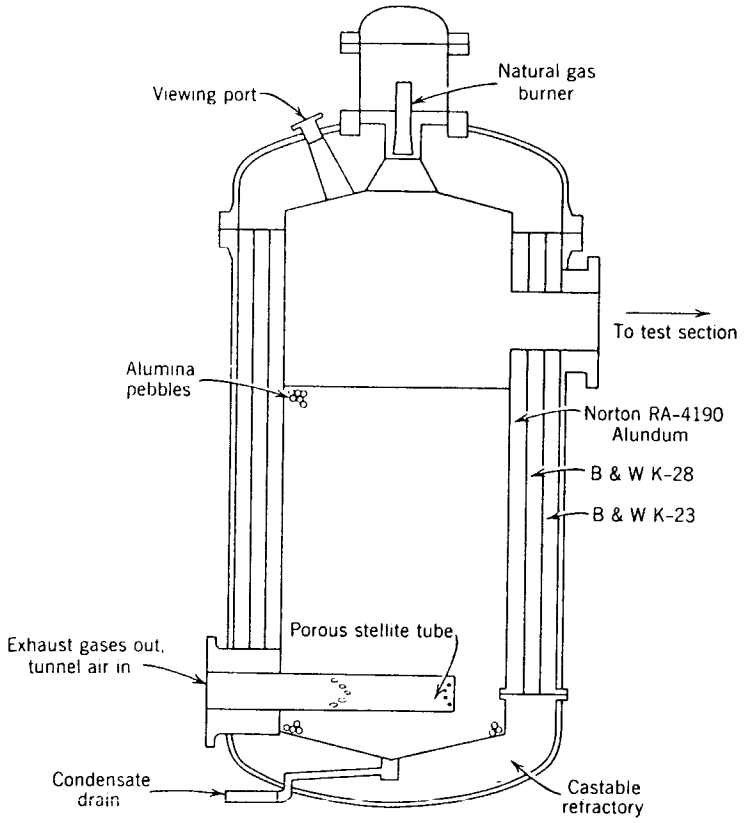


Fig. 4:3 Elements of a gas-fired pebble-bed heater.

in Fig. 4:3. In this heater natural gas and air are burned in the cavity above the pebbles and products of combustion are forced downward through the bed of pebbles during the period of heat soaking the pebbles. The gas-fired heater has the advantages of being more economical to operate and of allowing more rapid heating of the pebble bed. However, the electrically fired heater can provide air with less contamination.

After the development of the first aluminum oxide pebble-bed heater for air temperatures to 3000°R, the NASA developed a zirconium oxide pebble-bed heater for supplying air temperatures to 4000°R. The primary difference between the zirconium oxide and aluminum oxide heaters are the differences in materials; zirconium oxide will withstand temperatures of 4710°F without melting, whereas aluminum oxide will only withstand temperatures of 3660°F. All zirconium oxide pebble-bed heaters are gas fired with oxygen enrichment because suitable electrical heating elements

are not available and combustion of gas with air alone will not provide sufficiently high flame temperatures.

The most important problem in the design of pebble-bed heaters is that of pressure drop. The pebbles in existing heaters of this type are restrained only by gravity. If air flow in the heater causes a pressure drop across the bed sufficient to lift the pebbles, severe damage may be done to the heater and possibly to personnel. The pressure drop per unit bed length has been given by Carmen in Ref. 4:2 as

$$\frac{dp}{dx} = 2.4\left[\frac{\rho U}{\mu S}\right]^{-0.1} \frac{1-e}{e} \frac{\dot{w}^2}{\rho g a^2 d} \tag{4:3}$$

where a = flow area at any cross section of pebble bed, eA, ft²,
e = porosity of pebble bed, ratio of void volume to total volume, dimensionless,
A = cross-sectional area of empty container at subject station, ft²,
g = acceleration of gravity, 4.165×10^8 ft/hr²,
ρ = air density, lb/ft³,
d = pebble diameter, ft,
$\dot{w}$ = flow rate, lb/hr,
U = air velocity in heater bed based on empty container, ft/hr,
μ = air viscosity in bed (Fig. 4:4) lb/ft-hr,
S = area of pebble surface per unit volume of pebble bed, ft⁻¹.

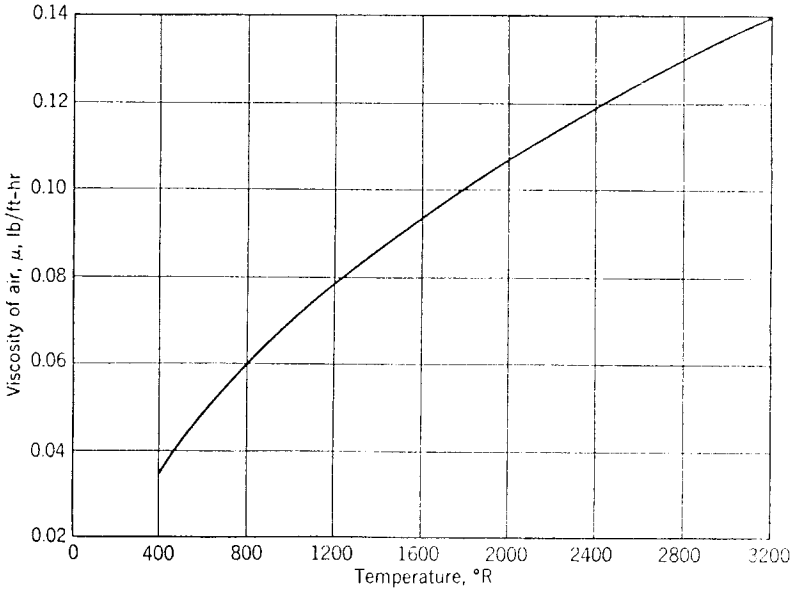


Fig. 4:4 Variation of viscosity of air with temperature.

Carman gives an accuracy of 18 per cent for eq. (4:3) and experimenters have found pressure drops within this range, as shown in Ref. 4:3.

The pressure drop through a pebble bed given by eq. (4:3) increases very rapidly with decreasing porosity e. Consequently, any heater design should include an accurate experimental determination of e. Experiments have indicated that values of e are likely to be near 0.33 in pebble-bed heaters with large bed to pebble-diameter ratios. Because the pressure is dropping and the density decreasing as air progresses through a pebble bed, the pressure drop is highest in the upper portion of the bed, even for cold operation. In heated operation, the density decreases much more rapidly as the air progresses through the bed because of its increasing temperature. Consequently pressure drop calculations are critical in the upper portion of the pebble bed. The pressure drop dp/dx becomes critical when it becomes equal to the bulk density of the pebble bed. (An artifice sometimes employed to reduce the probability of lifting the pebbles is to put a few inches of large pebbles on top of the bed of smaller ones.)

The convection heat transfer rate between spheres and a moving fluid is given by

$$h_c = 0.56 \frac{k}{d}\left(\frac{\rho U' d}{\mu}\right)^{0.6}\left(\frac{\mu C_p}{k}\right)^{0.33} \text{Btu/ft}^2\text{-hr-°R} \qquad (4:4)$$

where k = thermal conductivity of air (Fig. 4:5), Btu/ft-hr-°R,
U' = apparent velocity in bed based on the flow area, eA, ft/hr,
C_p = specific heat of air (Fig. 4:6), Btu/lb-°R.

For refractory pebbles being cooled by an airstream, the surface temperature of the pebbles will be below the average pebble temperature because of the poor conductivity of the pebble material. For precise calculations this effect is sometimes included. However, its use is not usually justified in pebble-bed heater designs.

In pebble-bed heater design it is customary to have pebble-bed depths two or more times that estimated on the basis of heat transfer calculations. One of the main reasons is that the heaters are usually designed for a temperature gradient in the lower portion of the bed so that less exotic structural materials are required for the pebble support grate.

Pebble heaters are frequently designed so that no cooling of the structural shell is required except by radiation and free convection. Adequate insulation can easily be installed inside the shell to prevent shell temperatures from exceeding 300 to 400°F with pebble-bed temperatures of 2500°F. The use of eqs. (4:3) and (4:4) for pebble-bed heater pressure drop and heat transfer design is best illustrated by the following example:

Example 4:2 Determine the dimensions of a pebble-bed heater required to heat 25,200 lb/hr (7 lb/sec) of air from 420°R to 3000°R for

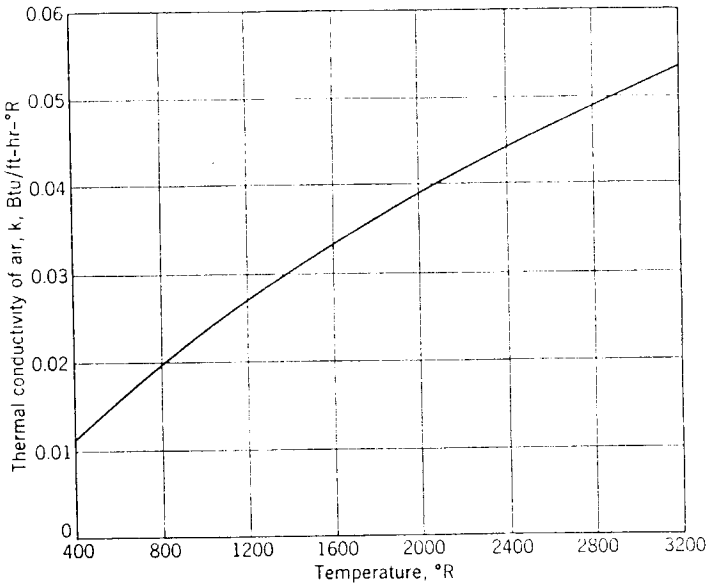


Fig. 4:5 Variation of thermal conductivity of air with temperature.

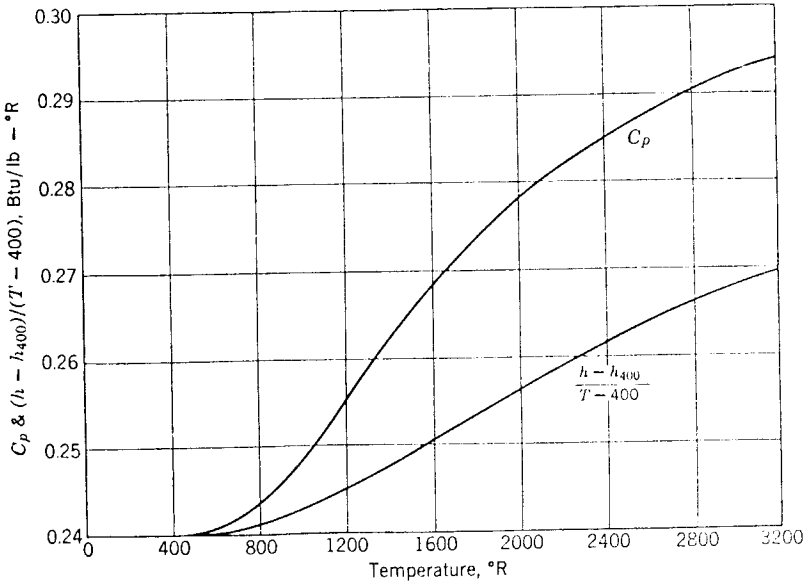


Fig. 4:6 Variation of specific heat at constant pressure and enthalpy function of air with temperature.

0.004 hr (14.4 sec) with a discharge pressure of 86,400 lb/ft². Assume an initial pebble bed temperature of 3100°R.

1. Define the pebble material and size and the porosity of the bed. For this example alumina pebbles are satisfactory. The pebble size will be arbitrarily selected as 0.0833 ft in diameter and the bed porosity will be assumed to be 33 per cent.

2. Determine a bed diameter required to prevent lifting of the pebbles. At the heater exit conditions

$$\rho = \frac{(86{,}400)}{(53.3)(3000)} = 0.54 \text{ lb/ft}^3$$

$$U = (25{,}200)/(0.54A) = 46{,}300/A \text{ ft/hr}$$

$$\mu = 0.0135 \text{ lb/ft-hr} \qquad \text{(Fig. 4:4)}$$

The volume of a sphere is $(4/3)\pi(d/2)^3$ and the surface area is $4\pi(d/2)^2$. For the sphere surface area in each cubic foot of the pebble bed we have

$$S = \frac{(1-e)4\pi(d/2)^2}{(4/3)\pi(d/2)^3} = \frac{6(1-e)}{d} = \frac{(6)(0.67)}{(0.0833)} = 48.2 \text{ ft}^2/\text{ft}^3$$

$$\frac{dp}{dx} = (2.4)\left[\frac{0.54 \times 46{,}300/A}{0.135 \times 48.2}\right]^{-0.1} \frac{0.67}{0.33} \frac{(25{,}200)^2}{(0.54)(4.165 \times 10^8)(0.33A)^2(0.0833)}$$

$$\frac{dp}{dx} = 660/A^{1.9}$$

The weight of alumina is about 240 lb/ft³ so the bulk density of the pebble bed is $0.67 \times 240 = 161$ lb/ft³. If the pressure drop exceeds this figure, the pebbles will lift. Thus the pebble-bed area is calculated for a pressure drop of 161 lb/ft³:

$$A^{1.9} = 660/161 = 4.10, \qquad A = 2.10 \text{ ft}^2$$

and the bed diameter is 1.64 ft.

3. Define constants needed for heat transfer calculations. The pebble surface area in each 1-ft length of the bed is

$$S' = (2.10)(48.2) = 101.2 \text{ ft}^2$$

The weight of pebbles in each 1-ft length of the bed is

$$W_P = (0.67)(2.10)(240) = 338 \text{ lb}$$

The specific heat of the pebbles is $C_{pP} = 0.24$.

4. Construct a graph of the variation of the heat transfer rate from eq. (4:4) with temperature. This graph is presented in Fig. 4:7.

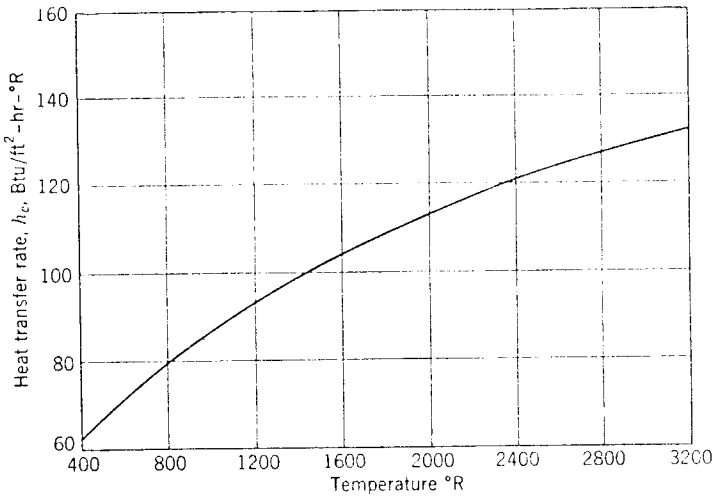


Fig. 4:7 Variation of heat transfer rate with air temperature for pebble-bed heater, example 4:2.

5. Set up heat balance equations for a 1-ft length of the bed. The heat added to the air in heating it from one temperature to another is:

$$Q_a = \dot{w}t\left[\frac{h_e - h_{400}}{T_e - 400}(T_e - 400) - \frac{h_i - h_{400}}{T_i - 400}(T_i - 400)\right] \text{ Btu,} \qquad (4:5)$$

where t = run time, hr,

h = air enthalpy, Btu/lb from Fig. 4:6,

and the subscript e denotes exit conditions and i denotes inlet conditions. The heat removed from the pebbles is

$$Q_P = W_P C_{pP}(T_{P0} - T_{P1}) \qquad (4:6)$$

where 0 denotes conditions at beginning of run, 1 denotes conditions at end of run, and P denotes pebbles.

The heat transferred from the pebbles to the air by convection is

$$Q = h_c S' t(T_{P(\text{ave})} - T_{\text{ave}}) \qquad (4:7)$$

where the subscript ave denotes average of initial and final pebble temperatures and average of inlet and exit air temperatures.

6. Rewrite eq. (4:5) to (4:7) including constants

$$Q_a = 101\left[\frac{h_e - h_{400}}{T_e - 400}(T_e - 400) - \frac{h_i - h_{400}}{T_i - 400}(T_i - 400)\right] \qquad (4:8)$$

$$Q_P = 81.1(T_{P0} - T_{P1}) \qquad (4:9)$$

$$Q = 0.405h_c(T_{P(\text{ave})} - T_{\text{ave}}) \qquad (4:10)$$

Table 4:1

Pebble-Bed Heater Calculations

T_r	$\frac{h_r - h_{100}}{T_r - 400}$	$h_r - h_{100}$	$h_e - h_i$	Q_a	T_{ave}	h	$T_{P(ave)} - T_{ave}$	$T_{P(ave)}$	$T_{P0} - T_{P1}$	T_{P1}	$T_{P(ave)}$
First 1 Foot of Length											
$T_i = 420$	1600	0.250	300	29,800	1010	87.0	847	1857	367	2733	2917
$\frac{h_i - h_{100}}{T_i - 400} = 0.240$	2000	0.256	409	40,900	1210	93.5	1080	2292	504	2596	2848
	2400	0.261	522	52,200	1410	99.0	1301	2711	643	2457	2779
	2800	0.266	638	63,900	1610	104.0	1512	3122	786	2314	2707
$h_i - h_{100} = 5$	*2455	0.262	537	53,700	1437	99.5	1335	2772	662	2438	2769
Second 1 Foot of Length											
$T_i = 2455$	2500	0.262	550	1,210	2477	122.0	25	2502	15	3085	3092
$\frac{h_i - h_{400}}{T_i - 400} = 0.262$	2800	0.266	638	10,100	2628	125.0	199	2827	124	2976	3038
	3200	0.269	754	21,800	2828	128.0	421	3249	268	2832	2966
$h_i - h_{400} = 538$	*2970	0.267	686	14,900	2712	126.0	292	3004	184	2916	3008
Third 1 Foot of Length											
$T_i = 2970$	3000	0.268	697	1,110	2985	130.0	21	3006	14	3086	3093
$\frac{h_i - h_{400}}{T_i - 400} = 0.267$	3100	0.269	727	4,140	3035	130.5	78	3113	51	3049	3075
	3200	0.269	754	6,870	3085	131.0	129	3214	85	3015	3057
$h_i - h_{400} = 686$	*3070	0.268	715	2,930	3020	130.0	56	3076	36	3064	3082

* Solution suggested by interpolation

7. Select several exit air temperatures between the inlet air temperature and the initial pebble temperature.
8. At each of these exit air temperatures
   a. Read values of the enthalpy functions of eq. (4:8) from Fig. 4:6.
   b. Solve eq. (4:8) for Q_a.
   c. Determine the average of inlet and exit air temperatures, T_{ave}.
   d. Read a value of the heat transfer rate corresponding to T_{ave} from Fig. 4:7.
   e. Set $Q = Q_a$ and solve eq. (4:10) for $T_{P(ave)}$.
   f. Set $Q_P = Q_a$ and solve eq. (4:9) for T_{P1}
   g. Calculate $T_{P(ave)}$ from $T_{P(ave)} = (T_{P0} + T_{P1})/2$
   h. Compare $T_{P(ave)}$ from items 8e and 8g. The equations are solved at the final air temperature for which these two values are equal.
9. Use the final air temperature from item 8h as the inlet air temperature for the second 1 ft length of the pebble bed and repeat items 7 through 9. Continue until the final air temperature is at the desired value. Samples of the above calculations are presented in Table 4:1. It is noted in the table that the air slightly exceeds the design temperature on leaving the third 1-foot layer of pebbles, indicating that somewhat less than 3 feet would have gotten the air to the design temperature.

Unfortunately, though it is not obvious, there is a way in which a gas-fired pebble-bed heater can put water into the air stream: During the heating cycle large amounts of water from the products of combustion pass into the pebble bed. The water that condenses on the initially cool pebbles in the bed is boiled away as the pebbles heat up. But near the walls the insulation is cool and stays cool and wandering currents of the products of combustion deposit moisture in the insulation which is not boiled off by heating. Also moisture will condense in the cool piping leading to and from the heater. Some of this gets picked up by the dry air during a run, and moist air is then delivered to the test section. A cure for this is "vacuum-boiling," that is, connecting the hot pebble heater to the vacuum supply for a period before the run. At one tunnel, one hour at 0.2 psia yields a satisfactory moisture level. Since electric heaters introduce no moisture into the system, they do not have this problem.

High-speed tunnels exhibit considerable sandblasting of the models being tested which varies from acceptable to extremely serious. Originally believed to be pebble particles broken off by bed movement, recent experience with both pebble and electric rod heaters suggests that the loose material is probably insulation. At some tunnels each usable run

is preceded by a dust removal run, a dolorous situation indeed. Force and pressure data are believed to be unaffected, but some concern is felt about heat transfer studies. A simple dust removal system that works well for continuous tunnels is in use at Tunnel S2 of the French ONERA. It consists of a small airscoop which continuously leads a small percentage of the tunnel air into a still air chamber where the dust drops out. The air is subsequently returned to the tunnel circuit.

4:4 Tunnel Start-Stop Valves

If the pressure-vacuum tunnel includes a pebble-bed heater, it is necessary to have a tunnel start-stop valve between the heater and the tunnel. Without the valve, starting the tunnel would entail a dynamic increase of pressure across the bed, which could cause pebble lifting. With the valve, the heater may be pressurized slowly. The alternative of starting the tunnel slowly is unacceptable from the standpoint of wasting run time.

With combustion heaters, there is a second reason for such a valve. Products of combustion include a great deal of water vapor. Without the valve large quantities of water vapor will get into the tunnel circuit and condense out on cool surfaces. This presents a considerable problem from the standpoint of maintaining dry air and also from the standpoint of designing all portions of the tunnel for corrosion resistance.

While such valves are almost a necessity in pressure-vacuum tunnels with pebble-bed heaters, good and reliable valves for the job are difficult to obtain. A low leakage rate is desirable to prevent pressure buildup in the vacuum tanks during the heater filling process. The valve is usually close to the heater cavity and must withstand a severe environment during both the heater firing and the tunnel running. It must be a quick-operating valve. These requirements are more than most commercial valve manufacturers care to tackle. Valves that have been used in this application include plugs that are driven into the nozzle inlet, sliding blades, and quarter-turn plug valves.

4:5 Thermal Mixers

In almost all hot air tunnels, the problem of designing so that the air will have a uniform temperature distribution as it enters the tunnel is a difficult one, particularly if the tunnel is to have a wide range of operating conditions. This problem is especially severe in pebble-bed heaters such as that of Fig. 4:3. With pebble-bed temperatures of 1000 to 2000°F and low operating mass flows, temperature stratifications to several hundred degrees in magnitude have been indicated in the head cavity near the heater outlet. If large temperature gradients due to stratification in the heater or in other sections of the circuit are allowed to persist until the air



Fig. 4:8 Cone-type thermal mixer for hypersonic wind tunnel settling chamber.

enters the nozzle, uniform test section flows cannot be expected. Hence, the need for thermal mixers.

A thermal mixer that is effective in this application is shown in Fig. 4:8. It is simply a cone frustrum with the apex facing downstream and with a series of holes in a plane along the horizontal centerline. It is positioned two or more duct diameters upstream of the nozzle inlet. The hole design is such as to provide accelerations of the air to Mach 0.2 or more as it passes through the holes.

Bringing hot air from the top and cold air from the bottom of the duct together, squeezing it through the small holes on the duct centerline, and then putting it through a turbulent mixing process apparently does a good job of mixing. The effectiveness of this type of mixer is illustrated in Fig. 4:9. A side benefit is a reduction in temperature fluctuations.

These mixers, like any mixers, have disadvantages. They create a pressure drop and a temperature loss that can be minimized by using low heat capacity (thin wall) design. They cause a high level of turbulence in the duct. Attempts to remove this turbulence by using screens has, at least in some cases at high temperatures, been quite disappointing. In these cases, the screens introduced additional temperature gradients. Thermal mixers begin to approach impracticality from a materials

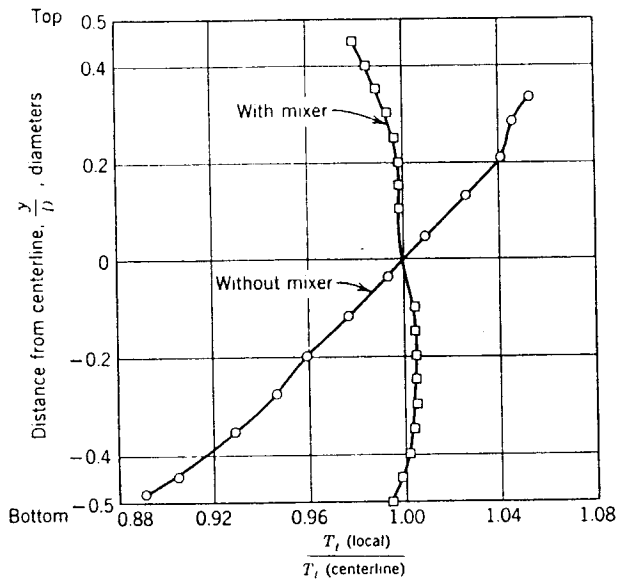


Fig. 4:9 Vertical distribution of temperature in settling chamber of a pebble-bed heated hypersonic wind tunnel with and without a thermal mixer. Heater temperature = 1500°F. Velocity in settling chamber = 22 fps.

standpoint at the higher temperatures of aluminum oxide pebble-bed heaters. No attempts at mixing with the higher temperatures of zirconia heaters are known.

4:6 Circuit Cooling

The rates of component heating in a pressure-vacuum tunnel are the same as those for a continuous tunnel operating at the same conditions. However, there is a major difference in that the pressure-vacuum tunnel will be subjected to these heating rates for periods of only several seconds. This allows a more simple and less expensive approach to the problem of cooling practically all tunnel components except the nozzle throat. For sections of the tunnel where heating rates are moderate, a heat sink (thick wall) design can be used. In this design, sufficient mass is provided so that the temperature rise during a run will not be a problem. The cooling is accomplished between runs by radiation and free convection. External fins or ribs will increase the rate of cooling.

Essentially any high-temperature tunnel will require water pumps for water cooling various hot spots, and it is well to bear in mind that either the electricity or the water (or both) may fail during a run. The consequences of such a failure can run into the tens of thousands of dollars,

and it is good design practice to prepare for it. An air turbine with an automatic switch-over arrangement can supplant the loss of electricity, and a water tower can supply the needed water. In either case it is not necessary to have the emergency supplies for more than stopping time.

4:7 Air Coolers

Air coolers of some sort are required in hot air pressure-vacuum tunnels. The amount of heat entering the vacuum tanks during a run is not usually sufficient to cause dangerously high tank wall temperatures. However, if the air is not cooled before it enters the vacuum tanks, the rate of pressure rise in the tanks will be relatively high because of the high temperature and the relatively large volume of air. The result will be a greatly increased vacuum tank volume required for the same run time.

Frequently if not usually, intermittent coolers are used. An intermittent cooler may consist of banks of metal rods similar in arrangement to those in the water cooler described in Section 5:3. These rods are solid instead of hollow and include sufficient mass to absorb the heat required during a run without reaching excessive temperatures. The design of a cooler of this type differs from that of a water cooler primarily in that the heat increase of the rods during a run must be considered.

Another scheme for cooling that has been used is the installation of a large number of tin cans in the first of three vacuum tanks. The air entering the vacuum tanks is cooled during its passage through the mass of cans (Fig. 1:4). The cans are quite inexpensive and easy to install.

Spraying water into the hot air stream, while being the most effective and simple means of cooling, has very significant disadvantages. These arise from the large volume of vapor created by the water, which causes the vacuum tank pressure to rise more rapidly. It also presents problems from the standpoint of evacuating the tanks following a run, and, of course, corrosion.

4:8 The Tunnel Circuit

The circuit of a pressure-vacuum tunnel requires most of the features of the blowdown tunnel and of the indraft tunnel. A valve is required between the tunnel and the vacuum tank in order that the tunnel may be opened with the tanks evacuated. A blowout patch is necessary between the vacuum valve and the tunnel start-stop valve to prevent inadvertent over-pressure in the circuit. If the tunnel is a hot air tunnel, bellows or sliding seals must be provided to allow for thermal expansion.

The increased hazard for personnel working on models in high-temperature wind tunnels has been greatly reduced by two features: some tunnels draw back the test section to expose the model ("railroad" tunnels), and

some are arranged for model injection. The latter provide a pressure-tight model box exterior to the tunnel and sealed off from it during tunnel start. After the tunnel is started a door is opened and the model is injected into the established airstream, using a mechanism with suitable shock absorbers so that inertia loads are not excessive. While a little more advantageous with continuous tunnels than with intermittent tunnels, model injection is an excellent feature that should be studied for every design. Its advantages are as follows:

1. Tunnel start is not limited by the presence of the model and its support strut.
2. Models and balances are not subjected to high starting and stopping loads.
3. Model installation is accomplished outside the tunnel.
4. Heat transfer tests do not need model shoes, and the model may easily be cooled between runs.
5. Tunnel flow may be maintained between runs (this is of interest only for continuous tunnels).

4:9 Design of Low-Density Tunnels

Low-density tunnels differ little in principle from other types of tunnels. However, both their purpose and their actual design are quite specialized. As the name implies, the purpose of the low-density tunnel is to allow experiments to be performed in rarefied air flows such as those which would exist during flight at very high altitudes. In this section a definition of what constitutes a rarefied air flow will be given and some of the unusual aspects of low-density tunnel design will be discussed.

Air consists of molecules, the number of which in any volume is dependent on the air density. Conversely, it may be said that each molecule occupies a specific volume. The molecules have a definite size and are in continuous motion. As each molecule moves in its random path it sweeps out a volume that is equal to the product of its cross-sectional area and the distance it travels. Speaking in terms of averages, when the volume swept out by a molecule equals the specific volume occupied by each molecule of the air, the molecule will collide with another molecule. The distance that the molecule must move before this occurs is called the mean free path. The mean free path is an important parameter in the definition and analysis of rarefied air flows and a plot of mean free path in the atmosphere as a function of altitude is given in Fig. 4:10 (Ref. 4:4).

At moderate altitudes, the mean free path of a molecule is microscopic. Any molecule striking a body passing through the air at these conditions will absorb momentum from the body and will be reflected from the body.

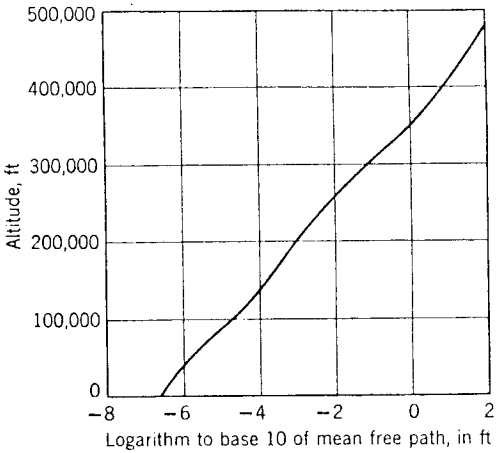


Fig. 4:10 Variation of molecular mean free path of air with altitude; Ref. 4:4.

Upon being reflected, the molecule will collide with another molecule after passing through a microscopic distance and will impart momentum to it. A chain reaction of molecular collisions will be set up in which the momentum imparted by the body is diffused throughout the air in the vicinity of the body. Flow of this type is called "continuum" and is the type that is assumed in all other sections of this book.

At very high altitudes (~100 miles) the mean free path of a molecule is several feet. Any molecule striking a body passing through the air at these conditions will, upon being reflected, travel several feet before it collides with another molecule. In other words, the effect of intermolecular collisions at these conditions has no effect at all on the air in the vicinity of the body, and the theory of continuum flow no longer is valid. When these conditions exist the flow is called "free molecule" flow.

Between these two extremes, two additional flow regimes are defined in the kinetic theory of gases. One, the "slip flow" regime, is that in which the mean free path is a few per cent of some characteristic length, such as the boundary layer thickness. In this regime, the flow field is predominantly determined by intermolecular collisions. However, there will be a number of molecules in the layer immediately adjacent to the body which do not receive momentum from the body and consequently do not contribute to the effect of the body on the flow field. The other regime, called "transition flow," is that between "slip flow" and "free molecule" flow. In this regime, the mean free path is of the same order as a typical body dimension and the effects of body surface and intermolecular collisions are of comparable importance. The "slip flow," "transition flow," and "free molecule" flow regimes are varying degrees of rarefied air flows.

The ratio of mean free path to a characteristic body length, which is the factor of importance with regard to defining the flow regime, is called the "Knudsen" number. Knudsen number has been defined as

$$K = 1.26(M/RN)\sqrt{\gamma} \qquad (4:11)$$

where K = Knudsen number,
γ = specific heat ratio,
M = Mach number,
RN = Reynolds number based on the same characteristic length as K.

Whereas the principle of design of a wind tunnel for studying the aerodynamics of rarefied flows do not differ greatly from those previously discussed, the low-density tunnel takes on an entirely different appearance and its design presents new problems.

A low-density tunnel as illustrated in Ref. 4:5 is primarily a large number of vacuum pumps connected to a vacuum chamber. The nozzle, test section, and supply system appear almost incidental when compared to the necessary large size of the pumps. One of the primary problems in the design of a low-density tunnel is that of designing a system which can be evacuated to very low pressures. The following are items of importance with regard to mechanical design features:

MATERIALS. Many materials that could be used in an unprotected form for the tunnel structure as far as strength is concerned, have poor sorption qualities. The oxides and hydroxides of iron and copper alloys, for instance, are hydroscopic and take up moisture upon exposure to atmospheric air. The removal of this moisture by diffusion is a slow process, and it is advisable to coat these substances with a low vapor pressure varnish. Other materials, such as glass, plastics, and rubbers, do not appear to cause trouble.

FABRICATION. Obviously, for the required internal pressures, leaks will not be tolerable, and when possible all joints should be welded or brazed. It is good practice to make all welds of the single-pass, continuous type with rather generous overlaps, rather than double welds (inside and outside passes), which could leave pockets of high-pressure air to bleed in like leaks. Thorough cleaning of the flux from the joint after welding has also been found necessary.

GASKET JOINTS. The joints for removable parts must be gasketed of course, and here the usual O-ring and round and square cord continuous gaskets have been found satisfactory. The sealing material may be nearly any of the synthetic compounds such as Neoprene, Hycar, or Silicone, and grooves that allow for 30 per cent diametrical deformation of round cross section gaskets or 10 per cent deformation of square cross section

material have been found satisfactory. For larger joints double gasket grooves may be used with a venture pipe between the seals to monitor any leaks. Motion seals with O-rings have been found satisfactory.

The evacuation system for maintaining very low densities in the tunnel is a considerable design problem. Commercial vacuum equipment in the form of mechanical pumps and mechanical oil diffusion pumps in series is readily obtainable with a minimum pressure capability of about one micron (one millionth part of a meter of mercury) or less. This pressure is low enough for studies of rarefied air flows. However, pumps with adequate capacity to handle flows through a nozzle at these very low pressures can be relatively large and expensive. Refrigeration has been used as an aid in reducing the pumping problem. If the air entering the vacuum chamber can be liquefied and frozen, its contribution to pressure in the chamber will be negligible.

The nozzle also presents a design problem. Low-density flows are conducive to thick boundary layers on nozzle walls. At very low densities, boundary layers can easily fill the large part of a nozzle. High Mach number nozzles are much worse in this respect than low Mach number nozzles. Refrigeration of the nozzle walls to freeze the boundary layer has been shown to be of help in solving this problem.

Substantial help in this specialized area will be found in Ref. 4:6.

References

4:1 Martin H. Bloom, A High Temperature Air Heater (Suitable for Intermittent Hypersonic Wind Tunnel Operations), WADC Technical Note 55-694, 1956.

4:2 P. C. Carman, Fluid Flow Through Granular Beds, Transactions Institute of Chemical Engineers, London, **15** (1937) p. 150.

4:3 D. E. Randall and S. S. Millwright, Experimental Determination of the Pressure Drop Through a Pebble Bed, Sandia Corporation SC-4354(TR), September 1959.

4:4 R. A. Minzer, W. S. Ripley, T. P. Condron, U.S. Extension to the ICAO Standard Atmosphere, Tables and Data to 300 Standard Geopotential Kilometers, U.S. Government Printing Office, 1958.

4:5 Ruth N. Weltmann and Perry W. Kuhns, Heat Transfer to Cylinders in Crossflow in Hypersonic Rarefied Gas Streams, NASA TN D-267, 1960.

4:6 L. Bernstein, Design Performance of the NPL Low Density Wind Tunnel, ARC 23, 234, September 1961.

Chapter five

Design of continuous closed-circuit tunnels

5:1 General

The advantages and disadvantages of the continuous closed-circuit wind tunnel over other types have been discussed in Section 1:1 and will not be repeated here. Let us say, however, that every wind tunnel engineer would like to have minutes of uniform flow test time instead of the seconds normally available in the intermittent tunnels. This would allow him to easily make some tests which are very difficult in intermittent tunnels, would give him time during a run to check data and repeat if necessary, and would reduce the problems he has in obtaining accurate measurements, particularly of pressure.

There are several aspects of the design of continuous high-speed wind tunnels that are in addition to or different from those of the blowdown and indraft tunnel. Probably the most important of these is the air supply problem. The compressor installation of the blowdown tunnel air supply system pumping continuously from an atmospheric inlet pressure to a constant discharge pressure will not suffice. For a tunnel with a significant Mach number range, the required operating pressures and mass flows vary widely, and a great deal of flexibility is required in the compressor installation.

The compressor for the continuous tunnel is adding energy and consequently heating the air continuously. Compressors used for continuous tunnels generally do not come equipped with aftercoolers for removing the heat of compression, so that a special cooler is usually required. Without such a cooler, the air temperatures in the circuit would rise continuously and the flow conditions of the test section would change accordingly. Also the circuit piping and the compressors would overheat.

The continuous tunnel may operate at hypersonic Mach numbers as well as at the lower Mach numbers that are common to blowdown and indraft tunnels. For hypersonic operation, the air must be heated upstream

of the nozzle to prevent liquefaction during the expansion in the nozzle (Section 1:11). When the air is so heated it must be cooled downstream of the nozzle to the point where the tunnel piping will not overheat and where the air can be safely handled by the compressors. Between the heater and the cooler, provisions must be made for continuously cooling all structural components. Major differences also exist between the piping and valving and the air drying system of continuous and blowdown or indraft tunnels.

The above design aspects of continuous tunnels will be discussed in the following sections. There are some very large (up to 16-foot test sections) continuous high-speed tunnels currently in operation. Tunnel design problems that are strictly the result of size, such as the design of special compressors, will not be included herein.

5:2 Compressors

The majority of continuous high-speed wind tunnels are driven by either axial flow or centrifugal compressors. These types of compressors are inherently high-speed machines designed especially for high-capacity flows, such as those required by the steel industry. They are normally driven by steam turbines or variable-speed electric motors. Although considerably less versatile, positive displacement piston and rotary sliding vane compressors have been used.

If the compressors are to be used for tunnels where the range of required operating conditions is limited, such as in a transonic tunnel, a single compressor is adequate. However, for operation over a large Mach number range, the compressor installation may have to be staged. This arises from the need for high pressure ratios and low mass flow for hypersonic tunnels compared to low pressure ratios and high mass flows for transonic operation. For example, three comparable compressors might be operated in parallel to obtain a high mass flow with a compression ratio of 3.0 for tunnel operation at one Mach number. For tunnel operation at a higher Mach number, these same three compressors could be rearranged with two in parallel discharging into the third, with the result of a lower mass flow at a higher pressure. Up to seven stages of compression are used in large hypersonic tunnels, where each compressor or parallel group of compressors is considered a stage.

When compressors are to be operated in series the volumetric flow capacities of each stage in the series must be carefully matched. This can be illustrated by considering the case of two positive displacement compressors in series. If the second-stage compressor has a greater capacity than the first-stage compressor, the pressure at the second-stage inlet will be reduced from the design discharge pressure of the first compressor

until the volume handled by the second stage corresponds to its displacement. On the other hand, if the second-stage compressor has a smaller capacity than the first-stage compressor, the inner-stage pressure would have to increase. Thus, if the two compressors are not properly matched, the efficiency of compression will suffer and it will be possible to achieve dangerously high inner-stage pressures. With centrifugal or axial flow compressors, dangerously high inner-stage pressures are not as likely because of the inherent "slip" possible in the flow through the compressors. However, if the two stages are not properly matched, the loss in efficiency can be quite severe. Also if the stages are not matched within limits, the range of stable operation of one of the compressors is likely to be exceeded, with the result that it will "surge" (rapidly speed up and slow down with a constant power input). This surge condition normally occurs when the flow into a compressor is somewhat less than that for which the compressor was designed at a given operating speed.

Compressors and compressor systems are seldom designed by the wind tunnel engineer and their design is consequently beyond the scope of this book. The primary responsibility of the tunnel designer is to specify accurately the required range of operating pressures and mass flows and then to make sure that he gets a compressor installation that will satisfactorily meet these specifications at a minimum cost.

The type of information that a compressor manufacturer will require before he can propose a compressor system is illustrated in Fig. 5:1. It is emphasized that the accuracy of compression-ratio–flow-rate data is extremely important. If the specified conditions are not adequate, the tunnel will not operate. On the other hand if the requirements are overly conservative the cost will be correspondingly high. In determining compression ratio requirement for continuous supersonic tunnels, the most important consideration as in blowdown tunnels is the efficiency of the diffuser. Pressure losses in the diffuser typically account for over 90 per cent of the total pressure losses in high Mach number tunnels. This is not true for nearsonic or transonic tunnels, however, where shock wave losses are small. In such tunnels, the losses in the ducting and the turns may be a larger portion of the total pressure losses, and it is then important to make every effort to minimize these losses.

In the event that a wind tunnel designer is called upon to prepare specifications for a new compressor system, the following items are noted as having given trouble to other wind tunnel engineers:

1. The manufacturer may not have enough power available to run the compressor up to full load. Definition and responsibility for performance should hence be carefully spelled out.

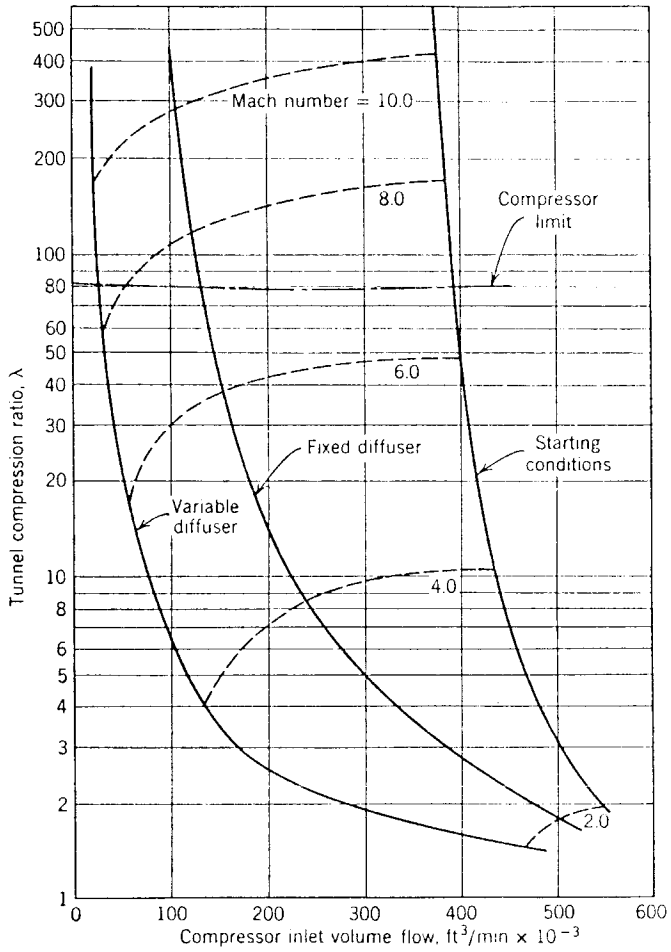


Fig. 5:1 A chart used for selecting a compressor for one particular tunnel.

2. It may also not be possible to check the oil seal performance until tunnel installation. Responsibility for this should also be spelled out.

3. It should be determined that compressor surge will not occur in the tunnel operating range.

4. The compressor manufacturer should be given the desired range of pressure and volume requirements for both starting and running, and his suggestions for achieving them should be considered. Minor changes in the specifications that would result in material decreases in cost should be solicited.

5. In commercial use, a compressor can rarely be subjected to more

than its own pressure, but in a wind tunnel this is not true; compressors frequently get shock loads from sudden valve closures and they may, in series operation, get far more than their rated pressure. Accordingly, another design parameter the manufacturer will need is the location of the compressor in the tunnel circuit and the type of operation or use that is likely to subject the compressor to maximum loads.

6. The compressors should be able to start and run under all possible tunnel conditions, at both high and low pressures. Depending on the tunnel design, it may be desirable to specify that the compressors can be run at idle against closed valves in order to "warm up" the compressor and drive system for use without air flow through the circuit.

7. Since the intake of the compressor will in all probability be below ambient pressure, it should be specified and demonstrated that the casing is free from leaks which would permit wet outside air to enter the tunnel.

The cost of the compressor in a supersonic tunnel usually justifies an expenditure in both installation and power to prevent failure of a model or failure to remove all tools and materials from the test section before starting the tunnel from causing serious damage to the compressors. Protective measures usually take one of two forms: grids and screens, or sumps.

a. Grids and screens. A good location for a model-catcher screen is at the trailing edge of the second set of corner vanes, since by the time the flying part reaches this point, it will have been slowed by contact with the corner guide vanes. When the vane and screen system is used it is necessary to add some cross members in the vane system so that large pieces may not turn and pass through. An alternate arrangement, which protects the corner vanes as well as the compressor, is a model breakup grid just ahead of the first turn. Such a grid costs power of course, but in all but the largest installations where 1 per cent is still a large absolute number, the loss is quite negligible. A breakup grid should be made of continuous bars, notched and welded at the crossovers, since the possibility of a flying model's knocking out a segment of a built-up grid is not worth risking.

The bars in a breakup grid should have a diameter of about 1 per cent of the test section diameter, and a mesh of about four bar diameters.

b. Sumps. Some tunnels are designed so that the diffuser air is dumped into a manifold, where it finally is picked up by the compressor inlet duct. Such a manifold design, which admittedly tolerates the very small loss of the diffuser dumping, is an admirable device for the collection of flying model parts. A grid, or corner vanes, are useful for assuring that the model parts will be broken up and will drop to the bottom of the sump. A light screen of about $\frac{1}{2}$-inch mesh and $\frac{1}{32}$-inch-diameter wires is a good cover for the lead-off from the manifold to the compressor inlet.

5:3 Coolers

Coolers are required in supersonic tunnels to remove the heat of compression before the air passes through the ducting to the nozzle-test section area. In the case of hypersonic tunnels using heaters immediately upstream of the nozzle to avoid air liquefaction in the nozzle, coolers are also required downstream of the diffuser to remove heat added by the heater. The purpose of the coolers is, of course, to eliminate temperature excesses in the tunnel ducting and in the compressors.

The basic design concepts of the two types of coolers are usually the same. They normally consist of water-carrying tubes crossing back and forth across the air flow passage with fins to provide maximum cooling effect. Water is normally pumped through the cooler, through a cooling tower, and then back through the cooler in a closed loop system. Water cooling temperatures leaving the coolers will typically be at least 10 or 20°F below the temperature for which the tunnel circuit is designed (typically 125 to 150°F).

Operational problems of the two types of coolers are also quite similar. The failure of a cooling system could result in severe damage to the wind tunnel, and safeguards must be provided to prevent it. These safeguards might take the form of devices to automatically reduce power to the compressors or to automatically shut down the heater in the event that safe air temperatures are exceeded. Coolers often develop leaks, though this possibility can be minimized by proper design to allow for a good deal of vibration, and by the selection of a location well away from any shock waves. In the design of the cooler, consideration must be given to the fact that leaks may develop at any point, and when one does occur, easy access is required for quick repair. Leaks are usually first detected by a rising dewpoint of the air in the tunnel. Small leaks are sometimes difficult to detect with the naked eye but can often be located quickly by adding a little fluorescein to the water and searching for the leak with an ultraviolet light. Cooling systems are subject to corrosion, scaling, and the precipitation of minerals on the inside of the cooling tubes, all of which reduce the effectiveness of the cooler. Requirements for avoiding this should be worked out with a cooling engineer who is familiar with local water conditions.

The design requirements of the two types of coolers are, however, much different. The cooler for removing the heat of compression is located immediately downstream of the compressor and will typically receive air at 300 to 400°F and then deliver it to the tunnel at a temperature of 125

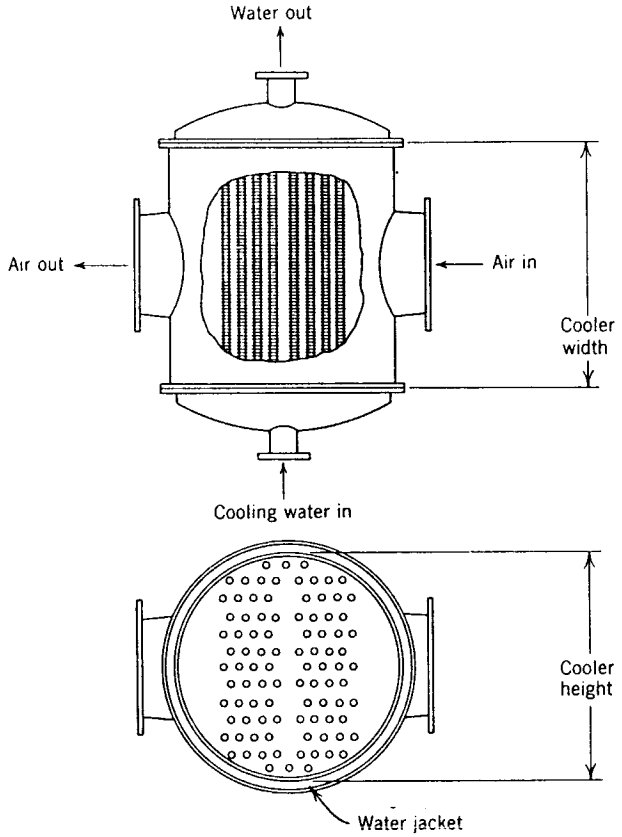


Fig. 5:2 Schematic drawing of cooler (the end has been removed in side view).

to 150°F. The air discharge temperature should be held constant because it is the stagnation temperature of the tunnel. Although these coolers are usually designed for a relatively low air pressure drop, drops of 1 psi are seldom of importance.

The cooler for removing the heat added to the air by a heater is normally located immediately downstream of the tunnel diffuser, where the air pressure is perhaps as low as 1 psia. These coolers will receive air at temperatures to 1500°F or more, depending on the heater capacity, and will typically deliver it to the compressor inlet at 125 to 150°F. This cooler must be designed for a minimum pressure drop, 2 to 5 inches of water being typical. With tunnel discharge pressures in the vicinity of 1 psia, small pressure drops have a large effect on the overall compression ratio required to operate the tunnel. Methods that have been used to minimize the pressure drop of this cooler include expanding the duct cross section

at the heater to flow areas as high as 20 times that of the tunnel test section and inclining the cooling tube bundles with respect to the direction of air flow.

Coolers are frequently if not usually designed as "double-pass" systems. In these systems, the cooling tubes will be separated into groups of rows. Water will be passed through one row in the downstream group, through one row in the upstream group, and then back to the cooling tower before recirculation. The double-pass system can be designed to provide almost as much cooling as a single-pass system and with half the water pump capacity. The design of a cooler having a large number of finned tubes has been described by Nagamatsu et al. in Ref. 5:1 and is shown in Fig. 5:2.

We shall now outline a procedure for cooler design. The procedure given is for a single-pass water system. However, it may be applied to the design of a double-pass system by considering the downstream group of tube rows as one complete cooler design and the upstream group of tube rows as a separate cooler design. The following data must be known before beginning a cooler design:

a. weight flow of air (lb/hr),
b. temperature of air entering the cooler (°R),
c. pressure of air entering the cooler (lb/ft²),
d. desired temperature of air leaving the cooler (°R),
e. temperature of water entering the cooler.

Once these data are available, the design steps are the following:

1. Compute the required rate of heat removal from the air from:

$$Q = \dot{w}(h_1 - h_2) \tag{5:1}$$

where Q = rate of heat removal from air, Btu/hr,
$\dot{w}$ = rate of air flow through the heater, lb/hr,
h_1 = enthalpy of air entering the cooler from Fig. 4:6, Btu/lb,
h_2 = enthalpy of air leaving the cooler, Btu/lb.

2. Assume a cooling water pump capacity and calculate the temperature rise of water flowing through the cooler which corresponds to the heat removed from the air:

$$\Delta T_w = Q/C_{pw} \cdot \dot{w}_w \tag{5:2}$$

where ΔT_w = temperature rise of water, °R,
C_{pw} = specific heat of water, 1 Btu/lb-°R,
$\dot{w}_w$ = weight flow of water, lb/hr.

3. Assume an average air velocity of 50 ft/sec through the unobstructed area of the cooler and compute the unobstructed area required using the

average of inlet and exit air temperature and using the inlet air pressure (the pressure drop should be insignificant):

$$A_f = \frac{\dot{w}}{(p/53.33T_A)(50 \times 3600)}$$

or

$$A_f = 0.0002963\dot{w}T_A/p \tag{5:3}$$

where A_f = free flow area through cooler, ft²,
p = air pressure at cooler inlet, lb/ft²,
T_A = average of air inlet and exit temperature, °R.

4. Assume that the unobstructed flow area through the cooler is two-thirds the total cooler cross-sectional area. Calculate the total cross-sectional area of the cooler. Assume a square cooling passage and calculate the dimensions of the cooler:

$$A_c = (\tfrac{3}{2})A_f$$
$$L_c = \sqrt{A_c}$$

where A_c = cooler cross-sectional area, ft²,
L_c = height and width of the cooler, ft.

5. Assume an arbitrary tube size. Calculate a Reynolds number corresponding to the airflow and the average of inlet and exit air temperature in the cooler T_A:

$$RN = \frac{(\dot{w}/A_f)d_o}{\mu} \tag{5:4}$$

where d_o = outside diameter of tube, ft,
μ = air viscosity at temperature T_A from Fig. 4:4, lb/ft-hr.

6. Read the Nusselts number Nu (non-dimensional heat transfer coefficient) from Fig. 5:3.

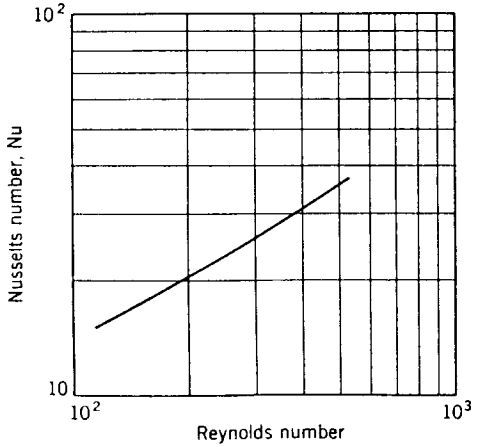


Fig. 5:3 Nusselt's number vs. Reynolds number for flow perpendicular to tubes.

7. Calculate the convection heat transfer coefficient from the air to the tubes from:

$$h = \frac{Nuk}{d_o}, \text{ Btu/ft}^2\text{-hr-°R} \tag{5:5}$$

where k = conductivity of air at T_A (from Fig. 4:5), Btu/ft-hr-°R.

8. Assume an average tube wall temperature 20° below the air exit temperature and calculate the total external tube surface area required from

$$A_{TE} = \frac{1.25Q}{h(T_A - T_B)} \tag{5:6}$$

where A_{TE} = total external surface area of tubes, ft²,
T_B = average tube wall temperature, °R.

The constant 1.25 is a safety factor term.

9. Calculate the external surface area of one tube and the number of tubes required:

$$a_{TE} = \pi d_o L_c$$
$$N_T = A_{TE}/a_{TE}$$

10. Calculate the combined internal cross-sectional and surface area of all tubes:

$$A_{TC} = \frac{N_T \cdot \pi(d_i)^2}{4}$$

$$A_{TI} = N_T \cdot \pi \cdot d_i \cdot L_c$$

where A_{TC} = internal tube cross-sectional area, ft²,
A_{TI} = internal tube surface area, ft²,
d_i = inside diameter of tube, ft.

11. Calculate a coefficient for heat transfer from the tube to the water by using the following equation from Ref. 5:8:

$$h_w = 0.023\,\frac{k_w}{d_i}\left(\frac{Gd_i}{\mu_w}\right)^{0.8}\left(\frac{\mu C_{pw}}{k}\right)^{0.4} \tag{5:7}$$

where h_w = coefficient of heat transfer from tube to water, Btu/ft²-hr-°R,
$G = \dot{w}_w/A_{TC}$, lb/ft²-hr,
T_{AW} = average of inlet and exit water temperature, °R,
C_p, μ, k, are for water at T_{AW} (μ and k are from Table 5:1).

12. Calculate an average tube wall temperature corresponding to the required heat flow from

$$Q = h_w A_{TI}(T_B - T_{AW})$$

or

$$T_B = \frac{Q}{h_w A_{TI}} + T_{AW}$$

Table 5:1

Viscosity and Conductivity of Water

Temp °R	μ lb/ft-hr	k Btu/hr-ft-°R
520	2.71	0.338
530	2.36	0.345
540	2.08	0.351
550	1.85	0.357
560	1.66	0.363
580	1.36	0.372
600	1.14	0.379
620	0.970	0.385
640	0.840	0.380
660	0.738	0.393

13. Compare the average tube wall temperature calculated with that assumed in item 8. If there are significant differences between the two values, an adjustment should be made to the value of T_B assumed in item 8, and items 8 through 12 should be repeated.

14. Calculate the number of tubes per row and the number of rows:

$$N = \frac{L}{3d_o}$$

$$N_R = \frac{N_T}{N}$$

where N = number of tubes per row,
N_R = number of rows.

15. Assume the tube arrangement shown in Fig. 5:4 and calculate the cooler length necessary for the required number of tubes. If the length is more than can be accommodated, it may be reduced by decreasing the tube diameter:

$$l = \frac{L}{N}$$

where $L = N_R l \cos 30°$,
l = distance between centerlines of tubes in one row, ft,
L = total cooler length, ft.

16. Calculate the pressure drop through the heater by using the following equation from Ref. 5:7:

$$\Delta P = 4fN_R(\tfrac{1}{2}\rho U^2) \qquad (5:8)$$

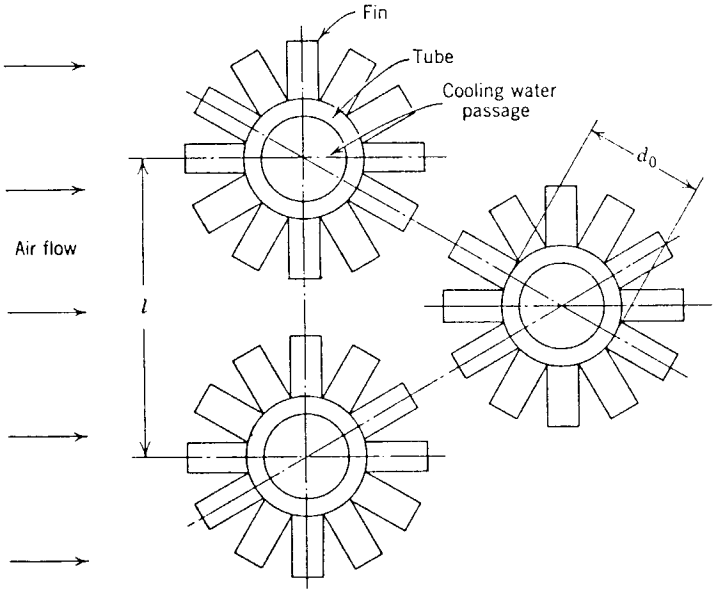


Fig. 5:4 Arrangement of cooling water tubes in a cooler.

where ΔP = pressure drop across cooler, lb/ft²,
ρ = average air density in the cooler, slugs/ft³,
U = average velocity through unobstructed area of cooler, ft/sec,

$$f = \left[0.23 + \frac{0.11}{(l/d_0 - 1)^{1.08}}\right]\frac{1}{RN^{0.15}} \qquad (5:9)$$

17. Determine whether the calculated pressure drop will make the tunnel operation doubtful. If so, the only way to decrease the pressure drop is to increase the open area through the heater and reduce the velocity.

Example 5:1 Design a single-pass cooler for cooling 4200 lb/hr of air at a pressure of 288 lb/ft² from 2260°R to 610°R. The inlet water temperature is 540°R.

1. $Q = (4200)(0.2596 \times 1860 - 0.2401 \times 210) = 1{,}816{,}000$ Btu/hr

2. Assume a cooling water pump capacity of 200 gal per minute = 12,000 gal per hour. The weight flow of cooling water is then

$$\dot{w}_w = (12{,}000)(8.34) = 100{,}100 \text{ lb/hr}$$

and $$\Delta T_w = (1{,}816{,}000)/(100{,}100) = 18.14°\text{R}$$

3. $$T_A = (2260 + 610)/2 = 1435°\text{R}$$

$$A_f = (0.0002963)(4200)(1435)/(288) = 6.201 \text{ ft}^2$$

4. $A_c = (\frac{3}{2})(6.201) = 9.302 \text{ ft}^2$

$L_c = \sqrt{9.302} = 3.050 \text{ ft}$

5. Assume that the cooling tubes will have an outside diameter of 0.0521 ft and an inside diameter of 0.0417 ft ($\frac{5}{8}$ inch and $\frac{1}{2}$ inch).

$$RN = \frac{(4200/6.201)(0.0521)}{0.0872} = 404.7$$

6. $Nu = 30.8$

7. $$h = \frac{(30.8)(0.0305)}{(0.0521)} = 18.03$$

8. $T_B = 590$

$$A_{TE} = \frac{(1.25)(1{,}816{,}000)}{(18.03)(1435 - 590)} = 149.0$$

9. $a_{TE} = \pi(0.0521)(3.05) = 0.4992$

$N_T = 149.0/0.4992 = 298.4$

10. $$A_{TC} = \frac{(299)(\pi)(0.0417)^2}{4} = 0.4084$$

$A_{TI} = (299)(\pi)(0.0417)(3.05) = 119.5$

11. $G = (100{,}100)/(0.4084) = 245{,}100$

$T_{AW} = 540 + 9.1 = 549.1$

$C_{pw} = 1.0$

$\mu_w = 1.87$

$k_w = 0.356$

$$h_w = (0.023)(0.356/0.0417)\left[\frac{(245{,}100)(0.0417)}{1.87}\right]^{0.8} \times (1.87/0.356)^{0.4} = 374$$

12. $$T_B = \frac{(1{,}816{,}000)}{(374)(119.5)} + 549.1 = 589.7^\circ\text{R}$$

13. The calculated tube wall temperature of 589.7°R is near enough to the assumed temperature of 590°R for practical purposes.

14. $$N = \frac{(3.05)}{(3)(0.0521)} \cong 19$$

$$N_R = \frac{299}{19} \cong 16$$

15. $l = (3.05)/(19) = 0.1605$

$L = (16)(0.1605)(0.8660) = 2.224$

16. $$\rho = \frac{(288)}{(1716)(1435)} = 0.000117$$

$$f = \left[0.23 + \frac{0.11}{\left(\frac{0.1605}{0.0521} - 1\right)^{1.08}}\right] \frac{1}{(404.7)^{0.15}} = 0.114$$

$$\Delta P = (4)(0.114)(16)(0.5)(0.000117)(50)^2 = 1.07 \text{ lb/ft}^2$$

17. This pressure drop at a pressure level of 288 lb/ft² is not sufficient to make the tunnel operation doubtful.

5:4 Heaters

From Fig. 1:39 we can see that conditions for equilibrium liquefaction of air in a wind tunnel will exist when air at room temperature is expanded to Mach numbers of about 4 to 5. We can also see that the amount of heating required to avoid conditions for equilibrium liquefaction increases quite rapidly as Mach number is increased. In spite of the fact that recent experiments indicate the effects of liquefaction on test data may in some cases be small, most hypersonic tunnels in this country have used the criterion of avoiding conditions for equilibrium liquefaction to specify minimum operating temperatures and thus minimum heater capabilities. There is also considerable interest in hypersonic wind tunnels with operating temperatures in excess of those required to avoid conditions for equilibrium liquefaction. Between Mach numbers of 2 and 3, air temperatures encountered by an aircraft in flight become high enough that real gas effects (Section 1:3) begin to be significant. As flight Mach numbers increase, air temperatures increase rapidly and the importance of the real gas effects has a corresponding increase. Duplication of real gas effects on flow properties in a wind tunnel requires duplicating flight temperatures. As Mach numbers increase this rapidly becomes impractical. However, air heaters for many hypersonic tunnels are designed for operation at temperatures considerably in excess of those required to avoid conditions for equilibrium liquefaction in order to come as close as possible to flight. The designs of heaters currently used in continuous hypersonic wind tunnels are quite varied. The following discussion is designed to describe some of the more generally used types of heaters together with some of the more important design considerations, and then to present a design procedure for a resistance wire heater.

5:5 Electrical Resistance Heated Tube Heater

A good example of an electric resistance heater is the one used for the Jet Propulsion Laboratory 290-square-inch continuous-operating hypersonic tunnel described in Ref. 5:2. This heater is designed for operation

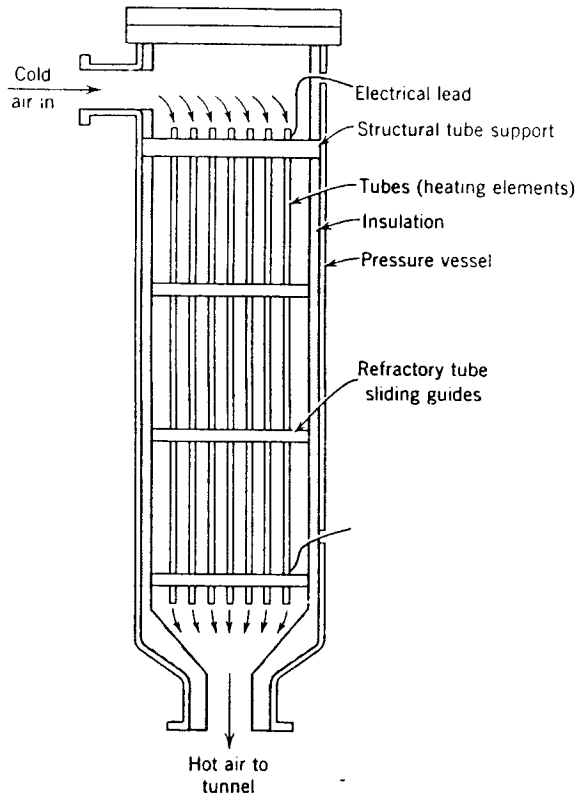


Fig. 5:5 Schematic of electric resistance tube heater.

of a Mach number 5 to 9 wind tunnel with maximum inlet pressures to 1000 psi and maximum exit temperatures to 1350°F, which is somewhat above the limit required to avoid liquefaction.

With this design, heating of the air is accomplished by passing the air downward through a bundle of parallel tubes suspended from the top of the heater (Fig. 5:5). Guides are positioned near the center and near the bottom of the heater to maintain the alignment of each tube relative to the other tubes and relative to the pressure vessel. These guides provide no vertical restraint and thus allow the tubes to expand and contract freely during heating and cooling. The tubes are made of Nichrome, which can be operated as a resistive heating element in air for an indefinite period of time at 1600°F. Each tube is electrically insulated from the other tubes and from the pressure vessel by means of quartz insulators. Resistance heating of the tubes is accomplished by a 4200 kw power supply.

This heater design has several advantages that are thoroughly discussed in Ref. 5:2. The most important of the advantages is the fact that the design does not require the hot tubes to withstand any significant pressure load; the pressure of air in the tubes and in the cavity of the pressure shell surrounding the tubes is essentially the same. Because the tubes do not have to withstand pressure, they can be designed to have a low thermal mass, which will allow relatively rapid response to changes in air flows or to changes in required temperatures. Complete electrical operation of the heater, from the power supply to the temperature sensing element, is another advantage in that it tends toward simplicity of operation. The large electrical power requirements of this type of heater may be a disadvantage in some cases, depending on the availability and cost of electrical power in large quantities.

One problem of importance in the design of a heater of this type was experienced by the Naval Ordnance Laboratory during early tests with a hypersonic tunnel. The tunnel utilized a vertical heater with a downward flow of air. During tests at high Mach numbers, excessive heating of the top cover of the heater vessel was noted. It was determined that the cause of the excessive heating was free convection. Upon being heated, some of the air in the heater was rising even though the normal flow velocity was downward. The problem was solved by increasing the flow velocities through the heater to values in excess of convective velocities by by-passing a considerable amount of air around the wind tunnel nozzle at the higher Mach numbers.

The problem of convection currents' carrying the hottest air upward may be important in any type of heater. It is usually associated with low flow velocities through the heater, and these are difficult to avoid when the heater is used for operation of a hypersonic tunnel over a large range of Mach numbers.

5:6 Resistance Wire Electrical Heater

This type of heater differs in principle from the tube-type heater in that air is heated by being passed over coils of electrically heated wire rather than through electrically heated tubes. Heaters of this type may be designed to provide air temperatures in excess of 2500°R. The first wind tunnels to provide continuous flows of air at hypersonic Mach numbers with temperatures in excess of 2500°R were designed by the Aerodynamics Laboratory of the Ohio State University using heaters of this type (Refs. 5:3 and 5:4). Figure 5:6 illustrates the heater and the heating coil design for this type of heater.

The heater consists of a cylindrical steel pressure vessel, a heating element assembly within the pressure vessel, and "Kanthal A-1" wire heating elements. The Fibrefrax insulation used within the heating

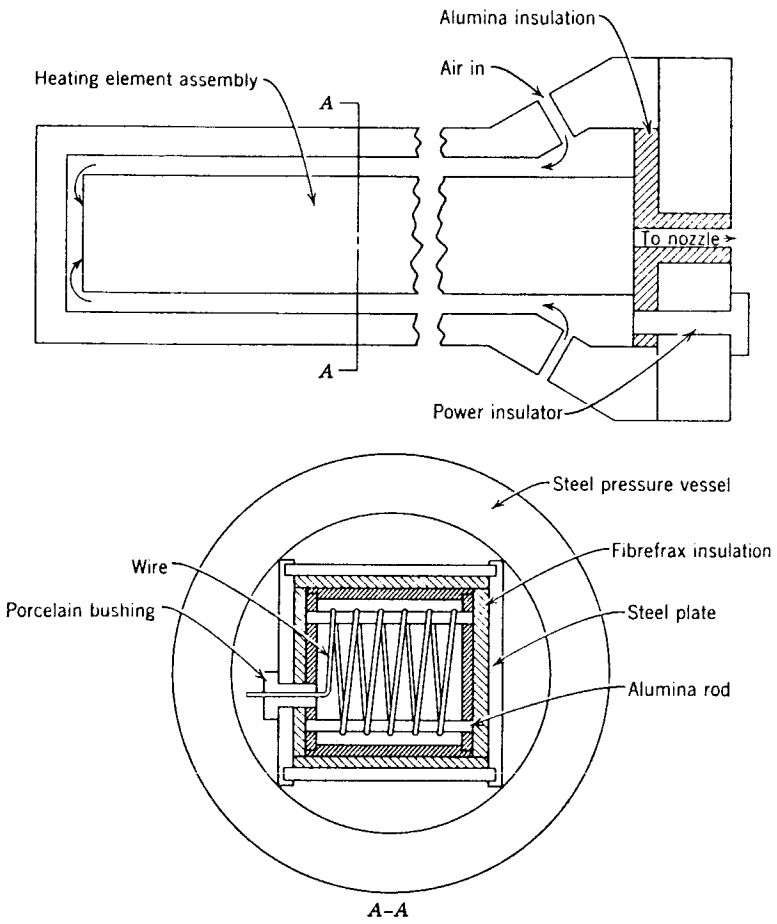


Fig. 5:6 Electric resistance wire heater.

element assembly has a melting temperature of 3760°R. The Kanthal A-1 wire has a melting point of 3210°R and a maximum use point of 2920°R. Air is introduced into the annulus between the heating element assembly and the pressure vessel at the downstream end of the heater. The air flows upstream through this annulus, keeping the pressure vessel walls cool and at the same time picking up heat from the outer walls of the heating element assembly. At the upstream end of the pressure vessel the air flows from the annulus into the heating element assembly and downstream over the wire heating coils.

Because of the thermal mass of the Fibrefrax tube and the pressure vessel, a significant operating time is required for all components to reach

a stable operating temperature. A heater of this type is suitable for use over a wide temperature range but is not suitable when rapid changes in operating pressures or temperatures are required.

Heaters of this type have been used at Mach numbers of 8 to 14 in tunnels to 12 inches in diameter at the Ohio State University and to 20 inches in diameter at the Aeronautical Research Laboratory. Such heaters would probably be suitable for use in larger tunnels, depending on the availability of power. Hoskins Alloy 875 is currently preferred over Kanthal A-1 for heater elements.

5:7 A Graphite Resistance Heater for Use with Nitrogen

A graphite resistance heater for use with nitrogen has been designed by the Gas Dynamics Laboratory of Princeton University and operated at 1000 psi pressures and exhaust temperatures of over 5000°R (Ref. 5:5). The heater development is directed toward the ultimate development of a continuous-operating Mach 20 nitrogen tunnel with stagnation pressures of 10,000 psi and stagnation temperatures of about 5000°R.

Using nitrogen as a test gas, the tunnel is not truly a "wind" tunnel. The following approach has been followed in the development of this heater: At Mach numbers of 20, flows of air over a vehicle in flight through the atmosphere will be influenced to a large extent by real gas effects, particularly dissociation of the diatomic molecules of oxygen and nitrogen, and ionization. The fundamental fluid mechanical effects at high Mach numbers are not yet thoroughly understood and facilities are required for studying these effects without the presence of the complicating real gas effects. Nitrogen has properties similar to those of air and can be expanded to a Mach number of 20 without liquefaction in the test section if the stagnation temperature is above 4500°R. At temperatures to somewhat above 5000°R; depending on pressure, nitrogen will not dissociate, and the only real gas effects are variations of specific heat ratios (γ) with temperature. Also, nitrogen is almost inert to graphite, which for this application is a very practical material for a heating element.

A photograph of the heating element of the heater is shown in Fig. 5:7. It consists of a solid cylindrical graphite rod with a machined spiral gas passage and a sleeve to fit snugly over the rod to contain the gas in the spiral passage. Gas enters the cylindrical heating element along its axis, flows through holes into the spiral passage and completely through the spiral passage, and flows out of the spiral passage through holes into a discharge chamber on the axis of the heating element.

Such a heater has one danger problem that must be monitored—the formation of cyanogen. At typical operating pressures this forms at 3500°K and occurs only rarely, when a heater element burns out.

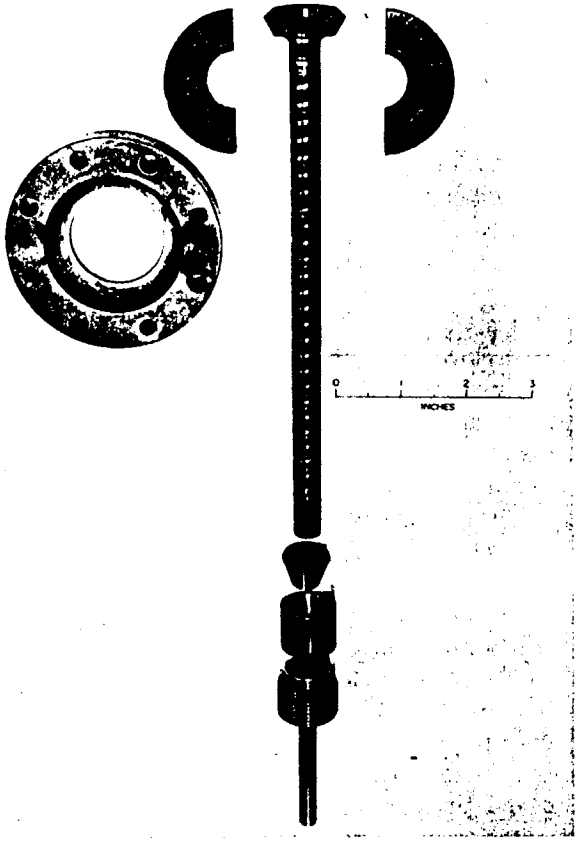


Fig. 5:7 Heating element for a graphite resistance heater; flow passage cover removed. (Courtesy Princeton University.)

5:8 Gas Fired Tube Heater

In this type of heater, air is heated by passage through tubes that are heated by passing products of combustion of gas and air over their exterior surfaces. A heater of this type is used for the continuous-operating 50-inch-diameter Mach 8 tunnel (tunnel *B*) of the Von Karman Gas Dynamics Facility at the Arnold Engineering Development Center. It is also used as a first stage of heating for the continuous-operating Mach 10 tunnel (tunnel *C*). This heater is used to provide air at a maximum temperature of 900°F.

The primary advantage of this type of heater over the electrically powered heaters is the generally greater availability and lower cost of gas in quantities required for supplying heated air for a large wind tunnel.

The primary disadvantage stems from the fact that the gas is fired at near atmospheric pressures and the heating tubes must therefore be designed as high-temperature pressure vessels with thick walls. Relative to the electrical heater illustrated in Fig. 5:5 the thick tubing walls result in a high tube cost. They also result in a high thermal mass which increases the time required for stabilization of operating conditions, and makes rapid changes in tunnel operating temperatures and pressure impractical.

5:9 Design Procedure for a Resistance Wire Heater

In a heater of the type described in Section 5:6, essentially all of the power dissipated in the heating coils will go toward increasing the air temperature. The Fibrefrax insulation surrounding the heating elements will be heated very rapidly when the heater is first turned on. However, because of the insulating qualities of the Fibrefrax, the steel housing for the heating element assembly will be much cooler than the inner walls of the heater. The cool air entering at the downstream end of the heater and flowing upstream over the steel housing before entering the heater proper will keep the housing relatively cool and will absorb most of the heat passing through the housing. Thus, practically all of the energy dissipated in the heating coils enters the air through convection heating. In the heater design it is assumed that all heating of the air is by convection as the air flows over the heating coils. This includes a safety factor in the coil design inasmuch as the heat added to the air during its flow upstream over the housing of the assembly will not have to be added by the coils.

The design of resistance wire heater is described in Ref. 5:4. The items that must be defined in order to begin the design of such a heater are

a. The weight flow of air through the heater,
b. The inlet air temperature,
c. The inlet air pressure,
d. The exit air temperature.

1. The first step in the design is to determine the total electrical power that must be dissipated by the heater coils from

$$Q = \dot{w}(h_{\text{out}} - h_{\text{in}}) \times 0.293 \times 10^{-3}\ \text{kw} \qquad (5:10)$$

where $\dot{w}$ = weight flow of air, lb/hr,
h = enthalpy of air, Btu/lb.

The subscript out indicates conditions at the heater outlet and in indicates conditions at the heater inlet. Values of the enthalpy of air as a function of temperature to 3200°R, including real gas effects, are presented in Fig. 4:6.

2. Assuming that the power requirements can be met, the next step is to determine the cross-sectional area of the heater. Two factors must be

considered in specifying the size of the heater. First, the maximum velocity in the heater must not be high enough to result in failure of the wires or supporting structure due to dynamic pressure loads. Second, the minimum velocity must be well above free convection velocities which would tend to result in uneven heating and consequent wire failure. Velocities from as low as 3 ft/sec to as high as 40 ft/sec at the exit end of the heater based on duct cross-sectional area are satisfactory. Velocities as low as 1 ft/sec at the inlet are tolerable though not desired. The higher velocities will result in improved heat transfer from the wire to the air and are to be desired. Assume a velocity of 30 ft/sec (108,000 ft/hr) in the duct downstream of the last heating element and calculate the duct cross section from

$$A_{HD} = \frac{\dot{w}}{(p_{\text{out}}/53.3T_{\text{out}})U_{\text{out}}}$$

where A_{HD} = cross-sectional area of heater duct, ft²,
p = pressure, lb/ft²,
T = temperature, °R,
U_{out} = air velocity at heater outlet based on duct cross section ft/hr.

3. Check the velocity in the duct at the heater inlet to ensure that it does not fall below 3 ft/sec (10,800 ft/hr) from

$$U_{\text{in}} = \frac{\dot{w}}{(p_{\text{in}}/53.3T_{\text{in}})A_{HD}}$$

If U_{in} falls below 3 ft/sec, the exit velocity should be increased above 30 ft/sec and a new heater duct area calculated.

4. Calculate the heater height Y_h, assuming a square cross section, from $Y_h = \sqrt{A_H}$.

5. Select a heating element material corresponding to the expected material operating temperature. This would probably be Nichrome for temperatures to 2000°R and Kanthal A-1 or Hoskins Alloy 875 for temperatures to 2850°R. Select a standard wire size based on strength and workability, and define a heating coil configuration with wire spacing such that about $\frac{2}{3}$ of the duct cross section is obstructed. Determine the length of wire L_w and the surface area of wire A_w in each element of the heater.

6. Assume that the average of the wire temperature in all heating elements will equal the desired exit air temperature and calculate a film temperature as follows:

$$T_{a,\text{ave}} = (T_{\text{in}} + T_{\text{out}})/2$$
$$T_{w,\text{ave}} = T_{\text{out}}$$
$$T_f = (T_{a,\text{ave}} + T_{w,\text{ave}})/2$$

where the subscript a,ave refers to average air temperature, w,ave refers to average wire temperature, and f refers to a film temperature.

7. Calculate a heat transfer coefficient from

$$h = 0.26\frac{k}{d_w}\left[\frac{(\dot{w}/A'_H)d_w}{\mu}\right]^{0.6}\left[\frac{\mu C_p}{k}\right]^{0.33} \text{Btu/ft}^2 - \text{hr} - {}^\circ\text{R} \quad (5:11)$$

where A_H = portion of heater duct area not obstructed, ft²,
d_w = wire diameter, ft,
and μ, k, and C_p are air properties defined in Figs. 4:4, 4:5, and 4:6 and evaluated at the film temperature T_f.

8. Calculate a number of heating elements required in series to provide the required heat input to the air from

$$N = \frac{(Q/0.293 \times 10^{-3})}{hA_w(T_{w,\text{ave}} - T_{a,\text{ave}})}$$

9. Assume that all heating elements are in series and calculate the amount of heat energy that must be dissipated from each element, Q/N. Note that the wire temperature will continue to rise until this amount of heat is dissipated from each element or until the wire of the element fails.

10. Calculate the enthalpy of the air entering the downstream element. For this element

$$h_{\text{in}(f)} - h_{400} = (h_{\text{out}} - h_{400}) - \frac{h_{\text{out}} - h_{\text{in}}}{N}$$

where the subscript f denotes the temperature of the air entering the downstream heater element. Determine the air temperature corresponding to $h_{\text{in}(f)}$.

11. Assume the heat transfer coefficient calculated in item 7 and calculate a wire temperature for the last element from

$$Q/N - hA_w(T_{wf} - T_{\text{in}(f)}) \times 0.293 \times 10^{-3}$$

or

$$T_{wf} = T_{\text{in}(f)} + \frac{Q/N}{hA_w \times 0.293 \times 10^{-3}}$$

12. Similarly, calculate the wire temperature of the first element, T_{w_1}.

13. If both the initial and final wire temperatures calculated are below the maximum use temperature of the wire, new average film temperatures based on these wire temperatures and local air temperatures and corresponding new heat transfer coefficients should be calculated for both the first and last heater element, as in items 6 and 7. Corresponding wire temperatures are then calculated as in items 10 to 12. Probably not more than two iterations of this type will be required for reasonable wire temperature accuracy.

If the initial heater element temperature is above the maximum use temperature of the wire, the power dissipation per element is too high. The number of elements must be increased and the preceding calculations repeated.

If the initial element temperature is low but the final element temperature is near or above the maximum use temperature of the wire, two alternatives exist. One is to increase the number of heater elements and reduce the power input per element. The other is to break the series elements into two or more banks wired in parallel with a higher power input per element to the bank or banks nearer the heater inlet. This latter approach is recommended because less hardware (heater elements and heater length) will be required. If this approach is used, each bank of heater elements should be treated as a complete heater insofar as the heat transfer calculations are concerned.

Example 5:4 Design a resistance wire electric heater to heat 4850 lb/hr (1.35 lb/sec) of air at 144,000 lb/ft² pressure from 560° to 2000°R.

1. $Q = 4850(0.2562 \times 1600 - 0.2401 \times 160) \times 0.293 \times 10^{-3}$
   $= 528$ kw

2. $A_{HD} = \dfrac{4850}{\dfrac{144{,}000}{53.3 \times 2000}(108{,}000)} = 0.0332$ ft²

3. $U_{\text{in}} = \dfrac{4850}{\dfrac{144{,}000}{53.3 \times 560}(0.0332)} = 30{,}300$ ft/hr
   $= 8.41$ ft/sec

4. $Y_H = \sqrt{0.0332} = 0.182$ ft

5. Kanthal A-1 is selected as the heating element material and a wire diameter of 0.144 in. (0.012 ft) is chosen. In the heater width of 0.182 ft, the number of coils of wire in the heating element is $(\frac{2}{3})(0.182/0.012)$, or 10. Assuming that each coil goes from bottom to top to bottom of the duct, the total wire length is

$$L_w = (10)(0.364) = 3.64 \text{ ft}$$

The wire surface area in the heating element is

$$A_w = \pi(0.012)(3.64) = 0.137 \text{ ft}^2$$

6. $T_{a,\text{ave}} = (560 + 2000)/2 = 1280°\text{R}$
   $T_{w,\text{ave}} = 2000°\text{R}$
   $T_f = (1280 + 2000)/2 = 1640°\text{R}$

7. $h = (0.26)\dfrac{0.0337}{0.012}\left[\dfrac{\dfrac{4850}{0.0332 \times 0.333}(0.012)}{0.095}\right]^{0.66}\left[\dfrac{0.095 \times 0.2691}{0.0337}\right]^{0.33}$
   $= 900$ Btu/ft²-hr-°R

8. $N = \dfrac{(528/0.293 \times 10^{-3})}{(900)(0.137)(2000 - 1280)} = 20$

9. $Q/N = 528/20 = 26.40$ *kW*

10. $h_{\text{in}(f)} - h_{400} = 410 - 371.5/20 = 391.4$
    $T_{\text{in}(f)} = 1934$

11. $T_{wf} = 1934 + \dfrac{26.40}{(900)(0.137)(0.293 \times 10^{-3})} = 2664°\text{R}$

12. $T_{wi} = 560 + \dfrac{26.40}{(900)(0.137)(0.293 \times 10^{-3})} = 1290°\text{R}$

13. The initial and final wire temperatures are well below the maximum use temperature. Refining the calculations, we get for item 6

$$T_{a,\text{ave}} = 1280°\text{R}$$
$$T_{w,\text{ave}} = (2664 + 1290)/2 = 1977°\text{R}$$
$$T_f = (1280 + 1977)/2 = 1629°\text{R}$$

This film temperature differs from that obtained by using the assumed average wire temperature of 2000°R by such a small amount that it is not necessary to refine the previous heat transfer and wire temperature calculations.

Note that the wire temperature in the final element is about 260°R below the maximum use temperature. This indicates that the power density could be increased somewhat above the 26.40 kw per element used in the preceding calculations. Calculations for a higher power density would be accomplished by selecting an average wire temperature somewhat above the exit air temperature assumed in the preceding calculations and repeating items 6 through 13. The number of heating elements required would thus be reduced.

It is further noted that the wire temperature of the initial element is only 730°R above the entering air temperature, whereas the maximum use temperature is 2360°R above the entering air temperature. This indicates that the power density in the first element could be increased by a factor of about 3. If the heating elements were divided into parallel banks with

a significantly increased power density in the first bank, a further reduction in the number of heating elements could be accomplished.

5:10 Tunnel Circuits

Continuous wind tunnel circuits generally require valves on both the upstream and downstream sides of the test section. This is necessary for complete isolation of the test section from the compressor during model changes. These valves do not normally have to be leakproof valves. However, they should be tight enough so that the model changer will not be in a draft and so that a large amount of ambient air will not find its way into a circuit filled with dry air (if the circuit is below atmosphere). If the tunnel uses heated air, it is more economical to locate these valves upstream of the heater and downstream of the cooler, so that they do not have to operate at high temperatures.

Expansion joints, bellows, or other devices must be installed at appropriate places in the circuit to allow for thermal expansion and contraction. Even though the tunnel may not use a heater, significant temperature changes in various portions of the tunnel must be expected. When these temperature changes affect long lengths of pipe, rigid restraint will cause high stresses and possibly buckling or failure.

Continuous closed-circuit tunnels are usually equipped with a by-pass line which allows circulation of air by the blowers while the tunnel is open. This by-pass line serves two major purposes. First, it allows the blowers to operate between runs, so that a long warm-up period is not required prior to each run. This warm-up period before the blowers can be operated to full power may be as long as one to two hours. Second, the by-pass line allows the tunnel to be started quickly. The blowers may be brought up to operating speed with the air circulating through the by-pass line. With the valves upstream and downstream of the test section open, the tunnel is started by simply closing a valve in the by-pass line. The quick start is highly desirable because models are normally subjected to high loads during the starting process and the shorter the starting time, the less the likelihood of losing a model.

As in the blowdown tunnel, the continuous tunnel must have blowout diaphragms at points where there is a possibility that the pressure can exceed the design limits. The continuous tunnel also requires numerous interlocks for safety and prevention of damage. For example, it must not be possible to close the valve in the by-pass line unless the valves upstream and downstream of the test section are open. Air heaters must be interlocked so that power cannot be turned on when air is not passing through the heater, and safe temperatures on the heating elements and at critical points on the tunnel circuit cannot be exceeded.

5:11 Dry Air Supply

Air driers are seldom if ever used within the circuit of continuous tunnels because of cost and pressure drop considerations. However, they are needed to supply dry air to charge the tunnel, to replace dry air that leaks from high-pressure portions of the tunnel, and to overcome the effects of wet air that gets in during model changes. Dry air must be used for makeup when the tunnel pressure is increased for high Reynolds number runs.

The normal dry air supply for a continuous tunnel includes a pressure-type drier system similar to that described in Section 2:12 together with a dry air storage tank. A typical storage tank would store the dry air at about 125 psia and would be of sufficient volume to fill the tunnel completely perhaps eight times at atmospheric pressure.

The dry air storage tank is normally tied into the return (low-pressure) leg of the tunnel circuit through an automatically operated back-pressure valve and through a manually operated valve. Initial drying of the air in the tunnel circuit is accomplished by removing air from the tunnel circuit and replacing it with dry air. One way of doing this is to open a valve on the pressure side of the tunnel circuit to release air and then open the manual valve to allow dry air to flow into the circuit. Over a period of time this continuous dilution of the tunnel air with dry air results in a circuit full of dry air. Another way is simply to evacuate the tunnel circuit to a low pressure and then fill it with dry air one to several times.

The back-pressure valve serves the dual purpose of maintaining a constant tunnel operating pressure and of keeping the tunnel air dry. For any required operating pressure, temperature, and compressor speed, the pressure in the return leg of the circuit will be a fixed value. Adjustment of the back-pressure valve to open when the pressure drops below this fixed value will serve to maintain a constant operating pressure by replacing air that has leaked out of the circuit.

If the return leg of the circuit is being operated below atmospheric pressure, there will be the possibility of leakage of ambient air into the return leg, and the back-pressure valve is of little value in keeping the tunnel air dry. For this type of operation, which is not at all uncommon, it is necessary to design for small leak rates into the return leg.

5:12 Cooling the Tunnel Components

One of the major problems associated with the design of continuous tunnels using heated air (usually hypersonic tunnels) is that of keeping the tunnel components cool. It is usually impractical from a cost standpoint to allow structural tunnel components to exceed about 500°F, which

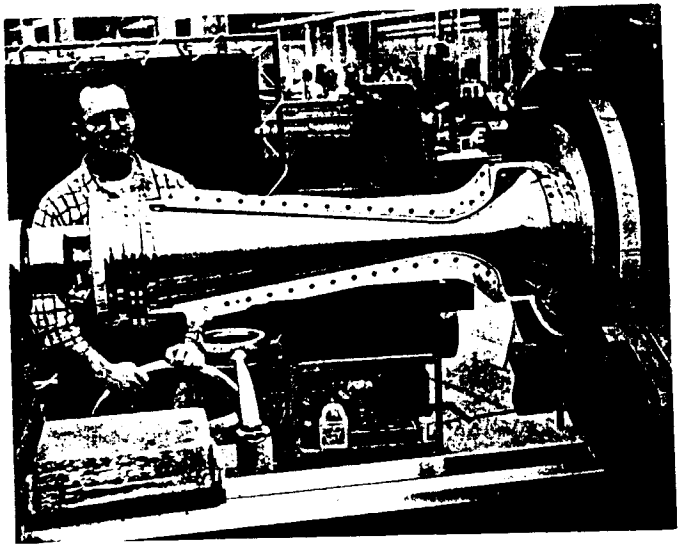


Fig. 5:8 Illustration of nozzle throat cooling water channels.

is well below operating air temperatures for many tunnels. Further, if the nozzle is allowed to operate hot, its contour dimensions are likely to change with the probability that the flow uniformity in the test section will be reduced. Consequently, considerable cooling is always used in hot air continuous tunnels.

The most severe heating problem is at the nozzle throat. At this point heat transfer rates with air temperatures frequently used can exceed the heat transfer rates at the throats of rocket engines using much higher temperatures. Figure 5:8 illustrates a nozzle throat designed for use with water cooling.

A coefficient of heat transfer from air to the walls of a nozzle in the vicinity of the throat, which has been used in the design of several wind tunnels, is as follows:

$$h = \rho U C_p St \tag{5:12}$$

where h = heat transfer coefficient, Btu/ft²-hr-°R,
ρ = air density, lb/ft³,
U = air velocity, ft/hr,
C_p = specific heat of air at T_f, Btu/lb-°R,
T_f = film temperature equal to the average of air and wall temperature, °R,
St = Stanton number (nondimensional) = 0.0014.

An illustration of heat transfer coefficients in the vicinity of a throat calculated from eq. (5:12) is presented in Fig. 5:9.

The rate of heat flow from the air into the wall of the nozzle is

$$Q_1 = h(T_o - T_{wi}); \text{ Btu/ft}^2\text{-hr} \tag{5:13}$$

where T_o = total or stagnation temperature of the air, °R,
T_{wi} = inside nozzle wall temperature, °R.

The rate of heat transfer through the wall of the nozzle by conduction is given by the following equations in the steady-state process. For a flat plate corresponding to a two-dimensional nozzle:

$$Q_2 = \frac{k(T_{wi} - T_{wo})}{\Delta x} \text{ Btu/ft}^2\text{-hr} \tag{5:14}$$

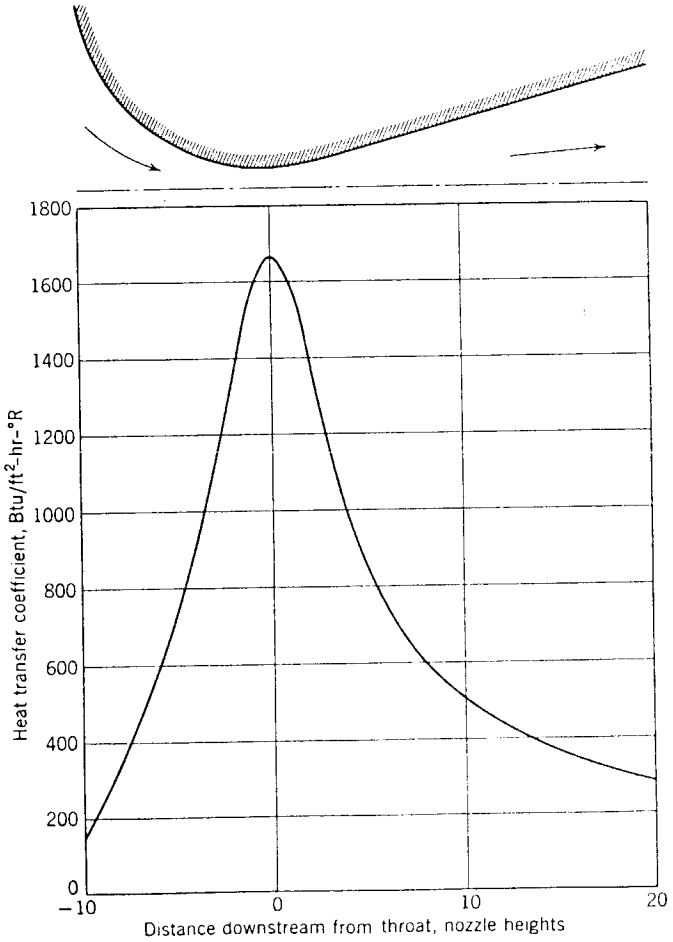


Fig. 5:9 Heat transfer rates in the vicinity of a two-dimensional nozzle throat with a supply temperature of 1460°R and a supply pressure of 650 psia.

where k = conductivity of the material of which the nozzle is made at the average of inside and outside wall temperature, Btu/ft-hr-°R,
T_{wo} = outside nozzle wall temperature, °R,
Δx = thickness of the nozzle wall, ft.

For a hollow cylinder corresponding to an axially symmetric nozzle

$$Q_2 = \frac{k(T_{wi} - T_{wo})}{r_i \ln (r_o/r_i)} \text{ Btu/ft}^2\text{-hr} \qquad (5:15)$$

where r_i = inside radius of metal forming nozzle wall, ft,
r_o = outside radius of metal forming nozzle wall, ft.

The rate of heat transfer from the outside wall to a coolant flowing through a passage adjacent to the wall is given by the following for the two-dimensional nozzle with rectangular cooling passages:

$$Q_3 = h_c(T_{wo} - T_c) \text{ Btu/ft}^2\text{-hr} \qquad (5:16)$$

where h_c = coefficient of heat transfer to the coolant, given by eq. (5:7) with d_i replaced by d_e,

d_e = equivalent diameter equal to $\dfrac{4 \times \text{free cross-sectional area,}}{\text{wetted perimeter}}$ ft,

T_c = coolant temperature, °R.

For the annular cooling passage corresponding to the axially symmetric nozzle, the rate of heat transfer is given by eq. (5:16) with h_c defined as follows:

$$h_c = h\left(\frac{r_c}{r_0}\right)^{0.45} \qquad (5:17)$$

where h = heat transfer coefficient defined by eq. (5:7) with d_i replaced by $2(r_c - r_o)$,
r_c = outside radius of coolant annulus, ft.

The procedure required for the design of a nozzle throat for proper cooling is as follows:

1. A material to be used is selected. This selection is based on strength at elevated temperatures (to withstand normally high air pressure loads), the heat conduction properties, and the thermal coefficient of expansion. A high thermal conductivity allows conduction of a larger amount of heat through the wall, which in turn results in a lower operating wall temperature. A low thermal coefficient of expansion is desired from the standpoint of dimensional stability of the throat and also from the standpoint of minimizing stresses due to thermal gradients in the material. All of these things considered, the most common material selected is high-strength beryllium copper. However, high-conductivity beryllium copper, high-purity nickel, and stainless steel have also been used.

2. Select a maximum allowable material temperature at the nozzle throat. This temperature will be somewhat arbitrary at this point but will depend on the effects of temperature on the material strength and other properties.

3. Using the maximum allowable temperature as the inside wall temperature, calculate the heat flow from the air to the wall, Q_1, at the throat by using eq. (5:13).

4. Equate the heat flow to the wall, Q_1, to the heat conducted through the wall, Q_2, (eq. (5:14) or (5:15) and calculate wall thicknesses corresponding to several outside wall temperatures lying between the inside wall temperature and the coolant temperature.

5. Calculate the maximum total stresses due to a combination of pressure loads to which the throat will be subjected and thermal stresses for each of the wall thicknesses and corresponding temperatures of items 3 and 4. Procedures for calculating thermal stresses in both plates and cylinders may be found in Ref. 5:6.

6. Select a wall thickness based on desirable stress levels and an outside wall temperature as high as possible. If the outside wall temperature for a suitable wall thickness is not considerably above an expected coolant temperature, it may be desirable to adjust the maximum allowable material temperature (item 1) or the desirable stress level.

7. Using this outside wall temperature at the throat together with a coolant temperature that is reasonable for the particular locale, calculate a coefficient of heat transfer to the coolant h_c required to make $Q_3 = Q_2 = Q_1$ (using eq. (5:16).

8. Select a coolant passage cross-sectional area at the throat arbitrarily, keeping in mind that small areas will cause high pressure drops in the coolant and that large areas will require high volume flows.

9. Determine a rate of coolant flow (lb/ft²-hr) required for Q_3 to equal Q_1 and Q_2. The coolant heat transfer coefficient involves eq. (5:7), which in turn involves a flow rate term.

10. Repeat the calculations of items 3, 4, and 7 at points from the beginning of the contraction upstream of the throat to a point downstream of the throat where the area is about ten times the throat area. In these calculations use the same inside and outside wall temperature at all points.

11. Determine a coolant passage cross section at each point of the calculations corresponding to the total coolant flow at the throat (lb/hr) determined in item 9 and satisfying the requirement $Q_3 = Q_2 = Q_1$.

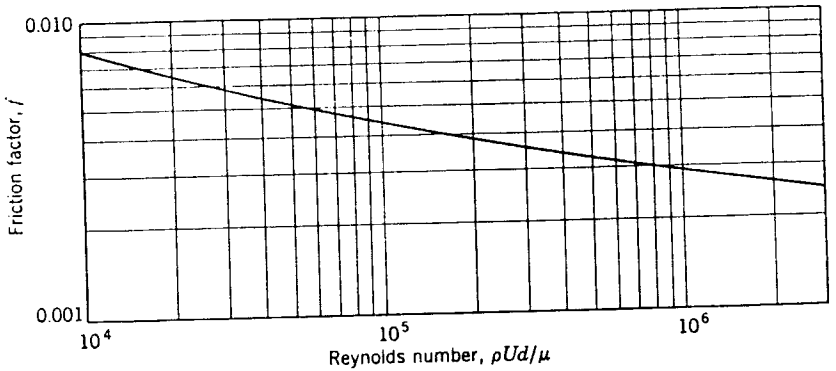


Fig. 5:10 Friction factors for turbulent flow in smooth circular tubes (Ref. 5:8).

12. Calculate a coolant water flow Reynolds number at each point and read a friction coefficient f from Fig. 5:10.

13. Calculate a coolant pressure drop term at each point from

$$\frac{\Delta p}{\Delta x} = f \cdot \frac{\rho U^2}{2g} \frac{S}{A} \tag{5:18}$$

where $\Delta p/\Delta x$ = pressure drop (lb/ft^2) per foot,
ρ = coolant density, lb/ft^3,
U = coolant velocity, ft/sec,
g = acceleration of gravity, 32.174 ft/sec^2,
A = cross-sectional area of coolant passage,
S = wetted perimeter of coolant passage, ft.

14. Plot $\Delta p/\Delta x$ as a function of coolant passage length and integrate to determine total pressure drop in the coolant passage.

15. Examine the coolant flow requirements and the coolant pressure drop. If either of these requirements is too severe, it will be necessary to repeat the calculations of items 8 to 14. It is noted that in some cases where water coolant velocities in excess of 100 ft/sec were used, cavitation occurred downstream of the throat and a high back-pressure was required to eliminate it.

At some point downstream of the throat the cooling requirements will generally be reduced to the point where thin wall cooling is not required and cooling tubes soldered to the outer surfaces of the nozzle at reasonably spaced intervals are quite adequate. This cooling arrangement is considerably more economical than the thin wall type previously discussed. In this lower heat transfer area, heat transfer coefficients of eq. (5:12) will generally be conservative.

For some portions of the circuit where the heat transfer coefficients are

relatively low, it will in some cases be possible to get by with free convection and radiation cooling. This is accomplished by lining the inside of the structure with an insulating material, most frequently castable alumina. Because of its good insulating qualities, the inside surface of the alumina will stabilize at a temperature very near the flow temperature and the surface of the alumina next to the *structure* will be relatively cool. With the inside surface temperature near flow temperature, the heat transfer to the alumina, and consequently to the structure will be low. With an adequate thickness of alumina, losses from the outside of the structure due to radiation and free convection can be made equal to the heat added to the inside of the structure with structure temperatures at reasonable values. Free convection and radiation heat transfer rates are discussed in detail in Refs. 5:7 and 5:8.

References

5:1 H. T. Nagamatsu et al., Feasibility and Design Study of GALCIT Hypersonic Leg #3, Appendix 3, Cooler, GALCIT Report, August 1953.

5:2 H. M. Schurmeier, Design and Operation of a Continuous-flow Hypersonic Wind Tunnel Using a Two-dimensional Nozzle, AGARDograph 38, May 1959.

5:3 John D. Lee, Preliminary Studies, Design and Theory for the Ohio State University Hypersonic Wind Tunnel, ASTIA Document 135635.

5:4 G. M. Gregorek and J. D. Lee, Design, Performance and Operational Characteristics of the ARL Twenty-inch Hypersonic Wind Tunnel, Aeronautical Research Laboratories Report 62-392, March 1962.

5:5 R. P. Shreeve, W. T. Lord, S. J. Boersen, and S. M. Bogdonoff, A Graphite Resistance Heater for a Hypersonic Wind Tunnel Using Nitrogen, Princeton University Report 560, June 1961.

5:6 S. Timoshenko, *Strength of Materials, Part II, Advanced Theory and Problems*, D. Van Nostrand Company, 1940.

5:7 W. H. McAdams, *Heat Transmission*, McGraw-Hill Book Company, 1942.

5:8 J. G. Knudsen and D. L. Katz, *Fluid Dynamics and Heat Transfer*, McGraw-Hill Book Company, 1958.

Chapter six

Air measuring devices

6:1 General

In the course of calibrating and using a high-speed wind tunnel the engineer is required to make many measurements to define the properties of the flow in the tunnel and its effect on a device being studied. Devices and techniques used in making these measurements (with the exception of "balances" for measuring air loads on wind tunnel models, which are discussed in Chapter 7) are discussed in this chapter. The reader is also referred to the work of Volluz (Ref. 6:1).

6:2 Pressure Measurements

The pressures that must be measured during the operation of high-speed wind tunnels cover an extremely wide range, an idea of which may be obtained from Fig. 6:1, where test section static pressures at various Mach numbers corresponding to perfect gas expansion from various total pressures are presented. The static pressures are those which would be measured on the wall of a tunnel test section. They approximate values that would be measured on portions of a model aligned with the air flow, and they are above values that would be measured on the base of a model at supersonic speeds. Thus, pressures down to a few thousandths of a pound per square inch absolute and lower must frequently be measured. Measurement of total pressure is required in every test in every tunnel and values of 1000 psia or higher are not uncommon. Determining pressures over such a range requires a variety of measuring instruments and techniques. Some of the more common of these are discussed in the following sections.

6:3 Barometers

An accurate barometer is a necessity for every high speed wind tunnel since pressures are invariably measured in terms of a difference in pressure from some known reference. By far the most common reference is local atmospheric pressure. For pressures measured with reference to atmospheric

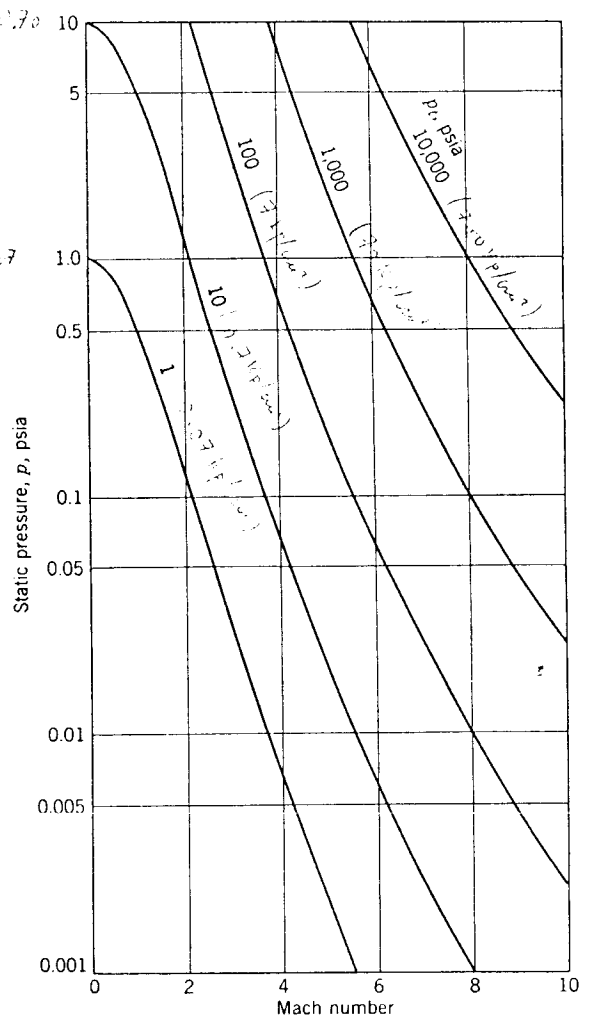


Fig. 6:1 Static pressure for a range of total pressures.

pressure, conversion to absolute pressures requires that atmospheric pressure be known. The common mercury barometer (Fig. 6:2) is quite satisfactory for this purpose. When equipped with a suitable device for viewing the meniscus of the mercury column and reading the mercury column height scale, a good barometer will allow measurement of atmospheric pressure with an accuracy of a small fraction of a millimeter of mercury. This is usually quite adequate for purposes of high-speed wind tunnel operation.

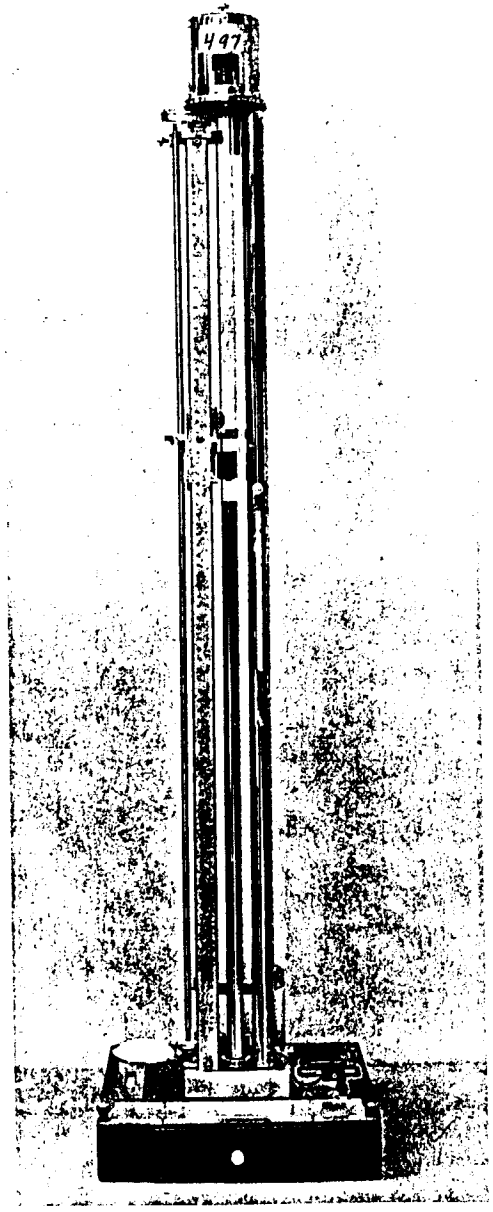


Fig. 6:2 A mercury barometer.

6:4 Manometers

Manometers are devices for measuring the difference between a known and an unknown pressure by observing the difference in heights of two fluid columns. Two common types of manometers are illustrated in Figs. 6:3 and 6:4. One, Fig. 6:3*a*, consists of two vertical glass tubes joined together with a U-type connection at the bottom. Each tube has a linear scale adjacent to it which is usually marked off in inches or millimeters. The tubes are filled with a fluid until the fluid level in the tubes is at about the center of the adjacent scales. A reference pressure is applied to the top of one of the tubes and the pressure to be measured is applied to the top of the other tube. The heights of the two columns of fluid will change until the difference between the two heights, h, is equal to the pressure to be measured in terms of fluid column height. The reference pressure for this type of manometer is most frequently atmospheric. However, in many cases the difference between atmospheric and measured pressure will represent more inches of the manometer fluid than can be accommodated by the tubes. In such cases, the only way to use the manometer (exclusive of changing fluids) is to adjust the reference pressure so that a smaller

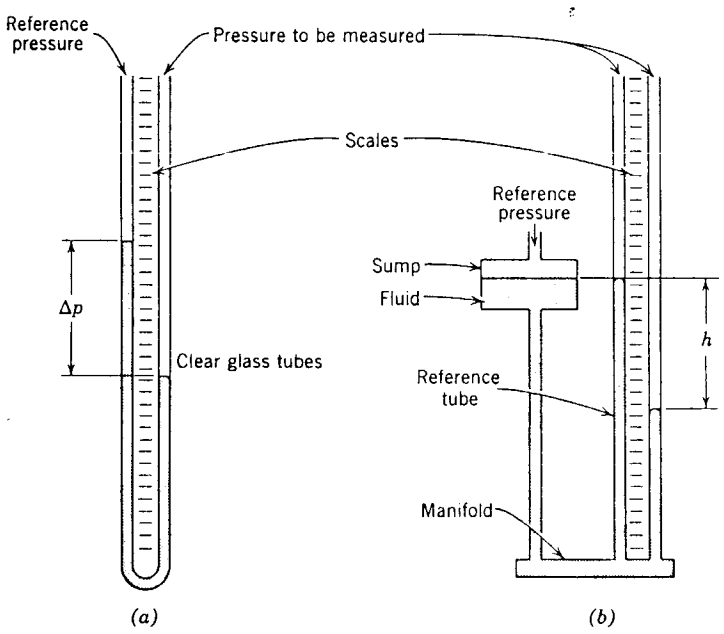


Fig. 6:3 (*a*) Schematic of U-tube manometer. (*b*) Schematic of sump and multiple-tube manometer.

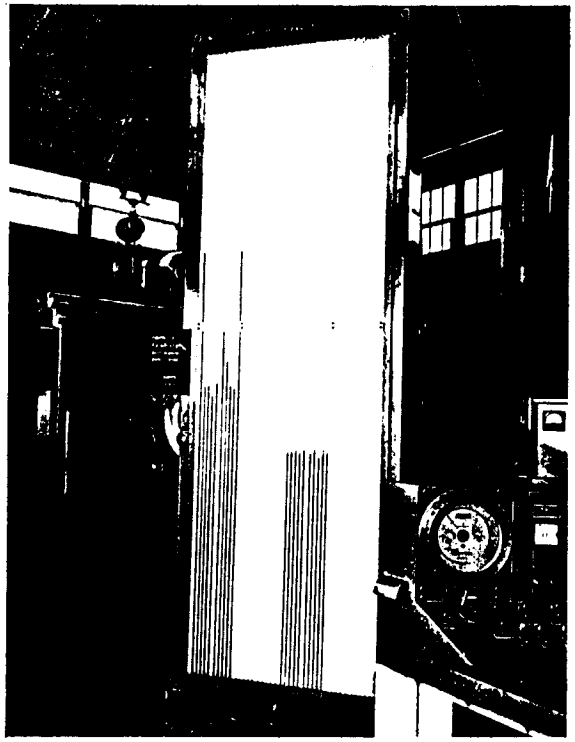


Fig. 6:4 Photograph of sump and multiple-tube manometer.

fluid height will be reached. This has the disadvantage of adding an intermediate pressure to measure.

The sump and tube manometer operates on the same principle as the U-tube manometer. However, in this manometer a large cross-sectional area sump takes the place of the tube to which the reference pressure is applied. The sump level is used as a reference and frequently a number of tubes are employed to form a multiple manometer. The sump and tube manometer has two advantages over the U-tube manometer. It can be used for the measurement of more than one differential pressure at a time and the reference level can be adjusted so that only one scale need be read, instead of two, to determine fluid column height.

Either of the two types of manometer may be, and sometimes is, constructed with tubes and scales that can be tilted. In this way an improvement in reading accuracy is obtained because a given distance along the scale will represent a smaller vertical height and consequently a smaller pressure.

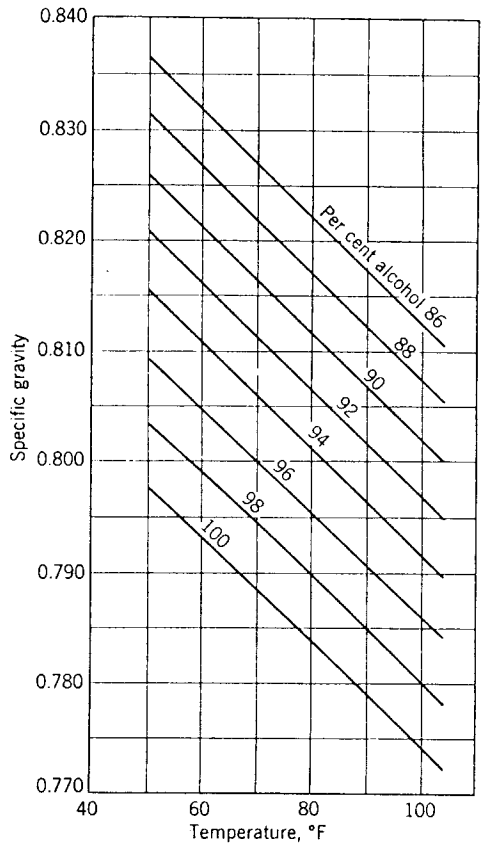


Fig. 6:5 The variation of the specific gravity of alcohol with temperature.

The following table shows some of the fluids commonly used in manometers and their nominal specific gravities.

Fluid	*Nominal Specific Gravity*
Water	0.998 at 70°F
Alcohol	0.8
Dibutyl-phthalate	1.047
Tetrabromoethane (TBE)	2.97
Mercury	13.7

The effects of temperature on the specific gravity of alcohol, tetrabromoethane and mercury, and dibutyl-phthalate are presented in Figs. 6:5, 6:6, and 6:7.

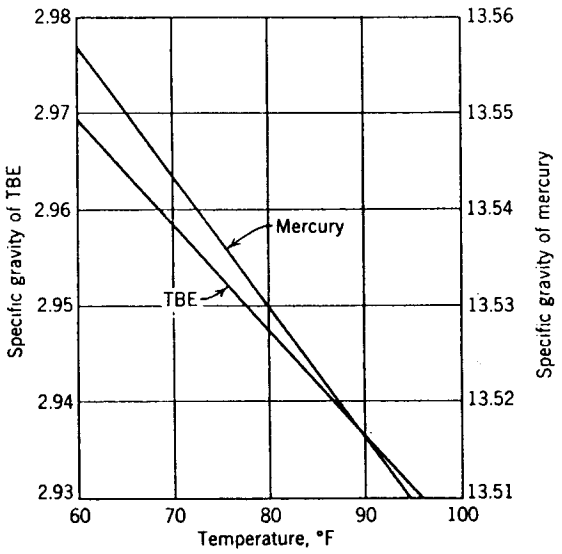


Fig. 6:6 The variation of the specific gravities of tetrabromoethane and mercury with temperature.

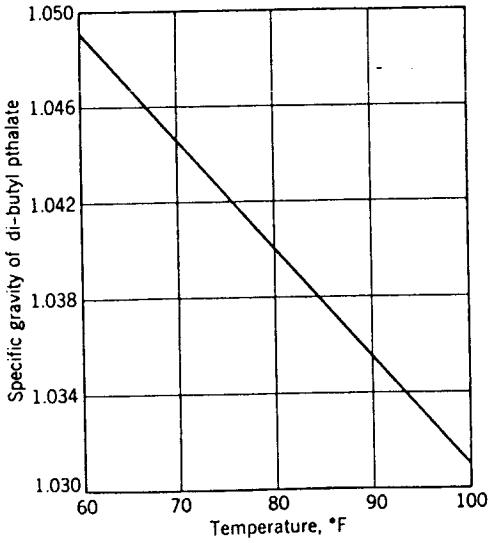


Fig. 6:7 The variation of the specific gravity of dibutyl-phthalate with temperature.

Water and alcohol have the advantages of good accuracy in measuring small pressure differences. Their disadvantages are a small pressure range on a normal manometer (which will have a height of less than 100 inches) and boiling at moderate vacuum levels. Tetrabromoethane and mercury are less desirable to use but allow the measurement of a greater range in pressures. Dibutyl-phthalate has a low specific gravity and a very low boiling pressure and is thus useful for accurate measurements at low pressure levels.

Manometers have been used very extensively for pressure measurements in wind tunnels in the past. Their use is on the decline for three major reasons. First, they are relatively slow response measuring devices because of relatively large volumes between the pressure port and the manometer fluid. This has almost precluded their use for accurate pressure measurements in intermittent tunnels, which comprise the major portion of wind tunnels now in use. Second, they tend to complicate the data-handling process. Excluding the few very expensive automatic reading manometers, they are usually read manually while the test is in progress, or photographed and the photographs read manually after the test. Either method requires a great deal more manual effort and time than the more modern pressure-measuring and recording systems. The third disadvantage is the difficulty of use. Many tunnel engineers can attest to the fact that it is not difficult to apply too high or too low a pressure to a manometer and wind up with manometer fluid all over the floor or in the tunnel. A little dirt in a tube, a bubble in a line, or condensate changing the fluid specific gravities can all produce anomalous readings.

6:5 Dial-Type Pressure Gages

Dial-type pressure gages (Fig. 6:8) usually operate on the principle of a bellows or a Bourdon tube deflecting as a result of a pressure change and driving the needle on a dial through a mechanical linkage. Gages of this type range in cost from a few dollars up, with cost being closely related to accuracy. Although gages of this type may be obtained with accuracies suitable for measuring wind tunnel pressures, they are not extensively used for this purpose. Their primary use is for visual monitoring of pressures in the many plumbing circuits required for the usual wind tunnels.

Dial-type gages do have the advantage over a manometer of being easier to read. Also, they can be obtained for pressure ranges well beyond those of the manometer. Their primary disadvantage is that they must be calibrated periodically to ensure that they continue to read correctly. A second disadvantage is that manometers are cheaper when there is a large number of pressures to be read, and a third, as with manometers, is that they cannot be easily read electronically.

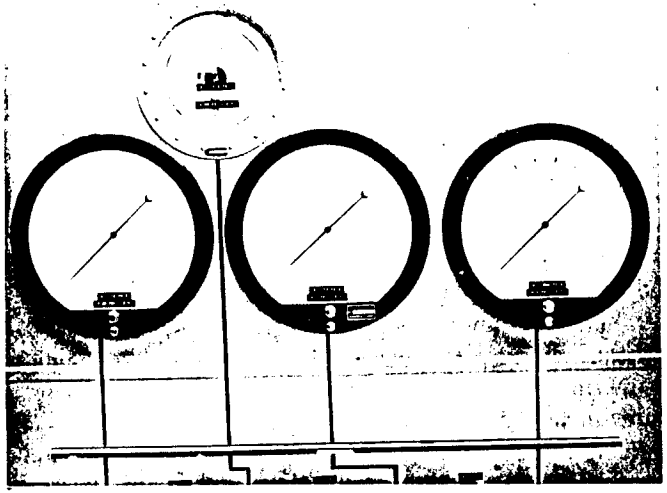


Fig. 6:8 Dial-type pressure gages.

6:6 Pressure Transducers

Pressure transducers are electromechanical devices that convert pressures to electrical signals which can be recorded with a data system such as that used for recording strain gage signals (Section 7:4). Several typical pressure transducers used in wind tunnel operation are shown in Fig. 6:9. The internal cavity of the transducer is divided into two parts by a thin metal diaphragm. The pressure to be measured is applied to one side of the diaphragm and a reference pressure is applied to the other side. The resulting differential pressure causes a bending of the thin metal diaphragm. The displacement of the diaphragm is sensed electrically. Common techniques are to let the movement of the diaphragm cause changes in tension of very fine resistance wires which are actually strain gages, or to use the movement of the diaphragm to change the inductance or capacitance of an electrical circuit. Pressure transducers can be bought commercially for measuring any pressure in the range normally required in wind tunnels except the very low pressures found in high Mach number tunnels. Design pressure ranges of 0 to 0.3 to 0 to 5000 psi (absolute or gage) are readily available and cost from about 200 dollars up, with the lower-range transducers costing more. They are generally precision instruments and often yield signals that are consistent to 0.1 per cent of design pressure or better when used properly.

Pressure transducers have the following advantages over manometers and other pressure gages: they provide a signal proportional to pressure

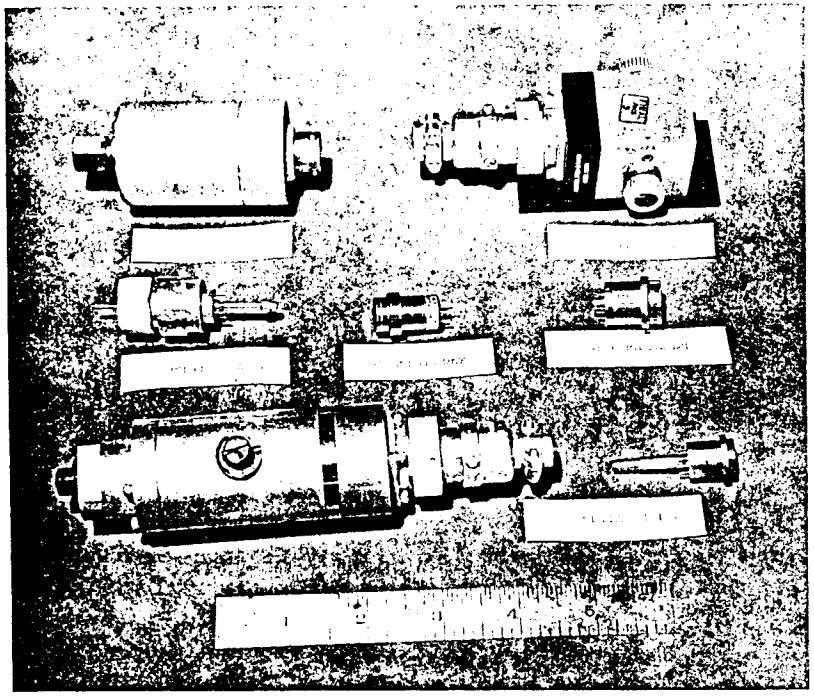


Fig. 6:9 Several pressure transducers.

which can be automatically recorded by the usual wind tunnel data system, they are relatively low volume devices and consequently respond more rapidly to pressure changes, and they are small enough to be mounted inside some wind tunnel models. Their major disadvantages relative to a good manometer is that they must be calibrated whereas the manometer with a known fluid can be considered a pressure standard.

Because of the relatively large cost of pressure transducers in quantity, a scheme has been devised for using one transducer to measure a number of pressures—up to 48 or more. This scheme is the commutation of pressures using a device known as a "pressure scanner valve" (Fig. 6:10). In using the scanner valve, model pressures are allowed to stabilize in the lines leading from the model through the stator of the scanner valve. The rotor is then turned through one revolution, connecting each model pressure in turn to the pressure transducer through a slot. Seals between the individual model pressures at the scanner valve are commonly maintained by the very close contact of the hardened steel surfaces of the stator and rotor which are lapped together. The force holding the two surfaces in close contact is sometimes provided by a pressure equal to or greater

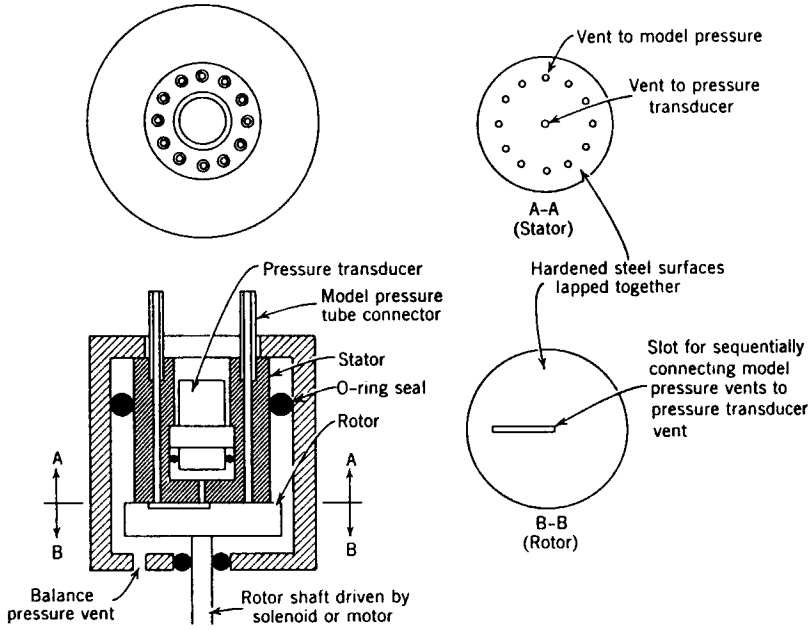


Fig. 6:10 Schematic of a pressure scanner valve.

than the highest model pressure. Obviously, the mating surfaces must be kept very clean in order to avoid leakage of pressures. If the two surfaces should be accidentally separated, for example by loosing the balance pressure, the rotor should be turned through several revolutions to pulverize any dirt that may have gotten between the surfaces. If the valve leaks after this has been done, it will be necessary to disassemble and clean the valve. Lens tissue is normally used for cleaning and a single drop of light silicone oil is put on the surface before reassembly.

When using a scanner valve in a blowdown wind tunnel, a common mode of operation is as follows. The pressure in the lines will be allowed to equalize over a period of time during the run. At the end of this time, a guillotine (or other type) clamp is used to trap the model pressures in these lines. The tunnel is then shut down and the lines are sequentially connected to the transducer and pressure readings taken. The volumes of the lines in which the pressures are trapped are large compared to the scanner valve and transducer volume (more than 100 times) so that the volume when vented to the transducer is not materially affected. This mode of operation requires a minimum use of air for blowdown tunnel operation. A photograph of such an installation is presented in Fig. 6:11.

Pressure scanner valves can be obtained with wide ranges of scanning

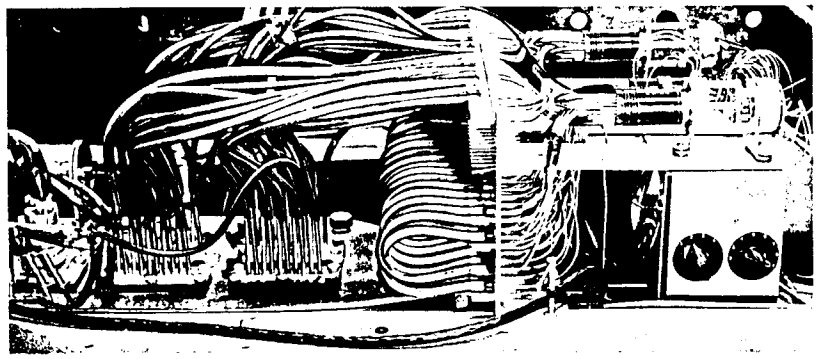


Fig. 6:11 A pressure scanner system installation.

speeds. The two major limitations are transducer stabilization time and data-recording time. A typical scanning rate is 100 pressure ports per minute. Scanner valves may be equipped with switches that indicate the position of the scanner valve each time a pressure is recorded. Common practice in the use of a scanner valve is to vent one or more of the pressure connectors to a known reference pressure to obtain an indication of any transducer drift.

6:7 Calibration of Pressure Gages or Transducers

Calibrating a pressure gage or transducer consists of applying a series of known pressures and obtaining a series of corresponding readings. If a dial gage is being calibrated, differences between actual and indicated pressures will be calculated. The differences will be examined to determine if they are random or if there is a consistent error that would warrant corrections to the dial readings. If a transducer is being calibrated, a straight line will be faired through a plot of pressure versus reading to determine a slope $d(\text{pressure})/d(\text{reading})$ to be used in reducing test data. The differences between the faired line and the experimental points will provide a good indication of the transducer performance. The most desirable and most accurate method of defining the straight line is by use of a least squares fit to the data. The following equations yield a slope and intercept for a least squares straight line through a set of data.

$$\frac{dr}{dp} = \frac{n\sum p_i r_i - \sum p_i \sum r_i}{n\sum p_i^2 - (\sum p_i)^2} \tag{6:1}$$

$$r_{(\text{at } p=0)} = \frac{\sum p_i^2 \sum r_i - \sum p_i \sum p_i r_i}{n\sum p_i^2 - (\sum p_i)^2} \tag{6:2}$$

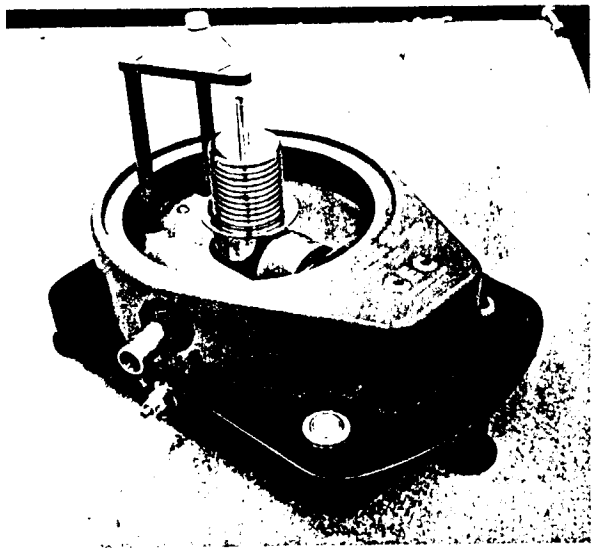


Fig. 6:12 A dead weight tester.

where Σ indicates a summation from $i = 1, \ldots, n$,

p = pressure, any units,

r = reading, counts,

n = number of data points of calibration.

Although the above may appear to indicate that pressure calibrations are simple, the large pressure range which must be considered can lead to very significant practical problems.

Manometers are the most readily available standards for measuring pressures and can be purchased with accurate scales in maximum lengths to about 100 inches, which for mercury corresponds to a pressure of about 50 psi. This value may be considered the upper limit for the use of a manometer as a pressure calibration standard. For higher pressures a second type of standard is required. The most frequently used is a dead-weight tester (Fig. 6:12). This consists of a piston in an oil-filled cylinder with the provision for applying precise weights to the piston to obtain precise oil pressures. The piston is rotated continuously during use in order to avoid erratic oil pressures due to friction between the piston and cylinder. Needless to say, the dead-weight tester is a precision device.

For pressure calibrations over ranges below about 0 to 10 psid,* the usual 100-inch mercury manometer begins to loose its usefulness. The scales provided for the usual 100-inch manometer can be easily read only to a fraction of a millimeter so reading accuracy becomes important.

* Differential between measured and reference pressure.

Further, such a manometer is very bulky and cannot be readily transported to the vicinity of a device needing calibration. Manometers are available in heights of about 30 inches with precise scales, verniers, and meniscus viewing arrangements which allow reading the height of the fluid column to about a 0.1 millimeter. The barometer of Fig. 6:2 is often used as a precision manometer by venting the top of the tube to a reference pressure or a pressure to be measured. When mercury is used as a fluid, manometers are adequate for calibrations down to ranges of about 0 to 1.0 psid. When oil is used as a fluid, they are adequate for calibrations down to ranges of about 0 to 0.1 psid. For calibrations over ranges significantly less than 0 to 0.1 psid, a special-purpose manometer called a "micromanometer" has been used. A manometer of this kind with a useful range of about 0 to 0.05 psid is illustrated in Fig. 6:13. This manometer uses oil with a low boiling pressure such as butyl-phthalate or DC-200 silicone oil. The difference between heights of the two fluid columns is measured by using micrometers that drive pointed plungers down until they break the surface tension of the fluid columns. Each fluid column can be read to 0.0001 inch with this arrangement and readings of column height have been found to be repeatable to about 0.0005 inch, which corresponds to about 1.8×10^{-5} psid.

When pressure-measuring devices need to be calibrated over a pressure

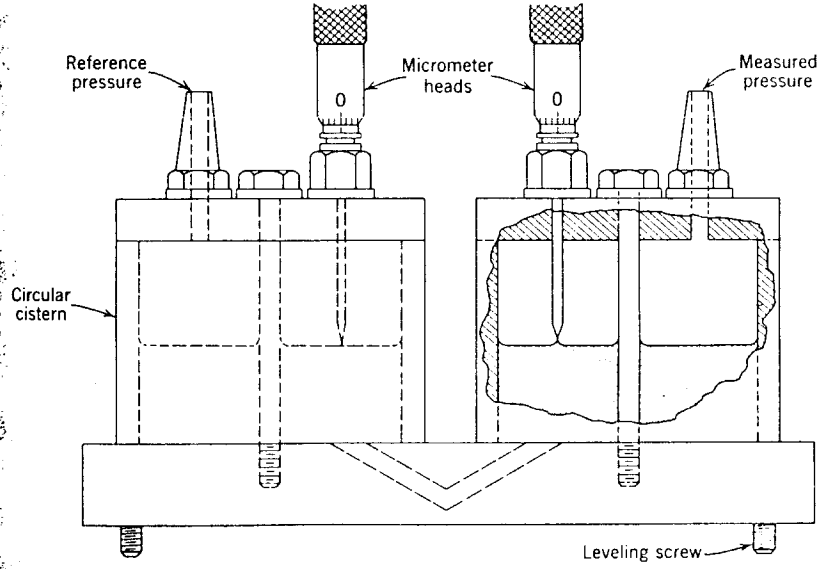


Fig. 6:13 A 2-inch cistern micromanometer. All joining surfaces have teflon "O" ring seals, not shown.

range of 0 to 2 psid or less, the pressure to be measured during a test will most frequently be near absolute zero. When this is true, the most convenient pressure to use as a reference is a pressure near enough to absolute zero that it may be considered absolute zero for purposes of calibration or testing. Such a pressure would typically be less than 0.1 per cent of the calibration range; that is, less than 0.002 psia for a 0 to 2 psia calibration. Absolute zero is the most convenient reference pressure because it is easier to get a pressure near enough to absolute zero and to know that you have it than it is to get some higher pressure and know what you have.

A schematic of an arrangement for calibrating low-pressure transducers is presented in Fig. 6:14. A pumping system is connected to a manifold through a valve. Connected to the manifold are the transducer to be calibrated, a device for rough monitoring of pressure in the manifold, a bleed valve, and two sides of a manometer through valves and traps. The traps are devices to catch the manometer fluid and prevent its entering the manifold and pumping system in the event that one of the manometer valves is operated at the wrong time. In use with the system at atmospheric pressure, the manifold shutoff valve and the valves to the manometer are opened, and the bleed valve closed. The pumping system is then turned on and the manifold pressure monitor observed until the pressure in the

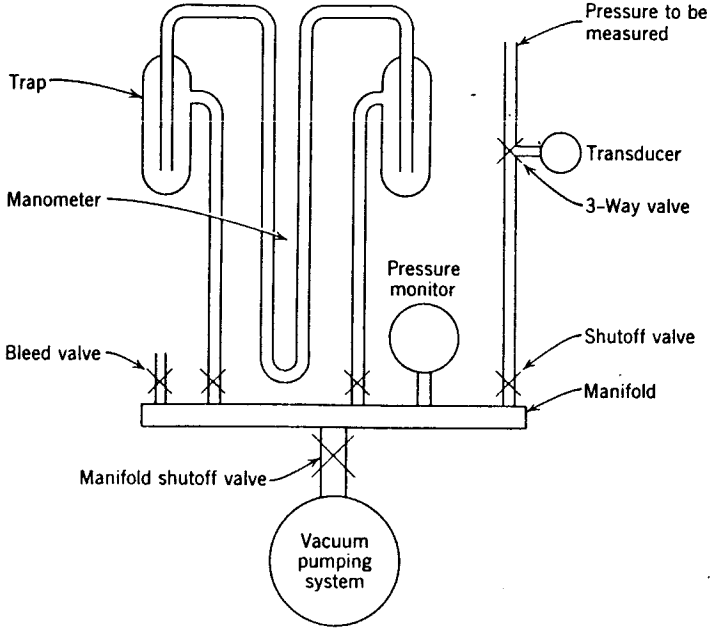


Fig. 6:14 Schematic of an arrangement for calibrating transducers at low pressure.

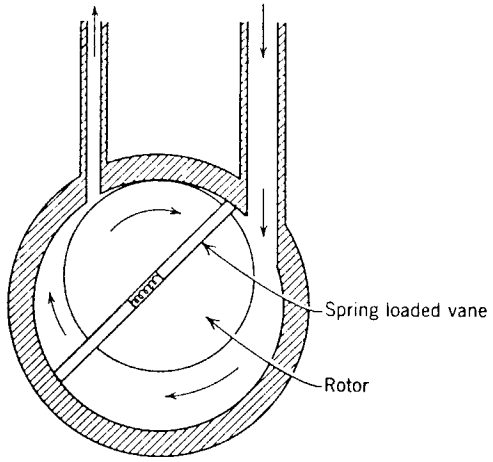


Fig. 6:15 Schematic of rotary piston vacuum pump.

manifold reaches a value low enough to be called zero for the purposes of the calibration. One of the manometer valves is then closed, trapping this reference pressure in one side of the manometer. The manifold shutoff valve is then closed and the bleed valve opened to let a small amount of air into the manifold. The difference between the manifold pressure and the reference pressure trapped in one side of the manometer is registered on the manometer. This difference is measured and recorded along with a reading from the transducer. The procedure is repeated several times until the pressure in the manifold reaches a maximum value corresponding to the limit of the calibration.

The vacuum pumping system always includes a mechanical pump, commercially obtainable with a capability of absolute pressures down to about one micron (one millionth of a meter of mercury or 1.93×10^{-5} psi). The principle of operation of a common mechanical vacuum pump is illustrated in Fig. 6:15. Mechanical pumps have a limited pumping capacity at the lower pressures and a diffusion pump is often used as a first stage in the pumping system. The diffusion pump is normally designed to operate at inlet pressures below 5 mm mercury absolute and to discharge into a mechanical type of vacuum pump. It has a considerably greater pumping capacity than a matching mechanical pump at pressures below about 5 mm mercury. Its principle of operation is illustrated in Fig. 6:16. Air molecules are widely separated at low pressures and the oil vapor jets trap the molecules and cause a relatively high concentration at the pump discharge port. A photograph of a mechanical-diffusion vacuum pumping system is shown in Fig. 6:17. Several types of gages are available for conveniently monitoring the manifold pressure with a satisfactory accuracy

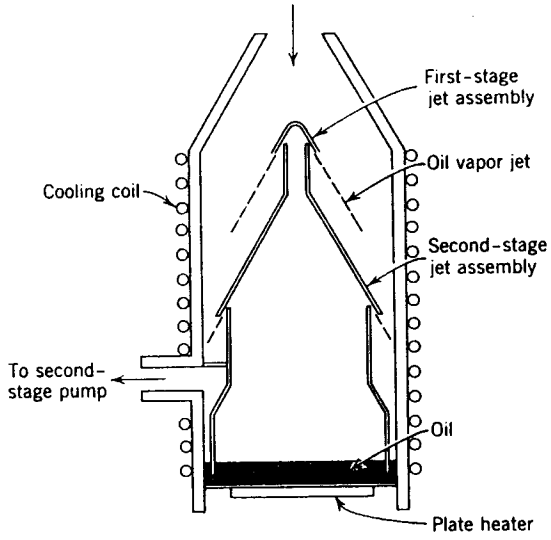


Fig. 6:16 Schematic of an oil diffusion pump.

at pressures of the order of 1 micron mercury absolute. Among the most common of these are the "thermocouple gage" and the "alphatron." The thermocouple gage uses a wire in the vacuum system with a constant rate of supply of electrical energy to the wire. At low pressures where convection heat losses are small, and at moderate temperatures where radiation

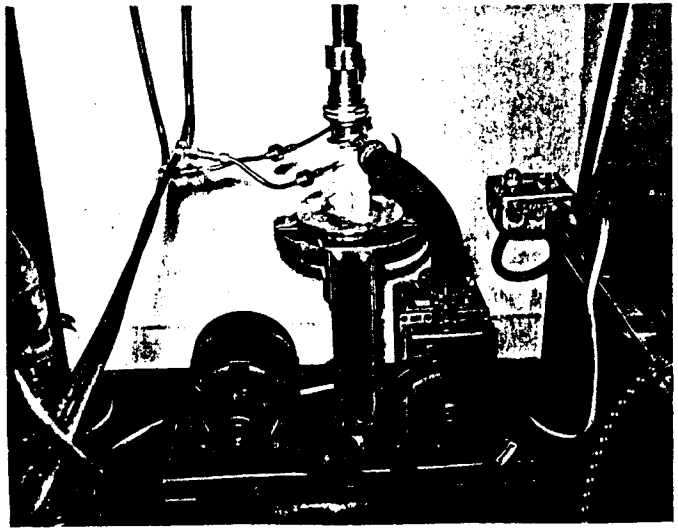


Fig. 6:17 A mechanical pump-diffusion pump vacuum pumping system installation.

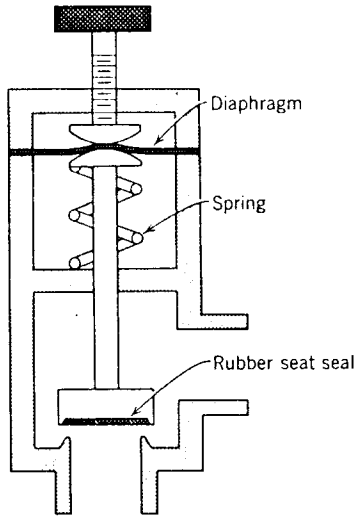


Fig. 6:18 Schematic of a high-vacuum valve.

heat losses are small, the temperature of the wire is dependent primarily on the conduction to the air surrounding the wire. The conduction heat losses are in turn a function of the pressure of the surrounding air. The temperature of the wire is monitored by a thermocouple attached to the wire and the output of the thermocouple is indicated by a suitable galvanometer. The alphatron *gage* includes a source of alpha particles (usually a gold radium alloy in a sealed capsule). A constant flow of the alpha particles through a chamber connected to the vacuum system causes an ionization of the air in the chamber. The ions are collected on a grid and produce a flow of current. The current flow is proportional to the rate of ionization which is in turn a function of the pressure. The ionization current is amplified and then indicated by a micro-ammeter.

Valves for use in vacuum systems are special-purpose valves but may be obtained commercially. A schematic of one type of high-vacuum valve is shown in Fig. 6:18. Copper, steel, aluminum, and bronze are commonly used for the permanently plumbed portions of a vacuum system such as the manifold and piping between the pumps and the manifold. Care is required in the assembly of such plumbing because the fluxes required in normal welding and brazing processes leave a residue that will be converted to gas at low pressures (outgas). If such joining processes are used, the design should be such that a minimum of the flux will be deposited on the vacuum side of the weld. Fluxless welding by using an electric arc in a shielding atmosphere of argon or helium or furnace brazing in an inert

atmosphere are preferred methods of joining metals for vacuum applications. (Also see Section 4:9.)

Rubber, neoprene, and polythene tubing are suitable for flexible connections in vacuum systems with pressures down to one micron. Many plastics, however, outgas very badly at these low pressures.

Semi-permanent joints between glass, metal, or ceramics may be made by using low vapor pressure waxes such as the "Apiezon W" waxes. Rubber gaskets and O-rings are extensively used in sealing temporary joints. "Apiezon" and silicone greases are suitable for use in vacuum applications. A thorough treatment of present-day vacuum technology is presented in Ref. 6:2.

6:8 Air Temperature Measurements

The measurement of air temperature is a routine part of the operation of most if not all wind tunnels. Air temperature is required for calculating Reynolds number. In unheated blowdown tunnels, the temperature must in some cases be monitored to avoid total temperatures low enough to allow condensation in the nozzle. In unheated continuous tunnels, the air temperature must be monitored to avoid overheating of the tunnel circuit due to failure of the aftercooler. In tunnels using air heated to 1000°R or above the temperature must be known for the reduction of routine force and moment data. Air temperature measurements are also required for tests involving boundary layer and heat transfer studies.

On any stationary device placed in an air stream a boundary layer will develop. In the boundary layer immediately adjacent to the exposed surfaces of the device the air will be at rest. This air at rest will have had the kinetic energy of the air stream converted back to temperature and will consequently be at the *total* temperature of the airstream rather than at the *static* temperature. Thus, any stationary device placed in an airstream will be subjected to the total temperature. In other words, static temperatures of a moving air stream cannot be measured with a stationary device.

6:9 Thermocouples

The measurement of air temperatures in high-speed wind tunnels are almost invariably made with thermocouples. Thermocouples are devices which operate on the principle that a flow of current in a metal accompanies a flow of heat. In some metals the flow of current is in the direction of heat flow. In other metals, the flow of current is in the direction opposite to that of the heat flow. Thermocouples consist of two dissimilar metals (usually in the form of wire) joined together at two points, one point being the place where the temperature is to be measured and the other point

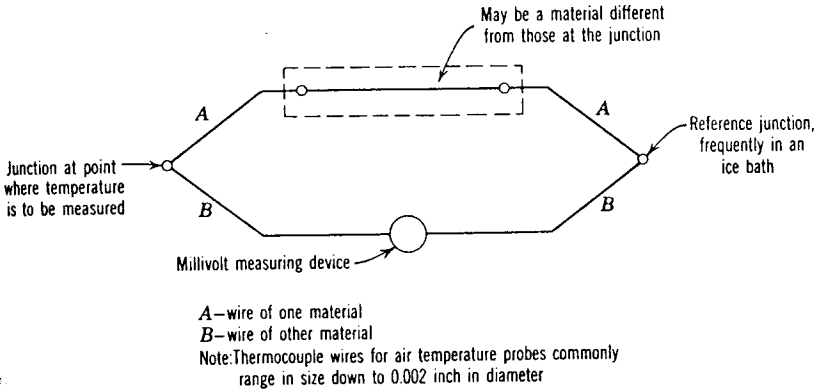


Fig. 6:19 Arrangement of a thermocouple.

being a place where the temperature is known (called the reference junction). The reference junction may be an ice bath at 32°F, an oven at some closely regulated temperature, or a junction with an associated circuit to yield the effect of some known reference temperature.

The most effective thermocouples are those having dissimilar metals with opposite directions of current flow for a given direction of heat flow. In such a case with a hot thermocouple junction, heat will be flowing away from the junction in each of the two dissimilar metals. Since the heat will be flowing in opposite directions in the circuit, the currents induced in the two dissimilar metals will be in the same direction and will be additive.

The voltage developed in a thermocouple circuit is independent of wire size A material different from the two dissimilar metals may be used in a thermocouple circuit without altering the induced voltage as long as the temperature of the third material does not vary over its length. If no third material is used, the induced voltage will be independent of the temperature of the wire connecting the two thermocouple junctions. A schematic of a thermocouple circuit is presented in Fig. 6:19. The voltages developed for a number of common thermocouple materials from Ref. 6:3 are presented in Table 6:1 as a function of temperature for a reference junction temperature of 32°F. It is noted that voltages developed are a function of the absolute temperature levels of the two junctions rather than the temperature difference between the two junctions. This fact should be considered in using the data of Table 6:1 to obtain voltage readings corresponding to a different reference junction temperature.

6:10 Supersonic Total Temperature Probes

These probes are devices to be used in a supersonic airstream, as in the test section of a wind tunnel. Supersonic stagnation temperature probes

Table 6:1

Temperature-Millivolt Tables for Commonly Used Thermocouple Materials

(Temperature in °F, Reference Junctions at 32°F)

Materials: A—Copper versus Constantan
B—Iron versus Constantan
C—Chromel versus Alumel
D—Platinum versus Platinum 10 per cent Rhodium

Temp, °F	Millivolts for: A	B	C	D	Temp, °F	Millivolts for: B	C	D	Temp, °F	Millivolts for: C	D
−300	—	−7.52	−5.51	—	850	24.85	18.70	3.775	2050	45.96	10.992
−250	—	−6.71	−4.96	—	900	26.40	19.89	4.046	2100	47.00	11.323
−200	—	−5.76	−4.29	—	950	27.95	21.07	4.319	2150	48.03	11.655
−150	—	−4.68	−3.52	—	1000	29.52	22.26	4.596	2200	49.05	11.989
−100	—	−3.49	−2.65	—	1050	31.12	23.44	4.874	2250	50.06	12.322
−50	—	−2.22	−1.70	—	1100	32.72	24.63	5.156	2300	51.05	12.657
0	−0.670	−0.89	−0.68	—	1150	34.36	25.81	5.440	2350	52.03	12.991
32	0	0	0	0	1200	36.01	26.98	5.726	2400	53.01	13.325
50	0.389	0.50	0.40	0.056	1250	37.71	28.15	6.015	2450	53.97	13.658
100	1.517	1.94	1.52	0.221	1300	39.43	29.32	6.307	2500	54.92	13.991
150	2.711	3.41	2.66	0.401	1350	41.19	30.49	6.601	2550	—	14.324
200	3.967	4.91	3.82	0.595	1400	42.96	31.65	6.897	2600	—	14.656
250	5.280	6.42	4.97	0.800	1450	—	32.80	7.196	2650	—	14.988
300	6.647	7.94	6.09	1.017	1500	—	33.93	7.498	2700	—	15.319
350	8.064	9.48	7.20	1.242	1550	—	35.07	7.803	2750	—	15.649
400	9.525	11.03	8.31	1.474	1600	—	36.19	8.110	2800	—	15.979
450	11.030	12.57	9.43	1.712	1650	—	37.31	8.420	2850	—	16.308
500	12.575	14.12	10.57	1.956	1700	—	38.43	8.732	2900	—	16.637
550	14.157	15.65	11.71	2.205	1750	—	39.53	9.048	2950	—	16.965
600	15.773	17.18	12.86	2.458	1800	—	40.62	9.365	3000	—	17.292
650	17.421	18.72	14.02	2.716	1850	—	41.70	9.686	3050	—	17.618
700	19.100	20.26	15.18	2.977	1900	—	42.78	10.009	3100	—	17.943
750	20.805	21.79	16.35	3.240	1950	—	43.85	10.334	3150	—	18.267
800	—	23.32	17.53	3.506	2000	—	44.91	10.662	3200	—	18.590

Fig. 6:20 Design of stagnation temperature probe. Thermocouple support and shield made of silica with all exposed surfaces platinum coated; thermocouple: iron-constantan, 0.01-inch diameter, fiberglass insulated; two vent holes (Ref. 6:4).

usually measure temperatures from slightly below to considerably below the true stagnation temperatures. The performance of such a probe is usually defined by a "recovery factor" as follows:

$$r = \frac{T_m - T}{T_t - T} \tag{6:3}$$

where r = recovery factor, dimensionless,
T_m = measured temperature, °R,
T = static temperature, °R,
T_t = total temperature, °R.

Sometimes, a single ratio T_m/T_t is used instead of the recovery factor in defining probe performance.

A sketch of one of the early stagnation temperature probes for use in test sections of high-speed wind tunnels is presented in Fig. 6:20 (from Ref. 6:4). Recovery factors for probes of this type (also from Ref. 6:4) are presented in Fig. 6:21 where it is seen that recovery factor drops very rapidly with increases in total temperature and also with increases in Mach number. Data are presented in Ref. 6:4 which indicate that a large portion of the losses of such a probe result from conduction of heat from the thermocouple junction into its support base; that with thermocouple wires extending 50 to 100 diameters from the support base to the junction, recovery factors for the conditions of Fig. 6:21 can be increased to 0.96 to 0.99.

Probes of the type shown in Fig. 6:20 were designed to be used in tunnels having test times long enough to allow stabilization of the temperature of all parts of the probe. In intermittent tunnels where test times are insufficient for temperature stabilization, a different approach is required. One such approach is described in Ref. 6:5 and Fig. 6:22. In this approach, the shield is an electrical heating element. A thermocouple

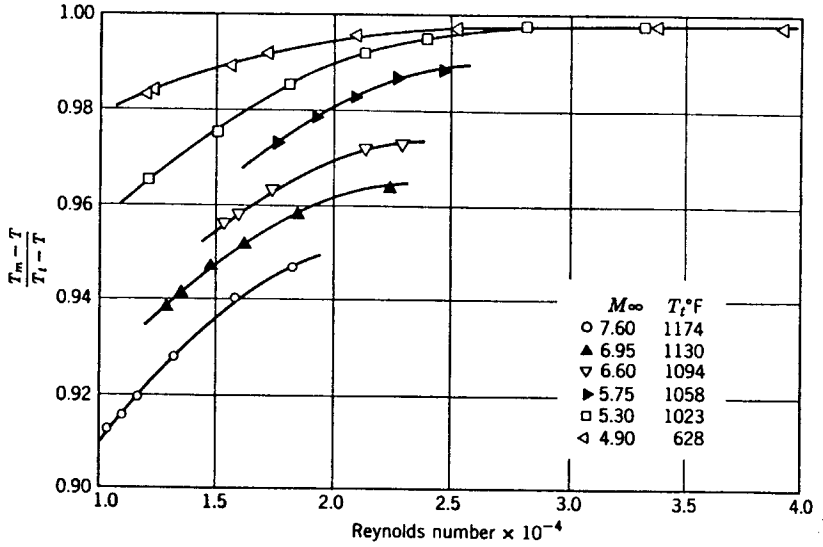


Fig. 6:21 Variation of probe temperature recovery factor with freestream Reynolds' number at various freestream Mach numbers from Ref. 6:4. Vent/entrance area = 1:5. Reynolds number based on probe entrance outside diameter. Ten wire diameters from support base to thermocouple junction.

is installed on the shield for indicating shield temperature. The outputs of the shield and air thermocouples are compared and electrical power is applied to the shield until the two outputs are equal, indicating that air and shield temperatures are equal. When this condition is reached the output of the air thermocouple is recorded. In a Mach 5 nozzle with air temperatures to 880°F in the settling chamber, this probe indicated test section temperatures 10°F below settling chamber temperatures. A large portion of this difference was attributed to a loss of total temperature between the settling chamber measuring station and the nozzle throat.

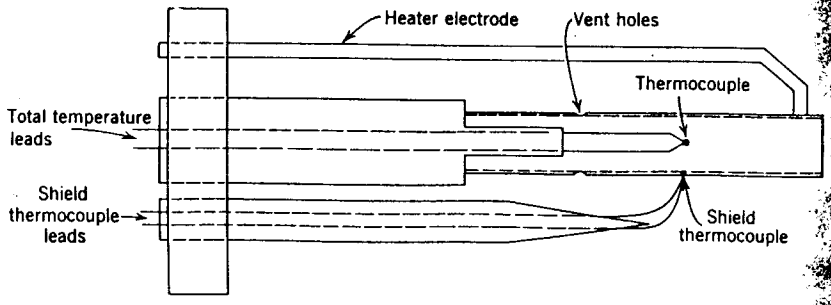


Fig. 6:22 Supersonic total temperature probe.

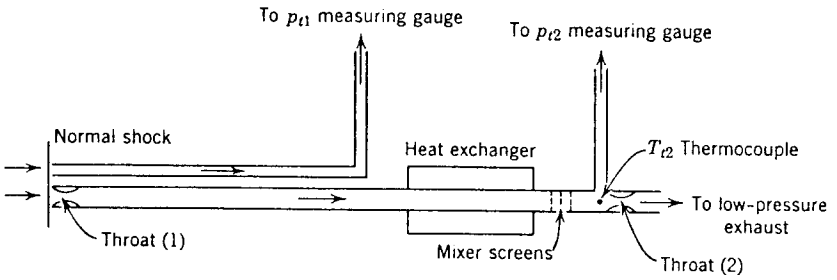


Fig. 6:23 Schematic of "sonic-pneumatic" total temperature probe.

Another approach that is applicable to intermittent tunnels is described in Ref. 6:6 and Fig. 6:23. The probe used in this approach has its greatest potential in the measurement of temperatures in airstream above the melting temperature of metals used for its fabrication, the reason being that the probe can be completely cooled without affecting the temperature measurement. The probe is called a "sonic-pneumatic probe." As indicated in Fig. 6:23, the probe includes two sonic throats with a heat exchanger between. Its operation is based on the principle that the mass flow through the two throats must be equal. Writing the equations for the mass flow through the two throats and equating them, we obtain

$$T_{t1} = \left(\frac{\rho_1}{\rho_{t1}}\frac{\rho_{t2}}{\rho_2}\right)^2 \frac{T_1}{T_{t1}}\frac{T_{t2}}{T_2}\frac{\gamma_1}{\gamma_2}\left(\frac{A_1}{A_2}\right)^2\left(\frac{p_{t1}}{p_{t2}}\right)^2 T_{t2} \qquad (6:4)$$

where T = temperature, °R,
ρ = density, slugs/ft³,
γ = specific heat ratio,
A = area, ft²,
p = pressure, lb/ft²,

and the subscript t indicates total conditions, 1 indicates a condition at the sonic point in the first throat, and 2 indicates conditions at the sonic point in the second throat.

When the air passing through the heat exchanger is cooled to near room temperature, γ_2, ρ_{t2}/ρ_2 and T_{t2}/T_2 are constant. In this case eq. (6:4) can be rewritten

$$T_{t1} = K\left(\frac{A_1}{A_2}\right)^2\left(\frac{p_{t1}}{p_{t2}}\right)^2 T_{t2} \qquad (6:5)$$

where K is a function only of T_{t1} with values as shown in Fig. 6:24.

Values of p_{t1}, p_{t2}, and T_{t2} are measured as indicated in Fig. 6:23. The ratio A_1/A_2 is obtained by calibration at air temperatures low enough for T_{t1} to be measured accurately. The value of T_{t1} is calculated using an iterative process with K dependent on T_{t1}.

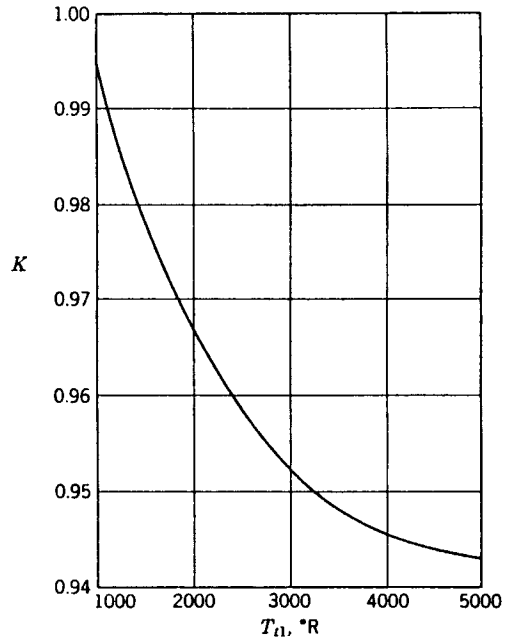


Fig. 6:24 Variation of constant in eq. 6:5 with total temperature. (Redrawn from Ref. 6:6.)

The value of this probe stems from the fact that the only temperature requiring measurement is a low temperature where an accurate measurement is possible. The probe has been used for the measurement of temperatures in a Mach 10 wind tunnel with total temperatures to 2700°R with a random scatter of up to ±3 per cent.

6:11 Settling Chamber Total Temperature Probes

The settling chamber is the usual place for monitoring air temperature for routine tunnel operation. It is also the place in the tunnel where temperature is monitored for determining a reference temperature for probes such as those described in the previous section.

There are many cases in which settling chamber temperatures can be accurately measured with a simple bare-wire thermocouple, that is, a thermocouple in which the two wires extend out of the base support with no shielding and with a large number of wire diameters between the base and the junction. Probes of this type are satisfactory when the temperatures to be measured are near room temperature. They have been used satisfactorily to above 2000°F in continuous tunnels. In such cases, the base

support reached temperatures very near air temperatures and the tunnel walls were hot, so that conduction and radiation losses from the junction were small.

In intermittent hypersonic tunnels, probes of this type may be expected to operate satisfactorily if the Reynolds numbers are high enough so that the convective heat transfer to the wire junction is sufficiently high relative to the conduction and radiation losses from the junction. It has not been shown, however, what Reynolds numbers are high enough. Usually in intermittent hypersonic tunnels many factors are present which tend to introduce errors in temperature measurement with a bare wire probe. At the highest Mach number of the tunnel, the velocity and consequently the Reynolds number of the flow are low. The run duration is usually short so that neither the base support nor the tunnel walls reach temperatures near air temperature. For use under such conditions shielded and aspirating thermocouple probes have been developed (Figs. 6:25 and 6:26). The aspirating probe uses the difference in pressure between the stagnation chamber and the room, or a low-pressure portion of the tunnel, to create a sonic flow in a tube. The thermocouple junction is located within this tube. Heat transfer rates in sonic flow are very high, so that all portions of the probe are quickly heated to near air temperatures. Heat losses from the thermocouple junction in this case are relatively small and the probe can be expected to indicate very near the total temperature of the air.

6:12 Dewpoint Measurements

It is necessary to monitor dewpoint in all high-speed wind tunnels to ensure that the dewpoint does not become high enough to allow condensation in the nozzle. When practical, the sample of air for which dewpoint is to be measured is taken from the settling chamber of the tunnel during tests. In intermittent tunnels it is sometimes more practical to take the dewpoint sample from the air storage tanks periodically and assume that the dewpoints indicated are representative of those during the test. This method is quite satisfactory as long as there are no sources of moisture between the air storage tanks and the tunnel.

The sample of air for which dewpoint is to be measured is normally regulated to a pressure and temperature near those of the room before its dewpoint is measured. Pressure regulation is normally accomplished by using a valve to control flow rate, and temperature regulation is normally accomplished by passing the air through an adequate length of tubing, usually copper, which is at room temperature.

One of the most basic devices for measuring dewpoint is illustrated in Fig. 6:27. In this device one end of a polished metal rod is submerged in a low-temperature chamber. At equilibrium conditions, the rod will have

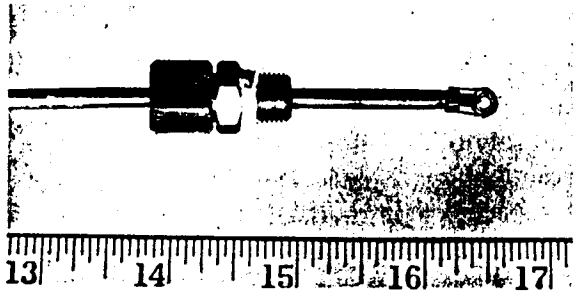


Fig. 6:25 A triple-shielded stagnation temperature probe.

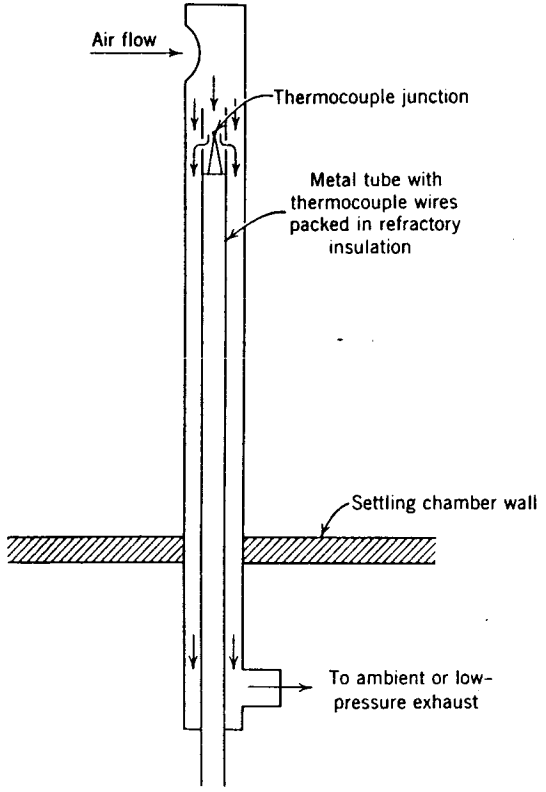


Fig. 6:26 Schematic of an aspirating probe for settling chamber temperature measurements.

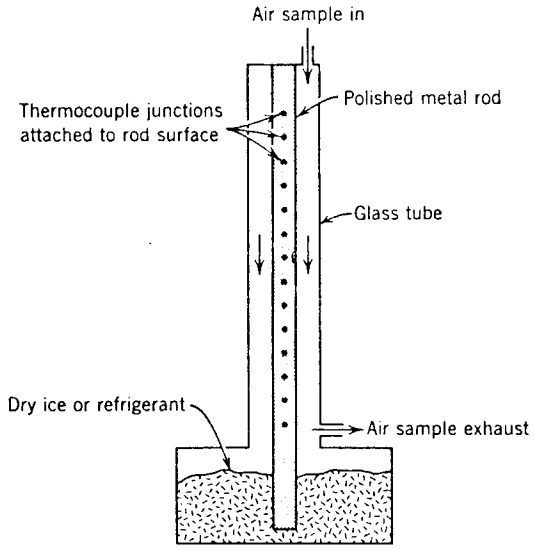


Fig. 6:27 Schematic of dewpoint measuring device.

a temperature gradient varying from that of the refrigerant at the submerged end to perhaps near room temperature at the exposed end. The air sample is introduced into a glass tube surrounding the rod at the exposed end and passed over the rod toward the cold end. When the sample of air reaches the portion of rod at the dewpoint temperature, moisture will condense on the rod and will be quite apparent on the polished surface. The temperature of the rod at points near the moisture line will be obtained from thermocouple measurements of rod temperature at adjacent points.

Another fairly basic device that is sometimes used for measuring dewpoints collects a sample of the air which is compressed by a hand pump to a known pressure. The temperature of the sample is monitored until it reaches a known temperature. The sample is then discharged into a viewing chamber at room pressure. The rapid expansion of the air sample to the lower pressure reduces its temperature. If the expansion reduces the temperature of the sample to below the dewpoint temperature, a cloud will form in the viewing chamber. In operating this device it is necessary to vary the pressure to which the samples are compressed until a pressure is reached at which only a faint trace of a cloud is visible. The temperature of the expanded sample is the dewpoint temperature. A direct relation exists between this temperature, the pressure ratio of the expansion, and the temperature before the expansion. Instruments with this mode of operation (Fig. 6:28) are commercially available at a modest cost.

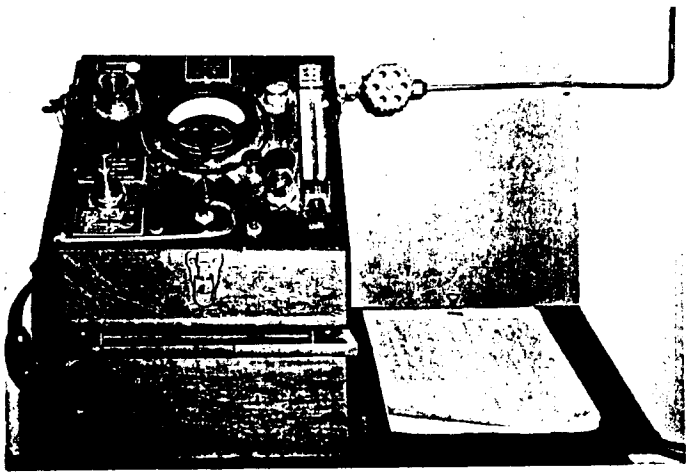


Fig. 6:28 Photograph of a manually operated dewpoint meter.

A less basic but more convenient dewpoint measuring device is one that operates on the principle of electrolysis (chemical decomposition) of water vapor. The sample of air is passed through a sensing element in which electrolysis takes place. The current of electrolysis, which is directly proportional to the mass flow of water vapor through the sensing element, is measured and indicated on a dial graduated in parts of water vapor per million parts of air by volume. Devices of this type are commercially available and extremely convenient to use in that they will continuously indicate the amount of water vapor in the sample without any manual operations. Their primary disadvantage is that they are relatively expensive. Also, the instrument does not correctly read the amount of water vapor present when hydrogen is present in the air sample.

With any of the above dewpoint measuring devices it is desirable to have a dry nitrogen purge system to get rid of excess moisture in the instrument after measurement of high dewpoint samples.

6:13 Heat Transfer Measurements

The measurement of the rate of heat transfer to the surface of a model in a high-speed wind tunnel is usually accomplished by what is called the "thin skin" technique. In this technique, the wall of the model in the region where the heat transfer is to be measured is made quite thin, so that the inside and outside wall temperatures will be nearly equal when the outside wall is being heated. Thermocouples are mounted on the inside surface of the model skin to measure temperature during the heating process. The measured temperature is assumed equal to the average local

skin temperature and the following heat balance equation is used as a basis for data reduction:

$$hA(T_{aw} - T_w)\,dt = wAlC_p\,dT_w \tag{6:6}$$

where h = heat transfer coefficient, Btu/ft²-sec-°R,
A = surface area, ft²,
T_{aw} = adiabatic wall temperature, i.e., the temperature the surface would reach at equilibrium conditions, °R,
T_w = wall temperature, °R,
w = specific weight of material being heated, lb/ft³,
l = wall thickness, ft,
C_p = specific heat of material of wall, Btu/lb-°R,
t = time, sec.

Equation (6:6) is a statement that the heat transferred to a specified area on the model surface during an increment of time is equal to the heat stored in the metal skin under that surface. If the model skin is isothermal and at a moderate temperature when the heating process is started, eq. (6:6) will be accurate for a short time following the start of heating. After a short time, temperature gradients in the skin will develop and this will result in heat transfer along the skin by conduction. Also, after some time the skin temperature will rise to a point where radiation heat transfer from the skin will be significant. When heat conduction along the skin and radiation from the skin become significant, eq. (6:6) is no longer accurate.

For use in data reduction eq. (6:6) is rearranged to obtain

$$h(T_{aw} - T_w) = wlC_p \frac{dT_w}{d_t} \tag{6:7}$$

Each variable of the right side of eq. (6:7) will be known from the geometry and thermal properties of the skin and from the temperature time history. The value of the right side of the equation is plotted versus time on log scale graph paper. Fairing the curve to time zero will yield a value of $h(T_{aw} - T_w)$ at time zero, where eqs. (6:6) and (6:7) are accurate. If T_{aw} is known, h can then be determined. If T_{aw} is unknown, more information is required before h can be determined. This is usually obtained by preheating the model before the test, allowing the model to set until the skin temperature is uniform and perhaps 100 to 200°F above ambient, making another aerodynamic heating run, and determining another value of $h(T_{aw} - T_w)$ at time zero. With the two values of $h(T_{aw} - T_w)$ and the corresponding two values of T_w at time zero, information is available to determine both h and T_{aw}. The wall is considered thin enough for this technique to be used when $(T_{aw} - T_{wi})/(T_{aw} - T_{wo})$ is less than 1.0 by not more than the accuracy expected of the experiment

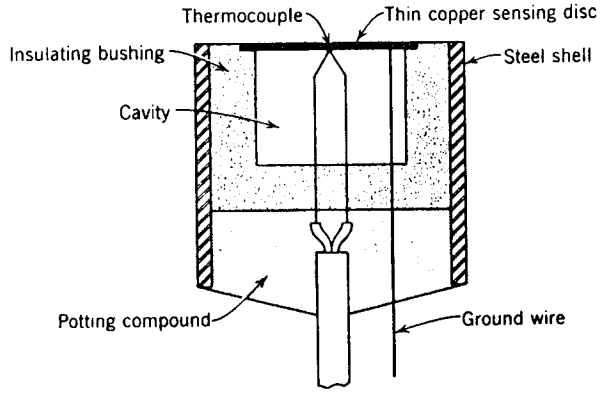


Fig. 6:29 Cross section of a cylindrical heat transfer gage.

(subscripts i and o refer to inside and outside, respectively). An estimate of the differences in temperature through the wall can be obtained by making the assumption that a steady state heat transfer process exists in which all the heat transferred to the wall at initial conditions is being transferred through the wall by conduction. Thus

$$h(T_{aw} - T_{wo}) = \frac{k(T_{wo} - T_{wi})}{l} \qquad (6:8)$$

where k = conductivity of wall material, Btu/ft-sec-°R,

or $$T_{wo} - T_{wi} = \frac{hl}{k}(T_{aw} - T_{wo})$$

Heat transfer tests are sometimes made by using heat transfer gages such as that shown in Fig. 6:29 with the sensing surface installed flush with the outside surface of the model at the point where the heating rate is required. Gages of this type may be obtained commercially. When heat transfer is required at many points on a model or at points where the installation of this type of gage is not feasible, the model is constructed with a thin wall, and thermocouples are installed on the inside surface of the wall. With either technique a temperature–time history is obtained and this together with the physical and thermal properties of the wall and the air temperature makes possible the determination of the heat transfer coefficient. Gages have recently become available commercially which provide an electrical signal proportional to heating rate (Btu/ft²-sec) instead of one indicative of temperature.

6:14 Hot Wire Anemometer

The hot wire anemometer is a device for the study of non-steady high-frequency flow phenomena. In wind tunnels it is used for determining

the turbulence level of the tunnel and for studying boundary layer and wake flows. Although the hot wire anemometer is not frequently used in normal wind tunnel testing, the wind tunnel engineer should have an idea of its construction and its principle of operation. It includes a probe placed in the airstream with a wire sensing element that is usually tungsten or platinum about 0.0002 inch in diameter and $\frac{1}{4}$ inch long. The sensing element is heated to a temperature above that of the stream. It is a part of an electronic system that may be designed either to supply a constant current to the sensing element and give an indication of the change in sensing element resistance, or to supply the amount of current required to maintain a constant sensing element resistance and give an indication of the change in current supplied. In either system, the electrical resistance (and therefore the wire temperature) and the current are known. From the resistance and current, the power dissipated in the wire is known and this dissipation goes into convective heating of the fluid stream. When the physical properties of the wire and the gross properties of the flow are adequately defined, the convective heat transfer can be related to the wire temperature and fluid velocity. Thus, variations in wire resistance or variations in current required to maintain a constant wire resistance are related to variations in fluid velocity. Since the wire has an extremely small thermal mass, it responds to very-high-frequency changes and can be used to obtain both the frequency and the magnitudes of turbulence in the flow.

6:15 Optical Systems

Density gradients in the vicinity of a model in a high-speed tunnel are often quite large, and optical systems have been developed for observing such gradients. Although the type of information that can be obtained from optical systems is generally qualitative, the use of such systems is very much a part of high-speed wind tunnel operation.

Three types of optical systems are available. These are the shadowgraph system, the schlieren system, and the interferometer. The first two of these are used very extensively in normal wind tunnel testing, whereas the third is seldom used. The cost of an optical system may range from a few dollars to many thousand dollars depending on the type and complexity.

6:16 Shadowgraph System

The shadowgraph system is the most simple and least expensive of the three optical systems. The general layout of the most simple shadowgraph system is illustrated in Fig. 6:30. This system includes a point source of high-intensity light (normally a spark gap) on one side of the test section and a film plate on the opposite side of the test section. The normal

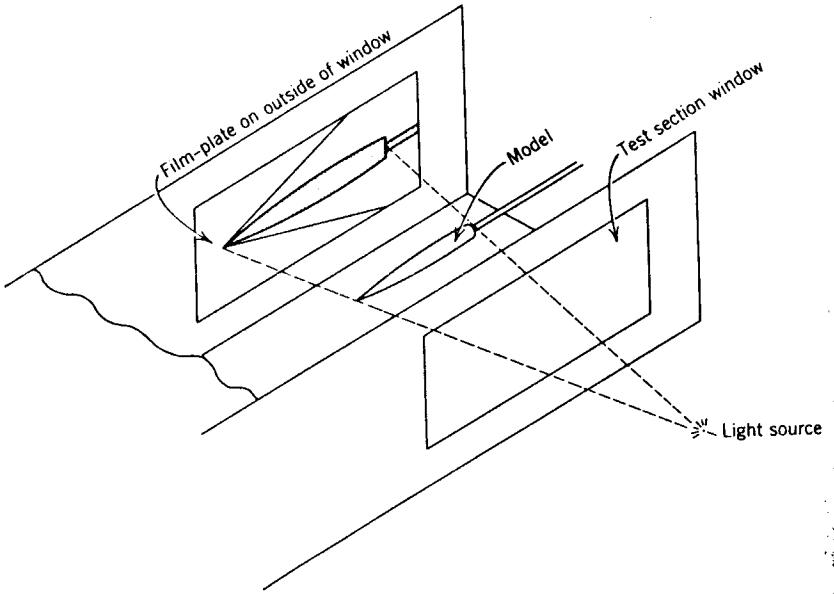


Fig. 6:30 General layout of shadowgraph system.

method of operation of this system is to darken the room, open the shutter of the film plate, trigger the spark gap once, and close the shutter of the film plate. A typical shadowgraph obtained in this manner is presented in Fig. 6:31.

Variations of the system described above are sometimes used. One is to replace the film plate with a screen and to photograph the screen with a camera located on the same side of the tunnel as the light source (Fig. 6:32). Another is to use a condensing lens or a parabolic mirror to make the light rays parallel before passing them through the flow field. However, neither of these variations may be expected to improve the quality of photographs obtained.

To obtain maximum clarity (minimum fuzzing) of shadowgraph pictures it is necessary to have a very short duration of light. Spark gaps with discharge times of one microsecond or less are desired. A typical spark gap configuration is illustrated in Fig. 6:33. It may be adjusted to have a duration of 2 μsec with a time of duration of half-intensity of 0.2 μsec A reasonable power supply would be 6 kv.

The principle of operation of the shadowgraph technique may be described as follows: As light rays pass through a medium of varying density, they will be deflected in proportion to the density gradient $\partial\rho/\partial x$, where ρ is the air density and x is a distance in any direction *parallel* to the

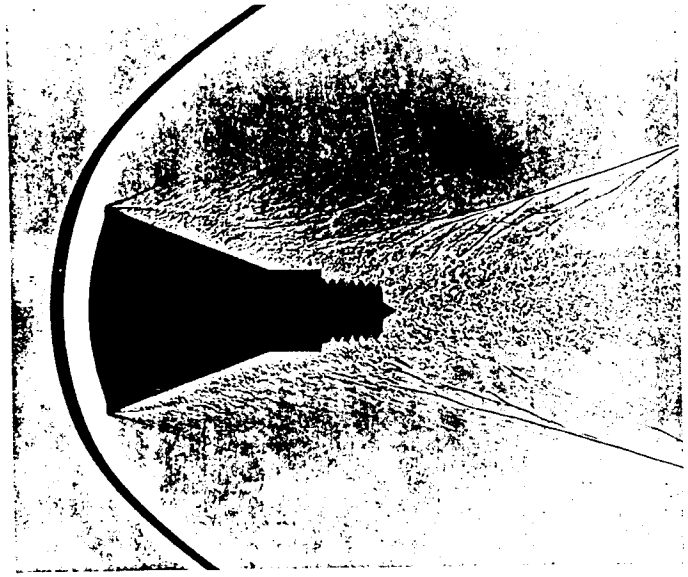


Fig. 6:31 Shadowgraph of Mercury capsule in free flight tunnel. (Courtesy National Aeronautics and Space Agency.)

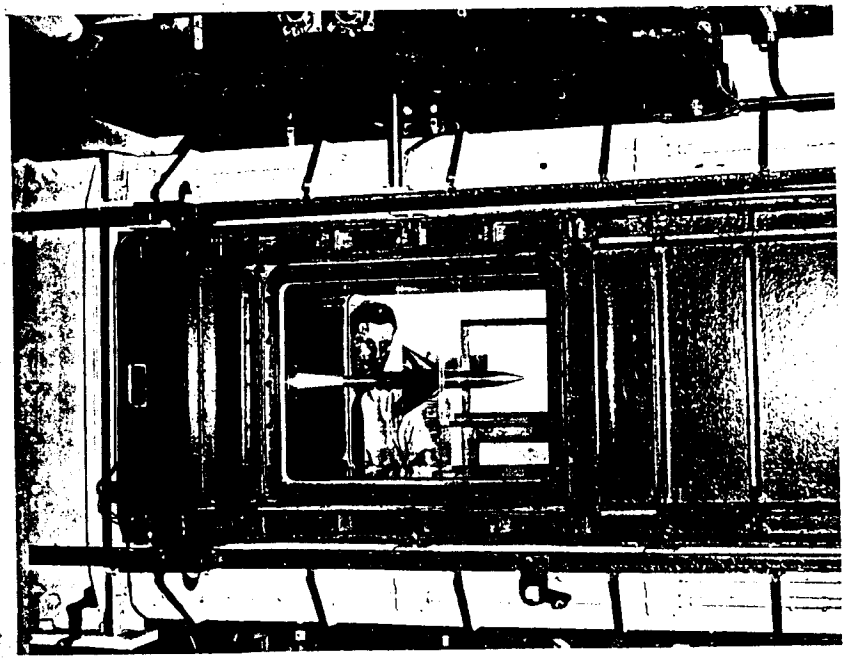


Fig. 6:32 Setup for observing shock waves on a ground glass screen. (Courtesy British Aircraft Corporation.)

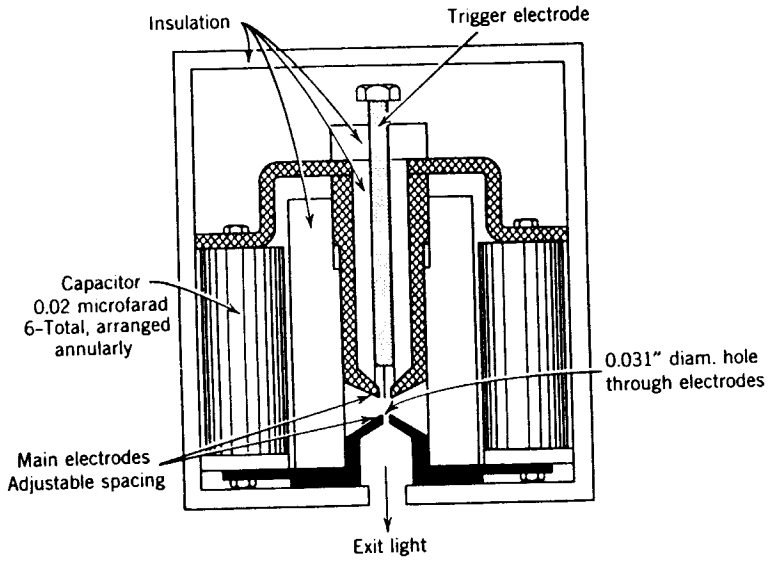


Fig. 6:33 A spark gap light source. Positive potential is shaded, ground is cross-hatched.

film plate. In a region where the density gradient is constant, all light rays passing through the field will be deflected by the same amount and the light intensity at the film plate will be constant. In regions where the density gradient is changing, the deflection of the light rays will not be constant and a variation in light intensity at the film plate will exist. Where the density gradient is increasing ($\partial^2\rho/\partial x^2$ is positive) the light rays passing through will diverge and the illumination of the corresponding place on the film plate will be decreased. Where the density gradient is decreasing, the light rays passing through will converge, causing an increased illumination of the corresponding place on the film plate. Hence, the dark line for the shock followed by the light line in Fig. 6:31.

Where sharp indications of flow discontinuities are desired, the shadowgraph is superior to other optical techniques. A point of interest with regard to interpreting shadowgraph pictures is that the bow shock on the model will often strike the test section window. The observer should not be misled into believing that the shadow at this intersection is a shock on the model.

6:17 Schlieren System

The most used optical system in wind tunnel operation is the schlieren system. This system gives a picture or an image representative of the

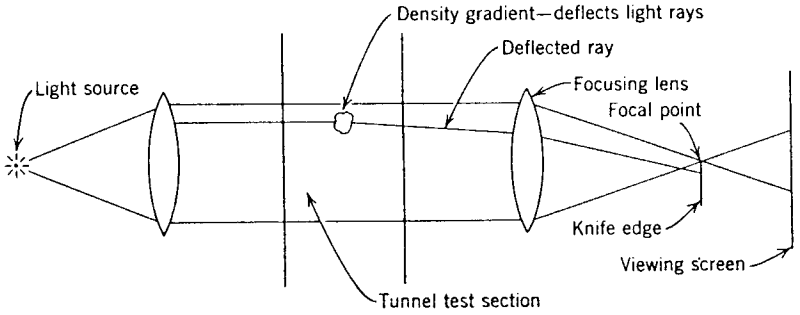


Fig. 6:34 Schematic of schlieren system.

variation of density throughout the complete flow field. A schematic of a schlieren system is presented in Fig. 6:34. Light from a point source is collected into a parallel beam and passed through the wind tunnel test section. The parallel beam is then focused and used to develop an image on a screen. In portions of the test section where the density is varying, the parallel light rays will be bent and consequently will not pass through the focal point. A knife edge is inserted at the focal point to eliminate rays that have been deflected in one direction from parallel. The elimination of these rays from the image results in a variation of illumination which is proportional to the density gradients in the test section. The knife edge may be used in any desired orientation. If perpendicular to the tunnel axis, symmetrical density gradients in the vicinity of a model on the tunnel axis will result in a symmetrical illumination pattern of the image. If the knife edge is parallel to the tunnel axis, the same density gradients will result in an antisymmetrical illumination pattern of the image. That is, a symmetrical shock wave will cause a decreased illumination on one side of the model and an increased illumination on the opposite side of the model. Figure 6:35*a* and *b* are schlieren pictures taken with the knife edge respectively perpendicular to and parallel to the tunnel axis. Schlieren systems used in most high-speed wind tunnels are more complex than that illustrated in Fig. 6:34. Instead of lenses for making the light rays parallel and then focusing them, parabolic mirrors are normally used. There are generally two important reasons for this. The first is that the quality of a front surface mirror required can be obtained more cheaply than a lens of the quality required for the same result. The second is that the mirror arrangement takes up considerably less room.

In wind tunnels where the test section density is very low, as in many hypersonic tunnels, it is difficult to obtain high-quality schlieren pictures. The densities to which satisfactory schlieren pictures can be obtained has been extended in some cases by using a "double-pass" system, that is, by

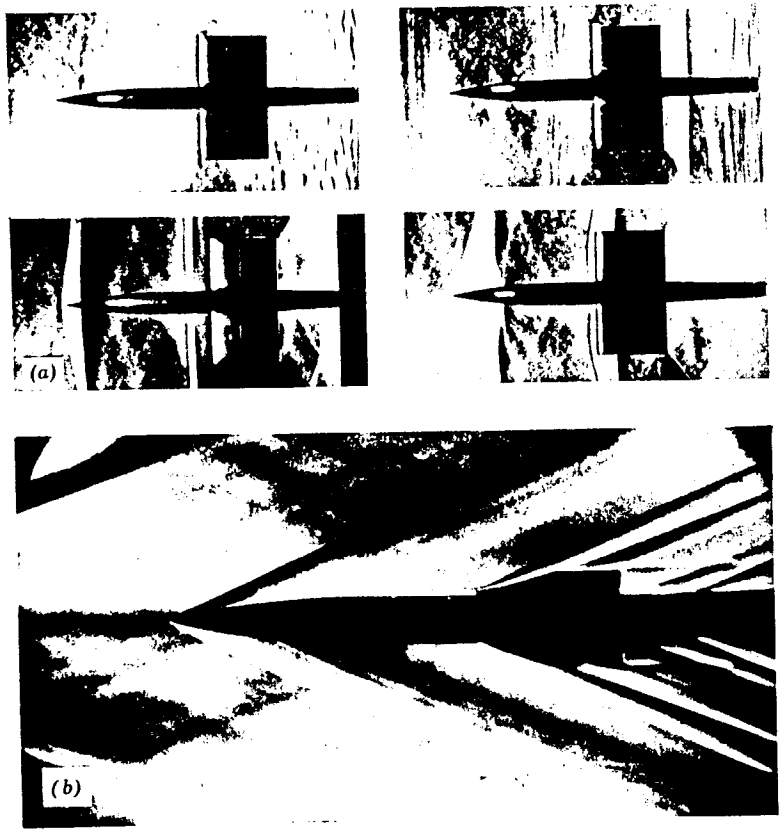


Fig. 6:35 Effect of schlieren knife-edge orientation: (*a*) perpendicular to tunnel axis; (*b*) parallel to tunnel axis.

passing the light rays through the test section twice. This is accomplished by using a circular arc mirror adjacent to one wall of the test section and a light source and mirror focal point as close together as possible on the opposite side of the test section.

Schlieren systems are often used for continuous viewing of a model during a test by projecting or transmitting the image to a point where the tunnel operator can view it. For this application mercury-vapor lamps can be obtained commercially for a continuous light source. The images can also be photographed using the mercury-vapor lamp as the light source. However, superior pictures are usually obtained when a spark gap similar to that described in the previous section is used.

One application of the schlieren system that is interesting though of questionable technical value is "color schlieren." In this application, the light from a source is broken into a spectrum by the use of a prism and a portion of the spectrum is passed through the tunnel. With proper adjustments, a picture can be obtained in which the background is some uniform color and density gradients show up as color variations.

In theory, schlieren pictures can be used to determine the actual density gradients of a flow field. In practice, they are seldom if ever used for this purpose. More common uses are for qualitative analyses of flow fields such as determining where shocks are located, whether the shocks are weak or strong, where the point of boundary layer transition is located, and whether separation occurs on the model.

The components that must be selected for a particular schlieren system are as follows: (*a*) base unit, (*b*) B-H6 light source, (*c*) spark gap and capacitor, (*d*) light source mirror assembly, (*e*) knife edge, (*f*) camera station assembly, (*g*) a-c power supply for B-H6, (*h*) d-c power supply for B-H6, (*i*) power supply for spark gap, (*j*) electrical power panel, (*k*) camera operation panel, (*l*) photo identification system.

6:18 Interferometers

Interferometers are seldom used in normal wind tunnel operation because of their relatively high cost and the high degree of precision required in their components and their use. They do, however, afford a means for determining the density of a flow field.

A schematic of an interferometer setup is presented in Fig. 6:36. Light from a point or a slit source is passed through a monochromatic filter and then through a lens which makes the rays parallel. The parallel rays strike a half-silvered mirror and are divided, half going straight through the mirror and half being reflected at right angles. The light passing through this first mirror is turned 90 deg by a second mirror, passes through the test section of the tunnel, and strikes a second half-silvered mirror where half of it is reflected to a camera. The light reflected by the first mirror is turned 90 deg by a second mirror, strikes the second half-silvered mirror where half of it passes through and is united at the camera with the rays that passed through the tunnel test section. On the film of the camera, "striae" or lines of interference are formed (Fig. 6:37). The pattern of these interference lines is related to the difference between the index of refraction of the mediums through which the divided rays passed before being reunited at the camera. The index of refraction of air is proportional to its density.

An idea of the theory on which an interferometer works may be obtained from the following explanation. Light is considered to be trains of waves emanating from a source with vibrations in a direction transverse to the direction of travel. All waves emanating from a single source at one time

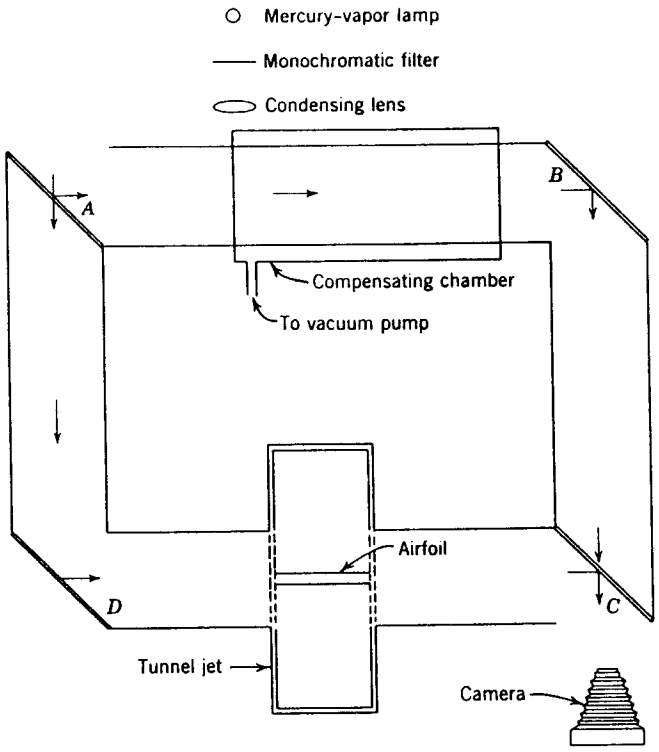


Fig. 6:36 Diagrammatic setup for striae system.

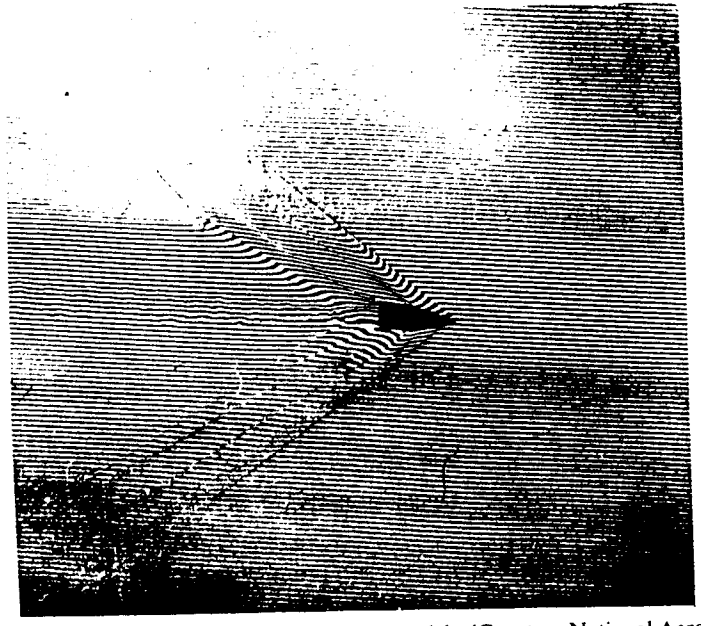


Fig. 6:37 Interferometer picture of free flight model. (Courtesy National Aeronautics

are in phase and will uniformly illuminate any object they strike. If a means is devised to change the phase relation between waves of adjacent trains, illumination of an object struck by the waves will not be uniform. At points where the waves are one-half cycle (π) out of phase, the waves completely cancel each other and the object struck by the waves will be dark. If light from a single source is divided, made to travel two separate paths, and then recombined, the phase relation of waves in adjacent trains can be altered by changing the distance traveled by adjacent trains or by changing the index of refraction of the medium through which they have traveled. If the phase relation of waves in the two beams are altered, the lines of interference will be formed on a plane object being struck by the beams after they are recombined. The alternate light and dark lines (Fig. 6:37) are regions where the waves of trains from the recombined beams are in phase and one-half cycle out of phase, respectively. The distance between alternate light and dark lines is related to the wavelength of the light and the distance of the viewing plane from the apparent origins of the two beams. When one of the beams is passing through a field of non-uniform index of refraction, such as the non-uniform flow field about a model in a wind tunnel, the lines of interference will change shape, and the change in shape, called "fringe shift," can be related to the change in air density. Interferometers use monochromatic light because the wavelength of light varies with color and a single color gives sharper interference lines than white light. An idea of the precision required in setting up and adjusting an interferometer is obtained when it is realized that the wavelength of light, on which the interference pattern depends, varies between 0.0004 and 0.0008 mm, depending on color.

6:19 Visualization of Boundary Layer Flow

In many wind tunnel investigations, it is desirable to be able to determine visually the type of boundary layer flow. Several techniques have been used for this purpose.

One technique frequently used on larger models is the "tuft" technique. Short strands of thread are fastened to the surface being studied by means of tape or other adhesive (see Fig. 6:38) in a manner to provide a minimum irregularity of the surface. The threads are small enough and light enough so that their behavior during operation is a good indication of the type of flow. If the flow is attached, the threads will be aligned in the direction of flow and will be fairly steady. If the flow is separated, the threads will be quite unsteady, and might even point in a direction 180 deg from the main flow direction.

Other flow visualization techniques described in Refs. 6:7, 6:8, and 6:9 are based on the principle that the rate of evaporation of a volatile liquid

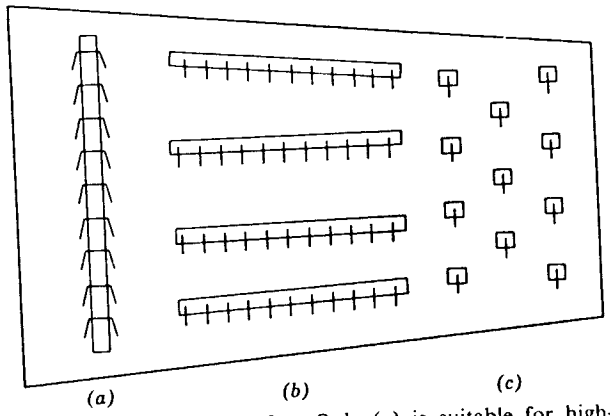


Fig. 6:38 Methods of attaching tufts. Only (*a*) is suitable for high-speed work.

from a model surface will be dependent on the type of boundary layer. That is, evaporation rates in a turbulent boundary layer will be much greater than those in a laminar boundary layer except for very thin laminar boundary layers near the leading edge.

In the "china clay" technique described in Ref. 6:7, the model surface is sprayed with a thin film of china clay suspended in lacquer. When the film is dry the model surface will have a smooth white finish and will be absorbent. For testing, the surface is sprayed with a volatile liquid having the same index of refraction as the china clay. The china clay film is invisible when wetted with the volatile liquid but becomes white again when the liquid evaporates. Suitable spray liquids include methyl salicylate (a fast drier), isosapol (medium), and eugenol (a slow drier).

Figure 6:39 is a sample china clay flow visualization photograph. The white surface near the cone leading edge is a region in which the laminar boundary layer is quite thin, has a relatively high shearing action and causes a high evaporation rate of the volatile liquid. The dark area extending over the greater portion of the cone surface is a region of thicker laminar boundary layer with consequent lower evaporation rates. The white region near the base of the cone indicates transition of the laminar boundary layer to a turbulent boundary layer. It is noted that the cone of Fig. 6:39 was prepared for the test by spraying only the model surface facing the camera with the volatile liquid. This explains the white regions on the top and bottom surfaces of the cone in the vicinity of the large dark area.

In the "liquid film" technique of Ref. 6:8, the model surface is first sprayed with a dull black lacquer, which is allowed to dry. It is then sprayed with a liquid mixture of glycerin, alcohol, and aerosol in the

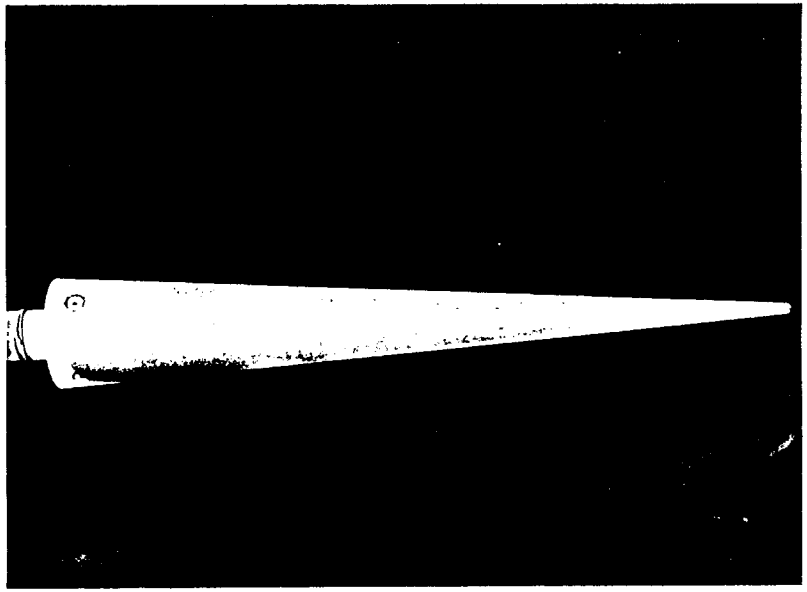


Fig. 6:39 China clay flow visualization photograph. (Courtesy Douglas Aircraft Co., Inc.)

volume ratio 1:9:2. With proper lighting, the wet and dry regions existing on the model after testing are quite apparent. These wet and dry regions can be accented for photographing by dusting with white talcum powder, which will adhere to the wet surface but not to the dry surface.

In the "luminescent lacquer" technique of Ref. 6:9, the model surface is sprayed with a phosphor pigment mixed in lacquer. The resulting film has the property of fluorescing with a bright yellow color under ultraviolet light when dry but exhibiting no fluorescence when wet.

For all of the volatile liquid film flow visualization techniques described above, proper application of the film is an art. If the film is too thick, it will run. If it is too thin, the timing of the tunnel run to get the desired flow patterns is difficult. If the film is not uniform, the flow patterns may be as dependent on the film non-uniformities as they are on the type of boundary layer. Needless to say, all the techniques are transient processes. If the model is left in the flow too long, all the volatile liquid will be evaporated, regardless of film thickness. If the model is not left in the flow long enough, none of the surfaces will be dry. In summary, much experimenting is generally required to develop the technique for use in any given wind tunnel.

In addition to the volatile liquid film techniques, an "oil flow" technique

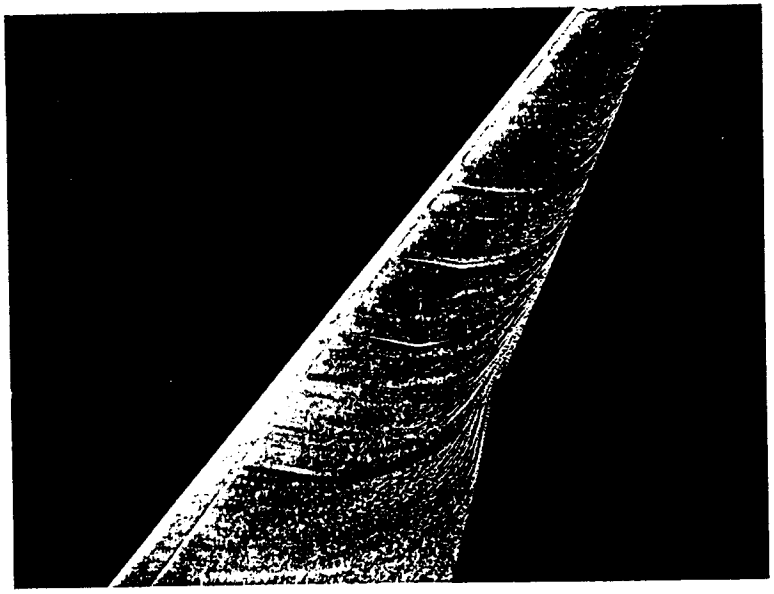


Fig. 6:40 Example of oil flow picture at a Mach number of 0.91 and an angle of attack of 2 deg. (Courtesy the De Havilland Aircraft Company Limited.)

is sometimes used. In this method, a mixture is prepared using oleic acid, 500 centi-stokes silicone oil, and titanium dioxide in the volume ratio 1:10:5. This mixture forms a fairly liquid paste, which is applied to the model with a brush. When the tunnel is started, the oil will flow according to the airflow on the model surface and will develop patterns as shown in Fig. 6:40.

A mixture of oil and lamplack may also be used to study surface flow directions. For this technique the proper consistency is determined by experiment, and discrete dots of the mixture are placed on the model surface. The near-fluid will flow in the local stream direction and, of course, the run must be stopped before it is all blown away. As a matter of interest, the oil and lampblack technique was probably the first flow visualization technique ever used. See also Ref. 6:10.

References

6:1 R. J. Volluz, Handbook of Supersonic Aerodynamics, Section 20, Wind Tunnel, Instrumentation and Operation, Naval Ordnance Laboratory, 1961.

6:2 M. Pirani and J. Yarwood, *Principles of Vacuum Engineering*, Reinhold Publishing Corporation, 1961.

6:3 Reference Tables for Thermocouples, NBS Circular 561, United States Department of Commerce, National Bureau of Standards, 1955.

6:4 E. M. Winkler, Stagnation Temperature Probes for Use at High Supersonic Speeds and Elevated Temperatures, NAVORD 3834, 1954.

6:5 J. L. Harkness, Final Report on Heat Transfer Investigations in Supersonic Flow, University of Texas Defense Research Laboratory Report 429, 1958.

6:6 D. E. Welshimer, The Experimental Application of Sonic Pneumatic Probe Systems to Temperature Measurements in a Hypersonic Airstream, Ohio State University RF-5593-62-6, Aeronautical Research Laboratory 62-364, 1962.

6:7 E. J. Richards and F. H. Burstall, The "China Clay" Method of Indicating Transition, Aero. Res. Council, Reports and Memoranda No. 2126, August 1945.

6:8 W. E. Gray, A Simple Visual Method of Recording Boundary Layer Transition (Liquid Film), Royal Aircraft Establishment, Technical Note No. Aero. 1816, August 1946.

6:9 J. R. Stalder and E. G. Slack, The Use of a Luminescent Lacquer for the Visual Indication of Boundary Layer Transition, NACA TN 2263, January 1951.

6:10 R. L. Maltby, Flow Visualization in Wind Tunnels Using Indicators, AGARDograph 70, April 1962.

DIRECCION DE PROYECTOS BIBLIOTECA

Chapter seven

Force and moment measuring devices

7:1 General Force and Moment Measurements

Any aircraft in flight through the atmosphere has six degrees of freedom. It is free to *translate* along three mutually perpendicular axes and to *rotate* about these three axes. Consequently, its motions during flight are dependent on forces along and moments about three mutually perpendicular axes as illustrated in Fig. 7:1. Force and moment measurements normally made in wind tunnels are for the purpose of obtaining forces along and/or moments about one or more of the axes produced by air loadings. The objective of such measurements is to obtain an estimate of loadings that will prevail on the full-scale aircraft in flight, both for structural integrity and for performance reasons.

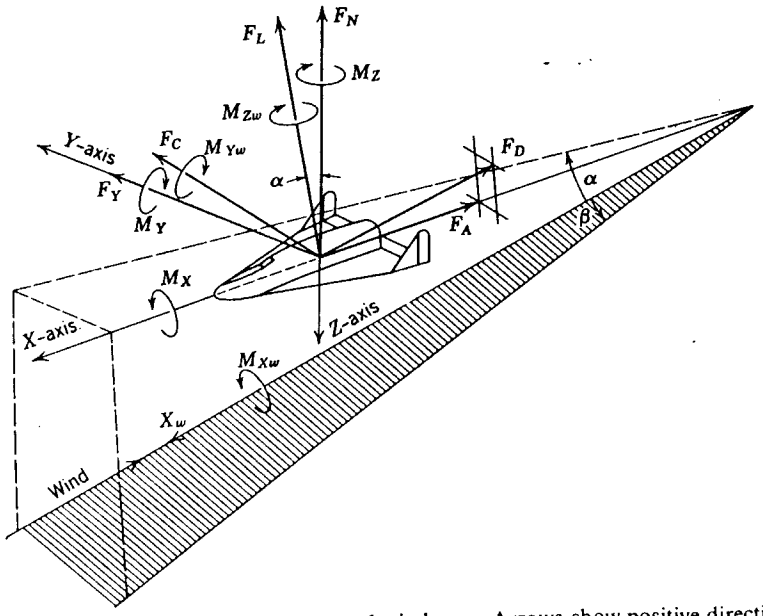


Fig. 7:1 The relation between body and wind axes. Arrows show positive directions.

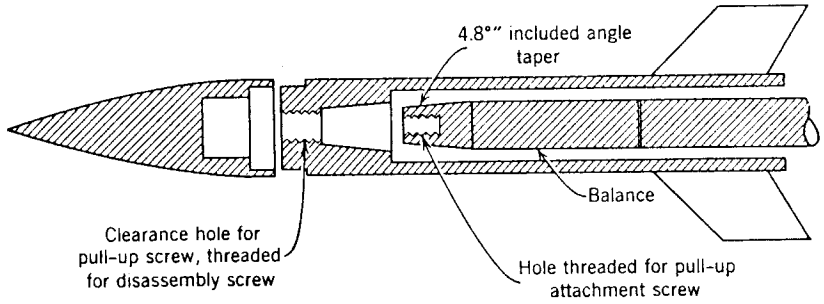


Fig. 7:2 Common method of mounting a high-speed wind tunnel model.

Forces and moments acting on an aircraft in flight or on a model in a wind tunnel are generally divided into the two broad categories of "static" and "dynamic" loadings. Static loadings are those resulting from the motion of air over an aircraft or model having a fixed alignment with respect to the relative wind. Referring to Fig. 7:1, this is saying that α and β are constant and the aircraft or model is not rolling about or accelerating along its axes. Conversely, dynamic loads are those resulting from variations with time of α, β, roll orientation, and/or linear accelerations.

Static loads are measured with devices called "balances," and dynamic loads are measured with devices called "dynamic test rigs." Static loads are, generally speaking, large in comparison to dynamic loads and are easier to measure with reasonable accuracy. The greater portion of wind tunnel test time is devoted to the measurement of static loads.

High-speed aircraft are normally propelled with some type of jet engine and this has fortuitously provided the wind tunnel engineer with a good means of supporting the model in a wind tunnel. Jet engines require blunt exits into which support mechanisms may be inserted with a minimum of interference to the air flow over a model (Fig. 7:2). This is fortunate because model mounting struts from the tunnel sidewalls, as normally used in low-speed tunnels, create disturbances that at high speeds can have large effects on the air flow over a model and consequently on the air loads on a model. In this section, various types of balances and dynamic test rigs in common use will be discussed.

7:2 Internal Balances

Internal balances are designed to fit within the hollowed-out cavity of a model as illustrated in Fig. 7:2. They are normally designed for the measurement of from 2 to 6 of the loading components. Maximum external dimensions range from less than $\frac{1}{2}$ inch to 2 or more inches and design loads vary from less than 10 pounds to several hundred pounds.

The cost of a six-component internal balance will typically be in the neighborhood of $10,000.

7:3 Strain Gages

Electric resistance "strain gages" are used extensively, if not exclusively, as the load-sensing element of the internal balance. An understanding of the principle of operation of the strain gage is essential to the design and intelligent use of an internal balance and this principle will be discussed in some detail before proceeding with a general discussion of internal balances.

The types of strain gage used most frequently in wind tunnel balances are illustrated in Fig. 7:3. The gages consist of a grid of very fine wire (0.0005 to 0.001 inch in diameter) or of very thin foil (less than 0.001 inch thick) embedded in a sheet of bakelite having a thickness comparable to that of heavy paper. The grid material is usually constantan, nichrome, or nichrome with small additions of iron and aluminum. Gages are available with grid lengths from about $\frac{1}{32}$ inch to several inches. In sizes and types used in wind tunnel balances, gages normally cost about $3.00 to $15.00 each.

Gages with the grid wires imbedded in paper instead of bakelite are available at a lower cost. However, they are not as stable as the bakelite gages and are seldom if ever used in internal balances. The theory of operation of the strain gage is as follows. When the bakelite body of the gage is intimately connected to the surface of a structure, it will stretch or contract as the outer fibers of the structure to which it is attached. With

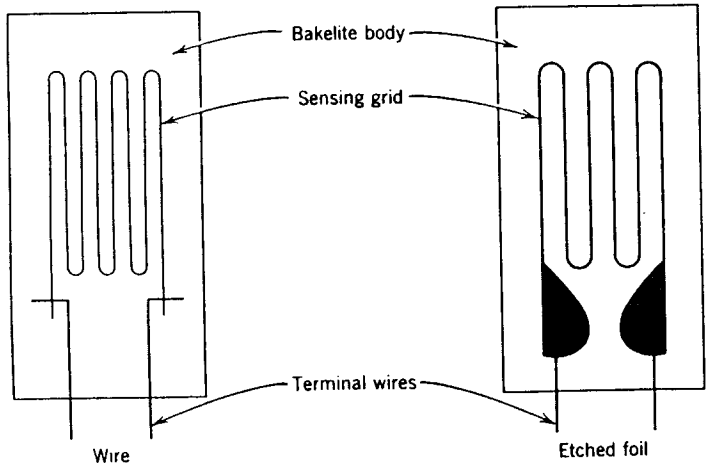


Fig. 7:3 Illustration of two types of strain gage.

the grid wires embedded in the bakelite, they will stretch or contract with the bakelite body and thus with the outer fibers of the structure. As the grid wires are stretched, their cross-sectional area decreases, causing an increase in electrical resistance. Similarly, as the grid wires are compressed, their cross-sectional area increases, causing a decrease in electrical resistance. In both instances the change in resistance is actually more than the change of area would indicate because of the change in length. It has been found in practice that the changes of resistance of the types of strain gages normally used in wind tunnel balances is directly proportional to the stress in the outer fibers of the structure to which it is attached.

It may be concluded from the theory of operation that great care must be exercised in the installation of the strain gage. If the grid wires of the gage are to have resistance changes in direct proportion to stresses of the structure, intimate and uniform attachment of the bakelite body to the structure is required. Typical strain gage installation instructions are as follow:

a. Scribe the metal for exact gage location.
b. Clean both gages and metal with very light sandblasting.
c. Dip both gages and metal in acetone.
d. Keep all oil away, do not touch glue surfaces.
e. Put light coats of Baldwin EPY-400 epoxy glue on both surfaces, and emplace gage.
f. Put layer of teflon tape over gage (to prevent sticking), then a layer of $\frac{1}{16}$-inch rubber, and clamp tight.
g. Cure in oven at 250 to 300°F for from 4 to 8 hours.
h. Heat the balance in a bath of 10W-30 motor oil or transformer oil at 170°F for a day. This, for some reason, seems to improve the quality of the gage installation.

Strain gages in wind tunnel balances are normally located on a member in which the desired component of loading is a bending moment. A typical strain gage installation is illustrated in Fig. 7:4.

Two gages are placed side by side on both the compression surface and the tension surface of the member. (On members where a side-by-side installation is not practical, satisfactory results have been obtained with the gages on one surface mounted end-to-end or one on top of the other.) The four gages are then wired together into a bridge circuit as illustrated in Fig. 7:5 and a supply voltage is applied. This supply voltage is typically between 5 and 10 volts and may be either direct or alternating current.

The four gages used in a strain gage bridge on a balance are usually closely matched for both initial resistance and rate of change of resistance with elongation or compression of the grid. Although not absolutely

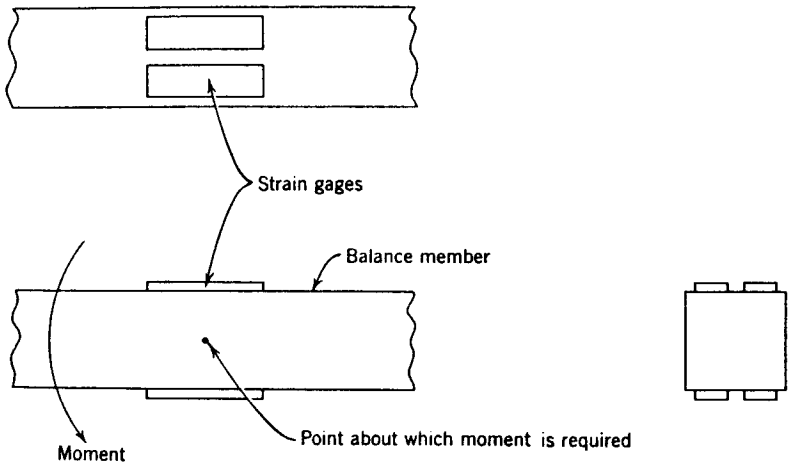


Fig. 7:4 A typical strain gage installation on a balance member. (Gage thickness is exaggerated for clarity.)

required for a usable bridge, this matching has two advantages. It has a tendency to minimize the sensitivity of the bridge to changes in temperature, and it maintains a near-zero output voltage under no load conditions. Matching of initial resistance of the gages can be accomplished prior to installation by use of a Wheatstone bridge. However, in matching for rate of change of resistance with elongation or compression, the manufacturer's specification of "gage factor" must be relied on. Gage factor is defined as $(\Delta R/R)/(\Delta L/L)$, where R and L are, respectively, initial electrical resistance and length of the grid, and where the Δ indicates incremental changes in these values.

The signal voltage from a strain gage bridge can be calculated as follows

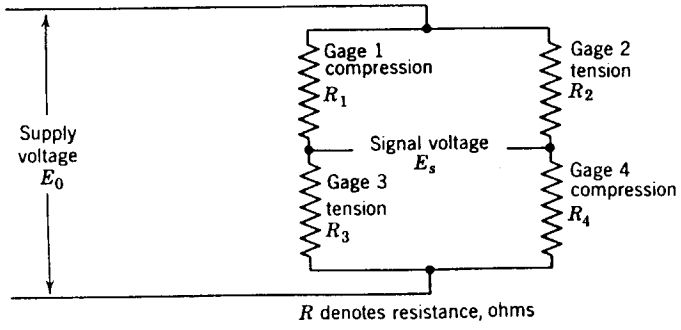


Fig. 7:5 The electrical arrangement of four strain gages in a bridge circuit.

using Ohm's law. The current flows through gages 1 and 3 and through gages 2 and 4 of Fig. 7:5 are

$$I_{13} = \frac{E_o}{R_1 + R_3}$$

$$I_{24} = \frac{E_o}{R_2 + R_4}$$

The voltage drops across gages 1 and 2 are

$$\Delta E_1 = I_{13}R_1 = E_o \frac{R_1}{R_1 + R_3}$$

$$\Delta E_2 = I_{24}R_2 = E_o \frac{R_2}{R_2 + R_4}$$

The signal voltage is equal to

$$E_s = (E_o - \Delta E_1) - (E_o - \Delta E_2)$$

which can be reduced to

$$\frac{E_s}{E_o} = \frac{R_2R_3 - R_1R_4}{(R_1 + R_3)(R_2 + R_4)} \tag{7:1}$$

With matched gages on a symmetrical section of the balance having both a bending load and an axial load, the resistances of the individual gages are

$$R_1 = R_4 = R_o - \Delta R_b + \Delta R_a$$

$$R_2 = R_3 = R_o + \Delta R_b + \Delta R_a$$

R_o = initial gage resistance

ΔR_b = increment in gage resistance due to bending stress

ΔR_a = increment in gage resistance due to axial stress

Using these relations, we obtain

$$\frac{E_s}{E_o} = \frac{4\,\Delta R_b(R_o + \Delta R_a)}{4(R_o + \Delta R_a)^2} = \frac{\Delta R_b}{R_o + \Delta R_a}$$

Since ΔR_a is normally very small in comparison to R_o, it can be considered equal to zero in the above equation. This indicates the insensitivity of a moment bridge on a wind tunnel balance to axial stresses under normal conditions.

Even though strain gages are matched as closely as practical prior to installation, it is often found that the signal voltage from the strain gage

bridge will be affected by temperature. These effects are usually small, but in many cases they are too large to be neglected, particularly if the balance is to be used in wind tunnels with heated air (see Section 11:12). These temperature effects result from unequal resistance changes due to temperature in the four gages of the bridge. They are usually detected by measuring the signal voltage with the balance at ambient temperature and then at the elevated temperature. The following is common procedure in checking for temperature effects:

a. Set up two oil baths in which the balance may be immersed, one at room temperature and one at perhaps 170°F.
b. Connect the balance gages to a signal-measuring device.
c. Immerse the balance in the room temperature bath and leave for 15 min to allow temperature stabilization.
d. Take gage signal readings.
e. Remove the balance from the room temperature bath, place it in the heated bath, and leave for 15 min.
f. Take gage signal readings.
g. Repeat the above process at least once.

If the readings taken at the end of 15 min in the hot bath differ significantly from those taken at the end of 15 min in the room temperature bath, the balance needs temperature compensation. Temperature compensation is accomplished as follows:

The bridge is connected to a signal-voltage-measuring device so that a positive load on the balance causes a positive reading, thus defining the gages which will be called tension gages and compression gages. Strain gages normally have a resistance increase with temperature and the direction of variation of signal reading with temperature is an indication of which gage or gages are more affected by temperature. If the reading increases with increasing temperature, one or more of the tension gages are too sensitive to temperature. Conversely, if the reading decreases with increasing temperature, one or more of the compression gages are too sensitive to temperature. Compensation is accomplished by placing temperature-sensitive resistance wire, usually No. 32 copper wire, in the bridge circuit. If the compensating wire has an increase in resistance with an increase in temperature, as all pure metals have, it is placed in series with one or both of the compression gages to compensate for too sensitive tension gages. Similarly it is placed in series with one or both of the tension gages to compensate for too sensitive compression gages. Although the amount of wire required is in practice finally reduced to inches of a specified wire for each count on the measuring device with a given temperature rise, an estimate of the amount required can be obtained in the

following manner. Referring to Fig. 7:5 let the compression gage with resistance R_1 be too sensitive to temperature, so that

$$R_1 = R_o + \Delta R_t$$
$$R_2 = R_3 = R_4 = R_o$$

Using these relations with equation (7:1) yields:

$$\frac{E_s}{E_o} = \frac{-\Delta R_t}{4R_o}$$

or

$$\Delta R_t = -4R_o \frac{E_s}{E_o}$$

The compensating wire to be inserted in series with one of the tension gages must have the same resistance increase with temperature:

$$\Delta R_t = R_c \alpha \Delta T$$

where R_c = resistance of compensating wire at the reference temperature, °R,
α = a constant defining rate of increase in resistance with temperature (ohm/ohm-°R),
ΔT = increase above reference temperature at which resistance change ΔR_t was determined, °R.

Thus

$$R_c = \frac{-4R_o \frac{E_s}{E_o}}{\alpha \Delta T}$$

The insertion of compensating wire into a strain gage bridge will affect the output signal at conditions of no load on the balance but is not likely to have a significant effect on the variation of output signal with applied moment.

To keep the strain gage within satisfactory limits of operation, wind tunnel balances made of steel are usually designed for a maximum stress under the gage of between 7500 and 30,000 psi. Greater stresses, corresponding to greater length changes of the gage, increase the likelihood of gage failure. On the other hand it is not desirable to design for low stresses under the gages. Electrical signals that can be obtained from strain gages are low, even at a stress of 30,000 psi, and stress reductions increase the difficulty of measuring signal voltages accurately. It is noted that deformation rather than stress is the important parameter in strain gage

applications and should be so considered in the design of balances using different materials. For instance, if aluminum is used for the balance material, the strain at a given stress is three times that of steel because of the lower modulus of elasticity of aluminum. Deformations of aluminum at stresses of about 2500 to 10,000 psi will correspond to those of steel at 7500 and 30,000 psi.

7:4 Strain Gage Signal-Measuring Devices

A detailed description of devices for measuring strain gage signals is beyond the scope of this work. However, a brief discussion of the principle involved is in order. The principle is the comparison of the strain gage signal voltage with a known reference voltage which is varied until reference and signal voltages are equal. This principle is illustrated by Fig. 7:6. A voltage E_1 is applied across the resistance of a potentiometer. This voltage is a small fraction of the voltage applied to the strain gage bridge, E_o, but is larger than the strain gage signal voltage E_s. The voltage E_1 is divided to provide a potential $E_{ref} = E_1 \times (R/R_t)$ between one end of the resistor and the movable contact of the potentiometer. One strain gage signal lead is attached to the end of the resistor and the other to the movable contact of the potentiometer through a galvanometer. The movable contact of the potentiometer is moved until the galvanometer indicates no current flow. (Reversing polarity of the strain gage signal

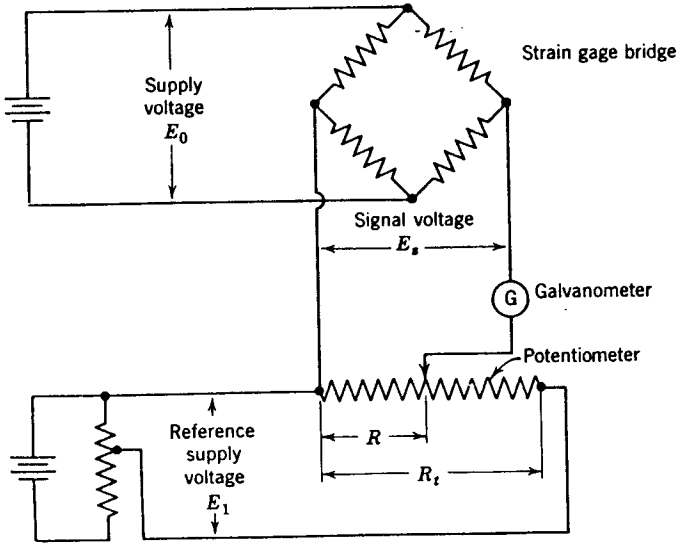


Fig. 7:6 Illustration for discussion of the principle used in the measurement of a signal voltage from a strain gage.

voltage will, of course, require interchanging the points of connection of the strain gage signal leads to the potentiometer in order to obtain no current flow through the galvanometer.) At this point of zero current flow the reference potential E_{ref} equals the strain gage signal voltage E_s. Knowing the voltage E_1 and the variation of potentiometer resistance with movable contact position, we can readily determine the signal voltage from contact position and the relation $E_s = E_{ref} = E_1(R/R_t)$.

Generally, in wind tunnels no manual operations are required in the above-described measurement of strain gage signals. With a system of the type illustrated, the current flow that operates the galvanometer is amplified and drives a motor, which in turn drives the movable contact of the potentiometer to a null position. Additional circuitry is provided to eliminate the necessity of reversing signal leads when the signal voltage from the strain gage changes polarity.

Measuring systems that are highly sophisticated in comparison to the one described are common in wind tunnels. However, they all use the basic principle described of comparing known reference voltages with the strain gage signal voltage until a matching is achieved.

7:5 Balance Design Considerations

There are several balance design considerations that are applicable regardless of the component or components to be measured. The most important of these are structural. It is generally considered unwise to build an expensive balance of anything except a high-quality steel. One steel that is considered satisfactory is ARMCO 17-4PH stainless steel heat treated to an ultimate tensile strength of 160,000 psi. If such a material is used and the balance is designed for maximum stresses of 30,000 psi or less due to air loads on a model inclined 10 to 20 deg with respect to the airstream, there is little likelihood of damaging the balance during tests at near sonic, transonic, or hypersonic speeds. However, at supersonic speeds this may not always be true because air loads on a model during starting and stopping of the tunnel are in some cases several times the steady-state air loads during the data-taking part of the test. Loads on models during supersonic tunnel starting and stopping are discussed in more detail in Chapter 10. The balance must be designed so that model loads encountered during a test will not cause deflections to the extent that the balance will come into contact with the after portion of the model. As previously mentioned, the balance should be designed for fairly high stresses under the gages at maximum test loads (up to about 30,000 psi for steel) in order to obtain the largest practical signals from the strain gages.

The design must also provide a satisfactory means for rigid attachment

between the balance and model. Any change of alignment between the balance and model during a test can result in erroneous data and, of course, poor attachment may result in the loss of a model. There are several satisfactory methods of attachment, one of the better of which is illustrated in Fig. 7:2. This method uses a locking taper for attachment. Conical tapers are ground on the forward portion of the balance and at some position inside the model which is convenient to the overall design. The taper half angle is selected so that its tangent will be less than the friction coefficient between the balance and model taper surfaces. When the model and balance are pulled together with such a taper, a resultant force is developed between the two surfaces which locks them together and a positive separating force is required. The friction coefficient between hardened and polished steel surfaces varies between 0.03 and 0.05, corresponding to taper half angles of 1.72 to 2.76 deg. A typical locking taper for a wind tunnel balance is 1 in 12, corresponding to an *included* taper angle of about 4.8 deg. The forward end of the balance is threaded for an attachment screw used to assemble the model and balance and lock the two together. The clearance hole in the model for the attachment screw is made somewhat oversize and threaded for a larger pulling screw. For disassembly, the attachment screw is removed and the larger pulling screw is screwed into the model until its end comes into contact with the end of the balance and breaks the taper joint.

Another important general consideration is to keep all the balance component strain gages located inside the model where there is a minimum circulation of air. Air flowing over the gages can cause local cooling or heating with accompanying local resistance changes in the gages which make the output signals from the strain gage bridges very erratic. Also, it is desirable to keep all power supply and signal wires to the strain gage bridges well shielded from the air flow, preferably by running them through a hole along the axis of the balance support sting.

7:6 Normal Force–Pitching Moment

Two separated strain gage bridges positioned on the body of the balance as shown in Fig. 7:7 are used for measuring these components. The body of the balance generally has axially symmetric cross sections because these are the easiest to fabricate. At positions where gages are to be mounted, equal amounts of the cross section are milled off at the top and bottom of the balance to provide flat mounting surfaces symmetrical about the balance centerline. The flats are required for ease of proper strain gage mounting, and symmetry affords equal and opposite bending stresses to which the tension and compression gages are subjected. In calibrations prior to tests the output signal from each bridge is obtained as a function

of bending moment at the effective gage location. Output signals obtained from the forward and aft bridges during the test are converted to moments M_f and M_a. The normal force is then obtained by dividing the difference between the two moments by the distance between the two effective bridge locations. $F_N = (M_a - M_f)/d$. The pitching moment about the reference point is obtained by linear interpolation between the two bridge moments.

$$\text{Pitching moment} = M_f + \frac{d_{ref}}{d} \times (M_a - M_f)$$

The equation for normal force indicates that if a given moment accuracy can be obtained regardless of bridge location, the most accurate normal force will be obtained when the bridges are as far apart as possible. The procedure followed in calculating pitching moment indicates that the best accuracy of this component will be obtained when the moment reference point is located *between* the two bridges. With the moment reference point between the two bridges, pitching moment is obtained by interpolation, whereas with the moment reference located elsewhere, extrapolation is required, and the moment error can increase by a factor of 10 or more.

7:7 Side Force–Yawing Moment

Balance design considerations for the measurement of these components are the same as for the measurement of normal force and pitching moment with the exception that the side force–yawing moment plane is perpendicular to the normal force–pitching moment plane. It is noted that milled flats for these strain gages should be as near as possible to 90 deg from flats for the normal force–pitching moment gages. Any deviation from 90 deg will result in a component of loading in one plane causing stresses in gages being used to measure loadings in the other plane.

Example 7:1 Design a normal force–side force balance according to the following specifications: A model similar to that of Fig. 7:7 has a

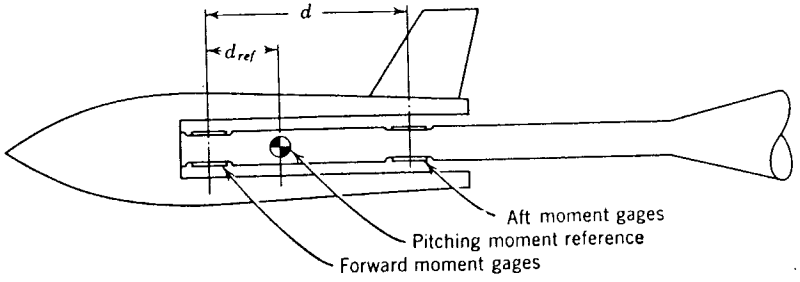


Fig. 7:7 Installation of forward and aft moment gages.

maximum allowable cavity diameter of 0.70-inch and a cavity depth of $5\frac{3}{4}$ inches from the model base to the beginning of the attachment taper. Normal force and side force loads of 60 lb are expected during the test with centers of pressure between $2\frac{1}{2}$ and 4 inches ahead of the model base.

The design proceeds as follows:

1. A maximum balance diameter of 0.5 inch is assumed. This will allow 0.1 inch clearance between the balance and the model to accommodate deflection of the balance due to loads and to facilitate assembly of the model and balance.

2. A maximum-dimension square cross section is calculated for the sections to be strain gaged. The sides of a maximum-dimension square that can be cut out of a circular cross section equals the circle diameter times cosine 45 deg, or in this case, $b = (0.5)(0.707) = 0.354$ inch. The maximum-dimension square cross section is selected because it gives the same strength in the two planes and allows the maximum width flat for placement of strain gages.

3. The gage stations are selected. An aft gage station $1\frac{1}{2}$ inches ahead of the model base is selected in order to get the gages well within the model cavity and thus minimize the effects of air circulation. A forward station 5 inches ahead of the model base is selected. This allows $\frac{3}{4}$ inch between the gage center and taper shoulder, which is adequate but not excessive.

4. The moments about the gage stations are calculated. With load centers of pressure $2\frac{1}{2}$ to 4 inches ahead of the base, the loads will be applied 1 to $2\frac{1}{2}$ inches ahead of the aft gage and 1 to $2\frac{1}{2}$ inches behind the forward gage. The maximum moment at each gage station is therefore (60 lb)($2\frac{1}{2}$ inches) or 150 inch-lb.

5. Calculate the stress in the outer fibers of the balance at the gage stations and at the maximum moment from the equation:

$$S = \frac{Mc}{I} \tag{7:2}$$

where S = stress, psi,
M = moment, inch-lb,
c = distance from the axis to the outer fibers of the balance, inches,
I = cross section moment of inertia, base × height^3/12, inches^4.

Thus
$$S = \frac{(150)(0.354/2)}{(0.354)(0.354)^3/(12)} = 20{,}300 \text{ psi.}$$

This design stress under the gages is not excessive assuming a high-quality steel and proper gage installation.

6. Determine the distance downstream of the base at which the cross section of the balance must be increased above $\frac{1}{2}$-inch diameter. Use eq. (7:2) with inertia given by $\pi d^4/64$.

$$S = \frac{M(0.25)}{\pi(0.5)^4/64} = 81.4\,M$$

Assume an allowable stress of 30,000 psi.

$$M = \frac{30{,}000}{81.4} = 368 \text{ inch-lb allowable.}$$

With a 60-lb load, this corresponds to a distance of 6.13 inches from the load or 2.13 inches downstream of the model base with the load center 4 inches ahead of the model base.

7. Calculate the displacement of the balance relative to the balance axis. Assume a uniform balance cross section equal to that at the gaged sections for simplicity and conservatism. For a uniform balance cross section, the deflection of the balance relative to the model axis at the model base is calculated by using the following equations:

$$y_b = \frac{Fx_b^3}{6EI}\left[\frac{3l}{x_b} - 1\right] \tag{7:3}$$

where y_b = displacement at model base station, inches,
F = applied load, lb,
x_b = distance from point of attachment of model balance to the model base, inches,
l = distance from point of attachment of model balance to the applied load,
E = modulus of elasticity of balance material, lb/inches^2,
I = section inertia, inches^4.

In this example, the maximum deflection will occur with the load in the most aft position. Using a value of $E = 30 \times 10^6$ for steel, we find

$$y_b = \frac{(60)(5.75)^3}{(6)(30 \times 10^6)(0.354)(0.354)^3/12}\left[\frac{(3)(3.25)}{5.75} - 1\right]$$

$$= 0.034 \text{ inch}$$

The deflection is not excessive and the balance design is satisfactory.

7:8 Rolling Moment

The measurement of rolling moment, which would correspond to torsion in the body of the internal balance, is not as straightforward as the previously discussed components. A steel shaft designed to support

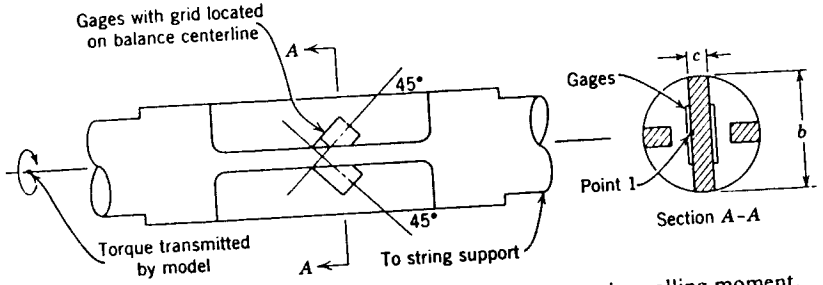


Fig. 7:8 An internal balance cruciform section for measuring rolling moment.

normal loads on a model is generally relatively stiff in torsion, making the accurate measurement of torsion difficult. Numerous schemes have been employed for the measurement of rolling moment with varying degrees of success. One of the more successful schemes is illustrated in Fig. 7:8.

The body of the balance is weakened to torsion by use of a cruciform section, and strain gages are installed at the center of the main web of the cruciform. The strain gages are inclined 45 deg from the balance axis and on each surface the two gages are mutually perpendicular. This arrangement requires "stacking" of the grids of the two gages on each side of the web (dual gages with grids at right angles may be purchased as a unit). Simple torque bar analysis indicates that this arrangement is such that on each surface one gage will be sensitive to the maximum tension stress in the member and the other gage will be sensitive to the maximum compression stress in the member. In spite of end support effects which prevent the main web from acting as a simple torque bar, this design with a cruciform length of less than 2 balance diameters has been found to yield linear variations of strain gage signal with applied torque.

The cruciform section is located near the axial position on the balance corresponding to model center of loading. In practice, this will probably always be between the two moment gages in the model pitch and yaw planes. With this axial location bending stresses in the cruciform section are kept to a minimum, thus allowing the cruciform to be designed for maximum sensitivity. A companion advantage of this location is that the portion of the signal from the rolling moment gage, which because of manufacturing imperfections is due to bending stresses, is kept to a minimum.

Referring to the section view of Fig. 7:8, the maximum stress of the cruciform occurs at point 1 and is given by

$$S = \frac{T}{\alpha b c^3} \tag{7:4}$$

where S = stress, psi,
T = torque applied to the main web, inch-lb,
b = height of main web, inches,
c = thickness of main web, inches,
α = a nondimensional function of section as follows:

b/c	1.0	1.5	2.0	4.0	6.0	8.0	10.0	∞
α	0.208	0.231	0.246	0.282	0.299	0.307	0.312	0.333
β	0.141	0.196	0.229	0.281	0.299	0.307	0.312	0.333

The angular deflection of a web in torsion is given by

$$\theta = \frac{T}{\beta G b c^3}$$

where θ = angular deflection, radians/inches of length,
β = a nondimensional function of section as shown above,
G = modulus of elasticity in torsion, 12×10^6 psi for steel.

For the cruciform section, the angular deflections of the main web and each of the short webs are equated, giving

$$\theta_m = \theta_s = \frac{T_m}{\beta_m G b_m {c_m}^3} = \frac{T_s}{\beta_s G b_s {c_s}^3} \tag{7:5}$$

where subscript m refers to the main web and subscript s refers to one of the short webs.

Equation (7:5) is rearranged to give

$$T_s = \frac{\beta_s}{\beta_m}\frac{b_s}{b_m}\left(\frac{c_s}{c_m}\right)^3 T_m \tag{7:6}$$

The design rolling moment will equal the sum of the torques taken out by the three webs:

$$\text{Rolling moment} = T_m + 2T_s \tag{7:7}$$

Equations (7:6) and (7:7) are combined to obtain the torque taken out by the main web. This torque is then inserted in eq. (7:4) to determine the stress under the gages.

7:9 Axial Force

The force acting along the axis of a model is the most difficult component of load to measure with an internal balance. One of the main reasons for this is that the forces normal to a model with lifting surfaces are usually large in comparison to axial force, particularly at angle of attack. Thus

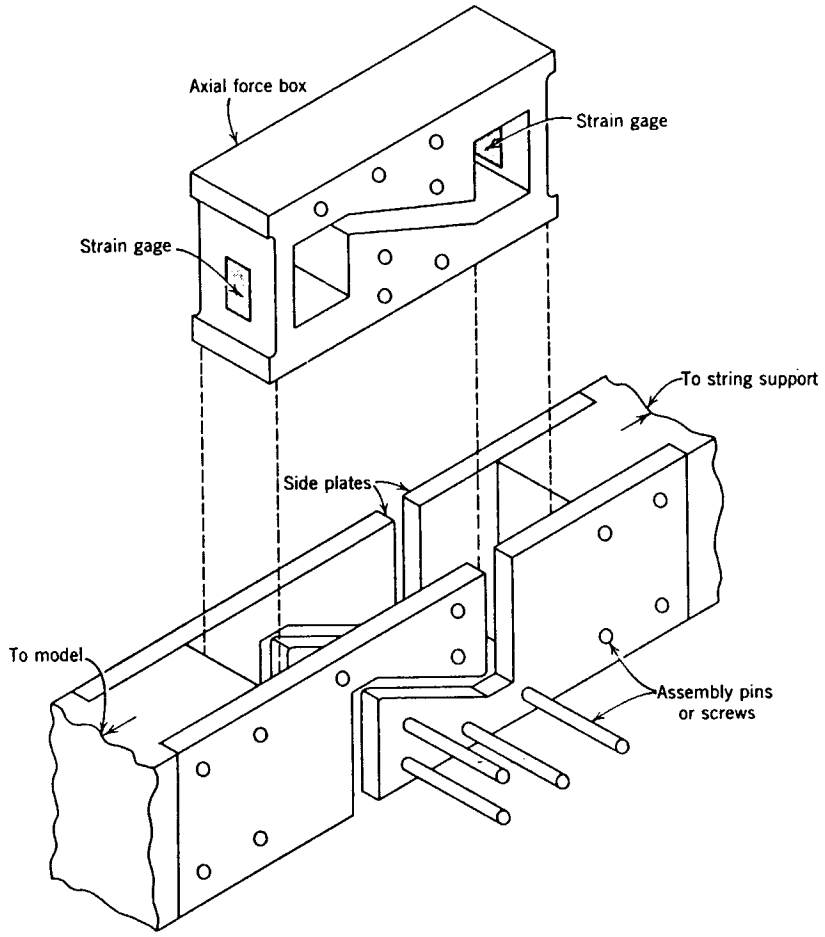


Fig. 7:9 Axial force measuring member of an internal balance.

the balance must be weak in the axial direction in order to be sensitive to axial loads and at the same time must have adequate strength in the normal force and side force directions to prevent undesirably large deflections. Designs have been worked out which satisfy these requirements fairly well. However, in many instances difficulty will be experienced in obtaining accurate axial force data at conditions of large normal force and/or side force because of the interaction of these large loads on the axial force readings. One principle of design frequently used is illustrated in Fig. 7:9.

Balances of the type shown in Fig. 7:9 have been built in sizes down to about 0.4 inch in diameter. An axial force member is built separately

from the balance with two thin webs through which all axial forces will be transmitted. These two thin webs each have strain gages installed on the surfaces which will have tension and compression stresses due to an axial force. The four gages thus installed are wired together to form the usual strain gage bridge. Then the axial force member is assembled with the forward and aft portions of the balance body in such a way as to maintain a stiff cross section for bending moments in the normal force and side force planes. As with the rolling moment member, the axial force member should be located near the load center of the model to keep bending moments due to normal and side forces as low as possible in the member. One of the critical considerations in the design of this type of internal balance is the method of attachment of the member to the balance body. Tight-fitting screws and alignment pins, which normally would be expected to give a rigid connection, have in many cases in practice allowed sufficient slippage of the connection to make the balance worthless. It will not generally be practical to use a welded or soldered connection because of heating of the gages of the axial force bridge. Also, as indicated by

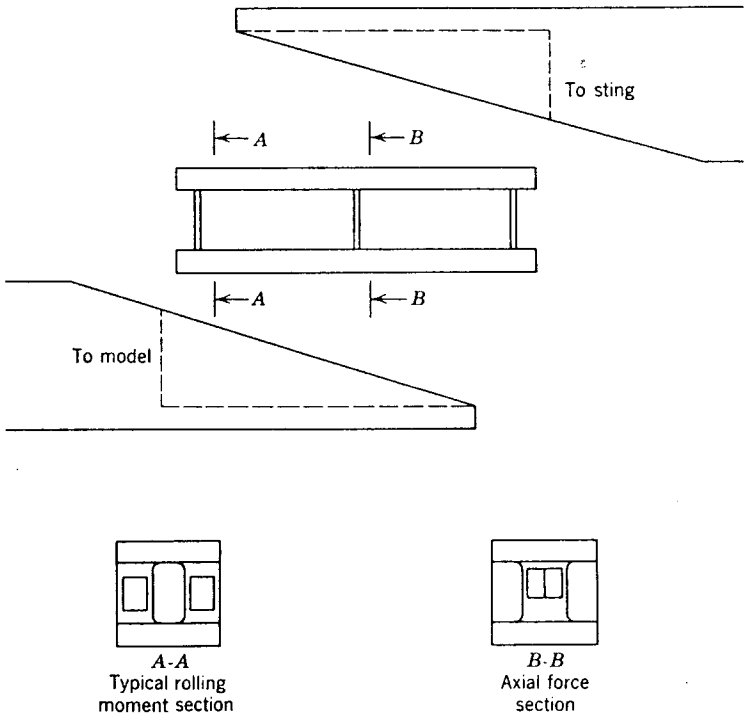


Fig. 7:10 Schematic of rolling moment–axial force measuring member of balance.

Fig. 7:9, the gages and wiring could not be reached for repair with a balance of this type after assembly. A method frequently used to overcome the slippage is to use a large number of screws so that the force holding the parts together will be very high.

A scheme that has been used for measuring both rolling moment and axial force on an internal balance is illustrated in Fig. 7:10. In this scheme, a box is made up using three webs, two for measuring rolling moment and one for measuring axial force. All three webs provide restraint in both axial force and rolling moment. However, the design is aimed at minimizing the axial restraint of the roll webs and the rolling restraint of the axial webs. The rolling moment webs provide roll restraint by pure tension and compression. The axial force web provides axial restraint by bending. The primary advantage of this arrangement is that axial force and rolling moment measuring members can both be located near the center of load on the model.

The machined parts for a six-component balance that uses still another scheme for simultaneous measurement of rolling moment and axial force is presented in Fig. 7:11. A photograph of an assembled six-component balance is presented in Fig. 7:12. Detailed design procedures for a six-component balance are discussed in Ref. 7:1.

7:10 Calibration of Internal Balances

Proper calibrations of balances are required for interpretation of wind tunnel test results in terms of the desired forces and moments. In general, calibrations comprise the mounting of the balance on a calibration rig outside the tunnel, loading the balance with known forces and moments which cover the range expected during a test, and recording strain gage readings at each force and moment combination. During the calibration the constancy of gage reading proportionality to force and moment is termed "linearity" and the difference between gage readings with no load taken before and after a loading is termed "gage drift."

Figure 7:13 shows a balance calibration rig. The rig is a fixture into which the balance can be mounted as it would be mounted in the tunnel. It includes mechanisms which allow the balance to be rotated about its axis through 360 deg and pitched in the vertical plane through perhaps ±5 deg. The provision for rolling the balance permits the application of positive or negative load to the balance in any balance plane (positive or negative normal force, positive or negative side force, and any combination of these at roll angles other than 0, 90, 180, and 270 deg). The provision for pitching the balance permits it to be maintained horizontal at all times and makes possible the measurement of balance and sting deflection.

A "calibration bar" is placed over the balance so that suitable loadings

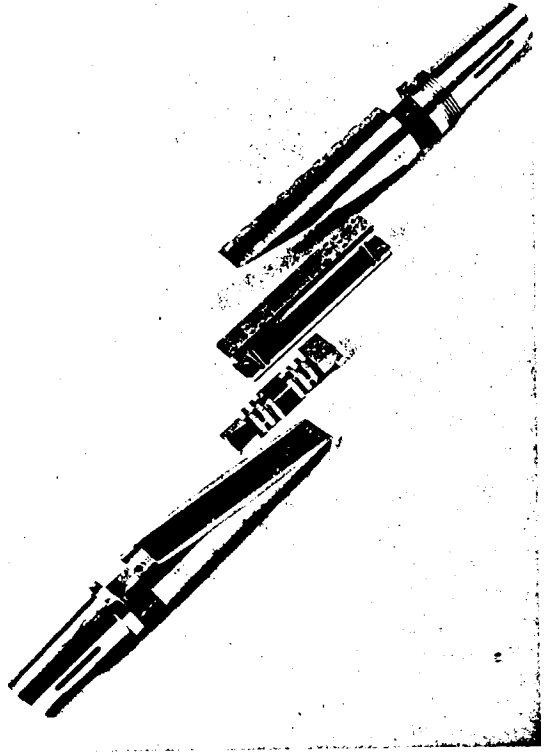


Fig. 7:11 Machined parts for a six-component internal balance. (Courtesy Ling-Temco-Vought Corporation.)

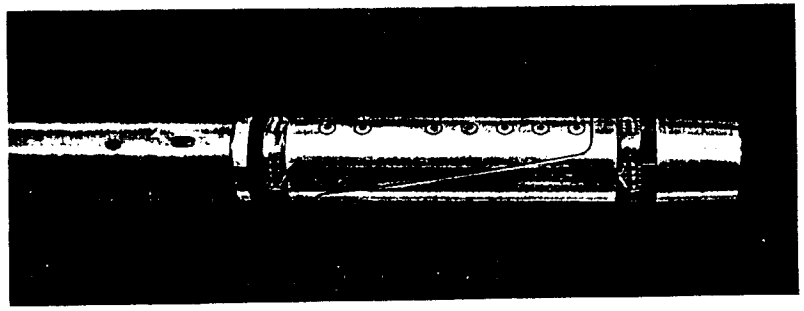


Fig. 7:12 Photograph of assembled internal strain gage balance.

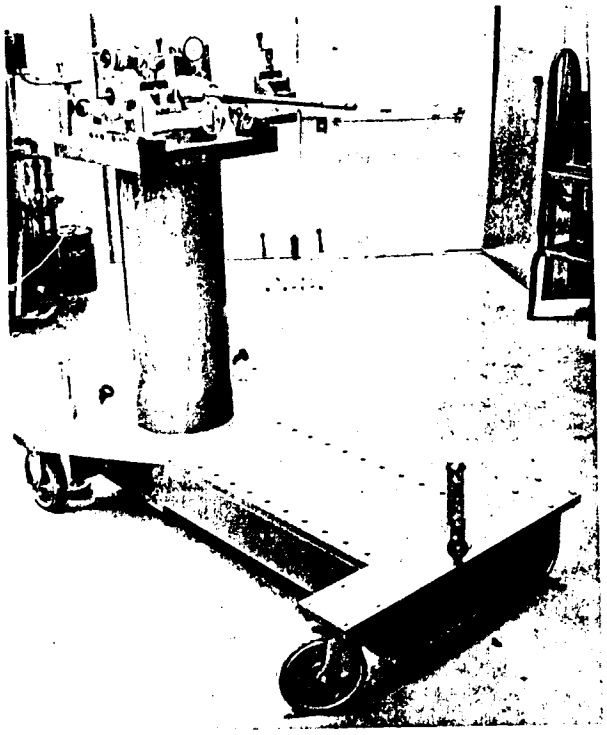


Fig. 7:13 A balance calibration rig.

can be applied. It has precisely located circular notches cut into its surface for positioning of calibration weights. Successive notches allow variations of moment about the moment gage stations while the normal force is held constant.

In Fig. 7:14, the rig is shown with the balance and calibration bar installed and with a normal force or side force loading, depending on whether the balance is at 0 or 90 deg roll. Figure 7:15 shows the rig with an axial force loading and Fig. 7:16 shows the rig with a rolling moment loading. One general consideration which is pertinent to any type of balance calibration is that of obtaining consistency of wiring and strain gage signal-measuring instrumentation between the calibration and the test. Because several strain gage signal magnitudes may be expected on a single balance, general practice is to make it possible to adjust the sensitivity of strain gage signal-measuring instrumentation to provide a range of instrument readings for one magnitude of strain gage signal. This adjustment is normally used to obtain the largest practical instrument reading due to model loads during a test, as a means of obtaining the most accurate

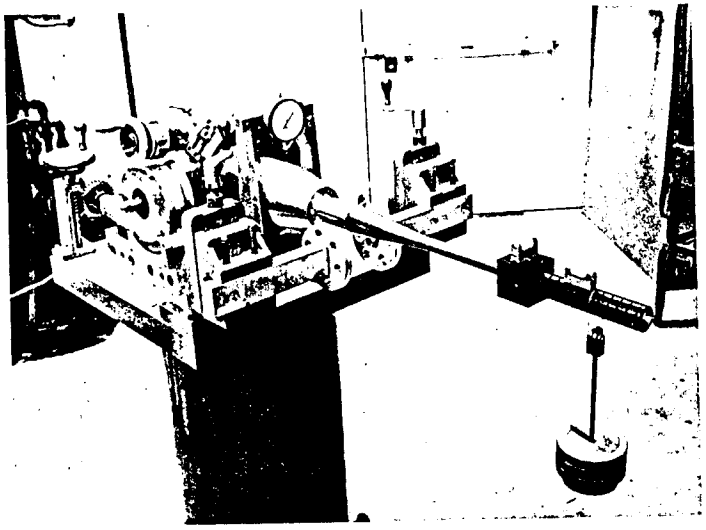


Fig. 7:14 Loading for normal force and pitching moment, or, with balance rotated 90 deg, side force and yawing moment.

test results. Variations of either the voltage supplied to the strain gage bridge or the reference supply voltage will have an effect comparable to changing sensitivities, so it is necessary that these voltages be maintained the same during calibrations and tests. Most wind tunnels are equipped with a group of measuring instruments so that data may be recorded

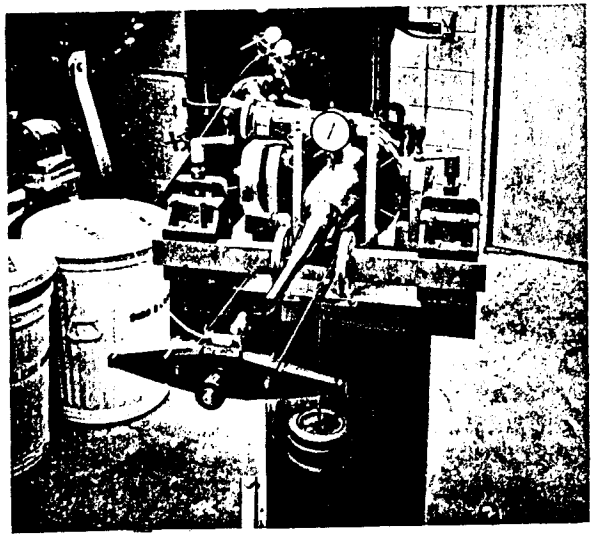


Fig. 7:15 Loading axial force.

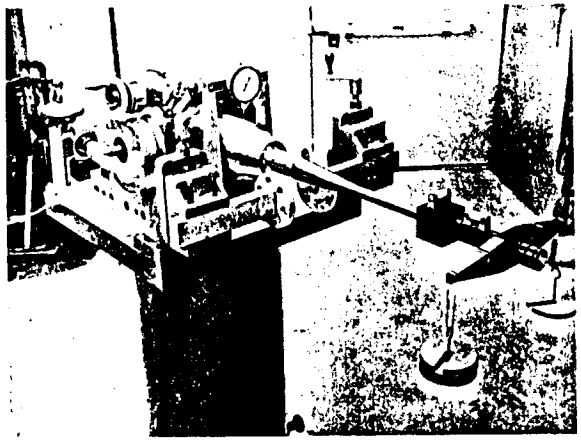


Fig. 7:16 Calibrating for rolling moment.

simultaneously from several strain gage bridges. This group of measuring instruments is usually interconnected to some extent. In such cases it is desirable to have all strain gages and other instrumentation that will be used during the test connected to the signal-measuring instruments during the calibration of any component of any balance. Also, experience has indicated the desirability of using the *same wiring and connections* throughout during the calibration and the test. Although the latter two considerations may be difficult to justify in some data-gathering systems with simple theory, the author's experience has indicated that they are sometimes quite important.

The first step in the calibration of an internal balance is to define some positive means of correlating the direction of applied loads (relative to the balance) with respect to the pertinent model planes during the test. For example, if some fixed plane of the balance is selected as the normal force plane during the calibration, and if the model is put on the balance with its normal force plane rotated 5 deg with respect to this plane, the correlation of loading direction will be poor and the resulting test data will be inaccurate.

If the relative orientation of the model and balance is fixed by keys or pins or by some other positive means, proper orientation of the balance for calibration is accomplished as follows. The model is placed on the balance, the balance–model assembly is rolled until the normal force plane of the model is in a vertical plane, the model is removed, and the calibration bar is installed without disturbing the balance orientation. At this point, the balance will be oriented so that weights applied to the calibration bar will be in the model normal force plane.

If the relative orientation of the model and balance is not fixed, as in the attachment method illustrated in Fig. 7:2, the method of obtaining proper orientation of the balance must be changed. A technique that has been used satisfactorily in this case may be described as follows. A point on the balance is selected where a weight may be hung prior to the installation of the calibration bar or model. A weight is hung at this point and the balance is rolled until the signal from a reference balance strain gage reaches zero. If the balance has gages only for normal force–pitching moment measurements, the reference gage may be either of the moment gages. In this case the balance is rolled exactly 90 deg from this point of zero signal in preparation for hanging calibration weights and for installing the model with its normal force plane in a vertical plane. If the balance has side force–yawing moment gages, one of the yawing moment gages is used as a reference. When this reference gage reads zero, the normal force plane of the balance is vertical.

Once the proper roll orientation of the balance has been achieved, the calibration bar and balance must be coaxial under zero load conditions for best calibration accuracy. A level is placed on the calibration bar and the calibration bar is leveled at zero load conditions. Then a series of weights are hung on the calibration bar at a series of stations covering the range of loadings likely to be encountered by the model during the test. At each weight and each station, the calibration bar is leveled and the deflection of the model support assembly is recorded. Leveling of the calibration bar is to ensure that the direction of load with respect to the balance is the same as that which would occur if the same load were acting at the same station on the model during a test. Measurements of deflection are also used for correcting indicated angles of attack recorded during a test.

The balance is then rolled precisely 180 deg, and the above procedure repeated, so that data will be obtained in both positive and negative directions in the normal force plane of the balance. If the balance also has side force gages, the procedure will be repeated with the balance rolled precisely 90 deg for loading in the side force plane. Calibrations at intermediate roll angles are also desired as a means of obtaining data with simultaneous loading in the normal force and side force planes of the balance. During all loadings of the balance, simultaneous readings of all balance gages will be recorded. Considering the theory of balance design with regard to one pitching moment gage, the gage is sensitive only to the moment in the normal force plane of the balance and at the gage station. Also, the gage reading is proportional to this moment. Thus, the theory suggests that

$$R = F_N(a + bx) \tag{7:8}$$

where R = reading due to applied load, counts,
F_N = applied normal force, lb,
a and b = constants to be determined from the calibration,
x = station at which the load is applied, inches from any reference point on the balance.

Actually, because of imperfections in manufacture, the pitching moment gage will be slightly sensitive to loadings in the side force plane of the balance. This effect of side force loading on a pitching moment gage reading is called an "interaction." Similarly, the effect of any loading on the reading of a gage not intentionally loaded is called an interaction. On a reasonably good balance, interactions will amount to only a few per cent of the primary gage reading at design load conditions but will not be negligible. And on such a balance, the interactions of loadings in the normal force plane on all other gages and of loadings in the side force plane on all other gages will be linear. When this is true, the actual readings of all gages due to normal force and side force loadings are as follows:

$$R = F_N(a + bx) + F_Y(c + dx) \tag{7:9}$$

where F_Y = applied side force, lb,
c, d = constants to be determined from the calibration.

When the reading being considered is a pitching moment gage reading, a and b are primary gage constants and c and d are interaction constants. When the reading being considered is a yawing moment gage reading, the reverse is true. And when the reading being considered is an axial force or rolling moment gage reading, all the constants are interaction constants.

As in all experimental measurements, the gage readings obtained during the calibration will be somewhat random and the determination of the constants of eq. (7:9) by a graphical procedure is difficult and inaccurate. Greater accuracy can be obtained with a little more time by a purely mathematical procedure. The procedure involves the "method of least squares" which is based on the premise that the most probable curve through a set of data will be the one for which the sum of the squares of the differences between the curve and the observed data are minimum. This method is developed as follows:

Rewriting eq. (7:9), we have

$$R_c = aF_N + bxF_N + cF_Y + dxF_Y \tag{7:10}$$

where R_c is the calculated reading and the constants are for the calculated curve.

Letting

$$V_i = R_{ci} - R_i \tag{7:11}$$

where V = difference between measured and calculated reading, counts,
i indicates a value at one condition of applied load (weight and station),

we have for the sum of squares of the differences

$$S = V_1^2 + V_2^2 + \cdots V_n^2 \tag{7:12}$$

where n is the total number of conditions for which data are available. In order to obtain constants for eq. (7:10) which corresponds to a minimum value of S, the following must be true:

$$\frac{\partial S}{\partial a} = \frac{\partial S}{\partial b} = \frac{\partial S}{\partial c} = \frac{\partial S}{\partial d} = 0 \tag{7:13}$$

$$\frac{\partial S}{\partial a} = 2V_1\frac{\partial V_1}{\partial a} + 2V_2\frac{\partial V_2}{\partial a} + \cdots 2V_n\frac{\partial V_n}{\partial a} \tag{7:14}$$

By letting Σ represent the summation from $i = 1$ to n, eq. (7:14) is rewritten

$$\frac{\partial S}{\partial a} = 2\sum V_i\frac{\partial V_i}{\partial a} \tag{7:15}$$

Combining eq. (7:15) with eqs. (7:10) and (7:11) yields

$$\frac{\partial S}{\partial a} = 2\sum (aF_{Ni} + bx_iF_{Ni} + cF_{Yi} + dx_iF_{Yi} - R_i)F_{Ni}$$

$$= 2\sum (aF_{Ni}^2 + bx_iF_{Ni}^2 + cF_{Ni}F_{Yi} + dx_iF_{Ni}F_{Yi} - R_iF_{Ni})$$

At $\dfrac{\partial S}{\partial a} = 0$,

$$a\sum F_{Ni}^2 + b\sum x_iF_{Ni}^2 + c\sum F_{Ni}F_{Yi} + d\sum x_iF_{Ni}F_{Yi} = \sum F_{Ni}R_i \tag{7:16}$$

Similarly for $\dfrac{\partial S}{\partial b} = \dfrac{\partial S}{\partial c} = \dfrac{\partial S}{\partial d} = 0$,

$$a\sum x_iF_{Ni}^2 + b\sum x_i^2F_{Ni}^2 + c\sum x_iF_{Ni}F_{Yi} + d\sum x_i^2F_{Ni}F_{Yi} = \sum x_iF_{Ni}R_i \tag{7:17}$$

$$a\sum F_{Ni}F_{Yi} + b\sum x_iF_{Ni}F_{Yi} + c\sum F_{Yi}^2 + d\sum x_iF_{Yi}^2 = \sum F_{Yi}R_i \tag{7:18}$$

$$a\sum x_iF_{Ni}F_{Yi} + b\sum x_i^2F_{Ni}F_{Yi} + c\sum x_iF_{Yi}^2 + d\sum x_i^2F_{Yi}^2 = \sum x_iF_{Yi}R_i \tag{7:19}$$

Equations (7:16) to (7:19) are four equations in terms of the four unknown constants and may be solved simultaneously to determine the four constants. Once the constants are determined, it is convenient from a

data reduction standpoint to alter them. For example, assume that eq. (7:9) represents the equation for the forward pitch gage reading. It will be necessary to know the effective location of the gage, which is called the "electrical center." This will be the point where the variation of reading with normal force is zero, and it is obtained as follows:

$$\frac{\partial R}{\partial F_N} = a + bx$$

$$x_{ec} = -\frac{a}{b} \tag{7:20}$$

It will also be necessary to know the variation of moment about the electrical center with reading. This is called the gage factor (GF) and is

$$GF = \frac{\partial(\text{Moment})}{\partial R} = \frac{\partial(F_N x)}{\partial R} = \frac{1}{b} \tag{7:21}$$

The amount of the gage reading which is due to side force and yawing moment interaction is obtained from

$$\frac{\partial R}{\partial F_y} = c + dx \tag{7:22}$$

$$\frac{\partial R}{\partial (F_y x)} = d \tag{7:23}$$

It is convenient for data reduction to set x in eq. (7:22) equal to the electrical center station of one of the side force gages so that the interaction can be represented by the sum of a reading due to side force and a reading due to moment about one of the side force gages.

The balance deflection angles measured at each weight and station are used to determine deflection constants. These deflection constants are needed to correct indicated angles α and β recorded during a test for balance bending due to air loads. Usually, the deflections of a balance can be represented by the following equations:

$$\Delta\alpha = F_N(e + fx) \quad \text{and} \quad \Delta\beta = F_Y(g + hx)$$

In determining the constants of the above equations which fit the calibration data, it is not necessary to consider data from combined loading (balance roll angles other than 0, ±90, 180 deg). For evaluating e and f, only the deflection angles measured during loadings with the balance at 0 deg and 180 deg need be considered. For evaluating g and h, only the deflection angles measured during loadings with the balance at ±90 deg need be considered.

The method for defining the constants using the least squares technique follows the procedure outlined previously for defining gage constants. The procedure is considerably shorter and less complicated because of the need to determine only two constants in each equation rather than four.

For use in data reduction, it will usually be convenient to rearrange the constants. For example, it is convenient to represent the deflection $\Delta\alpha$ by a constant multiplied by normal force plus another constant multiplied by moment about the forward pitching moment gage. These constants are determined as follows:

$$\frac{\partial \Delta\alpha}{\partial F_N} = e + fx_{ec1}$$

$$\frac{\partial \Delta\alpha}{\partial M_1} = f$$

where subscript 1 denotes the forward pitching moment gage.

Example 7:2 Determine the calibration constants for the following data obtained from one pitching moment gage during an internal balance calibration:

Balance Roll Angle, Deg	Applied Weight, lb	Reading (R, Counts) with Weight at Calibration Bar Station		
		0	2	4
180	100	−200	200	600
135	100	−163	148	460
135	50			230
90	100	−30	10	50

Roll angle is positive for clockwise rotation looking upstream and calibration bar station is in inches.

The coefficients of eqs. (7:16) to (7:19) are obtained by summations of Table 7:1.

Equations (7:16) to (7:19) are then rewritten

$$46{,}250a + 95{,}000b + 16{,}250c + 35{,}000d = 99{,}595$$

$$95{,}000a + 320{,}000b + 35{,}000c + 120{,}000d = 463{,}550$$

$$16{,}250a + 35{,}000b + 46{,}250c + 95{,}000d = 42{,}595$$

$$35{,}000a + 120{,}000b + 95{,}000c + 320{,}000d = 205{,}550$$

Table 7:1

Summations of Balance Calibration Terms for Example 7:2

Roll Angle	Wt.	x	F_N	F_Y	F_N^2	xF_N^2	F_NF_Y	xF_NF_Y	$x^2F_N^2$
180°	100.	0	100.	0	10,000	0	0	0	0
	100.	2	100.	0	10,000	20,000	0	0	40,000
	100.	4	100.	0	10,000	40,000	0	0	160,000
135°	100.	0	70.71	70.71	5,000	0	5,000	0	0
	100.	2	70.71	70.71	5,000	10,000	5,000	10,000	20,000
	100.	4	70.71	70.71	5,000	20,000	5,000	20,000	80,000
	50.	4	35.35	35.35	1,250	5,000	1,250	5,000	20,000
90°	100.	0	0	100.	0	0	0	0	0
	100.	2	0	100.	0	0	0	0	0
	100.	4	0	100.	0	0	0	0	0
	Summations Σ				46,250	95,000	16,250	35,000	320,000

$x^2F_NF_Y$	F_Y^2	xF_Y^2	$x^2F_Y^2$	F_NR	xF_NR	F_YR	xF_YR
0	0	0	0	−20,000	0	0	0
0	0	0	0	20,000	40,000	0	0
0	0	0	0	60,000	240,000	0	0
0	5,000	0	0	−11,525	0	−11,525	0
20,000	5,000	10,000	20,000	10,465	20,930	10,465	20,930
80,000	5,000	20,000	80,000	32,525	130,100	32,525	130,100
20,000	1,250	5,000	20,000	8,130	32,520	8,130	32,520
0	10,000	0	0	0	0	−3,000	0
0	10,000	20,000	40,000	0	0	1,000	2,000
0	10,000	40,000	160,000	0	0	5,000	20,000
120,000	46,250	95,000	320,000	99,595	463,550	42,595	205,550

Simultaneous solution of the equations at the bottom of page 269 yields

$$a = -1.995$$

$$b = 1.999$$

$$c = -0.322$$

$$d = 0.207$$

The gage electrical center from eq. (7:20) is:

$$x_{ec} = -\frac{(-1.995)}{(1.999)} = 0.998 \text{ (inches from station 0)}$$

The gage factor from eq. (7:21) is:

$$GF = \frac{1}{1.999} = 0.5003 \text{ inch-lb/count}$$

Assuming that yawing moment for calculating normal force interaction will be the moment about a side force gage located at the same station as the normal force gage, we obtain the interaction constants from eq. (7:22) and (7:23).

$$\frac{\partial R}{\partial F_Y} = (-0.322) + (0.207)(0.998) = -0.115 \text{ counts/lb}$$

$$\frac{\partial R}{\partial M_Y} = 0.207 \text{ counts/inch-lb}$$

These interaction terms may be converted from counts to inch-pounds by multiplying by the gage factor

$$\frac{\partial M}{F_Y} = (-0.115)(0.5003) = -0.0575 \text{ inch-lb/lb}$$

$$\frac{\partial M}{\partial M_Y} = (0.207)(0.5003) = 0.1036 \text{ inch lb/inch-lb}$$

7:11 Control Surface Hinge Moment and Bending Moment Balances

Control surface hinge moments and bending moments are generally difficult to measure in high-speed wind tunnel tests because of the small sizes of components involved. Because of the wide variety of types and locations of control surfaces and aircraft configurations, many schemes have been used to measure these components. We shall discuss two types which have been used successfully and which are applicable to a majority of familiar control surface configurations.

The first type to be discussed has been used to measure hinge moment and bending moments on flap-type or all-movable controls located adjacent to or near the body of an aircraft. The principle of this balance is illustrated by Fig. 7:17.

The balance is completely housed within the body of the model but does not touch the body except at the point of attachment. The control is fabricated with a support shaft which is inserted into a low-tolerance hole in the free end of the balance. At this point of attachment provision is made for indexing the control at desired angular positions. The balance is equipped with forward and aft moment strain gage bridges from which the normal force on the control and the moment of the control about its hinge axis can be determined. The balance is also equipped with a torsion bar strain gage bridge as discussed in Section 7:8. This gage is used to determine the moment of the control about the gage center. By using this moment together with the normal force on the control obtained from

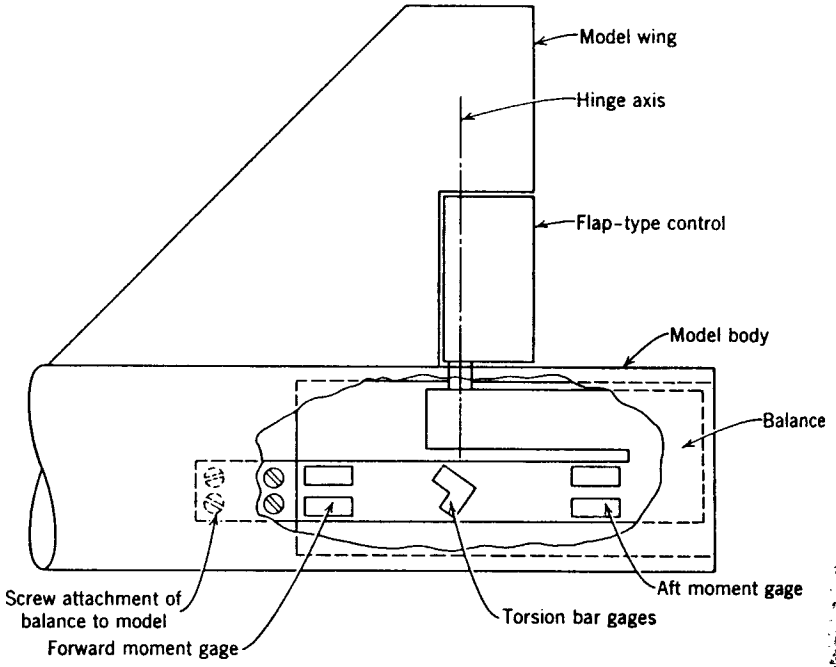


Fig. 7:17 A balance for measuring hinge moments and bending moments of a control surface located near the surface of the model body.

the other two gages, the bending moment of the control about a desired reference axis parallel to the balance axis may be calculated.

The second balance to be discussed has been used for measuring hinge moment only of aileron-type controls where space in the model for instrumentation is quite limited. This type of balance is illustrated in Fig. 7:18. The balance is simply a piece of thin metal bent to the angle of

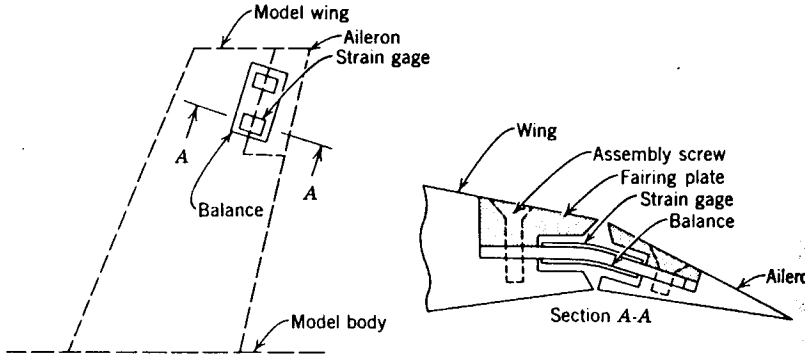


Fig. 7:18 A balance for measuring hinge moments of an aileron-type control

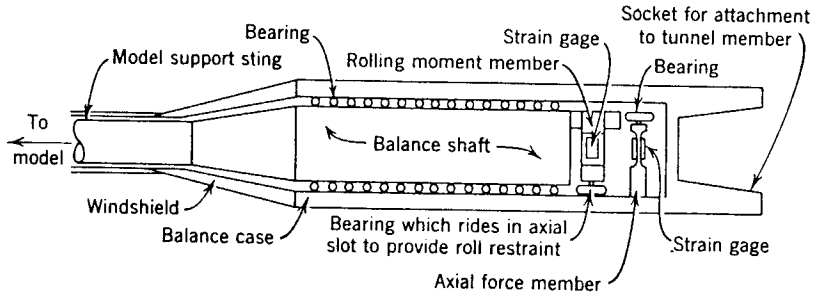


Fig. 7:19 A remote balance for measuring axial force and rolling moment.

aileron deflection desired and equipped with two strain gages on each of the upper and lower surfaces to form a single strain gage bridge. The wing and aileron are machined in such a way that the balance can be attached to both the wing and the aileron with its centerline along the chord plane of the wing and aileron. Fairing plates to place over the balance and provide the original surface contour are required. This balance arrangement leaves much to be desired but in some cases may be the only practical way to obtain aileron hinge moments.

7:12 Remote Rolling Moment and Axial Force Balances

In some cases, balances located on the model axis but downstream of the model in a pod have been used for the measurement of rolling moment and axial force. Such a balance is shown in Fig. 7:19. These balances were used extensively with reasonably satisfactory results before internal balances for measuring axial force were developed to their present state. The most important criteria for a satisfactory balance of this type are a stiff balance case, a high-quality job of bearing design and fabrication for freedom of the shaft relative to the case, and a balance case design that prevents air flow and consequent pressure gradients within the balance case.

7:13 Wall-Mounted Balances

A wall-mounting balance is a special-purpose balance that is used only when the model to be tested is a half-span (or smaller portion) model mounted directly from the tunnel wall or from a reflection plane near the tunnel wall. The balance may be a simple single-component balance or it may be designed to provide measurements of as many as six components. Because of the wide variations in applications of such balances, many different designs have been used. Most balances of this type in current use are strain gage balances and the fundamentals of strain gage balance design which have been discussed in previous sections will apply.

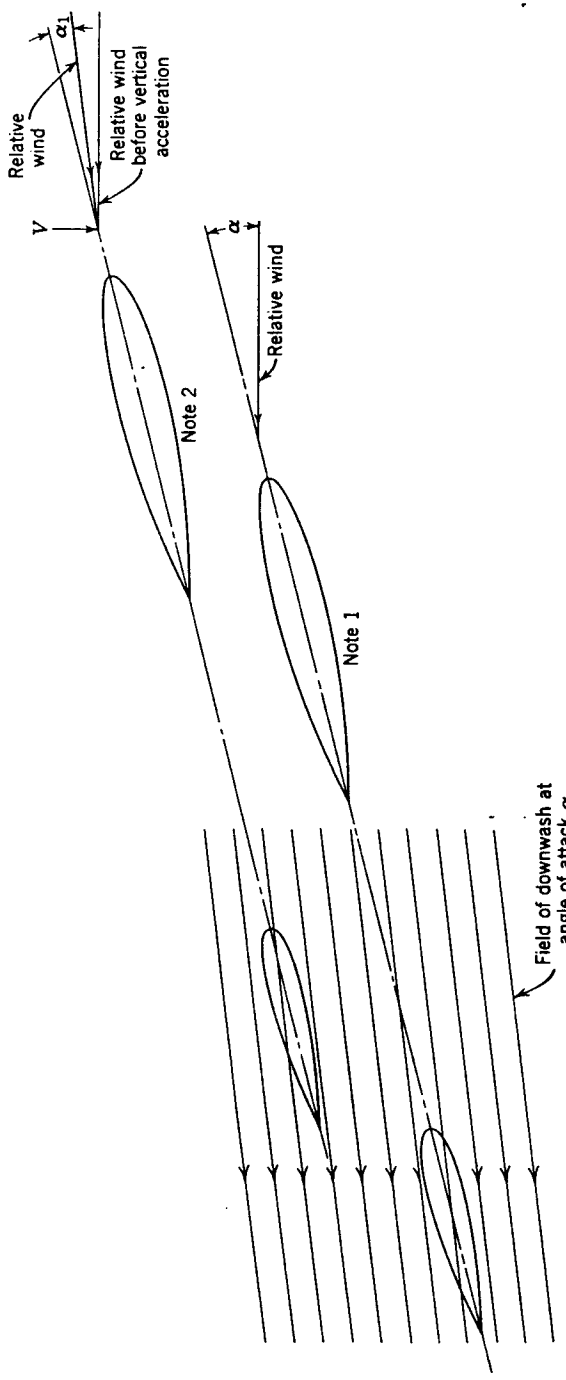


Fig. 7:20 Illustration of downwash lag effect during vertical acceleration.

Note 1: The aircraft is in steady flight at angle of attack α. The tail is operating in a downwash field corresponding to this α.
Note 2: The aircraft has been subjected to a vertical acceleration and has achieved a vertical velocity V. The components of vertical and forward velocity result in a new angle of attack α_1. However, the tail of the aircraft is still operating in the downwash fields corresponding to the previous angle of attack α. The downwash fields corresponding to steady flight at α and α_1 are different. Consequently, the air loads at α_1 during steady flight and flight with vertical acceleration are different.

7:14 External Balances

External balances are those located outside the wind tunnel and used to measure loads transmitted from the model located in the center of the test section, through the tunnel wall, and to the balance through one or more structural members. Balances of this type were used extensively in early low-speed wind tunnels and are at present used in some of these tunnels that are still operating. Their construction and use in recently built high-speed tunnels is so limited that the wind tunnel engineer is not likely to be concerned with them.

It is of interest to note that the design of early external balances was based on the mechanical separation of the various components of model loads by means of pivots and linkages and the mechanical balancing of each individual component by use of varying weights and/or varying moment arms. Balances of this type are quite complex in comparison with strain gage balances which have been discussed. Actually the term "balance," which is used for practically all wind tunnel force-measuring devices, arose from external balances in which loads on models were balanced with known weights. The decline of the external balance can be attributed primarily to two factors. First, the evolution of strain gage instrumentation has progressed to the point where measurement accuracy with strain gages is equal to or better than that with mechanical balances, and the strain gage affords simpler balance design. Second, at the higher speeds for which most wind tunnels have been built in recent years, struts used to transmit model loads to the external balance cause significant changes in the air loads on the model.

7:15 Dynamic Stability Rigs

Dynamic stability rigs are devices for measuring loads due to unsteady conditions during flight. Figures 7:20 to 7:22 are presented as aids for illustrating the cause of such loads.

In Fig. 7:20 are sketched the wing and tail of an aircraft in steady flight at one instant and an instant later after the aircraft has been subjected to a vertical acceleration. During a uniform vertical acceleration, the wind direction relative to the aircraft is continuously changing because of a continuously changing vertical velocity. The result is that the tail of an aircraft during a vertical acceleration is always operating in a field of downwash from the wing which was created earlier by the wing at a previous angle of attack. This lag effect causes the loadings on the aircraft to differ from those which would be experienced by the aircraft in steady flight at the same angle of attack. It is noted that this lag effect exists over the entire aircraft and not just over the tail. Downstream of the leading edge of the aircraft, every point is operating in a flow field which is

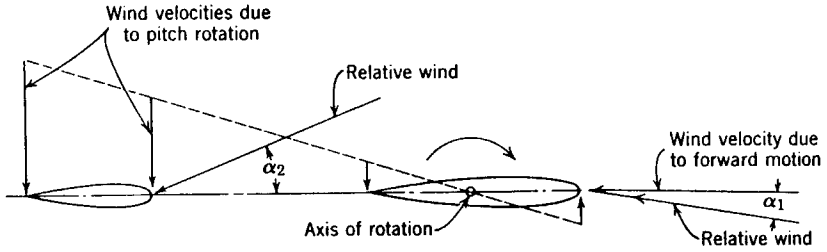


Fig. 7:21 Relative wind variation over an aircraft due to rotation in the pitch plane.

dependent on the flow over upstream points at earlier times. The lag effect is also present in the case of an aircraft which is rotating at a constant angular rate about an axis normal to the flight direction for the same reason.

Unsteady effects of angular rotation other than these lag effects and usually greater are present. These are illustrated by Fig. 7:21. During angular rotation, each point not on the axis of rotation has a velocity normal to the axis of the aircraft. The relative wind is a result of vector addition of this component of velocity and the component of velocity resulting from forward motion of the aircraft. Figure 7:21 illustrates the variation of the relative wind direction over an aircraft due to an angular-rotation.

When an aircraft is rolling about its axis, velocity components (and hence air loads) not present in steady flight are induced as shown in Fig. 7:22.

Dynamic air loads are difficult to measure in a wind tunnel because they are small relative to steady-state loads and because they must be measured with the model in motion. Dynamic stability tests in wind tunnels are generally limited to tests in which the model has one of two single degrees of freedom. These are a freedom to rotate about some

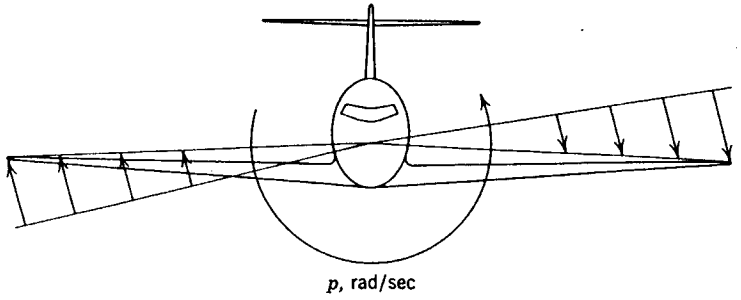


Fig. 7:22 Velocities on an aircraft wing due to rolling.

model pitching moment axis in dynamic pitch tests and a freedom to rotate about the model axis in dynamic roll tests.

Not a great deal of effort has been devoted to dynamic load measurements with a translational degree of freedom of the model. There are two major reasons for this. One is the difficulties involved in the measurements. The other is that damping moments, which are the primary requirement of dynamic tests, can be determined by using the simpler rotational degree of freedom system.

7:16 Dynamic Pitch Rigs

The most frequently used dynamic pitch rig is one in which the model is attached to a support member by means of bearings or flexures on the desired axis of rotation (Figs. 7:23 and 7:24). The model is locked to the support member while tunnel operation is established. The lock is released, the model is displaced from its equilibrium position (usually zero angle of attack), and then it is released. The motion after release is recorded, frequently by using a strain gage on a very flexible link between the support and the model. The time history of the oscillation is an indication of the dynamic loads.

The equation of motion for a single degree of freedom pitching system with no air loading or air damping but with a mechanical spring that tends to return the model to an equilibrium position is as follows:

$$I\ddot{\theta}_f + C_1\dot{\theta}_f + K_1\theta_f = 0 \qquad (7:24)$$

where I = Inertia of model about the axis of rotation, slug-ft^2,
θ = Angle of the model with respect to the equilibrium position, usually zero angle of attack, radians,
C_1 = A system damping constant, ft-lb/(radians/sec),
K_1 = A system spring constant, ft-lb/radians.

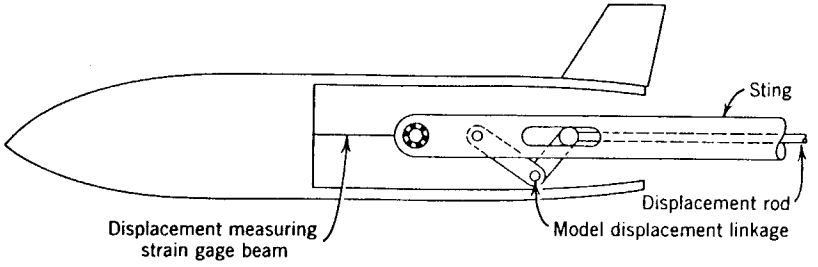


Fig. 7:23 Schematic of bearing-mounted free oscillation dynamic pitch rig. The bearings are sometimes ball-bearings, and more recently gas-bearings. The bearings are sometimes replaced by flexures.

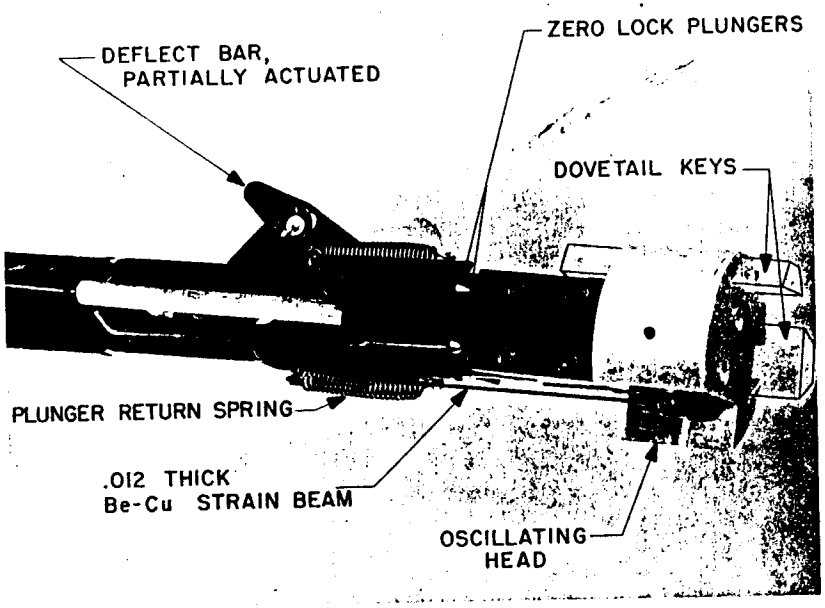


Fig. 7:24 Photograph of bearing-mounted free oscillation dynamic pitch rig.

The letter f denotes conditions with wind-off and the single and double dots above θ denote, respectively, the first and second derivatives with respect to time.

Equation (7:24) may be solved to obtain

$$\omega_f = \frac{1}{2\pi}\sqrt{\frac{K_1}{I} - \left(\frac{C_1}{2I}\right)^2} \tag{7:25}$$

$$P_f = \frac{1}{\omega_f} \tag{7:26}$$

$$C_1 = \frac{1.3863I}{(T_{1/2})_f} \tag{7:27}$$

$$K_1 = I\left[\frac{4\pi^2}{P_f^2} + \left(\frac{0.69315}{(T_{1/2})_f}\right)^2\right] \tag{7:28}$$

where ω = model pitching frequency, cycles/sec,
P = period of one cycle of oscillation, sec,
$T_{1/2}$ = the time required for the amplitude of model oscillation to decay from a reference value to a value equal to half the reference value, sec

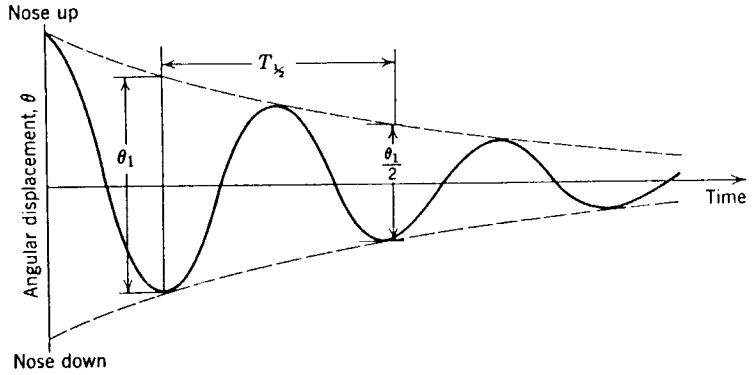


Fig. 7:25 Typical oscillation time history for a single degree of freedom model in a wind tunnel.

If the system considered above is placed in a vacuum chamber, displaced from its equilibrium position, and released, the values of P_f and $(T_{1/2})_f$ can be obtained directly from the displacement-time history. (See Fig. 7:25.) These values can then be used in eqs. (7:27) and (7:28) to obtain the system damping constant C_1 and the system spring constant K_1. If the same system is placed in an airstream and displaced, its equation of motion becomes

$$I\ddot{\theta} + (C_1 + C_2)\dot{\theta} + (K_1 + K_2)\theta = 0 \tag{7:29}$$

where C_2 = aerodynamic damping moment per unit value of θ, $-(M_q + M_{\dot{\alpha}})$, ft-lb/(radians/sec),
M_q = moment per unit value of $\dot{\theta}$ due to the effect illustrated in Fig. 7:21, ft-lb/(radians/sec),
$M_{\dot{\alpha}}$ = moment per unit value of $\dot{\theta}$ due to the effect illustrated in Fig. 7:20, ft-lb/(radians/sec),
K_2 = aerodynamic restoring moment per unit value of θ, $-M_\alpha$, ft-lb/radians,
M_α = aerodynamic moment per unit angle of attack, ft-lb/radians.

The solution of eq. (7:29) yields

$$\omega = \frac{1}{2\pi}\left[\frac{K_1 + K_2}{I} - \left(\frac{C_1 + C_2}{2I}\right)^2\right]^{1/2} \tag{7:30}$$

$$P = \frac{1}{\omega}$$

$$C_2 = -(M_q + M_{\dot{\alpha}}) = 1.3863I\left[\frac{1}{T_{1/2}} - \frac{1}{(T_{1/2})_f}\right] \tag{7:31}$$

$$K_2 = -M_\alpha = I\left\{4\pi^2\left(\frac{1}{P^2} - \frac{1}{P_f^2}\right) + (0.69315)^2\left[\frac{1}{(T_{1/2})^2} - \frac{1}{(T_{1/2})_f^2}\right]\right\} \tag{7:32}$$

By using the period and time to damp to half amplitude from the air-on oscillation in conjunction with similar values obtained from oscillation in a vacuum, the damping and static moment terms can be obtained from eqs. (7:31) and (7:32).

If the wind-off damping and spring constants are zero, the time to damp to half amplitude and the period with wind off $(T_{\frac{1}{2}})_f$ and (P_f) are infinite. Then, the damping and static-moment terms may be obtained by inserting infinity for these values in eqs. (7:31) and (7:32). Such a case would correspond to a dynamic rig with a frictionless bearing (for practical purposes) and no spring connection between the model and the fixed portion of the rig.

It is noted that negative values of the damping and static moment terms $M_q + M_{\dot{\alpha}}$ and M_α correspond to dynamic and static stability; that is, the damping moments tend to reduce the amplitude of oscillation and the static moments tend to restore the model to its undisturbed or "trim" position.

With models for which the inertia about the center of rotation cannot be easily calculated, it may be determined experimentally as follows: One end of a slender metal rod (typically 0.25 inch outside diameter by 4 ft long) is rigidly attached in a vertical position to some support with the free end hanging down. The free end of the rod is arranged in a way to allow rigid attachment of the model with its center of rotation on the rod axis. Three or four cylindrical rods having inertias about their centers which can be calculated and which bracket the model inertia are arranged so they can be mounted on the free end of the suspended rod. In turn, each of these rods is attached to the free end of the suspended rod, rotated to put a torque into the suspended rod, and released and allowed to oscillate freely in rotation. The cycles of oscillation in a given period of time are counted by visual observation or by using a torsion strain gage signal from the slender rod to obtain a frequency ω_f. A plot of ω_f versus calculated inertia is made. The model is then mounted on the suspended rod and its frequency ω_f determined. The model inertia is then obtained by entering the ω_f versus inertia curve at the value of ω_f for the model. This procedure is an experimental solution of eq. (7:25). Note that the procedure assumes that the air damping constant C_1 is the same for the rods and the model. Any errors due to this assumption can be eliminated by carrying out the procedure in a vacuum.

Note also that eqs. (7:24) to (7:32) are based on the assumption that the rig and aerodynamic damping and spring terms do not vary with angular position or rotational velocity. This is a good assumption when the amplitude of oscillation is small, but it may be very poor when the amplitude is large. The method is, nevertheless, sometimes used for

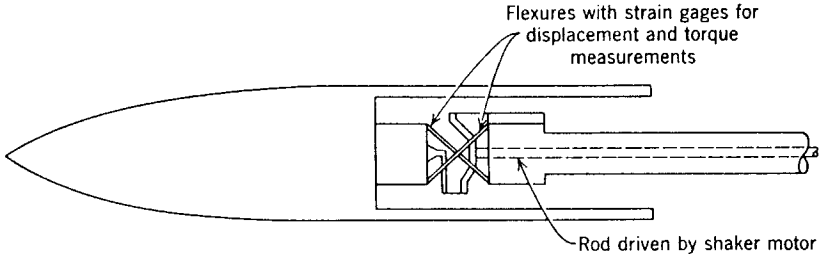


Fig. 7:26 Schematic of a forced oscillation dynamic pitch rig.

determining damping moments of models with variable M_α in the range of the oscillation. An approximate method has been developed in Ref. 7:2 for determining damping moment from time histories of the oscillation of a nonlinear system. Results are presented in Ref. 7:2 which indicate that the assumption of a linear system can result in appreciable errors in calculated damping moment if the system is nonlinear.

Dynamic pitch rigs sometimes are designed for a forced instead of a free oscillation. One such rig is discussed in Ref. 7:3 and is illustrated in Fig. 7:26. This rig together with the associated electronic circuitry is designed to vibrate a model at its undamped resonant frequency and at a constant amplitude. For this system, the equation of motion is

$$I\ddot{\theta} - M_{\dot{\theta}}\dot{\theta} - M_\theta\theta = T \qquad (7:33)$$

where $M_{\dot{\theta}}$ = damping moment per unit value of $\dot{\theta}$, including tare values, ft-lb/(radians/sec),

T = driving torque, ft-lb.

With the model being vibrated at a constant amplitude and at the undamped natural frequency of the system, the inertial moment and the restoring moment exactly balance each other and the driving torque T is equal to the damping moment $M_{\dot{\theta}}\dot{\theta}$. Tare values of $M_{\dot{\theta}}\dot{\theta}$ are obtained by vibrating the system in a vacuum (with no aerodynamic damping). The difference between values of $M_{\dot{\theta}}\dot{\theta}$ from the test and tare run is equal to the aerodynamic damping moment $M_q + M_{\dot{\alpha}}$. Reference 7:3 contains a description of the electronic circuits with which the model vibrating frequency and amplitude are controlled and the driving torque is measured.

7:17 Dynamic Roll Rigs

Dynamic roll rigs are used to measure the aerodynamic damping moments while the model is rolling as a result of the effects illustrated in Fig. 7:22. They may be either free roll or forced roll systems. With the free roll system the model is bearing mounted on a sting and one of two procedures is applied to obtain damping moment. For the first, the model

is forced in a rolling motion by an external power source until some desired speed is reached. It is then disconnected from the power source so that there is no mechanical restraint to the rolling motion. A record of roll position or velocity variation with time is recorded and is used to calculate damping moment. The equation of motion in this case is

$$I\ddot{\phi} - M_{\dot{\phi}}\dot{\phi} = M_x \tag{7:34}$$

where ϕ = angle of model roll with respect to a plane through the body axis, radians. One and two dots above ϕ indicate, respectively, the first and second derivatives of ϕ with respect to time,

$M_{\dot{\phi}}$ = roll damping moment per unit ϕ, ft-lb/(radians/sec);

M_x = aerodynamic moment about roll axis due to model asymmetry, such as control incidence, ft-lb.

With the rolling moment due to model asymmetries obtained from static tests, the record of roll position or velocity with respect to time from the dynamic test, and the model inertia known, eq. (7:34) is readily solved for roll damping moment.

Another procedure used with the free roll technique is to deflect the ailerons of the model to produce a known aerodynamic rolling moment when the tunnel is operated. In the tunnel this aerodynamic moment will accelerate the model in roll until the moment produced by the ailerons is equal to the damping moment. When this condition is reached, the model will have reached a constant roll velocity. The steady-state roll velocity is recorded and the damping moment is calculated from the following equation:

$$M_x - M_{\dot{\phi}}\dot{\phi} = 0 \tag{7:35}$$

The forced roll system is one in which the model is driven at constant roll velocities by use of an external power source with provisions for measuring rolling moments by use of strain gages. In a system of this type the model is driven by a motor located either between the stationary internal balance and the model or between the rolling internal balance and the tunnel. In the latter case electrical connections to the strain gage are made through slip rings usually consisting of copper–silver ("coin silver") rings and silver–graphite brushes with a pressure of about 30 psi between the rings and brushes. With the model being rotated at a constant speed, the damping moment is obtained from eq. (7:35) by setting the measured rolling moment equal to M_x. One item of particular importance in the design of a forced roll rig is to provide a drive system capable of a very constant drive speed. Inertia moments will occur if the rotation speed is not constant and these can easily exceed the damping moments in magnitude.

References

7:1 Samuel B. Moore, The Design and Evaluation of an Internal Six Component Strain Gage Balance, M.S. thesis presented to the Southern Methodist University, January 1961.

7:2 C. J. Welsh, L. K. Ward, and G. R. Ahsmuhs, Determination of Damping Derivatives from Free Oscillation Tests of Non-Linear Systems Using Energy Relations, AEDC TN 60-104, 1960.

7:3 C. J. Welsh, Q. P. Hance, and L. K. Ward, A Forced Oscillation Balance System for the von Karman Facility 40- by 40-Inch Supersonic Tunnel, AEDC TN 61-63, 1961.

Chapter eight

Models, testing, and data reduction

8:1 General

Whereas models to be used in low-speed wind tunnel tests often are made almost entirely of wood, high-speed wind tunnel models seldom include any wood at all. There are several reasons for this. (1) The dynamic pressures in high-speed wind tunnels, and consequently the aerodynamic loads, are usually much greater than in low-speed tunnels. (2) High-speed wind tunnels are usually smaller and consequently require smaller models. In order to obtain the same degree of geometric similarity to a prototype, the absolute tolerances allowable on a small model are less than on a large model. The tolerances allowable for the desired degree of similarity usually dictate the use of metal instead of wood. (3) At the higher speeds, particles of dust or other foreign materials which inevitably find their way into wind tunnel circuits, are much more abrasive than at low speeds. The surfaces of a hard metal model are much more resistant to pitting and abrasion than those of a wood model. (4) And, of course, in heated wind tunnels the need for metal instead of wood models is apparent.

Some of the simpler high-speed wind tunnel models are occasionally fabricated of aluminum. However, the great majority are steel. Mild steel is not uncommon and type-303 stainless steel, which is called a free-machining stainless, is used when the properties of stainless are desirable.

The scales to which wind tunnel models are built are quite varied. The general practice is to build the model of the maximum size the tunnel engineer feels confident can be tested in his tunnel (Section 1:6). Usually, the aerodynamicist would prefer larger models, especially since much high-speed wind tunnel testing is done with models of $\frac{1}{60}$ scale and smaller. However, models are generally far too expensive in both time and money to take a chance on getting a model too large for the tunnel it is to be tested in.

Models are always built as nearly as possible to the exact configuration

of the prototype. The place where this is often difficult and sometimes impossible is at the aft end of the fuselage. The model designer generally must have a blunt-base model to insert a balance inside the model or to make a sting attachment to the tunnel angle of attack mechanism. The base diameter required depends on the size and deflection of the balance to be used and therefore on the model loads. On the other hand, if the design does not have a jet engine exhausting from the aft end of the fuselage, it will be unlikely to have a blunt-base fuselage. At this point the model designer and the aerodynamicist must compromise. The designer must make every effort to minimize the changes in aerodynamic configuration and the aerodynamicist must allow changes that cannot be avoided. The aerodynamicist usually will have ideas on changes that can be made with a minimum effect on the aerodynamic data or changes for which he can predict the effect.

If normal good machine shop tolerances of 0.001 to 0.002 inch can be held on all model dimensions, the model will generally be satisfactory. This is much more difficult than it sounds, however. Models are almost invariably of composite construction, being made up of several parts that must be assembled. This type of construction is required for practical fabrication and also for providing a means of varying model configuration during testing. For an assembled configuration to be accurate within 0.001 to 0.002 inch, the accuracies of the individual parts must sometimes be much greater. For example, assume that a wing 5 inches long is to be attached to a fuselage at a $\frac{1}{2}$-inch flat surface within the fuselage. In order for the wing tip to be in a specified plane within a tolerance of 0.002 inch, the combined inaccuracies of the flats must not exceed 0.0002 inch in angularity or the inaccuracies of individual flats must not exceed 0.0001 inch. Tolerances of these magnitudes are not practical in most machine shops. Because of this a great deal of effort is required on the part of the designer to ensure that the final model is satisfactorily accurate. To minimize errors at assembly, the designer may elect to do final machining with some mating parts assembled. He may specify tooling fixtures for machining. Or he may in some cases use a cut-and-try technique. Some models are of complex shape and require the use of template controlled machines. In such cases the template tolerances are important to the accuracy of the completed model. Reference 8:1 gives the following list of information that must be supplied to the model designer:

1. All basic model dimensions.
2. The required test configurations that determine the extent of components which must be put on or taken off during a test.
3. The maximum angle range of tests in pitch, yaw, and roll, and the

approximate maximum applied loads on the model, including normal force, pitching moment, side force, and axial force.

4. Movable surfaces, if any, and desired angle settings, along with the approximate maximum hinge moment expected during the tests.

5. Which hinge moments are to be measured.

6. The number of load and moment components that are to be measured, along with their approximate maximum values, will assist in the selection of the proper balance to be used or indicate the need of the design of a new balance.

7. The desired number, size, and locations of all pressure orifices.

8. Any other special instrumentation that is required. Examples are provision for measuring forces on external stores, or for total vertical or horizontal tail loads.

9. The type and extent of model inspection required.

8:2 Force Models

Force models are used in the measurement of three forces and three moments which completely define the overall loading. They may be designed so that various wings, horizontal tails, and vertical tails may be



Fig. 8:1 Photograph of a model installed on the pitching strut of a high-speed wind tunnel. (Courtesy McDonnel Aircraft Corporation.)

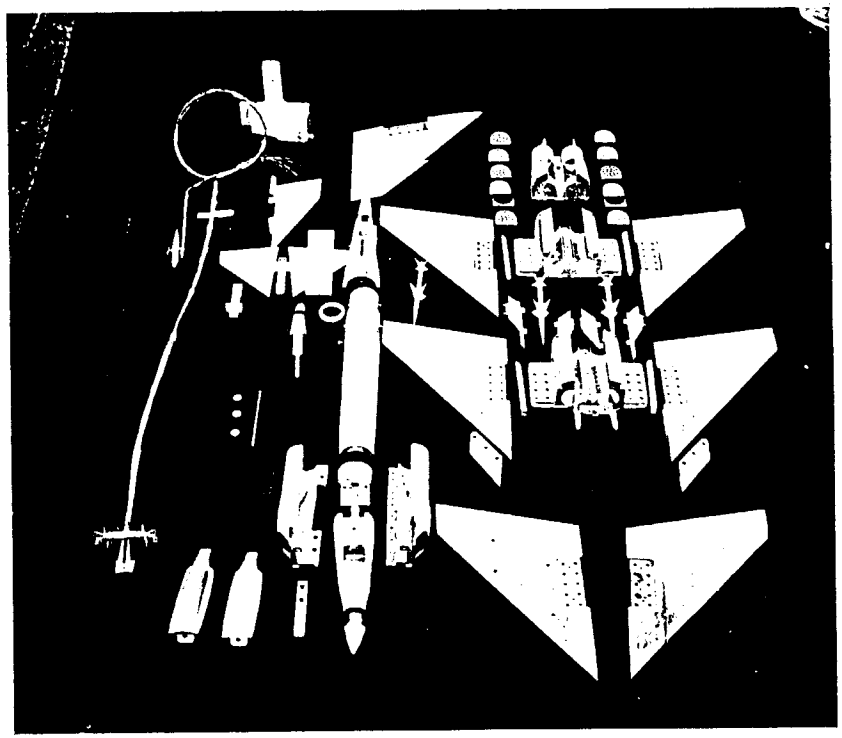


Fig. 8:2 Photograph of individual parts of wind tunnel model of a high-speed aircraft during the early development phase. (Courtesy McDonnell Aircraft Corporation.)

tested; designed for determining the effects on overall model loading of deflecting controls such as ailerons, flaps, and horizontal and vertical tails; or designed for determining the loading of control surfaces.

In order to supply all or most of the above information, it is apparent that the force model must be quite complex. An idea of the model's complexity and the many details with which the model designer is faced is best obtained by considering a typical example. Figure 8:1 is a photograph of a force model installed on the angle of attack mechanism of a high-speed tunnel. Figure 8:2 shows individual parts of the model during the early phases when the overall configuration of the aircraft was still being developed (note the three different wing planforms). Items of Fig. 8:2 which might puzzle the reader at this point are the series of perforated plates behind the wings. It will be noted that this aircraft has two engines with air inlets along the sides of the fuselage. The perforated plates are devices installed in the after portions of the engine tubes to change their air flow in simulation of various conditions of engine performance. Note

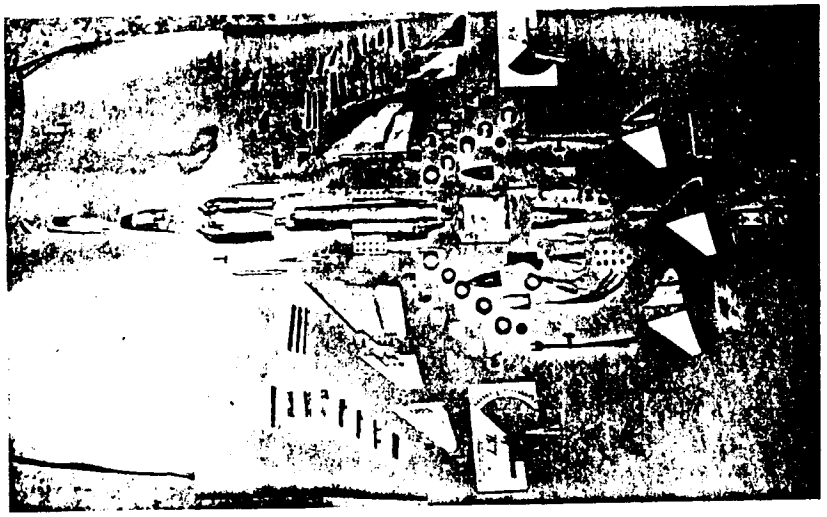


Fig. 8:3 Photograph of the individual parts of a high-speed wind tunnel model for evaluating control surfaces. (Courtesy McDonnell Aircraft Corporation.)

the small rakes at the extreme left of the figure. These are pressure-measuring rakes, which are installed in the after portion of the engine tubes to determine the amount of air flowing through the tubes.

Figure 8:3 is a photograph of the parts of a later model of the same aircraft. At this point the aircraft configuration was more firm and the emphasis was on evaluating control surfaces. Note the three different horizontal tails, the two different wing tip controls, and the control incidence setting fixtures.

With the multitude of individual parts of a single high-speed wind tunnel model, one of the most important parts of the designers job is to build the model so that configuration changes can be easily and quickly made. High-speed wind tunnel testing normally costs from a few hundred to well over a thousand dollars for each hour the model is in the tunnel. Difficult and time-consuming model changes are very costly.

8:3 Dynamic Stability Models

Dynamic stability models are subject to the same design considerations as force models with regard to exterior geometry. The model inertia about its axis of rotation and its center of gravity position are design considerations in some cases. Referring to Sections 7:16 and 7:17, we note that model inertia about the center of rotation must be known for all dynamic pitch testing and for one of the free roll techniques of dynamic roll testing. If it is desired to have flow fields about the model similar to those about

the prototype in these cases, the model inertia must be specified. This can be shown as follows. Consider Fig. 7:22 which illustrates that velocities normal to the direction of flight are induced by the rolling motion. The magnitudes of these velocities are equal to the product of roll rate and distance from the axis of rotation. If the induced velocities on the model are to be equal to the induced velocities on the prototype, then the products of roll rate and distance from the axis of rotation on the model and prototype must be equal. This means that a scale model must be rolling faster than the prototype by a factor equal to the inverse of the model scale. Similarly, a scale model must be pitching faster than the prototype by a factor equal to the inverse of the model scale in order to provide flow similarity. Thus, if flows over a model similar to those over the prototype at specified roll or pitch rates are required, the rates for the model are specified as is the model inertia.

The case in which the model center of gravity must be specified is that of the free oscillation technique where the oscillation is in a vertical plane. In this case, the model center of gravity must be at the center of rotation. Otherwise, the equation of motion (eq. (7:29)) is not correct. The necessity of this center of gravity location is sometimes avoided by oscillation in a horizontal plane.

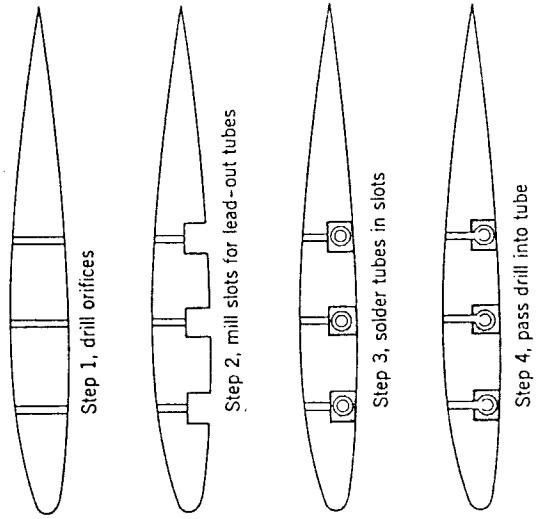
8:4 Pressure Models

When the aircraft design has progressed to the point where the aircraft configuration is fairly firm, pressure models are likely to be required. These are models for which the pressures at various points on the surface of the aircraft are measured. The purpose of pressure models is threefold:

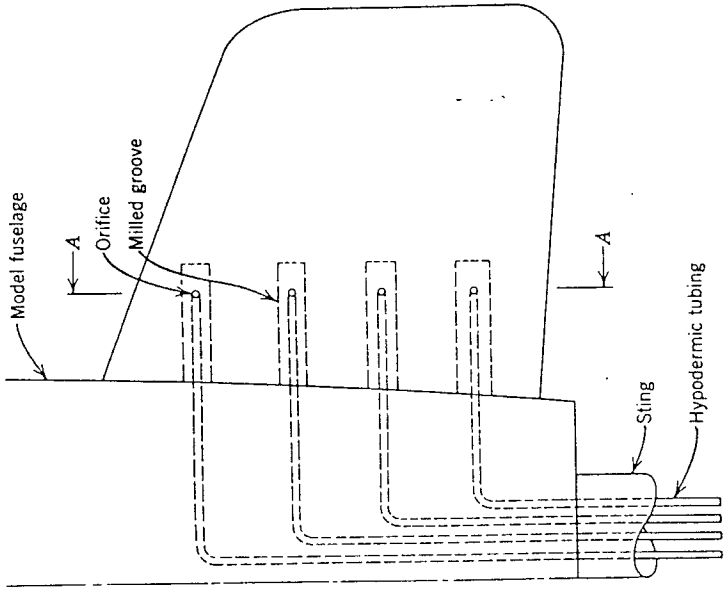
1. to obtain detailed loading information to be used for structural design of the various aircraft components,
2. for nearsonic tests to locate the points where the air flow first goes critical, and
3. for buffet tests. Here fast-response pressure measuring is required.

The pressure model is simpler in many respects than the force model in that few configuration changes will normally be required. What changes are required, however, are usually complicated because the aerodynamicists and the structures engineers almost invariably ask for more pressures than the designer can make arrangements for measuring.

One of the more common types of construction of pressure models is illustrated in Fig. 8:4. The component for which the surface pressure is to be measured, if it is a lifting or control surface such as a wing, tail, or flap, will have grooves milled in the surface opposite that on which the orifice is to be installed. These grooves will be for the installation of



(b)



(a)

Fig. 8:4 Illustration of orifice installation in a pressure model. (*a*) Plan views; (*b*) section A–A.

tubing to transmit the orifice pressures to measuring instruments. The tubing, which will normally be either mild steel or soft stainless steel, will be laid in the groove and the groove will then be filled with solder or some metal appropriate for the tunnel temperatures. The grooved surface will then be recontoured. One method of forming the orifice different from that illustrated in Fig. 8:4 is to drill a clearance hole normal to the model surface and countersink it slightly; insert the hypodermic tubing through the hole so that it extends a fraction of an inch above the orifice surface; solder the tube to the component in this position, making sure that solder fills the countersink and firmly attaches the tube to the component; bend the tube on the opposite side of the component so that it fits down into the bottom of the milled slot; fill the slot with solder so that the tubes are held tightly in place and so that the surface can be recontoured; cut the extended tubes off slightly above the orifice surface and then file the ends down until they are flush with the surface.

Usually, many pressure orifices are required in a single area. It is customary to design grooves for the tubing so that several tubes can be put in a single groove with each going to its respective orifice. When pressure measurements are required on both upper and lower surfaces of some component such as a wing or a tail, common practice is to install the orifices on one surface of one of the components and the opposite surface of the corresponding component on the opposite side of the aircraft.

In most pressure models, the tubing from all the individual models will be gathered into a bundle inside the fuselage which will pass through a hole in the sting which attaches the model to the tunnel. The bundle will be taken outside the tunnel where each individual tube is connected to a pressure-measuring device. The magnitude of the plumbing job with two hundred or more pressures, which is not unusual, may be seen in Fig. 8:5. If sufficient room is available inside the model, it is much more desirable to install one or more scanner valves (Section 6:6) inside the model and connect the pressure tubes to the scanner valve ports. Such an installation makes it possible to measure all the pressures by bringing a few wires outside the tunnel instead of bringing all the pressure tubes out. In Fig. 8:6, the model of Fig. 8:5 is shown with the tubes neatly bundled and attached to scanner valves in the rear of the model. In Fig. 8:7, the tubes have been covered with protective batting in preparation for installing the contoured shell of the model.

If it is necessary to bring the tubes outside the tunnel, it is highly desirable to arrange the plumbing so that no handmade pressure connections will be inaccessible with the model in the tunnel. The probability that handmade connections will develop leaks is several times the probability that continuous tubing will, and the test engineer shudders at the

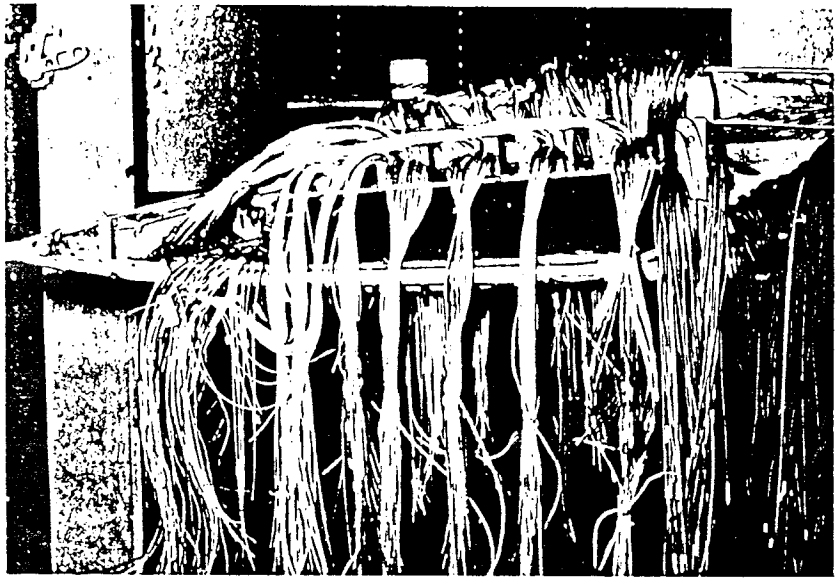


Fig. 8:5 Installing pressure leads on the Northrop T-38 wind tunnel model. (Courtesy Northrop Corporation.)

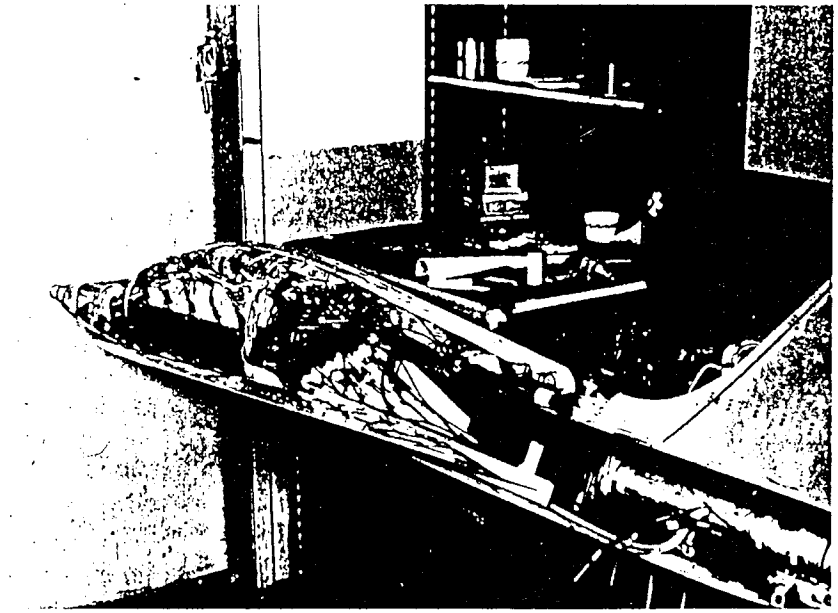


Fig. 8:6 Pressure tubes, connected to scanner valves. (Courtesy Northrop Corporation.)

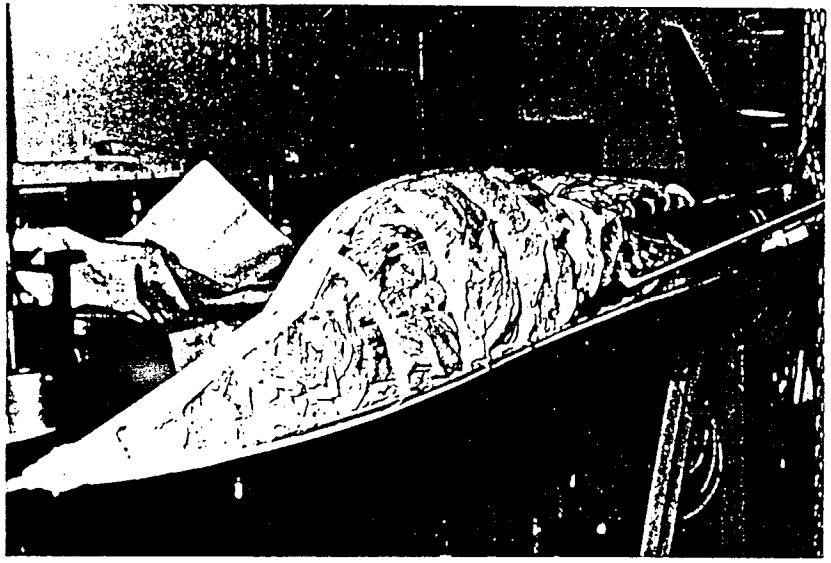


Fig. 8:7 Pressure model ready for port shell half.

thought of pulling a pressure model out of the tunnel to repair a few leaks when the test is in progress.

With an installation in which the pressure tubing must pass outside the tunnel, it is difficult to avoid a great deal of lag of the pressure-measuring instruments. The length of each tube will usually be several feet, each tube will have several bends in it which tend to constrict the flow, and the tube is almost always smaller than desired because of the physical impossibility of taking the required number of larger tubes through the sting. With all these factors tending to hinder flow in the tubing, a significant amount of time is necessary for pressure equalization between the orifice and the measuring instrument. In a continuous tunnel this is not too bad because almost any time required for stabilization is available. In an intermittent tunnel where the time for stabilization is limited, tubes that are too slow can result in no data at all. In the design of pressure models for intermittent tunnels, the tunnel engineer must be certain that the design will allow pressure stabilization during the run time he has available.

Note that pressure lag times are greater in going from a high pressure to a low pressure. When the pressure at the orifice is higher than that at the measuring instrument, the density in the tubing will be increasing as equilibrium is approached. Because density is increasing, the specific volume of air in the tubing will be decreasing. This will tend toward a

decreasing velocity in the tube and consequently lower pressure losses as equilibrium is approached. When the pressure at the orifice is below that at the measuring instrument, the specific volume of air in the tubing will be increasing, tending toward increasing velocity and consequently greater pressure losses as equilibrium is approached. This factor should be considered in selecting the size of tubing to be used. For a transducer and scanner valve installation in the model, pressure lag times will be reduced because of the shorter lengths of pressure tubing required. However, a few seconds of stabilization time are still required before the scanner valve is stepped from one pressure orifice to the next for recording data. When the transducer is housed within the fuselage, the model should be designed so that the transducer and all associated plumbing are readily accessible for installation and repair, and so that the transducer is isolated from any environment that affects its performance, such as vibration and heat.

8:5 Models for Engine Tests

Aircraft operating at speeds in the range of wind tunnels being considered herein normally use one of the following types of jet-propulsion engines: the turbojet, the continuous flow ramjet, the liquid-fuel rocket, or the solid-fuel rocket. Testing of complete scaled models of these jet engines in wind tunnels with burning is seldom done. The main reason is that burning is a time-dependent process and flow conditions at various stations in the hot gas portion of a scaled model would generally be expected to be considerably different from conditions at corresponding stations in the prototype. However, considerable scale model testing is done in wind tunnels to develop inlet and internal flow passage configurations that provide the desired flow at the air compressor inlet of the turbojet or at the fuel injection station of the ramjet with minimum drag.

Wind tunnel models for engine tests will usually be of somewhat larger scale than force models of the complete aircraft configuration. Accurate scaling, as with force models, will be accomplished externally in the vicinity of the inlet and internally back to the point at which the flow is to be determined. The downstream portions of the model may have little resemblance to the actual engine.

At the internal station of interest, probes for the measurement of total and static pressure of the flow will be installed (Fig. 8:8). Usually a rake will be used with enough probes to determine the uniformity of flow. From pressures measured, the compression efficiency of the inlet diffuser and all the flow parameters of importance to the engine operation can be determined. Downstream of the measuring station a variable area orifice will be installed for varying the amount of flow through the engine.

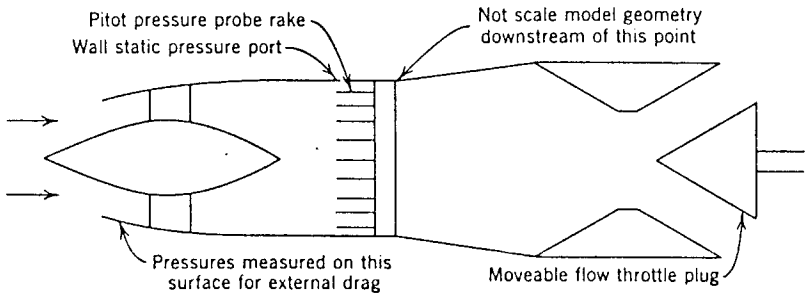


Fig. 8:8 Schematic of model arrangement for ramjet engine test.

Although devices have been designed for measuring inlet drag directly, they are quite complex and external drag determination is probably more frequently accomplished by using pressure orifices installed in the external surfaces of the model inlet.

8:6 General Testing Procedures

Discussions of the more common types of tests will be found in subsequent chapters and will be located in general according to whether the test is usually run at transonic speeds (Chapter 9), at supersonic speeds (Chapter 10), or at hypersonic speeds (Chapter 11). In this section some of the procedures that are independent of the type and speed range of a test are discussed.

Most high-speed wind tunnels are so expensive and so tightly scheduled that considerable pretest effort is required if the test is to be successfully and efficiently carried out. A pretest conference should be arranged between the project engineers desiring the data and the tunnel engineers responsible for getting the data at the earliest practical date. At this conference, the following items should be covered:

1. What test results are required (force, pressure, hinge moment, dynamic stability).
2. What model configurations will be tested. It is sometimes surprising to the neophyte to see how many runs are made with obviously unflyable configurations such as those with engines and horizontal or vertical tails off and the like. Data on such configurations are often worthwhile in that they allow the aerodynamicist to determine the contribution of individual components to the overall aircraft performance, the interactions between components, and what configuration changes may improve performance.
3. What tunnel operating conditions (pressure, temperature, and Mach number) the test will be run at.

4. What size the model will be.

5. What instrumentation will be required (balances, pressure transducers, manometers, pressure rakes, heat transfer gages).

6. What the run schedule will be in detail, what the purpose of each run will be, and what data are required to satisfy that purpose. The runs should be scheduled to minimize the tunnel down time required for model changes. Major model changes should be scheduled to be made overnight when possible for economy. Sometimes when a nice but not necessary run at the end of the tunnel day would preclude a major overnight model change, it should be eliminated.

7. What provisions will be made before the test to ensure that all model parts will fit together and that model and tunnel parts will match properly. One thousand dollars an hour, for instance, is an expensive price to pay for a minor change such as drilling a hole to make some part fit after the test is in progress.

8. What maximum model load limits will be cutoff points for terminating a run.

9. Whether there is a probability of model buffeting and if so what provisions should be made for monitoring it, and what severity of buffeting will be tolerated before terminating a run.

10. What amount of instrument drift during a run will be tolerated before a rerun is required.

11. Whether the test should be run with artificial boundary layer transition (see Section 9:7) and if so, where the transition strips should be placed.

Tests of a high-speed model in an inexpensive low-speed tunnel are sometimes made to get data that will augment high-speed results obtained later, to "practice" model configuration changes under actual test conditions, and to get a "feel" for model testing and instrumentation problems before the more expensive high-speed test is started. The test engineers conducting these tests should be the same ones who will later conduct the high-speed tests.

In actual preparation for a test all required instrumentation must be in a state of readiness. For a force test this would include at minimum the balance, a total pressure transducer, a model base pressure transducer, and the data recorders. The instruments will be attached to the recorders and a balance calibration carried out according to Section 7:10. Calibrations of the pressure transducers will be carried out according to Section 6:7. It is highly desirable to make these calibrations outside the tunnel during a tunnel down time, so that tunnel occupancy time is not charged for.

All instrumentation is installed in position in or on the tunnel ready for use, with the balance aligned according to Section 7:10. The model is installed on the balance with its vertical plane in the vertical plane of the tunnel, and is moved by using the sector or pitching strut until its horizontal plane is in the horizontal plane of the tunnel. "Zero" readings of all instrumentation are recorded for reference at this time. This includes "no air load" readings from the balance gages, atmospheric pressure readings from the pressure transducers, and a zero α reading from the position indicator of the sector or strut. At this point the model and instrumentation are set up for an angle of attack traverse.

Where preparations are being made for an angle of sideslip (β) traverse instead of an angle of attack traverse, the procedure varies only slightly. After the model has been installed on the balance with its vertical plane in the vertical plane of the balance, the model balance assembly is rolled precisely 90 deg. The model is then moved by using the sector or pitching strut until the *vertical* plane of the model is aligned with the horizontal plane of the tunnel. When this has been done it is time to record the instrumentation "zero" readings.

After the reference readings have been recorded, the tunnel will be started. The model will then be driven through an α or β range with data from all instruments being recorded at frequent intervals. Usually the model will be moved to the most negative angle, to the most positive angle and then back to zero before the tunnel is stopped. During this traverse the frequency of data recording is usually at increments between 1 and 2 deg.

The test engineer should be familiar with the instrumentation and calibration techniques. A highly desirable check that can be made at reasonable intervals during a test is to hang one or more weights on a model at a known position, obtain balance readings, and then check these against readings predicted by the balance calibration. If such a check is to be made, the test engineer should know before the test where and how much weight is to be hung and what balance readings are expected. Expensive tunnel time should not be used to make extensive slide rule calculations to see if the readings are what they should be.

8:7 Pressure Test Data Reduction

The reduction of data from tests in which model surface pressures are measured generally consists only of converting the measured pressures to the following coefficient form:

$$C_p = \frac{p_m - p}{q}$$

where p_m = model pressure, psia,
p = tunnel free stream static pressure, psia,
q = tunnel free stream dynamic pressure, psi.

The procedure followed in the pressure coefficient calculation is usually as follows:

$$C_p = \frac{(p_m/p_t) - (p/p_t)}{(q/p_t)} \tag{8:1}$$

The measured model pressure is divided by the corresponding measured total pressure to obtain (p_m/p_t). Values of (p/p_t) and (q/p_t) are obtained from the test section Mach number and eqs. (1:14) and (1:17).

8:8 Force and Moment Data Reduction

Forces and moments measured with an internal balance in a wind tunnel are relative to the body axes, whereas aerodynamic data relative to the wind axes are more frequently required (see Fig. 7:1). The transformation of forces and moments from the body axes to the wind axes is accomplished by using the following relations:

$$F_L = F_N \cos\alpha - F_A \sin\alpha \tag{8:2}$$

$$F_C = F_Y \cos\beta + F_N \sin\alpha \sin\beta + F_A \cos\alpha \sin\beta \tag{8:3}$$

$$F_D = F_A \cos\alpha \cos\beta + F_N \sin\alpha \cos\beta - F_Y \sin\beta \tag{8:4}$$

$$M_{Yw} = M_Y \cos\beta - M_X \cos\alpha \sin\beta - M_Z \sin\alpha \sin\beta \tag{8:5}$$

$$M_{Zw} = M_Z \cos\alpha - M_X \sin\alpha \tag{8:6}$$

$$M_{Xw} = M_X \cos\alpha \cos\beta + M_Z \sin\alpha \cos\beta + M_Y \sin\beta \tag{8:7}$$

It is quite apparent that forces and moments measured on a scaled model in a wind tunnel will be considerably different from those of an aircraft in flight. Because of this, forces and moments on a model in a wind tunnel are reduced to nondimensional coefficients that have meaning with regard to the full-scale aircraft. Forces are reduced to coefficient form by dividing by the product of dynamic pressure of the air flow, q, and a model reference area, S. Moments are reduced to coefficient form by dividing by the product of qS and a model reference length.

In high-speed wind tunnels the ratio of dynamic to total pressure, q/p_t, is a function of Mach number (eq. (1:17)). If the temperature of the air in the tunnel is above about 1000°R, the value of q/p_t also becomes a function of total temperature (see Fig. 1:12). In reducing force and moment data, a value of q/p_t corresponding to the tunnel operating conditions is calculated after calibration of the flow in the tunnel. During the test, tunnel total pressure is measured and multiplied by q/p_t to determine a value of q to be used in data reduction.

For airplanes the reference area S is normally the planform area of the wing including the part that would lie within the fuselage if the wing leading and trailing edges were extended to the fuselage centerline. In missiles and unmanned aircraft, the maximum cross-sectional area of the body of the vehicle is more commonly used for S.

For airplanes, the reference length used in reducing moment M_{Yw} (pitching moment) to coefficient form is normally the "mean aerodynamic chord $\bar{c}$ of the wing which is defined as:

$$\bar{c} = 2/S \int_0^{b/2} c^2 \, dy \tag{8:8}$$

where S = wing planform area, ft²,
b = wing span from tip to tip, ft,
c = local chord of wing, ft,
y = spanwise distance from aircraft axis to local chord of interest, ft.

For missiles and unmanned aircraft the reference length for reducing these moments to coefficients is more commonly the maximum body diameter.

The reference length normally used in reducing the rolling moment M_{Xw} and the yawing moment M_{Zw} to coefficient form is the wing span b. Thus, the normal coefficients are calculated as follows:

$$C_L = \frac{F_L}{qS} \tag{8:9}$$

$$C_C = \frac{F_C}{qS} \tag{8:10}$$

$$C_D = \frac{F_D}{qS} \tag{8:11}$$

$$C_{mw} = \frac{M_{Yw}}{qS\bar{c}} \quad \text{or} \quad \frac{M_{Yw}}{qSd} \tag{8:12}$$

$$C_{nw} = \frac{M_{Zw}}{qSb} \quad \text{or} \quad \frac{M_{Zw}}{qSd} \tag{8:13}$$

$$C_{lw} = \frac{M_{Xw}}{qSb} \tag{8:14}$$

At times, the wind tunnel engineer will be asked to provide data relative to the body axes. In this case the transformation of forces and moments is not required because the balance measures relative to the body axes. Body axes data are reduced to coefficient form by using the reference

where p_m = model pressure, psia,
p = tunnel free stream static pressure, psia,
q = tunnel free stream dynamic pressure, psi.

The procedure followed in the pressure coefficient calculation is usually as follows:

$$C_p = \frac{(p_m/p_t) - (p/p_t)}{(q/p_t)} \tag{8:1}$$

The measured model pressure is divided by the corresponding measured total pressure to obtain (p_m/p_t). Values of (p/p_t) and (q/p_t) are obtained from the test section Mach number and eqs. (1:14) and (1:17).

8:8 Force and Moment Data Reduction

Forces and moments measured with an internal balance in a wind tunnel are relative to the body axes, whereas aerodynamic data relative to the wind axes are more frequently required (see Fig. 7:1). The transformation of forces and moments from the body axes to the wind axes is accomplished by using the following relations:

$$F_L = F_N \cos\alpha - F_A \sin\alpha \tag{8:2}$$

$$F_C = F_Y \cos\beta + F_N \sin\alpha \sin\beta + F_A \cos\alpha \sin\beta \tag{8:3}$$

$$F_D = F_A \cos\alpha \cos\beta + F_N \sin\alpha \cos\beta - F_Y \sin\beta \tag{8:4}$$

$$M_{Yw} = M_Y \cos\beta - M_X \cos\alpha \sin\beta - M_Z \sin\alpha \sin\beta \tag{8:5}$$

$$M_{Zw} = M_Z \cos\alpha - M_X \sin\alpha \tag{8:6}$$

$$M_{Xw} = M_X \cos\alpha \cos\beta + M_Z \sin\alpha \cos\beta + M_Y \sin\beta \tag{8:7}$$

It is quite apparent that forces and moments measured on a scaled model in a wind tunnel will be considerably different from those of an aircraft in flight. Because of this, forces and moments on a model in a wind tunnel are reduced to nondimensional coefficients that have meaning with regard to the full-scale aircraft. Forces are reduced to coefficient form by dividing by the product of dynamic pressure of the air flow, q, and a model reference area, S. Moments are reduced to coefficient form by dividing by the product of qS and a model reference length.

In high-speed wind tunnels the ratio of dynamic to total pressure, q/p_t, is a function of Mach number (eq. (1:17)). If the temperature of the air in the tunnel is above about 1000°R, the value of q/p_t also becomes a function of total temperature (see Fig. 1:12). In reducing force and moment data, a value of q/p_t corresponding to the tunnel operating conditions is calculated after calibration of the flow in the tunnel. During the test, tunnel total pressure is measured and multiplied by q/p_t to determine a value of q to be used in data reduction.

For airplanes the reference area S is normally the planform area of the wing including the part that would lie within the fuselage if the wing leading and trailing edges were extended to the fuselage centerline. In missiles and unmanned aircraft, the maximum cross-sectional area of the body of the vehicle is more commonly used for S.

For airplanes, the reference length used in reducing moment M_{Yw} (pitching moment) to coefficient form is normally the "mean aerodynamic chord $\bar{c}$ of the wing which is defined as:

$$\bar{c} = 2/S \int_0^{b/2} c^2 \, dy \tag{8:8}$$

where S = wing planform area, ft²,
b = wing span from tip to tip, ft,
c = local chord of wing, ft,
y = spanwise distance from aircraft axis to local chord of interest, ft.

For missiles and unmanned aircraft the reference length for reducing these moments to coefficients is more commonly the maximum body diameter.

The reference length normally used in reducing the rolling moment M_{Xw} and the yawing moment M_{Zw} to coefficient form is the wing span b. Thus, the normal coefficients are calculated as follows:

$$C_L = \frac{F_L}{qS} \tag{8:9}$$

$$C_C = \frac{F_C}{qS} \tag{8:10}$$

$$C_D = \frac{F_D}{qS} \tag{8:11}$$

$$C_{mw} = \frac{M_{Yw}}{qS\bar{c}} \quad \text{or} \quad \frac{M_{Yw}}{qSd} \tag{8:12}$$

$$C_{nw} = \frac{M_{Zw}}{qSb} \quad \text{or} \quad \frac{M_{Zw}}{qSd} \tag{8:13}$$

$$C_{lw} = \frac{M_{Xw}}{qSb} \tag{8:14}$$

At times, the wind tunnel engineer will be asked to provide data relative to the body axes. In this case the transformation of forces and moments is not required because the balance measures relative to the body axes. Body axes data are reduced to coefficient form by using the reference

pressure, areas, and lengths of the wind axes coefficients. In the body axes, the coefficients are

$$C_N = \frac{F_N}{qS} \tag{8:15}$$

$$C_Y = \frac{F_Y}{qS} \tag{8:16}$$

$$C_A = \frac{F_A}{qS} \tag{8:17}$$

$$C_m = \frac{M_Y}{qS\bar{c}} \quad \text{or} \quad \frac{M_Y}{qSd} \tag{8:18}$$

$$C_n = \frac{M_Z}{qSb} \quad \text{or} \quad \frac{M_Z}{qSd} \tag{8:19}$$

$$C_l = \frac{M_X}{qSb} \tag{8:20}$$

There are special cases for which the moments and forces measured with an internal balance are not the true body axes forces and moments. These cases are ones in which the balance axis and the model body axis are not parallel or in which the balance axis does not pass through the model center of gravity. For example, if the model center of gravity were above the balance axis, the balance would indicate a pitching moment equal to the axial force times the distance of the center of gravity above the balance axis.

Also, in some cases tare corrections must be applied to obtain the net aerodynamic forces in the balance axes. The most common of these is an angle of attack correction to axial force. When the model angle of attack is other than zero (assuming model pitching in the vertical plane), a component of the model weight is being applied along the balance axis. This component of weight, equal to model weight times sin α, must be subtracted from the gross axial force indicated by the balance to obtain the aerodynamic axial force. If the model weight is significant in comparison to the aerodynamic normal forces, it will also be necessary to make corrections to the measured normal force and pitching moment at angle of attack. The component of weight normal to the balance axis equals model weight times $(1 - \cos \alpha)$ and the pitching moments measured are influenced by amounts depending on the location of the center of gravity of the model relative to the pitching moment reference. A common method of determining the axial force, normal force, and moment tares is to pitch the model through the α range of the test with no air flow and obtain balance readings at several angles of attack. Tare readings thus

obtained are applied to readings obtained at each corresponding α during the test.

Movable surface hinge moments such as those imposed on ailerons, elevators, rudders, dive brakes, landing gear doors, slats, spoilers, and all-movable controls surfaces are normally reduced to nondimensional coefficients as follows:

$$C_h = \frac{H}{qS_a\bar{c}_a} \tag{8:21}$$

where C_h = hinge moment coefficient,
H = hinge moment, inch-lb,
q = dynamic pressure, psi,
S_a = area aft of the hinge line, inches^2,
$\bar{c}_a$ = mean aerodynamic chord aft of the hinge line, inches.

Control surface hinge moments are also reduced to nondimensional coefficients in terms of dynamic pressure and an area moment. However, the area moment to be used in this case will depend on the desires of the structural engineer who is interested in the data.

Root bending moments are generally reduced by using dynamic pressure, exposed surface area, and panel exposed span. Dynamic stability data are reduced to nondimensional form by using the following equations:

$$C_{mq} + C_{m\alpha} = \frac{(M_q + M_{\dot{\alpha}})\dot{\theta}/qS\bar{c}}{\omega\bar{c}/2V} \quad \text{or} \quad \frac{(M_q + M_{\dot{\alpha}})\dot{\theta}/qSd}{\omega d/2V} \tag{8:22}$$

$$C_{lp} = \frac{M_{\dot{\phi}}\dot{\phi}/qSb}{\left(\frac{pb}{2V}\right)} \tag{8:23}$$

where ω = angular frequency of pitch oscillation, ($2\pi \times$ cycles per second), radians/sec,
V = air flow velocity, ft/sec,
p = angular velocity of roll, radians/sec.

The terms M_q, $M_{\dot{\alpha}}$, $M_{\dot{\phi}}$ are moments per unit angular velocity and $\dot{\theta}$ and $\dot{\phi}$ are units of angular velocity as defined in Sections 7:16 and 7:17.

It is noted that the quantities $\omega\bar{c}/2V$ and $\omega d/2V$ equal the angles of attack in radians induced by the pitching velocity (ω) at a distance of one-half the reference length ($\bar{c}$ or d) from the axis of rotation. Similarly, the quantity ($pb/2V$) equals the angle of attack in radians induced by the roll velocity at the tips of a wing or fin having a span of b feet. In reducing experimental data, eqs. (8:22) and (8:23) can be simplified by setting ω equal to $\dot{\theta}$ and p equal to $\dot{\phi}$.

pressure, areas, and lengths of the wind axes coefficients. In the body axes, the coefficients are

$$C_N = \frac{F_N}{qS} \tag{8:15}$$

$$C_Y = \frac{F_Y}{qS} \tag{8:16}$$

$$C_A = \frac{F_A}{qS} \tag{8:17}$$

$$C_m = \frac{M_Y}{qS\bar{c}} \quad \text{or} \quad \frac{M_Y}{qSd} \tag{8:18}$$

$$C_n = \frac{M_Z}{qSb} \quad \text{or} \quad \frac{M_Z}{qSd} \tag{8:19}$$

$$C_l = \frac{M_X}{qSb} \tag{8:20}$$

There are special cases for which the moments and forces measured with an internal balance are not the true body axes forces and moments. These cases are ones in which the balance axis and the model body axis are not parallel or in which the balance axis does not pass through the model center of gravity. For example, if the model center of gravity were above the balance axis, the balance would indicate a pitching moment equal to the axial force times the distance of the center of gravity above the balance axis.

Also, in some cases tare corrections must be applied to obtain the net aerodynamic forces in the balance axes. The most common of these is an angle of attack correction to axial force. When the model angle of attack is other than zero (assuming model pitching in the vertical plane), a component of the model weight is being applied along the balance axis. This component of weight, equal to model weight times sin α, must be subtracted from the gross axial force indicated by the balance to obtain the aerodynamic axial force. If the model weight is significant in comparison to the aerodynamic normal forces, it will also be necessary to make corrections to the measured normal force and pitching moment at angle of attack. The component of weight normal to the balance axis equals model weight times $(1 - \cos \alpha)$ and the pitching moments measured are influenced by amounts depending on the location of the center of gravity of the model relative to the pitching moment reference. A common method of determining the axial force, normal force, and moment tares is to pitch the model through the α range of the test with no air flow and obtain balance readings at several angles of attack. Tare readings thus

obtained are applied to readings obtained at each corresponding α during the test.

Movable surface hinge moments such as those imposed on ailerons, elevators, rudders, dive brakes, landing gear doors, slats, spoilers, and all-movable controls surfaces are normally reduced to nondimensional coefficients as follows:

$$C_h = \frac{H}{qS_a\bar{c}_a} \tag{8:21}$$

where C_h = hinge moment coefficient,
H = hinge moment, inch-lb,
q = dynamic pressure, psi,
S_a = area aft of the hinge line, inches^2,
$\bar{c}_a$ = mean aerodynamic chord aft of the hinge line, inches.

Control surface hinge moments are also reduced to nondimensional coefficients in terms of dynamic pressure and an area moment. However, the area moment to be used in this case will depend on the desires of the structural engineer who is interested in the data.

Root bending moments are generally reduced by using dynamic pressure, exposed surface area, and panel exposed span. Dynamic stability data are reduced to nondimensional form by using the following equations:

$$C_{mq} + C_{m\alpha} = \frac{(M_q + M_{\dot{\alpha}})\dot{\theta}/qS\bar{c}}{\omega\bar{c}/2V} \quad \text{or} \quad \frac{(M_q + M_{\dot{\alpha}})\dot{\theta}/qSd}{\omega d/2V} \tag{8:22}$$

$$C_{lp} = \frac{M_{\dot{\phi}}\dot{\phi}/qSb}{\left(\frac{pb}{2V}\right)} \tag{8:23}$$

where ω = angular frequency of pitch oscillation, ($2\pi \times$ cycles per second), radians/sec,
V = air flow velocity, ft/sec,
p = angular velocity of roll, radians/sec.

The terms M_q, $M_{\dot{\alpha}}$, $M_{\dot{\phi}}$ are moments per unit angular velocity and $\dot{\theta}$ and $\dot{\phi}$ are units of angular velocity as defined in Sections 7:16 and 7:17.

It is noted that the quantities $\omega\bar{c}/2V$ and $\omega d/2V$ equal the angles of attack in radians induced by the pitching velocity (ω) at a distance of one-half the reference length ($\bar{c}$ or d) from the axis of rotation. Similarly, the quantity $(pb/2V)$ equals the angle of attack in radians induced by the roll velocity at the tips of a wing or fin having a span of b feet. In reducing experimental data, eqs. (8:22) and (8:23) can be simplified by setting ω equal to $\dot{\theta}$ and p equal to $\dot{\phi}$.

8:9 Tunnel Wall Effects

The effects of the tunnel walls on data taken in nearsonic tunnels are profoundly different from those on data taken in transonic, supersonic, and hypersonic tunnels. For the *nearsonic* case, the solid walls alter the flow field extensively from that which would exist in free flight. In order to adjust the wind tunnel test results so that they are representative of the free flight case, it is necessary to make corrections for wake blocking, solid blocking, downwash, streamline curvature, and lift interference. These flow alterations are discussed in Ref. 8:2 and methods are presented for correcting the data. As the flow Mach number approaches 1.0, the corrections become very large and it is difficult to correct the wind tunnel data accurately.

The walls of *transonic* tunnels are vented to minimize their effects on the flow in the vicinity of a model. When a model is placed in the test section at subsonic speeds and the streamlines curve around the model, the vents allow a portion of the air in the outer streamlines to flow through the tunnel wall. This reduction of the air in the outer streamlines allows the air nearer the body to flow more nearly in the manner that it would if the model were in free flight.

At *supersonic* speeds, the effects of ventilated walls take on a different character. Shock waves which compress the air develop on the forward portion of the model and extend to the tunnel wall. When these shock waves strike a solid wall they are reflected back toward the model as compression waves. This reflected wave striking the model, as it always will at very low supersonic speeds, changes the air loads on the model from those that would be expected in free flight. On the other hand, if the test section has a completely free boundary, a shock wave striking the boundary will be reflected back toward the model as an expansion wave but will still affect the air loads on the model. The purpose of the wall venting is to try to reach the point between the solid and the free boundary cases where the shock is not reflected at all. This point will occur when conditions are such that the increased pressure behind a shock will force enough air through the vents behind the shock to reduce the pressure to exactly what it was ahead of the shock. It is easy to see what difficulties are involved in reaching this point, since shock strength at the wall will be dependent on Mach number, model size, model shape, and angle of attack. Assuming that such a point is reached, there is still a difficulty in achieving zero interference. Vents that let air flow out of the test section downstream of a shock will also let air flow in. Air flowing out of a vent immediately behind a shock wave is likely to flow back into the test section at a point slightly upstream or downstream. When this occurs the inflow will produce

a disturbance that affects the flow over the model. This effect has been minimized in some tunnels by using perforations inclined 30 deg with respect to the surface of the tunnel wall and in the direction of the mainstream flow.

Wall effects in transonic tunnels have been the subject of much theoretical, analytical, and experimental effort which cannot be adequately covered herein. An excellent summary of this work is, however, presented in Ref. 8:3.

In summary, it is noted that vented walls do not completely solve the problems of wall interference in transonic tunnels. Generally, transonic testing is carried out with models of small size (with cross sections of 1 per cent or less of the test section cross-sectional area) and it is assumed in data reduction that wall effects do not exist. In supersonic and hypersonic tunnels, the shock waves from the model are swept so far downstream that, with proper model sizing, there is no chance for their reflections to impinge on the model or on the model wake near enough to have a serious effect on the flow over the model. Thus, wall effects are not considered in such tunnels.

8:10 Corrections to the Data

Some high-speed tunnels have a slight pressure gradient in the test section due to imperfect nozzle and test section design. Such a gradient will have a positive or negative "buoyancy" effect on the model, depending on whether the gradient is positive or negative. This effect is normally important only with respect to the drag of the model. The correction which must be added to wind tunnel drag force to correct for the "buoyancy" effect is as follows:

$$\Delta F_{DB} = V_m \frac{dp}{dx} \tag{8:24}$$

where V_m = model volume, inches^3,

$\frac{dp}{dx}$ = pressure gradient in the direction of the flow, lb/inches^3.

The pressure gradient, if it exists, is easily determined from the Mach number gradient obtained during the tunnel calibration in the following way. Static to total pressure ratios at the nose and tail of the model corresponding to calibrated Mach numbers are obtained from Table 1:1. These ratios are multiplied by the operating total pressure of the tunnel to obtain static pressures. The differences in static pressure are then divided by the model length. Four further corrections that must be considered are the weight component of the model, which changes with angle of attack; the spurious base pressure due to the presence of the sting support; the

8:9 Tunnel Wall Effects

The effects of the tunnel walls on data taken in nearsonic tunnels are profoundly different from those on data taken in transonic, supersonic, and hypersonic tunnels. For the *nearsonic* case, the solid walls alter the flow field extensively from that which would exist in free flight. In order to adjust the wind tunnel test results so that they are representative of the free flight case, it is necessary to make corrections for wake blocking, solid blocking, downwash, streamline curvature, and lift interference. These flow alterations are discussed in Ref. 8:2 and methods are presented for correcting the data. As the flow Mach number approaches 1.0, the corrections become very large and it is difficult to correct the wind tunnel data accurately.

The walls of *transonic* tunnels are vented to minimize their effects on the flow in the vicinity of a model. When a model is placed in the test section at subsonic speeds and the streamlines curve around the model, the vents allow a portion of the air in the outer streamlines to flow through the tunnel wall. This reduction of the air in the outer streamlines allows the air nearer the body to flow more nearly in the manner that it would if the model were in free flight.

At *supersonic* speeds, the effects of ventilated walls take on a different character. Shock waves which compress the air develop on the forward portion of the model and extend to the tunnel wall. When these shock waves strike a solid wall they are reflected back toward the model as compression waves. This reflected wave striking the model, as it always will at very low supersonic speeds, changes the air loads on the model from those that would be expected in free flight. On the other hand, if the test section has a completely free boundary, a shock wave striking the boundary will be reflected back toward the model as an expansion wave but will still affect the air loads on the model. The purpose of the wall venting is to try to reach the point between the solid and the free boundary cases where the shock is not reflected at all. This point will occur when conditions are such that the increased pressure behind a shock will force enough air through the vents behind the shock to reduce the pressure to exactly what it was ahead of the shock. It is easy to see what difficulties are involved in reaching this point, since shock strength at the wall will be dependent on Mach number, model size, model shape, and angle of attack. Assuming that such a point is reached, there is still a difficulty in achieving zero interference. Vents that let air flow out of the test section downstream of a shock will also let air flow in. Air flowing out of a vent immediately behind a shock wave is likely to flow back into the test section at a point slightly upstream or downstream. When this occurs the inflow will produce

a disturbance that affects the flow over the model. This effect has been minimized in some tunnels by using perforations inclined 30 deg with respect to the surface of the tunnel wall and in the direction of the mainstream flow.

Wall effects in transonic tunnels have been the subject of much theoretical, analytical, and experimental effort which cannot be adequately covered herein. An excellent summary of this work is, however, presented in Ref. 8:3.

In summary, it is noted that vented walls do not completely solve the problems of wall interference in transonic tunnels. Generally, transonic testing is carried out with models of small size (with cross sections of 1 per cent or less of the test section cross-sectional area) and it is assumed in data reduction that wall effects do not exist. In supersonic and hypersonic tunnels, the shock waves from the model are swept so far downstream that, with proper model sizing, there is no chance for their reflections to impinge on the model or on the model wake near enough to have a serious effect on the flow over the model. Thus, wall effects are not considered in such tunnels.

8:10 Corrections to the Data

Some high-speed tunnels have a slight pressure gradient in the test section due to imperfect nozzle and test section design. Such a gradient will have a positive or negative "buoyancy" effect on the model, depending on whether the gradient is positive or negative. This effect is normally important only with respect to the drag of the model. The correction which must be added to wind tunnel drag force to correct for the "buoyancy" effect is as follows:

$$\Delta F_{DB} = V_m \frac{dp}{dx} \tag{8:24}$$

where V_m = model volume, inches^3,

$\frac{dp}{dx}$ = pressure gradient in the direction of the flow, lb/inches^3.

The pressure gradient, if it exists, is easily determined from the Mach number gradient obtained during the tunnel calibration in the following way. Static to total pressure ratios at the nose and tail of the model corresponding to calibrated Mach numbers are obtained from Table 1:1. These ratios are multiplied by the operating total pressure of the tunnel to obtain static pressures. The differences in static pressure are then divided by the model length. Four further corrections that must be considered are the weight component of the model, which changes with angle of attack; the spurious base pressure due to the presence of the sting support; the

deflection of sting and balance; and the internal duct drag of jet-engine installations. The weight component may be simply evaluated by a wind-off pitch run with the data obtained subtracted from the wind on data (see also Section 8:8). The base drag corrections are tied in with maintaining proper transition on the model and are discussed in Section 9:7. The deflection of the balance and sting due to loading is determined during the balance calibration. Deflection corrections to the indicated model angle of attack at each loading condition are made to define the true angles of attack during the test. In some large continuous tunnels, the loads on the model are monitored during the test and the indicated model angle of attack is corrected for deflection in order to provide the precise true angle desired. For the internal duct drag a rake of pitot probes are installed in the air flow exit of the engine nacelle. Through their use the rate of change of momentum of the air passing through the duct is determined and subtracted out, being later replaced by the net engine thrust which will exist in flight.

References

8:1 Joseph J. Muncey and David M. Pote, Design and Construction of Wind Tunnel Models, AGARD Report 20, 1956.
8:2 Alan Pope, *Wind Tunnel Testing*, John Wiley and Sons, 1954.
8:3 Bernhard H. Goethert, *Transonic Wind Tunnel Testing*, Pergamon Press, 1961.

Chapter nine

Calibration and use of nearsonic and transonic tunnels

9:1 General

Transonic tunnels operate at speeds varying from the speed at which compressibility effects become important (about Mach 0.5) through the speed of sound and to a maximum Mach number of about 1.4. Nearsonic tunnels cover the lower portion of this speed range up to something less than the speed of sound. Transonic tunnels have almost completely replaced nearsonic tunnels. But, because there are still a few nearsonic tunnels in operation, it is appropriate to discuss major differences between the two types, noting where these differences influence their calibration and use.

The nearsonic tunnel is basically a high-powered subsonic tunnel. It is normally a closed-circuit, fan-driven tunnel with continuous operation capability. The test section has the minimum cross section of the tunnel circuit. The air speed in the test section is increased simply by changing the fan speed or by changing the pitch of the fan blades. The walls of the test section are solid, and herein lies the major difference between the nearsonic and transonic tunnels. At subsonic speeds the solid tunnel walls do not allow the spread of the streamlines around the model which would occur in flight, and consequently there is a distorted flow field. In contrast, transonic tunnels have walls vented with slots or perforations in a way that minimizes the effects of the walls on the shapes of the streamlines in the vicinity of a model. As previously mentioned the test section of the nearsonic tunnel has the minimum cross-sectional area and hence the highest velocity of the circuit. When a model is placed in the test section, the minimum cross section occurs at the model. If we could assume that uniform flow existed in the vicinity of the model, we might expect that the nearsonic tunnel could be used for testing to Mach 1.0. In reality, the tunnel becomes "choked" in the vicinity of the model as conditions for Mach 1.0 are approached, with the result that the model is no longer in a

deflection of sting and balance; and the internal duct drag of jet-engine installations. The weight component may be simply evaluated by a wind-off pitch run with the data obtained subtracted from the wind on data (see also Section 8:8). The base drag corrections are tied in with maintaining proper transition on the model and are discussed in Section 9:7. The deflection of the balance and sting due to loading is determined during the balance calibration. Deflection corrections to the indicated model angle of attack at each loading condition are made to define the true angles of attack during the test. In some large continuous tunnels, the loads on the model are monitored during the test and the indicated model angle of attack is corrected for deflection in order to provide the precise true angle desired. For the internal duct drag a rake of pitot probes are installed in the air flow exit of the engine nacelle. Through their use the rate of change of momentum of the air passing through the duct is determined and subtracted out, being later replaced by the net engine thrust which will exist in flight.

References

8:1 Joseph J. Muncey and David M. Pote, Design and Construction of Wind Tunnel Models, AGARD Report 20, 1956.
8:2 Alan Pope, *Wind Tunnel Testing*, John Wiley and Sons, 1954.
8:3 Bernhard H. Goethert, *Transonic Wind Tunnel Testing*, Pergamon Press, 1961.

Chapter nine

Calibration and use of nearsonic and transonic tunnels

9:1 General

Transonic tunnels operate at speeds varying from the speed at which compressibility effects become important (about Mach 0.5) through the speed of sound and to a maximum Mach number of about 1.4. Nearsonic tunnels cover the lower portion of this speed range up to something less than the speed of sound. Transonic tunnels have almost completely replaced nearsonic tunnels. But, because there are still a few nearsonic tunnels in operation, it is appropriate to discuss major differences between the two types, noting where these differences influence their calibration and use.

The nearsonic tunnel is basically a high-powered subsonic tunnel. It is normally a closed-circuit, fan-driven tunnel with continuous operation capability. The test section has the minimum cross section of the tunnel circuit. The air speed in the test section is increased simply by changing the fan speed or by changing the pitch of the fan blades. The walls of the test section are solid, and herein lies the major difference between the nearsonic and transonic tunnels. At subsonic speeds the solid tunnel walls do not allow the spread of the streamlines around the model which would occur in flight, and consequently there is a distorted flow field. In contrast, transonic tunnels have walls vented with slots or perforations in a way that minimizes the effects of the walls on the shapes of the streamlines in the vicinity of a model. As previously mentioned the test section of the nearsonic tunnel has the minimum cross-sectional area and hence the highest velocity of the circuit. When a model is placed in the test section, the minimum cross section occurs at the model. If we could assume that uniform flow existed in the vicinity of the model, we might expect that the nearsonic tunnel could be used for testing to Mach 1.0. In reality, the tunnel becomes "choked" in the vicinity of the model as conditions for Mach 1.0 are approached, with the result that the model is no longer in a

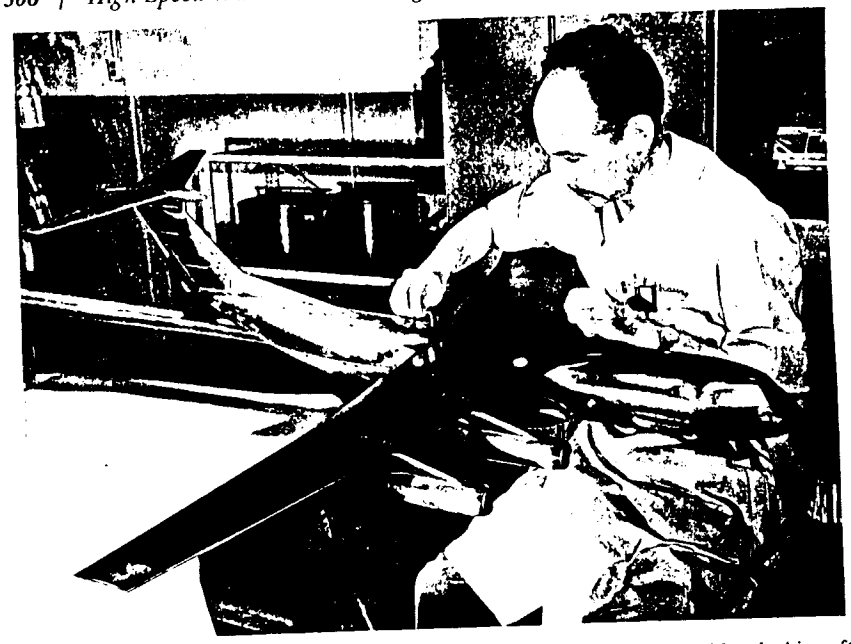


Fig. 9:1 Readying a model for a nearsonic test. (Courtesy Lockheed Aircraft Corporation.)

uniform flow field. This choking is noted in one of three ways: (1) by ratios of wall static pressure to total pressure at the axial station of the model which become equal to 0.528, indicating sonic flow at the wall and called "wall choke"; (2) by the failure of the reference Mach number indicated by upstream static pressures to increase with increasing power; (3) by the failure of an increase in power to produce an increase in forces on the model. The size of a model that can be tested in a nearsonic tunnel without choking becomes vanishingly small as Mach 1.0 is approached. Based on simple area ratios (eq. (1:18)) a model with a frontal area of 0.9 per cent of the test section cross section would cause choking with a reference Mach number of 0.9, and a model with a frontal area of 0.2 per cent would cause choking at Mach 0.95. Further, it is generally considered that data from a nearsonic tunnel will be erroneous if the reference Mach number is less than 0.02 below the choking Mach number.

In the transonic tunnel with vented walls, the flow Mach number can be increased continuously to and through Mach 1.0 without choking. The perforated section appears to offer better shock cancellation than the slotted section, but at a large increase in cost. A typical test section, for instance, may require 10,000 holes drilled 60 deg to the wall surface. While both types of test sections require small wall corrections, the fact

that they are not all theoretically defined (and those that are are hard to apply) has resulted in the use of small models (say 1 per cent of the test section area) and no corrections to the data.

A word of warning: Merely assuming that wall effects are negligible does not ensure that this is so, and the tunnel engineer should not dismiss a sharp deviation in a data curve (particularly a *moment* curve) as a "shock reflection." Its true nature may be investigated by moving the model off the tunnel centerline (in which case the "reflection" will move), or by using the schlieren system. In computing where a shock should reflect, one must not neglect the fact that it may be detached and hence originate ahead of the model nose. The location of the effective wall may be taken as being at the boundary layer displacement thickness. Although it is not possible to use a model small enough to avoid being hit by a reflected shock near $M = 1.0$, the shocks are weak in this speed regime.

As discussed in Section 1:10, the moisture content of the air in all high-speed wind tunnels is important to data obtained both in calibration and in testing. While the moisture problem is minimum in nearsonic and transonic tunnels, it cannot be dismissed, since still air at 80°F will expand to a temperature of −10°F at Mach 1.0 and −72°F at Mach 1.4. In several of the larger continuous nearsonic and transonic tunnels, atmospheric air is used without drying. In some of these tunnels, air is continuously discharged from the circuit and replaced with outside air as a means of controlling temperature buildup of the circuit. In such tunnels, condensation is probably always present to some extent at the higher test Mach numbers. A degree of control over condensation is exercised by letting the energy added to the air by the compressor heat the tunnel and the air to a maximum allowable operating temperature, perhaps 120°.

Note that at typical operating temperatures for nearsonic and transonic tunnels (say 100 to 120°F) the children's modeling clay that works so well at low temperatures for simple fairings becomes weak and gooey. A general-purpose filler suitable for the higher temperatures may be made from beeswax (80% by weight), Venice turpentine (20% by weight), and powdered rosin (½% by weight). The turpentine should be brought to a boil and the rosin stirred in. Then the beeswax is added and allowed to melt. After the constituents are thoroughly mixed, remove them from the fire and let cool until a surface crust forms. If desirable the filler may then be remelted and coloring added.

9:2 Transonic Theory

Unfortunately we do not have transonic theories comparable to perfect fluid theory for low subsonic speeds or linear, Busemann, and exact theories for the supersonic case. In the early days of high-speed flight an

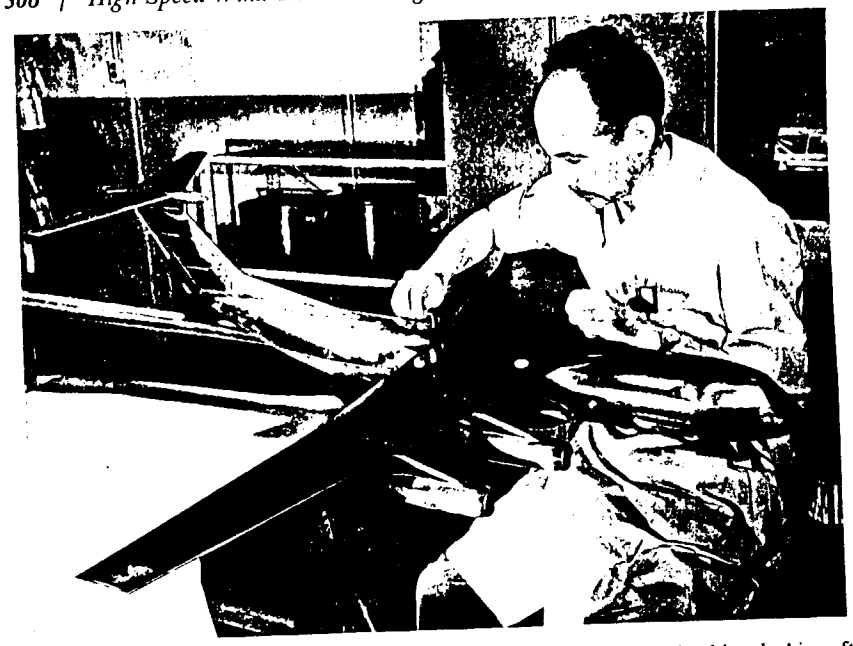


Fig. 9:1 Readying a model for a nearsonic test. (Courtesy Lockheed Aircraft Corporation.)

uniform flow field. This choking is noted in one of three ways: (1) by ratios of wall static pressure to total pressure at the axial station of the model which become equal to 0.528, indicating sonic flow at the wall and called "wall choke"; (2) by the failure of the reference Mach number indicated by upstream static pressures to increase with increasing power; (3) by the failure of an increase in power to produce an increase in forces on the model. The size of a model that can be tested in a nearsonic tunnel without choking becomes vanishingly small as Mach 1.0 is approached. Based on simple area ratios (eq. (1:18)) a model with a frontal area of 0.9 per cent of the test section cross section would cause choking with a reference Mach number of 0.9, and a model with a frontal area of 0.2 per cent would cause choking at Mach 0.95. Further, it is generally considered that data from a nearsonic tunnel will be erroneous if the reference Mach number is less than 0.02 below the choking Mach number.

In the transonic tunnel with vented walls, the flow Mach number can be increased continuously to and through Mach 1.0 without choking. The perforated section appears to offer better shock cancellation than the slotted section, but at a large increase in cost. A typical test section, for instance, may require 10,000 holes drilled 60 deg to the wall surface. While both types of test sections require small wall corrections, the fact

that they are not all theoretically defined (and those that are are hard to apply) has resulted in the use of small models (say 1 per cent of the test section area) and no corrections to the data.

A word of warning: Merely assuming that wall effects are negligible does not ensure that this is so, and the tunnel engineer should not dismiss a sharp deviation in a data curve (particularly a *moment* curve) as a "shock reflection." Its true nature may be investigated by moving the model off the tunnel centerline (in which case the "reflection" will move), or by using the schlieren system. In computing where a shock should reflect, one must not neglect the fact that it may be detached and hence originate ahead of the model nose. The location of the effective wall may be taken as being at the boundary layer displacement thickness. Although it is not possible to use a model small enough to avoid being hit by a reflected shock near $M = 1.0$, the shocks are weak in this speed regime.

As discussed in Section 1:10, the moisture content of the air in all high-speed wind tunnels is important to data obtained both in calibration and in testing. While the moisture problem is minimum in nearsonic and transonic tunnels, it cannot be dismissed, since still air at 80°F will expand to a temperature of −10°F at Mach 1.0 and −72°F at Mach 1.4. In several of the larger continuous nearsonic and transonic tunnels, atmospheric air is used without drying. In some of these tunnels, air is continuously discharged from the circuit and replaced with outside air as a means of controlling temperature buildup of the circuit. In such tunnels, condensation is probably always present to some extent at the higher test Mach numbers. A degree of control over condensation is exercised by letting the energy added to the air by the compressor heat the tunnel and the air to a maximum allowable operating temperature, perhaps 120°.

Note that at typical operating temperatures for nearsonic and transonic tunnels (say 100 to 120°F) the children's modeling clay that works so well at low temperatures for simple fairings becomes weak and gooey. A general-purpose filler suitable for the higher temperatures may be made from beeswax (80% by weight), Venice turpentine (20% by weight), and powdered rosin (½% by weight). The turpentine should be brought to a boil and the rosin stirred in. Then the beeswax is added and allowed to melt. After the constituents are thoroughly mixed, remove them from the fire and let cool until a surface crust forms. If desirable the filler may then be remelted and coloring added.

9:2 Transonic Theory

Unfortunately we do not have transonic theories comparable to perfect fluid theory for low subsonic speeds or linear, Busemann, and exact theories for the supersonic case. In the early days of high-speed flight an

effort was made to correlate subsonic drag rise with $1/\sqrt{1-M^2}$, and drag fall-off in the low supersonic range with $1/\sqrt{M^2-1}$ (for which there *is* a theoretical foundation), but no successful method has been found to compute the change of drag or lift curve slope, for instance, through the sonic range.

A practical improvement was put into use by the Germans late in World War II. This consisted of sweeping back the wings of aircraft, a method they had found effective in reducing drag. Probably this was an inspiration confirmed by wind tunnel testing. Today it is more generally explained by observing that the velocity of flow approaching a swept wing can be divided into two components, one normal to the leading edge and one parallel to the leading edge. The component of velocity parallel to the wing leading edge should have only secondary effects on the flow over the wing. The first-order effect would be due only to the velocity component normal to the wing leading edge, which would be reduced from the flight velocity by a factor equal to the cosine of the sweep angle. Thus, while an aircraft with a 45-deg sweptback wing is flying at Mach 0.9, the first approximation of the flow over the wing should be the same as that over the same wing unswept at a Mach number of $0.9 \times 0.707 = 0.64$. This "principle" is used with great amounts of sweep to keep the leading edge of wings "subsonic" while the flight speed is well into the supersonic range.

A second and substantial contribution to high-speed flight was the transonic "area rule" proposed by Whitcomb of the NACA (Ref. 9:1). In

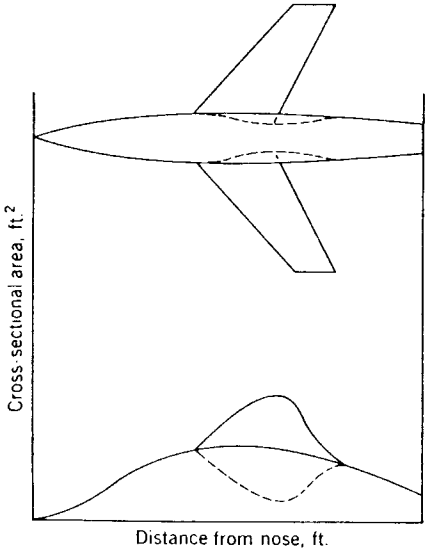


Fig. 9:2 Distribution of airplane cross-sectional area and (dashed) the area rule modification for it at sonic velocity.

essence this rule says that the drag rise of an aircraft with speed increasing into the transonic range will be a minimum for aircraft with the smaller values of maximum cross-sectional area and with the smoothest axial distribution of cross-sectional area. Thus, cutting cross-sectional area from the fuselage to make up for that of the wing will result in a decrease of drag at the speed of sound. A refairing of this type is shown in Fig. 9:2. Sweepback also tends to spread the cross-sectional area out along the axis of an airplane. Experimental tests have shown that aircraft pressure drag can be reduced by as much as 75 per cent by using the area rule.

The almost universal use of swept wings justifies some comment about their flow patterns, and in turn the problems the aerodynamicist may be investigating in the tunnel. First, from a theoretical standpoint, if we break the bound vortex of a swept wing at subsonic speed into a series of spanwise and chordwise components (Fig. 9:3), we see that the vortex component parallel to the line of flight induces an upwash increasing towards the wing tip. The net result is a tip stall tendency not present in unswept wings. The loss of lift due to the tip stall is easily replaced by a small increase of angle of attack, but the location of the stall—behind the airplane center of gravity—produces a loss of stability that can become too large for the pitch control to handle. A pitch-up may then occur, possibly of catastrophic consequence. Cures include reduced sweep; washout, or wing twist to provide smaller incidence angles at the tip than at the root; chordwise fences on the upper wing surface which break up the tipwise flow in the boundary layer; a leading edge extension near the wing tip which sheds a vortex of a sense to reduce tipwise flow in the boundary layer; devices which add high energy air to the boundary layer and thus delay the onset of separation; thicker airfoil tips which characteristically have higher stall angles; and wings with less taper so that local Reynolds number, and consequently local stall angle of attack, is higher. Vortex generators, which are small wings 1 or 2 inches high, are sometimes used to achieve the same effect as the leading edge extension. They are positioned normal to the upper surface of the wing on the aft half and at angles to produce outward loads. Their action can rarely be scaled in the wind tunnel satisfactorily.

Several other undesirable phenomena may result from tip stall: buffet, loss of aileron power, or even aileron reversal. The latter is unrelated to reversal due to aeroelastic twisting of the wing. It is characterized by a decrease in the angle of attack for $C_{L\max}$ with down flap angle. The stalling of the tip when the aileron is lowered and the unstalling when it is raised are bad because such asymmetric stall can cause severe reverse roll. Spoilers for roll control will not cause this effect.

Pitch-up may also be reduced by employing a low horizontal tail, which

effort was made to correlate subsonic drag rise with $1/\sqrt{1 - M^2}$, and drag fall-off in the low supersonic range with $1/\sqrt{M^2 - 1}$ (for which there *is* a theoretical foundation), but no successful method has been found to compute the change of drag or lift curve slope, for instance, through the sonic range.

A practical improvement was put into use by the Germans late in World War II. This consisted of sweeping back the wings of aircraft, a method they had found effective in reducing drag. Probably this was an inspiration confirmed by wind tunnel testing. Today it is more generally explained by observing that the velocity of flow approaching a swept wing can be divided into two components, one normal to the leading edge and one parallel to the leading edge. The component of velocity parallel to the wing leading edge should have only secondary effects on the flow over the wing. The first-order effect would be due only to the velocity component normal to the wing leading edge, which would be reduced from the flight velocity by a factor equal to the cosine of the sweep angle. Thus, while an aircraft with a 45-deg sweptback wing is flying at Mach 0.9, the first approximation of the flow over the wing should be the same as that over the same wing unswept at a Mach number of $0.9 \times 0.707 = 0.64$. This "principle" is used with great amounts of sweep to keep the leading edge of wings "subsonic" while the flight speed is well into the supersonic range.

A second and substantial contribution to high-speed flight was the transonic "area rule" proposed by Whitcomb of the NACA (Ref. 9:1). In

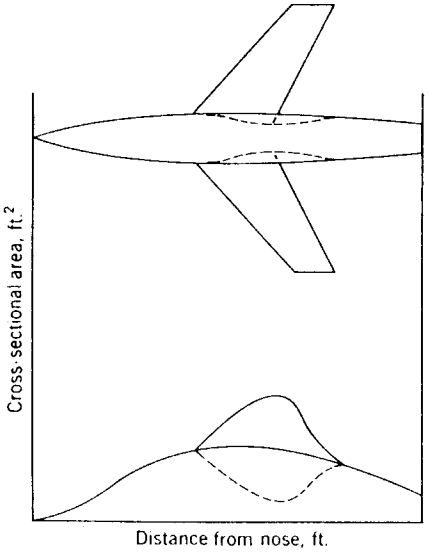


Fig. 9:2 Distribution of airplane cross-sectional area and (dashed) the area rule modification for it at sonic velocity.

essence this rule says that the drag rise of an aircraft with speed increasing into the transonic range will be a minimum for aircraft with the smaller values of maximum cross-sectional area and with the smoothest axial distribution of cross-sectional area. Thus, cutting cross-sectional area from the fuselage to make up for that of the wing will result in a decrease of drag at the speed of sound. A refairing of this type is shown in Fig. 9:2. Sweepback also tends to spread the cross-sectional area out along the axis of an airplane. Experimental tests have shown that aircraft pressure drag can be reduced by as much as 75 per cent by using the area rule.

The almost universal use of swept wings justifies some comment about their flow patterns, and in turn the problems the aerodynamicist may be investigating in the tunnel. First, from a theoretical standpoint, if we break the bound vortex of a swept wing at subsonic speed into a series of spanwise and chordwise components (Fig. 9:3), we see that the vortex component parallel to the line of flight induces an upwash increasing towards the wing tip. The net result is a tip stall tendency not present in unswept wings. The loss of lift due to the tip stall is easily replaced by a small increase of angle of attack, but the location of the stall—behind the airplane center of gravity—produces a loss of stability that can become too large for the pitch control to handle. A pitch-up may then occur, possibly of catastrophic consequence. Cures include reduced sweep; washout, or wing twist to provide smaller incidence angles at the tip than at the root; chordwise fences on the upper wing surface which break up the tipwise flow in the boundary layer; a leading edge extension near the wing tip which sheds a vortex of a sense to reduce tipwise flow in the boundary layer; devices which add high energy air to the boundary layer and thus delay the onset of separation; thicker airfoil tips which characteristically have higher stall angles; and wings with less taper so that local Reynolds number, and consequently local stall angle of attack, is higher. Vortex generators, which are small wings 1 or 2 inches high, are sometimes used to achieve the same effect as the leading edge extension. They are positioned normal to the upper surface of the wing on the aft half and at angles to produce outward loads. Their action can rarely be scaled in the wind tunnel satisfactorily.

Several other undesirable phenomena may result from tip stall: buffet, loss of aileron power, or even aileron reversal. The latter is unrelated to reversal due to aeroelastic twisting of the wing. It is characterized by a decrease in the angle of attack for $C_{L\max}$ with down flap angle. The stalling of the tip when the aileron is lowered and the unstalling when it is raised are bad because such asymmetric stall can cause severe reverse roll. Spoilers for roll control will not cause this effect.

Pitch-up may also be reduced by employing a low horizontal tail, which

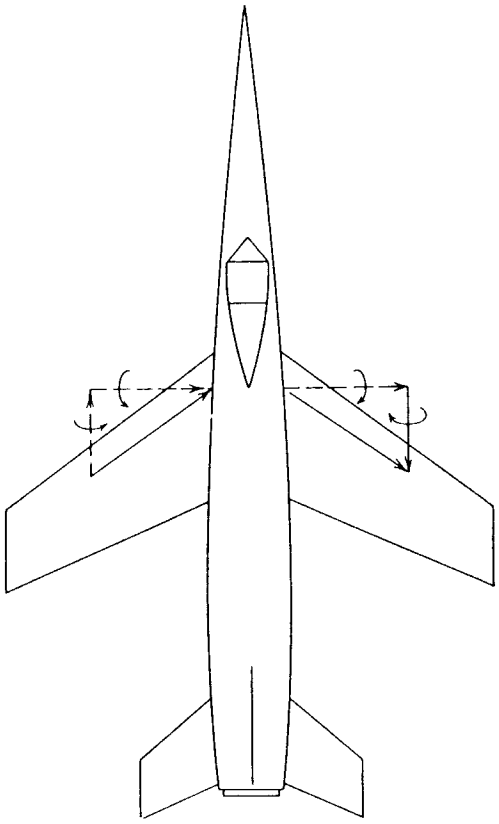


Fig. 9:3 Sketch showing the upwash toward the wing tips caused by the component of the bound vortex parallel to the airstream.

moves away from the area of greatest downwash with increasing angle of attack, instead of (with a raised horizontal tail) into it. Dihedral on a mid-set horizontal tail may keep it above the maximum downwash area for a high-aspect-ratio wing, while anhedral may get it through the high-downwash area at a low angle of attack.

9:3 Calibration

The calibration of these tunnels to determine flow Mach numbers in the test section is primarily a job of measuring static and total pressures of the flow. The relation between the ratio of static pressure to total pressure is then used to determine the flow Mach number according to eq. (1:14).

Frequently, if not usually, the static pressures are measured at orifices

on the surface of a "static pipe" on the tunnel centerline which starts in the settling chamber and extends through the test section (Fig. 9:4). The "static pipe" will typically have a cross-sectional area of 0.5 per cent or less of that of the test section, and will have static pressure orifices located at intervals along the pipe of about 0.05 tunnel height. Instead of the static pipe, a single static probe may be used for measuring static pressure, though this is seldom done in tunnel calibration. The static probe is typically made of tubing with an outside diameter of $\frac{1}{4}$ inch or less, and has a 10-deg included-angle conical tip. About 8 tube diameters downstream of the cone tip, 4 holes at 90-deg intervals are drilled to vent the tube cavity to the pressure on the tube surface. The tube extends downstream of these holes 20 diameters before being bent or having an increase in diameter for installation purposes. Though pressures measured by the static pipe may be expected to be slightly in error because of boundary layer growth on the pipe, the advantage of being able to measure pressures throughout the test section simultaneously is generally considered to overshadow these slight errors. In addition to the static pipe measurements, static pressures in nearsonic tunnels are usually measured on the tunnel wall. This is sometimes done in transonic tunnels also, though there is always the question of the effects of the vents. Much useful information on static pressure measurements may be found in Ref. 9:2.

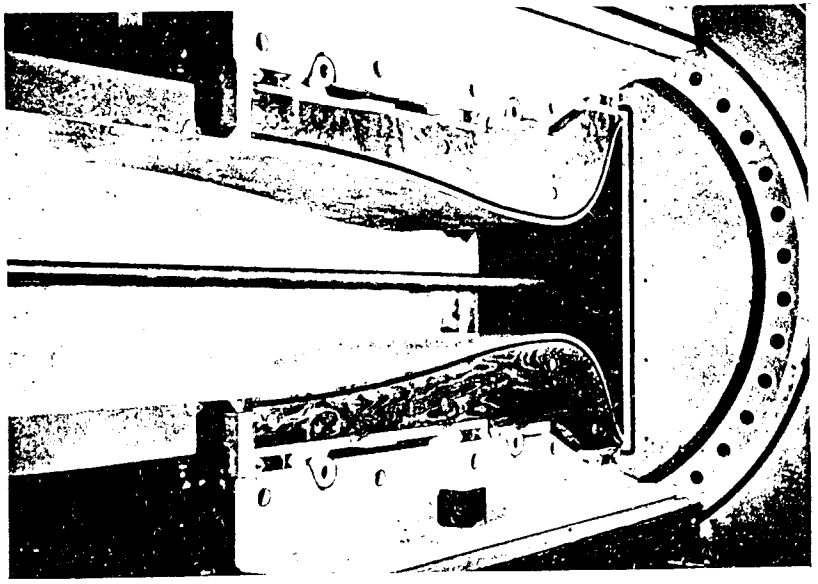


Fig. 9:4 Static pipe in the Sandia 12 × 12-inch transonic tunnel with supersonic throat blocks.

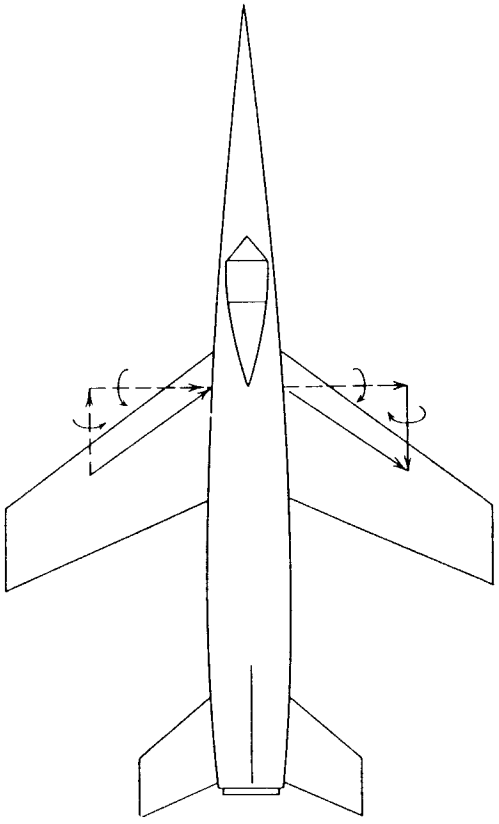


Fig. 9:3 Sketch showing the upwash toward the wing tips caused by the component of the bound vortex parallel to the airstream.

moves away from the area of greatest downwash with increasing angle of attack, instead of (with a raised horizontal tail) into it. Dihedral on a mid-set horizontal tail may keep it above the maximum downwash area for a high-aspect-ratio wing, while anhedral may get it through the high-downwash area at a low angle of attack.

9:3 Calibration

The calibration of these tunnels to determine flow Mach numbers in the test section is primarily a job of measuring static and total pressures of the flow. The relation between the ratio of static pressure to total pressure is then used to determine the flow Mach number according to eq. (1:14).

Frequently, if not usually, the static pressures are measured at orifices

on the surface of a "static pipe" on the tunnel centerline which starts in the settling chamber and extends through the test section (Fig. 9:4). The "static pipe" will typically have a cross-sectional area of 0.5 per cent or less of that of the test section, and will have static pressure orifices located at intervals along the pipe of about 0.05 tunnel height. Instead of the static pipe, a single static probe may be used for measuring static pressure, though this is seldom done in tunnel calibration. The static probe is typically made of tubing with an outside diameter of $\frac{1}{4}$ inch or less, and has a 10-deg included-angle conical tip. About 8 tube diameters downstream of the cone tip, 4 holes at 90-deg intervals are drilled to vent the tube cavity to the pressure on the tube surface. The tube extends downstream of these holes 20 diameters before being bent or having an increase in diameter for installation purposes. Though pressures measured by the static pipe may be expected to be slightly in error because of boundary layer growth on the pipe, the advantage of being able to measure pressures throughout the test section simultaneously is generally considered to overshadow these slight errors. In addition to the static pipe measurements, static pressures in nearsonic tunnels are usually measured on the tunnel wall. This is sometimes done in transonic tunnels also, though there is always the question of the effects of the vents. Much useful information on static pressure measurements may be found in Ref. 9:2.

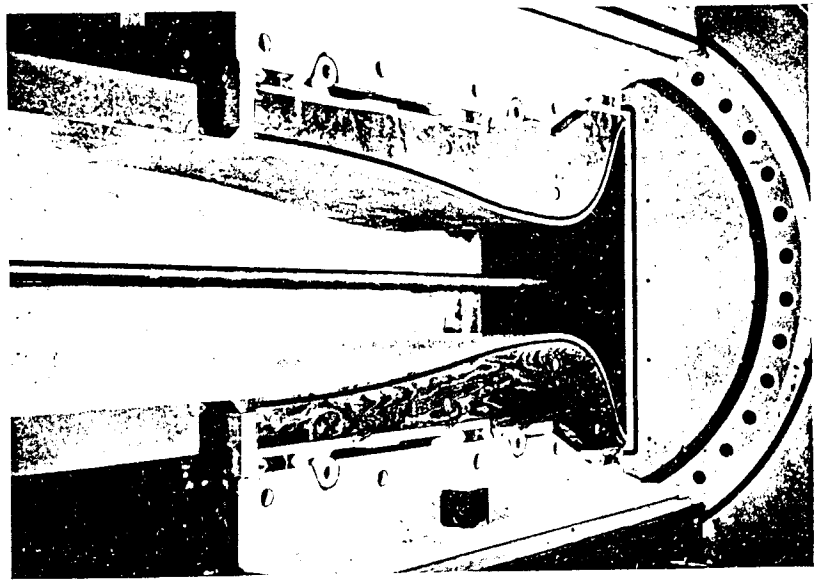


Fig. 9:4 Static pipe in the Sandia 12 × 12-inch transonic tunnel with supersonic throat blocks.

Two methods are used for measuring total pressure. One is to install several orifices around the periphery of the tunnel at a station immediately upstream of the contraction section, vent all of these orifices to a tube circling the tunnel (called a piezometer ring), and measure the pressure in this tube. If the flow velocity is small in this part of the tunnel, as it usually is, the static pressures sensed by the orifices are essentially total pressures. (The error is less than 0.2 per cent when the flow is at a Mach number of 0.05.) As discussed in Section 1:12 the total pressure at this point in the tunnel is equal to the total pressure in the test section when the flow between the two points is isentropic. This method of measuring total pressure is by far the most common. However, in nearsonic tunnels where the flow is always subsonic, an open-ended forward-facing tube is sometimes used to sense the impact pressure which is then equal to the total pressure.

In order to have a reference for use during testing of a model, the static pressure at a reference point is measured simultaneously with the test section static pressures during calibration. A Mach number is calculated for this reference static pressure along with those for the test section static pressures.

In the nearsonic tunnel, the reference point will normally be located in the forward end of the test section as far from the model as possible, but at a point where the Mach number is very near the same as at the place where the model will be mounted. Instead of a point measurement, a piezometer ring may be used. During a test with a model installed in the test section, the Mach number indicated by the reference static pressure will be the reference Mach number of the flow.

In the transonic tunnel, the reference static pressure is normally measured in the forward portion of the plenum surrounding the test section. A correlation between the reference and the test section Mach number is drawn. Then when a model is tested in the tunnel, the reference Mach number is calculated and the correlation is used to determine the Mach number in the test section. There will frequently be differences between the reference and test section Mach numbers in the transonic tunnel up to about 2 per cent. Typical results obtained from the calibrations of a transonic and a nearsonic tunnel are presented in Figs. 9:5 and 9:6.

In addition to determining Mach numbers in the test section, tunnel calibration often includes determining the inclination of flow with respect to the tunnel centerline. Devices used for this purpose are called yawmeters. Sketches of two yawmeters used in nearsonic and transonic tunnels are illustrated in Fig. 9:7 along with graphs depicting the sensitivity of each to flow angularity. One of the yawmeters consists of two open-ended pressure probes facing upstream and inclined 60 deg with

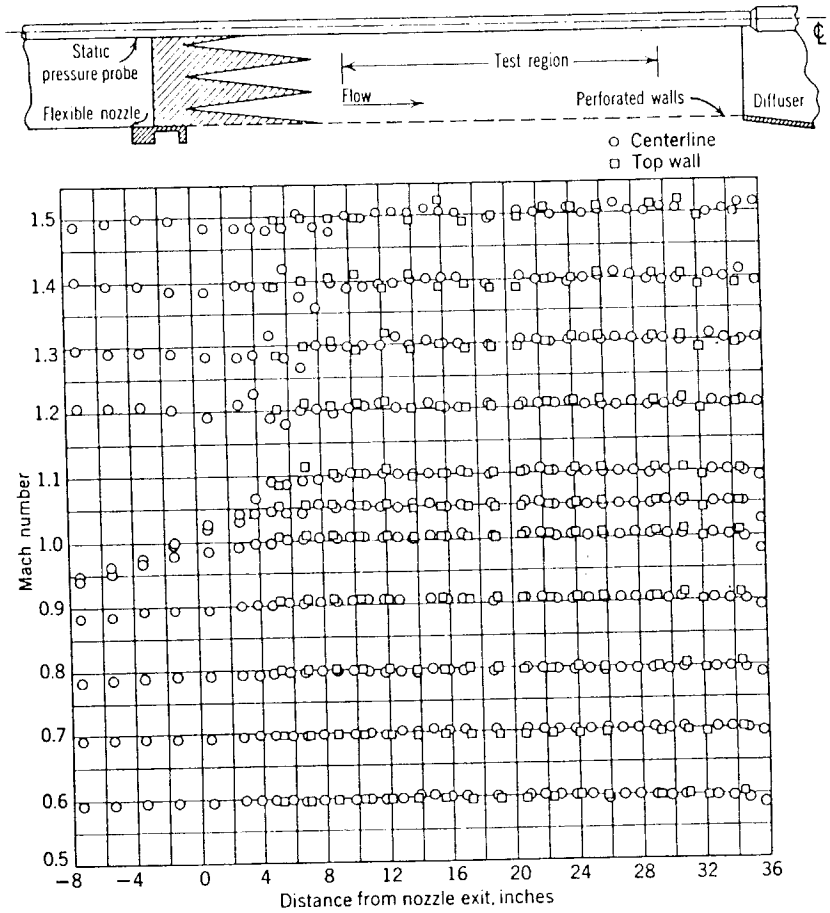


Fig. 9:5 Calibration plots for a transonic tunnel (from Ref. 9:3).

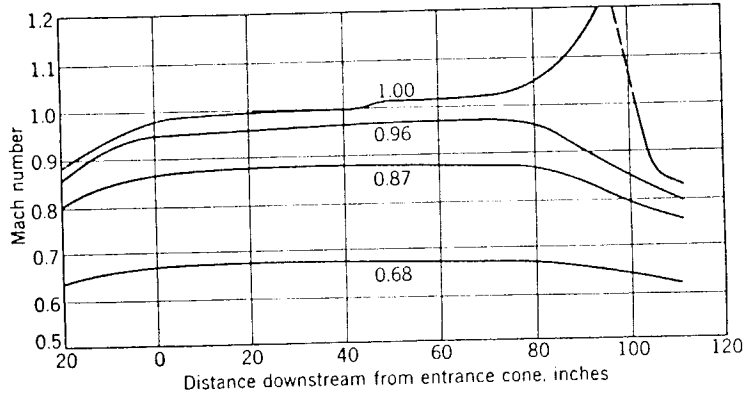


Fig. 9:6 Calibration plots for a nearsonic tunnel. Numbers are nominal Mach numbers.

Two methods are used for measuring total pressure. One is to install several orifices around the periphery of the tunnel at a station immediately upstream of the contraction section, vent all of these orifices to a tube circling the tunnel (called a piezometer ring), and measure the pressure in this tube. If the flow velocity is small in this part of the tunnel, as it usually is, the static pressures sensed by the orifices are essentially total pressures. (The error is less than 0.2 per cent when the flow is at a Mach number of 0.05.) As discussed in Section 1:12 the total pressure at this point in the tunnel is equal to the total pressure in the test section when the flow between the two points is isentropic. This method of measuring total pressure is by far the most common. However, in nearsonic tunnels where the flow is always subsonic, an open-ended forward-facing tube is sometimes used to sense the impact pressure which is then equal to the total pressure.

In order to have a reference for use during testing of a model, the static pressure at a reference point is measured simultaneously with the test section static pressures during calibration. A Mach number is calculated for this reference static pressure along with those for the test section static pressures.

In the nearsonic tunnel, the reference point will normally be located in the forward end of the test section as far from the model as possible, but at a point where the Mach number is very near the same as at the place where the model will be mounted. Instead of a point measurement, a piezometer ring may be used. During a test with a model installed in the test section, the Mach number indicated by the reference static pressure will be the reference Mach number of the flow.

In the transonic tunnel, the reference static pressure is normally measured in the forward portion of the plenum surrounding the test section. A correlation between the reference and the test section Mach number is drawn. Then when a model is tested in the tunnel, the reference Mach number is calculated and the correlation is used to determine the Mach number in the test section. There will frequently be differences between the reference and test section Mach numbers in the transonic tunnel up to about 2 per cent. Typical results obtained from the calibrations of a transonic and a nearsonic tunnel are presented in Figs. 9:5 and 9:6.

In addition to determining Mach numbers in the test section, tunnel calibration often includes determining the inclination of flow with respect to the tunnel centerline. Devices used for this purpose are called yawmeters. Sketches of two yawmeters used in nearsonic and transonic tunnels are illustrated in Fig. 9:7 along with graphs depicting the sensitivity of each to flow angularity. One of the yawmeters consists of two open-ended pressure probes facing upstream and inclined 60 deg with

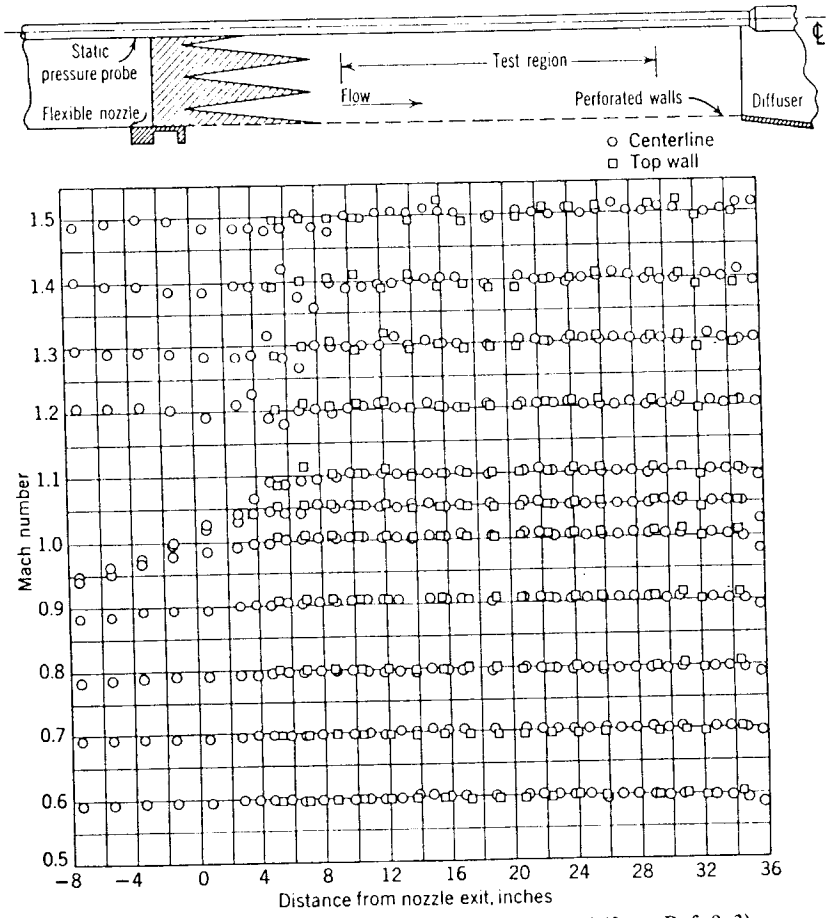


Fig. 9:5 Calibration plots for a transonic tunnel (from Ref. 9:3).

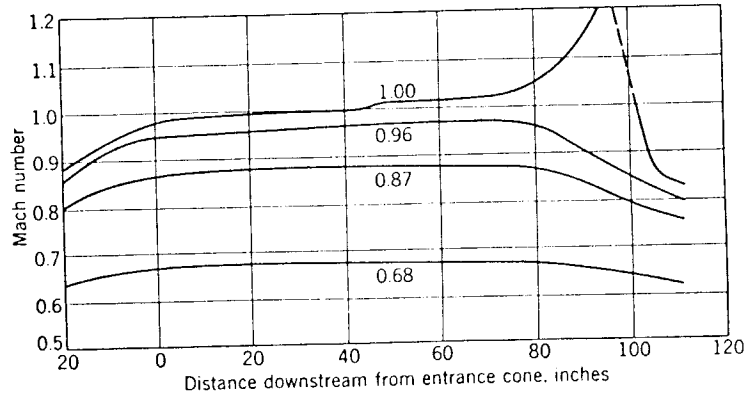


Fig. 9:6 Calibration plots for a nearsonic tunnel. Numbers are nominal Mach numbers.

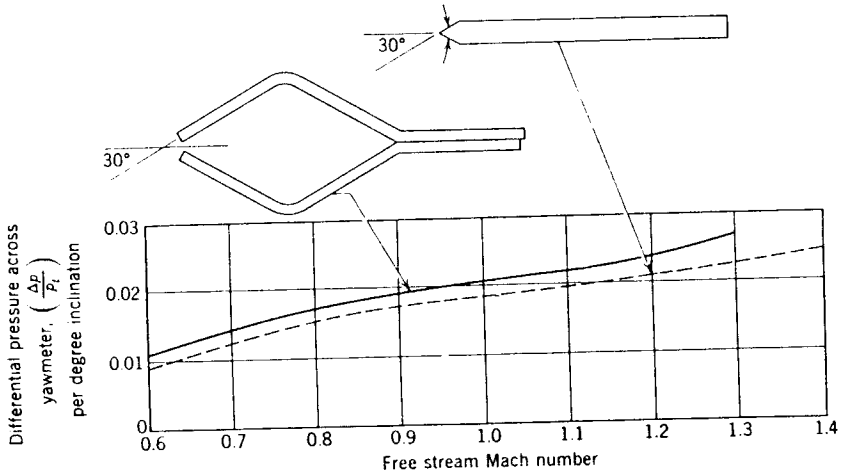


Fig. 9:7 Claw and conical yawmeters and their sensitivity to flow angularity. (From Ref. 9:9.)

respect to each other. The other consists of a 60-deg cone with static pressure orifices on the cone surfaces 180 deg apart.

Regardless of the type of yawmeter or the speed range in which it is used, it is necessary to make tests to determine the calibration of the meter, because the instrument will not be perfectly symmetrical. Yawmeter calibration is accomplished by measuring yawmeter pressures at appropriate tunnel operating conditions with the yawmeter axis at various small angles relative to the tunnel axis, and then rotating the yawmeter precisely 180 deg and repeating these measurements. The differences between pressures from the individual orifice are determined and are plotted as a function of angle relative to the tunnel axis (Fig. 9:8). If the plots from the 0 and 180-deg tests intersect at zero Δp, then the yawmeter has no aerodynamic error. If the intersection is not at zero, however, the instrument will have an aerodynamic error that can be evaluated as shown in Fig. 9:8. The rate of change of pressure difference with respect to flow angle, as shown in the graph of Fig. 9:7, can also be determined from the plots.

The calibration of any tunnel should be carried out at conditions representative of the complete Mach number range through which model tests are likely to be made. If the tunnel has the capability of being operated at various pressure or temperature levels, calibration data should be obtained at representative values. One other parameter which may sometimes be varied in transonic tunnels is the angular alignment of the vented walls with respect to the tunnel centerline. The effect of wall angle

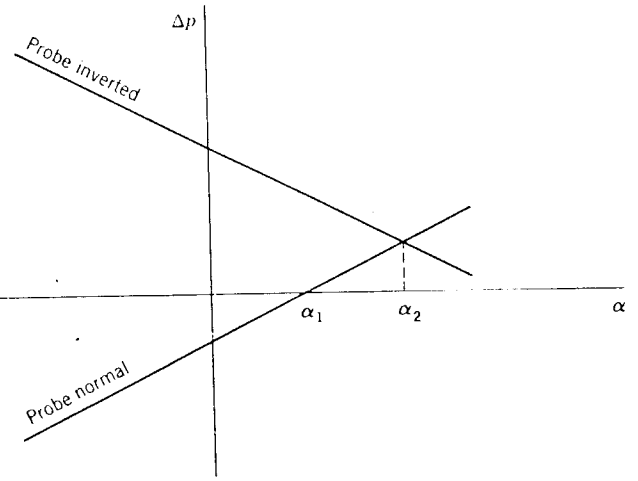


Fig. 9:8 The use of yawmeter probe-normal and probe-inverted data to define aerodynamic instrument error. From normal and inverted data: ε = flow inclination angle, $-\alpha_2$; δ = instrument error, $\alpha_2 - \alpha_1$. From data at $\alpha = 0$: $\varepsilon = \dfrac{\Delta p(\alpha = 0)}{\dfrac{d\,\Delta p}{d\alpha}} - \delta$.

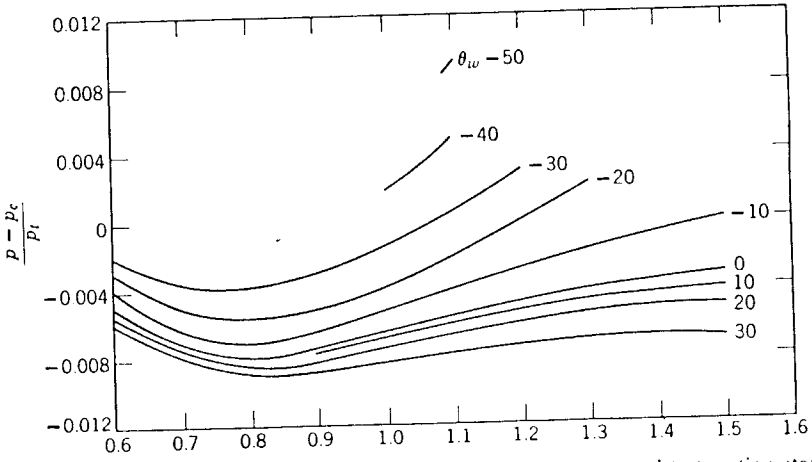


Fig. 9:9 Difference between plenum chamber static pressure p_c and test section static pressure p for a number of wall angles, θ_w, in minutes. From Ref. 9:3. Positive angles correspond to a section that expands in the down-stream direction.

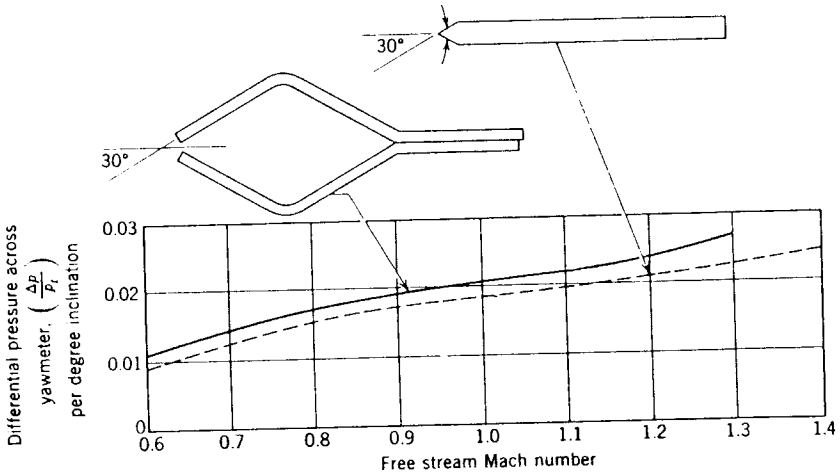


Fig. 9:7 Claw and conical yawmeters and their sensitivity to flow angularity. (From Ref. 9:9.)

respect to each other. The other consists of a 60-deg cone with static pressure orifices on the cone surfaces 180 deg apart.

Regardless of the type of yawmeter or the speed range in which it is used, it is necessary to make tests to determine the calibration of the meter, because the instrument will not be perfectly symmetrical. Yawmeter calibration is accomplished by measuring yawmeter pressures at appropriate tunnel operating conditions with the yawmeter axis at various small angles relative to the tunnel axis, and then rotating the yawmeter precisely 180 deg and repeating these measurements. The differences between pressures from the individual orifice are determined and are plotted as a function of angle relative to the tunnel axis (Fig. 9:8). If the plots from the 0 and 180-deg tests intersect at zero Δp, then the yawmeter has no aerodynamic error. If the intersection is not at zero, however, the instrument will have an aerodynamic error that can be evaluated as shown in Fig. 9:8. The rate of change of pressure difference with respect to flow angle, as shown in the graph of Fig. 9:7, can also be determined from the plots.

The calibration of any tunnel should be carried out at conditions representative of the complete Mach number range through which model tests are likely to be made. If the tunnel has the capability of being operated at various pressure or temperature levels, calibration data should be obtained at representative values. One other parameter which may sometimes be varied in transonic tunnels is the angular alignment of the vented walls with respect to the tunnel centerline. The effect of wall angle

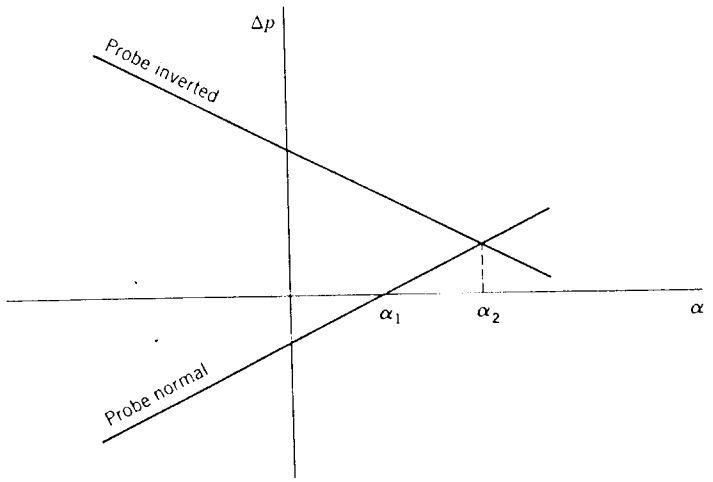


Fig. 9:8 The use of yawmeter probe-normal and probe-inverted data to define aerodynamic instrument error. From normal and inverted data: ε = flow inclination angle, $-\alpha_2$; δ = instrument error, $\alpha_2 - \alpha_1$. From data at $\alpha = 0$: $\varepsilon = \dfrac{\Delta p(\alpha = 0)}{\dfrac{d\,\Delta p}{d\alpha}} - \delta$.

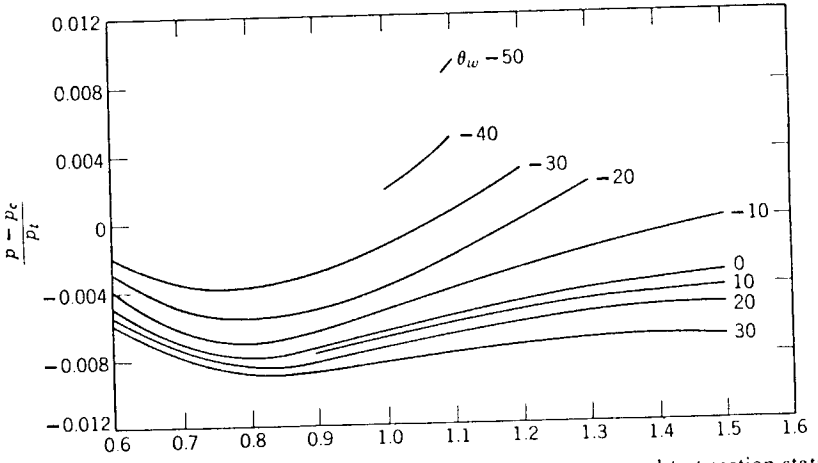


Fig. 9:9 Difference between plenum chamber static pressure p_c and test section static pressure p for a number of wall angles, θ_w, in minutes. From Ref. 9:3. Positive angles correspond to a section that expands in the down-stream direction.

on the differences between plenum chamber and test section static pressure for one transonic tunnel is illustrated by Fig. 9:9.

9:4 Setting Mach Number

We have noted that reference static pressures are measured during the calibration of nearsonic and transonic tunnels and correlated with the pressures of the flow in the part of the test section where the model will be located. These reference pressures are measured at points where the effect of model insertion on the pressure is expected to be negligible. During testing, the static pressure at this reference point and the total pressure are monitored. The ratio of this static pressure to total pressure is used in adjusting the operating conditions of the tunnel to the desired Mach number. Commercially available instruments called Machmeters are sometimes used for a rapid visual indication of tunnel Mach number. These instruments require the input of a static and a total pressure and are designed and calibrated to indicate the corresponding Mach number directly.

The primary method of varying Mach number in a nearsonic tunnel is to change the speed or pitch of the fan blades. One other device called an adjustable choke (Fig. 9:10) is occasionally used. This device provides a variable minimum cross-sectional area for the tunnel circuit somewhat downstream of the test section. With the adjustable choke the tunnel can be brought up to maximum-power operation, so that a sonic flow is established in the minimum area at the choke. The Mach number in the test section is a function of the ratio of area at the choke to test section area. Thus, by changing the choke position and consequently the minimum area, the test section Mach number is changed. The adjustable choke sometimes serves additional purposes in the nearsonic tunnel. If flow

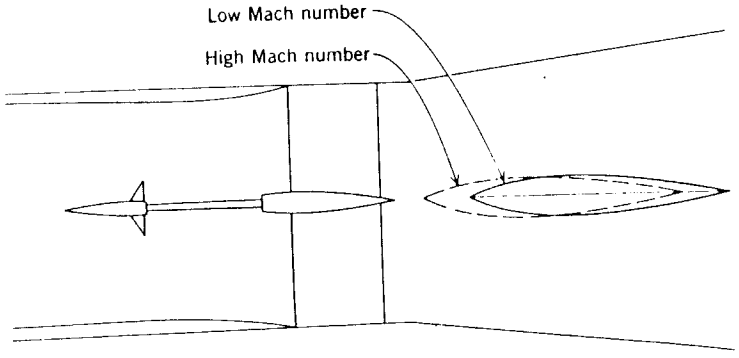


Fig. 9.10 Adjustable choke

pulsations occur in the diffuser, it is possible for disturbances from these pulsations to travel upstream into the test section if the flow is subsonic throughout the tunnel. However, the development of a sonic flow between the source of such pulsations and the test section prevents disturbances from traveling upstream into the test section. Also, small Mach number changes sometimes occur when model angle of attack is changed during a test. The choke can be used for compensating these small Mach number changes without the necessity of changing the speed or pitch of the fan blades.

The setting and control of *subsonic* Mach numbers in a transonic tunnel can be accomplished in either of the ways just described for the nearsonic tunnel. If the tunnel is blowdown instead of continuous, the control of the pressure regulator valve would of course replace the control of the fan. One additional method is to bleed or pump air from the plenum chamber (see Fig. 2:16). The setting and control of *supersonic* Mach numbers in a transonic tunnel may be accomplished by any of the above methods. In many transonic tunnels, supersonic Mach number control is accomplished by use of adjustable flaps at the test section exit (Fig. 2:16). These flaps allow the ejector action of the main tunnel flow to pump air out of the plenum chamber and accomplish the same result as direct bleeding or pumping from the plenum chamber.

9:5 Operating Range

Many if not most transonic and nearsonic tunnels may be operated at one Mach number with various pressure levels, or at constant dynamic pressure throughout the Mach number range. This can be achieved by using adjustable choke Mach number control in any tunnel. In continuous tunnels it is sometimes achieved by use of a designed-in capability for varying the pressure level of the complete tunnel circuit. Tunnels of this type are called "pressure tunnels." Figure 9:11 is a chart depicting the performance capabilities of one transonic tunnel in terms of the more important flow parameters.

9:6 Determining Turbulence Level

Transonic and nearsonic tunnels normally have a relatively high turbulence level. Turbulence level is important because it influences the point of boundary layer transition on a model, that is, the point at which the boundary layer changes from laminar to turbulent. The aerodynamic drag forces on a model are affected considerably by the point of transition at nearsonic and transonic speeds where the skin friction drag is a very important part of the total model drag. The turbulence levels of transonic and nearsonic tunnels are most frequently determined by using hot wire

on the differences between plenum chamber and test section static pressure for one transonic tunnel is illustrated by Fig. 9:9.

9:4 Setting Mach Number

We have noted that reference static pressures are measured during the calibration of nearsonic and transonic tunnels and correlated with the pressures of the flow in the part of the test section where the model will be located. These reference pressures are measured at points where the effect of model insertion on the pressure is expected to be negligible. During testing, the static pressure at this reference point and the total pressure are monitored. The ratio of this static pressure to total pressure is used in adjusting the operating conditions of the tunnel to the desired Mach number. Commercially available instruments called Machmeters are sometimes used for a rapid visual indication of tunnel Mach number. These instruments require the input of a static and a total pressure and are designed and calibrated to indicate the corresponding Mach number directly.

The primary method of varying Mach number in a nearsonic tunnel is to change the speed or pitch of the fan blades. One other device called an adjustable choke (Fig. 9:10) is occasionally used. This device provides a variable minimum cross-sectional area for the tunnel circuit somewhat downstream of the test section. With the adjustable choke the tunnel can be brought up to maximum-power operation, so that a sonic flow is established in the minimum area at the choke. The Mach number in the test section is a function of the ratio of area at the choke to test section area. Thus, by changing the choke position and consequently the minimum area, the test section Mach number is changed. The adjustable choke sometimes serves additional purposes in the nearsonic tunnel. If flow

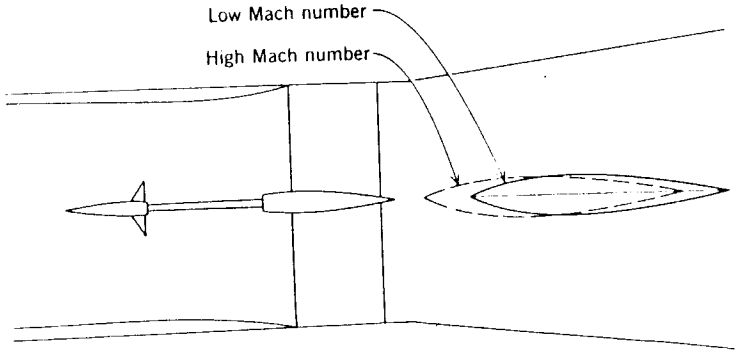


Fig. 9.10 Adjustable choke

pulsations occur in the diffuser, it is possible for disturbances from these pulsations to travel upstream into the test section if the flow is subsonic throughout the tunnel. However, the development of a sonic flow between the source of such pulsations and the test section prevents disturbances from traveling upstream into the test section. Also, small Mach number changes sometimes occur when model angle of attack is changed during a test. The choke can be used for compensating these small Mach number changes without the necessity of changing the speed or pitch of the fan blades.

The setting and control of *subsonic* Mach numbers in a transonic tunnel can be accomplished in either of the ways just described for the nearsonic tunnel. If the tunnel is blowdown instead of continuous, the control of the pressure regulator valve would of course replace the control of the fan. One additional method is to bleed or pump air from the plenum chamber (see Fig. 2:16). The setting and control of *supersonic* Mach numbers in a transonic tunnel may be accomplished by any of the above methods. In many transonic tunnels, supersonic Mach number control is accomplished by use of adjustable flaps at the test section exit (Fig. 2:16). These flaps allow the ejector action of the main tunnel flow to pump air out of the plenum chamber and accomplish the same result as direct bleeding or pumping from the plenum chamber.

9:5 Operating Range

Many if not most transonic and nearsonic tunnels may be operated at one Mach number with various pressure levels, or at constant dynamic pressure throughout the Mach number range. This can be achieved by using adjustable choke Mach number control in any tunnel. In continuous tunnels it is sometimes achieved by use of a designed-in capability for varying the pressure level of the complete tunnel circuit. Tunnels of this type are called "pressure tunnels." Figure 9:11 is a chart depicting the performance capabilities of one transonic tunnel in terms of the more important flow parameters.

9:6 Determining Turbulence Level

Transonic and nearsonic tunnels normally have a relatively high turbulence level. Turbulence level is important because it influences the point of boundary layer transition on a model, that is, the point at which the boundary layer changes from laminar to turbulent. The aerodynamic drag forces on a model are affected considerably by the point of transition at nearsonic and transonic speeds where the skin friction drag is a very important part of the total model drag. The turbulence levels of transonic and nearsonic tunnels are most frequently determined by using hot wire

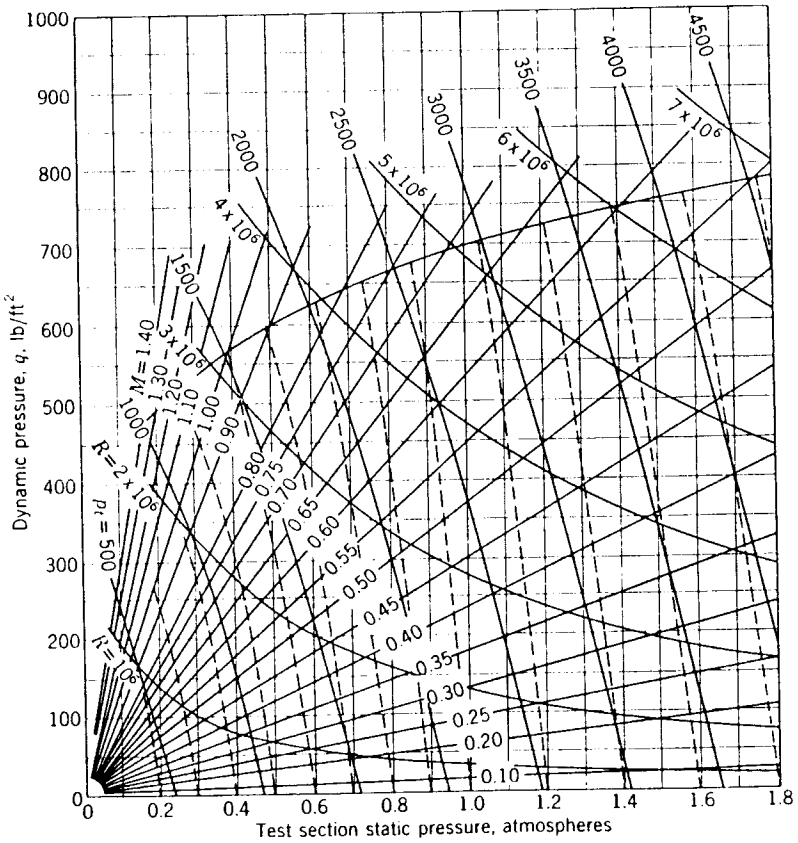


Fig. 9:11 Typical transonic pressure tunnel performance chart. R = Reynolds number per foot, p_t = absolute stagnation pressure, lb/ft². A tunnel run at constant mass operates approximately on the dashed lines. This chart was constructed assuming a stagnation temperature of 95°F and $\gamma = 1.4$. The line joining the ends of the dashed lines is a tunnel power limitation.

anemometers located in the tunnel settling chamber. It is generally believed that velocity fluctuations in the settling chamber will persist through the test section at the same magnitude, and thus that settling chamber turbulence measurements adequately define test section turbulence level.

9:7 Reynolds Number Effects

The primary effects of Reynolds number in transonic wind tunnel testing are on drag measurements. The aerodynamic drag of an aircraft can be considered to be made up of four parts: (1) the skin friction drag, which equals the momentum loss of air in the boundary layer; (2) the forebody

pressure drag, which is equal to the integration of pressure loads in the axial direction over all surfaces of the aircraft ahead of the base; (3) the base drag, which equals the product of base pressure differential and base area; and (4) the drag due to lift, which equals the component of normal force in the flight direction. The portions of drag described in (2) and (4) are essentially independent of model scale or Reynolds number and can be adequately evaluated from wind tunnel tests of small-scale models. This leaves the skin friction drag and base drag, both of which are affected by Reynolds number.

Transition and Skin Friction

At low subsonic speeds, the forebody pressure drag is very small and skin friction drag accounts for the major portion of the drag at zero lift. The importance of skin friction drag decreases as speed is increased but is still a major portion of total drag at transonic speeds. Skin friction drag is very closely related to Reynolds number and to the type of boundary layer (laminar or turbulent). This is illustrated by Fig. 9:12, which shows skin friction drag coefficient for plane surfaces as a function of Reynolds number for incompressible flow. Reference 9:8 includes results showing the effect of compressibility on skin friction drag. With both laminar and turbulent boundary layers, the skin friction drag coefficients decrease with increases in Reynolds number. As Reynolds number is increased with a laminar boundary layer, transition to a turbulent boundary layer occurs and the skin friction drag coefficient increases from the laminar to the turbulent value. While the absolute magnitudes of the skin friction drag coefficients are influenced by compressibility effects and surface geometry, the effects of Reynolds number illustrated in Fig. 9:12 are similar to those on more complex geometries at higher speeds.

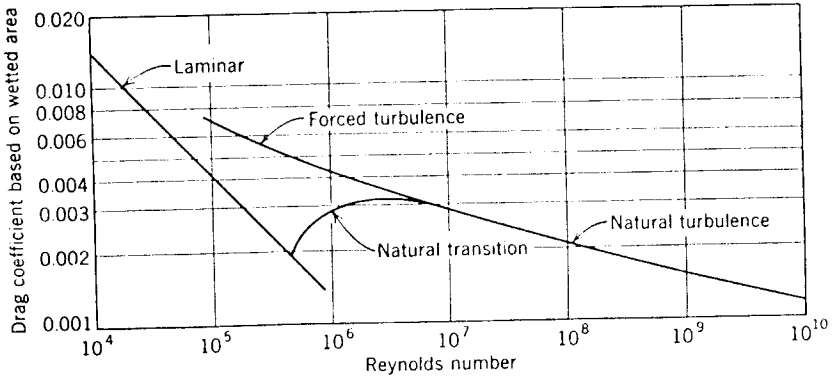


Fig. 9:12 Average skin friction drag coefficient based on wetted area for smooth plane surfaces in incompressible flow.

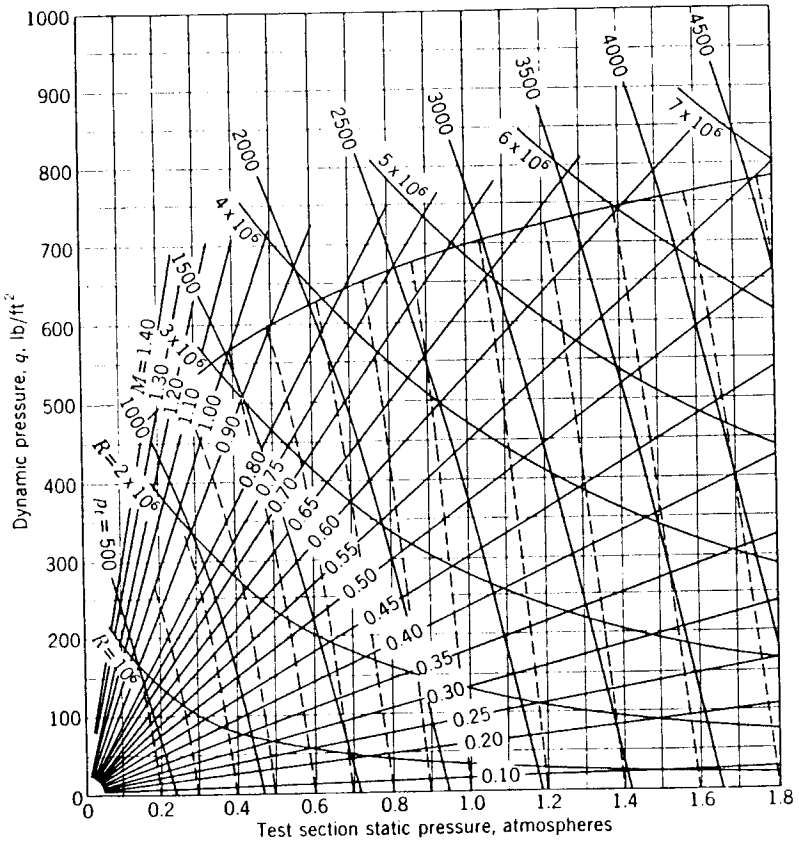


Fig. 9:11 Typical transonic pressure tunnel performance chart. R = Reynolds number per foot, p_t = absolute stagnation pressure, lb/ft². A tunnel run at constant mass operates approximately on the dashed lines. This chart was constructed assuming a stagnation temperature of 95°F and $\gamma = 1.4$. The line joining the ends of the dashed lines is a tunnel power limitation.

anemometers located in the tunnel settling chamber. It is generally believed that velocity fluctuations in the settling chamber will persist through the test section at the same magnitude, and thus that settling chamber turbulence measurements adequately define test section turbulence level.

9:7 Reynolds Number Effects

The primary effects of Reynolds number in transonic wind tunnel testing are on drag measurements. The aerodynamic drag of an aircraft can be considered to be made up of four parts: (1) the skin friction drag, which equals the momentum loss of air in the boundary layer; (2) the forebody

pressure drag, which is equal to the integration of pressure loads in the axial direction over all surfaces of the aircraft ahead of the base; (3) the base drag, which equals the product of base pressure differential and base area; and (4) the drag due to lift, which equals the component of normal force in the flight direction. The portions of drag described in (2) and (4) are essentially independent of model scale or Reynolds number and can be adequately evaluated from wind tunnel tests of small-scale models. This leaves the skin friction drag and base drag, both of which are affected by Reynolds number.

Transition and Skin Friction

At low subsonic speeds, the forebody pressure drag is very small and skin friction drag accounts for the major portion of the drag at zero lift. The importance of skin friction drag decreases as speed is increased but is still a major portion of total drag at transonic speeds. Skin friction drag is very closely related to Reynolds number and to the type of boundary layer (laminar or turbulent). This is illustrated by Fig. 9:12, which shows skin friction drag coefficient for plane surfaces as a function of Reynolds number for incompressible flow. Reference 9:8 includes results showing the effect of compressibility on skin friction drag. With both laminar and turbulent boundary layers, the skin friction drag coefficients decrease with increases in Reynolds number. As Reynolds number is increased with a laminar boundary layer, transition to a turbulent boundary layer occurs and the skin friction drag coefficient increases from the laminar to the turbulent value. While the absolute magnitudes of the skin friction drag coefficients are influenced by compressibility effects and surface geometry, the effects of Reynolds number illustrated in Fig. 9:12 are similar to those on more complex geometries at higher speeds.

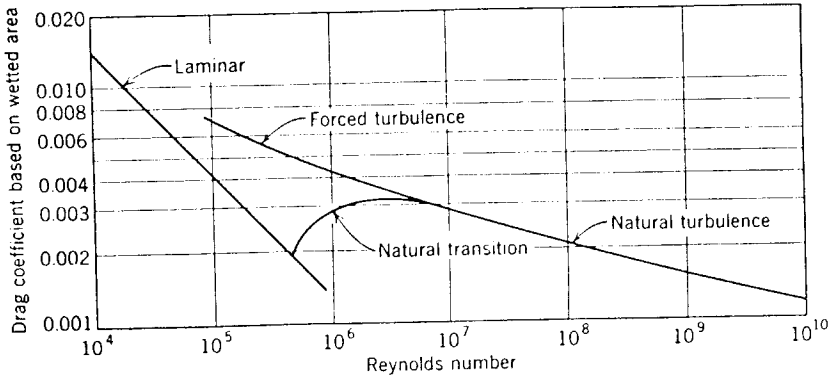


Fig. 9:12 Average skin friction drag coefficient based on wetted area for smooth plane surfaces in incompressible flow.

On a full-scale aircraft in flight, the Reynolds number is high and transition of the boundary layer from laminar to turbulent usually occurs on the forward portions of the aircraft surfaces. On a small-scale model of the same aircraft in a wind tunnel, the flow is likely to be laminar over most of the surfaces. The result is that drag coefficients measured in a wind tunnel with extensive laminar flow are likely to be considerably different from those of a full-scale aircraft in flight.

In some cases, transonic wind tunnel data are obtained with a smooth model having primarily laminar flow over all surfaces. When this is done, the aerodynamicist must estimate the skin friction drag of the model during the test and of the full-scale aircraft in flight and adjust the model drag measurements accordingly. This becomes a particularly difficult task when the actual extents of laminar and turbulent flow over the model during the test are not known.

Often, instead of testing a model with laminar flow and making these extensive calculations, one may test the model with transition fixed at points on the model corresponding to expected transition points on the full-scale aircraft. When this is done the extents of laminar and turbulent boundary layer on the model are known and are the same as on the aircraft. Expected differences between the drag coefficients of the wind tunnel test and the full-scale aircraft are then due to differences in Reynolds number level only. This Reynolds number level effect is easier for the aerodynamicist to cope with than the boundary layer effects involved in correcting smooth model drag (with excessive laminar flow) to full-scale aircraft drag.

Transition is fixed on the model by using strips of artificial roughness at the desired positions. These positions are usually about 5 per cent of

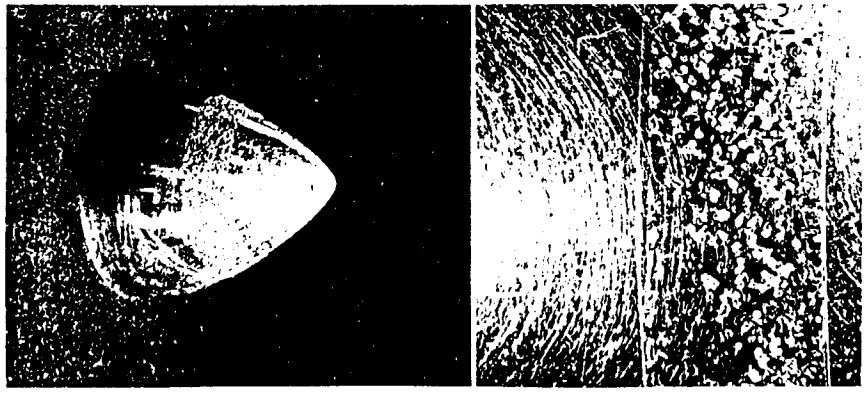


Fig. 9:13 Photograph and microphotograph of transition strip applied to the nose of a wind tunnel model.

the model length from the nose of the fuselage and at about the 5 per cent chord stations of wings or tails on both upper and lower surfaces. A common technique for applying roughness is to (1) mark off the desired transition lines on the model surface, (2) mask off the model surface with tape, leaving exposed strips along the transition lines $\frac{1}{4}$ inch wide or less depending on model size, (3) spray or brush a thin film of lacquer or shellac along the exposed strips, and (4) lightly sprinkle grit in the wet lacquer or shellac. A photograph of a model prepared in this manner is presented in Fig. 9:13.

Table 9:1

Commercial Carborundum Grit Numbers and Corresponding Particle "Diameters."

Grit Number	Nominal Grit Size (inches)
10	0.0937
12	0.0787
14	0.0661
16	0.0555
20	0.0469
24	0.0331
30	0.0280
36	0.0232
46	0.0165
54	0.0138
60	0.0117
70	0.0098
80	0.0083
90	0.0070
100	0.0059
120	0.0049
150	0.0041
180	0.0035
220	0.0029

The grit commonly used is carborundum because it is cheap and readily available in various sizes (Table 9:1). The size of grit particles used cannot be completely arbitrary. If they are too small, the boundary layer will not be "tripped." If they are too large, they will extend well through the boundary layer and cause drag in addition to that of the boundary layer. A formula suggested in Ref. 9:4 for selecting grit size is

$$D_g = \frac{12K}{R} \qquad (9:1)$$

On a full-scale aircraft in flight, the Reynolds number is high and transition of the boundary layer from laminar to turbulent usually occurs on the forward portions of the aircraft surfaces. On a small-scale model of the same aircraft in a wind tunnel, the flow is likely to be laminar over most of the surfaces. The result is that drag coefficients measured in a wind tunnel with extensive laminar flow are likely to be considerably different from those of a full-scale aircraft in flight.

In some cases, transonic wind tunnel data are obtained with a smooth model having primarily laminar flow over all surfaces. When this is done, the aerodynamicist must estimate the skin friction drag of the model during the test and of the full-scale aircraft in flight and adjust the model drag measurements accordingly. This becomes a particularly difficult task when the actual extents of laminar and turbulent flow over the model during the test are not known.

Often, instead of testing a model with laminar flow and making these extensive calculations, one may test the model with transition fixed at points on the model corresponding to expected transition points on the full-scale aircraft. When this is done the extents of laminar and turbulent boundary layer on the model are known and are the same as on the aircraft. Expected differences between the drag coefficients of the wind tunnel test and the full-scale aircraft are then due to differences in Reynolds number level only. This Reynolds number level effect is easier for the aerodynamicist to cope with than the boundary layer effects involved in correcting smooth model drag (with excessive laminar flow) to full-scale aircraft drag.

Transition is fixed on the model by using strips of artificial roughness at the desired positions. These positions are usually about 5 per cent of

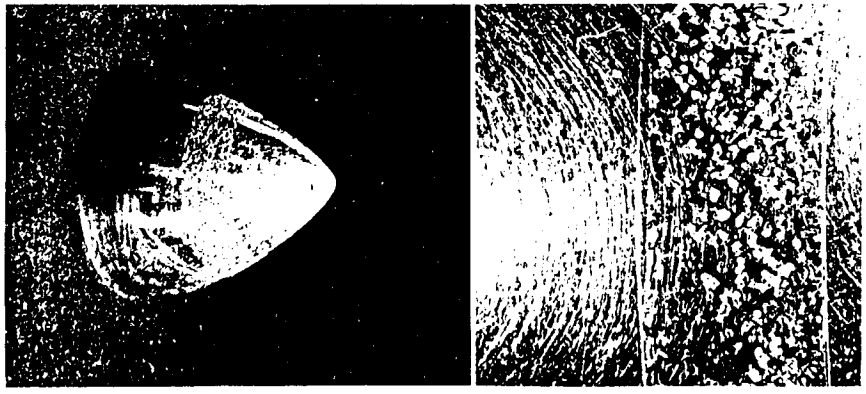


Fig. 9:13 Photograph and microphotograph of transition strip applied to the nose of a wind tunnel model.

the model length from the nose of the fuselage and at about the 5 per cent chord stations of wings or tails on both upper and lower surfaces. A common technique for applying roughness is to (1) mark off the desired transition lines on the model surface, (2) mask off the model surface with tape, leaving exposed strips along the transition lines $\frac{1}{4}$ inch wide or less depending on model size, (3) spray or brush a thin film of lacquer or shellac along the exposed strips, and (4) lightly sprinkle grit in the wet lacquer or shellac. A photograph of a model prepared in this manner is presented in Fig. 9:13.

Table 9:1

Commercial Carborundum Grit Numbers and Corresponding Particle "Diameters."

Grit Number	Nominal Grit Size (inches)
10	0.0937
12	0.0787
14	0.0661
16	0.0555
20	0.0469
24	0.0331
30	0.0280
36	0.0232
46	0.0165
54	0.0138
60	0.0117
70	0.0098
80	0.0083
90	0.0070
100	0.0059
120	0.0049
150	0.0041
180	0.0035
220	0.0029

The grit commonly used is carborundum because it is cheap and readily available in various sizes (Table 9:1). The size of grit particles used cannot be completely arbitrary. If they are too small, the boundary layer will not be "tripped." If they are too large, they will extend well through the boundary layer and cause drag in addition to that of the boundary layer. A formula suggested in Ref. 9:4 for selecting grit size is

$$D_g = \frac{12K}{R} \qquad (9:1)$$

where D_g = nominal grit size, inches (Table 9:1),
R = minimum Reynolds number per foot of length for the free stream flow,
K = a constant which depends on tunnel turbulence level and which may be assumed equal to 400 if data is lacking.

Results of a study made to determine the required grit size are presented in Fig. 9:14. With increases in grit size to about 0.003 inch, the drag coefficient increases quite rapidly. This is interpreted as an indication that a completely turbulent boundary layer has not been established downstream of the transition strip. Above a grit size of 0.004 inch, the rise of drag with grit size is considerably smaller and is constant. This indicates that transition is complete and that the increasing drag is a pressure drag on the transition strip. In this case, the grit size that should be used for testing is indicated to be between 0.003 and 0.004 inch. One method that has been used to obtain the drag at zero lift from results such as those in Fig. 9:14 is to extrapolate the data with fully established transition (grit sizes above 0.003) back to zero grit size as indicated by the dashed line. See also Ref. 9:4.

Transition and Base Drag

In the transonic speed range, the pressure acting on the blunt base of a model is an important part of the total model drag. The pressure acting over the base, and consequently the base drag, are dependent on both the type of boundary layer and the Reynolds number. Tripping the boundary layer on a model is expected to provide a base pressure coefficient nearer to that of the full-scale aircraft than would be obtained with a low

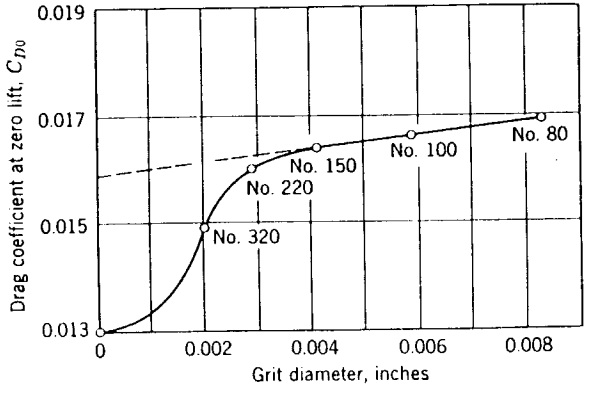


Fig. 9:14 Results of a transition study using a series of grit sizes. (Redrawn from data courtesy of Cornell Aeronautical Laboratory.)

Reynolds number laminar boundary layer. However, tripping the boundary layer does not ensure that accurate base drag will be obtained in wind tunnel tests. One of the major reasons for this is that base pressure is influenced to a large extent by the sting extending from the model base which supports the model in the tunnel. Effects of sting configuration on base pressure are illustrated in Fig. 9:15.

Fortunately, there are many tests in which the model base drag is not important. These are tests of models of aircraft that have jet engines exhausting from the major portion of the aircraft base area. In such cases the aerodynamicist will ask for data reduced to coefficients based on the assumption of zero base drag. To get total axial forces with the aircraft engine operating in flight, he will add engine thrust coefficient to the axial force coefficient from wind tunnel tests adjusted to zero base drag. To adjust wind tunnel axial force to zero base drag, the base pressure is measured during the test and the following equation is used:

$$F_{AC} = F_A - S_b(p - p_b) \tag{9:2}$$

where F_{AC} = axial force adjusted to zero base drag, lb,
F_A = axial force measured, lb,
S_b = model base area, inch^2,
p = free stream static pressure, psia,
p_b = model base pressure, psia.

When the model is of an aircraft that does not have a jet engine exhausting from the base, the problem of obtaining accurate base drag in wind tunnel tests is quite difficult. First, in such a case it is probable that the model base geometry has been altered for the installation of the balance. Second, there are the effects of the sting and the model boundary layer conditions on base pressure. Then, if proper care is not exercised, there is a good possibility that downstream disturbances such as those at the model support sector or in the diffuser will travel forward in the subsonic wake or in subsonic flow not in the wake and affect the base pressure.

With all these influences on base pressure, it is not possible to define total model drag accurately from tests of a sting-supported model. As a result, the best the tunnel engineer can do with data from such tests is to provide model drags corrected to zero base drag. If data cannot be found which satisfactorily define the base pressures for the configuration of interest (as they often cannot be), the approach is usually to design a test specifically to define model base pressures, insofar as possible, in the absence of the disturbing factors previously noted. Such a test could be one in which the model is supported in the tunnel by a minimum interference cantilever from a tunnel wall, by wires from the tunnel walls, or by a yoke support as illustrated in Fig. 9:16.

where D_g = nominal grit size, inches (Table 9:1),
R = minimum Reynolds number per foot of length for the free stream flow,
K = a constant which depends on tunnel turbulence level and which may be assumed equal to 400 if data is lacking.

Results of a study made to determine the required grit size are presented in Fig. 9:14. With increases in grit size to about 0.003 inch, the drag coefficient increases quite rapidly. This is interpreted as an indication that a completely turbulent boundary layer has not been established downstream of the transition strip. Above a grit size of 0.004 inch, the rise of drag with grit size is considerably smaller and is constant. This indicates that transition is complete and that the increasing drag is a pressure drag on the transition strip. In this case, the grit size that should be used for testing is indicated to be between 0.003 and 0.004 inch. One method that has been used to obtain the drag at zero lift from results such as those in Fig. 9:14 is to extrapolate the data with fully established transition (grit sizes above 0.003) back to zero grit size as indicated by the dashed line. See also Ref. 9:4.

Transition and Base Drag

In the transonic speed range, the pressure acting on the blunt base of a model is an important part of the total model drag. The pressure acting over the base, and consequently the base drag, are dependent on both the type of boundary layer and the Reynolds number. Tripping the boundary layer on a model is expected to provide a base pressure coefficient nearer to that of the full-scale aircraft than would be obtained with a low

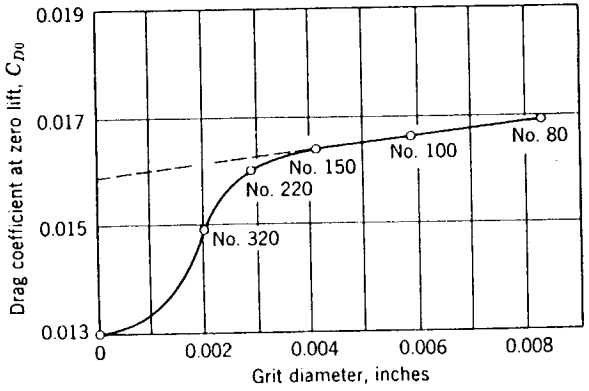


Fig. 9:14 Results of a transition study using a series of grit sizes. (Redrawn from data courtesy of Cornell Aeronautical Laboratory.)

Reynolds number laminar boundary layer. However, tripping the boundary layer does not ensure that accurate base drag will be obtained in wind tunnel tests. One of the major reasons for this is that base pressure is influenced to a large extent by the sting extending from the model base which supports the model in the tunnel. Effects of sting configuration on base pressure are illustrated in Fig. 9:15.

Fortunately, there are many tests in which the model base drag is not important. These are tests of models of aircraft that have jet engines exhausting from the major portion of the aircraft base area. In such cases the aerodynamicist will ask for data reduced to coefficients based on the assumption of zero base drag. To get total axial forces with the aircraft engine operating in flight, he will add engine thrust coefficient to the axial force coefficient from wind tunnel tests adjusted to zero base drag. To adjust wind tunnel axial force to zero base drag, the base pressure is measured during the test and the following equation is used:

$$F_{AC} = F_A - S_b(p - p_b) \tag{9:2}$$

where F_{AC} = axial force adjusted to zero base drag, lb,
F_A = axial force measured, lb,
S_b = model base area, inch^2,
p = free stream static pressure, psia,
p_b = model base pressure, psia.

When the model is of an aircraft that does not have a jet engine exhausting from the base, the problem of obtaining accurate base drag in wind tunnel tests is quite difficult. First, in such a case it is probable that the model base geometry has been altered for the installation of the balance. Second, there are the effects of the sting and the model boundary layer conditions on base pressure. Then, if proper care is not exercised, there is a good possibility that downstream disturbances such as those at the model support sector or in the diffuser will travel forward in the subsonic wake or in subsonic flow not in the wake and affect the base pressure.

With all these influences on base pressure, it is not possible to define total model drag accurately from tests of a sting-supported model. As a result, the best the tunnel engineer can do with data from such tests is to provide model drags corrected to zero base drag. If data cannot be found which satisfactorily define the base pressures for the configuration of interest (as they often cannot be), the approach is usually to design a test specifically to define model base pressures, insofar as possible, in the absence of the disturbing factors previously noted. Such a test could be one in which the model is supported in the tunnel by a minimum interference cantilever from a tunnel wall, by wires from the tunnel walls, or by a yoke support as illustrated in Fig. 9:16.

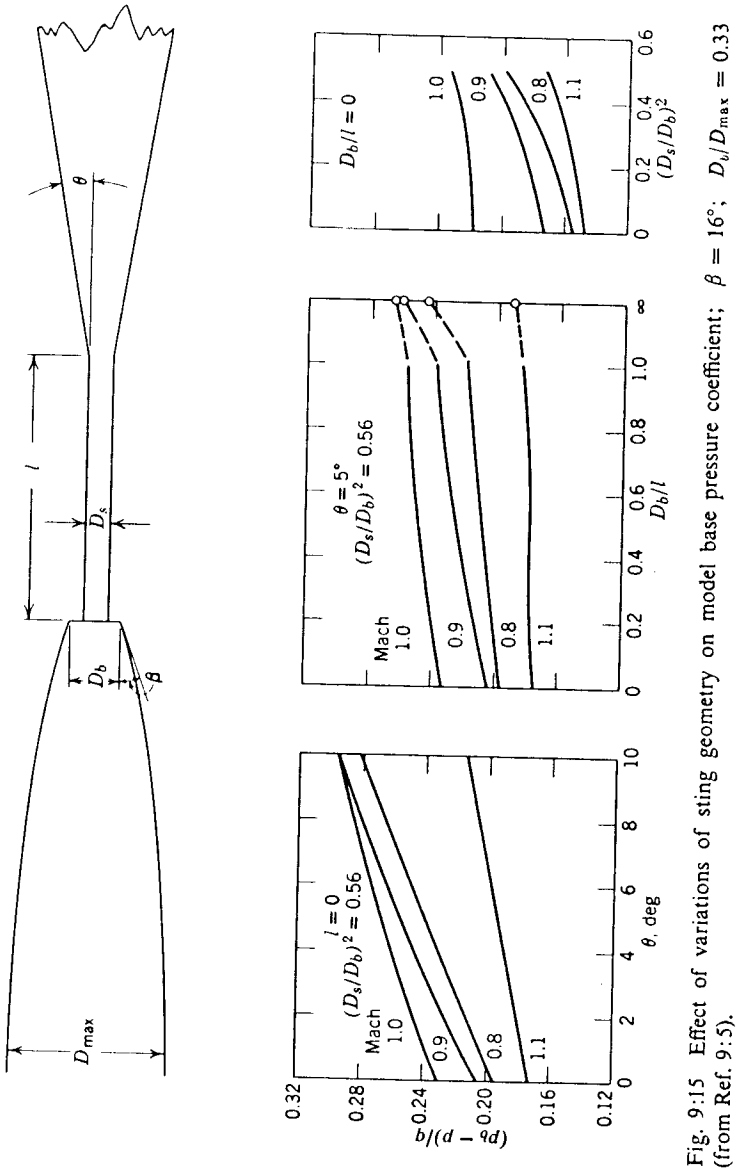


Fig. 9:15 Effect of variations of sting geometry on model base pressure coefficient; $\beta = 16°$; $D_b/D_{max} = 0.33$ (from Ref. 9:5).

During force tests, model base pressures are usually measured by using a piece of hypodermic tubing installed in a hole along the axis of the balance support sting. The tube terminates in the model cavity. The opposite end of the tube is connected by means of flexible tubing to a pressure-measuring instrument located outside the tunnel.

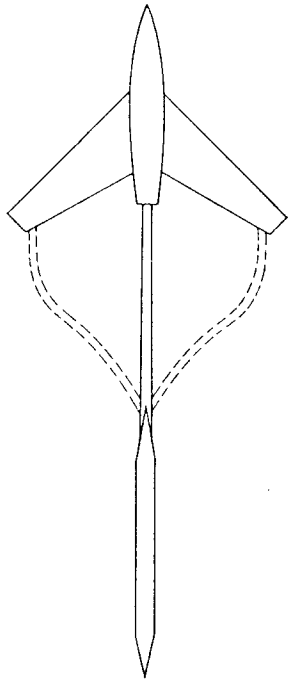


Fig. 9:16 Yoke method of evaluating base pressures.

Reynolds Number Effects on Stability

To this point, the Reynolds number effects discussed have been effects on drag. There are also effects of Reynolds number on lift and pitching moment data though these are usually secondary. If the aircraft is operating at relatively high angles of attack where boundary layer separation is possible, the type of boundary layer can become quite important. Lift and pitching moment data with aerodynamic hysteresis have been obtained with laminar boundary layers. The data have shown that with increasing angle of attack the flow will separate at one point and that with decreasing angle of attack, reattachment will be delayed to some earlier point. This aerodynamic hysteresis has been eliminated by use of fixed transition (Fig. 9:17). The reason the effects of Reynolds number on lift and pitching moment are usually secondary is that transonic aircraft do not frequently operate at high angles of attack and model angles of attack during wind tunnel tests are seldom high enough to cause a high degree of laminar boundary layer separation on the model.

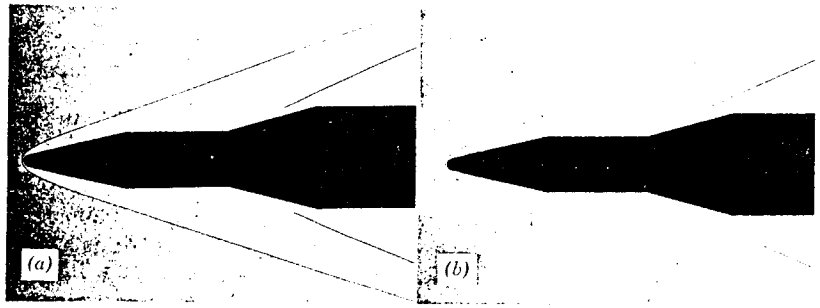


Fig. 9:17 Separation over forward cylinder (*a*) cured by transition roughness (*b*).

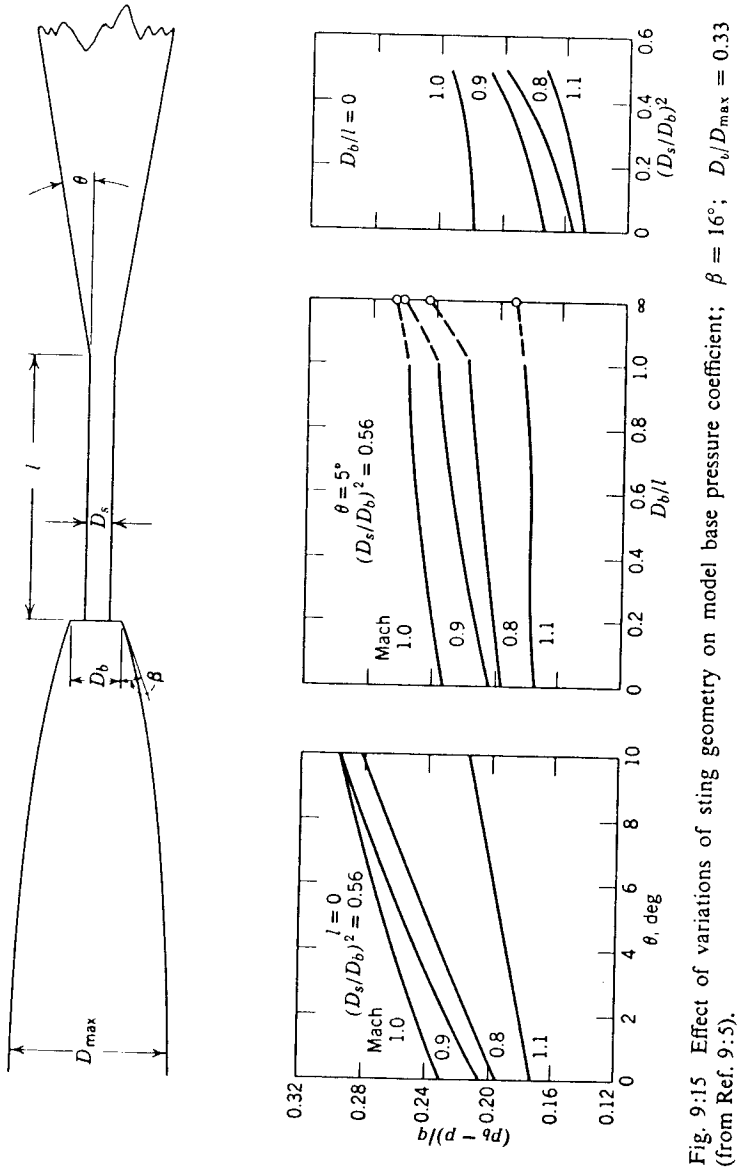


Fig. 9:15 Effect of variations of sting geometry on model base pressure coefficient; $\beta = 16°$; $D_b/D_{max} = 0.33$ (from Ref. 9:5).

During force tests, model base pressures are usually measured by using a piece of hypodermic tubing installed in a hole along the axis of the balance support sting. The tube terminates in the model cavity. The opposite end of the tube is connected by means of flexible tubing to a pressure-measuring instrument located outside the tunnel.

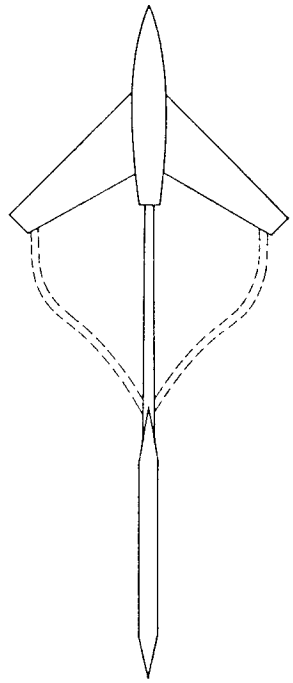


Fig. 9:16 Yoke method of evaluating base pressures.

Reynolds Number Effects on Stability

To this point, the Reynolds number effects discussed have been effects on drag. There are also effects of Reynolds number on lift and pitching moment data though these are usually secondary. If the aircraft is operating at relatively high angles of attack where boundary layer separation is possible, the type of boundary layer can become quite important. Lift and pitching moment data with aerodynamic hysteresis have been obtained with laminar boundary layers. The data have shown that with increasing angle of attack the flow will separate at one point and that with decreasing angle of attack, reattachment will be delayed to some earlier point. This aerodynamic hysteresis has been eliminated by use of fixed transition (Fig. 9:17). The reason the effects of Reynolds number on lift and pitching moment are usually secondary is that transonic aircraft do not frequently operate at high angles of attack and model angles of attack during wind tunnel tests are seldom high enough to cause a high degree of laminar boundary layer separation on the model.

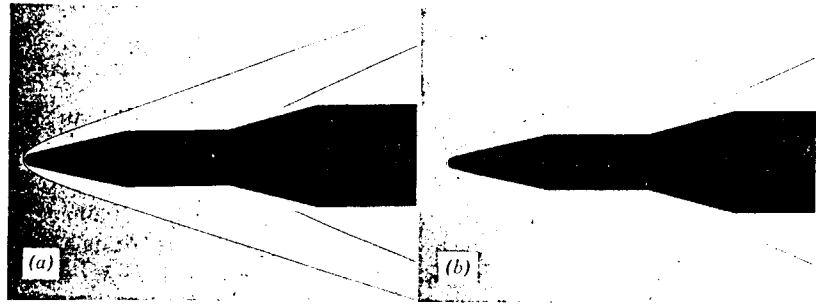


Fig. 9:17 Separation over forward cylinder (*a*) cured by transition roughness (*b*).

9:8 Testing Complete Airplanes

The wind tunnel program for a new transonic airplane is a lengthy and complex ordeal, exemplified by the 5400 hours of tunnel time (in four different tunnels) needed for the Boeing 727. In the transonic range the forces and moments on the airplane vary widely and rapidly, and airplanes and crews have been lost because of failure to interpret tunnel data properly or failure to take enough data. From a practical standpoint the tests are divided into those before a firm committment to build the airplane has been given ("Development Tests"), and those aimed very seriously at a specific airplane ("Flying Qualities, Research, and Loads"). The former are aimed at searching out enough confirmation for the paper study being used to sell the airplane, while the latter seek refinements that will result in the best airplane possible in every detail. Thus in actuality four types of people with four different interests follow the wind tunnel tests of a new airplane. The corporation president and sales staff worry about the performance's meeting specifications (or promises), the aerodynamicists and flight test engineers are concerned about flying qualities, the research aerodynamicists seek changes to improve future airplanes, and the structural engineers seek loads to which they must design. The test program, within limits, seeks to meet the above needs.

Development Tests

Following paper studies by the advanced design group, a series of models are built incorporating fairly gross changes: variations of wing sweep, tail size and position, engine position, and so forth. No movable controls are provided, although landing flaps and leading edge slats may be included toward the end of the program. Emphasis is placed on obtaining pitch plane data at Mach numbers throughout the proposed range with accent on lift to drag ratios and minimum drag. Transition studies are made to give confidence in the data. Development tests may include 50 or more configurations and take perhaps 1000 hours of tunnel time, as compared, for instance, with the total of 8000 hours spent on the supersonic B-58 and 12,000 on the supersonic F-111.

Flying Qualities, Research and Loads

Longitudinal Stability and Control Testing. The typical high-speed longitudinal data will be from a program similar to that of Table 9:2, expanded or contracted for the case at hand. The basic lift and pitching moment characteristics are usually obtained at values of α from about -5 to $+15$ deg or so. At each Mach number data through this α range will be recorded with the control deflections given in Table 9:2. Trailing edge downward is positive, by convention. In the transonic speed range,

the stability parameters vary rapidly and unpredictably with Mach number and it is necessary to obtain data at fairly small increments of Mach number; 0.01 near $M = 1.0$ is not uncommon. The discussion of force tests in this chapter will be generally applicable to tests in the supersonic and hypersonic as well as the transonic speed ranges, and will serve as the basis for force test discussion in later chapters. Section 10:28 contains additional details on supersonic tests, while general preparations for testing are in Section 8:6.

AIRPLANE BUILDUP. From the configurations shown in Table 9:2, it is seen that the drag evaluation tests of the canopy, nacelles, and horizontal tail are made without the wing in order to reduce the total force being measured and hence increase the accuracy for small contributions. The airplane aerodynamicists will have a feel for what an installation should cost with respect to drag from previous airplanes, and will at this time suggest changes if the data so indicate. Root bending moments and shears are taken for the relevant configurations.

LONGITUDINAL STABILITY AND CONTROL. The last three groups of runs in Table 9:2 determine the characteristics of the aircraft in longitudinal stability and control. Either the stabilizer or the elevator (or both) may be used for control or trim (condition where $C_m = 0$), and it is mandatory to know their effectiveness and which combination results in minimum drag. Deflection of the elevators (or stabilizer) results in a set of curves

Table 9:2

Longitudinal Stability and Control

Runs	Configuration	Deflections	Hinge Moments	Root Bending	Remarks
1-5	*B, BK, BKN, BKH, BKNWV*			*H, W*	Airplane buildup
6-9	*BKNVHE*	δ_H 0 to $-15°$	*E, H*	*H*	Horiz. stab. effectiveness
10-13	*BKNWVHE*	δ_H 0 to $-15°$	*E, H*	*H*	Downwash and q at tail
14-23	*BKNWVHE*	δ_H 0 to $-15°$ δ_E 0 to $-20°$	*E, H*	*H*	Elevator effectiveness

Configuration Code		Control Surface Deflections	
A	aileron	δ_A	aileron
B	body	δ_S	stabilizer
E	elevators	δ_R	rudder
F	flaps	δ_ρ	spoiler
H	horizontal tail	δ_n	leading edge
I	duct inlets	δ_E	elevators
K	canopy	δ_H	horizontal tail
N	nacelles		
R	rudder		
V	vertical tail		
W	wing		

9:8 Testing Complete Airplanes

The wind tunnel program for a new transonic airplane is a lengthy and complex ordeal, exemplified by the 5400 hours of tunnel time (in four different tunnels) needed for the Boeing 727. In the transonic range the forces and moments on the airplane vary widely and rapidly, and airplanes and crews have been lost because of failure to interpret tunnel data properly or failure to take enough data. From a practical standpoint the tests are divided into those before a firm committment to build the airplane has been given ("Development Tests"), and those aimed very seriously at a specific airplane ("Flying Qualities, Research, and Loads"). The former are aimed at searching out enough confirmation for the paper study being used to sell the airplane, while the latter seek refinements that will result in the best airplane possible in every detail. Thus in actuality four types of people with four different interests follow the wind tunnel tests of a new airplane. The corporation president and sales staff worry about the performance's meeting specifications (or promises), the aerodynamicists and flight test engineers are concerned about flying qualities, the research aerodynamicists seek changes to improve future airplanes, and the structural engineers seek loads to which they must design. The test program, within limits, seeks to meet the above needs.

Development Tests

Following paper studies by the advanced design group, a series of models are built incorporating fairly gross changes: variations of wing sweep, tail size and position, engine position, and so forth. No movable controls are provided, although landing flaps and leading edge slats may be included toward the end of the program. Emphasis is placed on obtaining pitch plane data at Mach numbers throughout the proposed range with accent on lift to drag ratios and minimum drag. Transition studies are made to give confidence in the data. Development tests may include 50 or more configurations and take perhaps 1000 hours of tunnel time, as compared, for instance, with the total of 8000 hours spent on the supersonic B-58 and 12,000 on the supersonic F-111.

Flying Qualities, Research and Loads

Longitudinal Stability and Control Testing. The typical high-speed longitudinal data will be from a program similar to that of Table 9:2, expanded or contracted for the case at hand. The basic lift and pitching moment characteristics are usually obtained at values of α from about -5 to $+15$ deg or so. At each Mach number data through this α range will be recorded with the control deflections given in Table 9:2. Trailing edge downward is positive, by convention. In the transonic speed range,

the stability parameters vary rapidly and unpredictably with Mach number and it is necessary to obtain data at fairly small increments of Mach number; 0.01 near $M = 1.0$ is not uncommon. The discussion of force tests in this chapter will be generally applicable to tests in the supersonic and hypersonic as well as the transonic speed ranges, and will serve as the basis for force test discussion in later chapters. Section 10:28 contains additional details on supersonic tests, while general preparations for testing are in Section 8:6.

AIRPLANE BUILDUP. From the configurations shown in Table 9:2, it is seen that the drag evaluation tests of the canopy, nacelles, and horizontal tail are made without the wing in order to reduce the total force being measured and hence increase the accuracy for small contributions. The airplane aerodynamicists will have a feel for what an installation should cost with respect to drag from previous airplanes, and will at this time suggest changes if the data so indicate. Root bending moments and shears are taken for the relevant configurations.

LONGITUDINAL STABILITY AND CONTROL. The last three groups of runs in Table 9:2 determine the characteristics of the aircraft in longitudinal stability and control. Either the stabilizer or the elevator (or both) may be used for control or trim (condition where $C_m = 0$), and it is mandatory to know their effectiveness and which combination results in minimum drag. Deflection of the elevators (or stabilizer) results in a set of curves

Table 9:2

Longitudinal Stability and Control

Runs	Configuration	Deflections	Hinge Moments	Root Bending	Remarks
1–5	*B, BK, BKN, BKH, BKNWV*			*H, W*	Airplane buildup
6–9	*BKNVHE*	δ_H 0 to $-15°$	*E, H*	*H*	Horiz. stab. effectiveness
10–13	*BKNWVHE*	δ_H 0 to $-15°$	*E, H*	*H*	Downwash and q at tail
14–23	*BKNWVHE*	δ_H 0 to $-15°$ δ_E 0 to $-20°$	*E, H*	*H*	Elevator effectiveness

Configuration Code		Control Surface Deflections	
A	aileron	δ_A	aileron
B	body	δ_S	stabilizer
E	elevators	δ_R	rudder
F	flaps	δ_p	spoiler
H	horizontal tail	δ_n	leading edge
I	duct inlets	δ_E	elevators
K	canopy	δ_H	horizontal tail
N	nacelles		
R	rudder		
V	vertical tail		
W	wing		

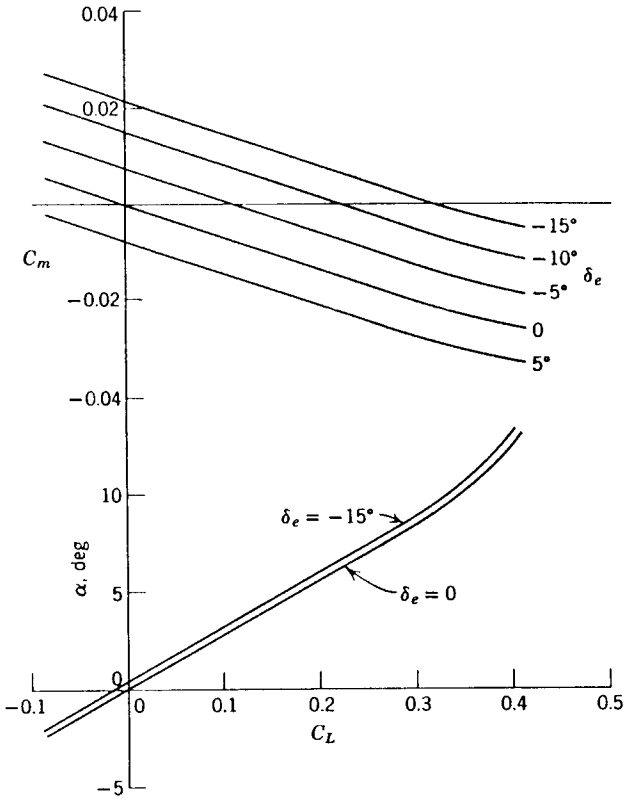


Fig. 9:18 Typical presentation of longitudinal stability data. Elevator deflection δ_e is positive for trailing edge down.

shown in Fig. 9:18. The curves typically show a negative slope of the moment coefficient against lift coefficient—a requirement for stability—and through crossplotting, a curve of elevator (or stabilizer) angle to trim (Fig. 9:19) is obtained. These types of runs are repeated for each Mach number, and both control surface hinge moments and root bending moments and shear of the horizontal tail are recorded. Further plots indicating the change of moment available per degree of elevator (or stabilizer) deflection, as shown in Fig. 9:20, may be obtained. The slope of the curve in Fig. 9:20, $\partial C_m/\partial \delta_e$ (also called $C_{m\delta}$) is the elevator effectiveness parameter. The available change in moment due to control deflection, combined with the moment of inertia of the aircraft, is an indication of available angular acceleration and therefore an indication of aircraft maneuverability. Figure 9:21 shows the change in α_{trim} with Mach number.

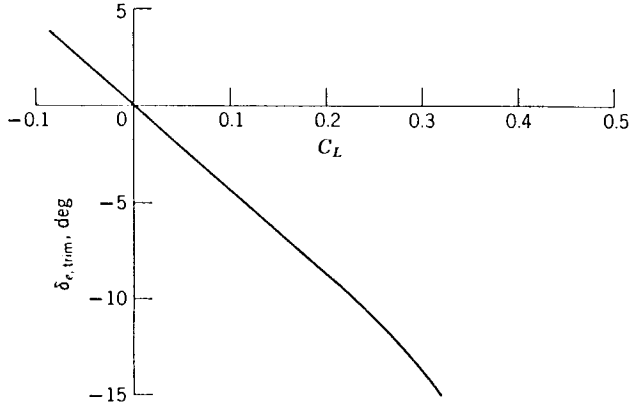


Fig. 9:19 Crossplot from Fig. 9:18 to define elevator angle for trim at various lift coefficients.

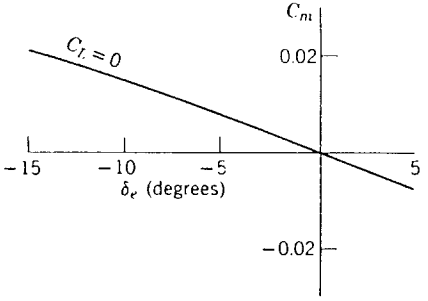


Fig. 9:20 Crossplot from Fig. 9:18 to define control effectiveness.

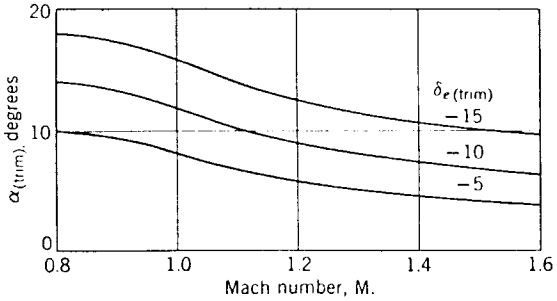


Fig. 9:21 Typical plot of $\alpha_{(trim)}$ variation with Mach number at transonic speeds.

In evaluating the horizontal-tail data the aerodynamicist will compare the performance of the tail with that predicted by theory, often ascribing the inevitable loss to a loss of dynamic pressure at the tail. He may request surveys of the fuselage boundary layer near the tail, or even a relocation of the tail.

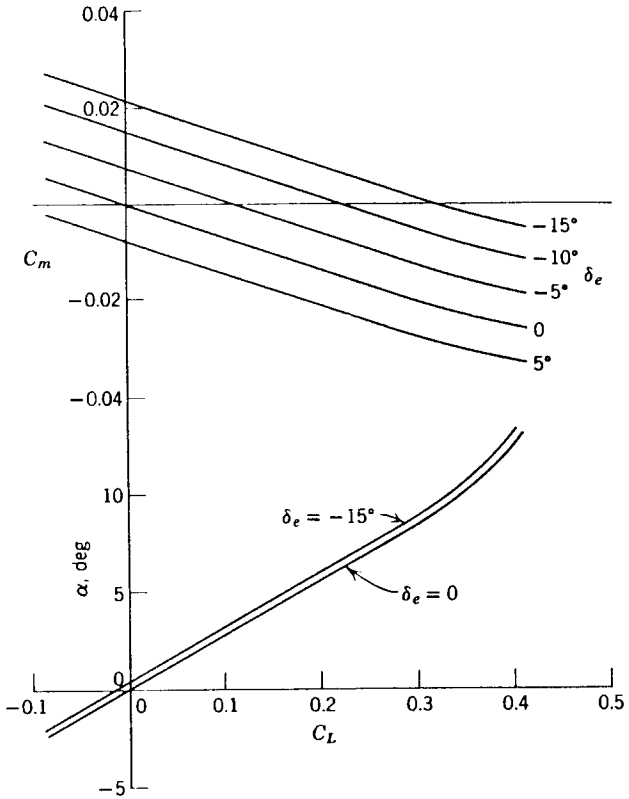


Fig. 9:18 Typical presentation of longitudinal stability data. Elevator deflection δ_e is positive for trailing edge down.

shown in Fig. 9:18. The curves typically show a negative slope of the moment coefficient against lift coefficient—a requirement for stability—and through crossplotting, a curve of elevator (or stabilizer) angle to trim (Fig. 9:19) is obtained. These types of runs are repeated for each Mach number, and both control surface hinge moments and root bending moments and shear of the horizontal tail are recorded. Further plots indicating the change of moment available per degree of elevator (or stabilizer) deflection, as shown in Fig. 9:20, may be obtained. The slope of the curve in Fig. 9:20, $\partial C_m/\partial \delta_e$ (also called $C_{m\delta}$) is the elevator effectiveness parameter. The available change in moment due to control deflection, combined with the moment of inertia of the aircraft, is an indication of available angular acceleration and therefore an indication of aircraft maneuverability. Figure 9:21 shows the change in α_{trim} with Mach number.

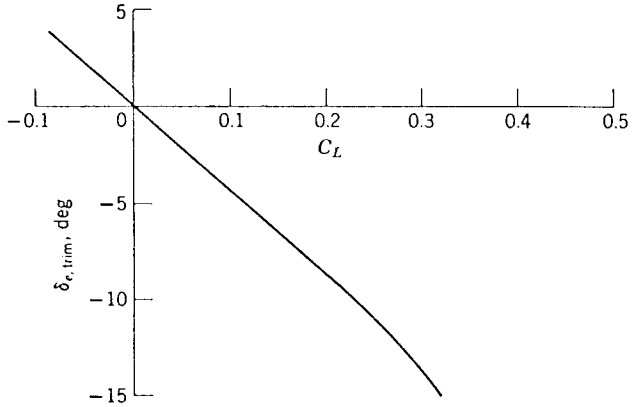


Fig. 9:19 Crossplot from Fig. 9:18 to define elevator angle for trim at various lift coefficients.

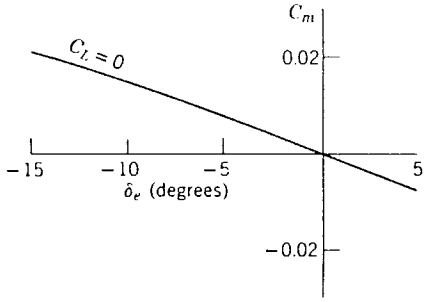


Fig. 9:20 Crossplot from Fig. 9:18 to define control effectiveness.

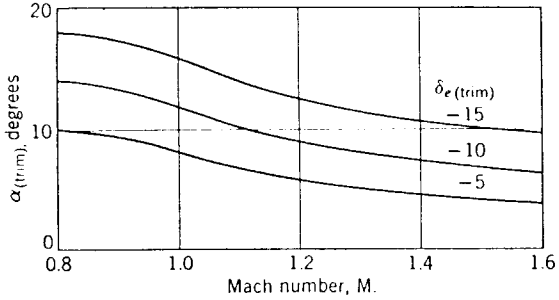


Fig. 9:21 Typical plot of $\alpha_{(trim)}$ variation with Mach number at transonic speeds.

In evaluating the horizontal-tail data the aerodynamicist will compare the performance of the tail with that predicted by theory, often ascribing the inevitable loss to a loss of dynamic pressure at the tail. He may request surveys of the fuselage boundary layer near the tail, or even a relocation of the tail.

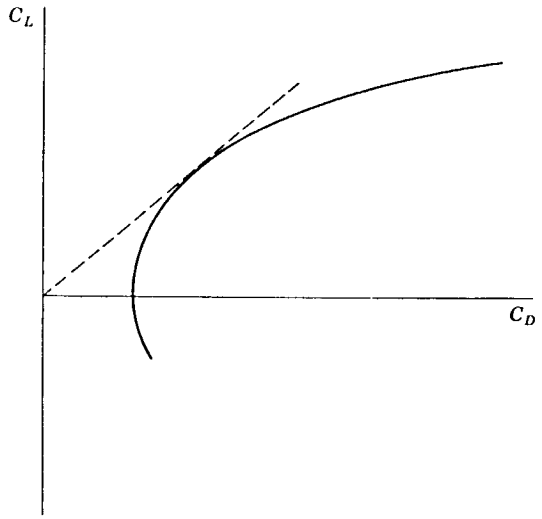


Fig. 9:22 Typical presentation of drag data.

DRAG. The aerodynamicist is primarily interested in drag of the aircraft at conditions of flight for which the aircraft is likely to fly for a significant period of time. This of course means flight at "trim" conditions. However, he will normally ask for drag data at all conditions for which longitudinal, directional, and lateral stability data are obtained.

A typical presentation of drag data is illustrated in Fig. 9:22. From graphs of this type at the appropriate control deflections, he can obtain the drag at trim conditions. The drag is, or course, the parameter that defines maximum aircraft speed for a specified engine and the maximum aircraft range for a specified engine and fuel capacity.

The dashed line in Fig. 9:22 defines both the maximum lift-to-drag ratio (L/D_{max}) and the lift coefficient at which it occurs. The aerodynamicist will endeavor to have this lift coefficient correspond to cruise conditions. Many additional drag studies are made for the variety of loads an airplane may be called upon to carry. See, for instance, Fig. 9:23.

Lateral-Directional Testing. A number of tests with the aircraft in a yawed condition are performed in the tunnel although yawed flight is an emergency rather than an intentional flight maneuver.* That is, high-speed airplanes are rarely if ever sideslipped, and flight with asymmetric

* One may also sadly note that in some cases performance regulations set up for low-speed aircraft are still being insisted upon for high-speed aircraft. One may hope that with the years these will be rescinded where inapplicable.

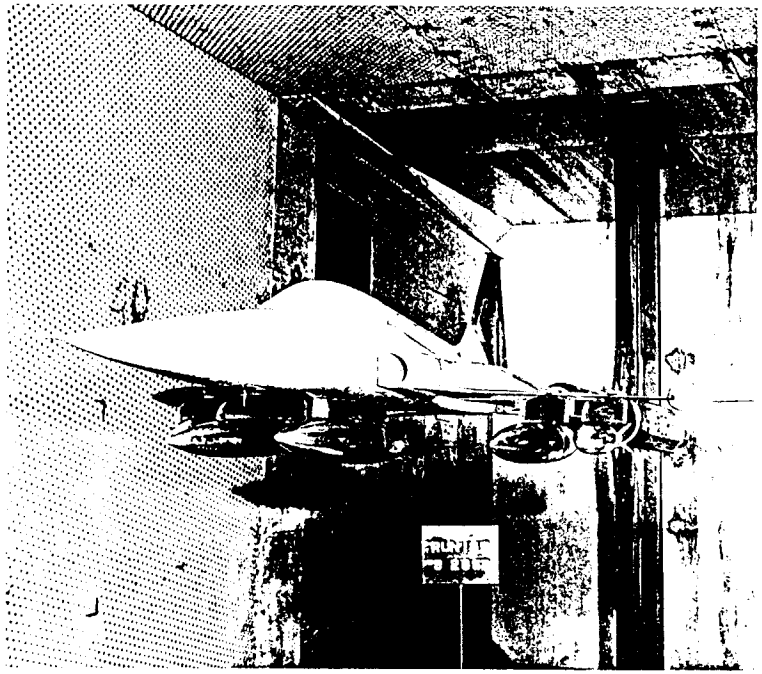


Fig. 9:23 Model during transonic drag study. (Courtesy Northrop Corporation.)

power is preferably accomplished by trimming to zero yaw. Nevertheless, for those inadvertent conditions—insufficient rudder power, battle damage, or a skidding maneuver—it is important to know that stability and control will remain. In turn, it becomes important to determine that obtaining stability and control in either trimmed unyawed flight or actual yawed flight is possible and may be obtained with the minimum drag penalty.

Table 9:3

Lateral-Directional Tests

Runs*	Configuration	Deflections	Hinge Moments	Root Bending	Remarks
1–36	*B, BK, BKN, BKNHE, BKNVR BKNWVRHE*	None	*F, A, H, E, R*	*W*	Airplane buildup
37–55	*BKNVRHE*	δ_V −5, 0, 5	*V*	*V*	Vertical-tail effectiveness
56–67	*BKNWVRHE*	δ_V −5, 5	*V*	*V*	Sidewash
68–86	*BKNWVRHE*	δ_R −5, −10, −15	–	–	Rudder effectiveness
122–158	*BKNWVRHE BKNWHE*	δ_A −10 to +20	*A*	*W*	Aileron power and effectiveness

* The run numbers allow for six angles of yaw: −15, −10, −5, 5, 10, 15.

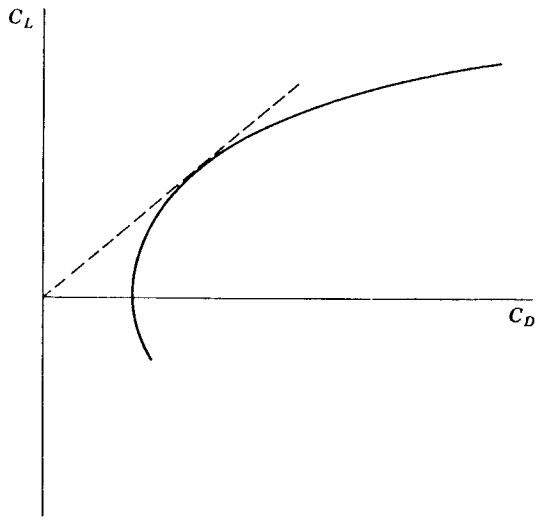


Fig. 9:22 Typical presentation of drag data.

DRAG. The aerodynamicist is primarily interested in drag of the aircraft at conditions of flight for which the aircraft is likely to fly for a significant period of time. This of course means flight at "trim" conditions. However, he will normally ask for drag data at all conditions for which longitudinal, directional, and lateral stability data are obtained.

A typical presentation of drag data is illustrated in Fig. 9:22. From graphs of this type at the appropriate control deflections, he can obtain the drag at trim conditions. The drag is, or course, the parameter that defines maximum aircraft speed for a specified engine and the maximum aircraft range for a specified engine and fuel capacity.

The dashed line in Fig. 9:22 defines both the maximum lift-to-drag ratio (L/D_{max}) and the lift coefficient at which it occurs. The aerodynamicist will endeavor to have this lift coefficient correspond to cruise conditions. Many additional drag studies are made for the variety of loads an airplane may be called upon to carry. See, for instance, Fig. 9:23.

Lateral-Directional Testing. A number of tests with the aircraft in a yawed condition are performed in the tunnel although yawed flight is an emergency rather than an intentional flight maneuver.* That is, high-speed airplanes are rarely if ever sideslipped, and flight with asymmetric

* One may also sadly note that in some cases performance regulations set up for low-speed aircraft are still being insisted upon for high-speed aircraft. One may hope that with the years these will be rescinded where inapplicable.

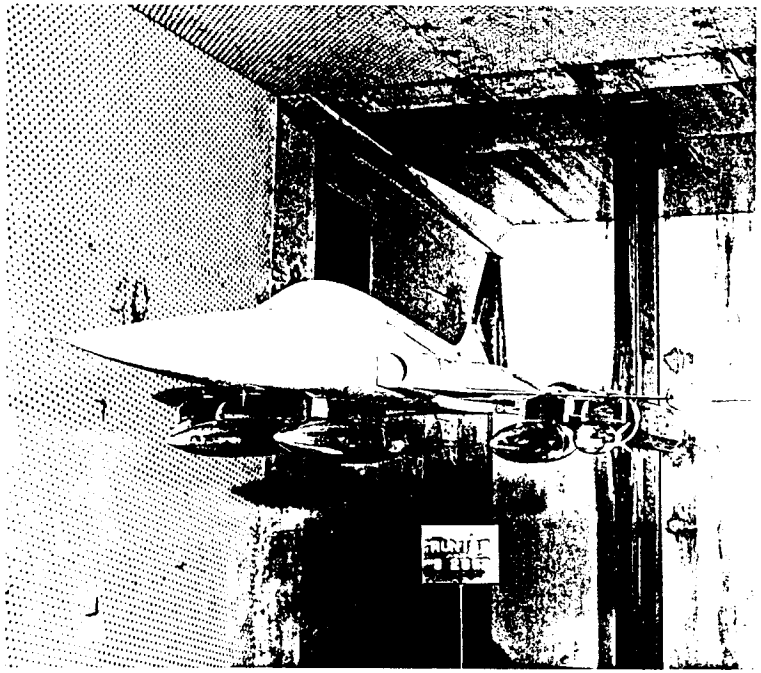


Fig. 9:23 Model during transonic drag study. (Courtesy Northrop Corporation.)

power is preferably accomplished by trimming to zero yaw. Nevertheless, for those inadvertent conditions—insufficient rudder power, battle damage, or a skidding maneuver—it is important to know that stability and control will remain. In turn, it becomes important to determine that obtaining stability and control in either trimmed unyawed flight or actual yawed flight is possible and may be obtained with the minimum drag penalty.

Table 9:3

Lateral-Directional Tests

Runs*	Configuration	Deflections	Hinge Moments	Root Bending	Remarks
1–36	*B, BK, BKN, BKNHE, BKNVR BKNWVRHE*	None	*F, A, H, E, R*	*W*	Airplane buildup
37–55	*BKNVRHE*	δ_V −5, 0, 5	*V*	*V*	Vertical-tail effectiveness
56–67	*BKNWVRHE*	δ_V −5, 5	*V*	*V*	Sidewash
68–86	*BKNWVRHE*	δ_R −5, −10, −15	–	–	Rudder effectiveness
122–158	*BKNWVRHE BKNWHE*	δ_A −10 to +20	*A*	*W*	Aileron power and effectiveness

* The run numbers allow for six angles of yaw: −15, −10, −5, 5, 10, 15.

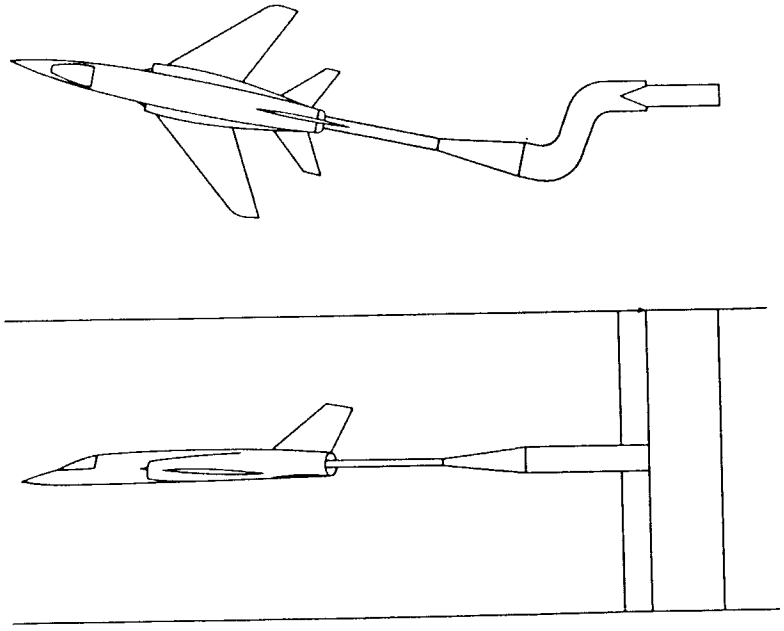


Fig. 9:24 Illustration of a bent support used to obtain longitudinal stability data with a yawed model, as well as directional stability data.

The lateral-directional program will be similar to Table 9:3. The ψ (angle of yaw, positive nose to the right) and α combinations depend upon the tunnel mechanism and should be arranged to obtain maximum angle coverage. Several procedures have been used according to the tunnel capabilities:

1. Using bent stings (Fig. 9:24) with split yaw adaptors so that yaw angles may be changed without breaking the balance and pressure leads.
2. Rolling the model and balance so that each position of the model pitch mechanism corresponds to a different value of ψ as well as α.
3. Employing a rig such that yaw, roll, and pitch may be set as desired (not commonly available).

In each case six-component data are taken at all Mach numbers.

AIRPLANE BUILDUP. The airplane buildup proceeds during yaw studies as during the runs in the pitch plane; the engineers evaluate each component in turn, and watch for anomalous slopes which would indicate flow separation. Hinge moment readings are taken on the flaps, ailerons, horizontal tail, elevators, and rudder, and root bending and shears are taken on the wing and horizontal tail.

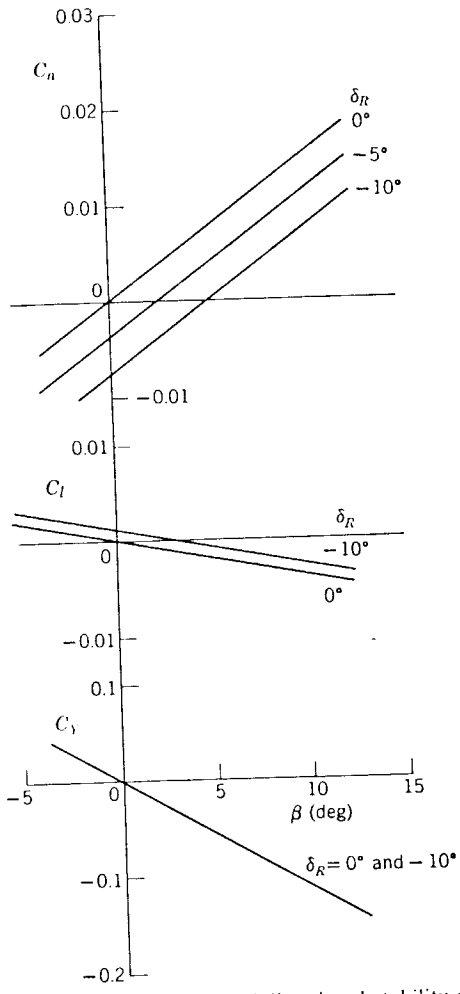


Fig. 9:25 A typical presentation of directional stability data.

DIRECTIONAL STABILITY AND CONTROL. During the yaw runs made for directional stability and control, the effectiveness of the vertical tail and rudder and their ability to trim a moment caused by asymmetrical power are evaluated. During these runs both the vertical tail and the rudder are deflected. The vertical-tail tests evaluate the slope of the vertical-tail lift curve, and hence determine whether it is performing as expected, rather than evaluating its use as a trim or control device. During these runs hinge moments on the surfaces and root bending moments are read. Plots of the directional data are illustrated in Fig. 9:25. The angle of yaw may

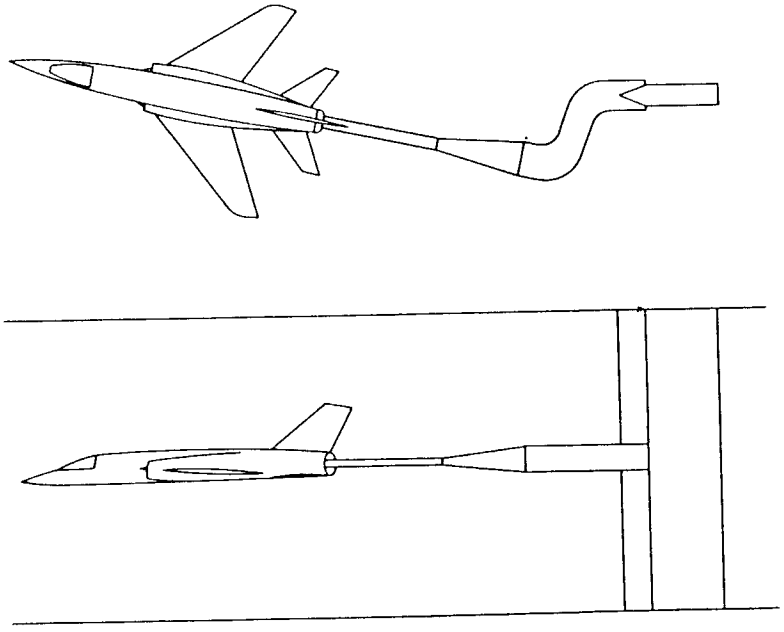


Fig. 9:24 Illustration of a bent support used to obtain longitudinal stability data with a yawed model, as well as directional stability data.

The lateral-directional program will be similar to Table 9:3. The ψ (angle of yaw, positive nose to the right) and α combinations depend upon the tunnel mechanism and should be arranged to obtain maximum angle coverage. Several procedures have been used according to the tunnel capabilities:

1. Using bent stings (Fig. 9:24) with split yaw adaptors so that yaw angles may be changed without breaking the balance and pressure leads.
2. Rolling the model and balance so that each position of the model pitch mechanism corresponds to a different value of ψ as well as α.
3. Employing a rig such that yaw, roll, and pitch may be set as desired (not commonly available).

In each case six-component data are taken at all Mach numbers.

AIRPLANE BUILDUP. The airplane buildup proceeds during yaw studies as during the runs in the pitch plane; the engineers evaluate each component in turn, and watch for anomalous slopes which would indicate flow separation. Hinge moment readings are taken on the flaps, ailerons, horizontal tail, elevators, and rudder, and root bending and shears are taken on the wing and horizontal tail.

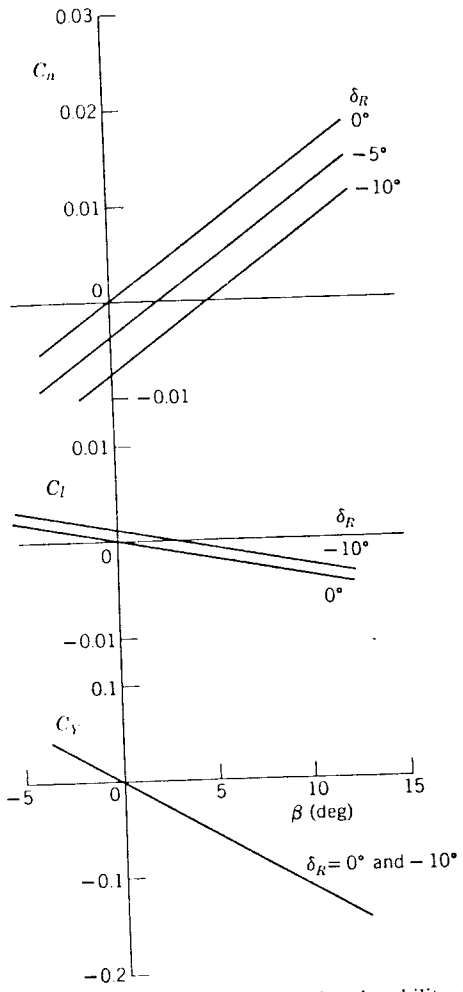


Fig. 9:25 A typical presentation of directional stability data.

DIRECTIONAL STABILITY AND CONTROL. During the yaw runs made for directional stability and control, the effectiveness of the vertical tail and rudder and their ability to trim a moment caused by asymmetrical power are evaluated. During these runs both the vertical tail and the rudder are deflected. The vertical-tail tests evaluate the slope of the vertical-tail lift curve, and hence determine whether it is performing as expected, rather than evaluating its use as a trim or control device. During these runs hinge moments on the surfaces and root bending moments are read. Plots of the directional data are illustrated in Fig. 9:25. The angle of yaw may

be indicated by ψ, which is positive for nose right, or β, which is positive for nose left. The aerodynamicist is primarily interested in the slope of the yawing moment curve $\partial C_n/\partial\beta$ (also called C_{n_β}), the rudder power parameter $\partial C_n/\partial\delta_R$ (also called $C_{n_{\delta R}}$), and the rudder angle required for trim at various values of sideslip.

AILERON POWER. The aileron tests encompass deflection of one aileron from say -10 to $+15$ deg throughout the range of yaw angles and Mach numbers. The purpose of deflecting only one stems from the normal procedure of using differential ailerons, i.e., different deflections of right and left aileron for a given stick deflection in order to reduce adverse yaw. During the tests, both the aileron hinge moments and the wing root bending moment will be recorded.

A knowledge of rolling moments due to aileron deflection is required for defining the maneuverability of the aircraft. This rolling moment in conjunction with the aircraft inertia about the roll axis allows the calculation of roll acceleration. In conjunction with aerodynamic damping moments due to rolling, it allows the calculation of maximum roll rate (see Section 7:17). Maximum required roll rates vary from 50 deg per second for a medium bomber to 150 deg per second for a highly maneuverable fighter. A knowledge of rolling moments is also required for defining the amount of aileron deflection required to trim out the rolling moment due to yawing. The aileron effectiveness parameter of interest to the

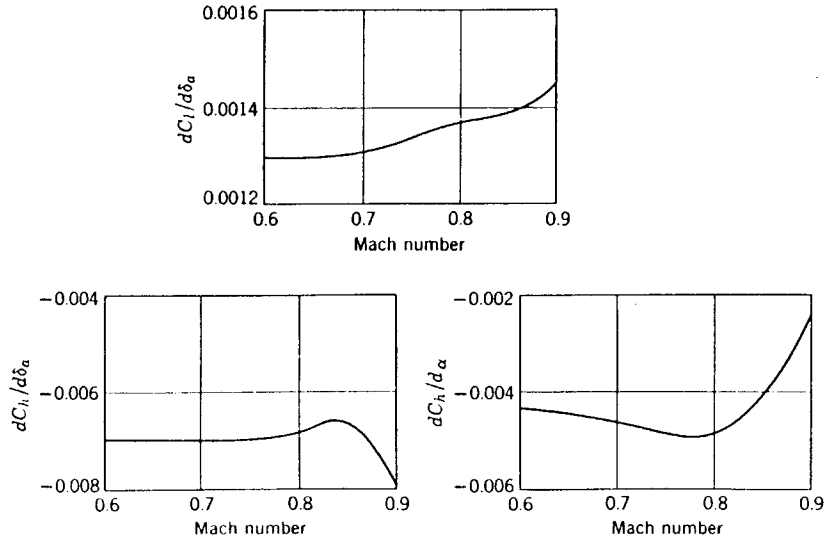


Fig. 9:26 Presentation of aileron power and hinge moment data. (Swept wing fighter.)

aerodynamicist is $\partial C_l/\partial\delta_a$, called $C_{l_{\delta a}}$. Figure 9:26 is a typical presentation of aileron data.

9:9 Reflection-Plane Testing

Since both aircraft and missiles have a plane of symmetry, in theory at least one should obtain satisfactory results by testing a half model on a reflection plane. Benefits one could expect include (1) A high Reynolds number owing to a larger model; (2) A cheaper model; (3) Elimination of sting or mounting strut interference; (4) Easy access for pressure leads; and (5) Simpler balances and oscillating rigs, since they may be outside the tunnel. In actual practice, our experiences with reflection-plane testing have been dolorous for all but items located well away from the reflection plane such as ailerons or engine nacelles. The difficulty is due mainly to the reflection-plane boundary layer, and to leakage around the model reflection-plane joint. Efforts to shim the model to get it out of the boundary layer reveal how sensitive the results are to minute changes, and how hopeless it is to be confident of the data. Figure 9:27 shows the comparison of reflection-plane and complete model testing for the nearsonic–high subsonic speed range; similar results have been found in the low supersonic range. Those considering reflection-plane tests should consult Ref. 9:6.

9:10 Testing for Dynamic Stability

Dynamic pitch tests are important in the transonic speed range, where dynamic instability is most likely to occur. They are most frequently made with all control surfaces set at zero angle of deflection, since damping moments are relatively insensitive to control surface deflection. With free oscillation dynamic pitch rigs, two types of dynamic stability tests in nearsonic and transonic tunnels are common. In one type the model is allowed to float freely as the tunnel speed is increased. The model itself or a visual signal from the model-attitude indicator is observed. The turbulence or vibrations of the tunnel will be high enough to cause the model to oscillate slightly. If a speed for dynamic instability is reached, the oscillations of the model will increase in amplitude rapidly. If such a point is reached, the model brake must be quickly applied to prevent oscillations from reaching destructive angles.

The second type of dynamic pitch testing, which is used at all speeds, is the following. The model brake is engaged while the desired tunnel operating speed is established. When steady flow has been achieved in the tunnel, the model brake is released, and the model is given a kick of perhaps 5 or 10 deg α by the displacement mechanism. The variation of model displacement with time is recorded. When this second technique

be indicated by ψ, which is positive for nose right, or β, which is positive for nose left. The aerodynamicist is primarily interested in the slope of the yawing moment curve $\partial C_n/\partial\beta$ (also called C_{n_β}), the rudder power parameter $\partial C_n/\partial\delta_R$ (also called $C_{n\,\delta R}$), and the rudder angle required for trim at various values of sideslip.

AILERON POWER. The aileron tests encompass deflection of one aileron from say -10 to $+15$ deg throughout the range of yaw angles and Mach numbers. The purpose of deflecting only one stems from the normal procedure of using differential ailerons, i.e., different deflections of right and left aileron for a given stick deflection in order to reduce adverse yaw. During the tests, both the aileron hinge moments and the wing root bending moment will be recorded.

A knowledge of rolling moments due to aileron deflection is required for defining the maneuverability of the aircraft. This rolling moment in conjunction with the aircraft inertia about the roll axis allows the calculation of roll acceleration. In conjunction with aerodynamic damping moments due to rolling, it allows the calculation of maximum roll rate (see Section 7:17). Maximum required roll rates vary from 50 deg per second for a medium bomber to 150 deg per second for a highly maneuverable fighter. A knowledge of rolling moments is also required for defining the amount of aileron deflection required to trim out the rolling moment due to yawing. The aileron effectiveness parameter of interest to the

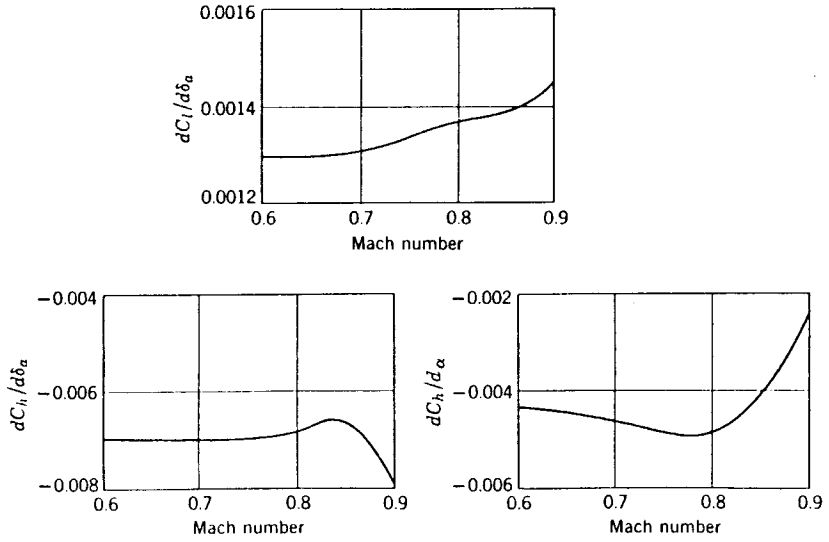


Fig. 9:26 Presentation of aileron power and hinge moment data. (Swept wing fighter.)

aerodynamicist is $\partial C_l/\partial\delta_a$, called $C_{l\,\delta a}$. Figure 9:26 is a typical presentation of aileron data.

9:9 Reflection-Plane Testing

Since both aircraft and missiles have a plane of symmetry, in theory at least one should obtain satisfactory results by testing a half model on a reflection plane. Benefits one could expect include (1) A high Reynolds number owing to a larger model; (2) A cheaper model; (3) Elimination of sting or mounting strut interference; (4) Easy access for pressure leads; and (5) Simpler balances and oscillating rigs, since they may be outside the tunnel. In actual practice, our experiences with reflection-plane testing have been dolorous for all but items located well away from the reflection plane such as ailerons or engine nacelles. The difficulty is due mainly to the reflection-plane boundary layer, and to leakage around the model reflection-plane joint. Efforts to shim the model to get it out of the boundary layer reveal how sensitive the results are to minute changes, and how hopeless it is to be confident of the data. Figure 9:27 shows the comparison of reflection-plane and complete model testing for the nearsonic–high subsonic speed range; similar results have been found in the low supersonic range. Those considering reflection-plane tests should consult Ref. 9:6.

9:10 Testing for Dynamic Stability

Dynamic pitch tests are important in the transonic speed range, where dynamic instability is most likely to occur. They are most frequently made with all control surfaces set at zero angle of deflection, since damping moments are relatively insensitive to control surface deflection. With free oscillation dynamic pitch rigs, two types of dynamic stability tests in nearsonic and transonic tunnels are common. In one type the model is allowed to float freely as the tunnel speed is increased. The model itself or a visual signal from the model-attitude indicator is observed. The turbulence or vibrations of the tunnel will be high enough to cause the model to oscillate slightly. If a speed for dynamic instability is reached, the oscillations of the model will increase in amplitude rapidly. If such a point is reached, the model brake must be quickly applied to prevent oscillations from reaching destructive angles.

The second type of dynamic pitch testing, which is used at all speeds, is the following. The model brake is engaged while the desired tunnel operating speed is established. When steady flow has been achieved in the tunnel, the model brake is released, and the model is given a kick of perhaps 5 or 10 deg α by the displacement mechanism. The variation of model displacement with time is recorded. When this second technique

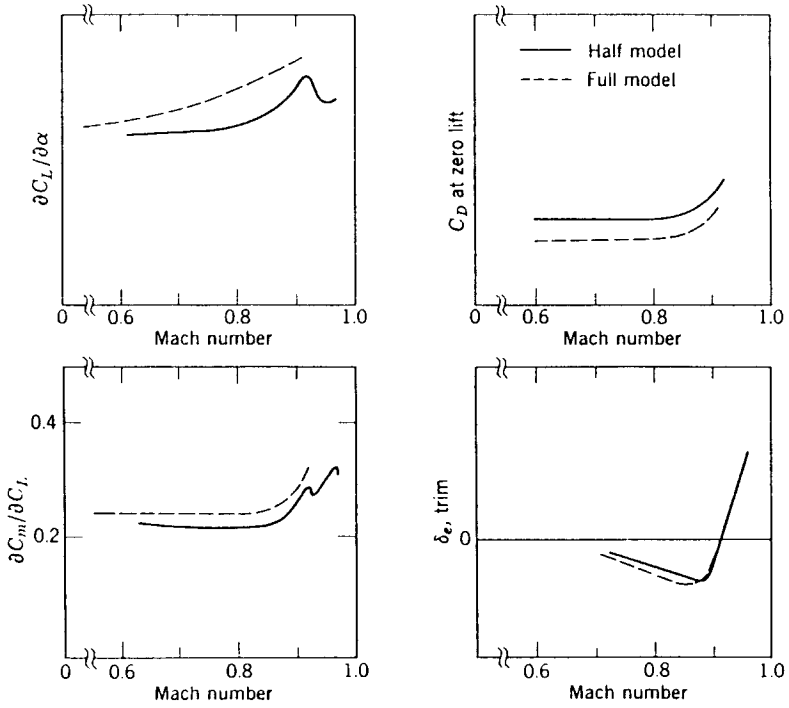


Fig. 9:27 Comparison of half model and complete model tests of F7U fighter. Ordinate values are available only for the moment data as shown. Redrawn from Ref. 9:6.

is used, the damping coefficient $(C_{mq} + C_{m\dot{\alpha}})$ is obtained as discussed in Section 7:16. It is noted that the value of M_α of eq. (7:29) is obtained from the slope $\partial C_m/\partial\alpha$ from force test data such as those illustrated in Fig. 9:18.

Forced oscillation dynamic stability tests are made in a manner similar to that for the second described free oscillation method. The model is locked in position while the tunnel speed is stabilized. The lock is then released and the forcing mechanism is energized. In forced oscillation tests the M_θ term of eq. (7:33) includes a moment-versus-displacement slope due to the spring action of the flexures, plus an aerodynamic moment slope from force test data such as those illustrated in Fig. 9:18. In flight, dynamic stability problems rarely occur at a constant velocity (as in tests made in a tunnel), and in relating tunnel tests to flight one should note that acceleration is stabilizing and deceleration, destabilizing. To understand how, for instance, the destabilization comes about during deceleration, consider a neutrally stable model oscillating at some particular

amplitude. After the model crosses through zero deflection it has an angular velocity that is resisted by aerodynamic restoring forces, which eventually reverse it and return it through zero, with an angular velocity that results in an equal swing on the other side. Now add a deceleration. The model swinging through zero meets a constantly decreasing dynamic pressure and takes longer to become turned around to swing back toward zero. It thus swings out to a greater amplitude, and on the next swing, meeting still lower restoring moments, executes a still-wider swing. The ensuing divergence is unstable rather than neutrally stable.

The loss of dynamic stability described above is particularly violent on vertically fired rockets, which besides being very rapidly decelerated after burnout, are proceeding into ever-less-dense air.

9:11 Testing for Buffet

Buffet is an unsteady flow phenomenon wherein intermittent boundary layer attachment and separation cause a local drumming. It is usually not catastrophic, but can be annoying and in some instances can lead to instrument or other failure through excessive vibration. Buffet arises when the flow is required to change direction abruptly, as near a wing root fillet or around a cone-cylinder juncture on a missile. Nearly all high-speed airplanes exhibit some degree of buffeting in the Mach number range of 0.80 to 0.95. The aerodynamicist is interested in determining the exact range of conditions for which buffeting exists on his particular airplane, in increasing the Mach number at which buffeting begins, and in reducing the severity of buffeting.

Several approaches have been used in the definition of operating conditions for which buffeting occurs in wind tunnel tests. These are (1) Measuring the bending moment of a wing by using strain gages along the region of attachment of the wing to the fuselage. When this technique is used, the buffet boundary is frequently defined as the point where the bending moment oscillations exceed 5 per cent of the mean level of the bending moment. For this criterion to be used, it is necessary for bending moment oscillations due to normal tunnel operation to be small relative to the 5 per cent figure. It is noted that a high-response instrument such as an oscillograph is required for monitoring wing bending moments for this purpose. (2) Measuring static pressures on the wing surface near the trailing edge and defining the buffet boundary as the point where the pressures oscillate by a specified amount, perhaps 10 per cent. (3) Placing small tabs along the trailing edge of the wing and defining the buffet boundary in terms of some magnitude of tab oscillation. (4) Monitoring the loads indicated by internal balance normal force gages and defining the buffet boundary in a manner similar to that described in (1); and (5)

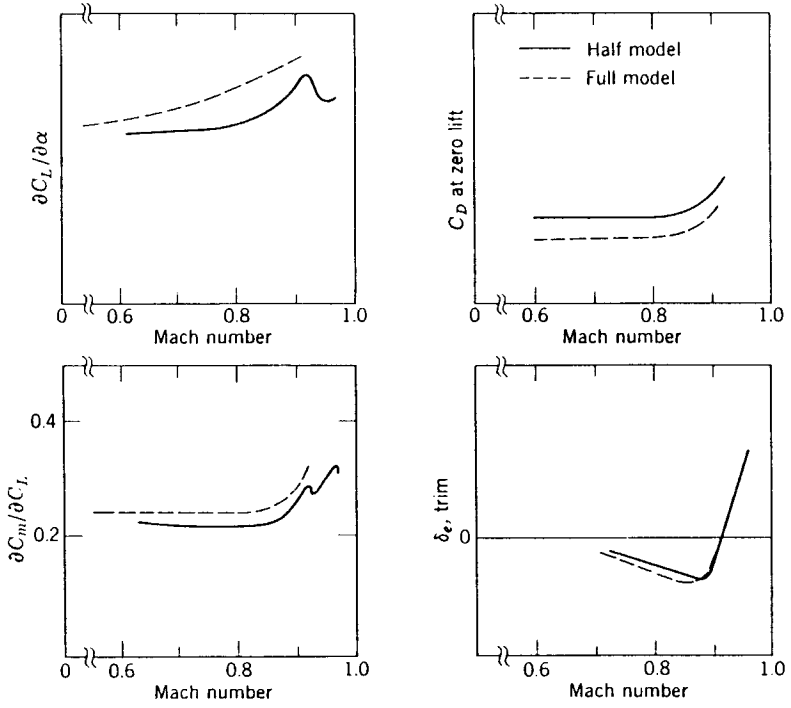


Fig. 9:27 Comparison of half model and complete model tests of F7U fighter. Ordinate values are available only for the moment data as shown. Redrawn from Ref. 9:6.

is used, the damping coefficient $(C_{mq} + C_{m\dot{\alpha}})$ is obtained as discussed in Section 7:16. It is noted that the value of M_α of eq. (7:29) is obtained from the slope $\partial C_m/\partial\alpha$ from force test data such as those illustrated in Fig. 9:18.

Forced oscillation dynamic stability tests are made in a manner similar to that for the second described free oscillation method. The model is locked in position while the tunnel speed is stabilized. The lock is then released and the forcing mechanism is energized. In forced oscillation tests the M_θ term of eq. (7:33) includes a moment-versus-displacement slope due to the spring action of the flexures, plus an aerodynamic moment slope from force test data such as those illustrated in Fig. 9:18. In flight, dynamic stability problems rarely occur at a constant velocity (as in tests made in a tunnel), and in relating tunnel tests to flight one should note that acceleration is stabilizing and deceleration, destabilizing. To understand how, for instance, the destabilization comes about during deceleration, consider a neutrally stable model oscillating at some particular

amplitude. After the model crosses through zero deflection it has an angular velocity that is resisted by aerodynamic restoring forces, which eventually reverse it and return it through zero, with an angular velocity that results in an equal swing on the other side. Now add a deceleration. The model swinging through zero meets a constantly decreasing dynamic pressure and takes longer to become turned around to swing back toward zero. It thus swings out to a greater amplitude, and on the next swing, meeting still lower restoring moments, executes a still-wider swing. The ensuing divergence is unstable rather than neutrally stable.

The loss of dynamic stability described above is particularly violent on vertically fired rockets, which besides being very rapidly decelerated after burnout, are proceeding into ever-less-dense air.

9:11 Testing for Buffet

Buffet is an unsteady flow phenomenon wherein intermittent boundary layer attachment and separation cause a local drumming. It is usually not catastrophic, but can be annoying and in some instances can lead to instrument or other failure through excessive vibration. Buffet arises when the flow is required to change direction abruptly, as near a wing root fillet or around a cone-cylinder juncture on a missile. Nearly all high-speed airplanes exhibit some degree of buffeting in the Mach number range of 0.80 to 0.95. The aerodynamicist is interested in determining the exact range of conditions for which buffeting exists on his particular airplane, in increasing the Mach number at which buffeting begins, and in reducing the severity of buffeting.

Several approaches have been used in the definition of operating conditions for which buffeting occurs in wind tunnel tests. These are (1) Measuring the bending moment of a wing by using strain gages along the region of attachment of the wing to the fuselage. When this technique is used, the buffet boundary is frequently defined as the point where the bending moment oscillations exceed 5 per cent of the mean level of the bending moment. For this criterion to be used, it is necessary for bending moment oscillations due to normal tunnel operation to be small relative to the 5 per cent figure. It is noted that a high-response instrument such as an oscillograph is required for monitoring wing bending moments for this purpose. (2) Measuring static pressures on the wing surface near the trailing edge and defining the buffet boundary as the point where the pressures oscillate by a specified amount, perhaps 10 per cent. (3) Placing small tabs along the trailing edge of the wing and defining the buffet boundary in terms of some magnitude of tab oscillation. (4) Monitoring the loads indicated by internal balance normal force gages and defining the buffet boundary in a manner similar to that described in (1); and (5)

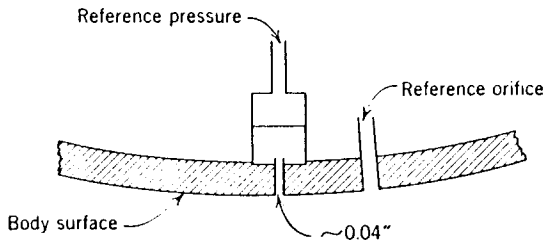


Fig. 9:28 Transducer installation for buffet study.

Accepting the break in the lift curve (the plot of C_L versus angle of attack) as the buffet boundary, inasmuch as the break is usually attributed to flow separation.

The methods described in items (2) and (3) leave a lot to be desired in that their effectiveness depends on the proper location of the pressure orifices or tabs. The method described in item (1) is not always adequate because the buffeting may be due to external bombs, fuel tanks, rockets, or other appendages that are attached to the fuselage instead of the wing, or it may be due to an unsteady downwash field acting on the tail. Method (4) at least has the advantage of pointing up a disturbance that will be of major concern to the crew and airframe.

Despite their disadvantages, pressure measurements are widely used. The hopefully-well-located pressure orifice is led to one side of a transducer, and a reference pressure (usually tunnel static pressure or pressure from a nearby orifice on the aircraft damped by running it through 40 or 50 feet of tubing) is fed to the other (Fig. 9:28). The tests consist of measuring both the static and fluctuating pressure over the Mach range as defined by flight conditions. In defining buffet a time-average pressure coefficient is defined as

$$C_p = \frac{p_{t,s} - p}{q} \tag{9:3}$$

where $p_{t,s} = \dfrac{1}{T}\displaystyle\int_0^T p_{t,u}\, dT$ lb/ft^2,

T = specific period of time, sec,

$p_{t,u}$ = unsteady pressure on model surface, lb/ft,^{2}

T = time, sec,

p = freestream static pressure, lb/ft^2,

q = freestream dynamic pressure, lb/ft^2.

The coefficient of the root-mean-square fluctuations of pressure about the time average is

$$(\Delta C_p)_{\text{rms}} = \frac{1}{q}\left[\frac{1}{T}\int_0^T (p_{t,u} - p_{t,s})^2\, dT\right]^{1/2} \tag{9:4}$$

The power spectral density of the fluctuating pressures is given by

$$\phi = \frac{(\text{psi})^2}{\text{cps}}$$

where psi = peak-to-peak pressure differential, psi,
cps = cycles per second of pressure oscillation.
Both the power spectral density and the frequency may be brought up to full-scale values by

$$\phi_{fs} = \phi_m \frac{q_{fs}^2}{q_m^2}\frac{D_{fs}}{D_m}\frac{V_m}{V_{fs}} \tag{9:5}$$

and

$$f_{fs} = f_m \frac{D_m}{D_{fs}}\frac{V_{fs}}{V_m} \tag{9:6}$$

where V = velocity, fps,
D = diameter or typical dimension, ft.
The subscript fs means full scale, and m means model. The values of dynamic pressure and velocity for the full-scale conditions must be obtained from the computed trajectory or flight condition at a point corresponding to the test Mach number. Equation (9:6) shows that model frequencies are higher than those of full scale.

The data may be presented as

(1) Curves of root-mean-square pressure coefficients against Mach number for constant angles of attack, using a separate curve for each transducer. One may expect peaks near $M = 1.0$.

(2) Plots of static and fluctuating (rms) pressure coefficients against model station for constant Mach number and selected angles of attack.

(3) Plots of power spectrum against frequency for constant Mach number. Here we typically find very small values of ϕ_{fs} above 20 cps.

The engineer will be interested in

(1) The frequency and intensity of full-scale buffet and its location. In assuring himself of a safe structure, he will take into account the time (i.e., number of cycles) his craft will be subjected to the buffet load as it passes through a critical Mach number region. For this he will scale the model pressure–time history according to

$$\Delta T_{fs} = \Delta T_m \frac{D_{fs}}{D_m}\frac{V_m}{V_{fs}} \tag{9:7}$$

where ΔT is the time per cycle.

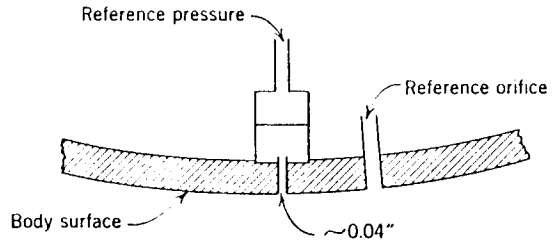


Fig. 9:28 Transducer installation for buffet study.

Accepting the break in the lift curve (the plot of C_L versus angle of attack) as the buffet boundary, inasmuch as the break is usually attributed to flow separation.

The methods described in items (2) and (3) leave a lot to be desired in that their effectiveness depends on the proper location of the pressure orifices or tabs. The method described in item (1) is not always adequate because the buffeting may be due to external bombs, fuel tanks, rockets, or other appendages that are attached to the fuselage instead of the wing, or it may be due to an unsteady downwash field acting on the tail. Method (4) at least has the advantage of pointing up a disturbance that will be of major concern to the crew and airframe.

Despite their disadvantages, pressure measurements are widely used. The hopefully-well-located pressure orifice is led to one side of a transducer, and a reference pressure (usually tunnel static pressure or pressure from a nearby orifice on the aircraft damped by running it through 40 or 50 feet of tubing) is fed to the other (Fig. 9:28). The tests consist of measuring both the static and fluctuating pressure over the Mach range as defined by flight conditions. In defining buffet a time-average pressure coefficient is defined as

$$C_p = \frac{p_{t,s} - p}{q} \tag{9:3}$$

where $p_{t,s} = \dfrac{1}{T}\displaystyle\int_0^T p_{t,u}\, dT$ lb/ft^2,

T = specific period of time, sec,

$p_{t,u}$ = unsteady pressure on model surface, lb/ft,^{2}

T = time, sec,

p = freestream static pressure, lb/ft^2,

q = freestream dynamic pressure, lb/ft^2.

The coefficient of the root-mean-square fluctuations of pressure about the time average is

$$(\Delta C_p)_{\text{rms}} = \frac{1}{q}\left[\frac{1}{T}\int_0^T (p_{t,u} - p_{t,s})^2\, dT\right]^{1/2} \tag{9:4}$$

The power spectral density of the fluctuating pressures is given by

$$\phi = \frac{(\text{psi})^2}{\text{cps}}$$

where psi = peak-to-peak pressure differential, psi,
cps = cycles per second of pressure oscillation.
Both the power spectral density and the frequency may be brought up to full-scale values by

$$\phi_{fs} = \phi_m \frac{q_{fs}^2}{q_m^2}\frac{D_{fs}}{D_m}\frac{V_m}{V_{fs}} \tag{9:5}$$

and

$$f_{fs} = f_m \frac{D_m}{D_{fs}}\frac{V_{fs}}{V_m} \tag{9:6}$$

where V = velocity, fps,
D = diameter or typical dimension, ft.
The subscript fs means full scale, and m means model. The values of dynamic pressure and velocity for the full-scale conditions must be obtained from the computed trajectory or flight condition at a point corresponding to the test Mach number. Equation (9:6) shows that model frequencies are higher than those of full scale.

The data may be presented as

(1) Curves of root-mean-square pressure coefficients against Mach number for constant angles of attack, using a separate curve for each transducer. One may expect peaks near $M = 1.0$.

(2) Plots of static and fluctuating (rms) pressure coefficients against model station for constant Mach number and selected angles of attack.

(3) Plots of power spectrum against frequency for constant Mach number. Here we typically find very small values of ϕ_{fs} above 20 cps.

The engineer will be interested in

(1) The frequency and intensity of full-scale buffet and its location. In assuring himself of a safe structure, he will take into account the time (i.e., number of cycles) his craft will be subjected to the buffet load as it passes through a critical Mach number region. For this he will scale the model pressure–time history according to

$$\Delta T_{fs} = \Delta T_m \frac{D_{fs}}{D_m}\frac{V_m}{V_{fs}} \tag{9:7}$$

where ΔT is the time per cycle.

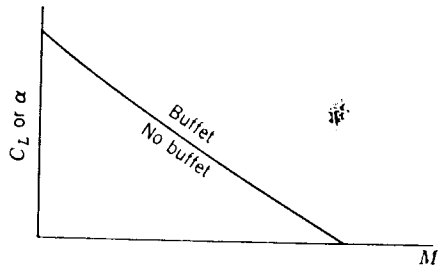


Fig. 9:29 Typical buffet zone variation with Mach number and angle of attack.

(2) The noise in decibels to which the craft will be subjected. This may be computed according to

$$p = (\Delta C_p)_{\text{rms}} \times q \tag{9:8}$$

and

$$\text{Noise level in decibels} = 20 \log_{10} \frac{p}{p_0} \tag{9:9}$$

where $p_o = 4.18 \times 10^{-7}$, lb/ft².
A value of $0.006q$ is sometimes taken as the noise from a turbulent boundary layer. The scaling up of values using eqs. (9:5), (9:6), and (9:7) may be done with confidence.

Example 9:1 The dynamic pressure 55 sec after lift-off is 690 lb/ft². What noise in decibels would be expected (a) from the turbulent boundary layer and (b) from $(\Delta C_p)_{\text{rms}} = 0.16$

(a) $p = 0.006q = 4.14$ lb/ft²

$$\text{Decibels} = 20 \log_{10} \frac{4.14}{4.18 \times 10^{-7}} = 140.0$$

(b)
$$\text{Decibels} = 20 \log_{10} \frac{0.16 \times 690}{4.18 \times 10^{-7}} = 168.4$$

The presentation of a typical buffet boundary for an airplane is illustrated in Fig. 9:29. Further data covering these types of tests are in Ref. 9:7.

9:12 Testing for Hinge Moments

The aerodynamic moments of control and other surfaces (landing gear doors, etc.) about their hinge lines, called hinge moments, must be determined for the design of the surface, its support, and its actuating mechanism. Hinge moment tests are made for all the conditions of the longitudinal and lateral-directional tests. When conditions require it, the hinge moment tests may be made separately from the stability and control tests.

On small, low-speed aircraft a lot of effort is expended to ensure that the hinge moments will be small enough for the pilot to handle manually, and also that they will increase continuously with effectiveness of the control. Efforts along this line have continued into the range of higher-speed and larger aircraft, though the emphasis is considerably reduced. Power boost systems are now used to multiply the work supplied by the pilot to deflect controls. "Artificial feel" systems are used to provide the pilot with the sensation of a consistent relation between the hinge moment and control effectiveness.

The total hinge moment and hence the size of its support and actuating mechanism can be reduced by "balanced controls" or "tabs." Balanced controls have a portion of their lifting surface ahead of the hinge line. Tabs are small lifting devices at the trailing edge of a control which are deflected in a direction opposite to that of the main surface. They may be differentially linked to the control so that the pilot's deflection of the control causes an opposite tab deflection. Also, they may be arranged so that the pilot deflects the tab, which in turn deflects the control by its aerodynamic moment. With the latter arrangement it is extremely important that the pilot have some emergency means of deflecting the control as well as the tab. One new transport was lost when the control surface and tabs were stalled and all longitudinal control effectiveness was lost.

9:13 Testing Speed Brakes

Nearly all high-speed aircraft require speed brakes both to reduce speed and to permit a steeper glide angle. The designer seeks adequate braking and minimum buffeting. Above all, the trim change, if any, should be *nose up* and small. Secondary effects on nearby surfaces may also be checked.

Speed brakes may be split trailing edges or flush panels which emerge from fuselage or wing. Readings are made of the usual six components of force and moment, of brake hinge moments, and in many cases of several surface pressures for defining local loads.

It is advisable to include a few runs, maximum and minimum dynamic pressure, for instance, with the brakes on one side undeflected and with full deflection on the other. This unintentional condition should be within the capability of the controls to trim out.

9:14 Testing for Aeroelastic Effects

Although the wind tunnel engineer may only rarely be called upon to design a high-speed model having bending and torsional stiffness similar to that of a proposed full-scale airplane or missile, he should realize that the all-steel model he will test will be far stiffer than the "real thing," and

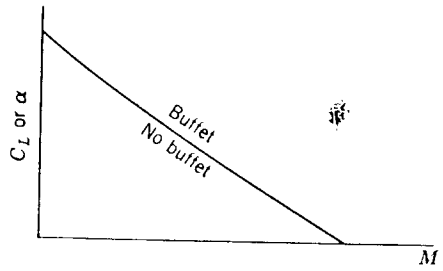


Fig. 9:29 Typical buffet zone variation with Mach number and angle of attack.

(2) The noise in decibels to which the craft will be subjected. This may be computed according to

$$p = (\Delta C_p)_{\text{rms}} \times q \tag{9:8}$$

and

$$\text{Noise level in decibels} = 20 \log_{10} \frac{p}{p_0} \tag{9:9}$$

where $p_o = 4.18 \times 10^{-7}$, lb/ft².
A value of $0.006q$ is sometimes taken as the noise from a turbulent boundary layer. The scaling up of values using eqs. (9:5), (9:6), and (9:7) may be done with confidence.

Example 9:1 The dynamic pressure 55 sec after lift-off is 690 lb/ft². What noise in decibels would be expected (a) from the turbulent boundary layer and (b) from $(\Delta C_p)_{\text{rms}} = 0.16$

(a) $p = 0.006q = 4.14$ lb/ft²

$$\text{Decibels} = 20 \log_{10} \frac{4.14}{4.18 \times 10^{-7}} = 140.0$$

(b)
$$\text{Decibels} = 20 \log_{10} \frac{0.16 \times 690}{4.18 \times 10^{-7}} = 168.4$$

The presentation of a typical buffet boundary for an airplane is illustrated in Fig. 9:29. Further data covering these types of tests are in Ref. 9:7.

9:12 Testing for Hinge Moments

The aerodynamic moments of control and other surfaces (landing gear doors, etc.) about their hinge lines, called hinge moments, must be determined for the design of the surface, its support, and its actuating mechanism. Hinge moment tests are made for all the conditions of the longitudinal and lateral-directional tests. When conditions require it, the hinge moment tests may be made separately from the stability and control tests.

On small, low-speed aircraft a lot of effort is expended to ensure that the hinge moments will be small enough for the pilot to handle manually, and also that they will increase continuously with effectiveness of the control. Efforts along this line have continued into the range of higher-speed and larger aircraft, though the emphasis is considerably reduced. Power boost systems are now used to multiply the work supplied by the pilot to deflect controls. "Artificial feel" systems are used to provide the pilot with the sensation of a consistent relation between the hinge moment and control effectiveness.

The total hinge moment and hence the size of its support and actuating mechanism can be reduced by "balanced controls" or "tabs." Balanced controls have a portion of their lifting surface ahead of the hinge line. Tabs are small lifting devices at the trailing edge of a control which are deflected in a direction opposite to that of the main surface. They may be differentially linked to the control so that the pilot's deflection of the control causes an opposite tab deflection. Also, they may be arranged so that the pilot deflects the tab, which in turn deflects the control by its aerodynamic moment. With the latter arrangement it is extremely important that the pilot have some emergency means of deflecting the control as well as the tab. One new transport was lost when the control surface and tabs were stalled and all longitudinal control effectiveness was lost.

9:13 Testing Speed Brakes

Nearly all high-speed aircraft require speed brakes both to reduce speed and to permit a steeper glide angle. The designer seeks adequate braking and minimum buffeting. Above all, the trim change, if any, should be *nose up* and small. Secondary effects on nearby surfaces may also be checked.

Speed brakes may be split trailing edges or flush panels which emerge from fuselage or wing. Readings are made of the usual six components of force and moment, of brake hinge moments, and in many cases of several surface pressures for defining local loads.

It is advisable to include a few runs, maximum and minimum dynamic pressure, for instance, with the brakes on one side undeflected and with full deflection on the other. This unintentional condition should be within the capability of the controls to trim out.

9:14 Testing for Aeroelastic Effects

Although the wind tunnel engineer may only rarely be called upon to design a high-speed model having bending and torsional stiffness similar to that of a proposed full-scale airplane or missile, he should realize that the all-steel model he will test will be far stiffer than the "real thing," and

he should have some understanding of how his data will be used by the aero structures engineer.

Aeroelastic effects are *steady state* (loss of control, control reversal, and reduction of lift and stability) or *dynamic* (flutter and buzz). The effects are in general worsened by reducing the thickness of lifting surfaces, flying at higher dynamic pressures, and aerodynamic heating. They are helped by using materials of higher modulus of elasticity such as titanium.

The steady-state difficulties may be divided into (1) torsional and (2) bending. The upward load of a down aileron at the wing trailing edge twists the wing so that the leading edge goes down, reducing the wing lift until finally down aileron yields a net downward force and right stick results in left roll, a disconcerting maneuver. This is a dynamic pressure effect, but probably the structures engineer will want it plotted against velocity or Mach number so that he may talk of an "aileron reversal speed." If aileron reversal occurs in the flight regime, it may be cured by increasing the wing torsional stiffness, or, if that is impractical, by moving the aileron inboard. Some modern jet transports have both inboard and outboard ailerons, the outer ones being disconnected during high-speed flight. A loss in elevator effectiveness can occur as a result of the same twisting action of the elevator on the horizontal tail. Here the cure must come from increased torsional stiffness.

A loss in lift curve slope proportional to q and amounting to as much as 25 per cent can also arise out of the twisting due to bending of a swept or delta wing under load. One may also encounter a 3 to 5 per cent forward movement of the wing center of pressure, although the changes in lift and center of pressure tend to cancel so there may be little change in trim. There may also be a decrease in elevator deflection required per G of acceleration.

The dynamic aeroelastic effect of flutter depends on the flexural and dynamic characteristics (inertia, natural frequency, mass) of a wing or fin in both bending and torsion, as well as the aerodynamic loading. Under the proper combination of these characteristics a disturbance will start an oscillation which rapidly increases in amplitude and which almost always destroys the wing or fin. Wind tunnel testing to define conditions for flutter is extremely important but is not widely practiced.

Unless a flexible model is provided, all this may make little difference to the wind tunnel engineer except to increase the number of runs to cover ailerons of various span.

9:15 List of Transonic Wind Tunnels

Table 9:4 gives a partial list of the transonic wind tunnels in this country and around the world.

Table 9:4

Transonic Wind Tunnels

Organization	Tunnel	Location	Type	Mach Number Range	Test Section Size	Remarks
A. GOVERNMENT						
AEDC	Transonic model tunnel	Tullahoma, Tenn.	Continuous	0.55–1.5	12″ × 12″	
AEDC	PWT	Tullahoma, Tenn.	Continuous	0.5–1.6	16′ × 16′	100,000 hp
DTMB	7 × 10-foot	Carderock, Md.	Continuous	0.3–1.17	7′ × 10′	27,000 hp
NASA, Ames	1 × 3½-foot	Moffett Field, Calif.	Continuous	0.5–1.1	12″ × 35″	
NASA, Ames	2 × 2-foot	Moffett Field, Calif.	Continuous	0–1.4	2′ × 2′	
NASA, Ames	14-foot	Moffett Field, Calif.	Continuous	0.6–1.2	13.5′ × 13.5′	
NASA, Ames	6 × 6-foot	Moffett Field, Calif.	Continuous	0.65–2.2	6′ × 6′	
NASA, Ames	11 × 11-foot	Moffett Field, Calif.	Continuous	0.7–1.4	11′ × 11′	200,000 hp
NASA, Ames	16-foot	Moffett Field, Calif.	Continuous	0–0.95	16′ round	27,000 hp
NASA, Ames	12-foot	Moffett Field, Calif.	Continuous	0–0.97	12′ round	11,000 hp
NASA, Langley	Aero-elasticity	Langley Field, Va.	Continuous	0–1.2	24″ × 24″	
NASA, Langley	22-inch transonic	Langley Field, Va.	Indraft	0.5–1.4	20″ octagonal	

he should have some understanding of how his data will be used by the aero structures engineer.

Aeroelastic effects are *steady state* (loss of control, control reversal, and reduction of lift and stability) or *dynamic* (flutter and buzz). The effects are in general worsened by reducing the thickness of lifting surfaces, flying at higher dynamic pressures, and aerodynamic heating. They are helped by using materials of higher modulus of elasticity such as titanium.

The steady-state difficulties may be divided into (1) torsional and (2) bending. The upward load of a down aileron at the wing trailing edge twists the wing so that the leading edge goes down, reducing the wing lift until finally down aileron yields a net downward force and right stick results in left roll, a disconcerting maneuver. This is a dynamic pressure effect, but probably the structures engineer will want it plotted against velocity or Mach number so that he may talk of an "aileron reversal speed." If aileron reversal occurs in the flight regime, it may be cured by increasing the wing torsional stiffness, or, if that is impractical, by moving the aileron inboard. Some modern jet transports have both inboard and outboard ailerons, the outer ones being disconnected during high-speed flight. A loss in elevator effectiveness can occur as a result of the same twisting action of the elevator on the horizontal tail. Here the cure must come from increased torsional stiffness.

A loss in lift curve slope proportional to q and amounting to as much as 25 per cent can also arise out of the twisting due to bending of a swept or delta wing under load. One may also encounter a 3 to 5 per cent forward movement of the wing center of pressure, although the changes in lift and center of pressure tend to cancel so there may be little change in trim. There may also be a decrease in elevator deflection required per G of acceleration.

The dynamic aeroelastic effect of flutter depends on the flexural and dynamic characteristics (inertia, natural frequency, mass) of a wing or fin in both bending and torsion, as well as the aerodynamic loading. Under the proper combination of these characteristics a disturbance will start an oscillation which rapidly increases in amplitude and which almost always destroys the wing or fin. Wind tunnel testing to define conditions for flutter is extremely important but is not widely practiced.

Unless a flexible model is provided, all this may make little difference to the wind tunnel engineer except to increase the number of runs to cover ailerons of various span.

9:15 List of Transonic Wind Tunnels

Table 9:4 gives a partial list of the transonic wind tunnels in this country and around the world.

Table 9:4

Transonic Wind Tunnels

Organization	Tunnel	Location	Type	Mach Number Range	Test Section Size	Remarks
A. GOVERNMENT						
AEDC	Transonic model tunnel	Tullahoma, Tenn.	Continuous	0.55–1.5	12″ × 12″	
AEDC	PWT	Tullahoma, Tenn.	Continuous	0.5–1.6	16′ × 16′	100,000 hp
DTMB	7 × 10-foot	Carderock, Md.	Continuous	0.3–1.17	7′ × 10′	27,000 hp
NASA, Ames	1 × 3½-foot	Moffett Field, Calif.	Continuous	0.5–1.1	12″ × 35″	
NASA, Ames	2 × 2-foot	Moffett Field, Calif.	Continuous	0–1.4	2′ × 2′	
NASA, Ames	14-foot	Moffett Field, Calif.	Continuous	0.6–1.2	13.5′ × 13.5′	
NASA, Ames	6 × 6-foot	Moffett Field, Calif.	Continuous	0.65–2.2	6′ × 6′	
NASA, Ames	11 × 11-foot	Moffett Field, Calif.	Continuous	0.7–1.4	11′ × 11′	200,000 hp
NASA, Ames	16-foot	Moffett Field, Calif.	Continuous	0–0.95	16′ round	27,000 hp
NASA, Ames	12-foot	Moffett Field, Calif.	Continuous	0–0.97	12′ round	11,000 hp
NASA, Langley	Aero-elasticity	Langley Field, Va.	Continuous	0–1.2	24″ × 24″	
NASA, Langley	22-inch transonic	Langley Field, Va.	Indraft	0.5–1.4	20″ octagonal	

Table 9:4 (*continued*)

Organization	Tunnel	Location	Type	Mach Number Range	Test Section Size	Remarks
			A. GOVERNMENT			
NASA, Langley	26-inch blowdown	Langley Field, Va.	Blowdown	0.6–1.4	26″ octagonal	
NASA, Langley	Transonic-dynamic	Langley Field, Va.	Continuous	0.01–1.0	16′ × 16′	20,000 hp
NASA, Langley	16-foot	Langley Field, Va.	Continuous	0.2–1.3	15.5′ octagonal	60,000 hp
NASA, Langley	Transonic pressure	Langley Field, Va.	Continuous	0–1.2	86″ × 86″	25,000 hp
NASA, Langley	8-foot transonic	Langley Field, Va.	Continuous	0–1.28	87″ dodecagonal	16,000 hp
NASA, Langley	7 × 10-foot transonic	Langley Field, Va.	Continuous	0–1.2	6.6′ × 9.6′	10,000 hp
NASA, Lewis	8 × 6-foot	Cleveland, Ohio	Continuous	0.8–2.1	8′ × 6′	
NASA, Marshall	Trisonic	Huntsville, Ala.	Blowdown	0.4–4.0	14″ × 14″	
Naval Ordnance Lab.	No. 1	White Oak, Md.	Indraft	0.2–1.3	16″ × 16″	
Naval Ordnance Lab.	No. 2	White Oak, Md.	Blowdown	0.2–1.3	16″ × 16″	
Sandia Corp.	Trisonic	Albuquerque, N.M.	Blowdown	0.4–3.0	12″ × 12″	
USNMC	Transonic	Pt. Mugu, Calif.	Continuous	0.5–1.6	16″ × 16″	15,400 hp
			B. COLLEGES AND INDUSTRY			
Boeing Co.	Transonic	Seattle, Wash.	Continuous	0–1.3	8′ × 12′	54,000 hp
Cornell Aero Lab.	Transonic	Buffalo, N.Y.	Continuous	1.3	8′ × 8′	
Convair	Transonic	San Diego, Calif.	Blowdown	0.5–2.0	4′ × 4′	
Douglas Aircraft Corp.	Trisonic	El Segundo, Calif.	Blowdown	0.2–4.8	12″ × 12″	
Fluidyne	20-inch	Minneapolis, Minn.	Indraft	1.35	20″ × 22″	600
Ling-Temco-Vought Corp.	High-speed tunnel	Dallas, Tex.	Blowdown	0.2–1.8	4′ × 4′	
MIT	Transonic	Cambridge, Mass.	Blowdown	0.7–1.3	22″ octagonal	
MIT	Naval supersonic tunnel	Cambridge, Mass.	Continuous	0.8–1.2	18″ × 18″	
McDonnell Aircraft	Polysonic	St. Louis, Mo.	Blowdown	0.5–5.0	4′ × 4′	
University of Minnesota	Transonic	Rosemount, Minn.	Continuous	0–1.2	16″ × 16″	
North American Aviation	Trisonic	Inglewood, Calif.	Blowdown	0.2–3.5	7′ × 7′	
Ohio State University	Transonic	Columbus, Ohio	Blowdown	0–1.5	12″ × 12″	
Republic Aviation	Transonic	Farmingdale, N.Y.	Blowdown	1.4	26″ octagonal	
United Aircraft Corp.	17-inch	East Hartford, Conn.	Blowdown	0.5–1.5	17″ × 17″	
United Aircraft Corp.	8-foot	East Hartford, Conn.	Continuous	0–0.90	8′ octagonal	7,000 hp

Table 9:4 (*continued*)

Organization	Tunnel	Location	Type	Mach Number Range	Test Section Size	Remarks
			C. FOREIGN			
ARA	Transonic	Bedford England	Continuous	0.3–1.4	8′ × 9′	38,000 hp
ARA	Transonic	Bedford, England	Continuous	1.6	27″ × 30″	
ARA	8-foot	Bedford, England	Continuous	0.7–1.6	8′ × 8′	30,000 hp
ARC	Transonic	Melbourne, Australia	Continuous	0–1.3	25″ × 32″	
ARL	10-inch	Whitley, England	Blowdown	0.2–1.2	8″ × 10″	
ARL	24-inch	Whitley, England	Continuous	0.3–1.25	20″ × 24″	10,000 hp
Armstrong-Whitworth	18-inch	Coventry, England	Continuous	0.8–1.6	18″ × 14″	18,000 hp
BAC	4-foot	Wharton, England	Blowdown	0–1.7	18″ × 18″	
DeHaviland	Transonic	Hatfield, England	Continuous blow-down	1.3	24″ × 24″	Three ghosts*
DVL	Cascade tunnel	Braunschweig, Germany	Continuous	1.1	—	1300 kw
English Electric	Transonic	Wharton, England	Continuous blow-down	1.1	12″ × 12″	One Nene*
English Electric	Transonic	Wharton, England	Blowdown	1.6	18″ × 18″	
FFA	Transonic	Stockholm, Sweden	Continuous	1.3	35″ × 35″	
Handley-Page	Nearsonic	Radlett, England	Continuous indraft	1.0	3′ × 4′	Three Nenes*
Hawker-Siddeley	Transonic	Coventry, England	Indraft	1.6	8″ × 10″	
KTH	13-inch	Stockholm, Sweden	Indraft	1.8	13″ × 13″	270 hp
NAE	Transonic	Bedford, England	Continuous	1.3	8′ × 9′	38,000 hp
NAL	7-inch	Tokyo, Japan	Continuous	1.4	7″ × 7″	530kw
NLRL	Transonic	Amsterdam, Netherlands	Continuous	0–1.3	5′4″ × 6′8″	20,000 hp
NLRL	Small transonic	Amsterdam, Netherlands	Continuous	0–1.0	18″ × 18″	1500 hp
NPL	9-inch	Teddington, England	Indraft	1.8	9.5″ × 9.5″	
NPL	20-inch	Teddington, England	Indraft	1.6	8″ × 20″	
ONERA	S3CH	Chalais-Meudon, France	Continuous	0.1–1.1	39″ round	2000 kw
ONERA	S1MA	Modane, France	Continuous	0.2–1.03	25′ round	110,000 hp
RAE	2-foot	Farnborough, England	Continuous	1.4	18″ × 24″	8000 hp
RAE	3-foot	Bedford, England	—	1.25	3′ × 3′	
RAE	35-inch	Bedford, England	—	1.2	27″ × 35″	
RAE	6 × 8	Farnborough, England	Continuous	1.2	6′ × 8′	20,000 hp
Saab	Transonic	Linkoping, Sweden	Open circuit	0–1.4	2.3′ × 3.3′	Four DH Goblins
SNECMA	Nearsonic	Villaroche, France	Blowdown	0.97	13″ × 22″	
Short Bros.	Transonic	Belfast, N. Ireland	—	1.2	30″ × 30″	
Sud-Aviation	Transonic	Cannes, France	—	1.6	8″ × 8″	120 hp
TCEA	S-1	Rhode-Saint-Genèse, Belgium	Continuous	1.2	16″ × 16″	615 kw
Vickers-Armstrong	Transonic	Weybridge, England	Continuous	0.90	3′ × 2′	1700 hp

* Jet engines.

References

9:1 Richard T. Whitcomb, Recent Results Pertaining to the Application of the Area Rule, NACA RM L53I15a, 1953.

9:2 William Gracey, Measurements of Static Pressure on Aircraft, NACA TN 4184, 1957.

9:3 William M. Chew, Jr., Determination of Optimum Operating Parameters for the 1-foot Transonic Tunnel Utilizing Cone-Cylinder Bodies of Revolution, AEDC TN 60-69, 1960.

9:4 A. L. Braslow and E. C. Knox, Simplified Method for Determination of Critical Height of Distributed Roughness Particles for Boundary-Layer Transition at Mach Numbers from 0 to 5, NASA TN 4363, September 1958.

9:5 Maurice S. Cahn, An Experimental Investigation of Sting Support Effects on Drag and a Comparison with Jet Effects at Transonic Speeds, NACA Report 1353, 1958.

9:6 J. A. van der Bliek, Notes on Half Model Testing in Wind Tunnels, AGARD 298, 1959.

9:7 John W. McKee and T. A. Byrdsong, A Wind-Tunnel Investigation of Pressure Fluctuations on the Upper Vertical Tail of the X-15 When Mated to the B-52 Carrier Airplane, NASA TN D-1359, 1962.

9:8 E. R. Van Driest, Turbulent Boundary Layer in Compressible Fluids, *JAS*, **18** (3), March 1951.

9:9 J. S. Thompson and D. W. Holder, Notes on Wind Tunnel Pressure Measurement from the Operators Point of View, RAE TN 2547, 1958.



Chapter ten

Calibration and use of supersonic tunnels

10:1 General

Supersonic tunnels operate in the Mach number range of about 1.4 to 5.0. They usually have total operating pressures from about atmospheric to 300 psia and total operating temperatures of about ambient to 250°F. They require contoured nozzles and their test sections usually have solid walls.

Figures 10:1 to 10:3 illustrate large supersonic tunnels. Figure 10:1 is a drawing of a complete tunnel circuit, Fig. 10:2 shows a console test section area, and Fig. 10:3 shows a tunnel drive compressor room.

Larger models can usually be tested in supersonic tunnels than in near-sonic and transonic tunnels, because of both blocking and wave reflection considerations. Maximum model cross-sectional areas up to 4 per cent of the test section area are not uncommon and larger models have been tested. Model size is limited by tunnel choking considerations discussed in Section 1:6, and shock wave reflections discussed in Section 2:20. When proper consideration is given to choking and wave reflections in sizing a model, there will be no effects of the wall on the flow over the models because reflected disturbances will pass downstream of the model, but there will be a buoyancy effect (eq. (8:24)) if there is a pressure gradient in the tunnel. Fortunately typical pressure gradients are small, and buoyancy effects usually negligible. The Mach number in a supersonic tunnel with solid walls cannot be adjusted because it is set by the geometry of the nozzle. Small increases in Mach number usually accompany large increases in operating pressure in that the boundary layer thickness is reduced and consequently the effective area ratio is increased.

Condensation of moisture is a problem to be avoided in all supersonic tunnels, both in calibration and in testing. The moisture levels of air required to avoid condensation at various Mach numbers are discussed in Section 1:10. To ensure that condensation will not be present in

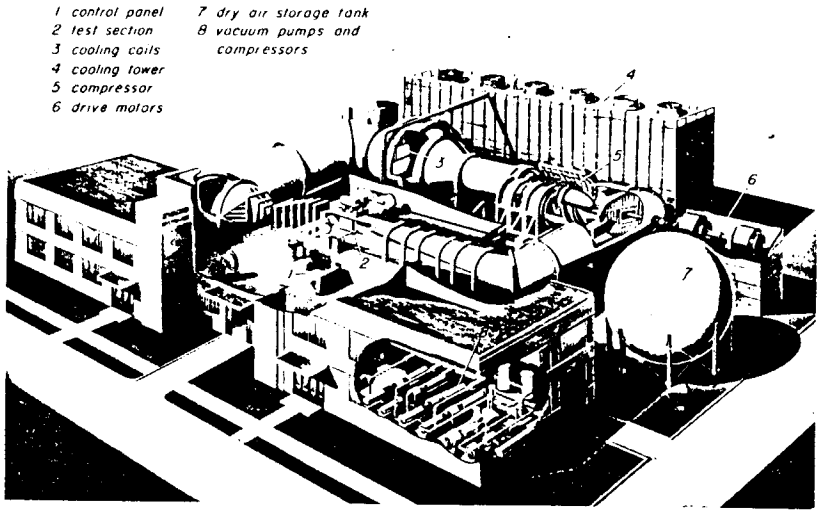


Fig. 10:1 Pictorial drawing of the Ames 6 × 6-foot supersonic tunnel. (Courtesy National Aeronautics and Space Agency.)

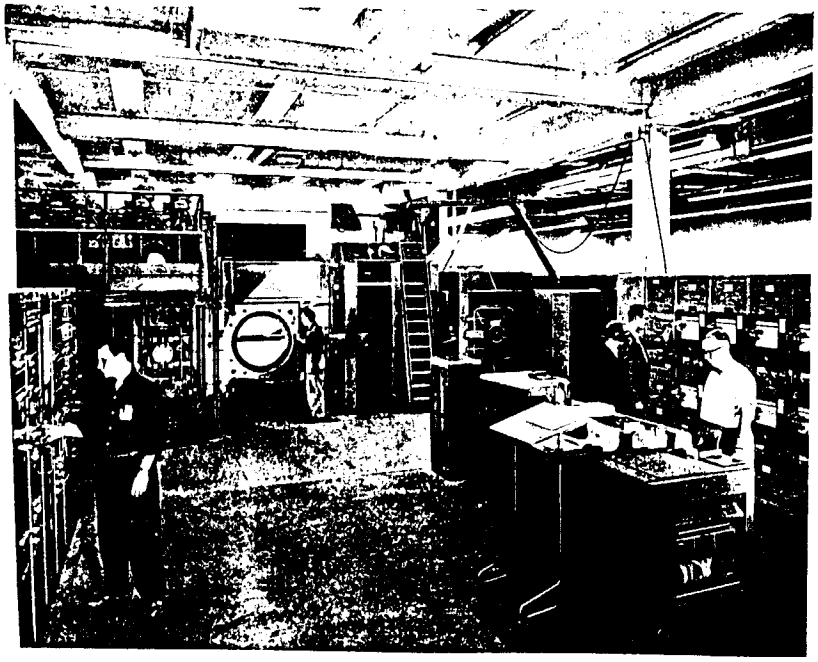


Fig. 10:2 Operating area of a modern high-speed wind tunnel. Few tunnels are this spacious or have such a good view of the test section. (Courtesy Boeing Company.)

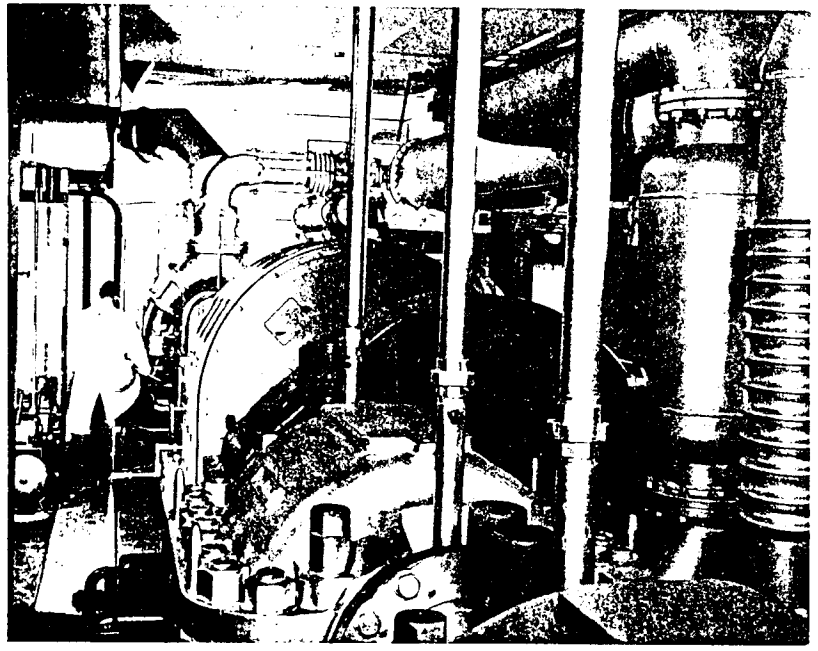


Fig. 10:3 A compressor room. (Courtesy Convair San Diego.)

significant amounts, the tunnel air dewpoint in practically all supersonic tunnels is monitored continuously during tunnel operation.

The calibration of a supersonic tunnel differs considerably from that of transonic and nearsonic tunnels, whereas the testing procedures in the three types of tunnel are quite similar. In this chapter, calibration procedures and testing procedures are discussed mainly with respect to differences from procedures described in Chapter 9. In addition, specific types of tests that are often carried out in transonic tunnels as well as in supersonic tunnels are discussed.

10:2 Theory

A tremendous amount of theory has been derived for the flow over wings and bodies at supersonic speeds. The most simple and probably the most useful theory to the tunnel engineer is that for the flow over a two-dimensional flat plate. This theory, which applies to any portion of an infinitely thin flat plate not affected by disturbances from the ends of the plate, yields

$$\frac{p_s - p}{q} = \frac{2\alpha}{57.3\sqrt{M^2 - 1}} \qquad (10:1)$$

where p_s = pressure on either surface of the flat plate, psia,
p = freestream static pressure, psia,
q = freestream dynamic pressure, psi,
α = angle of attack of the plate, positive when windward side pressure is being calculated and negative when leeward side pressure is being calculated, deg,
M = Mach number.

Equation (10:1) can be used to determine the lift coefficient slope as follows:

$$C_{L\alpha} = \frac{4}{57.3\sqrt{M^2 - 1}} \tag{10:2}$$

Although there are very definite limitations to the theory, it often does a good job of predicting lift coefficients. Any wing will, of course, have end effects, being attached to a fuselage and having a free tip. At the tip, there is a loss of lift because air can flow around it. However, there is an upwash around the fuselage which increases lift over the inner portion of the wing, tending to compensate the tip loss. Equations (10:1) and (10:2) are directly applicable only to wings with no sweepback. However, to a surprising degree, eq. (10:2) seems to work for many complete airplanes. For wings having Mach waves from the wing–fuselage juncture which are ahead of the wing leading edge, the surface pressure coefficient cannot be predicted by this method because the flow normal to the wing leading edge is subsonic.

10:3 Calibration

The calibration of a supersonic tunnel includes determining the Mach number of the flow throughout the range of operating pressures for each nozzle, determining flow angularity, and determining an indication of turbulence level effects.

10:4 Determining Mach Number

The Mach numbers in supersonic tunnels are usually obtained from close to the speed of sound up to $M = 1.6$ by measuring the static pressure in the test section and the total head in the settling chamber and using eq. (1:14). Above $M = 1.6$ it is more accurate to use the pitot pressure in the test section with the total head in the stagnation chamber and eq. (1:24). This comes about because the loss of total head above $M = 1.6$ yields a sufficient difference between the pitot pressure and the stagnation pressure for a useful ratio to be obtained. A further advantage is that the static pressure is a more difficult quantity to measure, at best.

Although less accurate than the pitot pressure method at the higher Mach numbers, the measurement of static pressure can also be used for determining Mach number as can the measurement of shock wave angles from schlieren photographs or shadowgraphs.

Whereas Mach numbers in nearsonic and transonic tunnels are usually determined only on the tunnel centerline and at the tunnel walls, Mach numbers in supersonic tunnels are usually obtained *off* the tunnel centerline as well. The reason is that much larger non-uniformities of flow are possible in supersonic nozzles because they can be caused by shock waves. An average flow Mach number in the vicinity of a model is desired for testing and data reduction purposes and the cross-sectional area survey will give a better average Mach number than the centerline survey. If the centerline Mach number distribution is constant or varies gradually but continuously, the centerline survey is usually adequate. However, the characteristics of this distribution are not known when the calibration is started.

10:5 Measuring Pitot Pressures

Pitot pressures are measured by using a simple device called a pitot probe. The pitot probe is simply a tube with a blunt end facing into the airstream. The tube will normally have an inside to outside diameter ratio of $\frac{1}{2}$ to $\frac{3}{4}$, and a length aligned with the airstream of 15 to 20 tube diameters. The pressure orifice is formed by the inside diameter of the tube at the blunt end. A rake of nine pitot probes used for calibration traverses of a test section is shown by the photograph of Fig. 10:4. We may add that the pitot tube is both simple to construct and accurate to use. It should always have a squared-off entry, and the largest practical ratio of hole diameter to outside diameter. It will be insensitive to angle of attack up to 10 deg for an orifice diameter only 10 per cent of the outside diameter and up to 15 deg for one 98 per cent of the outside diameter.

Calibration errors due to angle of attack and hole size within the above ranges are much less than actual flow deviations found in any reasonable tunnel. (Also see Ref. 10:12.)

At this point we may make the clarification that an open-ended tube facing into the airstream *always* measures the stagnation pressure (a term identical in meaning to "total head") it sees. Above $M = 1.0$ the shock wave that forms ahead of the tube means that it sees not the *freestream* stagnation pressure but the stagnation pressure behind a normal shock. This new value is called *pitot pressure* and in modern terminology implies a supersonic stream, although there is no error in calling the pressure so measured in a subsonic stream "pitot pressure."

Pressures measured by pitot probes are influenced significantly by very low Reynolds numbers based on probe diameter. This effect is seldom a

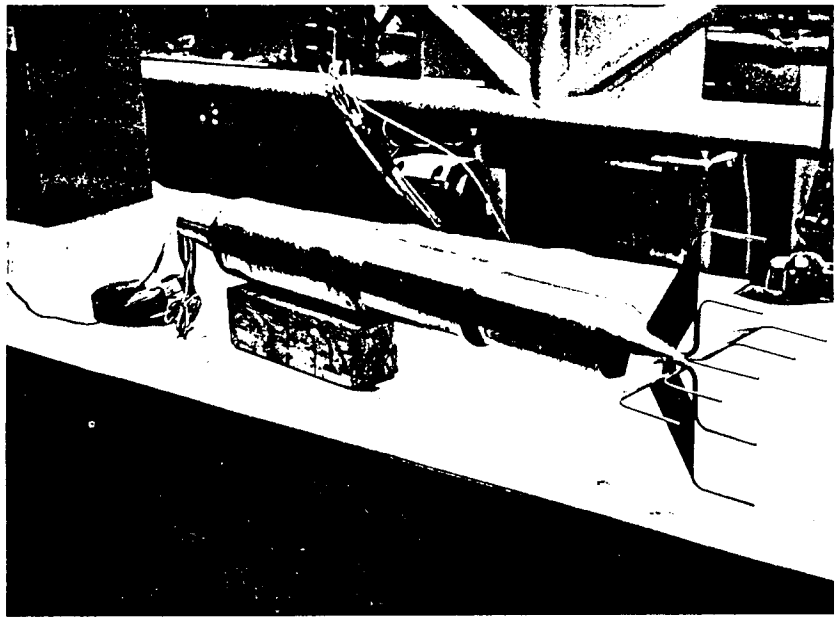


Fig. 10:4 Photograph of a traversing rake of nine pitot probes.

problem in supersonic tunnels, however, because a reasonable-sized probe will usually have a Reynolds number well above 500 or 1000, which is the range where trouble starts.

10:6 Measuring Static Pressures

Static pressures in a supersonic flow are much more difficult to measure than static pressures in a subsonic flow and pitot pressures in a supersonic flow. The "static pipe" described for calibrating nearsonic and transonic tunnels is rarely used because its presence in the tunnel will affect the flow in the test section. It changes the area ratio of the nozzle by subtracting from the effective throat and test section area, and it also interferes with the expansion pattern required for the development of uniform flow.

While static pressure probes are not used extensively for calibrating supersonic tunnels, a great deal of effort has been devoted to the development of accurate static pressure probes for other applications. The result has been the development of probes that have an application in wind tunnel calibration and use.

The primary problem in the use of static pressure probes at supersonic speeds is that any probe will have a shock wave at its forward end which causes a rise in static pressure. If the probe consists of a cone tip followed

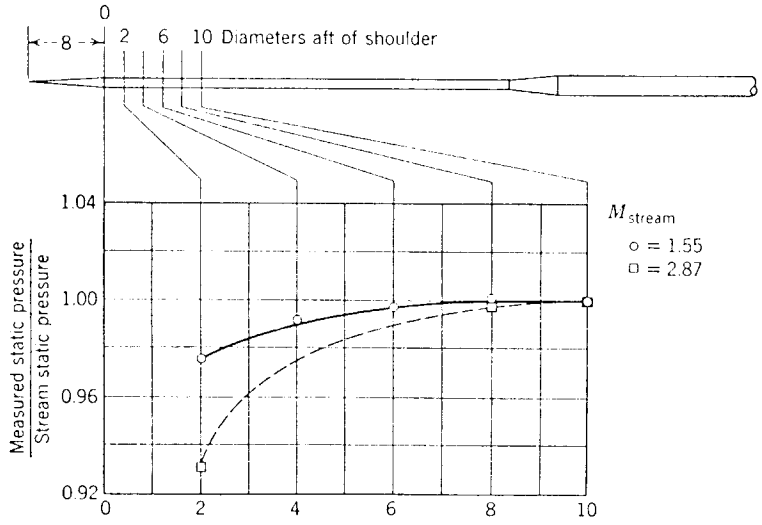


Fig. 10:5 Effect of orifice distance from shoulder on measured static pressure. From Ref. 10:1.

by a cylinder, the air passing the shoulder will be expanded to a pressure below static. Then as distance from the shoulder is increased, the pressure on the probe will approach the true static pressure of the stream.

Pressure measurements on a cone-cylinder probe with a 7-deg included angle cone followed by a cylinder 30 diameters in length are presented in Fig. 10:5. These results show negligible errors in static pressure measurements for orifices located 10 diameters downstream of the shoulder.

Another type of probe designed for the accurate measurement of static pressures over a large Mach number range is illustrated in Fig. 10:6. Errors of static pressure measured with this probe are presented in Fig. 10:7. They were obtained by reference to a static pressure calculated from a measured pitot and total pressure. Flow angularity during these tests was of no consequence, since the tunnel employed had extremely even

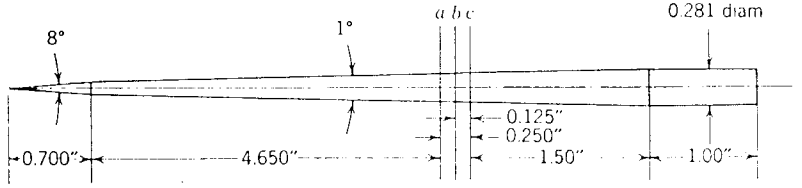


Fig. 10:6 Approximate dimensions of supersonic static pressure probe; see Ref. 10:2 for complete details. There are three interdigitated rings of holes at *a*, *b*, and *c*.

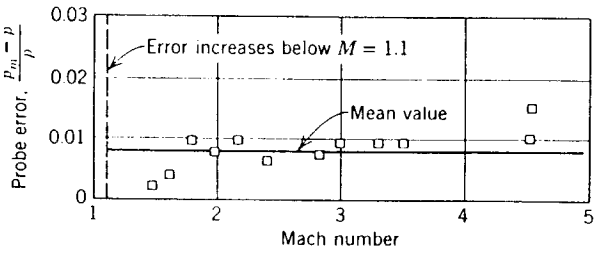


Fig. 10:7 Error in static pressure measured p_m in fraction of the true static pressure p.

flow. However it was found impossible to get consistent results until the pitot probe mentioned above and the static probe were mounted in the test section on a vertically moving support system so that either could be moved into centerline calibration position without a tunnel shutdown and with little time interval between measurements. Evidently for the extreme accuracy being sought (of the order of 0.01 *per cent* of q or 0.1 per cent of p), minute tunnel changes due to controls or thermal expansion became significant.

Static pressures on the walls of supersonic tunnels are often used for rough estimation of test section Mach numbers. It is noted, however, that wall pressures do not necessarily correspond to pressures on the tunnel centerline because of the possibility of compression or expansion waves between the wall and the centerline. When Mach number is to be determined from static pressure measurements, the total pressure of the stream is measured in the settling chamber simultaneously with the test section static pressure. Mach number is then calculated from these two pressures and the relation of eq. (1:14).

10:7 Measuring Wave Angles on Wedges and Cones

Although the method is seldom used in tunnel calibration, it is possible to determine Mach number by measuring the angles of waves produced by known wedges or cones from schlieren pictures or shadowgraphs. Charts and tables are available in the literature (see, for example, Ref. 1:1) which give wave angles for cones and two-dimensional wedges as a function of leading-edge angles. It is noted in Ref. 1:1 that there are limiting angles for both wedges and cones for shock attachment. That is, if the angle becomes too great at a given Mach number, the shock wave will be detached and Mach number cannot be determined from the wave angle. Whatever usefulness wave angle has for determining Mach number is pretty well limited to the supersonic range, as above $M = 6$ or so wave angle changes but little with Mach number.

10:8 Measuring Pressures on Wedges and Cones

Mach number can also be obtained by measuring pressures on the surface of cones or two-dimensional wedges, although this is seldom done in calibration. Literature that presents wave angles for wedges and cones will usually also include the ratios of surface pressure to total pressure as a function of Mach number. Thus, the surface pressure and tunnel total pressure are measured. The charts or tables are entered with the ratio of these pressures and the leading-edge angle to determine a corresponding Mach number. In practice the exact wedge or cone angle to use is obscure because of the undefined depth of the boundary layer. Ref. 10:17 has further data in this area.

10:9 Mach Number Calibration Results

Results of calibrations to determine Mach number from tunnel wall static pressures and tunnel axis pitot pressures are presented in Fig. 10:8. This figure illustrates the differences that may exist between the tunnel wall and centerline due to expansion waves between the two. Results of a very thorough Mach number survey at one axial station of a tunnel are presented in Fig. 10:9, and an even more complete survey along the plane of the horizontal axis is shown in Fig. 10:10.

The importance of calibrating over the range of Reynolds numbers (pressures if the temperature is constant) at which the tunnel will be operated is illustrated by the plots of Fig. 10:11. A change in Reynolds number from 0.06 to 0.4 $\times$ 10^6 per inch causes a Mach number deviation of 0.06 at a nominal Mach number of 5.0. As mentioned previously, this

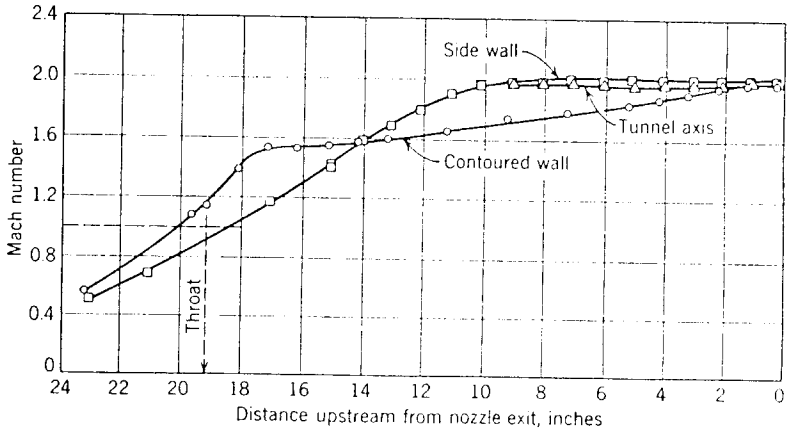


Fig. 10:8 Wall and tunnel axis calibration data from $M = 2.0$ nozzle. Redrawn from Ref. 10:3.

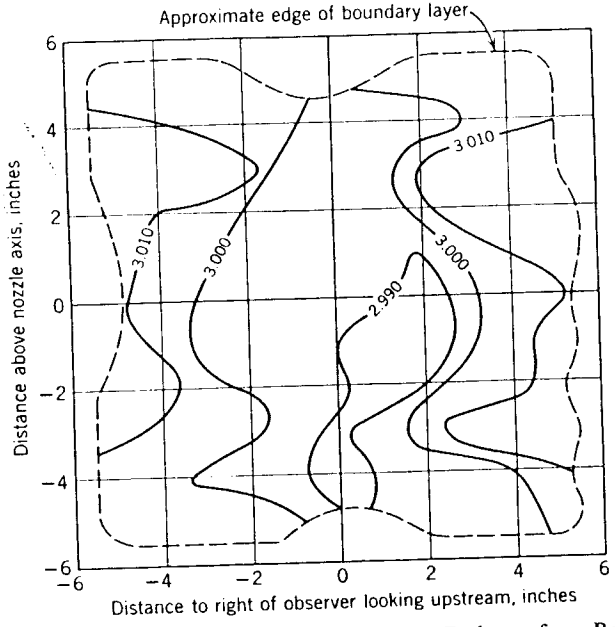


Fig. 10:9 Contour plot of $M = 3.0$ nozzle. Redrawn from Ref. 10:3.

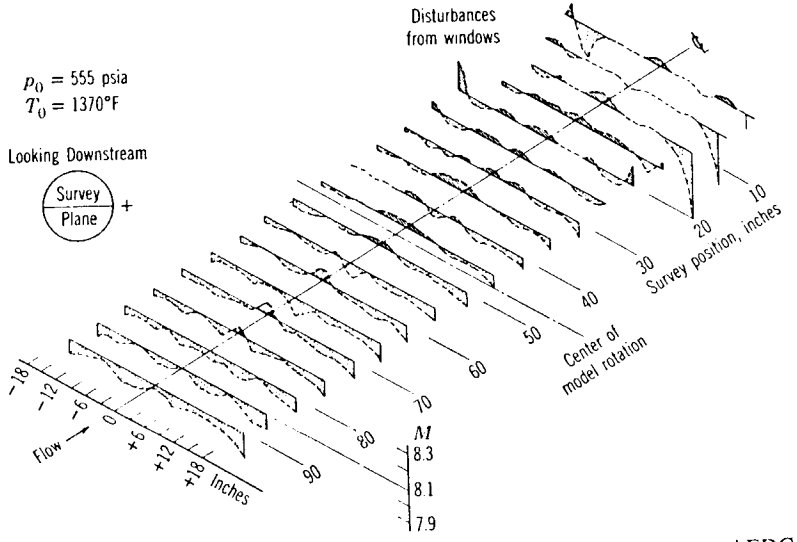
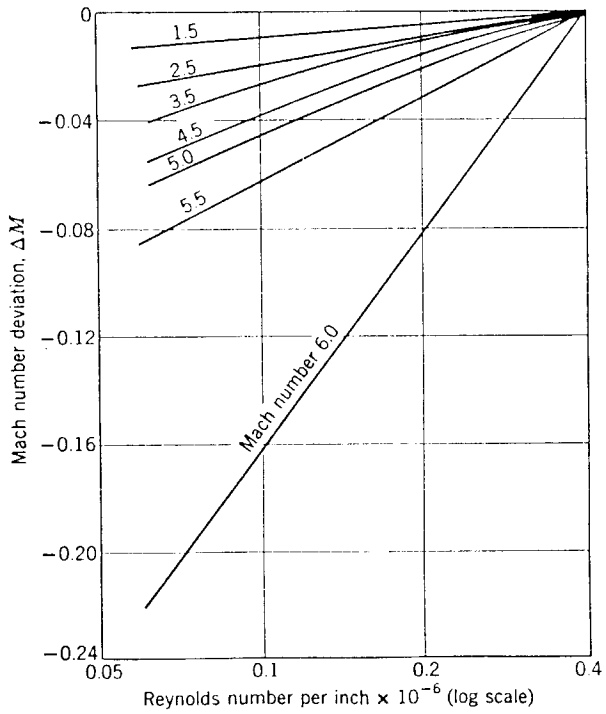


Fig. 10:10 Mach number distribution in the Mach 8 tunnel (B). (Courtesy AEDC.)



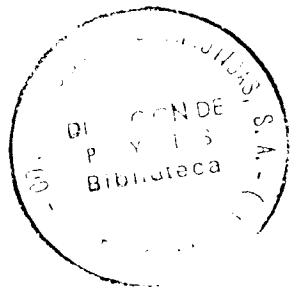


Fig. 10:11 Variation of centerline Mach number with Reynolds number, 40-inch tunnel. Redrawn from Ref. 10:4.

effect results from changes in boundary layer thickness and consequently effective nozzle area ratio.

As a matter of interest, many supersonic tunnels run at constant dynamic pressure throughout their Mach number range. This is in contradistinction to low speed testing where q increases with the test parameter V^2. Constant q helps with handling balance loads, and (although it is of small matter) with data reduction.

10:10 Determining Flow Angularity

The flow angularity in a supersonic tunnel is usually determined by using either cone or wedge yawmeters. The sensitivities of several yawmeters for use in supersonic tunnels are presented in Fig. 10:12. It is noted that the sensitivities of these yawmeters are maximum when the wedge or cone angles are maximum. They work below Mach numbers for which wave detachment occurs, and are so used. The cone yawmeter is used more extensively than the wedge yawmeter because it is easier to fabricate. A photograph of a wedge yawmeter is presented in Fig. 10:13.

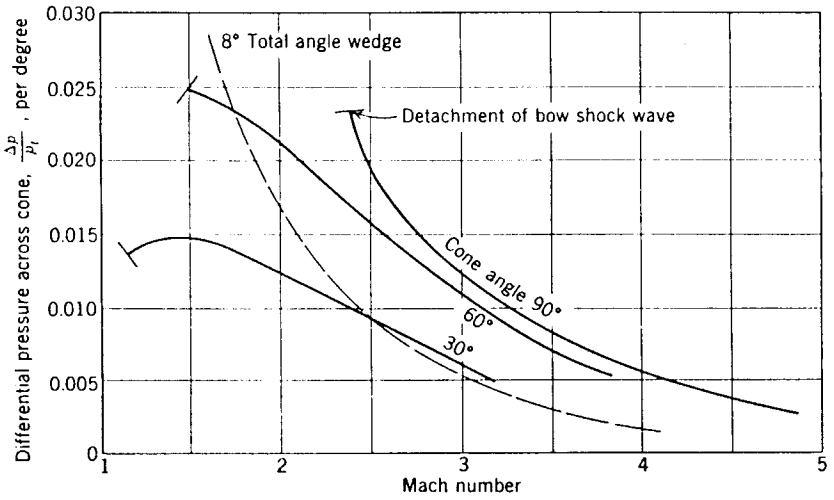


Fig. 10:12 Sensitivities of several yawmeters at supersonic speeds, pressure ratio per degree.

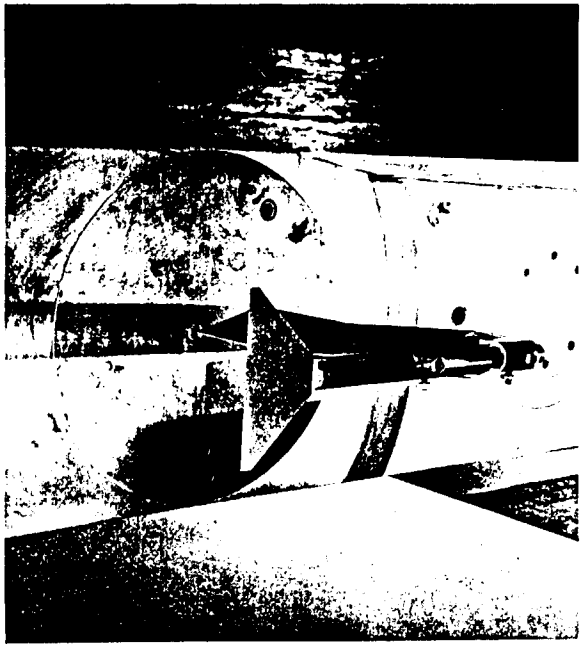


Fig. 10:13 A wedge yawmeter. (Courtesy Jet Propulsion Laboratory.)

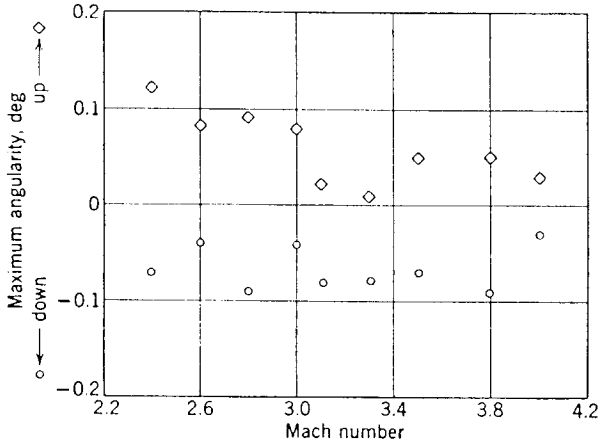


Fig. 10:14 Maximum up and down flow in Jet Propulsion Laboratory 12-inch supersonic tunnel for about 0.7 tunnel height up and downstream of balance center. From Ref. 10:5.

Note that the use of the yawmeter at supersonic speeds requires a calibration to determine the aerodynamic error, as discussed in Section 9:3 for transonic tunnels. A typical summary of results from tests to determine flow angularity in a wind tunnel is presented in Fig. 10:14.

10:11 Determining Turbulence Level

Measurements with a hot-wire anemometer demonstrate that there are high-frequency fluctuations in the airstream of supersonic tunnels that do not occur in free air. These fluctuations, broadly grouped under the heading of "turbulence," consist of small oscillations in velocity, stream temperature (entropy), and static pressure (sound). Values from one tunnel are given in Table 10:1.

Table 10:1

Turbulence in Settling Chamber and Test Section of a Supersonic Tunnel

	Settling Chamber	Test Section	
Mach number	All	2.2	4.5
Sound, $\frac{\Delta P_t}{P_t}$	Less than 0.1%	0.2%	1%
Entropy, $\frac{\Delta T_t}{T_t}$	Less than 0.1%	Less than 0.1%	
Vorticity, $\frac{\Delta V}{V}$	0.5 to 1%	Less than 0.1%	

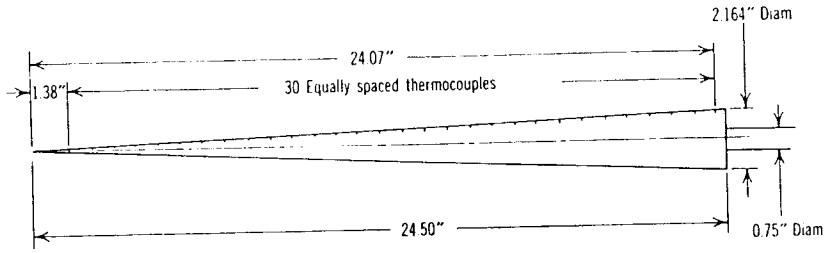


Fig. 10:15 Dimensions of Jet Propulsion Laboratory transition cone. From Ref. 10:6.

The fluctuations arise from a variety of causes, mostly from the pressure regulator valve, the drive system, the aftercooler, and the test section boundary layer. Velocity fluctuations emanating from upstream causes may be reduced at low and moderate Mach numbers by the addition of screens in the settling chamber. At high Mach numbers, upstream pressure and velocity effects are usually less, since the large nozzle contraction ratios damp them out. Temperature fluctuations are unaffected by the contraction ratio. The existence of such fluctuations is, of course, of less interest than their effect. Here the calibration procedure has been to determine the transition Reynolds number on smooth cones and compare this with values obtained in other tunnels.

By common usage, transition cones have either 5- or 10-deg included angles and highly polished surfaces. Various methods have been used to determine the point of transition on the cone. These have been (1) optical methods in which schlieren pictures or shadowgraphs were made and inspected to determine the point at which a sudden thickening of the boundary layer occurred; (2) traversing along the cone a constant

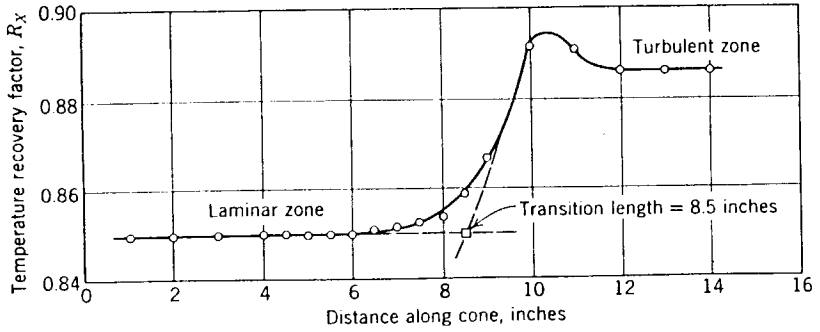


Fig. 10:16 Typical determination of transition Reynolds number on a cone. Free-stream Reynolds number per foot, 4.31×10^6; transition Reynolds number 3.055×10^6. From Ref. 10:7.

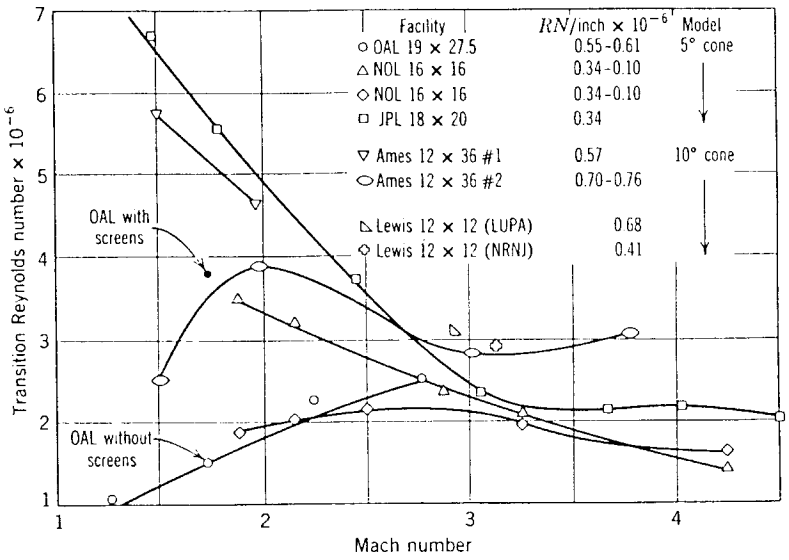


Fig. 10:17 Transition Reynolds number on 5- and 10-deg cones as measured at several facilities. From Ref. 10:8.

distance away from the surface with a small pitot probe that is within the turbulent boundary layer and noting the point at which the probe pressure changes from a steady to a fluctuating pressure; (3) making similar traverses with a hot-wire anemometer; and (4) measuring temperatures of the surface by using thermocouples on the inner surface of a thin-walled cone.

The dimensions of a cone for use with the surface temperature technique are presented in Fig. 10:15. Surface temperatures of this cone were used to obtain a recovery factor, R_x, as follows:

$$R_x = \frac{T_{aw} - T}{T_t - T} \tag{10:3}$$

where T_{aw} = adiabatic wall temperature, °R,
T_t = stream total temperature, °R,
T = stream static temperature, °R.

Figure 10:16 is plot of the resulting data which indicates the method of locating the point of transition. A summary of transition Reynolds numbers in several wind tunnels is presented in Fig. 10:17.

10:12 Determining the Presence of Test Section Noise

Test section "noise" is defined as pressure fluctuations. Noise may result from unsteady settling chamber pressure fluctuations due to upstream

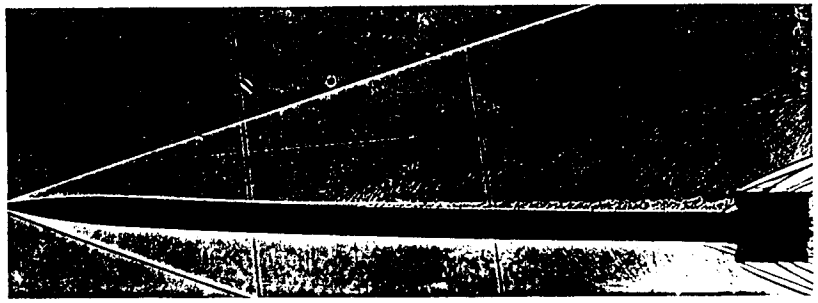


Fig. 10:18 Noise emanating from the turbulent boundary layer on a missile model. $M = 3.5$; $RN = 2 \times 10^6$/inch. Note the diminution of wavelet strength as the distance from the source is increased. (From Fig. 4(*y*) of Ref. 10:18.)

flow conditions. It may also be due to weak unsteady shocks originating in a turbulent boundary layer on the tunnel wall. Such weak shocks to which noise is attributed are illustrated by the shadowgraph of Fig. 10:18. Noise in the test section of a wind tunnel is very likely to influence the point of boundary layer transition on a model. Although it is possible that other effects on tests results may exist, there has not yet been evidence showing that they do.

Test section noise can be detected by either hot-wire anemometry measurements or by high-response pitot pressure measurements. The method used to determine if the noise is coming from the test section boundary layer is to make measurements in the tunnel settling chamber as well as in the test section. It is then possible to determine if fluctuations in the two places are related. It has been found that test section noise generally increases as tunnel operating pressure increases, and, that test section noise originating in the settling chamber generally decreases as tunnel Mach number increases.

10:13 The Use of Calibration Results

The Mach number in the vicinity of a model during a test is assumed equal to an average of those obtained in the same portion of the test section during calibrations. With this known Mach number and values of total pressure measured in the settling chamber, it is possible to define the dynamic pressure used in data reduction by using eq. (1:17). If total temperature is also measured in the settling chamber, all of the properties of the flow in the test section are defined by relations given in Section 1:2. The flow angularities measured during the calibration are used to adjust

model angles set with respect to the tunnel axis to a mean flow direction reference. The most concrete use of results of transition point and noise measurements made during the calibration normally lies in taking steps to decrease the tunnel turbulence and noise level.

10:14 Starting the Tunnel

Supersonic tunnels are usually started simply by opening a quick-operating valve, which causes air to flow through the tunnel proper. In continuous tunnels, the compressors are normally brought up to the desired operating speed with air passing through a by-pass line. When operating speed is reached, a valve in the by-pass line is closed, which forces the air through the tunnel. In blowdown tunnels a valve between the pressure storage tanks and the tunnel is opened.

Quick starting is desirable in all supersonic tunnels because the model is usually subjected to high loads during the starting process. The quick start of the blowdown tunnel also conserves air.

A method for determining when the tunnel is started is to observe the pressure at an orifice in the test section wall near the forward model station. When this pressure suddenly drops to a value near the static pressure for the design Mach number, the tunnel is started. If the model is blocking the tunnel, this pressure will not drop. With experience in operating a tunnel, the wind tunnel engineer can usually tell by the sound whether the tunnel has started.

Some tunnels are equipped with variable second-throat diffusers designed to decrease the pressure ratio required for tunnel operation. These diffusers are designed to allow the setting of a cross-sectional area large enough for starting the tunnel and then to allow the setting of a lesser cross-sectional area for more efficient tunnel operation. When used as designed, the variable diffuser is closed to a predetermined area as soon as the tunnel starts.

10:15 Starting Loads

Whenever a supersonic tunnel is being started or stopped, the normal shock system passes through the test section and large forces are imposed on the model. The model oscillates violently at the natural frequency of the model support system and normal force loads of 5 times those which the model would experience during steady flow in the same tunnel at $\alpha = 10$ deg are not uncommon. Experience has indicated that in a two-dimensional tunnel, starting loads will be higher when the major lifting surfaces (wings) of the model are in a plane parallel to the nozzle plane of symmetry.

The magnitudes of starting loads on a given model in a given tunnel are quite random and exactly what causes the large loads is not yet understood. However, it has been proposed that they may be due to a highly unsymmetrical flow in which separation from one of the contoured walls occurs, producing large flow angularities, accompanied by supersonic flow on one side of the lifting surface and subsonic flow over the other. A low pressure accompanies the supersonic flow over the one side and a high pressure accompanies the subsonic flow over the opposite side. The result of such a flow field is a large load. If it is assumed that the supersonic flow on the one side is at the design nozzle Mach number and that the



Fig. 10:19 Cooling and protective shoes in partially extended condition. (Courtesy Douglas Aircraft Corporation.)

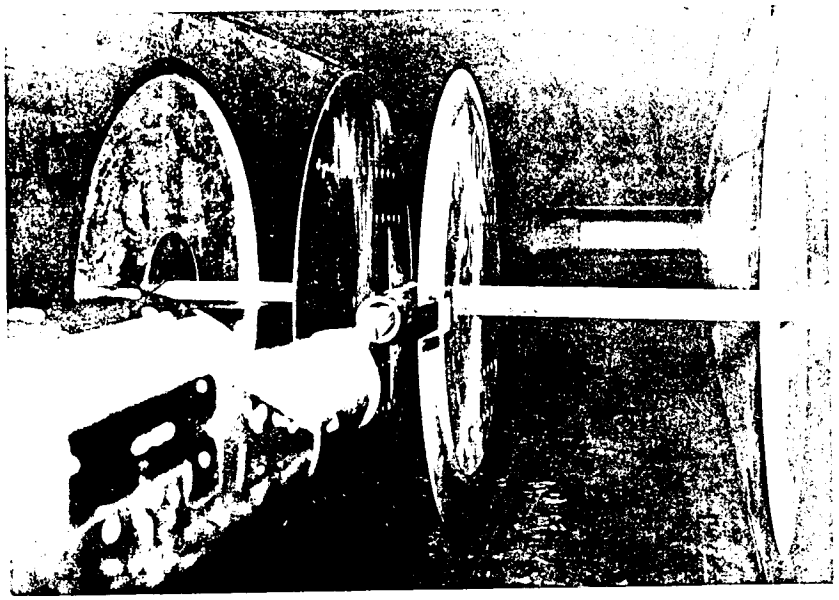


Fig. 10:20 Proximity plates protecting an AGARD B model shown with wings vertical. (Courtesy Convair San Diego.)

subsonic flow on the opposite side is that behind a normal shock at the design Mach number, the flow field described would yield

$$C_{N_s} = \frac{F_{Nm}}{p_t S} = \frac{2\gamma(M^2 - 1)}{(\gamma + 1)\left[1 + \frac{\gamma - 1}{2} M^2\right]^{\gamma/(\gamma-1)}} \qquad (10:4)$$

where C_{N_s} = a starting load normal force coefficient due to the assumed flow fields,
F_{Nm} = maximum normal force, lb,
p_t = total pressure of tunnel flow at the time the shock system passes over the model, psia,
S = lifting surface planform area, inches^2,
γ = specific heat ratio for air, 1.4,
M = design Mach number of the nozzle.

Equation (10:4) has now been broadly accepted as a correlation parameter for starting load information.

Starting loads present a serious problem in the design of balances for wind tunnel models. If the balances are strong enough to withstand these severe starting loads, it is difficult to obtain sensitivities adequate for resolving the much smaller aerodynamic loads during tests. Various methods have been used for alleviating this problem. Among them are

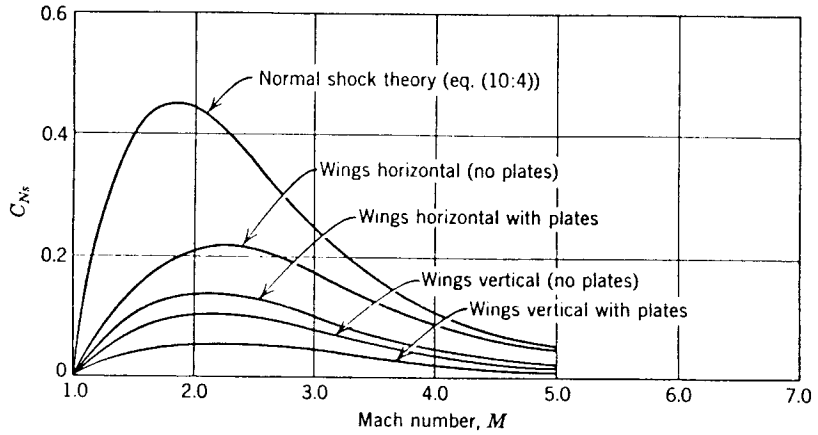


Fig. 10:21 Effect of plates for reducing starting loads on AGARD model B.

(1) starting at a reduced total pressure in continuous tunnels; (2) clamping the model; (3) shielding the model with retractable protective shoes (Fig. 10:19); (4) shielding the model with two retractable flat plates (Fig. 10:20); and (5) injecting the model into the airstream after the tunnel is started.

Results of studies of starting loads on one model in one wind tunnel are presented in Fig. 10:21. These results, as well as most starting loads studies, indicate that eq. (10:4) overestimates starting loads considerably, particularly at low Mach numbers. The studies confirm that starting loads are higher when the wing is in the nozzle plane of symmetry (horizontal) than when it is 90 deg from this plane. They also show the effectiveness of protective plates in reducing starting loads.

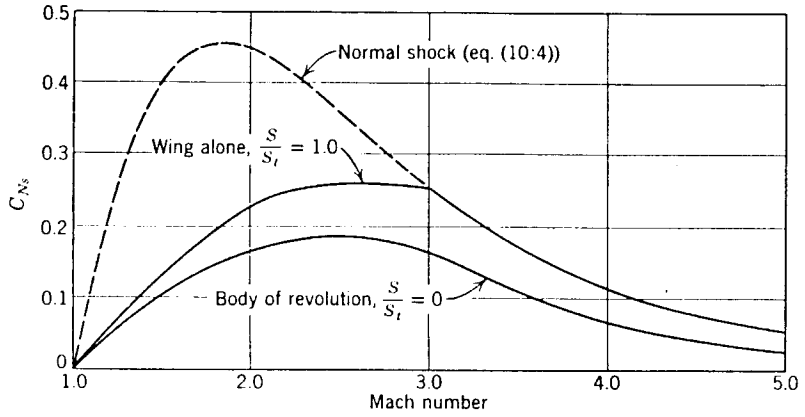


Fig. 10:22 Suggested starting loads coefficients. (From Ref. 10:9, refaired.)

It is noted that eq. (10:4) is derived specifically for models with lifting surfaces and makes no provision for models without lifting surfaces. Noting that starting loads are also large on body-alone models, Ref. 10:9 suggests that the total planform area is the important criterion rather than the lifting surface planform area. Thus the starting load normal force coefficient should be defined as

$$C_{Ns} = \frac{F_{Nm}}{p_t S_t} \tag{10:5}$$

where S_t = total model planform area, inches^2. With this definition of C_{Ns}, published starting loads data were compiled in Ref. 10:9 and the empirical correlation curves of Fig. 10:22 were derived. Models and balances capable of withstanding the normal force loads indicated in Fig. 10:22 should experience no difficulty in most tunnels.

10:16 Reynolds Number Effects

The effects of Reynolds number on wind tunnel data at supersonic speeds are the same as those described for transonic conditions in Section 9:7, namely scaling problems with skin friction and the effect of the proper boundary layer on the base drag. The situation is helped somewhat in the supersonic case by the fact that skin friction is then a smaller part of the total drag due to the increased pressure drag over the forebody. It is still quite significant and fixed transition is frequently employed. Although the probability of downstream disturbances affecting base pressures and hence base drag is lessened because of the inability of downstream disturbances to move upstream in supersonic flow, enough changes make their way through the subsonic wake to cause substantial base interference effects as discussed in the next section.

10:17 Model Mounting-Sting Effects

Any sting extending downstream from the base of a model will have an effect on the flow and is therefore likely to affect model base pressure. This is illustrated by Fig. 10:23 which shows an effect of stings smaller than 0.1 model diameter. For actual tests the stings must be considerably larger than that to withstand the tunnel starting loads and to allow testing to the maximum steady load condition with a reasonable model deflection. Sting diameters of $\frac{1}{4}$ to $\frac{3}{8}$ model base diameters are typical in wind tunnel tests, though values outside this range are sometimes used. The effects on base pressure of typical sting diameters indicated by Fig. 10:23 are significant but represent less than 1 per cent of the dynamic pressure and therefore a small amount of the total drag of many but not all models.

Figure 10:24 (from Ref. 10:11) is a plot of a typical variation of base pressure with Reynolds number. This plot shows that base pressure is

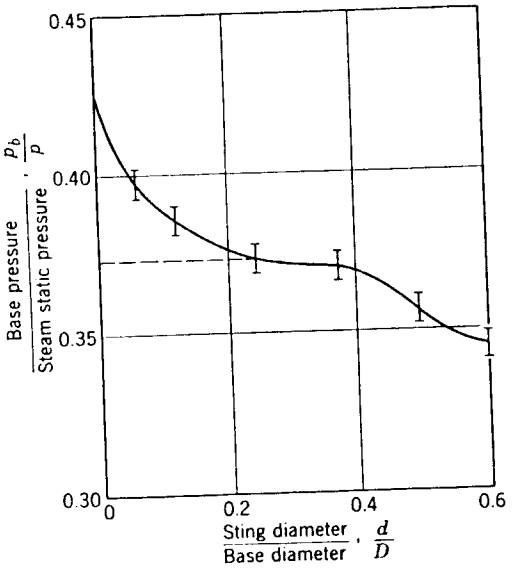


Fig. 10:23 The effect of sting diameter to model base diameter ratio on the ratio of base pressure to stream pressure p_b/p for an ogive cylinder model; $RN = 15 \times 10^6$, $M = 2.97$. (From Ref. 10:10.)

highly sensitive to Reynolds number when the model boundary layer is laminar but is relatively insensitive to boundary layer when transition occurs well forward on the model. From data of the type shown in this figure, it has been concluded that an accurate base drag on a small-scale model in a wind tunnel requires a turbulent boundary layer (assuming that the full-scale vehicle has a turbulent boundary layer).

The results of tests to determine the lengths of constant diameter stings

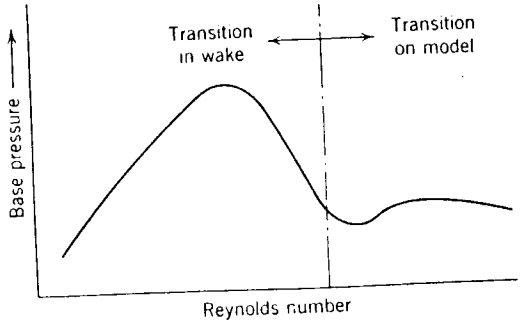


Fig. 10:24 Typical variation of base pressure with Reynolds number (redrawn from Ref. 10:11.)

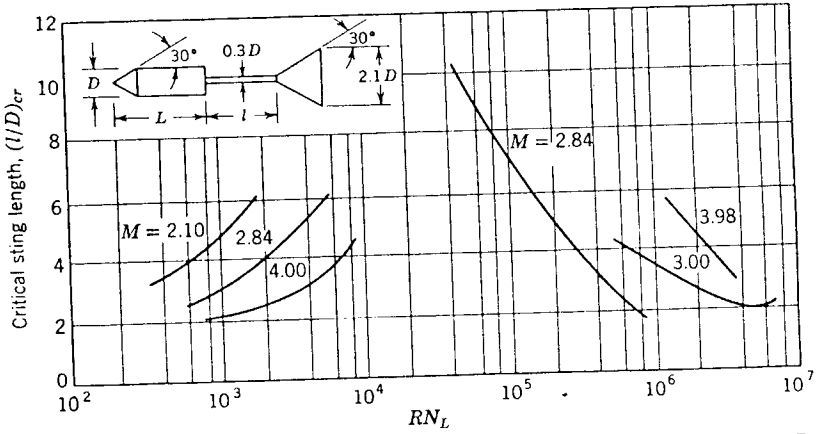


Fig. 10:25 The effect of Reynolds number on critical sting length. (From Ref. 10:11.)

required to avoid effects of the enlarged portion of the sting on base pressure ("critical sting length") are presented in Fig. 10:25.

10:18 Force Tests

There are essentially no differences between force tests for a given purpose in transonic and supersonic tunnels. Thus, the discussion of airplane force tests in Section 9:8 is directly applicable to supersonic testing. Further data on airplane testing appear in Section 10:28. There are force tests of many types which differ somewhat in technique, if not in principle, from airplane force tests and these are also discussed herein. Force and moment coefficients for missiles, unguided rockets, and stores are usually obtained in terms of characteristic lengths and areas which are different from those of airplanes, as discussed in Section 8:8.

10:19 Testing Guided Missiles

One respect in which many guided missiles differ markedly from airplanes is in their maneuverability and power. Missiles are often designed for accelerations in maneuvers such as climbing, rolling, and turning which are several times those of airplanes in the same maneuvers. To achieve this high maneuverability, control surfaces are often complete wings or tail surfaces. In flight, the maneuvers are accompanied by high angles of the missile relative to the direction of flight. Thus, wind tunnel tests of missiles are likely to require considerably higher angles of attack than tests of airplanes (up to 30 deg are not uncommon). It is in these cases that the bent sting of Fig. 9:24 is likely to be used most.

Another way in which many missiles differ from airplanes is that the missiles may fly with any roll orientation. Equal vertical and horizontal

wings and tails provide this capability. Because of this capability, wind tunnel data through an angle-of-attack range at several roll attitudes is often required. An alternate method of getting the required data of this type in some wind tunnels is to fix the model angle of attack, roll the model balance assembly through the desired angle range with a remote roll device and record data while rolling, change the angle of attack, and repeat the rolling and data recording. In missiles there will sometimes be combinations of roll angle and angle of attack where very severe changes of stability occur. In order to ensure that such conditions are not missed, a very thorough coverage of possible flight attitudes in the wind tunnel is required.

10:20 Testing Unguided Rockets

Unguided rockets are used for carrying instrumentation or some other payload to a specific point in or out of the atmosphere or for carrying the payload so that it experiences a specified altitude–velocity time history (Fig. 10:26). Unguided rockets are always equipped with three or four stabilizer fins located near their base. They are usually "spin-stabilized"; that is, they are designed to roll continuously during flight so that vehicle imperfections such as those due to fin misalignment do not cause the vehicle to veer from the desired trajectory. Spin stabilization is usually accomplished by slight differential deflections of the fins (say $\frac{1}{4}$ to $\frac{1}{2}$ deg) to provide a rolling moment during flight. Small rockets canted with respect to the vehicle axis have also been used.

The rocket engineer will usually be interested in aerodynamic data from near zero velocity to the maximum velocity of the rocket. Typically, he might ask for normal force, pitching moment, rolling moment, and drag data at Mach numbers of 0.4, 0.6, 0.8, 0.9, 0.95, 1.00, 1.05, 1.10, 1.40, 2.0, 3.0, and 5.0. He will not usually be interested in data at more than a few degrees angle of attack because his fins will probably break off if high angles of attack occur. However, he will typically *ask* for data at angles of attack of perhaps −4 deg to 12 deg. Also, he will typically ask for data with fins in the "plus" (vertical and horizontal) and "cross" (rolled 45 deg from "plus") configurations. Figure 10:27 shows typical detailed and summary data plots for two rocket configurations.

One of the major problems faced by the rocket engineer, which has a bearing on the configurations he will test in the wind tunnel, is one of dynamics. The rocket must be spun in order to achieve a reasonably predictable trajectory. During its flight the rocket will be subjected to disturbances which will have a tendency to cause a continuous pitching motion of small amplitude at the pitch natural frequency. If the roll frequency is within about 20 per cent of the pitch natural frequency, there

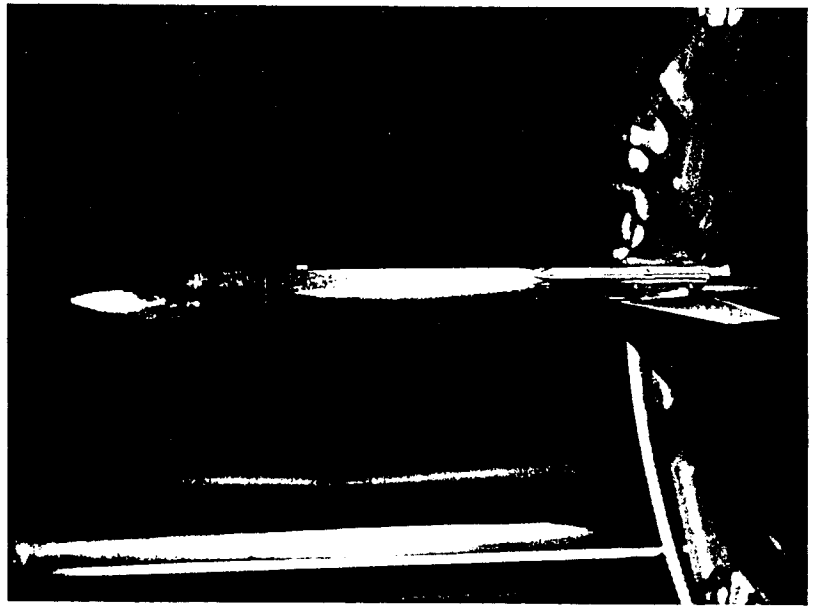


Fig. 10:26 Photograph of a wind tunnel model of an unguided rocket.

is a danger that a "roll–pitch coupling" will occur. In such a case, the rolling motion will amplify the pitching motion, causing high fin loads, seriously increased drag, and possible rocket destruction. It is of interest to consider the manner in which wind tunnel static force and moment data are used in studies relating to the roll–pitch coupling problem.

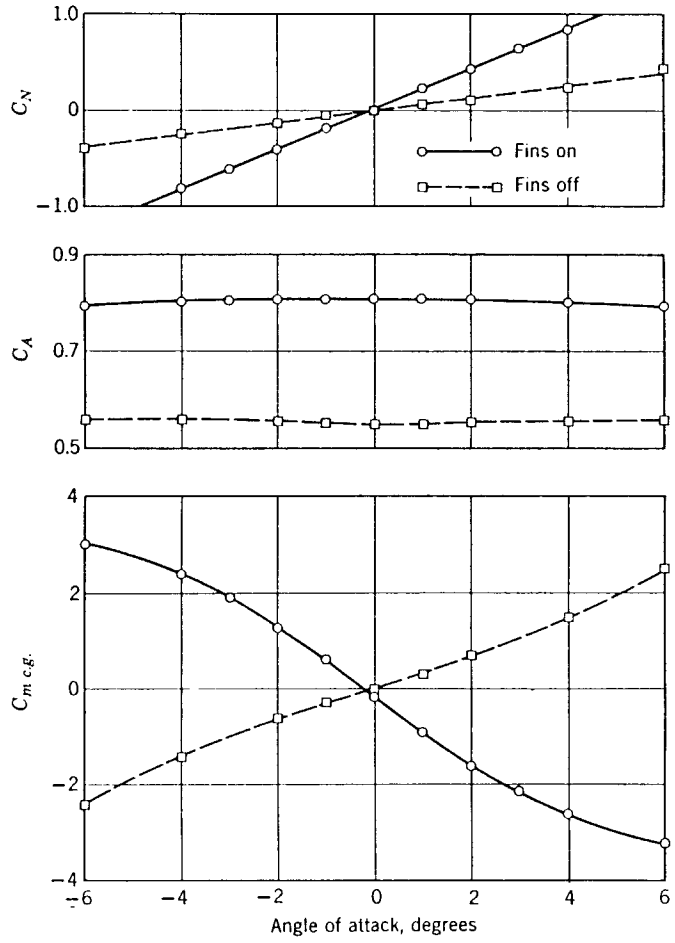
The vehicle pitching frequency is calculated from eq. (7:30) with the full-scale value of M_α calculated from the product of the flight value of dynamic pressure (q), the reference surface area (S) of the vehicle, the reference length (d) of the vehicle, and the value of $dC_m/d\alpha$ (per radian) from the wind tunnel test. The damping moment term of eq. (7:30) (in brackets) has a relatively small effect on pitch frequency for unguided rocket configurations and is usually neglected.

The vehicle roll acceleration is calculated from eq. (7:34). The full-scale value of rolling moment M_x of eq. (7:34) is calculated from the product of qSb (b is the fin span) for the vehicle in flight and the value of C_l from the wind tunnel test. The full-scale flight value of damping moment is calculated from the following:

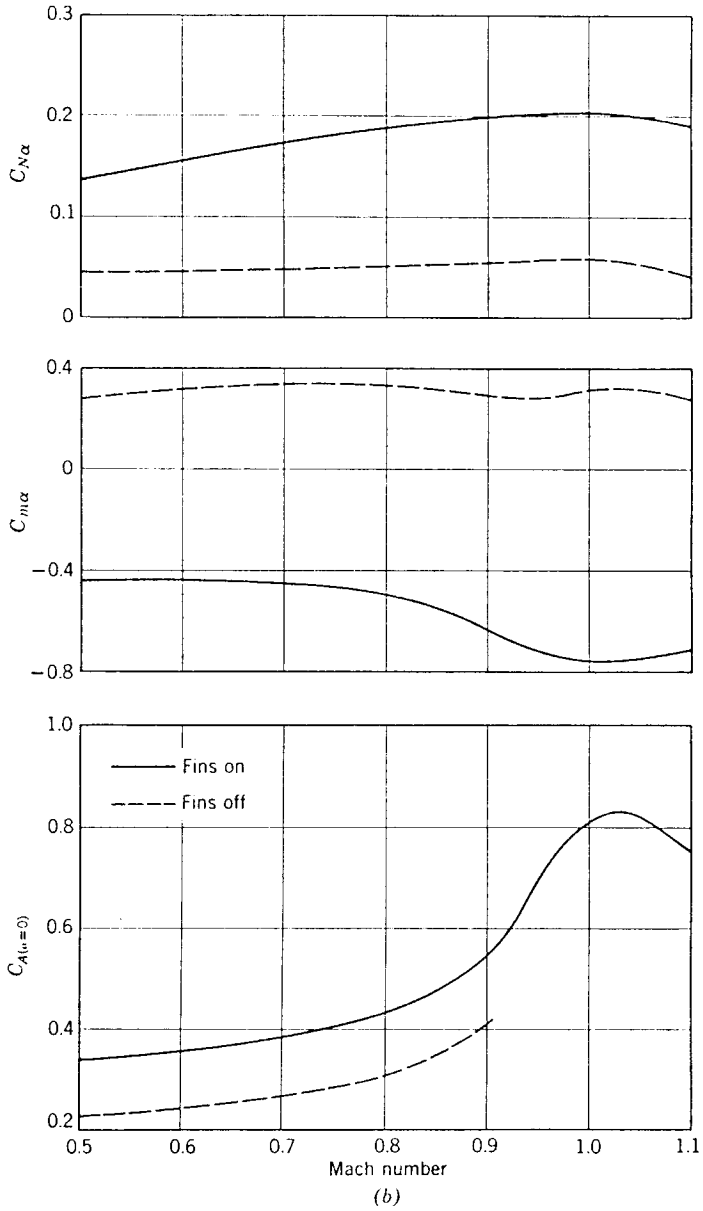
$$M_\phi = qSbC_{l_p} \tag{10:6}$$

$$\phi = \frac{pb}{2V} \tag{10:7}$$

Insertion of the above determined values of M_x and $M_{\dot{\phi}}\dot{\phi}$ into eq. (7:34), together with the vehicle inertia about the roll axis, allows the determination of a value of roll acceleration in terms of $(pb/2V)$. A solution of eq. (7:34) to determine the rolling frequency p, and of eq. (7:30) to determine the pitch frequency ω is obtained by a high-speed computer "trajectory program." In this program the complete rocket flight is divided into small time intervals and the changes in attitude, position, and velocity of the rocket which occur during each time interval as a result of all forces and moments acting on the rocket are calculated. During the first time interval, $(pb/2V)$ is assumed equal to zero and a roll



(a)



(b)

Fig. 10:27 Presentation of unguided rocket data; center of gravity at 66 per cent of the model length from the nose. Coefficients based on maximum body area and maximum diameter. (*a*) Effect of angle attack, $M = 1.0$; (*b*) effect of Mach number on major parameters.

acceleration is calculated from eq. (7:34). With this roll acceleration acting during the first time interval, the roll velocity at the end of the interval can be calculated. This gives a second value of $(pb/2V)$ to be used for calculating a second value of acceleration. An example of results of a roll–pitch coupling study for a 100-mile-high, two-stage rocket system is presented in Fig. 10:28. It is noted in this figure that the roll and pitch frequency curves cross and that there is therefore a danger of the disastrous roll–pitch coupling.

It is usually quite difficult to make substantial changes in either rocket moment of inertia or center of gravity. The only means available for increasing C_{m_α} is an increase of fin size. In turn, increases of fin size are undesirable because they make the vehicle more sensitive to local winds during the launch phase and consequently increase the deviation of the rocket from the desired trajectory. Similarly, increases in roll rate may result in centrifugal loads too large for the instrumentation to handle,

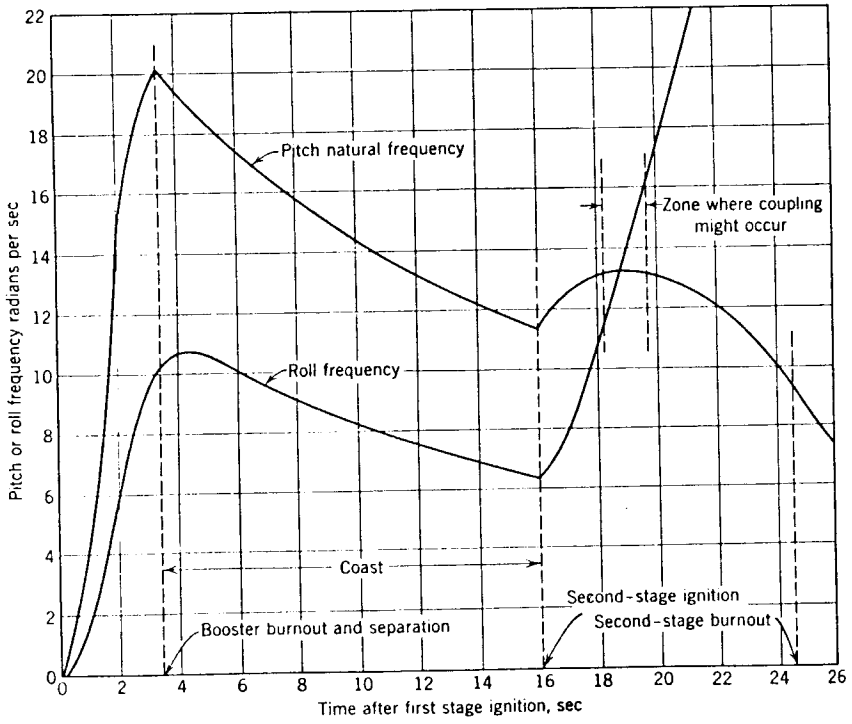


Fig. 10:28 Results of a roll–pitch coupling study for a two-stage Nike-Tomahawk rocket system.

and decreases in roll rate yield additional deviations from the desired flight path. In short, many rocket systems are really difficult problems.

10:21 Testing Bombs

Bomb shapes are frequently tested in a tunnel primarily to determine their static stability and secondarily to get a first cut at the drag. Tests are run at Mach numbers from 0.4 to perhaps 2.0 with close intervals of

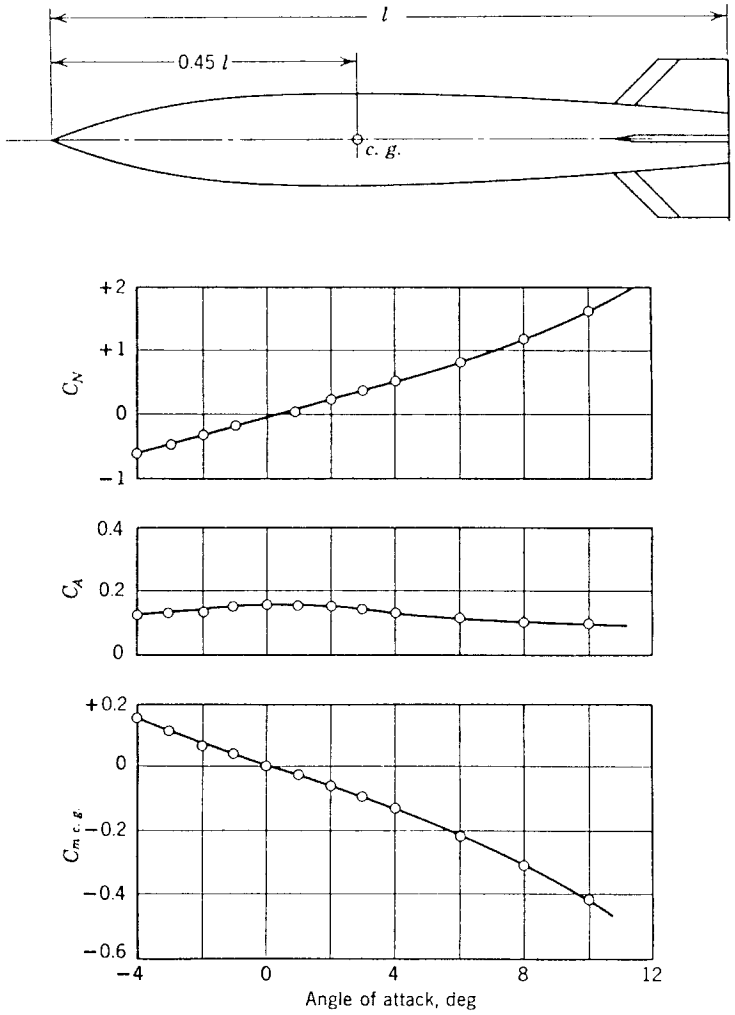


Fig. 10:29 Streamlined bomb data; $M = 0.90$. Coefficients based on maximum cross-sectional area and model length.

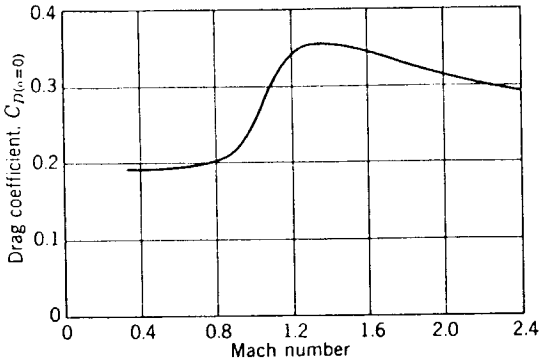


Fig. 10:30 Typical variation of streamlined bomb drag with Mach number, $\alpha = 0°$.

Mach number employed in the transonic range where the various parameters are varying most rapidly. The angle of attack schedule might run from −4 deg to +4 deg in 1 deg increments on up to a maximum angle of 45 deg, using larger increments above +4 deg. Preliminary tests may well go only up to say 15 deg. Several fin configurations may be tried. Center of gravity positions typically vary from 40 to 50 per cent of the bomb's length measured from the nose.

Whether or not to use transition roughness must be decided by the staff of the particular tunnel being employed, using an estimate by the bomb designer of whether the full-scale bomb will have a laminar or a turbulent boundary layer flow, the desire being to duplicate the type of flow expected. The bomb designer is seeking a C_{m_α} of −0.01 per degree or more negative based on maximum cross-sectional area and body length, although he may express this as, say, a "20 per cent static margin, based on body length."*

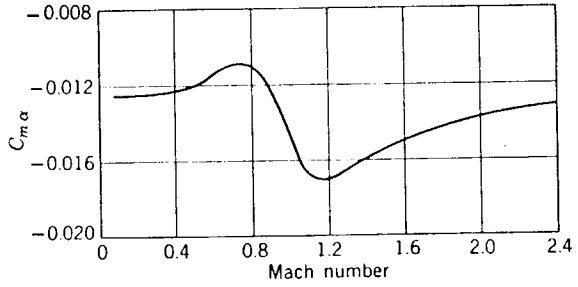


Fig. 10:31 Typical variation of the slope of the moment coefficient curve for a streamlined bomb with Mach number, per degree.

* Static margin is the nondimensional distance of the center of pressure behind the center of gravity.

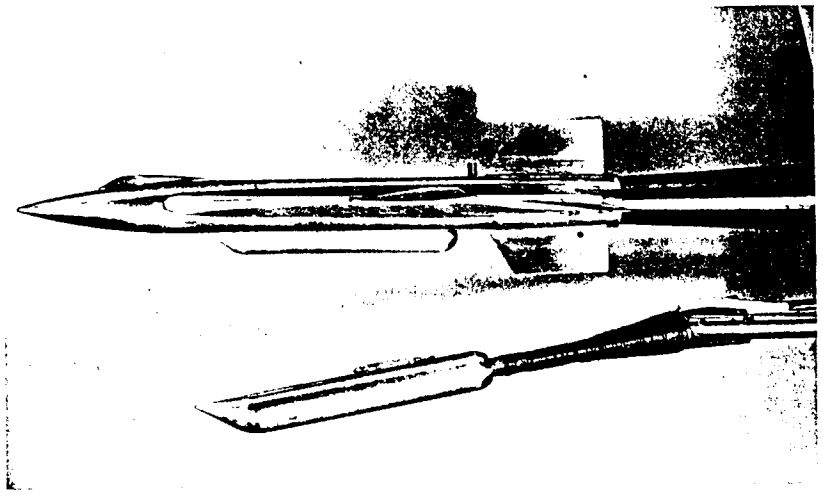


Fig. 10:32 Setup for proximity test. (Courtesy National Aeronautics and Space Agency.)

Data for one bomb shape at one Mach number are shown in Fig. 10:29 and variations of important parameters with Mach number are shown in Figs. 10:30 and 10:31. Sometimes the pitching moment data are plotted against C_N rather than against α, and any parameters may be plotted against Mach number at a constant angle of attack. This type of plot will require replotting from the original data, since sting and balance deflection usually result in the points' not being exactly at even increments of angle of attack.

The effect of the sting and the Reynolds number on drag is such that a 20 per cent error between tunnel and full scale either way may be expected particularly at transonic speeds. The effect on C_{m_α} is believed to run somewhat better, but is hard to determine from full-scale tests because the bomb in flight is usually rolling as well as pitching.

As mentioned in Section 10:20, one seeks to avoid having a bomb roll at the natural pitch frequency in order to avoid roll–pitch coupling. The natural pitch frequency of a great number of full-scale bombs seems to run about one cycle per second. For such shapes one should avoid rolling at one revolution per second. Aerodynamicists are interested in "installed" drag of a bomb as well as that in free flight, since when a bomb is mounted on an airplane externally the interference typically increases its drag by a factor of 2 or 3 or even more, plus, of course, the drag of the pylon. For a first approximation, the minimum overall drag usually occurs when the

pylon places the bomb about a diameter away from the airplane; more pylon adds excessive pylon drag; less increases the mutual interference. The fact that bombs might be small relative to their carriers or that the carriers themselves might be temperature limited as far as top speed is concerned is no argument to slight bomb drag: several bombs might be carried so that the overall drag becomes consequential; and even temperature limited airplanes suffer a loss in range. Sometimes interference and/or buffet is reduced by cambering the pylons, nose-in in most cases.

10:22 Proximity Tests

One of the more difficult types of force tests made in wind tunnels are the aircraft-store and booster–second-stage interference tests. These tests, for aircraft, are made to obtain data for estimating the early part of the store release trajectory, so that collision will not occur. It is also desirable to avoid excessive pitch-up in order to prevent radar-fused bombs from ranging on the delivery aircraft. The latter action has occurred in flight and is irritating to the crew of the delivery aircraft.

In the aircraft-store interference test, the store model is mounted on one balance and the aircraft model is mounted on a separate balance or sting (Fig. 10:32). Mechanisms are required which allow translation of the store with respect to the aircraft as well as rotation of the store about its center of gravity. Translation and rotation in the side force plane are sometimes required in addition to these movements in the pitch plane. If the store is located off the aircraft centerline, side loads will probably be significant and can be very large. And, of course, there will be a relative speed between the aircraft and store so that axial movement of the store is required.

Interference tests are sometimes made by taking data during a pitch traverse and during a yaw traverse of the store at a number of vertical and axial stations relative to the wing. When an accurate definition of the stability parameters has been obtained through the region of interference, it is possible for the aerodynamicist to predict a trajectory by a series of point-to-point calculations. The difficulty is that a tremendous amount of data must be taken in order to have information at each angle and location.

Considerably more sophisticated systems have been built for some tunnels, notably at the Cornell Aeronautical Laboratory. These systems provide the capability for remote and automatic rotation and traversing of the store relative to the aircraft. The store is positioned next to the aircraft. Signals from the store balance are fed into a computer, which calculates the amount of translation and rotation of the store that would occur in a specified time interval due to the loads indicated by the balance.

The computer sends a signal to the control for automatic rotation and traversing of the store, which causes the calculated motions to occur. The procedure is repeated a number of times until the store is out of the region of interference or far enough away from the aircraft.

The booster–second-stage separation is a somewhat simpler problem, involving as it does separation only along the axis of symmetry. Frequently the engineer is satisfied to take pressures around the booster head cap, or only to measure the separate drag on each body. The difficulty arises from the need for two balances along the same sting.

10:23 Magnus Force Tests

Magnus forces are forces associated with vehicles that are roll stabilized, such as rockets, bombs, and projectiles from guns. They arise when a spinning vehicle acquires an angle of attack owing to a disturbance. The source of the force may be visualized by considering a low-speed flow normal to a nonspinning cylindrical vehicle in flight. Flow normal to the cylinder will be symmetrical and will cause a force in the direction of the relative wind because of separation on the leeward side. If the vehicle is spun, one point on the cylinder will be moving toward the relative wind at the roll velocity while a point 180 deg away on the cylinder is moving away from the relative wind at the same speed. When this occurs the separation points are rotated from their no-spin positions. The resulting separation pattern is not symmetrical about a plane aligned with the flow and passing through the vehicle axis. This nonsymmetry causes a cross flow component of force called Magnus force, which in turn results in a Magnus moment.

Wind tunnel tests to determine Magnus forces require that the body be driven in roll by use of either an internal motor or fins at differential incidence. Indeed, simply providing bearings for rotation may result in surprising rates of roll although the fins are set to zero incidence within measurable tolerances. At high angles or attack *autorotation* may occur and the model should have a brake.

10:24 Drop Tests

The separation of bombs from the bomb bays of aircraft and sometimes the separation of stores are studied by simply dropping or ejecting them from the model as they would be dropped or ejected from the full scale aircraft. Although it is not possible to scale a drop test accurately at high speeds, much valuable information has been obtained from wind tunnel drop tests.

One of the main problems in scaling drop tests is gravity, though there

are others. A scaled model object dropped from a scaled model airplane in a wind tunnel will be subjected to an acceleration of 1 g and at the end of a fraction of a second will be a certain distance away from the aircraft. When the full-scale object is dropped from the full-scale aircraft, the distance between the two at the end of a time interval will be the same as the distance between a model aircraft and a model store at the end of the same time interval. In the case of the model the distance of separation might be 10 model lengths whereas it will be only one aircraft length in the full-scale case. Obviously, the interference effects are not the same. At the end of a given time interval a shock wave from the full-scale object could be striking the tail of the airplane while a shock wave from the scaled object would pass well downstream of the scaled airplane.

With regard to tunnel operation during drop tests, the tunnel engineer has two primary problems. One is to obtain accurate information on the position and attitude of the model during the drop. This is usually accomplished by the use of two synchronized cameras, one looking at the model from the side and the other looking from the bottom. Sometimes

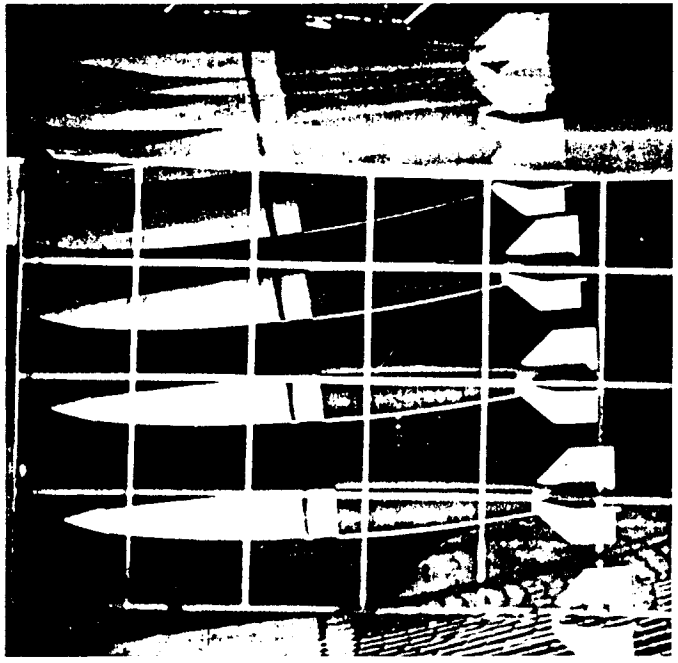


Fig. 10:33 Multiple flash drop picture. The illusion that the store is entering the catch-net is due to the net's being in every flash and thus appearing more intense.

a multiple flash technique is used (Fig. 10:33). The other problem is to ensure that dropped models do not cause damage to personnel or to the wind tunnel circuit. One solution used is to have a model-catching screen or grid. Another is to use frangible models, which are essentially pulverized upon impact with the tunnel walls.

10:25 Testing Airfoils

Two-dimensional airfoil tests are not nearly so common in high-speed wind tunnels as in the low-speed tunnels. However, it is sometimes desired to make tests with two-dimensional airfoils or flat plates to study pressure distribution, boundary layer, or heat transfer rates. When such tests are required it is customary to mount the model between two side walls of the tunnel with little or no gap between the ends of the model and the wall. A common method of doing this is to replace the glass schlieren windows with steel plugs and attach the model to the steel plugs. Where optical measurements were desired, the models have been clamped between the glass windows. Needless to say, this is a delicate operation. In addition to the dangers of glass breakage, stresses set up in the glass are likely to have a significant effect on schlieren photographs.

For two-dimensional testing, it is necessary that the area of the model being investigated be outside the region of influence of the tunnel walls; this may be taken as Mach cones emanating from the juncture of the airfoil and the tunnel wall. Thus the airfoil chord must be less than $(w/2)\cot\alpha_m$, where w = tunnel width, and α_m = the Mach angle.

10:26 Engine Tests

Some of the very large supersonic wind tunnels are equipped for full-scale tests of turbojet and ramjet engines. These wind tunnels are often equipped with scavenger systems to remove the products of combustion from the engine, so that full-scale burning tests can be made. The main object of such tests is usually to study the interaction between internal and external flows.

In the more modestly sized wind tunnels, engine testing is most frequently limited to studies of the characteristics of turbojet or ramjet inlets. The type of model usually used in tests of ramjet engine inlets (and similarly in tests of turbojet engine inlets) is described in Section 8:5. These tests are strictly pressure tests designed to determine the uniformity of flow entering the burner portion of the engine at various operating conditions (angle of attack, Mach number, and inlet configuration), and to determine the efficiency of the inlet in terms of how much air it will deliver to the burner and at what pressure. A series of pitot pressure probes in the duct downstream of the inlet diffuser (Fig. 8:8) are arranged to provide a

representative profile of the pitot pressure throughout the duct. At the survey station, the flow is normally subsonic, so that the pitot pressures are total pressures. The "pressure recovery" of the inlet is defined as the ratio of this total pressure in the inlet duct to the total pressure of the freestream tunnel flow. Schemes have been used in which the duct cross section was divided into a number of equal areas with a pitot probe on the center of each area. With this scheme, the average pressure recovery for the inlet is obtained by averaging the values obtained from the individual tubes.

In addition to total pressures, static pressure measurements are made in the vicinity of the pitot probes, either with static pressure probes or with duct wall orifices. From these pressure measurements together with measurements of total pressure and temperature of the tunnel flow it is possible to determine the "capture area ratio." Capture area ratio is a parameter used in determining inlet performance. It is defined as the ratio of the air passing through the duct to the air flowing in a streamline of the undisturbed test section that has a cross-sectional area equal to the cross-sectional area of the inlet lip. Using relations of Section 1:2 and assuming adiabatic flow, we can calculate the capture area ratio from the following equation:

$$\frac{A_c}{A_i} = \frac{p_{td}}{p_{t\infty}} \frac{(\rho/\rho_t)_d}{(\rho/\rho_t)_\infty} \frac{M_d}{M_\infty} \frac{A_d}{A_i} \sqrt{\frac{(T/T_t)_d}{(T/T_t)_\infty}} \qquad (10:8)$$

where A = cross-sectional area, ft²,
p = pressure, lb/ft²,
ρ = density, slugs/ft³,
M = Mach number,
T = temperature, °R.

The subscript t denotes total conditions, d denotes conditions at survey station in duct, and ∞ denotes conditions in the tunnel freestream.

An alternative method of determining capture area ratio is sometimes used which avoids the necessity of knowing static pressure and Mach number in the duct. The minimum flow area is determined at the downstream plug, which is used to control the flow through the inlet (see Fig. 8:8). The flow is normally sonic at this minimum area during the inlet test. The capture area ratio in this method is determined by letting the d subscript of eq. (10:8) denote conditions at the downstream plug, where the flow is at Mach 1.0.

The inlet performance is defined by a plot of pressure recovery versus capture area ratio as shown in Fig. 10:34. The variations of duct flow during the test are achieved by moving the exit throttle plug and thus changing the exit area of the duct.

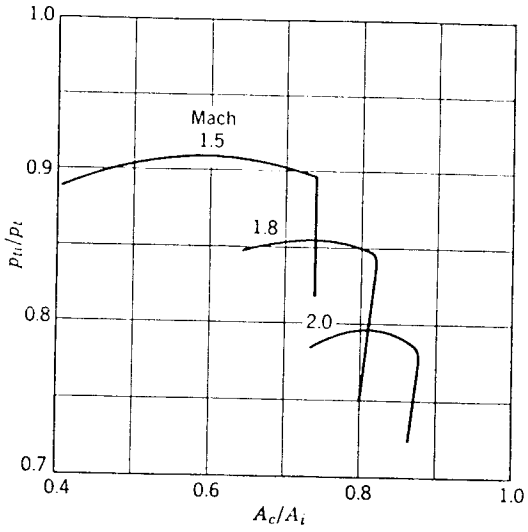


Fig. 10:34 Typical pressure recovery versus capture area ratio plot for a ramjet engine inlet (A_c/A_i = ratio of stream tube area captured by the inlet to the inlet area; p_{ti}/p_t = ratio of total pressure in the engine to total pressure of the freestream).

A problem often encountered during tests of ramjet engines is a violent flow instability called "buzz" during certain operating conditions. This is a condition that sometimes occurs when the pressure recovery is just about right to hold a normal shock in the converging portion of the inlet diffuser. Some small flow instability, probably of a viscous nature, is just right to cause the shock to pop out of the inlet diffuser and then right back in. This phenomenon may occur at a frequency of a few to many cycles per second. It is violent in nature and the model must be well built and well secured to avoid its being lost.

10:27 Testing Retro-Rockets

Retro-rockets are rockets that have a jet exhaust in the direction of flight rather than opposite the direction of flight as do conventional rocket engines. The purpose of the rockets is, of course, to slow a vehicle at some time during its flight. Though studies with which the authors are familiar indicate the superiority of parachutes for this purpose from a weight and volume standpoint, retro-rockets are incorporated in some vehicles and wind tunnel tests are sometimes required.

In typical tests of retro-rockets, high-pressure air is piped to the rocket motor from outside the tunnel through the model sting. The total pressure of the air supplied to the rocket motor is varied to cover an expected range of thrust conditions. Pressures are measured over the surfaces of the

model and integrated to determine total aerodynamic loads on the model. Shadowgraph or schlieren photographs are usually taken.

The thrust coefficient of the retro-rocket is an important parameter in such tests and is determined from the sum of momentum and pressure area product as follows:

$$T = \rho_j A_j V_j^2 + (p_j - p)A_j \qquad (10:9)$$

where T = thrust, lb,
ρ_j = air density at jet exit, slugs/ft³,
A_j = cross-sectional area of jet exit, ft²,
V_j = air velocity at jet exit, ft/sec,
p_j = pressure at jet exit, lb/ft²,
p = freestream static pressure, lb/ft².

Using the perfect gas relation $q = (\gamma/2)pM^2$ for defining flow conditions at the jet exit and rearranging eq. (10:9), we obtain the thrust coefficient from

$$C_t = \frac{A_j}{S}\frac{p_t}{q}\left[\frac{p_{t_j}}{p_t}\frac{p_j}{p_{t_j}}(1 + \gamma_j M_j^2) - \frac{p}{p_t}\right] \qquad (10:10)$$

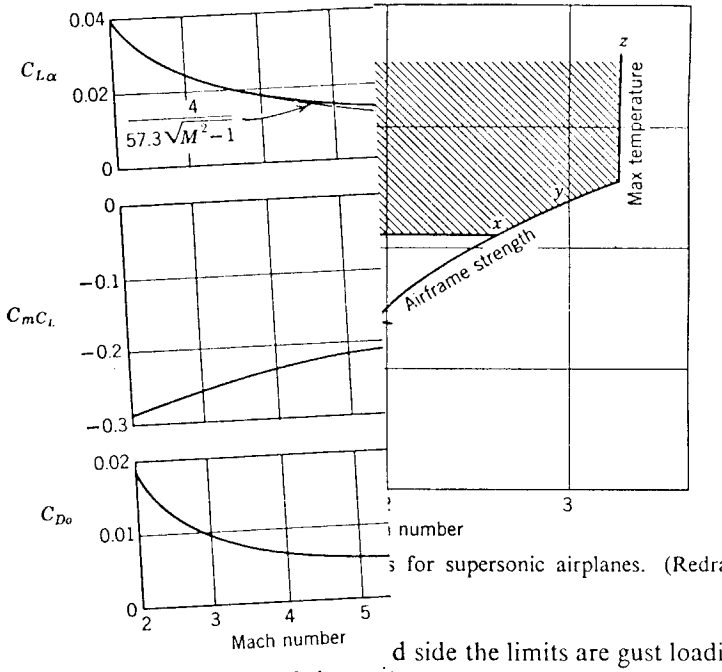
where C_t = thrust coefficient,
S = reference area, ft²,
p_t = total pressure of freestream flow, lb/ft²,
q = dynamic pressure of freestream flow, lb/ft²,
p_{t_j} = total pressure of retro-rocket flow, lb/ft²,
γ_j = specific heat ratio of retro-rocket flow,
M_j = Mach number of retro-rocket flow at jet exit.

The effects of the retro-rocket on stability and drag data from wind tunnel tests have sometimes appeared quite erratic. Model normal forces at positive angles of attack have in some cases become negative. Also, the forward model surface pressures have indicated a loss of pressure drag due to the jet exhaust.

Data commonly required from retro-rocket tests are plots of C_t versus p_{t_j}/p_t and plots of the normal force, pitching moment, and axial force coefficients versus angle of attack for various values of p_{t_j}/p_t.

10:28 Testing Complete Airplanes

Wind tunnel tests of a complete supersonic airplane follow the general testing procedure outlined in Section 8:6 and the programs outlined in Section 9:8 for transonic airplanes. Here we will only add a few comments on the data and their presentation for the supersonic case. The following remarks apply primarily to the case of a supersonic fighter, which customarily has low values of stability because of the need for maximum maneuverability.



s for supersonic airplanes. (Redrawn

Fig. 10:35 Presentation of the maj ıation temperature—line *uvwxyz*. supersonic airplane. Values should no e may be ignored.)

d side the limits are gust loading,

ing qualities of such aircraft are around $C_L = 0.1$, $(L/D)_{max}$ decr high altitudes where the low air values of L/D are hard to obta usual long aircraft fuselage with $M = 2.0$ and 5.0 at $M = 3.0$ be ntrol and stability augmentation

A representative summary o creates more work for the tunnel Fig. 10:35. that the airplane will be flyable

Most supersonic aircraft emp e.

vertical tail surfaces, and have psonic transports have yielded the moments. In such cases the mo

he does not have to provide mo aircraft now flying, remarkable hinge moment balances. To ma rerunners of more sophisticated normally be several tail sizes an g designers that in the not too generally somewhat larger tha rsonic transports may equal that ±30 deg. ll come about through improved

Some comments on superson lage interference, and improve- is designed to *cruise supersonic* dash capability. Such a craft is

economic ones) as shown in Fing span to the wing planform area, first limited by stall speed, then

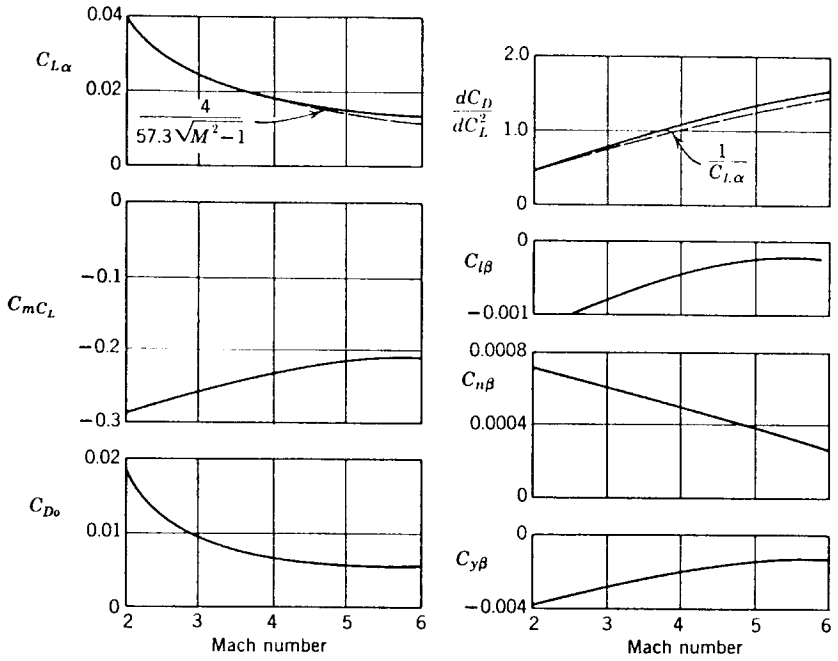


Fig. 10:35 Presentation of the major stability and performance parameters for a supersonic airplane. Values should not be taken as typical.

around $C_L = 0.1$, $(L/D)_{max}$ decreases with increasing Mach number. High values of L/D are hard to obtain at supersonic speeds, a value of 6.0 at $M = 2.0$ and 5.0 at $M = 3.0$ being very good.

A representative summary of the data described above is shown in Fig. 10:35.

Most supersonic aircraft employ completely movable horizontal and vertical tail surfaces, and have power boost to overcome the surface hinge moments. In such cases the model designer will be relieved to learn that he does not have to provide movable elevators, for instance, with internal hinge moment balances. To make up for that saving, however, there will normally be several tail sizes and locations required. Deflection angles are generally somewhat larger than for subsonic aircraft, perhaps up to ±30 deg.

Some comments on supersonic transports follow. This type of airplane is designed to *cruise supersonically* rather than only to have a supersonic dash capability. Such a craft is beset by many operational limits (besides economic ones) as shown in Fig. 10:36. On the low-speed side flight is first limited by stall speed, then by buffet, and finally by engine flame-out

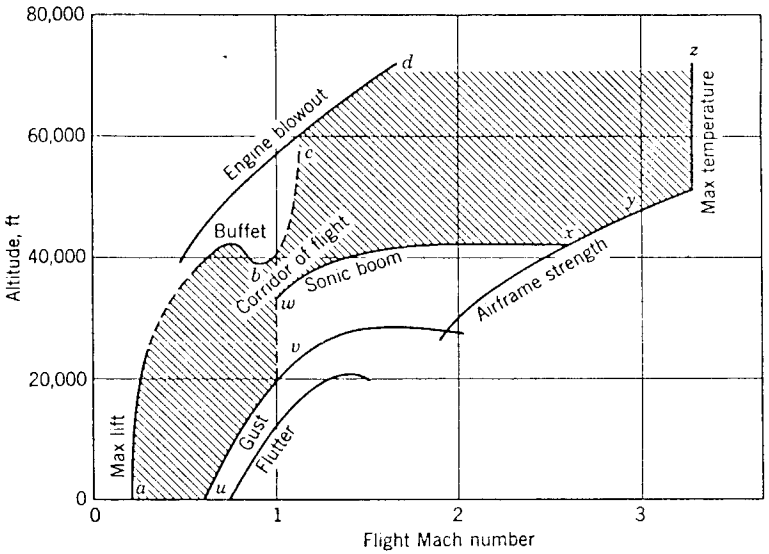


Fig. 10:36 The many operational boundaries for supersonic airplanes. (Redrawn from Ref. 10:14.)

as seen from line *abcd*. On the high-speed side the limits are gust loading, sonic boom, airframe strength, and stagnation temperature—line *uvwxyz*. (For military aircraft the sonic boom line may be ignored.)

Besides performance problems, the flying qualities of such aircraft are apt to be marginal. They will fly at very high altitudes where the low air density will result in poor damping for the usual long aircraft fuselage with low aspect ratio* wings. Usually, both control and stability augmentation devices will be necessary. This normally creates more work for the tunnel engineer who must obtain data to ensure that the airplane will be flyable with the augmentation devices inoperative.

Comments from the designers of supersonic transports have yielded the following information.

1. Performance. The many supersonic aircraft now flying, remarkable as they are, must still be considered the forerunners of more sophisticated designs. Indeed, there is a feeling among designers that in the not too distant future the overall efficiency of supersonic transports may equal that of current jet airliners. This hopefully will come about through improved wing warpage, more favorable wing-fuselage interference, and improvements in turbine inlet and exit design.

* Aspect ratio is the ratio of the square of wing span to the wing planform area, b^2/S.

2. Longitudinal Stability. Many of the design parameters required for supersonic flight contribute to difficulties in the pitch performance of the aircraft; for example, the fixed arrow wing has an undesirable nonlinear variation of lift and moment with angle of attack. This situation may be improved by wing slats or notches or by tail relocation or cathedral (opposite of dihedral).

3. Lateral-Directional Stability. The needlelike configurations proving most promising for supersonic aircraft (particularly transport designs) have far higher ratios of the moment of inertia about the yaw axis to that about the roll axis (say 8) than those usually found for subsonic aircraft (say 2). This leads to coupling between the directional and roll controls such that the airplanes show excessive roll in response to the directional controls. Decreasing the magnitude of the effective dihedral (C_{l_β}) while increasing the directional stability (C_{n_β}) is desirable, but not easy. Two or three short span vertical tails (instead of one tall tail with the same tail volume coefficient) will reduce C_{l_β}, but an additional retractable or folding vertical tail may be needed to hold sufficient C_{n_β} at the higher end of the speed range, or at high angles of attack. Changes in fuselage cross section may be of help in this regard.

The results of testing one supersonic transport configuration are given below. They are from Ref. 10:15.
Weight, $W = 300{,}000$ lbs.
Wing area, $S = 4040$ ft^2.
Wing span, $b = 76.8$ ft.
Mean aerodynamic chord, $\bar{c} = 62.73$ ft.
Slope of the lift curve, $dC_L/d\alpha = 1.55$ per radian.
Lift variation with elevator deflection, $dC_L/d\delta_E = 0.375$ per radian.
Elevator power, $dC_m/d\delta_E = 0.25$ per radian.
Static stability, $dC_m/d\alpha = -0.36$ per radian.
Damping in roll due to rolling velocity, $C_{l_p} = -0.125$ per radian/sec.
Aileron power, $dC_l/d\delta_a = -0.011$ per radian.
Damping in roll due to yawing velocity, $C_{l_r} = 0.102$ per radian/sec.
Roll due to yaw, $C_{l_\beta} = -0.0862$ per radian.
Static directional stability, $dC_n/d\beta = 0.075$ per radian.
Damping in yaw due to yawing velocity, $C_{n_r} = -0.453$ per radian/sec.
Damping in yaw due to rolling velocity, $C_{n_p} = 0.014$ per radian/sec.
Rudder power, $dC_n/d\delta_r = -0.028$ per radian.
Yawing moment due to aileron deflection, $dC_n/d\delta_a = -0.0092$ per radian.
Side force due to yaw, $dC_Y/d\beta = -0.347$ per radian.
Side force due to rudder deflection, $dC_Y/d\delta_r = 0.042$ per radian.
Drag coefficient at zero lift, $C_{D,0} = 0.0082$, nondimensional.

Drag rise with lift, $dC_D/dC_L{}^2 = 0.585$, nondimensional.
Static stability, $dC_m/dC_L = -0.232$, nondimensional.
Moment of inertia about X-axis, $I_X = 1{,}000{,}000$ slug-ft^2.
Moment of inertia about Y-axis, $I_Y = 10{,}000{,}000$ slug-ft^2.
Moment of inertia about Z-axis, $I_Z = 11{,}000{,}000$ slug-ft^2.

10:29 Testing for Sonic Boom

The increased use of supersonic velocities and the advent of the supersonic transport have centered interest in both the strength of the overpressure on the ground and the possibility of simulating the conditions in a wind tunnel for alleviation studies. Indeed, the current discussion of eliminating the lower surface shock impingement on the ground by reflecting it upward from a small reflecting surface mounted below the wing may stimulate studies in this area.

A primary difficulty in making sonic boom tests in a wind tunnel arises from the necessity of providing a model small enough that large distances (measured in terms of airplane body lengths) are realizable. Model scales of 0.0005 (physically 1.5 inches long) become necessary (see Fig. 10:37). Theory indicates that they should have as near the full-scale distribution of cross-sectional area versus length as possible. Duct area may be subtracted. For a test one then sets the tiny model at the angle of attack corresponding to cruise condition (allowing for tunnel flow angularity) and measures the static pressures along a line parallel to the tunnel axis as far away as one can get and still stay out of the tunnel boundary layer. Although theory (Ref. 10:13) indicates that one should see a classical N pressure pattern with a sharp rise and fall (dashed line, Fig. 10:38*a*), tunnel pressure patterns fall short of the ideal, usually showing a rounded off profile as seen in Fig. 10:38*a* or a shouldered profile as in Fig. 10:38*b*. The shoulder is probably due to failure to have enough distance for complete melding of the bow and wing–fuselage juncture shocks. Rounding off may be due to vibration of the model. A reasonable procedure is to extend the $\Delta p/p$ curve until the two shaded areas in Fig. 10:38 are equal and reading a new extrapolated maximum value. In the above pressure patterns the rise indicates the pressure intensity and the length its wavelength. Both depend on airplane geometry and flight conditions. The pressure rise on the ground is reduced by reducing Mach number, increasing the airplane size for a given weight, or increasing the flight altitude.

Correlation of wind tunnel and flight data of sonic boom has been good.

10:30 Acceleration Wind Tunnels

At the present time several wind tunnels have been built and others are under study or construction which would impose accelerations on the

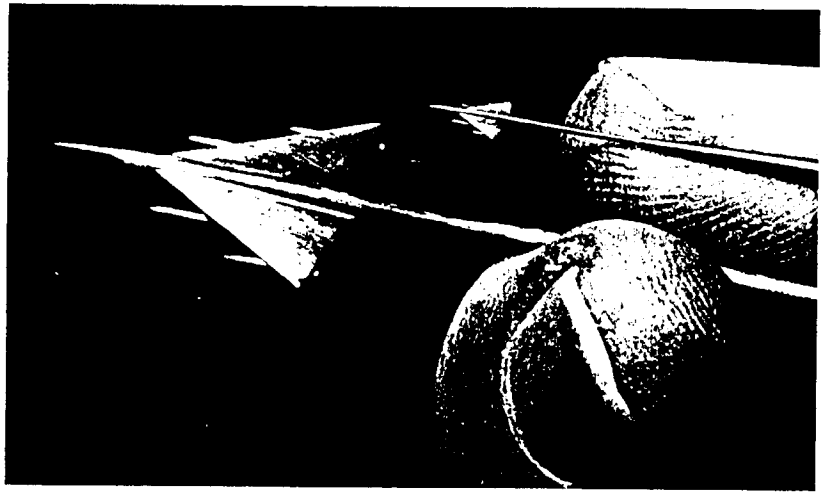


Fig. 10:37 The tiny wind tunnel models needed for studying sonic boom.

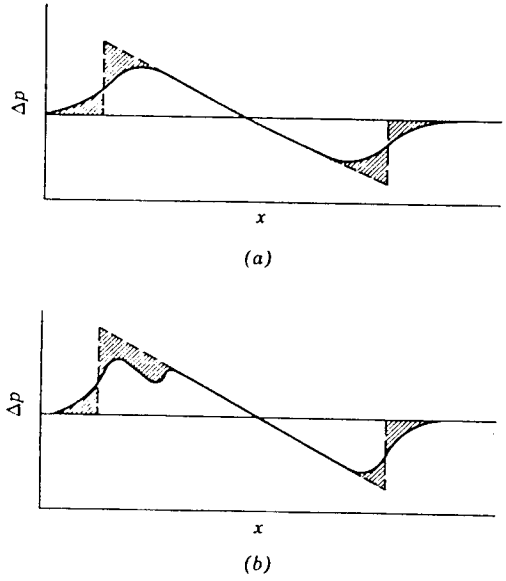


Fig. 10:38 Typical sonic boom pressure patterns as measured in wind tunnels.

model or airstream or both, usually by mounting the complete tunnel on a centrifuge. Studies that may be made in a tunnel of this type include turbine cascade studies with acceleration to more nearly approach conditions in the actual turbine, studies to determine the effects of an acceleration field on condensation on a cool surface, and studies to determine the effects of acceleration on vehicle stability, jet flows, and ablation. The acceleration approach offers an opportunity to expand the whole field of wind tunnel testing.

10:31 Testing for Unsteady Pressures

Many missile shapes exhibit unsteady pressures at the juncture of the nose cone and the body cylinder, particularly if the joint is abrupt. The pressure may be due to separated boundary layers as well as to those alternately separated and attached. The peak-to-peak pressure readings may range up to 65 per cent or so of the dynamic pressure, and hence constitute a potential source of trouble, normally worse in the transonic range where q is a maximum.

Transducers with leads to their respective orifices kept as short as possible can be installed in wind tunnel models to see if this phenomenon is present, but unfortunately the fluctuations seem to be affected by model size and more work needs to be done in this area before good extrapolation to full scale can be made. Reference 10:16 may be consulted for further information on tests of this special type.

10:32 Testing Missile Base Heating

Missiles that have single nozzles often have a base heating problem due to (a) recirculation of hot exhaust gases into the base region as a result of jet–freestream interactions; (b) radiation from the hot exhaust; and (c), for some types of liquid-fuel rockets, burning of the fuel-rich turbopump gases entrained in the base region. When several nozzles are employed, mutual interference can lead to base heating. In one installation temperatures of 2000°F were measured on the missile base plate, and 3000°F on the flame plate in the plane of the nozzles.

Missile base heating may be well simulated in the wind tunnel, but with substantial hazard if the full temperature of the hot exhaust is duplicated. Normally both high- and low-speed tests are needed, and tests should be run with various nozzles inoperative.

10:33 List of Supersonic Wind Tunnels

Table 10:1 gives a partial list of the supersonic wind tunnels in this country and around the world.

Table 10:1

Supersonic Wind Tunnels

Organization	Tunnel	Location	Type	Mach Number Range	Test Section Size	$p_{t(max)}$, psia	$T_{t(max)}$, °R	Remarks
			A. GOVERNMENT					
AEDC	E-1	Tullahoma, Tenn.	Blowdown	1.5–5.0	12″ × 12″	1 to 60	660	
AEDC	PWT	Tullahoma, Tenn.	Continuous	1.5–4.0	16′ × 16′	0.3 to 1.0	1100	216,000 hp
AEDC	A	Tullahoma, Tenn.	Continuous	1.5–6.0	40″ × 40″	1.3 to 200	800	100,000 hp
ASD	2-ft	Wright Field, Ohio	Continuous	1.5–5.0	24″ × 24″	0.3 to 45	—	Deactivated
ATL	17 × 21-inch	Pt. Mugu, Calif.	—	1.6–2.5	17″ × 21″	—	—	Deactivated
ATL	14 × 16-inch	Pt. Mugu, Calif.	—	2.5	14″ × 16″	—	—	Deactivated
BRL	No. 1	Aberdeen, Md.	Continuous	1.4–5.0	15″ × 13″	7–100	560	13,000 hp
BRL	No. 3	Aberdeen, Md.	Continuous	1.3–4.9	20″ × 15″	15–60	560	
DTMB	9-inch	Carderock, Md.	Indraft	0.1–4.5	9.5″ × 9.5″	15	540	
DTMB	12-inch	Carderock, Md.	Indraft	1.3–4.0	12″ × 12″	15	540	
DTMB	18-inch	Carderock, Md.	Indraft	0.2–4.5	18″ × 18″	15	540	
NASA, Ames	6-foot	Moffett Field, Calif.	Continuous	0.65–2.2	6′ × 6′	4–15	—	50,000 hp
NASA, Ames	8 × 7-foot	Moffett Field, Calif.	Continuous	2.4–3.5	8′ × 7′	2–30	—	200,000 hp
NASA, Ames	9 × 7-foot	Moffett Field, Calif.	Continuous	1.5–2.5	9′ × 7′	2–30	—	
NASA, Ames	1 × 3-foot	Moffett Field, Calif.	Continuous	1.4–6.15	12″ × 34″	20–60	690°	10,000 hp
NASA, JPL	20-inch	Pasadena, Calif.	Continuous	1.2–5.6	18″ × 20″	0.3–70	700	
NASA, Langley	4 × 4-foot	Langley Field, Va.	Continuous	1.47–2.87	4′ × 4′	2–60	760	60,000 hp
NASA, Langley	4 × 4-foot	Langley Field, Va.	Continuous	2.29–4.65	4′ × 4′	3–150	760	83,000 hp
NASA, Langley	4.5 × 4.5-foot	Langley Field, Va.	Continuous	1.41–2.2	4.5′ × 4.5′	2–40	610	
NASA, Langley	20-inch	Langley Field, Va.	Blowdown	2–4.5	20″ × 20″	25–130	660	
NASA, Langley	9 × 6-foot	Langley Field, Va.	Blowdown	3.0	8.8′ × 6′	55–200	1120	
NASA, Lewis	6 × 8-foot	Cleveland, O.	Continuous	0.8–2.1	6′ × 8′	15–25	720	100,000 hp
NASA, Lewis	10-foot	Cleveland, O.	Continuous	2–3.5	10′ × 10′	1–35	1160	250,000 hp
NASA, Marshall	7-inch	Huntsville, Ala.	Indraft	5.0	7″ × 7″	15	460	
NASA, Marshall	14-inch	Huntsville, Ala.	Blowdown	0.4–5.0	14″ × 14″	17–100	660	
NOL	No. 1	White Oak, Md.	Indraft	0.2–5.0	16″ × 16″	15	Ambient	
NOL	No. 2	White Oak, Md.	Continuous	0.2–5.0	16″ × 16″	12–45	600	
NOL	3-Mw arc	White Oak, Md.	Blowdown	3.5	2″ round	150–750	10,000	3-Mw arc tunnel
Sandia Corp.	Trisonic	Albuquerque, N.M.	Blowdown	0.4–3.0	12″ × 12″	15–75	550	
Sandia Corp.	Plasma arc	Albuquerque, N.M.	Continuous	3	3″ round	—	—	1 Mw
USNMC	20-inch	Point Mugu, Calif.	Continuous	1.6–6.0	20.8″ × 17″	15–165	1150	

Table 10:1 (*continued*)

Organization	Tunnel	Location	Type	Mach Number Range	Test Section Size	$P_{t(max)}$, psia	$T_{t(max)}$, °R	Remarks
B. INDUSTRY AND COLLEGES								
Boeing Co.	4 × 4-foot	Seattle, Wash.	Blowdown	1.2–4.2	4′ × 4′	18–126	520	
Douglas Aircraft Corp.	Trisonic	El Segundo, Calif.	Blowdown	0.2–3.5	12″ × 12″	20–100	540	
Douglas Aircraft Corp.	48 × 48-inch	El Segundo, Calif.	Blowdown	0.2–3.5	48″ × 48″	20–350	600	600-psi Storage
Fluidyne	13-inch	Minneapolis, Minn.	Blowdown	1.5–5	13″ diam	150	520	
Fluidyne	14-inch	Minneapolis, Minn.	Blowdown	2–5	14″ × 14″	150	520	
General Dynamics	48 × 48-inch	San Diego, Calif.	Blowdown	0.5–5.0	48″ × 48″	20–350	600	525-psi Storage
Grumman Aircraft Corp.	12-inch	Bethpage, N.Y.	Blowdown	1.4–4.0	12″ × 12″	37–600	520	3000-psi Storage
Lockheed-California Co.	4-foot	Burbank, Calif.	Blowdown	0.2–5.0	48″ × 48″	20–320		
Ling-Temco-Vought Corp.	4-foot	Dallas, Tex.	Blowdown	1.2–50	48″ × 48″	20–350	660	525-psi Storage
MIT	NSL supersonic	Cambridge, Mass.	Continuous	0.4–40	18″ × 24″	1–40	600	10,000 hp
McDonnell Aircraft Corp.	Polysonic	St. Louis, Mo.	Blowdown	0.5–5.8	48″ × 48″	20–400	800	
University of Michigan	8 × 13-inch	Ann Arbor, Mich.	Indraft	1.4–4.0	8″ × 13″	4–15	500	
University of Michigan	4 × 5-inch	Ann Arbor, Mich.	Indraft	1.3–5.0	4″ × 5″	4–90	500	
University of Minnesota	6 × 9-inch	Rosemount, Minn.	Continuous	1.5–5.6	6″ × 9″	120	900	600°F
North American Aviation	Trisonic	Inglewood, Calif.	Blowdown	0.4–3.5	7′ × 7′	15–140	550	
North American Aviation	Hyperthermal	Inglewood, Calif.	Blowdown	3.0	3.5″ round	—	—	1-Mw arc jet
Northrop Corp.	2-foot	Hawthorne, Calif.	Blowdown	1.5–5.0	24″ × 24″	9–600	500	
Ohio State University	12-inch	Columbus, O.	Blowdown	2.5–4.3	12″ × 12″	30–1500	500	1100 hp
Princeton University	4 × 8-inch.	Princeton, N.J.	Blowdown	2–4	4″ × 8″	50–900	—	4000-psi Storage
Republic Aviation	15-inch	Farmingdale, N.Y.	Blowdown	1.5–4.0	15″ × 15″	500	500	
United Aircraft Corp.	**17-inch**	**East Hartford, Conn.**	**Blowdown**	**1.5–5.0**	**17″ × 17″**	**40–300**	**540**	
C. FOREIGN								
ARA	2½-foot	Bedford, England	Continuous	1.4–3.2	27″ × 30″	—	—	13,000 hp
ARA	12 × 16-inch	Bedford, England	Blowdown	4–5	12″ × 16″	300	—	
ARA	27-inch	Bedford, England	Continuous	1.5–5.0	27″ × 27″	—	—	18,000 hp
ARDE	Low density	Ft. Halstead, England	Continuous	6.0	—	—	—	
ARL	16-inch	Whitley, England	Continuous	2.96	14″ × 16″	40	550	10,000 hp
Armstrong-Whitworth	18-inch	Coventry, England	Continuous	3.4	18″ × 14″	—	—	18,000 hp
Armstrong-Whitworth	24-inch	Coventry, England	Continuous	3.0	20″ × 24″	—	—	7700 hp
AVA	24-inch	Göttingen, Germany	Indraft	2.0	24″ × 24″			
AVA	3-foot	Göttingen, Germany	Continuous	0.4–2.5	3′ × 3′			
Avro	Supersonic	Woodford, England	—	1.6	20″ × 20″	—	—	
Avro	4-foot	Woodford, England	Blowdown	2–4.5	3′ × 4′	—	—	
Avro	Supersonic	Woodford, England	Blowdown	3.5	27″ × 30″			
BAC	20-inch	Weybridge, England	Indraft	1.4–3.5	20″ × 20″	—	—	
BAC	4-foot	Warton, England	Blowdown	0.2–4.0	48″ × 48″	600	550	
Bofors	12-inch	Karlskoga, Sweden	Blowdown	3.8	12″ diam	—	—	
Bristol Aircraft	20-inch	Bristol, England	Continuous Blow-down	1.7–4.5	20″ × 15″	150		24,000 hp
CAGI (new)	T-106	Moscow, USSR	—	2.0	—	—		
DFL	20-inch	Braunschweig, Germany	Blowdown	1.5–4.0	20″ × 20″	4000		250 kw
DVL	8-inch horizontal	Aachen, Germany	Blowdown	2.2	8″ × 8″	3000	1000	

Table 10:1 (*continued*)

Organization	Tunnel	Location	Type	Mach Number Range	Test Section Size	$p_{t(max)}$, psia	$T_{t(max)}$, °R	Remarks
DVL	12-inch	Aachen, Germany	—	6.0	12″ × 12″	—	—	
DVL	24-inch	Cologne, Germany	Blowdown	4.5	24″ × 24″	—		
DVL	Vertical	Aachen, Germany	Blowdown	2.2	8″ round	3750		
English Electric	18-inch	Wharton, England	Continuous	6.0	18″ × 18″	—	—	
English Electric	4-foot	Wharton, England	Blowdown	2–6.0	4′ × 4′	—	—	
ETH	16-inch	Zurich, Switzerland	Continuous	2.3	16″ × 16″			*
FFA	S-1 to S-4	Stockholm, Sweden	Indraft	0.5–3.6	To 22″	—	—	Four tunnels
FFA	Trisonic	Stockholm, Sweden	Blowdown	4.0	20″ × 20″	180	1400	
Flygmotor	18-inch	Trollhaten, Sweden	Blowdown	3.6	18″ × 18″	—	—	745 hp
Hawker-Siddeley	Supersonic	Coventry, England	Continuous	3.0	20″ × 24″	30	—	10,000 hp
KTH	Supersonic	Stockholm, Sweden	Blowdown	3.0	8.5″ × 8.5″	140	—	
LRBA	No. 1	Vernon, France	Continuous	4.4	16″ × 16″	160	—	20,000 hp
LRBA	No. 3	Vernon, France	Indraft	3.5	8″ × 8″	14.7	—	
LRBA	No. 4	Vernon, France	Indraft	2.1	8″ × 8″	14.7	—	
MAI	24-inch	Moscow, USSR	Continuous	3.0	24″ × 24″	—	—	11,000 hp
NAE	5-foot	Ottawa, Canada	Blowdown	0.2–4.5	5′ × 5′	20–200	500	
NAE	30-inch	Ottawa, Canada	Indraft	0.3–2.0	16″ × 30″	15	500	
NAE	3-foot	Bedford, England	Continuous	2.0	3′ × 3′	—	—	1200 hp
NAE	8-foot	Bedford, England	Continuous	2.7	8′ × 8′	—	—	68,000 hp
NAL	4-foot	Bangalore, India	Blowdown	0–3.5	4′ × 4′	—	—	
NAL	8-inch	Tokyo, Japan	Continuous Blow-down	2.6	7″ × 8″	50	700	
NAL	1-meter	Tokyo, Japan	Blowdown	3.0	39″ × 39″	—	—	
NLRL	SST	Amsterdam, Netherlands	Blowdown	1.2–4.0	4′ × 4′	15–220	500	6500 hp
NLRL	CSST	Amsterdam, Netherlands	Blowdown	0.6–6.0	12″ × 12″	15–600	700	
NLRL	4-foot	Amsterdam, Netherlands	Blowdown	1.2–4.0	4′ × 4′	600	—	
Nord-SFECMAS	Supersonic	Paris, France	Continuous Blow-down	1.9	14″ × 14″	—	—	Nene jet engine
Nord-SFECMAS	Transonic	Paris, France	Blowdown	2.0	8″ × 8″			
NPL	9.5-inch	Teddington, England	Induction	1.8	9.5″ × 9.5″			
NPL	9 × 3-inch	Teddington, England	Induction	1.8	9″ × 3″			
NPL	11-inch	Teddington, England	Continuous	2.8	11″ × 11″			
NPL	14-inch	Teddington, England	Continuous	2.6	11″ × 14″	20	—	
NPL	14 × 18-inch	Teddington, England	Induction	3.0	14″ × 18″	45		
NPL	20-inch	Teddington, England	Indraft	1.8	20″ × 25″	14.7	—	
NPL	36-inch	Teddington, England	Indraft	4.0	14″ × 36″	14.7	—	
ONERA	Aux 1	Modane, France	Blowdown	2.0	29″ × 37″	—	—	
ONERA	Aux 2	Modane, France	Blowdown	2.6	—	—	—	
ONERA	Aux 3	Modane, France	Blowdown	2.0	30″ diam	—	—	
ONERA	R1 Ch	Paris, France	Blowdown	2–5	8″ round	30–600	900	
ONERA	S5 Ch	Chalais-Meudon, France	Continuous	1–3.2	12″ × 12″	7–15	540	1400 kw

* World's first continuous supersonic tunnel.

Table 10:1 (*continued*)

Organization	Tunnel	Location	Type	Mach Number Range	Test Section Size	$p_{t(max)}$, psia	$T_{t(max)}$, °R	Remarks
ONERA	LC	La Courneuve, France	Continuous	0.75–2.3	6″ × 12″	7–22	540	
ONERA	S2 Ma	Modane, France	Continuous	0.9–3.2	6′ × 5′8″	—	—	55,000 kw
RAE	10-inch	Farnborough, England	Indraft	2.6	9″ × 10″	—	—	
RAE	10 × 10	Farnborough, England	Indraft	4.8	10″ × 10″	—	—	
RAE	18-inch	Farnborough, England	Continuous	1.4–3.0	18″ × 18″	40	—	7000 hp
RAE	3-foot	Bedford, England	Continuous	2.4	3′ × 3′	—	—	40,000 hp
RAE	8-foot	Bedford, England	Continuous	4.5	8′ × 8′	60	—	
WRE	15-inch	Salisbury, Australia	Continuous	1.4–3.0	15″ × 15″	45	670	4000 hp
ZAEA	Tunnel 8	Moscow, USSR	—	3.0	5.5″ round	—		
ZAEA	Tunnel 9	Moscow, USSR	—	1.3–2.0	4.7″ × 5.5″	—		
ZAEA	Tunnel 10	Moscow, USSR	—	1.8–2.2	14″ × 19″	—		

References

10:1 L. W. Walter and E. J. Redman, Needle Static Pressure Probes Insensitive to Flow Inclination in a Supersonic Stream, NAVORD Report 3694, 1954.

10:2 H. R. Vaughn, A Direct Reading Static Pressure Probe for a Supersonic Stream, Letter to the Editor, *JAS*, **27** (7), July 1960.

10:3 J. D. Lee and G. L. Von Eschen, Critical Performance Parameters of an Intermittent High-Pressure Free-Jet Supersonic Wind Tunnel, Ohio State University Proj. 344, 1954.

10:4 C. J. Schueler and W. T. Strike, Calibration of a 40-Inch Continuous-Flow Wind Tunnel at Mach Number 1.5 to 6.0, AEDC TN-59-136, 1959.

10:5 G. G. Gorensen *et al.*, A Method for the Calibration of Flexible Plate Supersonic Wind Tunnels and Calibration Results for the 12-Inch Wind Tunnel at the Jet Propulsion Laboratory, Report 20-110, 1957.

10:6 Hugh Franklin, Transister Reynolds Number Measurements in the CWI Supersonic Cart Using a 5-Degree Cone, CWT Rept. K-329, 1959.

10:7 Albert O. Ross, Determination of Boundary Layer Transition Reynolds Numbers by Surface-Temperature Measurements of a 10° Cone in Various NACA Supersonic Tunnels, NACA TN-3020, 1953.

10:8 K. L. Goin, Summary Calibration Report of the Ordnance Aerophysics Laboratory Supersonic Wind Tunnel, OAL Report 340-2.

10:9 R. C. Maydew, Compilation and Correlation of Model Starting Loads from Several Supersonic Tunnels, Sandia Corporation SC-4691(RR), June 1962.

10:10 K. R. Sivier and S. M. Bogdonoff, The Effect of Support Interference on the Base Pressure of a Body of Revolution at High Reynolds Numbers, Princeton University Report 332, 1955.

10:11 Jack D. Whitfield, Support Interference at Supersonic Speeds, AEDC TN-58-30, 1958.

10:12 William Gracey, Wind Tunnel Investigation of a Number of Total-Pressure Tubes at High Angles of Attack, Subsonic, Transonic, Supersonic Speeds, NACA TR 1303, 1957.

10:13 F. Walkden, The Shock Pattern of a Wing-Body Combination Far from the Flight Path, *Aero Quarterly*, **IX**, Pt. 2, May 1958, pp. 164–194.

10:14 William J. Alford and Cornelius Driver, Recent Supersonic Transport Research, *Astronautics and Aeronautics*, September 1964.

10:15 M. D. McLaughlin and James B. Whitten, Pilot Evaluation of Dynamic Stability Characteristics of a Supersonic Transport in Cruising Flight Using a Fixed-Base Simulator, NASA TN-D-2436, 1964.

10:16 H. L. Chevalier and J. E. Robertson, Unsteady Pressure and Scale Effects on Models of the Titan B Mark 4 Re-Entry Body at Transonic Speeds, AEDC TDR-62-178, 1962.

10:17 D. R. Andrews and W. G. Sawyer, The Calibration of a 60° Cone to Measure Mach Number, Total Pressure, and Flow Angles at Supersonic Speeds, HMSO, 1963.

10:18 Carlton S. James, Observations of Turbulent-Burst Geometry and Growth in Supersonic Flow, NASA TN 4235, 1958.

Chapter eleven

Calibration and use of hypersonic tunnels

11:1 General

Hypersonic tunnels operate in the Mach number range of 5 to 10 or higher. They usually operate with stagnation pressures of 150 to 1500 psia and stagnation temperatures from 150°F to 3500°F. They have solid-walled test sections and require contoured nozzles which are most frequently axially symmetric instead of two-dimensional (Fig. 11:1).

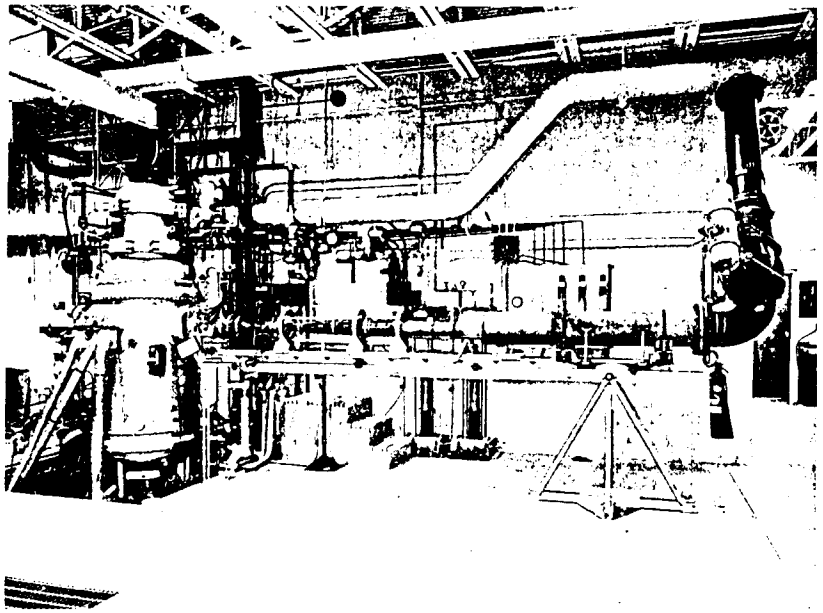


Fig. 11:1 Small hypersonic tunnel. Gas-fired pebble heater is at left, followed by gate valve, nozzle, test section, diffuser, and vacuum valve. (Courtesy Sandia Corporation.)

Models that can be tested in hypersonic tunnels are usually larger than those which can be tested in supersonic tunnels, and sometimes have frontal areas up to 10 per cent of the test section area. Model size will probably be limited by the large model wake, which takes up too much flow area in the diffuser and blocks it during tunnel starting. The tunnel wall is unlikely to affect the flow over the model.

Hypersonic tunnels use air that is heated to avoid liquefaction during expansion to the high Mach numbers and corresponding low temperatures (Section 1:11) and to facilitate heat transfer studies. The use of heated air is the major factor that causes hypersonic tunnels to be more complicated than supersonic tunnels. The air in hypersonic tunnels must also be dry (as in supersonic tunnels) to avoid condensation effects due to the expansion of the air to high Mach numbers and the consequently low temperatures. This is usually a less serious problem than in supersonic tunnels because in the process of compressing the air to the necessary high pressures for hypersonic flow, most of the natural water is simply squeezed out (Section 2:10).

11:2 Theory

A theory frequently used in the analysis of hypersonic flows is called the Newtonian Impact Theory. This theory is based on the premise that a stream approaching an object will impart to the object the component of its momentum normal to the surface of the object and that the tangential component of the freestream momentum will remain unchanged. From Fig. 11:2, the normal component of the freestream momentum affecting any unit surface area of an object is $\rho_\infty(U_\infty \sin \delta)^2$. If this momentum is imparted to the object, it represents a force per unit area or a pressure. A pressure coefficient is defined as

$$C_p = \frac{p - p_\infty}{q} \tag{11:1}$$

where p = pressure at some point on an object, lb/ft² abs,
p_∞ = freestream static pressure, lb/ft² abs,
q = freestream dynamic pressure, $\frac{1}{2}\rho_\infty U_\infty^2$, lb/ft².

The pressure due to momentum transfer represents a rise in pressure above ambient so that:

$$C_p = \frac{\rho_\infty(U_\infty \sin \delta)^2}{q} = 2 \sin^2 \delta \tag{11:2}$$

The angle between the approaching airstream and any portion of a conical segment of the surface of an axially symmetric body (body of revolution) δ is defined by

$$\sin \delta = \sin \eta \cos \alpha + \cos \eta \sin \alpha \cos \phi \tag{11:3}$$

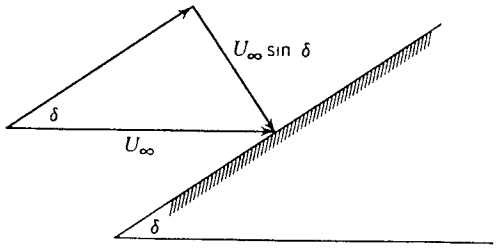


Fig. 11:2 Velocity component of flow of importance to Newtonian Impact Theory.

where α = angle of attack,
η = cone half angle,
ϕ = angle between two planes passing through the axis of the conical segment; one lies in the angle of attack plane and the other passes through the point of interest. When the point of interest is on the windward surface intersection with the angle of attack plane, $\phi = 0$ deg.

Equations (11:2) and (11:3) may be combined to obtain the pressure coefficient at any point on a body that is not in the shadow of upstream portions of the body. For example, the pressure coefficient may be obtained at all points on the surface of a cone that has an angle of attack less than the cone half angle η. When α exceeds η, portions of the cone will be in the shadow of upstream portions. The Newtonian theory is not applicable in these "shadow" regions.

Integration of the Newtonian pressure distribution over the surface of a cone yields the following forebody pressure force coefficients with reference to the cone base area:

$$C_N = 2 \cos^2 \eta \sin \alpha \cos \alpha \tag{11:4}$$

$$C_{N\alpha} = 2 \cos^2 \eta(\cos^2 \alpha - \sin^2 \alpha) \tag{11:5}$$

$$C_{A(\alpha=0)} = 2 \sin^2 \eta \tag{11:6}$$

where $C_{N\alpha}$ = slope of C_N vs. α per radian.

The axial force coefficient of eq. (11:6) does not include the force due to pressures acting on the base of the cone or to skin friction. The axial force coefficient due to base pressures on a cone or any other body of revolution, with reference to the base area, is often approximated by

$$C_{A(\text{base})} = \frac{1}{M^2} \tag{11:7}$$

where M = Mach number.

The addition of the force coefficients from eqs. (11:6) and (11:7) gives the total axial force coefficient due to pressure. However, this result will be less than the total axial force coefficient by the amount due to skin friction. The effects of skin friction on the normal force coefficients will be insignificant.

Any body with a blunt nose or blunt leading edge is preceded by a normal shock at supersonic speeds, and the pressure at the stagnation point of such a body is defined by normal shock relations. For such bodies, the Newtonian approximation of eq. (11:2) is modified to provide a pressure coefficient at the stagnation point which is consistent with normal shock relations:

$$C_p = C_{p_s} \sin^2 \delta \tag{11:8}$$

where C_{p_s} = pressure coefficient at the stagnation point behind a normal shock, equal to $\dfrac{(p_{t_2}/p_{t_1}) - (p/p_t)}{(q/p_t)}$, where the ratios are defined by eqs. (1:14), (1:17), and (1:24).

The value of C_{p_s} is quite insensitive to Mach number, varying only from about 1.81 at Mach 5 to 1.84 at Mach 20. A close approximation to eq. (11:8) for bodies with blunt leading surfaces can hence be written

$$C_p = 1.82 \sin^2 \delta \tag{11:9}$$

The force coefficients due to forebody pressures for some simple blunt bodies can be readily obtained from eq. (11:9). Using the body base area for reference, we find for some of these:

$$\text{for a flat-faced cylinder,} \quad C_{A(\alpha=0)} = 1.82; \tag{11:10}$$

$$\text{for a hemisphere cylinder,} \quad C_{A(\alpha=0)} = 0.91. \tag{11:11}$$

For a hemisphere cone, where the hemisphere radius is a small fraction of the cone base radius, the following approximations are reasonable:

$$C_N = 1.82 \cos^2 \eta \sin \alpha \cos \alpha \tag{11:12}$$

$$C_{N\alpha} = 1.82 \cos^2 \eta(\cos^2 \alpha - \sin^2 \alpha) \tag{11:13}$$

$$C_{A(\alpha=0)} = 1.82 \sin^2 \eta \tag{11:14}$$

11:3 Calibration

The calibration of the test section of a hypersonic tunnel is generally the same as that of a supersonic tunnel. However, it is much more important in hypersonic tunnels to calibrate over the complete range of conditions through which the tunnel will operate. Nozzle wall boundary layers are much thicker and subject to larger changes in thickness due to operating pressure and temperature than in supersonic tunnels. Also, the real gas effects make test section Mach number quite sensitive to total temperature. For example, the area ratio required for Mach 7 increases about 24 per

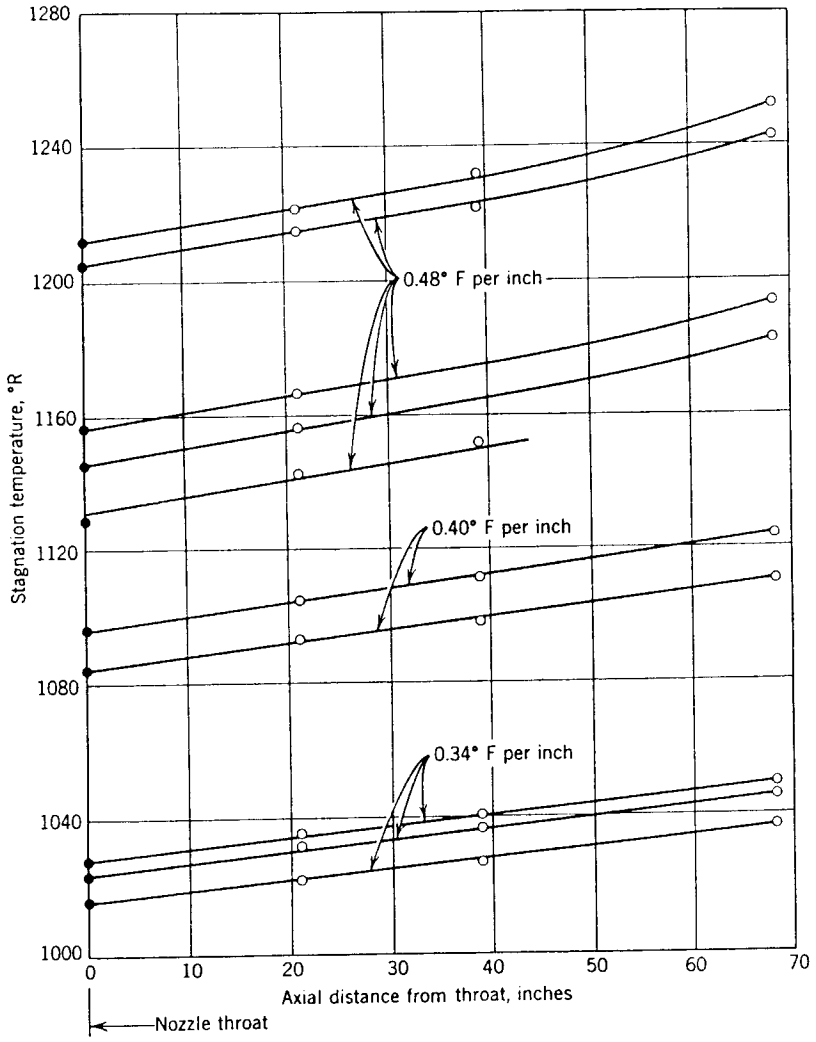


Fig. 11:3 Measurements of the stagnation temperature along the axis of the settling chamber of a 6 × 6-inch heated wind tunnel. The solid circles are from measurements made in the test section, not the throat as plotted. (From Ref. 11:7.)

cent as the operating temperature increases from 1000 to 3000°R (see Fig. 1:13). Also, a significant axial temperature gradient may exist in the settling chamber, with the temperature decaying as the nozzle throat is approached as shown in Fig. 11:3. The solid circles of Fig. 11:3 plotted at the nozzle throat station are from test section temperature measurements. The way they fit in with the settling chamber temperature data

indicates that there is no temperature loss between the throat and the test section. Instead of trying to eliminate the axial gradient the practical solution is to measure settling chamber temperature as near the throat as possible and to determine what the losses are between the measuring station and the throat so that they can be applied to the calibration and test data.

In addition to axial gradients, serious lateral temperature gradients in the settling chamber are the rule rather than the exception. These must be eliminated before uniform flow can be achieved in the test section (Section 4:5).

When a conical nozzle is being calibrated it is necessary to make detailed surveys of the portion of the tunnel in which models will be tested. Flow gradients will exist and the local Mach number and the gradients must be known to reduce and evaluate the data properly.

11:4 Tunnel Operation Charts

While the tunnel engineer spends a great deal of effort determining that the flow is good in his tunnel, of equal interest to the user are the operational charts which delineate the available pressure, temperature, and Mach number ranges in which he can test. For nearsonic, transonic, and supersonic tunnels, operating temperature is constant and the whole operational range may be plotted on a single sheet for a typical temperature. Off-design temperature effects are small and the tunnel engineer may see at a glance the Reynolds number per foot he will obtain for various tunnel pressures and Mach numbers. (See Fig. 9:11.)

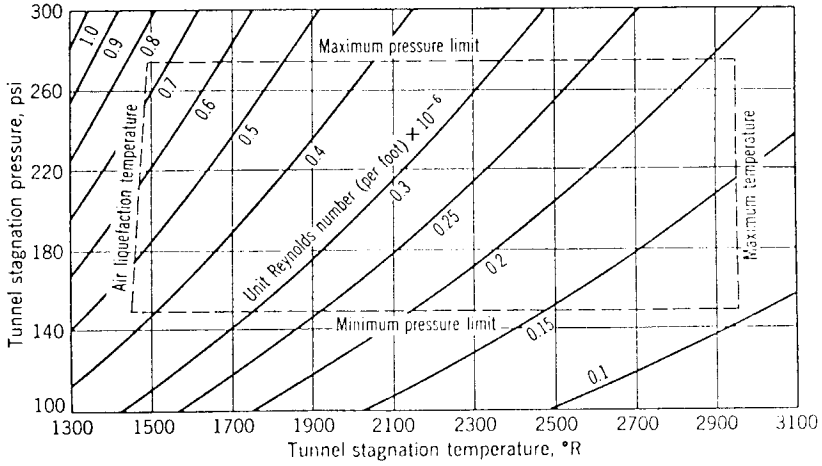


Fig. 11:4 Method of presenting hypersonic tunnel operating range. Mach number = 9.0.

For hypersonic tunnels the wide variation in temperatures plus the variation of Reynolds number with temperature makes necessary an operational chart for each Mach number. One such chart is shown in Fig. 11:4. The curves are unique and would work for any tunnel in the described temperature and pressure range, but the cutoff lines are for one particular tunnel. They are determined from a practical tunnel operation standpoint. The *maximum pressure* line may be a heat transfer limit, pebble-bed lifting, a structural limit, or just "all the pressure we got." The *maximum temperature* line may be a heater limit or a heat transfer limit. The *minimum pressure* line is from the practical pressure ratio limit. The *air liquefaction* line is from theory and could be adjusted in the light of the more recent data of Ref. 1:13.

11:5 Determining Mach Number

As in supersonic tunnels, Mach numbers in hypersonic tunnels are almost always obtained by using pitot probe measurements, which differ from those in supersonic tunnels in pressure and Reynolds number range. Pitot pressures in hypersonic tunnels will, in many cases, be lower. Checks should be made to ensure that the Reynolds number based on probe diameter is above 500 (or preferably 1000) because inaccurate measurements are likely if it is lower.

After the ratio of pitot pressure to total pressure is obtained, the determination of Mach number is considerably complicated if the air temperature is 1000°R or above because of the real gas effects discussed in Section 1:3. The procedure for determining Mach number from the ratio p_{t2}/p_{t1} and a measured total temperature T_t is the following.

1. Enter the perfect gas tables (Table 1:2) with the pressure ratio and determine a corresponding Mach number.
2. Enter Fig. 1:17 at this Mach number and at the measured T_t and determine a ratio $(p_{t2}/p_{t1})_{\text{therm perf}} \div (p_{t2}/p_{t1})_{\text{perf}}$.
3. Divide the experimental pressure ratio by the ratio determined in (2) to obtain a corresponding value of $(p_{t2}/p_{t1})_{\text{perf}}$.
4. Enter the perfect gas tables with this value of p_{t2}/p_{t1} and determine a corresponding Mach number.
5. If the Mach number obtained in (4) does not equal that used in (2), enter (2) with the Mach number from (4) and repeat. When the two Mach numbers agree, the iteration is complete.

This method of determining Mach number from measured pressure ratios is both laborious and inaccurate. A high-speed computer is highly desirable for the task. The iteration method is shown in Example 11:1.

Example 11:1 Determine the Mach number and dynamic pressure of an airstream when measured values are pitot pressure (p_{t2}) = 9.17 psia, total pressure (p_t) = 100 psia, and total temperature (T_t) = 3000°R.

1. Calculate a pressure ratio $p_{t2}/p_{t1} = 0.0917$.
2. Enter Table 1:2 at this pressure ratio and determine the Mach number corresponding to perfect gas equations. This is 4.5.
3. Enter Fig. 1:17 at Mach 4.5 and $T_t = 3000°\text{R}$ and determine a value of

$$\frac{(p_{t2}/p_{t1})_{\text{therm perf}}}{(p_{t2}/p_{t1})_{\text{perf}}} = 0.839.$$

4. Divide the experimental ratio of (1) by the ratio of (3) and obtain a new perfect gas value of $p_{t2}/p_{t1} = 0.0917/0.839 = 0.1093$.
5. Enter Table 1:2 at this pressure ratio and determine the corresponding Mach number, which is 4.286.
6. The Mach number of (5) does not agree with that of (2), so an iteration is required. Enter Fig. 1:17 at Mach 4.286 and $T_t = 3000°\text{R}$ and determine a value of

$$\frac{(p_{t2}/p_{t1})_{\text{therm perf}}}{(p_{t2}/p_{t1})_{\text{perf}}} = 0.841.$$

7. Divide the experimental ratio of (1) by the ratio of (6) and obtain a new perfect gas value of $p_{t2}/p_{t1} = 0.0917/0.841 = 0.1090$.
8. Enter Table 1:2 at this pressure ratio and determine the corresponding Mach number which is 4.289.
9. The Mach number of (8) is very near the Mach number of (5), so no further iterations are required. Within the accuracy of the readings from Fig. 1:17 and the interpolations from Table 1:2, the Mach number of the flow may be called 4.288.
10. Enter Table 1:1 at a Mach number of 4.288 and determine the value of q/p_t corresponding to perfect gas equations. This value is 0.05816.
11. Enter Fig. 1:12 at a Mach number of 4.288 and a total temperature of 3000°R and determine the value of

$$\frac{(q/p_t)_{\text{therm perf}}}{(q/p_t)_{\text{perf}}} = 0.832.$$

12. Multiply the value from (10) by the value from (11) to determine the thermally perfect value of q/p_t. This yields a value of $q/p_t = 0.05816 \times 0.832 = 0.04839$.

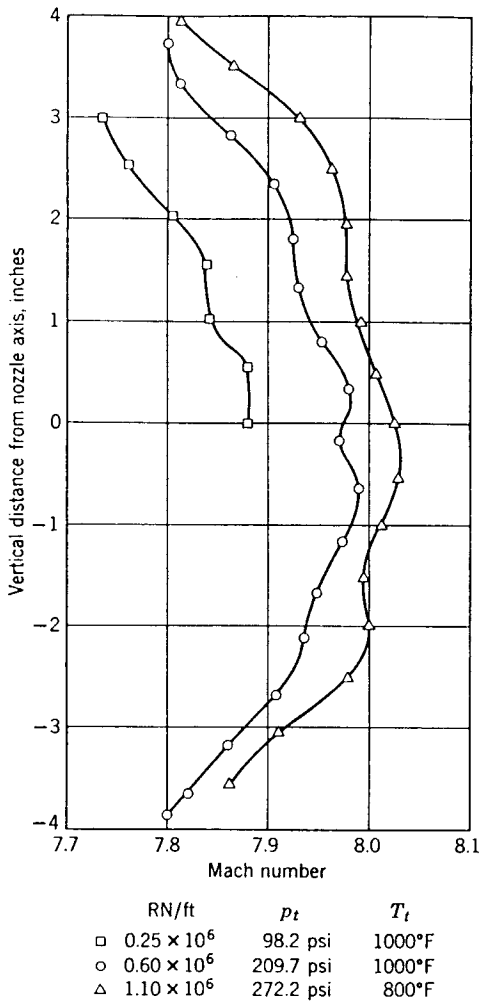


Fig. 11:5 Effect of Reynolds number on Mach number and Mach number distribution in one tunnel, Redrawn from Ref. 11:8.

13. Multiply the value of q/p_t from (12) by the total pressure to determine the dynamic pressure of the flow. This yields $q = 0.04839 \times 100 = 4.84$ psi.

The use of wave angles for determining hypersonic Mach numbers is very inaccurate because of the relative insensitivity of wave angle to Mach number changes. For example, variations in Mach number from 5 to 10 cause the Mach wave angle to change only from 11.54 deg to 5.74 deg.

Static pressures on cones and wedges have not to the authors' knowledge been used for calibrating hypersonic tunnels. Neither have static pressure probes been used. Although detailed evaluations of static pressure probes in hypersonic flow are not available, it is expected that a reliable probe will be more difficult to define than for supersonic flow, since boundary layers are considerably thicker at the higher Mach numbers. The boundary layer build-up on a cylindrical probe will have the same effect on pressure measurements as extending the probe to the edge of the boundary layer displacement thickness and removing the boundary layer. Aside from these aerodynamic problems, the static pressures in a hypersonic tunnel are quite low and in a range where accurate pressure measurements are extremely difficult. Typical results of calibrations to determine test section Mach numbers in a hypersonic tunnel are presented in Fig. 11:5.

11:6 Determining Flow Angularity

Flow angularity in hypersonic tunnels is most frequently determined by using cones employing included angles of 20 deg to 90 deg. The shock waves on cones with the higher angles are detached throughout the hypersonic speed range and the surface pressure variation with angle of attack cannot be easily calculated. A variation of probe angle of attack is the most simple method of determining probe sensitivity (the variation of differential surface pressure with angle of attack) as well as the only method of determining probe aerodynamic errors (see Fig. 9:8).

The cone is a very poor yawmeter in the hypersonic speed range, as indicated by the sensitivity plots of Fig. 10:12. One method that has been used to obtain increased sensitivity is to measure the difference between pitot pressures slightly above the surface of the cone at 180-deg intervals.

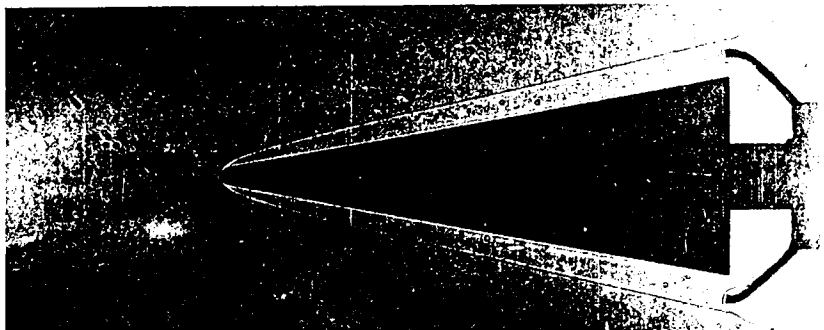


Fig. 11:6 Shadowgraph of pilot pressure flow angularity probe. (Courtesy Arnold Engineering Development Center.)

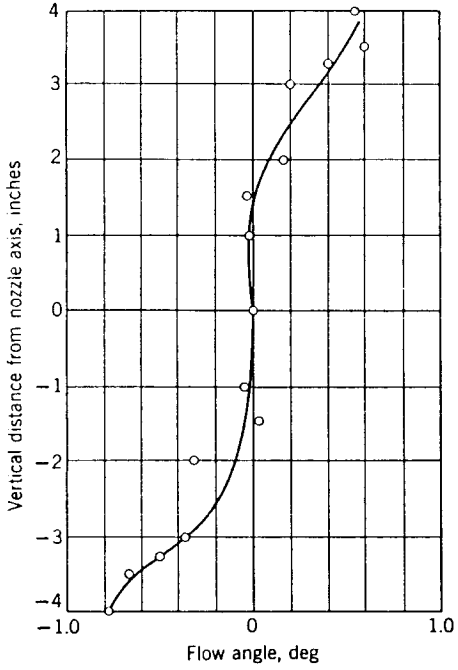


Fig. 11:7 Flow angularity data, $M = 7.2$. Redrawn from Ref. 11:8.

A shadowgraph illustrating a probe that uses this method is presented in Fig. 11:6. Data from flow angularity studies in one wind tunnel are presented in Fig. 11:7.

11:7 Determining Turbulence Level

To our knowledge, no significant effort has been devoted to the determination of turbulence levels of hypersonic tunnels. The large contraction ratios of most hypersonic tunnels have a tendency to reduce the turbulence percentage level in the test sections to insignificant proportions.

11:8 Surveying the Boundary Layer

Surveys of the boundary layer of a hypersonic tunnel are usually required only when the tunnel flow is not what it was designed to be and the tunnel engineer is trying to find out why, or when a new nozzle is being designed and the tunnel engineer wants to find out if the boundary layer estimates used in the design of a previous nozzle were sufficiently accurate.

Boundary layer surveys are made with pitot probes. A single probe may be used to traverse the boundary layer or a rake of several pitot

probes may be used to measure pressures at several positions in the boundary layer simultaneously. The open end of the probe should have a diameter that is small relative to the boundary layer thickness in order to avoid averaging a range of local pressures. One method that has been used in the fabrication of probes for thin boundary layers is the following: take an 0.040-inch internal diameter brass tube and draw it to an internal diameter of 0.008 inch. Hone it to a wall thickness of 0.003 inch, and flatten to obtain an orifice 0.005 inch high by 0.010 inch wide. The pressures measured by the pitot probe at each position in the boundary layer are divided by measured tunnel total pressures to obtain values of the ratio p_{t2}/p_{t1}. A typical plot of this ratio with distance from the nozzle wall in one hypersonic tunnel is presented in Fig. 11:8.

The most important boundary layer parameter with regard to nozzle design is the displacement thickness δ^*. In order to determine displacement thickness from the ratios p_{t2}/p_{t1} it is necessary to make two assumptions:

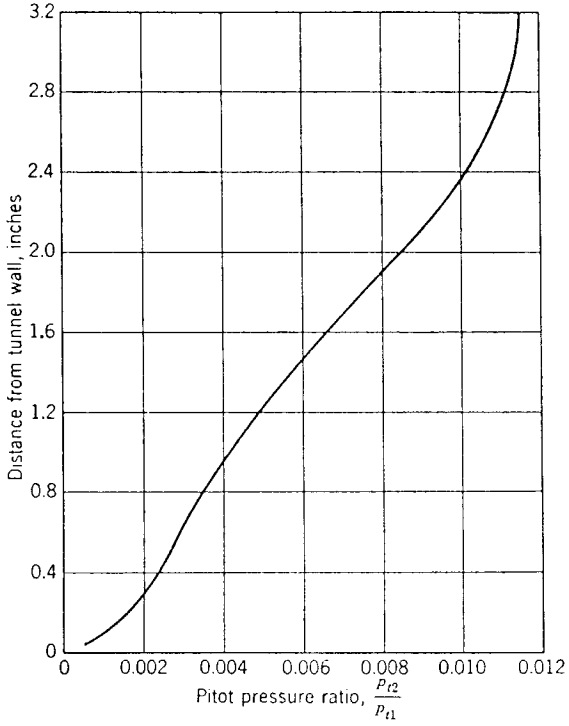


Fig. 11:8 Variation in the ratio of pitot pressure in the boundary layer, p_{t2}, to free-stream total pressure p_{t1} with distance from the tunnel wall; 18-inch hypersonic tunnel, $M = 7.3$.

(1) that the static pressure is constant through the boundary layer and equal to the static pressure of the local freestream, and (2) that the total temperature in the boundary layer has a linear variation with local velocity and varies from the freestream value at the edge of the boundary layer to the wall temperature at the nozzle wall. That is,

$$\frac{U}{U_\infty} = \frac{T_t - T_w}{T_{t\infty} - T_w} \tag{11:15}$$

where U = local velocity in boundary layer, ft/sec,
U_∞ = local velocity in the freestream just outside the boundary layer, ft/sec,
T_t = local total temperature in boundary layer, °R,
T_w = temperature of the nozzle wall, °R,
$T_{t\infty}$ = total temperature in the freestream just outside the boundary layer, °R.

While it is possible to make boundary layer calculations including real gas effects, this is seldom done because the calculations require iteration and become very complex. Fortunately, the real gas effects in many hypersonic wind tunnels are of second-order importance. The usual calculations assume that air is a perfect gas. For surveys of a boundary layer made with constant tunnel total temperature and pressure, the usual calculation steps are the following:

1. Values of pitot pressure measured in the freestream part of the survey (out of the boundary layer) are averaged. The resulting average is divided by the measured tunnel total pressure to obtain a freestream pitot to total pressure ratio p_{t2}/p_{t1}.
2. Table 1:2 is entered at this value of p_{t2}/p_{t1} to obtain a freestream Mach number M_∞ (the subscript ∞ denotes freestream).
3. Table 1:1 is entered at the freestream Mach number to obtain freestream pressure, temperature, and density ratios, $p_\infty/p_{t\infty}$, $T_\infty/T_{t\infty}$, and $\rho_\infty/\rho_{t\infty}$.
4. Freestream conditions are then completely defined using the freestream Mach number of (2), the ratios of (3), and the measured total temperature and pressure:

$$T_\infty = T_{t\infty}(T_\infty/T_{t\infty})$$
$$p_\infty = p_{t\infty}(p_\infty/p_{t\infty})$$
$$\rho_\infty = (p_{t\infty}/R_1 T_{t\infty})(\rho_\infty/\rho_{t\infty})$$
$$U_\infty = M_\infty\sqrt{\gamma R_1 T_{t\infty}(T_\infty/T_{t\infty})}$$

See Section 1:2 for nomenclature definition. The calculation of ρ_∞ makes use of the equation of state (eq. (1:1)) and the calculation of U_∞ makes use of eqs. (1:6) and (1:7).

At each point in the boundary layer where a pitot pressure is measured, the following steps are required.

5. The measured pitot pressure is divided by the measured tunnel total pressure to obtain the ratio $p_{t2}/p_{t\infty}$.
6. The ratio of $p_\infty/p_{t\infty}$ from (3) is divided by the ratio of $p_{t2}/p_{t\infty}$ from (5) to obtain the ratio of p_∞/p_{t2}. Since the static pressure in the boundary layer is assumed equal to the freestream static pressure, this ratio is the local value of p_1/p_{t2} in the boundary layer.
7. Table 1:2 is entered at this value of p_1/p_{t2} to obtain the local Mach number in the boundary layer, M.
8. Table 1:1 is entered at this value of Mach number to obtain ratios of p/p_t, T/T_t, and ρ/ρ_t.
9. From eqs. (1:6) and (1:7), the following relation between velocity and total temperature is obtained:

$$U = M\sqrt{\gamma R_1(T/T_t)T_t} \tag{11:16}$$

Equations (11:15) and (11:16) are combined to obtain the following quadratic in T_t:

$$U_\infty T_t - M(T_{t\infty} - T_w)\sqrt{\gamma R_1(T/T_t)}\sqrt{T_t} - U_\infty T_w = 0 \tag{11:17}$$

Equation (11:17) is solved for T_t by using measured values of $T_{t\infty}$ and T_w, the value of Mach number from (7), the temperature ratio from (8), and the freestream velocity from (4).

10. Equation (11:16) is solved for the local velocity U by using values of M from (7), T/T_t from (8), and T_t from (9).
11. The value of p_∞ from (4) is divided by the value of p/p_t from (8) to obtain a value of p_t.
12. By using the value of T_t from (9) and the value of p_t from (11), the equation of state (eq. (1:1)) is solved for the density ρ_t. This value of density is multiplied by the density ratio from (8), ρ/ρ_t, to obtain the local density ρ.
13. The local velocity from (10) and the local density from (12) are multiplied to obtain the local velocity-density product ρU. The freestream velocity from (4) and the freestream density from (4) are multiplied to obtain the freestream velocity-density product $\rho_\infty U_\infty$. Using these velocity-density products, one can determine the boundary layer displacement thickness from the following integration:

$$\delta^* = \int_0^{y_r}\left[1 - \frac{\rho U}{\rho_\infty U_\infty}\right] dy \tag{11:18}$$

where y = distance from the nozzle wall to the survey station. The subscript e denotes the edge of the boundary layer.

14. The integration of eq. (11:18) is accomplished by numerical or graphical means.

11:9 Blockage Tests

During the calibration phase of putting a hypersonic tunnel into operation it is desirable to make "blockage" tests to determine the sizes of models that may be tested in the tunnel and what the effect of model size is on the starting and operating compression ratios for the tunnel. These tests will yield results that make it possible to minimize the likelihood of building a model for some future test which is so large that the tunnel cannot be started. Blockage tests may make use of any shape model that is likely to be tested in the tunnel, though the more usual shapes are cone cylinders and hemisphere cylinders. In these tests the pressures in the settling chamber of the tunnel and in a zero- or low-speed portion of the tunnel downstream of the diffuser are measured with pressure transducers. A nozzle wall static pressure in the vicinity of the model in the test section is also measured with a transducer. The tunnel is brought up to typical operating conditions gradually by increasing the operating pressure of an intermittent tunnel or by increasing the compressor speed of a continuous tunnel. When the shock system passes through the test section, the wall static pressure will decrease suddenly, indicating that the tunnel has started. The starting compression ratio is calculated from the settling chamber and downstream pressures indicated at this time of tunnel starting. The operating pressures are then gradually reduced. When the shock system moves upstream past the model, the wall static pressure will rapidly rise. The minimum tunnel operating compression ratio is calculated from the settling chamber and the downstream pressures indicated at this time of tunnel stopping.

This test procedure will be followed for gradually increasing model sizes until the starting or operating compression ratios are unreasonably high or until the tunnel will not start at all. In addition to serving as a useful guide for sizing future models, the data thus obtained define the required operating conditions for compressors of continuous tunnels, and make possible available run-time calculations for intermittent tunnels.

11:10 Starting Loads

To our knowledge, no data on model starting loads in hypersonic tunnels have been published. However, limited personal experience at Mach 7.5 has indicated that starting loads are not nearly so severe as indicated for supersonic tunnels in Section 10:15.

11:11 Reynolds Number Effects

Boundary layers at hypersonic speeds are relatively thick and more prone to separate in the presence of unfavorable pressure gradients than at supersonic speeds. Also, there are likely to be important interactions between shock waves and boundary layers. For example, on a cone or wedge leading edge the shock at hypersonic speeds will lie very close to the surface. The boundary layer on the surface of the wedge or cone will be an important part of the distance between the surface and the shock. Under these conditions, loads on the model can no longer be considered simply as those due to an inviscid flow field which exerts pressures through the boundary layer and onto the model surface. Since the boundary layer has a primary dependence on Reynolds number, we are saying that the complete flow field around a vehicle at hypersonic speeds is dependent to a significant extent on Reynolds number. Thus, force and moment coefficients in addition to drag are likely to be affected by Reynolds number.

The boundary layers on models in hypersonic tunnels are normally mostly, if not completely, laminar. However, it is not clear that tripping the boundary layer is the answer to the problem of obtaining comparable flow fields over the model in the tunnel and the full-scale vehicle in flight. In flight at hypersonic speeds, the full-scale vehicle is likely to have long runs of laminar flow if it has reasonably smooth surfaces. Reynolds numbers as high as 70,000,000 without transition have been reported on rockets. This points up the difficulty of predicting where transition will occur on an aircraft in flight and consequently where or if a boundary layer trip should be used. The general practice at present is to test models without transition strips in hypersonic tunnels. If it is found that the smooth model has extensive boundary layer separation at some point at which it is not expected on the vehicle in flight, then a transition strip may be tried as a means of eliminating this separation. This may not be easy. With increasing Mach number the boundary layer becomes increasingly hard to trip; finally, at say $M = 10$ to 15 or above, boundary layers remain untripped by $\frac{3}{8}$-inch balls welded to the surface, and one may surely say tripping is impossible.

Reference 11:5 suggests that in the range $1.5 > M > 3$ the trip Reynolds number evaluated at the top of the roughness

$$R_T = \frac{\rho u k}{\mu}$$

where u = velocity, ft/sec,
ρ = density, slugs/ft^3,
μ = viscosity, lb-sec/ft^2
k = roughness height, ft,

should increase from 850 at $M = 1.6$ to 2000 at $M = 3.0$. Some experiments have indicated that a further increase of as much as 50 per cent may be necessary.

The added drag due to the minimum roughness is proportional to the fraction of the surface made rough relative to the total surface. Reasonable values for ΔC_D due to roughness run from 0.0001 to 0.0004. An alternative to using carborundum grit is the use of very tiny glass balls, now available commercially in diameters up to 0.01 inch. They may be glued on with a thin layer of epoxy. A little color added to the epoxy makes it easier to spread a thin layer. See also Ref. 11:6.

If boundary layer separation does not occur on the model and if the boundary layer is not extremely thick relative to model dimensions, reasonably good stability data can be obtained with test Reynolds numbers low relative to full-scale flight Reynolds numbers. Under these conditions, model drag may be expected to be less of a problem than in transonic and supersonic tunnels, even without fixed transition. With increasing speed the pressure drag increases in importance relative to the skin friction drag. Also, the base pressure drag decreases in importance. The static pressure of the flow becomes a small portion of the dynamic pressure, so that variations of base pressure between absolute zero and static pressure cannot be expected to cause large changes in drag. Hence boundary layer conditions and sting effects should be of secondary importance.

11:12 Force Tests

Force tests in hypersonic tunnels do not differ in procedure from those in supersonic tunnels. However, there are a few problems in hypersonic tunnel force tests that do not exist in the lower-speed tunnels.

Hypersonic tunnels almost invariably use heated air and the models are therefore heated during the tests. Care must be taken to ensure that the model heating and the heated air do not affect the electrical signals from the strain gage balance. There will probably be significant temperature effects on balance readout at temperatures well below those for which the cement holding the gages to the flexures fails. These effects are likely to be due to uneven heating of the model or to circulation of air from the model base through the balance cavity of the model. With the model at an angle of attack, surface heating rates of the model will be higher on the windward side than on the leeward side. If this heat is conducted through the walls of the model, there will be hotter surfaces in proximity to the strain gages on the windward side of the balance than on the leeward side. This condition will cause uneven heating of tension and compression gages of moment bridges with a consequent strain gage signal due to temperature. If air is circulating from the model base through the balance cavity, it

is almost certain that gages on one side of the balance will be heated more than gages on the other side. These cases of uneven balance heating are not taken care of by temperature compensation of the bridges of the balance.

Methods used to help solve the variable balance temperature problem are designed to keep the balance temperature essentially constant and at a near ambient value during the test. In continuous wind tunnels, where the test may last for several minutes, schemes have been worked out for using cooling water piped in from outside the tunnel. Nitrogen cooling has also been used. In intermittent tunnels, where the test will usually last less than one minute, the same results have been achieved by insulating the inside walls of the model and using a minimum clearance between the balance sting and the model base to minimize circulation of hot air in the balance cavity.

In addition to effects on balance readings, uneven heating on the windward and leeward model surfaces may cause model distortion of significant proportions, particularly if the length to diameter ratio is high. This effect is, of course, alleviated by model cooling. In intermittent operating tunnels it may also be alleviated by increasing model wall thickness or by using a material such as Invar, which has a low coefficient of thermal expansion.

Another problem in hypersonic force tests is low model loads, particularly at the higher Mach numbers. Aerodynamic loads in some cases may be considerably less than the weight of the model. This presents a real problem in balance design. The balance must obviously be strong enough to hold the model but it must also be weak enough to be sensitive to loads smaller than the model weight. A problem likely to develop under these conditions is a continuous low-frequency oscillation of the model during a test. The oscillation can easily be of sufficient magnitude to cause model inertia loads to become a significant portion of the aerodynamic loads to be measured. Under these conditions, satisfactory data cannot be obtained unless the data readout system is equipped with suitable electronic filtering.

In hypersonic tunnels which operate with air temperatures above about 1000°R, consideration must be given to real gas effects in determining dynamic pressures for reducing data to coefficient form. As in other tunnels, an average Mach number in the test section is determined by calibration. At this Mach number, a perfect gas value of the ratio of dynamic to total pressure (q/p_t) is determined as shown in Example 11:1.

11:13 Flow Visualization

As mentioned in Section 6:17, schlieren systems for high-speed tunnels are often designed for passing the light through the test section two times

(using a double-pass system) in order to increase the system sensitivity. However, it has been found difficult to obtain good schlieren pictures of the flow around a model when the pressures in the test section of a wind tunnel are less than about 1 mm mercury absolute, even with these double-pass systems. Pressures below 1 mm mercury are common in wind tunnels operating at Mach 8 and above.

To obtain better flow visualization at low test section pressures, the Jet Propulsion Laboratory has used an electric current to ionize the air in the flow field of a model. An electrode is placed a few inches upstream and a few inches above the model in the test section. A potential of 5000 v direct current is established between the electrode and the model with a

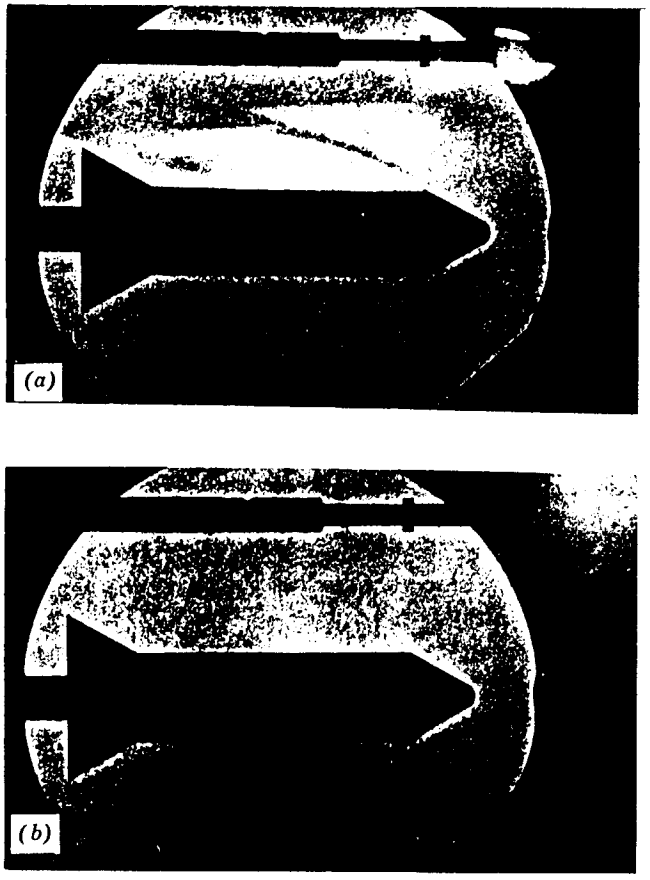


Fig. 11:9 Schlieren pictures from a hypersonic tunnel with and without ionization of the flow field.

current flow of 0.4 amp. The flow of current ionizes the flow field, with the result that shock waves are clearly shown in regular photographs and are much more visible in schlieren photographs than in schlieren photographs taken without ionization (Fig. 11:9). The power system should be interlocked (possibly with a low pressure switch) to prevent injury to personnel.

11:14 Testing Nose Cones

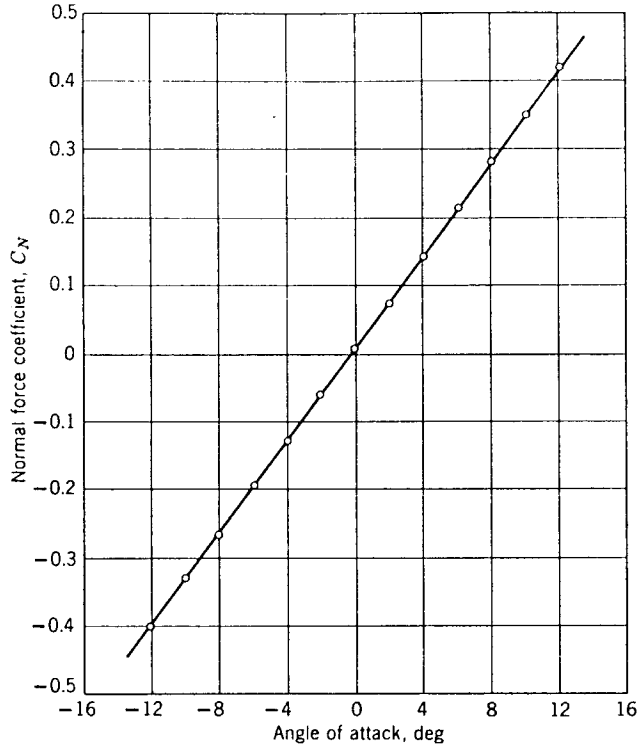
Nose cones differ from manned re-entry bodies (as far as wind tunnel tests are concerned) in being of far higher W/C_DA (500 to 4000 lb/ft^2), in having much smaller nose half-angle (from 5 to 10 deg), and in seeing far higher dynamic pressures (say 150,000 lb/ft^2) during re-entry. We find two types of nose cones, maneuvering and non-maneuvering. Maneuvering nose cones have controls and a smaller static margin in order to reduce the restoring moments that must be overcome by controls.

In general, nose cones see high angles of attack (say ± 30 deg) during the high-altitude low-G part of the trajectory, and low angles (± 4 deg) during the low-altitude high-G part. Nevertheless, since the vehicle may be subjected to enemy countermeasures that may tumble it, designers will want three-component data throughout the full 180-deg angle-of-attack range. For the maneuvering types the effect of control surface deflection, extension, or jet efflux will require six-component data.

Models are usually made of stainless steel or fiberglass, and are tested without transition strips. Ablation may be simulated by a rippled surface for static tests.

Since hypersonic coefficients change but little with Mach number, large increments in Mach number are used for wind tunnel tests. For example, increments of 5 would be adequate for the Mach number range between 5 and 20. Force data will normally be obtained at angle of attack increments of 1 or 2 deg near zero and at increments of perhaps 5 deg through the rest of the range. Maneuvering nose cones will normally not need to be tested over as wide a range of angle of attack as nonmaneuvering nose cones. A typical test for a maneuvering nose cone might include maneuvering flap deflections of 0, 10, 20 and 30 deg; angles of attack of -15 to $+15$ deg; and yaw angles of 0 and 10 deg. Basic data from a 10 deg half angle nose cone test at Mach 10 are shown in Fig. 11:10. The correlation of wind tunnel data with full-scale parameters is generally good, though drag adjustments due to Reynolds number differences may be required.

Slender nose cone data are usually reduced by using total length for a reference length, and base area for a reference area, while for the blunter types base area and diameter may be used for reference. Since the bodies are symmetric, no roll data are taken.



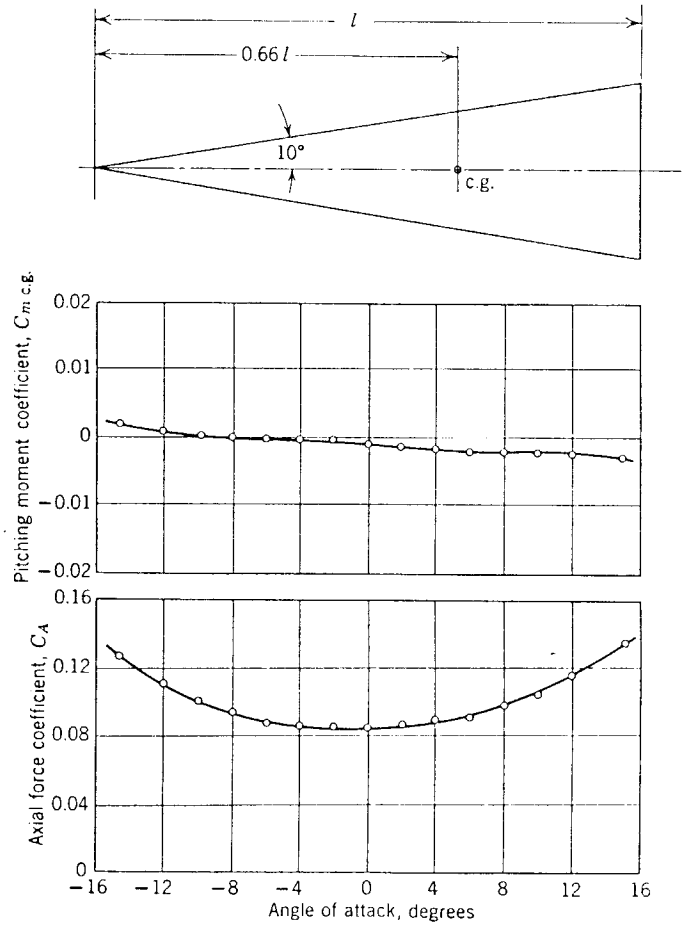
(a)

Fig. 11:10 Nose cone data, $M = 10$. Coefficients based on model length and base area. Part (*b*) is given on facing page.

A word of warning: The equations of motion for re-entry flight trajectories have been worked out by non-aerodynamic engineers and the wind tunnel engineer will do well to accept the new nomenclature for aerodynamic parameters and save argument, even though he may find himself using such sacreligious symbols as C_L for rolling moment, and so forth.

11:15 Testing Man-Carrying Re-entry Bodies

The non-man-carrying re-entry vehicles utilize great dynamic pressures and hence have great decelerations and heating rates, but the man-carrying types must avoid high q and its consequent high decelerations. This is accomplished by using a low W/C_DA (of the order of 50 lb/ft²) for the non-maneuvered types such as Mercury (Fig. 11:11) and Apollo and very critical trajectories for the maneuvering-Dynasoar-type vehicles whose



(b)

W/C_DA is more of the order of 700 lb/ft². A few words on the aerodynamic problems of each and the manner in which wind tunnel tests are needed are given below.

Non-Maneuvering Vehicles. The non-maneuvering man-carrying re-entry vehicles such as the Mercury (Fig. 11:11) and the Apollo adjust their attitude so that they have their axes of symmetry aligned along the flight path during re-entry. Their energy then is dissipated in a single plunge ending at terminal velocity for the vehicle and requiring a parachute for water or land impact without serious consequences to the astronauts. While their intended attitudes encompass small angles relative to the flight path, the possibility of errors demands that they be stable throughout



Fig. 11:11 Readying a test of the Mercury escape system. (Courtesy National Aeronautics and Space Agency.)

the entire angle-of-attack range, and have trim possible only at $\alpha = 0$ deg. Accordingly, wind tunnel tests must be made over the entire angle range using a series of sting mounts as described in Fig. 11:12. Angles of yaw are unnecessary because of the complete symmetry. Data from such a test are shown in Fig. 11:13.

Maneuvering Vehicles. The man-carrying maneuverable re-entry vehicle offers the opportunity to maneuver so that landing may occur anywhere in an area the size of the United States or larger after a high-speed glide of from 5000 to 25,000 miles horizontal range.

To accomplish such maneuvers a vehicle must have high drag and a maximum L/D value of about 2.0. One proposal is shown in Fig. 11:14. The blunt shape reduces concentrated heating loads, and a planform area is provided sufficient to permit landing at reasonable speed. Two markedly different though outwardly similar types are possible. For orbital velocities (say 25,000 ft/sec) it appears possible to cool the vehicle by radiation cooling, thus obviating the need for ablation material. For this type of vehicle the design and operation must be compatible with a selected maximum *heating rate*. For supercritical velocities (say 35,000 ft/sec and above) re-entry temperatures above present-day radiation cooling techniques will be developed, and ablation material must be provided. In this case the

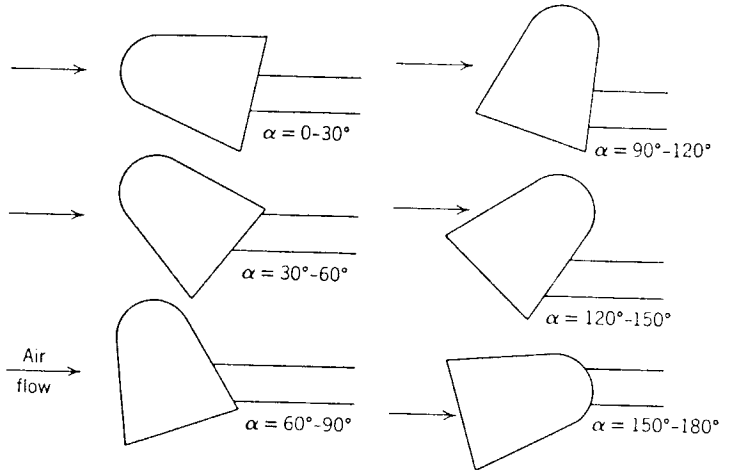


Fig. 11:12 Typical model mounting arrangements for high angle of attack re-entry body tests.

design criterion is to be able to handle the *integrated heat load.* The burn-off of the ablation material reduces the vehicle mass 10 to 20 per cent and tends to move the center of gravity rearward, whereas the expenditure of control fuel usually moves it forward.

For either vehicle (radiative or ablative cooled) re-entry must be made at a small angle (say 4 to 12 deg) below the tangent to the earth's horizontal, while the vehicle itself is initially at a high angle of attack (around 40 deg). As the re-entry begins and the vehicle altitude decreases, the dynamic pressure rises. The vehicle angle of attack is progressively decreased from its initial value in a manner to cause a controlled zoom (acceleration) of say 10G. This acceleration causes the vehicle to rise up 50,000 to 100,000 feet to perhaps 400,000 feet altitude. The purpose of the zoom is to slow the vehicle down so that its final re-entry trajectory will result in a smaller value of G_{max}. The number of zooms required will increase with the initial vehicle velocity. Following the zooms when the vechicle is on its equilibrium re-entry trajectory, the vehicle may be rolled as a means for range control. For example, if the vehicle at a positive angle of attack were rolled 90 deg to the right and maintained in this attitude for a period of time, then rolled to a 90-deg left attitude and maintained in this attitude for a period of time, its impact point could be on the initial line of flight but at a lesser range than without the roll. For the fastest re-entries, the vehicle may be maintained in a 180-deg roll attitude for extended periods as a means of reducing the negative G loading on the pilot during the re-entry. As for wind tunnel tests, maneuvering re-entry vehicles must

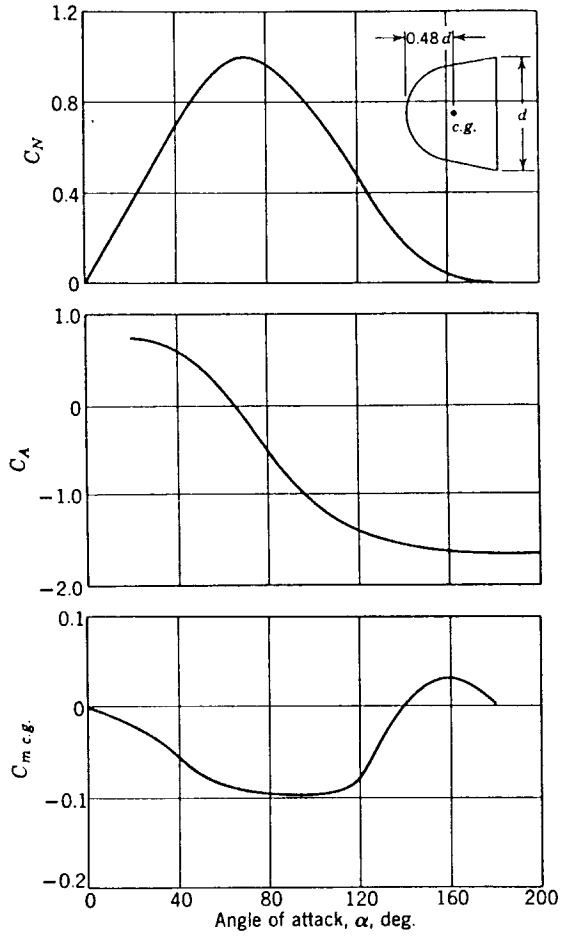


Fig. 11:13 Nose cone data for 180-deg angle of attack range; $M = 5.5$. Coefficients based on base area and diameter.

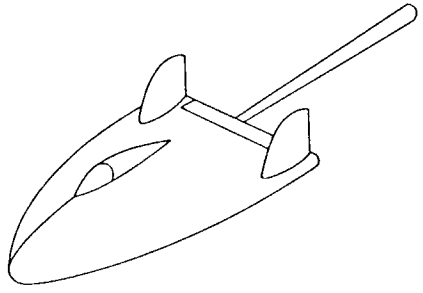


Fig. 11:14 Sketch of re-entry glider model.

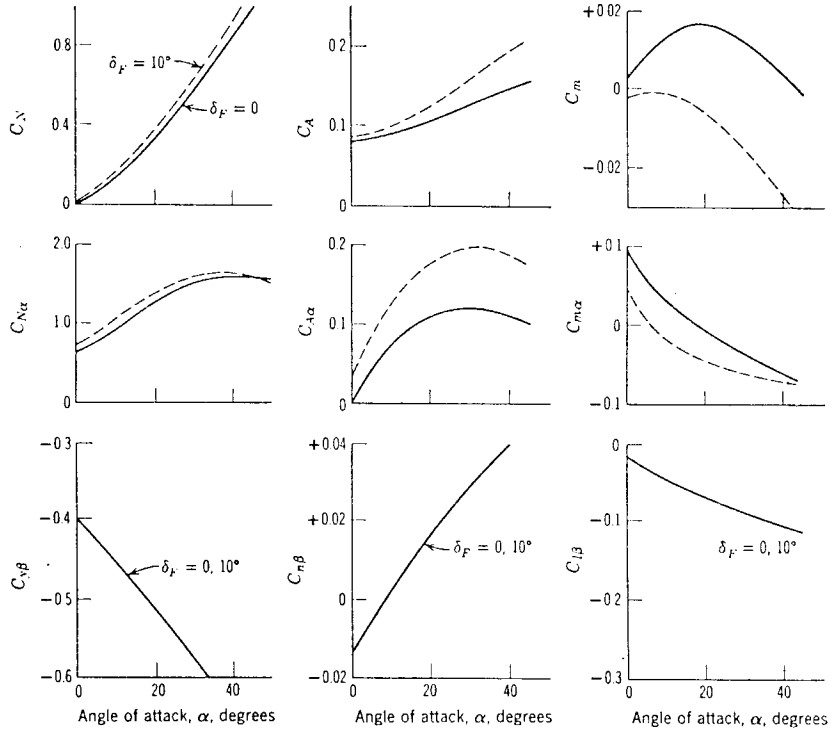


Fig. 11:15 Data from tests of a re-entry glider, landing flap 0 and 10°. Slopes are per radian.

be tested at hypersonic speeds past the angle corresponding to $C_{L\max}$. Since no sharp breaks in the coefficients are common, wide gaps in the angles may be employed (say 5 deg), but all six components of forces and moments must be taken. In addition a number of control settings must be evaluated. Deflections that move the control into the shadow of the flow may be expected to be far less effective (say one-fourth as effective) than those moving it into the flow. Typically in the hypersonic range the coefficients will vary but little with Mach number and only a few widely spaced Mach numbers need be tested.

Correlation of wind tunnel with full-scale data for the stubby body such as that shown in Fig. 11:15 is very limited. What exists seems to show good equality for C_N and C_A, and fair equality for C_m, but for some unexplained reason shows poor correlation with the yawing data.

11:16 Testing for Dynamic Stability

In addition to the use of dynamic stability rigs, two other techniques are receiving some attention at the higher speeds. One of these is the free

oscillation technique using a cross-strut model support system as shown in Fig. 11:16. In this system the model is pivoted on a shaft extending through the sides of the model instead of from the model base. This method of model support undoubtedly creates an interference on the aft portion of the model not present with the sting support. However, some evidence has been obtained indicating that this is not extremely important with regard to damping moment measurements of models of the type shown in Fig. 11:16.

The other technique receiving some attention is a novel free-flight technique developed by the Jet Propulsion Laboratory (Ref. 11:1). In this technique a model is suspended in the test section by means of a taut wire extending from the top to the bottom of the tunnel. The wire is weakened inside the model so that it will break with a slight increase in tension. After the tunnel is operating, the needed increase in tension is applied and the wire is pulled out of the model from the top and bottom, leaving the model in free flight in the airstream at an angle of attack. The motion of the model subsequent to release is recorded by high-speed photography, sometimes making use of the optics of the schlieren system. A reference grid is photographed along with the model to provide a reference for measuring model angles relative to the flow direction and for measuring model displacement. The camera film speed is accurately timed so that the time interval between subsequent frames is known. Thus a time history of model attitude is obtained. The damping moment coefficients are then obtained by inserting trial damping coefficients, together with static aerodynamic coefficients, into a high-speed computer trajectory program until the observed trajectory is matched.

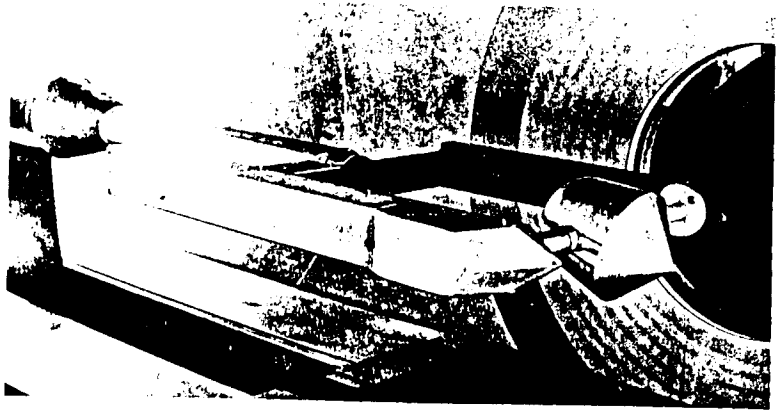


Fig. 11:16 Cross-strut model support assembly for dynamic stability testing. (Courtesy Jet Propulsion Laboratory.)

For this technique, estimates of the model aerodynamic characteristics must be available. When these estimates are obtained it is possible to design the model with a weight, center of gravity position, and moment of inertia so that it will have an adequate number of pitch cycles while it is in the field of view of the camera.

It is interesting to note that this free-flight technique has also been used to obtain drag measurements. It has the advantage in this respect that a sting is not present to alter the flow in the vicinity of the model base.

In addition to free flight testing using the wire support technique, models have been fired upstream into the flow from a point downstream of the test section windows. This technique allows the model to remain in the field of view of the windows twice as long as does the wire support technique. This allows more cycles of model oscillation for data reduction. Details of a pneumatic launcher and of model design and fabrication methods are presented in Ref. 11:2.

Dynamic testing at hypersonic speeds is relatively new. It embraces both fixed geometry models and those with ablating surfaces. Any tests planned in the field should include adequate variations of the test setup to give confidence in the data. These might include studies of the effects of sting interference, Reynolds number, the reduction of tare damping through the use of air bearings, and sensitive schlieren systems to help in the understanding of the boundary layer behavior. A fairly significant step forward in this area has been made by the Fluidyne Engineering Corporation where a material has been developed that ablates at tunnel temperatures just as the normally used ablating coverings do in the 15,000°F range (Ref. 11:4). Results studying dynamic stability with ablating models seem to indicate that for once the previously unknown effects work in the right direction-toward increasing stability as the surface ablates. A pitfall to avoid in the area of nonlinear coefficients is comparing data obtained from small oscillations with that obtained from large oscillations.

11:17 Testing for Heat Transfer

Heat transfer depends (among other things) on a difference in temperature between the body in question and the stagnation temperature of the airstream. Accordingly, one may conduct heat transfer studies in a tunnel using either a refrigerated model and an airstream at moderate temperatures, or a heated airstream and a model at moderate temperatures. In general, one would be happy with a temperature differential of 500°F to work with; some tests have been made with as little as 100°F

Heat transfer rate measurements in hypersonic (and supersonic) wind tunnels are made by using either the thin model skin technique or the heat

transfer gage as described in Section 6:13. In continuous wind tunnels, the model must be protected from the airstream during the time flow is being stabilized in the tunnel. Both the thin model skin and the heat transfer gages have a low thermal mass and exposure to the airstream for a matter of one or two minutes is likely to cause the temperatures being measured to approach equilibrium, with the result that essentially no heat transfer takes place after the flow is stabilized. One other reason for protecting the model during tunnel flow stabilization is that the temperature rise sensed by the thermocouple for determining heat transfer will be dependent to some extent on heat transfer between the gage and the material of the surrounding surface at a different temperature. Protection of the model during tunnel stabilization will tend to minimize model surface temperature gradients during the actual heat transfer measurements.

In addition to the above reasons for protecting the model, it is often desired to measure the heat transfer with the ratio of airstream to model surface temperature at a specified level. In hypersonic tunnels, the air temperatures are generally much lower than those of the air through which the full-scale aircraft will be flying. In order to obtain a ratio of airstream to model surface temperature corresponding to flight, it is necessary to cool the model considerably in addition to simply protecting it from the airstream.

Two techniques have been used for protecting a model from the airstream during tunnel stabilization. One consists of two protective shoes mounted from the tunnel sidewalls which completely enclose the model (Fig. 10:19). When it is time to make the heat transfer measurements the shoes are quickly withdrawn, one from each side. When a cold model is desired at the beginning of a test, these shoes may be equipped with internal cooling passages through which liquid nitrogen is circulated prior to the test. Or they may be equipped with a tube through which liquid nitrogen is brought into the tunnel and caused to flow directly over the enclosed model. The other technique is to have the model completely out of the tunnel while the flow is stabilized and then to inject it quickly into the test section for recording data. The latter technique is much more complex from the standpoint of hardware required.

In intermittent tunnels, it may not be necessary to cool the model if the flow in the tunnel can be reasonably well stabilized in less than 2 seconds. With proper design of the thin skin or the heat transfer gage, the temperature rise of the gages and the surrounding model skin during the flow stabilization will have no deleterious effect on heat transfer measurements. By proper design, it is meant that temperature gradients in the vicinity of the measuring points will be small, and that the temperature at the measuring point will be much lower than airstream temperature and much

lower than the design operating temperature of the gage when flow is established.

Heat transfer rates are highest at the nose of a body, at the leading edge of a wing or fin, in the vicinity of junctures between wing or fin and body, and in the vicinity of protuberances from a smooth surface. However, heat transfer measurements may be required at any point on any model of an aircraft designed for high supersonic or hypersonic speeds.

11:18 Testing for Ablation

Testing for ablation is largely in the cut-and-try stage, where various configurations and various materials are subjected to heat fluxes that will ablate their surfaces. The models that last longest are the best. Data-taking consists of photographing the manner of ablation and weighing and measuring the model after testing. In some instances thermocouples are buried in the ablation material to give additional information on local conditions. The progress of ablation on one model is shown in Fig. 11:17.

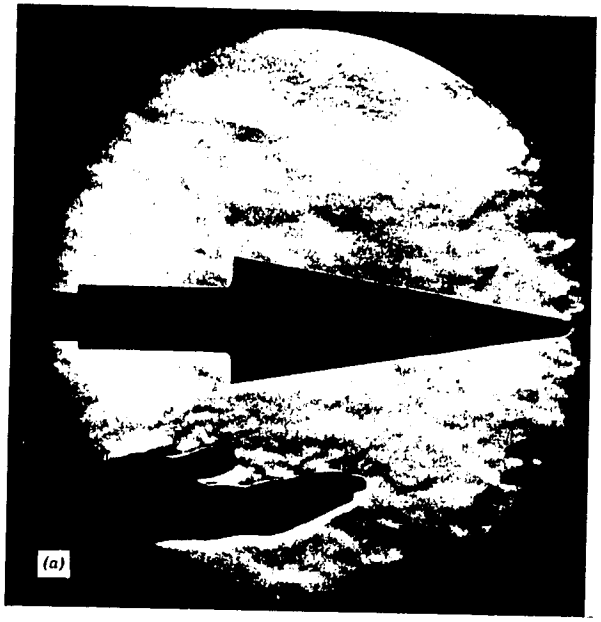
11:19 Testing Hypersonic Airplanes

While only a few hypersonic airplanes have reached the wind tunnel testing stage, when it does occur the testing is different and worthy of comment. Basically three new phenomena occur.

1. The slope of the lift curve of thin airfoils decreases to where the usual ratios for horizontal and vertical tail surfaces relative to the wing (15 and 20 per cent, respectively, say) become far too small and additional surface must be provided.
2. The flow many chord lengths behind a lifting wing is divided into sharply defined regions in which the dynamic pressure may be several times larger than freestream, or much less than freestream, and may have substantial variations in flow direction from the freestream direction. Hence the flow fields in which the horizontal and vertical tails operate become profoundly important.
3. The aerodynamic design, from an efficiency standpoint, becomes subservient to the design that will enable the aircraft to survive the aerodynamic heating environment.

The flow zones mentioned in (2) above affect the directional and lateral stability by putting the normal vertical tail in a region of decreased q as α increases (resulting in a loss of directional and lateral stability). A simple cure is a ventral fin, which in turn yields a negative dihedral effect.

The difficulty of tripping the boundary layer at hypersonic speeds and the difficulty of supplying Reynolds numbers in the tunnel equal to flight combine to make reliable comparisons between wind tunnel tests and



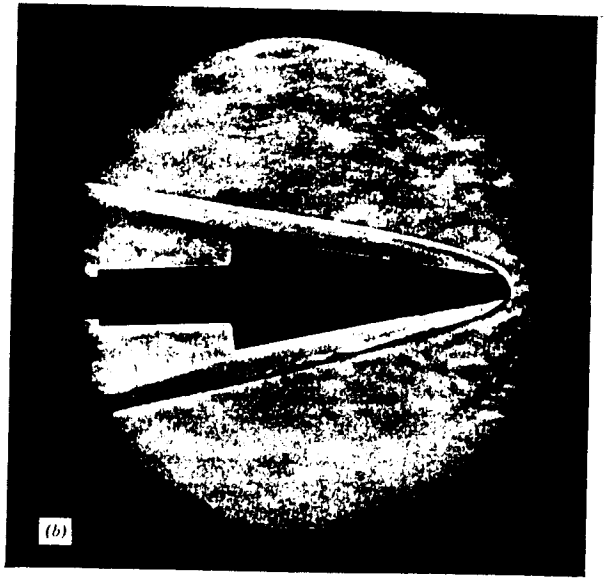
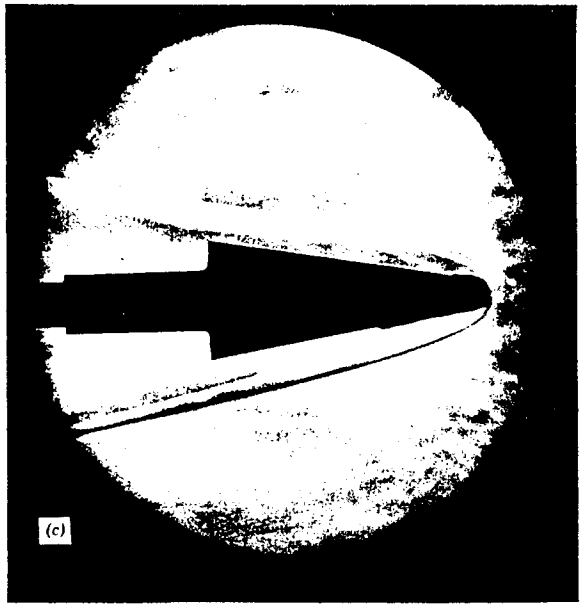
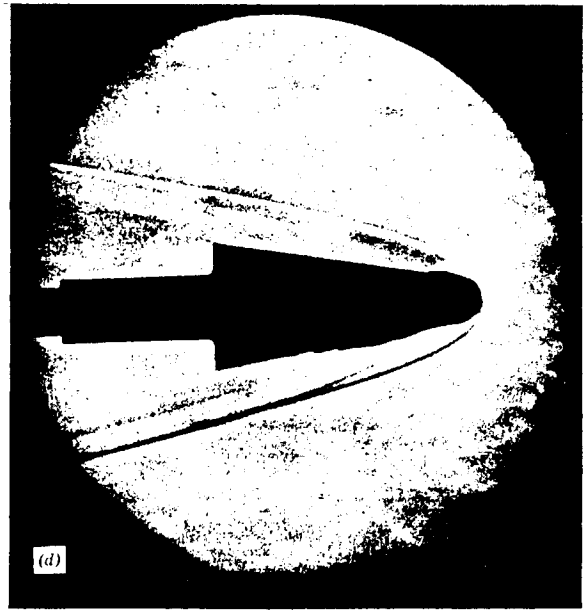


Fig. 11:17 Ablation tests at $M = 10.0$, 1800°F. Heat waves from hand shown in (*a*) demonstrate the sensitivity of the Schlieren system. (*a*) $t = 0$, $v = 0$; (*b*) $t = 20$ sec; (*c*) $t = 40$ sec; (*d*) $t = 60$ sec. (Courtesy Northrop Corporation.)





flight difficult. Studies of what little data exist seem to indicate that the flight slope of the normal force curve will be within 10 per cent of the tunnel data; drag will be about within 8 per cent, and the center of pressure will be within 6 per cent of the body length. The net result is that one must provide enough margin for safe flight in case the variations are in the wrong direction.

11:20 List of Hypersonic Wind Tunnels

Table 11:1 gives a partial list of hypersonic wind tunnels in this country (largely from Ref. 11:3) and around the world.

Table 11:1

Hypersonic Wind Tunnels

Organization	Tunnel	Location	Type	Mach Number Range	Test Section Size	$p_{t(max)}$, psia	$T_{t(max)}$, °R	
A. GOVERNMENT								
AEDC	E-2	Tullahoma, Tenn.	Pressure-vacuum	5–8	12″ × 12″	40–1300	1360	
AEDC	B	Tullahoma, Tenn.	Continuous	8	50″ round	100–800	1360	
AEDC	C	Tullahoma, Tenn.	Continuous	10–12	50″ round	180–2400	2000	
ARL	6-inch	Wright Field, O.	Continuous open jet	8–17	6″ round	400–3000	2400	
ARL	20-inch	Wright Field, O.	Blowdown open jet	10–15	20″ round	400–25,000	2400	
ARL	30-inch	Wright Field, O.	Pressure-vacuum open jet	14–21	30″ round	400–2900	4000	
ARL	4-inch	Wright Field, O.	Continuous open jet	8–17	4″ round	400–3000	2400	
ASD	24-inch	Wright Field, O.	Pressure-vacuum	6–14	24″ round	1200	4700	
ASD	EGF	Wright Field, O.	Arc-heated blow-down	4–17	To 24″ round	1500	13,500	
ASD	2-foot	Wright Field, O.	Indraft	3–6	2′ × 2′	1–15	750	
BRL	HWT-4	Aberdeen, Md.	Continuous	6–9.2	14″–18″ round	150–2000	2000	
DTMB	Hypersonic test facility	Carderock, Md.	Blowdown	5–10	13.5″ round	1–600	2500	
NASA, Ames	14-inch	Moffett Field, Calif.	Blowdown	10–25	14″ round	50–2000	530	Uses helium
NASA, Ames	20-inch	Moffett Field, Calif.	Blowdown	8–26	20″ round	360–4200	610	Uses helium

Table 11:1 (*continued*)

Organization	Tunnel	Location	Type	Mach Number Range	Test Section Size	$p_{t(max)}$, psia	$T_{t(max)}$, °R	
			A. GOVERNMENT					
NASA, Ames	Free-flight	Moffett Field, Calif.	Free-flight	—	24″ round	450–45,000	—	To 23,000 fps
NASA, Ames	Free-flight	Moffett Field, Calif.	Free-flight	—	17″ × 21″	1–150	—	To 20,000 fps
NASA, Ames	3.5-foot	Moffett Field, Calif.	Blowdown	5–15	3.5′ round	50–2000	3500	
NASA, Ames	Mass transfer	Moffett Field, Calif.	Blowdown	5–20	30″ round	100–1500	—	
NASA, Ames	Entry simulator	Moffett Field, Calif.	Free-flight	—	60″ × 60″	60–150	15,000	To 23,000 fps
NASA, JPL	21-inch	Pasadena, Calif.	Continuous	4–11.5	21″ × 21″	15–750	1350	
NASA, Langley	20-inch $M = 6.0$	Langley Field, Va.	Continuous	6.0	20″ × 20″	30–550	1060	
NASA, Langley	22-inch $M = 8.5$	Langley Field, Va.	Blowdown	8.5	20″ round	1800–3000	1510	
NASA, Langley	22-inch, helium	Langley Field, Va.	Blowdown	15–25	22″ round	500–4000	1060	
NASA, Langley	$M = 8.0$ Variable-density	Langley Field, Va.	Blowdown	8.0	18″ round	300–2500	1500	
NASA, Langley	$M = 6.0$ Low-density	Langley Field, Va.	Blowdown	6.0	12″ × 14″	15–600	1060	
NASA, Langley	Aerothermo facility	Langley Field, Va.	Blowdown	17.0	24″ round	1500–15,000	4000	Uses nitrogen
NASA, Langley	Ceramic heated	Langley Field, Va.	Blowdown	13.0	12″ round	600	4100	
NASA, Langley	Elasticity tunnel	Langley Field, Va.	Blowdown	7, 15	24″ round	15–1200	530	Uses helium
NASA, Langley	15-inch hypersonic flow	Langley Field, Va.	Blowdown	10.4	15″ round	300–1500	1960	
NASA, Langley	2-foot low-density	Langley Field, Va.	Continuous	3–7	24″ × 24″	3–50	1200	
NASA, Langley	10-Mw arc tunnel	Langley Field, Va.	Blowdown	8.0	24″ round	600–10,000	16,000	
NASA, Langley	Arc-heated	Langley Field, Va.	Blowdown	12–14	20″ round	1000	10,000	
NASA, Langley	10-inch ceramic heated	Langley Field, Va.	Blowdown	4, 6	10″ round	1125	4000	
NASA, Langley	31-inch hypersonic	Langley Field, Va.	Continuous	10, 12	31″ × 31″	225–2250	2000	
NASA, Langley	$M = 13.0$ ceramic	Langley Field, Va.	Blowdown	13.0	27″ round	1000–1200	4500	
NASA, Langley	Hyperthermal	Langley Field, Va.	Blowdown	—	4′ round	60–1500	—	8000–20,000 fps
NASA, Langley	Helium	Langley Field, Va.	Blowdown	10, 20	3′–5′ round	30–4000	1060	
NASA, Langley	Structures	Langley Field, Va.	Blowdown	7.5	8′ round	450–4000	4500	6300–7300 fps
NASA, Langley	1-foot arc tunnel	Langley Field, Va.	Blowdown	11–13	12″ round	400	8000	
NASA, Langley	4-foot arc-tunnel	Langley Field, Va.	Blowdown	12–20	4′ round	1500	12,000	
NASA, Langley	Helium blow-down	Langley Field, Va.	Blowdown	30–40	4″–22″ round	15,000	1060	Uses helium
NASA, Langley	11-inch	Langley Field, Va.	Blowdown	6.8–18.0	11″ × 11″	1600	1700	Uses air or helium
NASA, Lewis	24-inch	Cleveland, O.	Continuous	7.0	24″ round	200–480	1260	
NOL	No. 8	White Oak, Md.	Blowdown	5–10	To 25″ round	75–2500	2000	
Sandia Corp.	Hypersonic	Albuquerque, N.M.	Pressure-vacuum	4–9	18′ round	15–275	3000	
NOL	No. 4	White Oak, Md.	Blowdown	14–18	12″ round	2000	4500	Uses nitrogen

Table 11:1 (*continued*)

Organization	Tunnel	Location	Type	Mach Number Range	Test Section Size	$p_{t(max)}$, psia	$T_{t(max)}$, °R	
			B. COLLEGES AND INDUSTRY					
Boeing Co.	12-inch	Seattle, Wash.	Blowdown	5, 6, 7	12″ round open jet	1600	1000	
Brooklyn Polytech. Inst.	Hypersonic	Freeport, N.Y.	Blowdown	6, 8, 12	12″–44″ round	30–600	2600	
Cornell Aero. Lab.	Wave superheater	Buffalo, N.Y.	Blowdown	6–15	To 7′ round	300–3000	8000	
Douglas Aircraft Co.	2-ft hypersonic	El Segundo, Calif.	Blowdown	6, 8, 10	24″ round	75–2200	2000	
Fluidyne	8-inch	Minneapolis, Minn.	Blowdown	7.0	8″ diam	150	600	
Fluidyne	10-inch	Minneapolis, Minn.	Blowdown	5–8	10″ diam	450	1000	
Fluidyne	20-inch	Minneapolis, Minn.	Blowdown	20.0	20″ diam	2000	4000	
General Dynamics	Arc-jet	Fort Worth, Tex.	Arc-heated blow-down	1–12	8″ round	15–450	15,000	
Lockheed-California Co.	Propulsion	Burbank, Calif.	Blowdown	8.0	30″ round	600	3500	
Lockheed-California Co.	Hypersonic	Burbank, Calif.	Blowdown	6–12	30″ round	600	1700	
University of Minnesota	No. 2	Rosemount, Minn.	Blowdown	1.5–10	12″ × 12″	1000	1440	
University of Minnesota	No. 4	Rosemount, Minn.	Blowdown	5.5–10	12″ × 12″	50–160	3000	
University of Minnesota	6 × 9-inch	Rosemount, Minn.	Blowdown	2.7–8.2	6″ × 9″	600	1400	
MIT	Hypersonic core	Cambridge, Mass.	Continuous	7.6	12″ round	100	1300	
North American Aviation	12-inch	Inglewood, Calif.	Blowdown	5, 7	12″ round	30–330	1360	
North American Aviation	Arc discharge	Inglewood, Calif.	Blowdown	11–22	12″ round	15,000	12,000	
Northrop Corp.	Hypersonic	Hawthorne, Calif.	Blowdown	6–14	30″ round	3000	3200	
Ohio State University	Hypersonic	Columbus, O.	Blowdown	6–14	12″ round	50–1500	2800	
Princeton University	5-inch nitrogen	Princeton, N.J.	Blowdown	15	5″ round	1500	580	Uses nitrogen
Princeton University	7-inch	Princeton, N.J.	Blowdown	16	7″ round	500	900	Uses helium
Princeton University	8-inch	Princeton, N.J.	Blowdown	18–25	8″ round	5000	5700	Uses nitrogen
Purdue University	Hyperthermal	Lafayette, Ind.	Blowdown	10.0	12″ round	450	12,000	
Republic Aviation	Hypersonic	Farmingdale, N.Y.	Blowdown	6, 14	36″ round	50–3000	3500	
Republic Aviation	Arc tunnel	Farmingdale, N.Y.	Blowdown	2–10	8″ round	15,000	15,000	1.4-Mw
University of Southern Calif.	Low-density tunnel	Los Angeles, Calif.	Continuous	9	—	Small	540	2.5″ core in 30″ jet
Stanford University	Hypersonic	Stanford, Calif.	Blowdown	5	6″ round		5000	
United Aircraft Corp.	6-inch	East Hartford, Conn.	Blowdown	10.0	6″ × 6″	900	1800	
			C. FOREIGN					
ARA	Hypersonic	Bedford, England	Blowdown	7.0	12″ round	3000	1000	
BAC	18-inch	Stevanage, England	Blowdown	1.5–6.0	18″ × 18″	600	560	
FFA	Hypersonic 500	Stockholm, Sweden	Pressure-vacuum	10.0	20″ diam	1600	1800	
FFA	Hypersonic 200	Stockholm, Sweden	Pressure-vacuum	7.3	8″ diam	1600	2400	
NAE	Helium	Ottawa, Canada	Pressure-vacuum	9, 18	9″ round	3000	560	Uses helium
NAL	Hypersonic	Tokyo, Japan	Continuous blow-down	5.0			1350	
NAL	20-inch	Tokyo, Japan	Blowdown	11.0	20″ round	—	—	

Table 11:1 (*continued*)

Organization	Tunnel	Location	Type	Mach Number Range	Test Section Size	$p_{t(max)}$, psia	$T_{t(max)}$, °R	
NLRL	9-inch	Amsterdam, Netherlands	Blowdown	6.0	9″ × 9″	—	—	
NPL	—	Teddington, England	—	7.0	—	—	—	
NPL	Hypersonic	Teddington, England	Blowdown	7.0	10″ × 15″	220	1100	
ONERA	S4 MA	Modane, France	Pressure-vacuum	12	28″ diam	—	—	
ONERA	Hypersonic	Chalais-Meudon, France	Pressure-vacuum	10–16	12″ round	—	—	
ONERA	R3 Ch	Chalais-Meudon, France	Blowdown	8–10	12″ round	2100	2000	
ONERA	S3 MA	Modane, France	Pressure-vacuum	0.7–6.5	30″ × 30″	1270	1080	
ONERA	R2 Ch	Chalais-Meudon, France	Blowdown	5–7	12″ round	1200	1260	
RAE	7-inch	Farnborough, England	Blowdown	8.5	7″ × 7″	—	—	200 hp
RAE	3 × 4-foot	Bedford, England	Blowdown	5	3′ × 4′	180	800	

References

11:1 Bain Dayman, Jr., Simplified Free Flight Testing in a Conventional Wind Tunnel. Jet Propulsion Laboratory Tech. Report No. 32-346, 1962.

11:2 H. P. Holway, J. G. Herrera, and B. Dayman, Jr., A Pneumatic Launcher for Free Flight Testing in a Conventional Wind Tunnel. JPL Tech. Memorandum 33-177, July 1964.

11:3 F. A. Vicente and Nancy S. Foy, Hypersonic Wind Tunnel Facilities in the United States. Aerospace Corporation Report TOR-169(3305)-1, March 1963.

11:4 James H. Grimes, Jr., Dynamic Stability Testing with Ablation at Mach 14 in a Long Duration Wind Tunnel, Fluidyne Engineering Corporation, Minneapolis, 1964.

11:5 E. R. Van Driest and C. B. Blume, Boundary Layer Transition as Supersonic Speeds, *JASS* **29** (8), 1962.

11:6 Paul F. Holloway and James R. Sterrett, Effect of Controlled Surface Roughness on Boundary Layer Transition at Mach Numbers of 4.8 and 6.0, NASA TN-D-2054, 1964.

11:7 Grover L. Alexander, Development of Subsonic and Supersonic Total Temperature Probes for a Blowdown-Type Wind Tunnel. ASTIA AD-126 456, June 1957.

11:8 R. E. Thomas and J. D. Lee, Calibrations of the 12-inch No. 2 Hypersonic Nozzle Having Interchangeable Throats. Ohio State University TN(ALOSU) 659-3, 1959.

Chapter twelve

Hypervelocity facilities

12:1 General

There are a number of experimental aerodynamic facilities that allow testing and research to be done at velocities considerably above those achieved in tunnels of the types described in the preceding chapters. Usually in these facilities the high velocities are achieved at the expense of some other test parameter, such as Mach number, pressure, and/or run time.

Generally speaking, these facilities have come into being because the aerodynamicist does not believe that the aerodynamic problems of high-speed flight are completely answered by tests in hypersonic wind tunnels, where the tunnel operating temperature is only high enough to avoid liquefaction. There are several reasons for this skepticism. In order for the static temperatures and pressures in the test section of a wind tunnel to equal values at some altitude in the atmosphere at the same time that the velocity in the wind tunnel equals the flight velocity of an aircraft at that altitude, the total temperatures and pressures in the wind tunnel must be very high. This is illustrated for velocities and altitudes in the range of current interest by Fig. 12:1. The importance of duplicating static temperature, static pressure, and velocity in the test section arises from the fact that only in this way will the temperatures and pressures in the vicinity of a model (behind shock waves and in boundary layers) correspond to conditions for the vehicle in flight. Having the proper temperatures and pressures in the vicinity of the model is considered important because at high temperatures, the characteristics of air are completely different from those at low temperatures. The enthalpy no longer increases linearly with temperature and the gas law $P = \rho RT$ is no longer valid. The variation of enthalpy with temperature at high temperature levels is illustrated by Fig. 12:2. It is noted that the enthalpy at high temperatures is dependent on pressure as well as temperature.

The process taking place in air at high temperatures which causes the gas law $P = \rho RT$ to be invalid and which has a major effect on the enthalpy

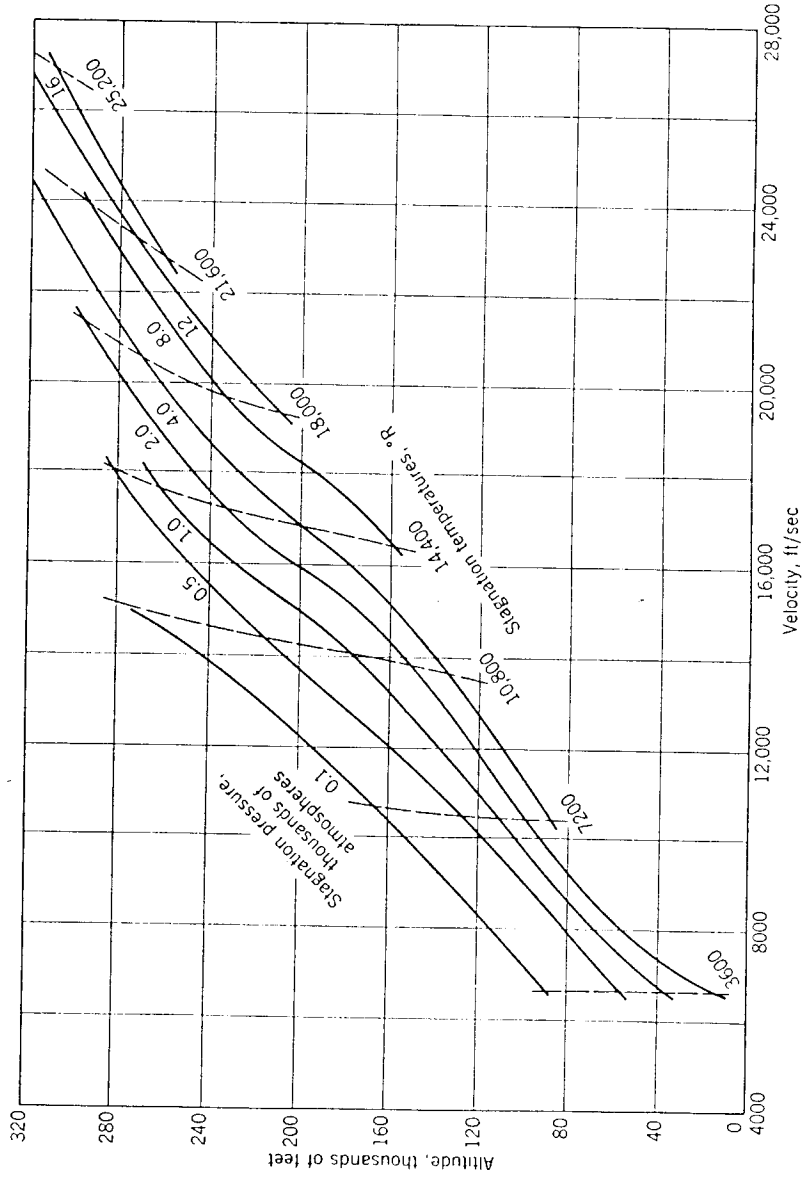


Fig. 12:1 The stagnation pressures and temperatures required to duplicate flight conditions over a wide range of speeds and altitudes.

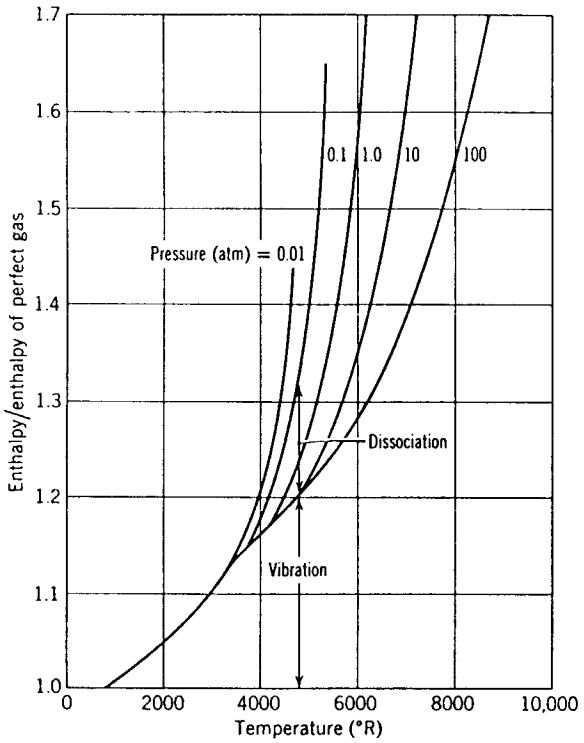


Fig. 12:2 Variation of enthalpy of air with temperature (from Ref. 12:1).

is called dissociation. Dissociation is the term given to the process in which diatomic molecules of oxygen and nitrogen (O_2 and N_2) are broken up into atomic oxygen and nitrogen (O and N). At some temperature, which is dependent on pressure, the internal energy level of the air becomes high enough that the two atoms of the diatomic molecules begin to loose their bonds and fly apart. This occurs after the vibrational degree of freedom discussed in Section 1:3 is fully excited. Considerable energy is required for breaking the diatomic molecules into atoms. This explains the unusual variation of enthalpy with temperature at high temperature levels. The gas law is not valid when dissociation is present because the number of molecules present is increased. Each molecule of O_2 that is dissociated becomes two molecules of O.

Dissociation is not an instantaneous process. It begins at one temperature and the number of diatomic molecules that are dissociated increases with increasing temperature until all the molecules are dissociated. The dissociation noted in Fig. 12:2 in the vicinity of 4000°R is that of oxygen.

The dissociation of nitrogen does not become significant until temperatures about twice this high are reached.

At temperatures near the maximum of Fig. 12:2, another real gas effect begins to reach significance. This effect is called ionization. Ionization is a process in which electrons orbiting about the nucleus of their atom are broken out of their orbits and become individual parts of the total gas mixture. Ionization progresses gradually, as does dissociation, and has an effect similar to that of dissociation on the gas properties.

Understandably, when the air in the vicinity of a vehicle in flight is dissociated or dissociated and ionized, the validity of data taken in a wind tunnel at the same Mach number without dissociation is subject to question. Because of this, a tremendous effort has been devoted to the development of facilities that provide more realistic flow conditions. Unfortunately, no facility has yet been developed in which complete duplication of the flow conditions of flight can be obtained at the higher Mach numbers. There are three primary reasons for this. The first is the inability of available materials to withstand the extreme temperature and pressure environments (Fig. 12:1) without burning or some form of erosion. The result is much contamination of the flow and a rapid destruction of tunnel components at the higher temperatures. The second is the inability to maintain the high temperatures required long enough to obtain data because of extremely high heat losses from the air due to radiation. The third reason deals with the previously described dissociation phenomenon. After the air is heated it must be expanded through a nozzle in order to achieve high velocities. In the process of expansion through the nozzle it cools very rapidly. If this cooling were to take place at a slow enough rate, all of the dissociated molecules would recombine so that the air entering the test section and approaching the model would have the same composition as atmospheric air; that is, it would be a mixture of molecules of O_2 and N_2. However, it develops that the rate of cooling during the expansion in any practical nozzle is too fast for the recombination to occur. The result is that the air reaching the test section will be in the dissociated state at a low temperature. This phenomenon is called "flow freezing" and is discussed in Refs. 12:2 to 12:4. Flow freezing affects the Mach number and other flow parameters in the test section and results in a test medium that may differ a great deal from the desired mixture of molecules of O_2 and N_2.

Facilities which have been developed in the process of trying to provide realistic flow conditions at high speeds and which are now used fairly extensively in high-speed testing include hotshot tunnels, plasma jets, shock tubes, shock tunnels, and light gas guns. These facilities are discussed briefly in the following sections.

12:2 Hotshot Tunnels

Hotshot tunnels (Refs. 12:5 and 12:6) are short-duration test devices in which the high temperatures and pressures required for operation are obtained by rapidly discharging a large amount of electrical energy into an enclosed small volume of air, which then expands through a nozzle and a test section.

The major components of a hotshot tunnel are shown in Figs. 12:3 and 12:4, and typical data from a hotshot test are shown in Fig. 12:5. The principle of operation is described with reference to Figs. 12:3 and 12:4 as follows. The arc chamber is filled with air at pressures up to 10,000 psia and the remainder of the circuit is evacuated to a very low pressure (usually to a few microns). The high- and low-pressure portions of the circuit are separated by a thin plastic or metal diaphragm located slightly upstream of the nozzle throat. Electrical energy from a capacitance or inductance energy storage system is discharged into the arc chamber over a time interval of a few milliseconds. The energy added to the air in the arc chamber causes an increase in its temperature and pressure, and this in

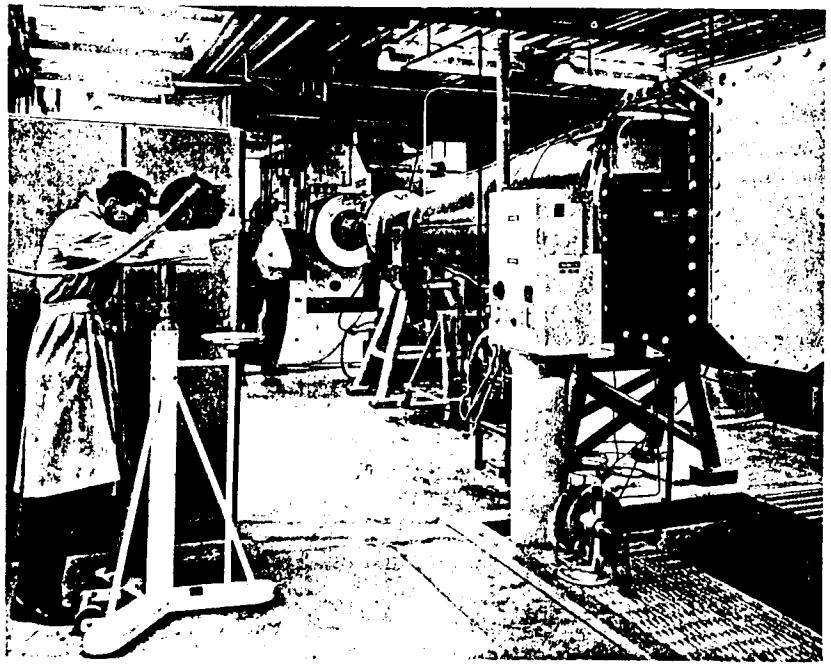


Fig. 12:3 General view of a hotshot tunnel at the Arnold Engineering Development Center. The arc chamber is in the background, with the nozzle, test section, and vacuum tank to the right. (Courtesy Arnold Engineering Development Center.)

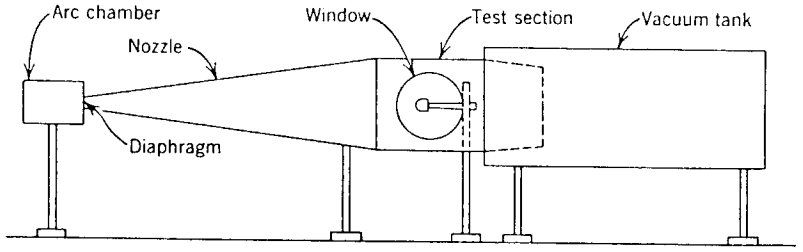


Fig. 12:4 Schematic drawing of hotshot tunnel.

turn causes a rupture of the diaphragm between the arc chamber and the nozzle throat. When the diaphragm ruptures, the high-temperature–high-pressure air in the arc chamber expands through the nozzle and establishes a high-velocity flow. The high-velocity flow typically lasts for periods of 10 to 100 msec but varies continuously during the periods. The flow variation is due to a decay with time of the pressure and temperature in

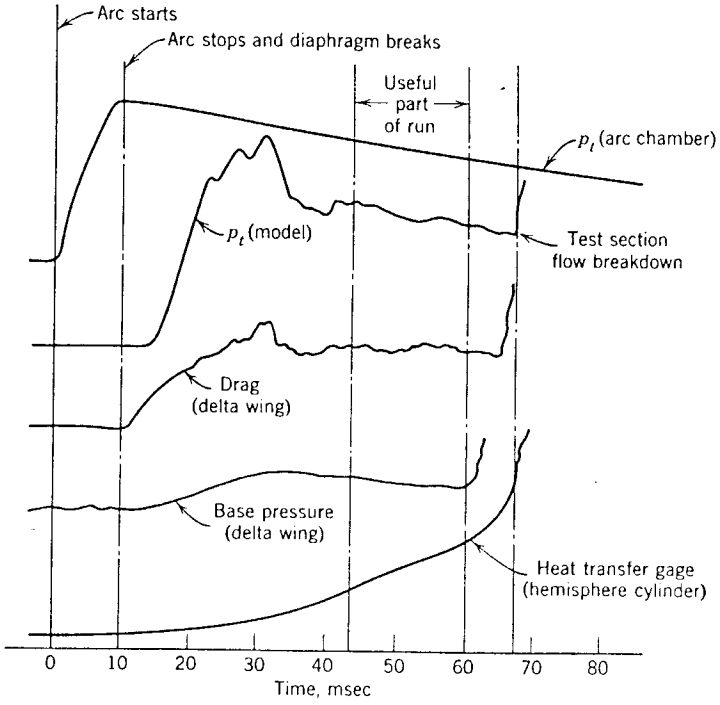


Fig. 12:5 Oscillograph traces illustrating the timewise variation of typical data components during a test in a hotshot tunnel.

the arc chamber due to the outflow of air and heat losses. The high-velocity flow is terminated when the shock that passed through the tunnel in starting the flow is reflected from the downstream end of the vacuum tank and arrives back upstream at the model.

Hotshot tunnels have been designed to operate at arc chamber pressures as high as 100,000 psia and at arc chamber temperatures of 18,000°R and higher. From Fig. 12:1 it is seen that these stagnation conditions correspond to flight duplication for about 20,000-ft/sec velocities at about 250,000-ft altitudes. Early tests in hotshot tunnels at stagnation conditions approaching these design values were quite disappointing. The metal liner, the electrode insulation, and the electrodes in the arc chamber were severely eroded by the arc discharge. The result was an excessive contamination of the air by metal and other products of the erosion. The mass flow of metal through the tunnel was many times the mass flow of air. Another problem was the erosion of the nozzle throat due to the severity of heating.

Many improvements were made in the arc chamber design in an effort to alleviate the erosion problem. To date, none of these appears to offer a solution for operation at pressures and temperatures approaching 100,000 psia and 18,000°R. Studies of the throat erosion problem were similarly disappointing. The calculated times at which a tungsten throat will begin to erode during tunnel operation at various arc chamber temperatures and pressures are presented in Fig. 12:6. In this figure it is indicated that with a stagnation temperature of 18,000°R, melting of the throat will begin in about 1 msec at a stagnation pressure of 100 atm (1470 psia), and that the run time before throat melting will decrease rapidly with increasing stagnation pressure. Results of the type presented in Fig. 12:6 are particularly disappointing in view of the fact that tungsten has the highest melting temperature of available metals.

Because of the inability thus far to solve the arc chamber and throat erosion problems, the general tendency in hotshot tunnel operation has been to reduce operating temperatures or pressures or both. Common operating conditions now are pressures of 30,000 psia, temperatures of 7200°R, and Mach numbers to 20 and above, although there is much variation between facilities. Also, it has been found that less flow contamination and throat erosion occurs if nitrogen is used instead of air for the test gas. A second advantage of using nitrogen instead of air, from the standpoint of tunnel operation, is the alleviation of the previously mentioned flow freezing problem, since dissociation of nitrogen is not significant at 7200°R.

The general trend to reduce operating temperatures and sometimes use nitrogen instead of air for the test gas has resulted in flow conditions in

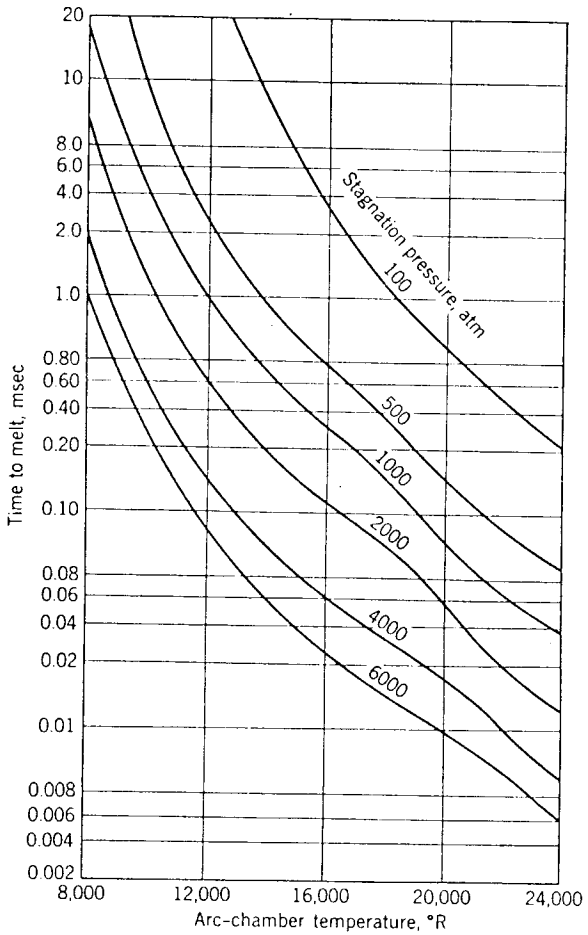


Fig. 12:6 Time required to melt a 0.1-inch diameter tungsten throat in a hotshot wind tunnel (Ref. 12:7).

the vicinity of models which do not have the real gas properties of dissociation and ionization that are characteristic of very-high-velocity flight. However, temperatures of 7200°R allow the generation of flow Mach numbers much higher than are possible in the more conventional hypersonic tunnels discussed in preceding chapters.

The problems of obtaining data in hotshot tunnels are much more difficult than in the more conventional tunnels because of the short run times. The high-response instrumentation required is beyond the scope of this book, but an insight into the problems involved may be obtained from Ref. 12:8 to 12:10. One interesting facet is the problem involved in

measuring forces with an internal balance. When the tunnel starting shock passes over the model, the model is disturbed and begins to oscillate. The model oscillation causes inertial forces to be induced on the internal balance. The tunnel run time is so short that it is very difficult to design a model balance system in which the model inertial forces do not interfere with the desired balance signals due to aerodynamic loads. The clever solution to this problem discussed in Ref. 12:8 consists of installing accelerometers in the model with signals calibrated to be the same as balance signals due to model oscillation. During the test the difference between the balance and the accelerometer signals are measured and give reliable data for aerodynamic loads.

Typical flow conditions for the useful portion of a hotshot tunnel run are stagnation pressures of 4000 to 20,000 psia, stagnation temperatures of 4000 to 8000°R, Mach numbers near 20, and dynamic pressures of about 0.5 psia. Typically the tunnel will be evacuated before the run to a pressure of 1 to 10 μ and the run will last for 50 msec.

12:3 Plasma Arc Tunnels

Plasma arc tunnels use a high-current electric arc to heat a test gas to a very high temperature. They may be operated for periods of time up to many minutes, using either direct or alternating current. Temperatures are developed in the test gas to more than 25,000°R.

The plasma arc tunnel (Fig. 12:7) consists of an arc chamber, a nozzle usually for a Mach number less than 3, an evacuated test chamber into which the nozzle discharges, and a vacuum system for maintaining the test chamber at a low pressure. In operation, a flow of cold test gas is established through the arc chamber and nozzle. An electric arc is established through the test gas between an insulated electrode in the arc

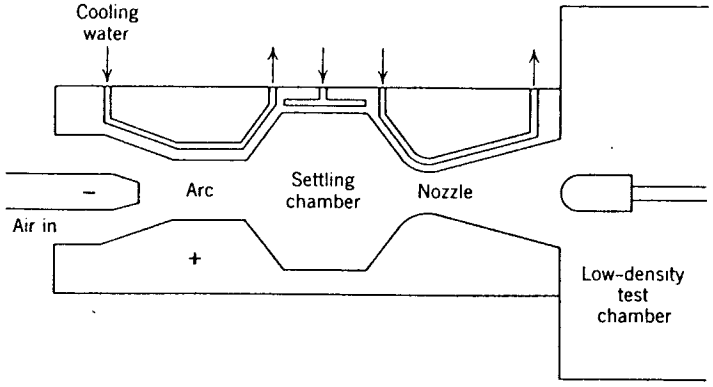


Fig. 12:7 Sketch of a low-density arc tunnel.

chamber and some surface of the arc chamber proper. The electric arc raises the temperature of the test gas to an ionization level, with the result that the test gas becomes a mixture of free electrons, positively charged ions, and neutral atoms. This mixture is called a "plasma" and it is from this that the plasma arc gets its name.

Plasma arc tunnels usually operate with low stagnation pressures (less than 100 psia) and with gases other than air. The enthalpy level of the test gas, and consequently the temperature and velocity in a given nozzle, are higher for a given power input when the pressure is low. Argon is frequently used as the test gas instead of air because a higher temperature and higher degrees of ionization can be achieved with a given power input, and because oxidation of the electrodes is eliminated.

For high-power operation, the problems of flow contamination and nozzle throat erosion discussed in Section 12:2 for hotshot tunnels exist. In existing facilities, electrode erosion has been controlled to some extent by water-cooling, by introducing the test gas into the arc chamber through a porous electrode for cooling purposes, and by rotating the arc continuously, using a magnetic field. Nozzle throat erosion at the high temperatures is controlled to an extent by operation at low pressures.

One great difficulty with a plasma jet is the variation of the qualities of the plasma over the test section. There is an actual large loss of energy through radiation so that both the temperature and the enthalpy decrease with distance downstream. In one small plasma arc $\frac{1}{4}$ inch in diameter, the temperature fell off along the centerline from 23,000°R to 15,000°R in 0.6 inch, and laterally from 23,000°R to 17,000°R in 0.1 inch. Such variation scarcely makes for good testing.

Plasma arc tunnels as generally used are not aerodynamic test facilities in the true sense of the word. They have an application in the field of aerodynamics, however, because the high heating rates that can be developed (300 Btu/ft²-sec) are useful in the study of materials for re-entry vehicles. Surface material ablation tests, which are not possible in low-temperature tunnels or high-temperature–short-duration tunnels, can be made. In these tests, the manner in which material is dissipated from the surface of a test model either by melting and run-off or by vaporization is studied. More basic studies which can be made in plasma arc tunnels and which have application in the field of aerodynamics are those on "magneto-aerodynamics" and plasma chemistry. In these studies, the electrical and chemical properties of the highly ionized gas in the flow field around a model are studied.

Some consideration is being given to the use of plasma arc chambers as heaters for more conventional high Mach number wind tunnels. See Ref. 12:21 for a list of plasma facilities in the United States.

12:4 Shock Tubes

Shock tubes are devices that use a high-pressure gas to set up a shock wave which will compress a low-pressure gas and heat it to very high temperatures. As shown in Fig. 12:8, the shock tube is simply two tubes separated by a diaphragm. One of the tubes is filled with a "driver" gas at a high pressure and the other tube is filled with a "driven" or working gas at a low pressure. The diaphragm between the two tubes is ruptured and the high-pressure driver gas rushes into the driven section, setting up a shock wave which compresses and heats the driven gas. The pressure variations through the shock tube at the instant of diaphragm rupture

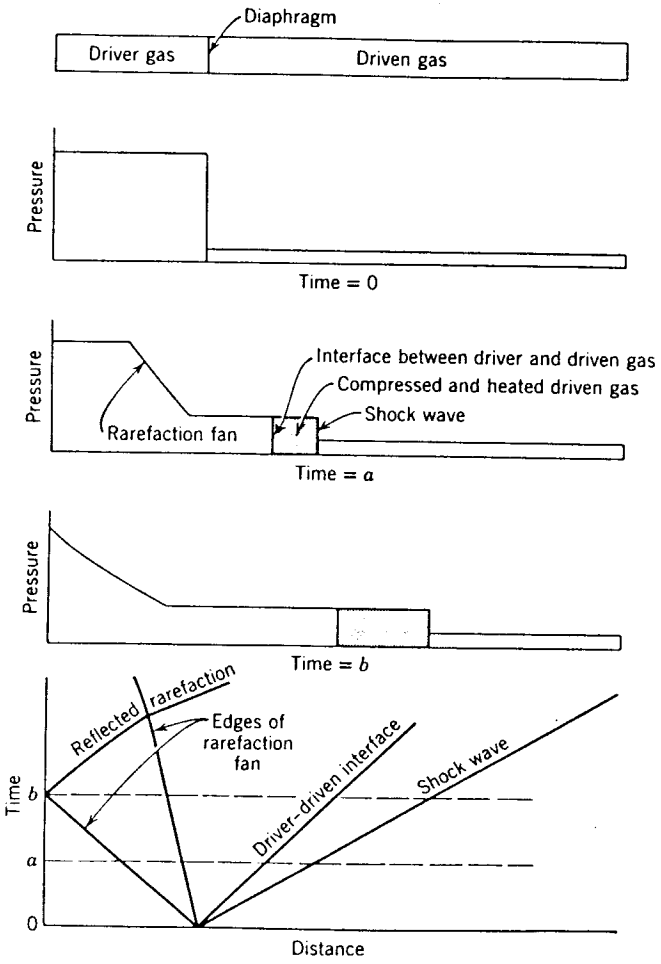


Fig. 12:8 Pressure and wave diagrams for a shock tube.

and at two short time intervals later are shown in Fig. 12:8. Also shown in Fig. 12:8 is a time–distance wave diagram, which is frequently used in depicting shock tube operation. The wave diagram simply shows the positions of the important waves as a function of time. In Fig. 12:8, at time 0 the diaphragm is broken and the shock starts moving through the driven tube at some velocity U. This is depicted on the time-distance plot as a line with a slope Δ time/Δ distance $= 1/U$. Similarly, the slopes of the lines for the driver–driven interface and the rarefaction waves are shown.

When the shock wave reaches the end of the driven tube, all of the driven gas will have been compressed and will have a velocity in the direction of shock wave travel. The shock wave, upon striking the end of the tube, will be reflected and start traveling back upstream. As it passes through the driven gas and brings it to rest, additional compression and heating is accomplished. The compressed and heated gas sample at the end of the shock tube will retain its state except for heat losses until one of two things happens: Either the shock wave reflected from the end of the tube passes through the driver gas-driven gas interface and sends a reflected wave back through the stagnant gas sample, or the rarefaction wave reflected from the end of the driver section reaches the gas sample.

The effectiveness of a shock tube for generating high temperatures is usually denoted by the shock Mach number, that is, the Mach number corresponding to the speed at which the initial shock wave travels through the driven gas. The shock Mach number that can be obtained in a shock tube is dependent on the "ratio" of initial pressures in the driver and the driven tubes, on the ratios of the speeds of sounds in the driver and driven gases at initial conditions, and on the specific heat ratios of the two gases. Equations normally used for defining shock tube operation are presented in Ref. 12:11. Higher shock Mach numbers are obtained by using large ratios of driver to driven gas pressures and by using light driver gases with high speeds of sound. The more powerful shock tubes use heated hydrogen or helium for the driver gas. Shock Mach numbers to 30 or above have been generated in such shock tubes.

Shock tubes are not normally used for the types of aerodynamic studies for which wind tunnels are used because of the very short duration of the high-velocity flows. However, the high-temperature gas samples that can be generated make the shock tube useful for studies of the chemical physics problems of high-speed flight, such as dissociation and ionization.

12:5 Shock Tunnels

Shock tunnels are wind tunnels that operate at Mach numbers to 25 or higher for time intervals up to a few milliseconds by using air heated and

compressed in a shock tube. The shock tunnel (Figs. 12:9 and 12:10) includes a shock tube, a nozzle attached to the end of the driven section of the shock tube, and a diaphragm between the driven tube and the nozzle. When the shock tube is fired and the generated shock reaches the end of the driven tube, the diaphragm at the nozzle entrance is ruptured. The shock is reflected from the end of the driven tube and the heated and compressed air behind the reflected shock is available for operation of the tunnel.

As the reflected shock travels back through the driven section it travels only a relatively short distance before striking the contact surface between the driver and the driven gas. Upon striking this contact surface, it will be reflected back toward the end of the driven section. When this reflected shock reaches the end of the driven section it will result in a change in pressure and temperature of the gas adjacent to the end of the driven section. If the change in conditions of the driven gas is significant, the flow in the nozzle will be unsatisfactory and the useful test time will be terminated. In early shock tunnels, periods of steady flow conditions were thus limited to a fraction of a millisecond. In the process of shock tunnel development it was found that testing times could be increased by almost an order of magnitude by using a "tailored-interface" (Ref. 12:13).

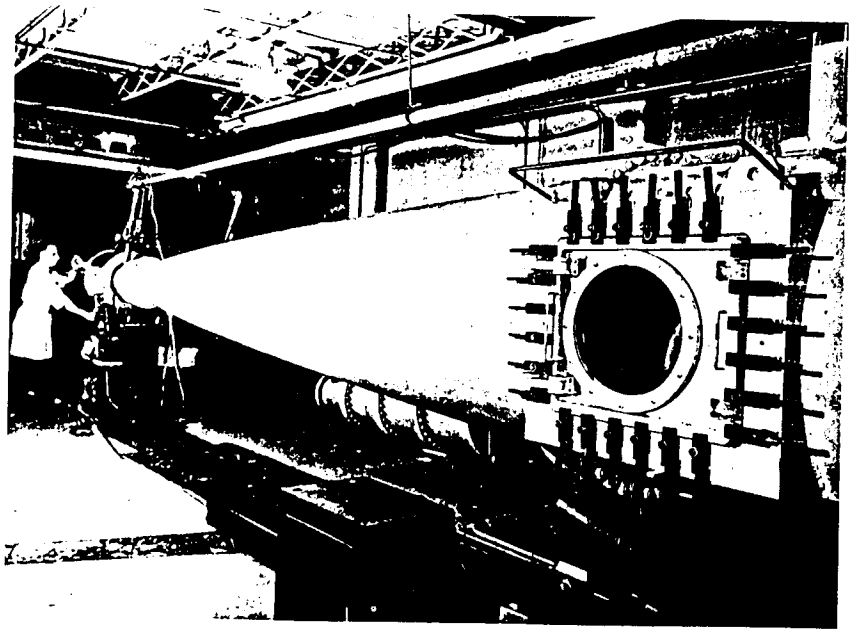


Fig. 12:9 A 48-inch hypersonic shock tunnel. (Courtesy Cornell Aeronautical Laboratory.)

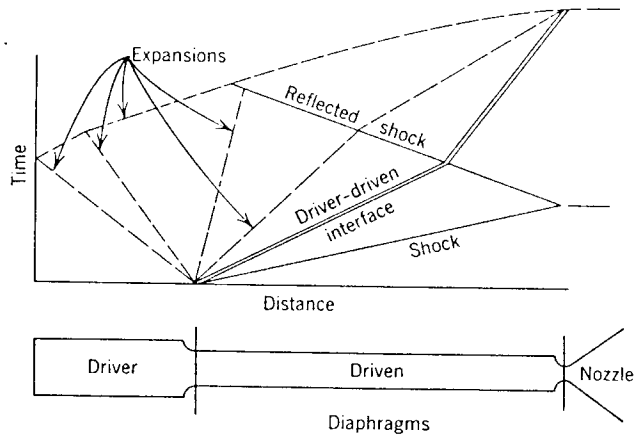


Fig. 12:10 Schematic of shock tunnel together with wave diagram.

A tailored-interface refers to conditions for which the pressure rise across the shock reflected from the nozzle end of the driven tube will be the same in the driven and the driver gas. When this condition is met, the shock will pass through the interface without being reflected. In this case the available test time will be increased and will be terminated by the flow of the last of the driven gas through the nozzle or by the reflected rarefaction waves from the driver section which reach the nozzle end of the driven tube. It has been found by experiment (Refs. 12:12 and 12:14) that significant deviations from conditions for the tailored-interface can be tolerated without a large decrease in useful run time. If the conditions do not deviate too far from those for tailoring, the shock will be reflected when it strikes the interface and will cause a significant change in pressure when it strikes the nozzle end of the driven tube the second time. However, subsequent reflections will be weak and the pressure will remain essentially constant for the duration of the run.

Shock tunnels currently in use have been designed to provide stagnation conditions to about 2000 atm pressure and 14,400°R temperature and to provide test times to about $6\frac{1}{2}$ msec. Facilities designed for higher operating pressures and temperatures are being constructed. As in hotshot tunnels, flow contamination is something of a problem at the more extreme operating conditions of shock tunnels. Figure 12:11 is a schlieren photograph of a re-entry body being tested in a hypersonic shock tunnel.

12:7 Gun Tunnels

The gun tunnel (Figs. 12:12 and 12:13) is quite similar in operation to the shock tunnel. It includes a high-pressure driver section and a low-pressure driven section with a diaphragm separating the two. A piston is

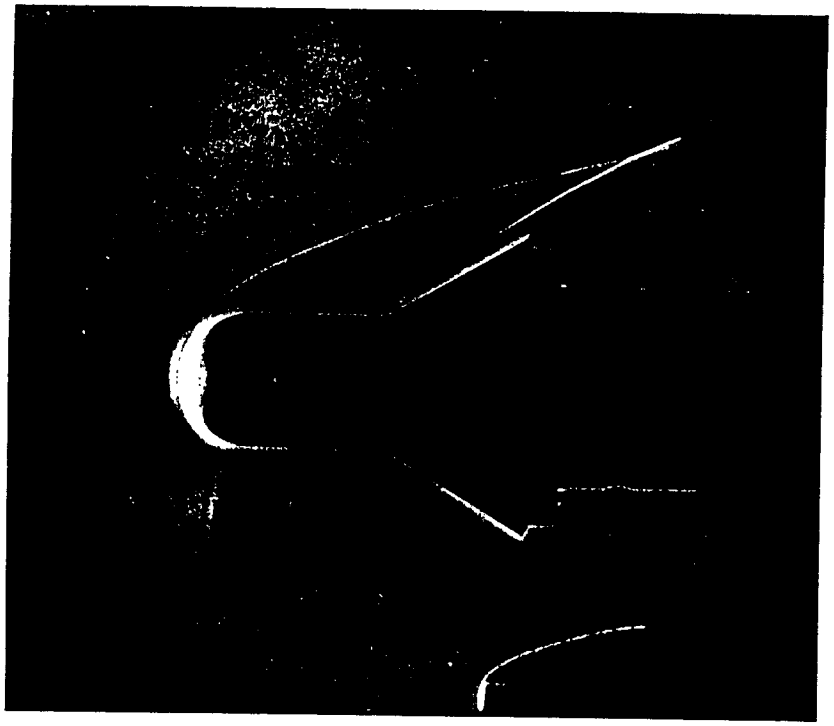


Fig. 12:11 Schlieren photograph of re-entry body under test in a hypersonic shock tunnel. (Courtesy Cornell Aeronautical Laboratory.)

placed in the driven tube adjacent to the diaphragm so that when the diaphragm ruptures, the piston is propelled through the driven tube, compressing the gas ahead of it. The piston used is very light so that it can be accelerated to velocities considerably above the speed of sound in the driven gas. This causes a shock wave to precede the piston through the driven tube and heat the gas. The shock wave will be reflected from the end of the driven tube to the piston, causing further gas heating. The piston comes to rest with equal pressure on its two sides, and the heated and compressed driven gas ruptures a diaphragm and flows through the nozzle. As the piston travels through the driven section it overshoots its equilibrium position, causing a pressure peak. This transient rapidly disappears, and the pressure of the driven gas remains essentially constant until the gas is exhausted or until an expansion wave from the driver section reaches the piston.

Gun tunnels are limited in the maximum temperature that can be achieved by the piston design. The piston must be very light in order to be accelerated to supersonic speeds in short driven sections (typical weights

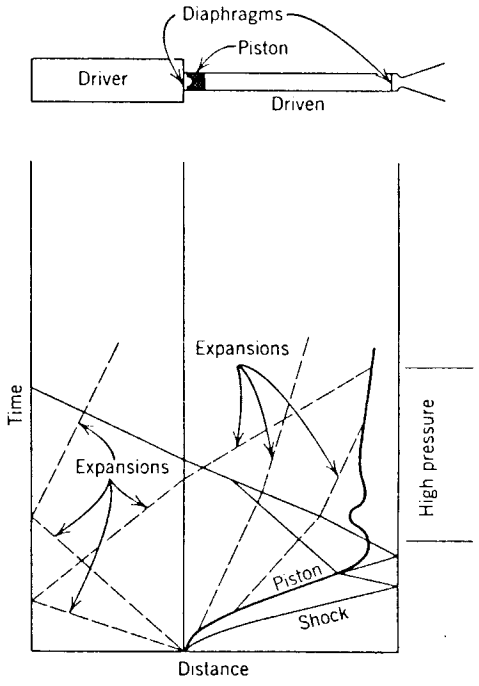


Fig. 12:12 Gun tunnel and wave diagram.

are 4 to 15 grams for a $1\frac{1}{2}$-inch diameter driven section). Also, the piston must be quite rugged to withstand very high accelerations, high temperatures, and non-uniform loading which occur during the initial diaphragm rupture. Because of piston limitations the ratios of driver to driven pressure are normally considerably less than in shock tubes and shock tunnels. Consequently the shock strength is considerably less and the temperatures achieved are considerably lower than in shock tubes and shock tunnels. The maximum temperatures normally achieved are less than 3600°R (Refs. 12:15 and 12:16), although Ref. 12:17 reports temperatures to about 5400°R. With the need to limit the ratio of driver to driven gas pressure and the desirability of a high operating pressure common to most hypersonic tunnels, the pressure and mass in the driven tube are higher than in the normal shock tube. The result is more run time (at essentially constant pressure) when the expansion wave from the driver section can be delayed. Run times an order of magnitude higher than in shock tunnels are reported in Refs. 12:15 and 12:16. Large and rapid decays in stagnation temperature have been noted during the period of essentially constant pressure. As an example, Ref. 12:15 reports a temperature decay from about 2200 to 1850°R during a 23-msec run. In

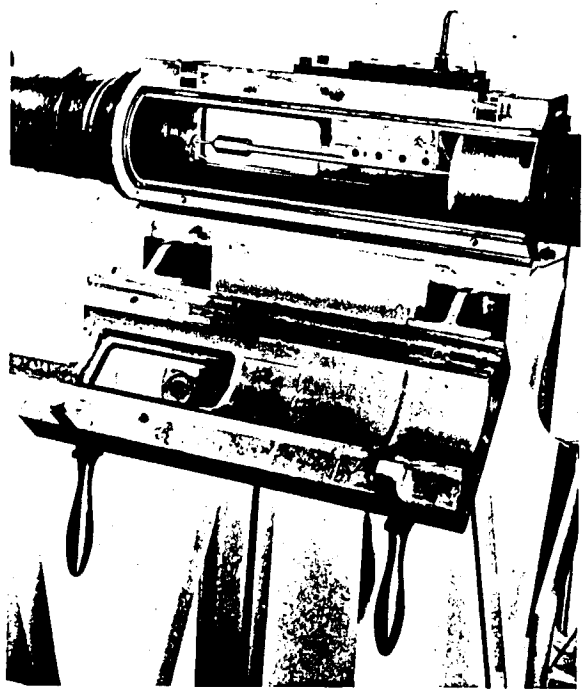


Fig. 12:13 Test section of hypersonic gun tunnel. (Courtesy FFA, Sweden.)

general, the types of tests that can be carried out in gun tunnels are the same as those in the hotshot tunnels and the shock tunnels.

12:6 Light Gas Guns

Although the light gas gun is not a wind tunnel in any sense, its importance as a hypervelocity test facility is increasing and it is therefore worthy of mention in this book. The gun is a device that accelerates a projectile to very high velocities in free flight.

Conventional guns using the standard nitrocellulose gunpowder are limited in the maximum muzzle velocities that can be achieved by the maximum speed of sound in the products of combustion of the powder and by the weight of the combustion gases which must be accelerated along with the projectile. The limiting velocity with this type of gun has appeared to be less than 10,000 ft/sec. In the light gas gun, hydrogen or helium, which are light gases with a high speed of sound, are heated and compressed and used to accelerate a projectile. With guns of this type, muzzle velocities to 30,000 ft/sec have been achieved.

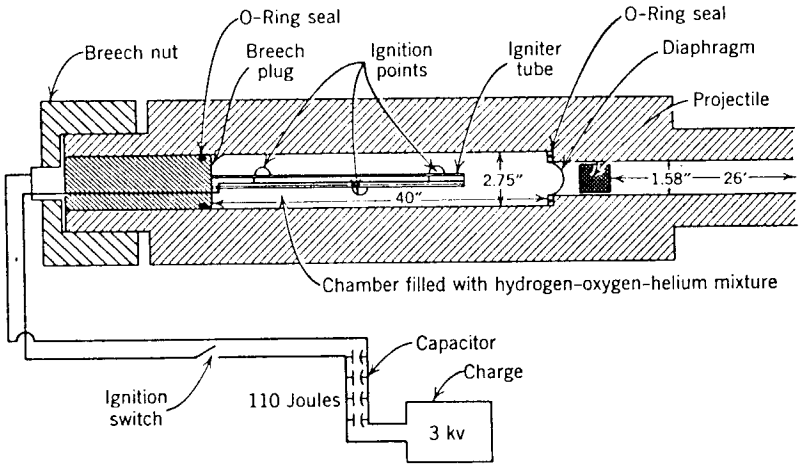


Fig. 12:14 Schematic of a single-stage light gas gun. (Ref. 12:18.)

Two types of light gas guns currently in use are illustrated in Figs. 12:14 and 12:15. The combustion chamber of the gun shown in Fig. 12:14 is filled with a mixture of helium, hydrogen, and oxygen. Discharge of the capacitors through the ignitor tube causes ignition of the hydrogen and oxygen and consequent heating of the helium. When combustion has progressed to the desired point, the diaphragm between the combustion chamber and the projectile is ruptured by the high pressure and the projectile is accelerated through the bore of the gun. The gun illustrated in Fig. 12:15 is a two-stage gun. The powder chamber is filled with a standard gunpowder. When this gunpowder is ignited it accelerates the piston to a supersonic velocity as it travels through the reservoir filled with one of the light gases. The piston moving through the reservoir causes heating and compression of the gases in the reservoir by means of a shock wave which precedes the piston. When the light gas has been compressed to the desired pressure and temperature, a diaphragm is

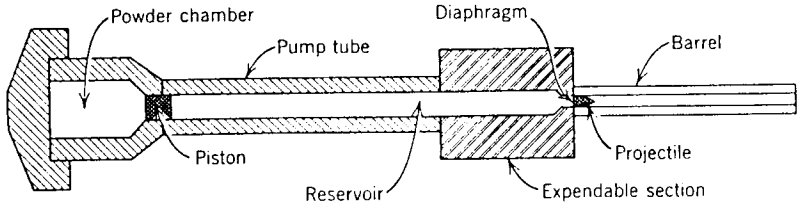


Fig. 12:15 Schematic drawing of two-stage light gas gun. (Ref. 12:19.)

ruptured by the high pressure. This allows the high-pressure and high-temperature gases in the reservoir to come in contact with the base of the projectile and accelerate it through the gun bore.

By firing the projectile into a tank of air at controlled pressure and temperature, the pressures, temperatures, and velocities of a vehicle in flight at very high velocities can be duplicated. This facility thus provides the most realistic environment of any of the hypervelocity test facilities. It does, however, have the limitation that projectiles have thus far been limited to a relatively small scale for any typical flight vehicle.

The task of obtaining data on the aerodynamic characteristics of a projectile traveling at a very high velocity is considerably more complex than that of obtaining data from a stationary wind tunnel model. A large portion of data taken to date have been photographic. Cameras are stationed at various positions along the path of flight of the projectile with shutters opened. A flash of light is triggered by the projectile passing through a light beam or some other device. Velocity of a projectile is sometimes obtained by using a number of printed circuit cards at precise locations in the line of fire of the gun. As the projectile passes through each card, the printed circuit is broken. The time at which each circuit is broken is recorded by an oscilloscope. A great deal of work has been directed toward the development of a system for telemetering data from the projectile to a fixed receiver (Ref. 12:20). This work has met with success to the degree that pressure measurements have been telemetered from a projectile traveling at more than 1500 ft/sec. The complexity of this technique is obvious when it is realized that the projectile (and any instrumentation housed in the projectile) is subjected to accelerations of 10^5 to 10^6 g.

12:7 List of Hypervelocity Wind Tunnels

Table 12:1 gives a partial list of the hypervelocity wind tunnels in this country.

Table 12:1

List of Hypervelocity Wind Tunnels

Organization	Tunnel	Location	Type	Jet Size
		A. GOVERNMENT		
ASD	Electrodynamics facility	Wright Field, O.	—	24″ diam
AEDC	Hotshot 2	Tullahoma, Tenn.	Hotshot	50″ diam
AEDC	Tunnel F	Tullahoma, Tenn.	Hotshot	100″ diam
NASA, Langley	Hyperthermal facility	Langley Field, Va.	—	48″ diam
NOL	Hypersonic shock tunnel # 1	Silver Spring, Md.	Shock	8″ models
NOL	Hypersonic shock tunnel # 2	Silver Spring, Md.	Shock	8″ models
NOL	Hypersonic shock tunnel # 3	Silver Spring, Md.	Shock	20″ models
		B. COLLEGES AND INDUSTRY		
Aerospace Corp.	Hypersonic shock tunnel	El Segundo, Calif.	Shock	66″ diam
AVCO-RAD	Shock tunnel	Wilmington, Del.	Shock	12.5″ diam
Boeing Co.	Hotshot wind tunnel	Seattle, Wash.	Hotshot	44″ diam
Boeing Co.	8-inch hotshot	Seattle, Wash.	Hotshot	8″ diam
Convair	Shock tunnel	San Diego, Calif.	Shock	27.6″ diam
Cornell Aero. Lab.	48-inch shock tunnel	Buffalo, N.Y.	Shock	48″ diam
Cornell Aero. Lab.	High-energy shock tunnel	Buffalo, N.Y.	Shock	96″ diam
Cornell Aero. Lab.	Wave superheater	Buffalo, N.Y.	Driven by sequential discharge from many shock tubes	114″ diam
Douglas Aircraft Corp.	Impulse tunnel	Santa Monica, Calif.	Shock	30″ diam
General Electric Co.	30-inch shock tunnel	Valley Forge, Pa.	Shock	30″ diam
Grumman Aircraft Corp.	Hypersonic shock tunnel	Bethpage, N.Y.	Shock	18″ diam
Ling-Temco-Vought Corp.	Hypervelocity tunnel	Dallas, Tex.	Hotshot	13″ diam
Lockheed-California Co.	Hypervelocity tunnel	Burbank, Calif.	Shock	100″ diam
Lockheed Missiles and Space Co.	Spark-heated tunnel	Palo Alto, Calif.	Hotshot	24″ diam
Lockheed Missiles and Space Co.	Spark-heated tunnel	Palo Alto, Calif.	Shock	5″ diam
Martin Marietta Corp.	Hotshot tunnel	Baltimore, Md.	Hotshot	12″ diam

Table 12:1 (*continued*)

Organization	Tunnel	Location	Type	Jet Size
McDonnell Aircraft Corp.	Impulse tunnel	St. Louis, Mo.	Hotshot	50″ diam
University of Michigan	Hotshot tunnel	Ann Arbor, Mich.	Hotshot	19″ diam
North American Aviation	12-inch hotshot	Los Angeles, Calif.	Hotshot	12″ diam
North American Aviation	12-inch shock tunnel	Los Angeles, Calif.	Shock	12″ diam
North American Aviation	Electrodynamic facility	Downey, Calif.	Hotshot	12″ diam
Republic Aviation	Shock tunnel	Farmingdale, N.Y.	Shock	24″ diam
Rhodes and Bloxom	60-inch tunnel	Canoga Park, Calif.	Hotshot	60″ diam
Stanford University	Hotshot	Stanford, Calif.	Hotshot	
United Aircraft Corp.	Hotshot tunnel	East Hartford, Conn.	Hotshot	59.5″ diam

References

12:1 R. Smelt, Test Facilities for Ultra High Speed Aerodynamics, AEDC TR 55-6, 1955.

12:2 K. N. C. Bray, Departure from Dissociation Equilibrium in a Hypersonic Nozzle, ARC 19, 983, 1958.

12:3 J. Gordon Hall, and Anthony L. Russo, Studies of Chemical Non-equilibrium in Hypersonic Nozzle Flows, paper presented at Combustion Institute Meeting, Western States Section, Los Angeles, California, November 2–5, 1959, by Cornell Aeronautical Laboratory, Inc.

12:4 D. W. Boyer, A. Q. Eschenroeder, and A. L. Russo, Approximate Solutions for Nonequilibrium Airflow in Hypersonic Nozzles, AEDC-TN-60-181, 1960.

12:5 R. W. Perry and W. N. MacDermott, Development of the Spark-Heated, Hypervelocity, Blowdown Tunnel-Hotshot, AEDC-TR-58-6, 1958.

12:6 J. A. van der Bliek, Further Development of Capacitance- and Inductance-Driven Hotshot Tunnels, AEDC-TDR-62-50.

12:7 Jackson R. Stalder, Morris W. Rubesin, and David K. Eberly, Study of Real-Gas and Heat-Transfer Effects on the Design of Hotshot Wind Tunnels, Sandia Corporation Report 166, 1960.

12:8 E. E. Edenfield, and R. L. Ledfor, Compensation of Dynamic Sting Effects in Hotshot Force Measurements, AEDC TDR-62-122, 1962.

12:9 G. R. Duryea, J. F. Martin, and L. M. Stevenson, Instrumentation for Force and Pressure Measurements in a Hypersonic Shock Tunnel, Proceedings of the Second Symposium on Hypervelocity Techniques, University of Denver, March 1962.

12:10 R. J. Vidal, Model Instrumentation Techniques for Heat Transfer and Force Measurements in a Hypersonic Shock Tunnel, Cornell Aeronautical Laboratory Report No. AD-917-A-1, 1956.

12:11 Walter Bleakney and R. J. Emrich, High Speed Problems of Aircraft and Experimental Methods, Section J, Princeton University Press, 1961.

12:12 A. Hertzberg, and Charles Wittliff, Summary of Shock Tunnel Development and Application to Hypersonic Research, Cornell Aeronautical Laboratory Report No. AD-1052-A12.

12:13 C. E. Wittliff, M. R. Wilson, and A. Hertzberg, The Tailored-Interface Hypersonic Shock Tunnel, Journal Aero/Space Sciences, **26**, 4, April 1959.

12:14 D. W. Holder and D. L. Schultz, The Duration and Properties of Flow in a Hypersonic Shock Tunnel, Proceedings of the ARS International Hypersonics Conference, August 1961.

12:15 K. N. C. Bray, Evaluation of The Hypersonic Gun Tunnel, Proceedings of the ARS International Hypersonic Conference, August, 1961.

12:16 R. N. Cox and D. F. T. Winter, A Theoretical and Experimental Study of an Intermittent Hypersonic Wind Tunnel Using Free Piston Compression, ARDE Report (B), September 1961.

12:17 Bo Lemcke, An Investigation of the Stagnation Conditions in the Shock Compression Heater of a Gun Tunnel, FFA Report 90, Stockholm, 1962.

12:18 M. E. Lord, Performance of a 40-mm Combustion Heated Light Gas Gun Launcher, AEDC-TN-60-176, 1960.

12:19 J. Eckerman, W. McKay, R. Ouellete, R. Schweiger, and G. Theophanis, Ballistic Range Developments at AVCO Research and Development Division, 1960.

12:20 P. L. Clemens, and M. K. Kingery, Development of Instrumentation for a Hypervelocity Range, AEDC-TN-60-230, 1960.

12:21 D. J. Tillian, Plasma Arc Facilities in the United States. Ling-Temco-Vought 0-71000/3R-22, November 1963.

Appendix

Numerical constants and conversion of units

1. Speed of Sound, V_c.
   $a = 49.01\sqrt{^\circ R} = 65.77\sqrt{^\circ K}$, ft/sec.
   $^\circ R = ^\circ$Fahrenheit + 459.6.
   $^\circ K = ^\circ$Centigrade + 273.0.
2. Standard Sea-Level Conditions.
   Pressure $p_0 = 14.7$ lb/inch$^2 = 29.92$ inches mercury.
   Density $\rho_0 = 0.002378$ slug/ft^3.
   Viscosity $\mu_0 = 3.74 \times 10^{-7}$ lb-sec/ft^2.
   Speed of sound $a_0 = 761$ mph $= 1116$ ft/sec.
   Temperature $t_0 = 59^\circ$F.
3. Standard Atmosphere.

Temperature decreases 1°F for each 280 ft of altitude until 36,500 ft. From 36,500 to 82,000 ft temperature is constant at −69.7°F.

Pressure decreases according to

$$p = (1.910 - 0.01315Z)^{5.256}$$

up to 36,500 ft, and according to

$$p = 6.94e^{(1.69-0.0478Z)}$$

from 36,500 to 82,000 ft. In both formulas above, Z is in thousands of feet, and p is in inches of mercury. Density decreases according to

$$\rho = \rho_0 \frac{p}{p_0} \frac{T_0}{T}$$

Viscosity varies with temperature according to

$$\mu = 2.27 \frac{(^\circ R)^{1.5}}{^\circ R + 198.6} \times 10^{-8} \frac{\text{lb-sec}}{\text{ft}^2}$$

4. Conversion Factors

A. Length

Multiply	*by*	*to obtain*
Inches	2.54	centimeters
Feet	30.48	centimeters
	0.3048	meters
Miles	5280	feet
	1.609	kilometers
	0.8684	nautical miles
Centimeters	0.3937	inches
Meters	39.37	inches
	3.281	feet
	1.094	yards
Kilometers	3281	feet
	0.6214	miles
	1094	yards

B. Area

Square inches	6.452	square centimeters
Square feet	929.0	square centimeters
	144	square inches
Square centimeters	0.1550	square inches
Square meters	10.76	square feet

C. Volume

Cubic feet	1728	cubic inches
	0.02832	cubic meters
	7.4805	U.S. gallons
Imperial gallons	0.1605	cubic feet
	4.546	liters
	277.4	cubic inches
U.S. gallons, liquid	0.1337	cubic feet
	231	cubic inches
	0.83267	imperial gallons
	4	U.S. quarts
Cubic meters	35.31	cubic feet
	1.308	cubic yards
	264.2	U.S. gallons

D. Velocity

Feet/minute	0.01667	feet/second
	0.01136	miles/hour

Multiply	*by*	*to obtain*
Feet/second	1.097	kilometers/hour
	0.5921	knots
	0.6818	miles/hour
Miles/hour	0.447	meters/second
	1.467	feet/second
	1.609	kilometers/hour
	0.8684	knots
Kilometers/hour	0.9113	feet/second
	0.5396	knots
	0.6214	miles/hour
	0.2778	meters/second
Meters/second	3.281	feet/second
	3.6	kilometers/hour
	2.237	miles/hour
Knots	1.152	miles/hour

E. Weight

Ounces (avoirdupois)	0.0625	pounds (avoirdupois)
Pounds (avoirdupois)	16.0	ounces (avoirdupois)
Tons (short)	2000	pounds (avoirdupois)
	907.18	kilograms
	0.90718	tons (metric)
Tons (long)	2240	pounds (avoirdupois)
	1016	kilograms
Tons (metric)	1000	kilograms
	2205	pounds
	1.1025	tons (short)
Kilograms	2.2046	pounds

F. Pressure

Pounds/square inch	51,710	microns
	0.06804	atmospheres
	2.036	inches of mercury
	703.1	kilograms/square meter
Pounds/square foot	0.1924	inches of water
	4.883	kilograms/square meter
Atmospheres	76.0	centimeters of mercury
	29.92	inches of mercury
	1.033	kilograms/square centimeters
	14.7	pounds/square inch
	2116	pounds/square foot

Multiply	*by*	*to obtain*
Inches of water	5.204	pounds/square foot
	25.40	kilograms/square meter
	0.07355	inches of mercury
Kilograms/square meter	0.2048	pounds/square foot
Microns (of mercury)	0.00001934	pounds/square inch

G. TEMPERATURE

To change Fahrenheit to Centigrade

1. Add 40.
2. Multiply by $\frac{5}{9}$.
3. Subtract 40.

To change Centigrade to Fahrenheit

1. Add 40.
2. Multiply by $\frac{9}{5}$.
3. Subtract 40.

Index

Ablation testing, 431
Acceleration wind tunnels, 391
Activated alumina, 83
Adiabatic wall temperature, 363
Aeroelastic effects, 341
Aftercooler, 79
Aileron, 272
  power, 334
  reversal speed of, 342
Air coolers, 161
Air driers, 81, 139, 191
  for indraft tunnels, 139
  pressure drop in, 141
Air inlet, 137
Air loads, 242
Air storage tanks, 87
  painting of, 88
Airfoil flow, 10
Airplane testing, 431
Alcohol, 203
Alphatron, 215
Aluminum oxide, 150
Anemometer, hot wire, 228
Area rule, 308
Axes, body, 298
  body to wind, 298
Axial force, 257
  corrections, 323

Back-pressure valve, 87
Balances, axial force, 273
  calibration of, 260
  design of, 251
  external, 275
  heating of, 418
  hinge moments, 271
  internal, 243
  remote, 273
Balances, rolling moment, 273
  six-component, 261
  wall-mounted, 273
Balloonets, 143
Barometer, 198
Base drag, 322
Base heating testing, 393
Bending moment, control, 271
Blockage test, 416
Body axes, 298
Boundary layer, 10, 33, 52, 412
  displacement thickness of, 51
  laminar, 50, 319
  separation of, 33
  survey of, 412
  turbulent, 50, 319
  visualization of, 237
    china clay, 238
    liquid film, 238
    luminescent lacquer, 239
    oil flow, 239
Buffet, 337
Buoyancy, 63, 303
Buzz, 385

Calculating air flow rates, 70
Calibration, 62, 310, 352
  of balances, 265
  hypersonic tunnels, 405
  nearsonic tunnels, 305
  pressure, 209
  transonic tunnels, 311
  use of, 364
Capture area ratio, 384
Center of pressure, 63
Characteristic line, 28
Characteristics, method of, 39
  reflection of, 43

China clay, 238
Choke, adjustable, 316
  body, 106
Choking, 305
  wall choke, 306
Circuit, tunnel, 161, 190
Coefficients, force and moment, 298
Compressible flow theory, 5
Compression, 9
  drying, 80
  ratio, 31
Compressors, 75, 133, 167
  centrifugal, 167
  staging, 167
  surge of, 168
Condensation, 53, 307, 349
Conductivity, of air, 153
  of water, 176
Continuity equation, 13
Continuous tunnels, 4
Continuum flow, 163
Control, flap-type, 272
Convection current, 102
Conversion of units, 465
Coolers, air, 161, 171, 191
  design of, 173
Cooling, ablative, 425
  radiative, 425
Corrections to data, 303
  reduction of, 284

Deadweight tester, 210
Desiccant, 83
  amount needed, 140
Development tests, 326
Dewpoint, 56, 84, 223
  meters for, 57, 223
Diaphragms, 99
Dibutyl-phthalate, 203
Diffuser, 97, 104, 117, 126, 133
  adjustable, 127
  efficiency of, 118
  flaps, 126
  wide-angle, 97
Diffusion pump, 214
Directional stability and control, 333
Dissociation, 444
Doors, test section, 112
  tunnel inlet, 137
Downwash lag, 274
Drag, 63, 330

Driers, 133
Driven gas, 452
Drop test, 381
Dry air, 191
Dynamic roll rig, 281
Dynamic stability, 275, 301, 335
  forced oscillation, 281, 336
  free oscillation, 277
  pitch rig, 278
  reduction of, 301
  rigs for, 275, 277
  testing for, 335, 427

Ejectors, 128
Energy equation, 13
Engines, 294
  tests of, 383
Equations of motion, pitching, 277
Equation of state, 12
Expansion, 9

Fail-safe, 95
Fibrefrax, 182
Flaps, diffuser, 104
Flow, angularity, 359, 411
  freezing, 445, 448
  ionization, 420
  qualities, 62
  rate, 70
  separation of, 33
  spreaders, 98, 99
  streamline, 8
  visualization, 237, 419
Flutter, 342
Fool-proofing, 131
Force data, 298
  measurement of, 242
  reduction of, 298
  tests, 371, 418
Forces, 242
Forces and moments; wind axes, 298
  body axes, 298
Free-flight technique, 428
Free jets, 116, 117
  enclosed, 118
Free molecule flow, 163
Friction factor, 196
Fringe shift, 237

Gage factor, 246
Glass, 112

Globars, 149
Grit, carborundum, 321
  table of, 321
Gun tunnels, 453

Heat transfer, measurement of, 226
  nozzle throat, 192
  testing for, 429
Heaters, combustion, 158
  design of, 185
  electrical resistance, 179
  gas-fired, 150
  graphite, 183
  need for, 58
  nitrogen, 183
  pressure drop in, 151
  resistance tube, 179
  resistance wire, 181, 183
  storage, 148
Hinge moments, 301
  control, 271
Hotshot tunnels, 446
Hot-wire anemometers, 361
Hypersonic tunnels, calibration of, 402
  definition of, 402
  facilities, 442
  list of, 434
Hypervelocity facilities, list of, 460

Ideal flow, 22
Indraft tunnels, 5
  design of, 135
Inertia, measurement of, 280
Injectors, 128
Inlets, 384
  engine, 294
Interference tests, 380
Interferometer, 235
Intermittent tunnels, 1
  drawings of, 2, 3
Ionization, 445
Ionized flow, 420
Isentropic relations, 13
  table of, 15

Joule-Thomson flow, 94

Kanthal, 181
Knife edges, 233
Knudsen number, 164

Lateral-directional testing, 330, 390
Least squares, 209, 266
Light gas gun, 458
Liquefaction, 58
  detection of, 60
Liquid film, 238
Longitudinal stability and control, 326, 390
Luminescent lacquer, 239

Mach number, 1
  calibration of, 352, 357
  control, transonic, 316
  determination of, 352, 408
Mach wave, 8
Magnus force test, 381
Manometers, 201
  fluids for, 203, 211
  multiple, 201
  U-tube, 201
Mass flow, 70
Mean aerodynamic chord, 299
Mean free path, 162
Measuring devices, 198
  for forces, 242
  for moments, 242
  for total temperature, 217
Mercury, 203
Method of characteristics, 39
Micromanometers, 211
Mixers, 146, 158
Model catchers, 142, 170
Modeling clay, 307
  for high temperatures, 307
Models, 284
  dynamic stability, 288
  engine test, 294
  filler for, 307
  force, 286
  half-span, 124
  heating, 419
  length, 109
  mounting, 110
  pressure, 289
  size, 37, 112, 303
  support systems, 119, 123
Moisture, 54
Moments, 242
Momentum equation, 13

Newtonian theory, 403
Noise, 95, 363

Normal forces, 252
Normal shock, 9, 18, 29, 33
  relations for, 19
Nozzle, 103
  boundary layer for, 52
  design of, 44
  flexible plate, 107
  three-dimensional, 50
Numerical constants, 465
Nusselts number, 174

Oblique shock, 9
Oil filter, 81
Operating pressure, 67
Operating range, transonic, 317
Optical systems, 229
  shadowgraph, 229
  schlieren, 121, 232
  interferometer, 235

Pebble beds, 148
Piping, 96
Pitching moment, 63, 252
Pitch-pause, 124
Pitot pressure, 64, 353
Pitot tubes, 353
Plasma arc tunnels, 450
Plenum chamber, 104
Porous walls, 103
Prandtl-Meyer flow, 9
  table for, 40
Pressure calibration, 212
  coefficient, 297
  control, 93
  data, 297
  drop, 152
  gage, dial type, 205
    calibration of, 209
  lag, 293
  measurement, 198
  ratios, 34, 35
    definition of, 30
  recovery, 384
  regulators, 92, 133
  transducers, 206
Pressure-vacuum tunnels, 4
  design of, 146
Proximity tests, 380
Pumping time, 75, 77, 144
  vacuum, 143
Pumps, diffusion, 213

Real gas, 21, 408
Recovery factor, 219, 363
Reflection-plane testing, 335
Refrigeration, 165
Reynolds number, 50
Reynolds number effect, 318, 369, 417
  on base pressure, 370
  on stability, 325
  on transition, 363
Roll damping, 276
Roll-pitch coupling, 373
Roll rates, 334
Rolling moment, 255
Rotation, angular, 276
Rotational speed, model, 123
Roughness, 321, 378
Run frequency, 74
Run time, 69
  blowdown tunnels, 71
  indraft tunnels, 135

Safety, 131, 144
Safety discs, 88, 99
Safety grids, 170
Sandblasting, 157
Scanner valve, pressure, 207, 291
Schlieren systems, 112, 121, 232, 419
  color, 234
  double-pass, 233
Screens, 100, 159, 170
  pressure drop, 101
Second throat, 28, 32
Separation, boundary layer, 325
Setting Mach number, 316
Shadowgraph, 229
Shock tubes, 452
Shock tunnels, 453
Shock waves, 8, 28
  oblique, 9
Side force, 253
Signal measuring, 250
Signal voltage, 246
Silencers, 127
Silica gel, 83
Silicone oil, 211
Skin friction, 319
Slip flow, 163
Slots, 103
Small classroom tunnels, 132
Sonic boom testing, 391
Sonic-pneumatic probes, 221

Sound, speed of, 13
Sound waves, 6
Spark gap, 230
Specific gravity, table of, 203
  variations with temperature, 204
Specific heat, air, 153
Speed brakes, 341
Stability, Reynolds number effects, 325
Starting loads, 365, 416
  reduction of, 367
Starting supersonic tunnels, 29
Static pipe, 311
Static pressure, 63, 354
  measurement of, 312, 354
  pipe, 311
  probes, 354
Stings, 110, 120
  effects of, 323, 324, 369
Storage tanks, 133
Strain gages, 244
  bridge, 245
Stream tubes, 8
Streamline flow, 8
Stress, balance, 249
Strut, sector, 121
  twin screw, 121
  vertical, 120
Sumps, 170
Supercooling, 56
Supersonic transport, 388
Supersonic wind tunnels, calibration of, 393
  list of, 349, 357
  reduction of starting loads, 38
Support systems, model, 119
Swept wings, 308

Tailored interface, 454
Tare corrections, 300
Temperature, compensating for, 248
  gradients, 407
  measurement of, 138, 216
  probes, 222
  settling chamber, 406
Test, pressure, 297
Test section, 109, 133
  auxiliary suction for, 106
  free jet, 116
  plenum for, 106
  ventilation of, 104
  windows, for, 112
Testing, ablation, 431
Testing aeroelastic effects, 341
  aileron power, 334
  airfoils, 383
  bombs, 377
  complete airplanes, 326, 386
  drag, 300
  drop models, 381
  engines, 383
  free-flight, 428
  heat transfer, 429
  hinge moments, 420
  hypersonic airplanes, 431
  guided missiles, 371
  longitudinal stability, 327
  for Magnus forces, 381
  missile base heating, 393
  nose cones, 421
  procedures, 295
  re-entry bodies, 422
  retro-rockets, 385
  for sonic boom, 391
  speed brakes, 341
  unguided rockets, 372
  unsteady pressures, 393
Tetrabromoethane, 203
Theories, compressible flow, 5
  linear, 351
  supersonic, 351
Thermal mixer, 158
Thermocouples, 216
Throat, nozzle, 192
Tip stall, 309
Total head, 64
  measurement of, 312
Total temperature probe, 217, 222
Transducer, 206
  calibration of, 328
  installation of, 212
Transition, 32, 319, 326, 370
  on cone, 362
  determination of, 362, 363
  fixed, 320
  flow, 163
  Reynolds number, 362
  strip, 320
Transonic tunnels, list of, 342
Tubing, 291
Tunnel, blowdown, 1, 2, 5, 66
  design of, 68
  low-density, 162
  operational chart, 407

Tunnel, pressure vacuum, 1, 3, 146
  settling chambers, 99
  size, 68
  starting, 29, 36, 365
  test sections, 109
  wall effects, 302
Turbulence, 100, 336, 361, 412
  determination of, 317
  level of, 317

Vacuum boiling, 157
Vacuum pumps, 213
Vacuum tank, 142
Valves, back-pressure, 87
  ball, 97
  butterfly, 96, 136
  downstream, 142
  gate, 97, 133
  plug, 97
  vacuum, 142, 215
Vents, nozzle, 103
Vibration, 21
Vibrational effects, 22
Viscosity, of air, 151
  of water, 176

Wall angle, 314
Wall effects, 302
Water, conductivity, 176
  vapor, 54
  viscosity, 176
Wave-angle measurement, 356
Wave diagram, 452
Wedges, 357
Windows, 112
Window specifications, 116

Yawmeters, 312, 360
  hypersonic, 411

Zirconium oxide, 150